
FLUID DYNAMICS

Theory, Computation, and Numerical Simulation

Accompanied by the software library *FDLIB*

by

C. Pozrikidis

*University of California, San Diego
La Jolla, California 92093-0411
U.S.A.*

Email: cpozrikidis@ucsd.edu

Internet URL: http://stokes.ucsd.edu/c_pozrikidis



KLUWER ACADEMIC PUBLISHERS
Boston / Dordrecht / London

Distributors for North, Central and South America:

Kluwer Academic Publishers
101 Philip Drive
Assinippi Park
Norwell, Massachusetts 02061 USA
Telephone (781) 871-6600
Fax (781) 681-9045
E-Mail <kluwer@wkap.com>

Distributors for all other countries:

Kluwer Academic Publishers Group
Distribution Centre
Post Office Box 322
3300 AH Dordrecht, THE NETHERLANDS
Telephone 31 78 6392 392
Fax 31 78 6546 474
E-Mail <services@wkap.nl>



Electronic Services <<http://www.wkap.nl>>

Library of Congress Cataloging-in-Publication Data

Pozrikidis, C.

Fluid dynamics: theory, computation, and numerical simulation / by C. Pozrikidis
p.cm.

"Accompanied by the software library FDLIB. "

Includes bibliographical references and index.

ISBN 0-7923-7351-0 (acid-free paper)

1. Fluid dynamics. I. Title

QA911 .P63 2001
532'.05—dc21

2001029458

Copyright © 2001 by Kluwer Academic Publishers

All rights reserved. No part of this publication may be reproduced, stored in a retrieval system or transmitted in any form or by any means, mechanical, photocopying, recording, or otherwise, without the prior written permission of the publisher, Kluwer Academic Publishers, 101 Philip Drive, Assinippi Park, Norwell, Massachusetts 02061.

Printed on acid-free paper.

Printed in the United States of America.

Preface

Ready access to computers at an institutional and personal level has defined a new era in teaching and learning. The opportunity to extend the subject matter of traditional science and engineering disciplines into the realm of scientific computing has become not only desirable, but also necessary. Thanks to portability and low overhead and operating costs, experimentation by numerical simulation has become a viable substitute, and occasionally the only alternative, to physical experimentation.

The new environment has motivated the writing of texts and monographs with a modern perspective that incorporates numerical and computer programming aspects as an integral part of the curriculum: methods, concepts, and ideas should be presented in a unified fashion that motivates and underlines the urgency of the new elements, but does not compromise the rigor of the classical approach and does not oversimplify.

Interfacing fundamental concepts and practical methods of scientific computing can be done on different levels. In one approach, theory and implementation are kept complementary and presented in a sequential fashion. In a second approach, the coupling involves deriving computational methods and simulation algorithms, and translating equations into computer code instructions immediately following problem formulations. The author of this book is a proponent of the second approach and advocates its adoption as a means of enhancing learning: interjecting methods of scientific computing into the traditional discourse offers a powerful venue for developing analytical skills and obtaining physical insight.

The goal of this book is to offer an introductory course in fluid mechanics, covering traditional topics in a way that unifies theory, computation, computer programming, and numerical simulation. The approach is truly introductory, in the sense that a minimum of prerequisites are required. The intended audience includes not only advanced undergraduate and entry-level graduate students, but also a broad class of scientists and engineers with a general interest in scientific computing.

The discourse is distinguished by two features. First, solution procedures and algorithms are developed immediately after problem formulations. Second, numerical methods are introduced on a need-to-know basis and in increasing order of difficulty: function interpolation, function differentiation, function integration, solution of algebraic equations, finite-difference methods, etc.

A supplement to this book is the FORTRAN software library *FDLIB* whose programs explicitly illustrate how computational algorithms translate into computer code instructions. The codes of *FDLIB* range from introductory to advanced, and the problems considered span a broad range of applications; from laminar channel flows, to vortex flows, to flows in aerodynamics. The input is either entered from the keyboard or read from data files. The output is recorded in output files in numerical form so that it can be read and displayed using independent graphics, visualization, and animation applications on any computer platform. Computer problems at the end of each section ask the student to run the programs for various flow conditions, and thus study the effect of the various parameters characterizing a flow. Instructions for downloading the source code and a description of the library contents are given on page 651.

In concert with the intended usage of this book as a stand-alone text and as a tutorial on numerical fluid dynamics and scientific computing, references are not provided in the text. Instead, a selected compilation of introductory, advanced, and specialized references on fluid dynamics, calculus, numerical methods, and computational fluid dynamics are listed in the bibliography on page 666. The reader who wishes to focus on a particular topic is directed to these resources for further details.

I would like to extend special thanks to Vasilis Bontozoglou for his friendship and encouragement, and to Yuan Chih-Chung, Rhodalynn Degracia, Audrey Hill, and Kurt Keller for helping me with the preparation of the manuscript.

C. Pozrikidis

San Diego

January, 2001

Email: cpozrikidis@ucsd.edu

Book internet site: http://stokes.ucsd.edu/c.pozrikidis/FD_TCNS

Contents

<i>Preface</i>	ix
1. Fluid Motion: Introduction to Kinematics	1
1.1 Fluids and Solids	1
1.2 Fluid Parcels and Flow Kinematics	2
1.3 Coordinates, Velocity, and Acceleration	4
1.4 Fluid Velocity and Streamlines	15
1.5 Point Particles and Their Trajectories	18
1.6 Material Surfaces and Elementary Motions	27
1.7 Interpolation	38
2. Fluid Motion: More on Kinematics	49
2.1 Fundamental Modes of Fluid Parcel Motion	49
2.2 Fluid Parcel Expansion	61
2.3 Fluid Parcel Rotation and Vorticity	62
2.4 Fluid Parcel Deformation	68
2.5 Numerical Differentiation	72
2.6 Areal and Volumetric Flow Rate	77
2.7 Mass Flow Rate, Mass Conservation, and the Continuity Equation	87
2.8 Properties of Point Particles	93
2.9 Incompressible Fluids and Stream Functions	101
2.10 Kinematic Conditions at Boundaries	106
3. Flow Computation Based on Kinematics	111
3.1 Flow Classification Based on Kinematics	111

3.2	Irrotational Flows and the Velocity Potential	114
3.3	Finite-Difference Methods	122
3.4	Linear Solvers	131
3.5	Two-Dimensional Point Sources and Point-Source Dipoles	135
3.6	Three-Dimensional Point Sources and Point-Source Dipoles	149
3.7	Point Vortices and Line Vortices	154
4.	Forces and Stresses	164
4.1	Body Forces and Surface Forces	164
4.2	Traction and the Stress Tensor	166
4.3	Traction Jump across a Fluid Interface	173
4.4	Stresses in a Fluid at Rest	181
4.5	Viscous and Newtonian Fluids	185
4.6	Simple Non-Newtonian Fluids	194
4.7	Stresses in Polar Coordinates	197
4.8	Boundary Condition on the Tangential Velocity	203
4.9	Wall Stresses in Newtonian Fluids	205
5.	Hydrostatics	208
5.1	Equilibrium of Pressure and Body Forces	208
5.2	Force Exerted on Immersed Surfaces	217
5.3	Archimedes' Principle	224
5.4	Shapes of Two-Dimensional Interfaces	227
5.5	A Semi-Infinite Interface Attached to an Inclined Plate	231
5.6	Meniscus between Two Parallel Plates	235
5.7	A Two-Dimensional Drop on a Horizontal Plane	241
5.8	Axisymmetric Shapes	246

6. Equation of Motion and Vorticity Transport	252
6.1 Newton's Second Law for the Motion of a Parcel	252
6.2 Integral Momentum Balance	258
6.3 Cauchy's Equation of Motion	263
6.4 Euler's and Bernoulli's Equations	270
6.5 The Navier-Stokes Equation	281
6.6 Vorticity Transport	288
6.7 Dynamic Similitude, the Reynolds Number, and Dimensionless Numbers in Fluid Dynamics	296
7. Channel, Tube, and Film Flows	306
7.1 Steady Flow in a Two-Dimensional Channel	306
7.2 Steady Film Flow Down an Inclined Plane	315
7.3 Steady Flow through a Circular or Annular Tube	319
7.4 Steady Flow through Channels and Tubes with Various Cross-Sections	327
7.5 Steady Swirling Flow	336
7.6 Transient Flow in a Channel	339
7.7 Oscillatory Flow in a Channel	347
7.8 Transient and Oscillatory Flow in a Circular Tube	354
8. Finite-Difference Methods	364
8.1 Choice of Governing Equations	364
8.2 Unidirectional Flow; Velocity/Pressure Formulation	366
8.3 Unidirectional Flow; Velocity/Vorticity Formulation	377
8.4 Unidirectional Flow; Stream Function/Vorticity Formulation	382
8.5 Two-Dimensional Flow; Stream Function/Vorticity Formulation	386
8.6 Velocity/Pressure Formulation	395
8.7 Operator Splitting and Solenoidal Projection	399

9. Flows at Low Reynolds Numbers	410
9.1 Flows in Narrow Channels	411
9.2 Film Flow on a Horizontal or Down Plane Wall	424
9.3 Two-Layer Channel Flow	436
9.4 Flow Due to the Motion of a Sphere	443
9.5 Point Forces and Point Sources in Stokes Flow	450
9.6 Two-Dimensional Stokes Flow	459
9.7 Flow near Corners	465
10. Flows at High Reynolds Numbers	475
10.1 Changes in the Structure of a Flow with Increasing Reynolds Number	476
10.2 Prandtl Boundary-Layer Analysis	479
10.3 Prandtl Boundary Layer on a Flat Surface	485
10.4 Von Kàrmàn's Integral Method	501
10.5 Instability of Shear Flows	512
10.6 Turbulent Motion	525
10.7 Analysis of Turbulent Motion	539
11. Vortex Motion	548
11.1 Vorticity and Circulation in Two-Dimensional Flow	549
11.2 Motion of Point Vortices	551
11.3 Two-Dimensional Flow with Distributed Vorticity	566
11.4 Vorticity, Circulation, and Three-Dimensional Flow Induced by Vorticity	581
11.5 Axisymmetric Flow Induced by Vorticity	586
11.6 Three-Dimensional Vortex Motion	600
12. Aerodynamics	606
12.1 General Features of Flow Past an Aircraft	607
12.2 Airfoils and the Kutta-Joukowski Condition	609

12.3 Vortex Panels	612
12.4 Vortex Panel Method	620
12.5 Vortex Sheet Representation	629
12.6 Point-Source-Dipole Panels	638
12.7 Point-Source Panels and Green's Third Identity	645
FDLIB Software Library	651
FDLIB Directories	653
References	666
Subject Index	668

FDLIB Software Library

The software library *FDLIB* contains a collection of FORTRAN 77 programs and subroutines that solve a broad range of problems in fluid dynamics using a variety of numerical methods. At the time of this printing, *FDLIB* consist of thirteen main directories, each containing a multitude of nested subdirectories. The contents of the subdirectories are listed on pages 655-667.

Downloading

The source codes of *FDLIB* and accompanying *User Guide*, available in the pdf format, can be downloaded from the internet site:

http://stokes.ucsd.edu/c_pozrikidis/FDLIB

Installation and compilation on UNIX or LINUX

- The library has been archived using the tar UNIX facility into the file *FDLIB.tar*. To unravel the directories on a UNIX or LINUX system, please execute the UNIX command:
`tar xvf FDLIB.tar`
- The downloaded package does not contain object files or executables. An application can be built using the makefile provided in each subdirectory. A makefile is a UNIX script that instructs the operating system how to compile the main program and subroutines, and then link the object files into an executable using an f77 compiler.
- To compile the programs using a FORTRAN 90 compiler, simply make appropriate compiler call substitutions in the makefiles.
- To compile the application named *pindos*, go to the subdirectory where it resides, and type:
`make pindos`
- To remove the object files and output files of the application named *pindos*, go to the subdirectory where it resides, and type:
`make purge`

- To remove the object files, output files, and executable of the application named *pindos*, go to the subdirectory where it resides, and type:
`make clean`

Installation and compilation on Windows and Macintosh

- To unravel the directories on a Windows or Macintosh platform, double-click on the archived tar file and follow the on-screen instructions of the invoked application.
- To compile the link the programs, follow the instructions of your FORTRAN 77 or FORTRAN 90 compiler.

CFDLAB

A subset of *FDLIB* has been combined with the X11 graphics library *vogle* into an integrated application that visualizes the results of the simulations. The source code of *CFDLAB* can be downloaded from the internet site:

http://stokes.ucsd.edu/c_pozrikidis/CFDLAB

FDLIB Directories

	Subject	Directory	Units
1	Numerical methods	<i>01_num_meth</i>	89
2	Grids	<i>02_grids</i>	22
3	Hydrostatics	<i>03_hydrostat</i>	5
4	Various	<i>04_various</i>	27
5	Lubrication	<i>05_lub</i>	4
6	Stokes flow	<i>06_stokes</i>	33
7	Potential flow	<i>07_ptf</i>	25
8	Hydrodynamic stability	<i>08_stab</i>	15
9	Vortex motion	<i>09_vortex</i>	16
10	Boundary layers	<i>10_bl</i>	3
11	Finite difference methods	<i>11_fdm</i>	2
12	Boundary element methods	<i>12_bem</i>	6
13	Turbulence	<i>13_turbo</i>	1

Directory Contents

The thirteen main directories consist of subdirectories that include main programs, assisting subroutines, and utility subroutines. Linked with drivers, the utility subroutines become stand-alone modules; all drivers are provided. A list of the subdirectories with a brief statement of their contents follows. The indicated number of units is the sum of the number of main programs and utility subroutines; assisting subroutines and drivers of utility subroutines are not counted. An extensive description of the problem statement, mathematical formulation, and numerical methods can be found in the *FDLIB User Guide* available from the *FDLIB* internet site.

01_num_meth
*General purpose numerical methods in scientific computing.*¹

<i>Subdirectory</i>	<i>Topic</i>	<i>Units</i>
01_num_comp	General aspects of numerical computation.	14
02_lin_calc	Linear algebra and linear calculus.	11
03_lin_eq	Systems of linear algebraic equations.	10
04_nl_eq	Nonlinear algebraic equations.	8
05_eigen	Eigenvalues and eigenvectors of matrices.	9
06_interp_diff	Function interpolation and differentiation.	8
07_integration	Function integration.	10
08_approximation	Function approximation.	8
09_ode_ivp	Ordinary differential equations; initial-value problems.	1
10_ode_bvp	Ordinary differential equations; boundary value problems.	2
11_pde	Partial differential equations.	5
12_spec_fnc	Computation of special functions.	10

¹This directory accompanies the book: C. Pozrikidis 1998 *Numerical Computation in Science and Engineering*, Oxford University Press.

02_grids

Adaptive discretization, parametrization, representation, and meshing of planar lines, three-dimensional lines, and three-dimensional surfaces.

<i>Subdirectory</i>	<i>Topic</i>	<i>Units</i>
grid_2d	Discretization of a planar line into a graded mesh of straight or circular elements.	3
prd_2d	Adaptive parametrization of planar lines.	5
prd_3d	Adaptive parametrization of three-dimensional lines.	5
prd_ax	Adaptive parametrization of planar lines representing the trace of axisymmetric surfaces in a meridional plane.	3
rec_2d	Interpolation through a rectangular grid.	1
rec_2d_strml	Streamline pattern by interpolation through a rectangular grid.	1
sm_3d_cl_df	Smoothing of a function on a closed surface by surface diffusion.	1
sm_3d_cl_tr	Smoothing of a function on a closed surface by Legendre spectrum truncation.	1
trgl_octa	Triangulation of a closed surface.	1
trgl_octa_hs	Triangulation of an open surface.	1
trgl_sq	Triangulation of a square patch.	1

*03_hydrostat**Shapes of interfaces in hydrostatics.*

<i>Subdirectory</i>	<i>Topic</i>	<i>Units</i>
drop_2d	Shape of a two-dimensional pendant or sessile drop on a plane.	1
drop_ax	Shape of an axisymmetric pendant or sessile drop on a plane.	1
men_2d	Shape of a two-dimensional meniscus between two parallel plates.	1
men_2d_plate	Shape of a two-dimensional meniscus attached to an inclined plate.	1
men_ax	Shape of an axisymmetric meniscus in a circular tube.	1

04_various
Structure and kinematics of various flows.

<i>Subdirectory</i>	<i>Topic</i>	<i>Units</i>
flow_1d	Steady unidirectional flow in a tube with arbitrary cross section.	1
flow_1d_osc	Oscillatory unidirectional flow in a tube with arbitrary cross section.	1
flow_1d_shear	Unidirectional shear flow over an array of cylinders.	1
spf	Similarity solutions for stagnation-point flows.	1
strml	Streamline patterns of a broad range of flows.	1
strml1	Light version of strml.	1
uni_flow	Steady unidirectional flows with rectilinear or circular streamlines.	15
uni_flow_u	Unsteady unidirectional flows with rectilinear or circular streamlines.	8

05_lub
*Nearly unidirectional lubrication flows
at low Reynolds numbers.*

<i>Subdirectory</i>	<i>Topic</i>	<i>Units</i>
bear_2d	Dynamical simulation of the motion of a slider bearing pressing against a wall.	1
chan_2l_exp	Dynamical simulation of the evolution of two superposed viscous layers in a horizontal or inclined channel, computed by an explicit finite-difference method.	1
chan_2l_imp	Dynamical simulation of the evolution of two superposed viscous layers in a horizontal or inclined channel, computed by an implicit finite-difference method.	1
films	Evolution of an arbitrary number of superposed films on a horizontal or plane wall.	1

*06_stokes**Viscous flows at vanishing Reynolds numbers.*

<i>Subdirectory</i>	<i>Topic</i>	<i>Units</i>
caps_2d	Dynamical simulation of the motion of a two-dimensional drop or elastic capsule, for a variety of flow configurations.	1
caps_3d	Dynamical simulation of the motion of a three-dimensional elastic capsule.	1
caps_ax	Dynamical simulation of the motion of an axisymmetric drop or elastic capsule, for a variety of flow configurations.	1
cop_ax	Shear flow over an axisymmetric cavity, orifice, or protrusion.	1
drop_3d	Dynamical simulation of the motion of a three-dimensional drop with constant or varying surface tension.	1
drop_3dw	Dynamical simulation of the deformation of a three-dimensional drop adhering to a plane wall.	1
em_2d	Dynamical simulation of the motion of a suspension of two-dimensional drops or elastic capsules, for a variety of flow configurations.	1
films	Dynamical simulation of the motion of superimposed layers in a channel, or two films flowing down a plane wall.	1
flow_2d	Two-dimensional flow in a domain with arbitrary geometry.	1
layers	Dynamical simulation of the motion of an arbitrary number of layers in a channel, or films flowing down a plane wall.	1
prtcl_2d	Flow past a fixed bed of two-dimensional particles with arbitrary shapes, for a variety of flow configurations, computed by a boundary-element method.	1

*06_stokes (Continued)**Viscous flows at vanishing Reynolds numbers.*

<i>Subdirectory</i>	<i>Topic</i>	<i>Units</i>
prctl_2d_se	Flow past a fixed bed of two-dimensional particles with arbitrary shapes for a variety of flow configurations, computed by a spectral-element method.	1
prctl_3d	Flow past, or due to the motion of, a three-dimensional particle, for a variety of configurations, computed by a boundary-element method.	1
prctl_ax	Flow past, or due to the motion of, a collection of axisymmetric particles, computed by a boundary-element method.	1
prctl_sw	Swirling flow produced by the rotation of an axisymmetric particle, computed by a boundary-element method.	1
sgf_2d	Green's functions of two-dimensional Stokes flow.	6
sgf_3d	Green's functions of three-dimensional Stokes flow.	5
sgf_3dax	Green's functions of Stokes flow in an axisymmetric domain.	1
sgf_ax	Green's functions of axisymmetric Stokes flow.	4
susp_2d	Dynamical simulation of the motion of a suspension of two-dimensional rigid particles with arbitrary shapes, for a variety of flow configurations, computed by a boundary-element method.	1
susp_2d_se	Dynamical simulation of the motion of a suspension of two-dimensional rigid particles with arbitrary shapes, for a variety of flow configurations, computed by a spectral-element method.	1
thread_ax	Dynamical simulation of the evolution of a fluid thread or annular layer.	1

*07_ptf**Potential flows.*

<i>Subdirectory</i>	<i>Topic</i>	<i>Units</i>
airf_2d	Shapes of airfoils.	1
airf_2d.cdp	Flow past an airfoil computed by the constant-dipole-panel method.	1
airf_2d.csdp	Flow past an airfoil computed by the constant-source-dipole-panel method.	1
airf_2d.lvp	Flow past an airfoil computed by the linear-vortex-panel method.	
body_2d	Flow past, or due to the motion of, a two-dimensional body, computed by a boundary element method.	1
body_ax	Flow past, or due to the motion of, an axisymmetric body, computed by a boundary element method.	
bubble_3d	Dynamical simulation of the deformation, collapse, or oscillations of a three-dimensional bubble.	1
cvt_2d	Flow in a rectangular cavity, computed by a finite difference method.	1
drop_3d	Dynamical simulation of the surface-tension induced oscillations of a three-dimensional inviscid drop suspended in vacuum.	1
flow_2d	Two-dimensional flow in an arbitrary domain, computed by a boundary element method.	1
lgf_2d	Green and Neumann functions of Laplace's equation in two dimensions.	8
lgf_3d	Green and Neumann functions of Laplace's equation in three dimensions.	5
lgf_ax	Green and Neumann functions of Laplace's equation in axisymmetric domains.	3
tank_2d	Dynamical simulation of liquid sloshing in a rectangular tank, computed by a boundary integral method.	1

*07_ptf (Continued)**Potential flows.*

<i>Subdirectory</i>	<i>Topic</i>	<i>Units</i>
wave_3d	Simulation of gravity and capillary waves	1

*08_stab**Hydrodynamic stability.*

<i>Subdirectory</i>	<i>Topic</i>	<i>Units</i>
ann_2l	Linear stability of two coaxial annular layers placed between two concentric cylinders.	4
chan_2l_stk	Linear stability of two superposed layers in a channel, in Stokes flow.	1
film_stk	Linear stability of a viscous film in Stokes flow.	1
prony	Prony fitting of a times series with a sum of exponentials.	1
ray_tay_stk	Rayleigh-Taylor instability of an interface separating two semi-infinite fluids in Stokes flow.	1
ray_tay_stk_w	Rayleigh-Taylor instability of an interface separating a layer from a semi-infinite fluid in Stokes flow.	1
sf_inv	Linear instability of an inviscid shear flow with an arbitrary velocity profile.	1
thread_inv	Linear instability of an inviscid thread suspended in an inert ambient fluid.	1
thread_stk	Linear instability of a viscous thread suspended in another viscous fluid, in Stokes flow.	1
vl	Linear instability of a uniform vortex layer.	1
vs	Linear instability of a vortex sheet.	1
wave_fitting	Decomposition of linear waves into exponentially growing or decaying normal modes.	1

*09_vortex**Vortex motion.*

<i>Subdirectory</i>	<i>Topic</i>	<i>Units</i>
lv_lia	Dynamical simulation of the motion of a three-dimensional line vortex, computed by the local-induction approximation (LIA).	1
lvr	Velocity induced by line vortex rings.	2
lvrm	Dynamical simulation of the motion of a collection of coaxial line vortex rings.	1
pv	Velocity induced by point vortices.	5
pvm	Dynamical simulation of the motion of a collection of point vortices.	1
pvm_pr	Dynamical simulation of the motion of a periodic collection of point vortices.	1
ring	Self-induced velocity of a vortex ring with core of finite size.	1
vl_2d	Dynamical simulation of the evolution of compound periodic vortex layers.	1
vp_2d	Dynamical simulation of the evolution of a collection of two-dimensional vortex patches.	1
vs_3d	Self-induced motion of a closed three-dimensional vortex sheet.	1
vp_ax	Dynamical simulation of the evolution of a collection of axisymmetric vortex rings and vortex patches.	1
vs_3d_2p	Self-induced motion of a doubly-periodic three-dimensional vortex sheet.	1

 10_bl
Boundary layers.

<i>Subdirectory</i>	<i>Topic</i>	<i>Units</i>
falskan	Computation of Falkner-Skan boundary layers.	1
kp_cc	Boundary layer around a circular cylinder computed by the Karman-Pohlhausen method.	1
pohl_pol	Profiles of the Pohlhausen polynomials.	1

 11_fdm
Finite difference methods.

<i>Subdirectory</i>	<i>Topic</i>	<i>Units</i>
cvt_pm	Transient flow in a rectangular cavity computed by a projection method.	1
cvt_sv	Steady flow in a rectangular cavity computed by the stream function/vorticity formulation.	1

 12_bem
Boundary element methods.

<i>Subdirectory</i>	<i>Topic</i>	<i>Units</i>
ldr_3d	Solution of Laplace's equation with Dirichlet boundary conditions in the interior or exterior of a 3D region (boundary-integral formulation).	1
ldr_3d_2p	Solution of Laplace's equation with Dirichlet boundary conditions in a semi-infinite region bounded by a doubly-periodic surface (double-layer formulation).	1
ldr_3d_ext	Solution of Laplace's equation with Dirichlet boundary conditions in the exterior of a 3D region (double-layer formulation).	1
ldr_3d_int	Solution of Laplace's equation with Dirichlet boundary conditions in the interior of a 3D region (double-layer formulation).	1
lnm_3d	Solution of Laplace's equation with Neumann boundary conditions in the interior or exterior of a 3D region (boundary-integral formulation).	1

 13_turbo
Turbulent flows.

<i>Subdirectory</i>	<i>Topic</i>	<i>Units</i>
stats	Statistical analysis of a turbulent time series.	1

References

Further discussion on fluid mechanics, applied mathematics, and numerical methods can be found in the following highly recommended texts.

Introductory on classical mechanics:

- MARION, J. B. 1970 *Classical Dynamics of Particles and Systems*, Harcourt Brace.

Introductory on fluid dynamics:

- BIRD, R. B., STEWART, W. E. & LIGHTFOOT, E. N. 1960 *Transport Phenomena*, Wiley.
- PAPANASTASIOU, T. C. 1994 *Applied Fluid Mechanics*, Prentice Hall.

Advanced on fluid dynamics:

- BATCHELOR G. K. 1967 *An Introduction to Fluid Dynamics*, Cambridge University Press.
- BRODKEY, R. S. 1967 *The Phenomena of Fluid Motions*, Dover.
- POZRIKIDIS, C. 1997 *Introduction to Theoretical and Computational Fluid Dynamics*, Oxford University Press.
- WARSI, Z. U. A. 1993 *Fluid Dynamics; Theoretical and Computational Approaches*, CRC Press.
- WHITE, F. M. 1974 *Viscous Fluid Flow*, McGraw Hill.

Computational fluid dynamics:

- FERZIGER, J. H. & PERIĆ, M. 1996 *Computational Methods for Fluid Dynamics*, Springer-Verlag.
- HIRSCH, C. 1988 *Numerical Computation of Internal and External Flows, Volume I and II*, Wiley
- POZRIKIDIS, C. 1997 *Introduction to Theoretical and Computational Fluid Dynamics*, Oxford University Press.

Low-Reynolds-number flow:

- HAPPEL, J. & BRENNER, H. 1973 *Low Reynolds Number Hydrodynamics*, Martinus Nijhoff.
- POZRIKIDIS, C. 1992 *Boundary Integral and Singularity Methods for Linearized Viscous Flow*, Cambridge University Press.

Aerodynamics:

- ANDERSON, J. D. 1990 *Modern Compressible flow with Historical Perspective*, McGraw-Hill.
- ANDERSON, J. D. 1991 *Fundamentals of Aerodynamics*, McGraw-Hill.
- KATZ, J. & PLOTKIN, A. 1991 *Low-Speed Aerodynamics; from Wing Theory to Panel Methods*, McGraw-Hill.

Numerical methods:

- POZRIKIDIS, C. 1999 *Numerical Computation in Science and Engineering*, Oxford University Press.

Calculus:

- BOAS, M. L. 1983 *Mathematical Methods in the Physical Sciences*, Wiley.
- HILDEBRAND, F. B. 1976 *Advanced Calculus for Applications*, Prentice-Hall.

Mathematical handbooks:

- ABRAMOWITZ, M. & STEGUN, I. A. 1972 *Handbook of Mathematical Functions*, Dover.
- GRADSHTEYN, I. S. & RYZHIK, I. M. 1980 *Table of Integrals, Series, and Products*, Academic Press.
- KORN, G. A. & KORN, T. M. 1968 *Mathematical Handbook for Scientists and Engineers*, McGraw-Hill.

Chapter 1

Fluid Motion: Introduction to Kinematics

- 1.1 Fluids and solids
- 1.2 Fluid parcels and flow kinematics
- 1.3 Coordinates, velocity, and acceleration
- 1.4 Fluid velocity and streamlines
- 1.5 Point particles and their trajectories
- 1.6 Material surfaces and elementary motions
- 1.7 Interpolation

We begin the study of fluid mechanics by pointing out the differences between fluids and solids, and by describing a flow in terms of the motion of elementary fluid parcels. As the volume of a fluid parcel becomes infinitesimal, the parcel reduces to a point particle, and the average velocity of the parcel reduces to the local fluid velocity computed well before the molecular nature of the fluid becomes apparent. The study of the motion and deformation of material lines and surfaces consisting of collections of point particles reveals the nature, and illustrates the diversity of motion in the world of fluid mechanics. Numerical methods allow us to study the kinematical structure of a flow with a specified velocity distribution obtained by analytical, numerical, or experimental methods.

1.1 Fluids and solids

Casual observation of the world around us reveals objects that are classified as solids and fluids; the second category includes gases and liquids. What are the distinguishing features of these two groups? The answer may be given on a wide variety of levels; from the molecular level of the physicist, to the macroscopic level of the engineer and oceanographer, to the cosmic level of the astronomer.

From the perspective of mainstream fluid mechanics underlying this book, the single most important difference between fluids and solids is that fluids must assume the shape of the container within which they are placed, whereas solids is able to stand alone sustaining their own shape. As a consequence, a mass of fluid is not able to resist a shearing force exerted on its surface, that is, a force that is parallel to its boundaries, and must keep deforming forever when subjected to it. In contrast, a solid is able to deform and assume a new stationary shape. A certain class of materials, including polymeric melts and solutions, exhibits properties that are intermediate between those of fluids and solids. This advanced class, however, will not concern us in this book.

The physicist attributes the differences between fluids and solids to the intensity of the forces holding the molecules together to form a coherent piece of material. Indeed, the inability of a fluid to assume its own shape is due to the weakness of the potential energy associated with the intermolecular forces relative to the kinetic energy associated with the vibrations of the individual molecules; the molecules are too busy vibrating to hang onto one another and thus form a long-lived crystal.

Fluids may be transformed into solids, and vice versa, by manipulating the relative magnitude of the potential energy due to intermolecular forces and the kinetic energy due to thermal motion. In practice, this is done by heating or by changing the pressure of the ambient environment.

Problem

Problem 1.1.1 *Nature of a liquid/solid suspension.*

Fluids containing suspended solid particles abound in nature, physiology, and technology. One example, is blood; another example is a slurry used in the petroleum industry for the fluidic transport of particulates. Discuss whether a suspension should be classified as a fluid or solid with reference to the volume fraction of the suspended solid phase.

1.2 Fluid parcels and flow kinematics

The motion of a non-deformable solid body, called a rigid body, may be described in terms of two vectors: the velocity of translation vector, and the angular velocity of rotation vector, where the rotation occurs around a specified center. A rigid body moves as a whole in the direction

of the velocity vector, while rotating as a whole around the angular velocity vector that is pinned at the designated center of rotation. In contrast, the motion of a fluid may not generally be described in terms of two vectors alone. A more advanced framework that allows for an extended family of motions is required.

1.2.1 Decomposition of a fluid into parcels

To establish this extended framework, we consider a body of fluid, and subdivide it into parcels. For simplicity, we assume that all molecules comprising the parcels are identical, that is, the fluid is homogeneous. Each molecule of a certain parcel moves with its own highly fluctuating velocity, but if the parcel exhibits a net motion, then the velocities of the individual molecules must be coordinated to reflect, or more accurately, give rise, to the net motion. A molecule of a gas frequently collides with other molecules after having travelled a distance comparable to the mean free path.

On a macroscopic level, the motion of a small fluid parcel may be described in terms of its velocity of translation, which can be quantified in terms of the average velocity of the individual molecules, as will be discussed in Section 1.3. If the parcel is sufficiently small, rotation may be neglected to a first approximation.

1.2.2 Relative parcel motion

A key observation is that the motion of a fluid may be described in terms of the *relative* motion of the individual fluid parcels. For example, if all parcels move with the same velocity, in which case the relative velocity vanishes, then the fluid translates as a rigid body. Moreover, it is possible that the velocity of the parcels is coordinated so that the fluid rotates as a whole like a rigid body around a designated center or rotation.

Consider now a fluid-filled flexible rubber tube that is closed at both ends, and assume that the tube is stretched, thereby extending the fluid enclosed by it along its length. The fluid has undergone neither translation nor rotation, but rather a new type of motion called pure deformation. Combinations of translation, rotation, and pure deformation whose relative strength varies with position in the fluid gives rise to a wide variety of fluid motions.

1.2.3 Kinematics as a field of fluid dynamics

Establishing in quantitative terms the relationship between the relative motion of fluid parcels and the structure of a flow, is the main objective of an introductory discipline of fluid mechanics called “flow kinematics”. “Kinematics” derives from the Greek work *κίνησις* which means “motion”. The complementary discipline of “flow dynamics” addresses the forces exerted on a fluid by an ambient force field, such as the gravitational field, as well as the forces developing in a fluid as the result of the motion.

1.3 Coordinates, velocity, and acceleration

To describe the motion of a molecule, we work under the auspices of *classical mechanics*. We begin by introducing three mutually orthogonal axes forming the Cartesian coordinate system (x, y, z) , as illustrated in figure 1.3.1. A point in the fluid may be identified by its *Cartesian coordinates*, that is, by the values of x , y and z , collected into the ordered triplet

$$\mathbf{x} = (x, y, z). \quad (1.3.1)$$

Each point in the fluid has an associated *position vector* which starts at the origin of the Cartesian axes and ends at the point. The Cartesian coordinates of the point are equal to the components of the position vector, defined as the positive or negative projections of the position vector onto the corresponding axes. Accordingly, the Cartesian coordinates of a point have a dual interpretation: they form an ordered triplet of real numbers, and they represent a geometrical entity associated with the position vector.

1.3.1 Unit vectors

The three position vectors:

$$\mathbf{e}_x = (1, 0, 0), \quad \mathbf{e}_y = (0, 1, 0), \quad \mathbf{e}_z = (0, 0, 1), \quad (1.3.2)$$

point in the positive directions of the x , y , or z axis, and the end-points represented by them lie on the x , y , or z axis at distances equal to one unit of length away from the origin. We say that the vectors \mathbf{e}_x , \mathbf{e}_y and \mathbf{e}_z are mutually orthogonal Cartesian unit vectors.

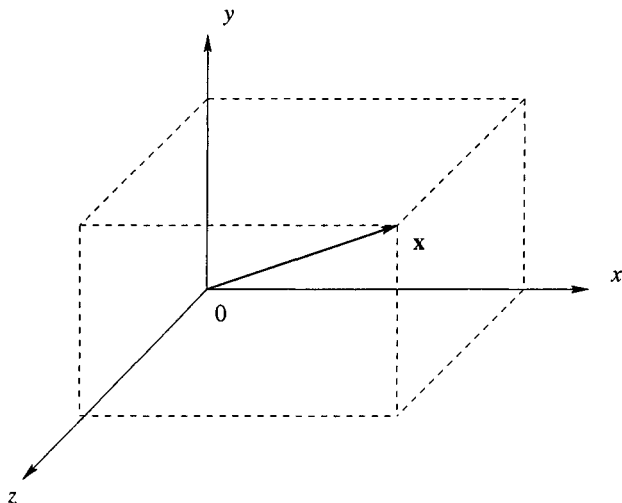


Figure 1.3.1 Three mutually orthogonal axes defining a Cartesian coordinate system (x, y, z) , and the position vector corresponding to the point \mathbf{x} .

Combining the preceding definitions, we write

$$\mathbf{x} = x \mathbf{e}_x + y \mathbf{e}_y + z \mathbf{e}_z. \quad (1.3.3)$$

In physical terms, this equation states that, to reach the point \mathbf{x} departing from the origin, we may move along each one of the unit vectors \mathbf{e}_x , \mathbf{e}_y , \mathbf{e}_z , by respective distances equal to x , y , or z units of length; the order of motion along the three directions is immaterial.

1.3.2 Velocity

Because a molecule moves with a highly fluctuating velocity, its position is a rapidly changing function of time. Formally, we say that the coordinates of the molecule are functions of time t , denoted by

$$x = X(t), \quad y = Y(t), \quad z = Z(t). \quad (1.3.4)$$

To economize our notation, we introduce the vector function

$$\mathbf{X}(t) = (X(t), Y(t), Z(t)). \quad (1.3.5)$$

and consolidate expressions (1.3.4) into the form

$$\mathbf{x} = \mathbf{X}(t). \quad (1.3.6)$$

Now, by definition, the velocity of a molecule is equal to the rate of change of its position, displacement per time elapsed. If, during an infinitesimal period of time dt , the x coordinate of the molecule has changed by the infinitesimal displacement dX , then $v_x = dX/dt$. Writing the counterparts of this equation for the y and z components, we obtain

$$v_x = \frac{dX}{dt}, \quad v_y = \frac{dY}{dt}, \quad v_z = \frac{dZ}{dt}, \quad (1.3.7)$$

which may be collected into the ordered triplet

$$(v_x, v_y, v_z) = \left(\frac{dX}{dt}, \frac{dY}{dt}, \frac{dZ}{dt} \right). \quad (1.3.8)$$

In vector notation,

$$\mathbf{v} = \frac{d\mathbf{X}}{dt}. \quad (1.3.9)$$

The velocity of a molecule is a vector described by its three Cartesian components v_x , v_y , and v_z ; these are the positive or negative distances subtended between the projection of the last and first point of the velocity vector onto the x , y , or z axis. The distances are then multiplied by a scaling factor to acquire dimensions of velocity, that is, length divided by time. A negative value for v_x indicates that the x coordinate of the last point of the velocity vector is lower than the x value of the first point, and the motion occurs toward the negative direction of the x axis; similarly for the y and z components. In terms of the unit vectors defined in equations (1.3.2), the velocity vector is given by

$$\mathbf{v} = v_x \mathbf{e}_x + v_y \mathbf{e}_y + v_z \mathbf{e}_z. \quad (1.3.10)$$

It is evident from the preceding definitions that the velocity is a *free Cartesian vector*, which means that it may be translated in space to any desired location. In contrast, the first point of the position vector is always pinned at the origin.

1.3.3 Cylindrical polar coordinates

A point in space may be identified by the values of the ordered triplet (x, σ, φ) , where x is the projection of the position vector onto to the

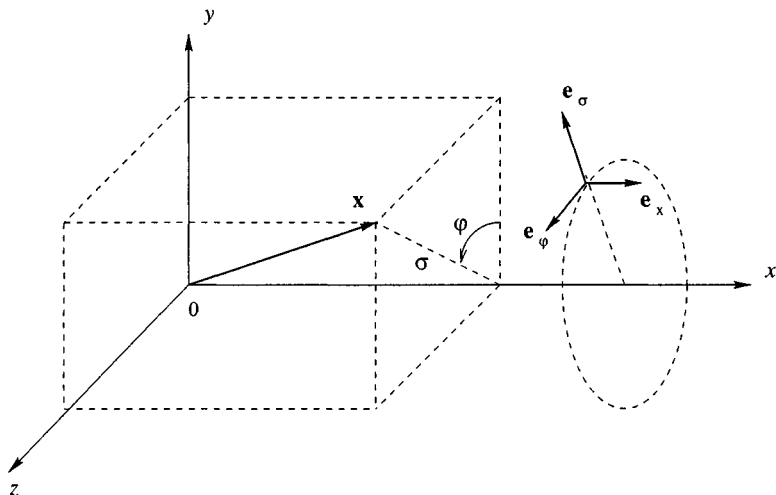


Figure 1.3.2 A system of cylindrical polar coordinates (x, σ, φ) defined with reference to the Cartesian coordinates (x, y, z) .

straight (rectilinear) x axis passing through a designated origin; σ is the distance of the point from the x axis; and φ is the meridional angle measured around the x axis. The value $\varphi = 0$ corresponds to the xy plane, as illustrated in figure 1.3.2. The axial coordinate x takes values in the range $(-\infty, +\infty)$, σ takes values in the range $[0, \infty)$, and φ takes values in the range $[0, 2\pi)$.

Using elementary trigonometry, we derive the following relations between the Cartesian and associated polar cylindrical coordinates,

$$y = \sigma \cos \varphi, \quad z = \sigma \sin \varphi, \quad (1.3.11)$$

and the inverse relations

$$\sigma = \sqrt{y^2 + z^2}, \quad \varphi = \arccos\left(\frac{y}{\sigma}\right). \quad (1.3.12)$$

Unit vectors

Considering a point in space, we define three vectors of unit length, denoted by \mathbf{e}_x , \mathbf{e}_σ , and \mathbf{e}_φ , pointing, respectively, in the direction of the x axis, normal to the x axis, and in the meridional direction of varying angle φ , as depicted in figure 1.3.2. Note that the orientation of the

unit vectors \mathbf{e}_σ and \mathbf{e}_φ changes with position in space; in contrast, the orientation of \mathbf{e}_x is fixed and independent of position in space. In terms of the local unit vectors \mathbf{e}_x , \mathbf{e}_σ , the position vector is given by

$$\mathbf{x} = x \mathbf{e}_x + \sigma \mathbf{e}_\sigma. \quad (1.3.13)$$

where the dependence on the meridional angle φ is mediated through the unit vector \mathbf{e}_σ on the right-hand side. The absence of \mathbf{e}_φ from the right-hand side of (1.3.13) is explained by noting that the distance from the origin, expressed by the position vector \mathbf{x} , is perpendicular to the unit vector \mathbf{e}_φ .

Correspondingly, the velocity vector \mathbf{v} is given by

$$\mathbf{v} = v_x \mathbf{e}_x + v_\sigma \mathbf{e}_\sigma + v_\varphi \mathbf{e}_\varphi. \quad (1.3.14)$$

The coefficients v_x , v_σ , and v_φ are the cylindrical polar components of the velocity.

Relation to Cartesian vector components

Using elementary trigonometry, we derive the following relations between the Cartesian and cylindrical polar unit vectors,

$$\mathbf{e}_\sigma = \cos \varphi \mathbf{e}_y + \sin \varphi \mathbf{e}_z, \quad \mathbf{e}_\varphi = -\sin \varphi \mathbf{e}_y + \cos \varphi \mathbf{e}_z, \quad (1.3.15)$$

and the inverse relations

$$\mathbf{e}_y = \cos \varphi \mathbf{e}_\sigma - \sin \varphi \mathbf{e}_\varphi, \quad \mathbf{e}_z = \sin \varphi \mathbf{e}_\sigma + \cos \varphi \mathbf{e}_\varphi. \quad (1.3.16)$$

The corresponding relations for the components of the velocity are

$$v_\sigma = \cos \varphi v_y + \sin \varphi v_z, \quad v_\varphi = -\sin \varphi v_y + \cos \varphi v_z, \quad (1.3.17)$$

and

$$v_y = \cos \varphi v_\sigma - \sin \varphi v_\varphi, \quad v_z = \sin \varphi v_\sigma + \cos \varphi v_\varphi. \quad (1.3.18)$$

Rates of change

The counterparts of expressions (1.3.4) for the cylindrical polar coordinates are

$$x = X(t), \quad \sigma = \Sigma(t), \quad \varphi = \Phi(t). \quad (1.3.19)$$

The rate of change of the unit vectors following the motion of a molecule is given by the relations

$$\frac{d\mathbf{e}_x}{dt} = \mathbf{0}, \quad \frac{d\mathbf{e}_\sigma}{dt} = \frac{d\Phi}{dt} \mathbf{e}_\varphi, \quad \frac{d\mathbf{e}_\varphi}{dt} = -\frac{d\Phi}{dt} \mathbf{e}_\sigma. \quad (1.3.20)$$

Substituting expressions (1.3.19) into the right-hand side of (1.3.13), taking the time derivative of both sides of the resulting expression, identifying the left-hand side with the velocity, expanding out the derivatives of the products on the right-hand side, using relations (1.3.20) to eliminate the time derivatives of the unit vectors, and then comparing the result with expression (1.3.14), we find the counterparts of equations (1.3.7),

$$v_x = \frac{dX}{dt}, \quad v_\sigma = \frac{d\Sigma}{dt}, \quad v_\varphi = \Sigma \frac{d\Phi}{dt}. \quad (1.3.21)$$

1.3.4 Spherical polar coordinates

Alternatively, a point in space may be identified by the values of the ordered triplet (r, θ, φ) , where r is the distance from a designated origin; θ is the azimuthal angle subtended between the x axis, the origin, and the chosen point; and φ is the meridional angle measured around the x axis. The value $\varphi = 0$ corresponding to the xy plane, as depicted in figure 1.3.3. The radial distance r takes values in the range $[0, \infty)$, the azimuthal angle θ takes values in the range $[0, \pi]$, and the meridional angle φ takes values in the range $[0, 2\pi)$.

Using elementary trigonometry, we derive the following relations between the Cartesian, cylindrical, and spherical polar coordinates,

$$\begin{aligned} x &= r \cos \theta, & \sigma &= r \sin \theta, \\ y &= \sigma \cos \varphi = r \sin \theta \cos \varphi, \\ z &= \sigma \sin \varphi = r \sin \theta \sin \varphi, \end{aligned} \quad (1.3.22)$$

and the inverse relations

$$\begin{aligned} r &= \sqrt{x^2 + y^2 + z^2} = \sqrt{x^2 + \sigma^2}, \\ \theta &= \arccos \frac{x}{r}, & \varphi &= \arccos \frac{y}{\sigma}. \end{aligned} \quad (1.3.23)$$

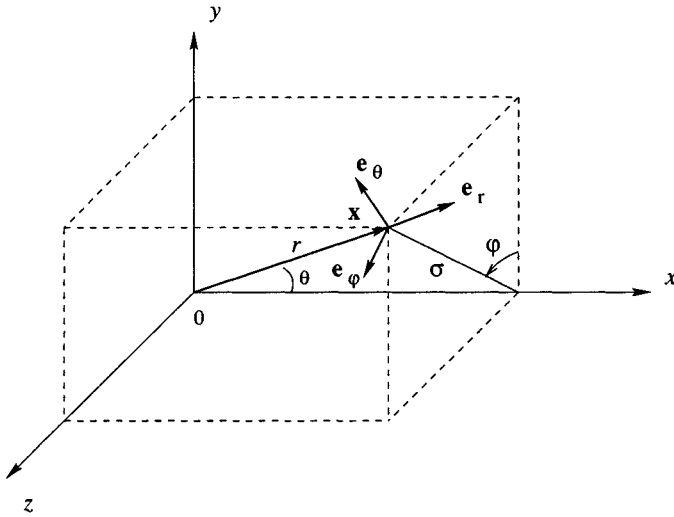


Figure 1.3.3 A system of spherical polar coordinates (r, θ, φ) defined with reference to the Cartesian coordinates (x, y, z) .

Unit vectors

Considering a point in space, we define three vectors of unit length \mathbf{e}_r , \mathbf{e}_θ , and \mathbf{e}_φ , pointing, respectively, in the radial, azimuthal, and meridional direction, as illustrated in figure 1.3.3. Note that the orientation of all of these unit vectors changes with position in space; in contrast the orientation of the Cartesian unit vectors \mathbf{e}_x , \mathbf{e}_y , and \mathbf{e}_z is fixed.

In terms of the local unit vectors \mathbf{e}_r , \mathbf{e}_θ , and \mathbf{e}_φ , the position vector is given by

$$\mathbf{x} = r \mathbf{e}_r. \quad (1.3.24)$$

where the dependence on θ and φ is mediated through the unit vector \mathbf{e}_r on the right-hand side. The absence of \mathbf{e}_θ and \mathbf{e}_φ from the right-hand side of (1.3.24) is explained by noting that the distance from the origin, expressed by the position vector \mathbf{x} , is perpendicular to the unit vectors \mathbf{e}_θ and \mathbf{e}_φ . Correspondingly, the velocity vector \mathbf{v} is given by

$$\mathbf{v} = v_r \mathbf{e}_r + v_\theta \mathbf{e}_\theta + v_\varphi \mathbf{e}_\varphi, \quad (1.3.25)$$

where the coefficients v_r , v_θ , and v_φ are the spherical polar components of the velocity.

Relation to Cartesian vector components

Using elementary trigonometry, we derive the following relations between the spherical polar, cylindrical polar, and Cartesian unit vectors,

$$\begin{aligned}
 \mathbf{e}_r &= \cos \theta \mathbf{e}_x + \sin \theta \cos \varphi \mathbf{e}_y + \sin \theta \sin \varphi \mathbf{e}_z \\
 &= \cos \theta \mathbf{e}_x + \sin \theta \mathbf{e}_\sigma, \\
 \mathbf{e}_\theta &= -\sin \theta \mathbf{e}_x + \cos \theta \cos \varphi \mathbf{e}_y + \cos \theta \sin \varphi \mathbf{e}_z \\
 &= -\sin \theta \mathbf{e}_x + \cos \theta \mathbf{e}_\sigma, \\
 \mathbf{e}_\varphi &= -\sin \varphi \mathbf{e}_y + \cos \varphi \mathbf{e}_z.
 \end{aligned} \tag{1.3.26}$$

The corresponding relations for the components of the velocity are

$$\begin{aligned}
 v_r &= \cos \theta v_x + \sin \theta \cos \varphi v_y + \sin \theta \sin \varphi v_z \\
 &= \cos \theta v_x + \sin \theta v_\sigma, \\
 v_\theta &= -\sin \theta v_x + \cos \theta \cos \varphi v_y + \cos \theta \sin \varphi v_z \\
 &= -\sin \theta v_x + \cos \theta v_\sigma, \\
 v_\varphi &= -\sin \varphi v_y + \cos \varphi v_z.
 \end{aligned} \tag{1.3.27}$$

Rates of change

The counterparts of expressions (1.3.4) for the spherical polar coordinates are

$$r = R(t), \quad \theta = \Theta(t), \quad \varphi = \Phi(t). \tag{1.3.28}$$

The rate of change of the unit vectors following the motion of a molecule is given by the relations

$$\begin{aligned}
 \frac{d\mathbf{e}_r}{dt} &= \frac{d\Phi}{dt} \sin \theta \mathbf{e}_\varphi + \frac{d\Theta}{dt} \mathbf{e}_\theta, & \frac{d\mathbf{e}_\theta}{dt} &= \frac{d\Phi}{dt} \cos \theta \mathbf{e}_\varphi - \frac{d\Theta}{dt} \mathbf{e}_r, \\
 \frac{d\mathbf{e}_\varphi}{dt} &= -\frac{d\Phi}{dt} \cos \theta \mathbf{e}_\theta - \frac{d\Theta}{dt} \sin \theta \mathbf{e}_r.
 \end{aligned} \tag{1.3.29}$$

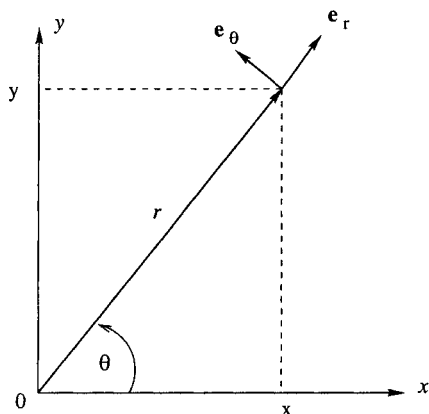


Figure 1.3.4 A system of plane polar coordinates (r, θ) in the xy plane.

Substituting the first of (1.3.28) into the right-hand side of (1.3.24), taking the time derivative of both sides of the resulting equation, identifying the left-hand side with the velocity, expanding out the derivatives of the products on the right-hand side, using the first relations (1.3.29) to eliminate the time derivative of the radial unit vector, and then comparing the result with expression (1.3.25), we find the counterparts of equations (1.3.7),

$$v_r = \frac{dR}{dt}, \quad v_\theta = R \frac{d\Theta}{dt}, \quad v_\varphi = R \sin \theta \frac{d\Phi}{dt}. \quad (1.3.30)$$

1.3.5 Plane polar coordinates

A point in the xy plane may be identified by the values of the doublet (r, θ) , where r is the distance from the designated origin, and θ is the angle subtended between the x axis, the origin, and the chosen point measured in the counterclockwise sense, as depicted in figure 1.3.4. The radial distance r takes values in the range $[0, \infty)$, and θ takes values in the range $[0, 2\pi)$.

Using elementary trigonometry, we derive the following relations between the Cartesian and plane polar coordinates,

$$x = r \cos \theta, \quad y = r \sin \theta, \quad (1.3.31)$$

and the inverse relations

$$r = \sqrt{x^2 + y^2}, \quad \theta = \arccos \frac{y}{r}. \quad (1.3.32)$$

Unit vectors

Considering a point in the xy plane, we define two vectors of unit length \mathbf{e}_r and \mathbf{e}_θ pointing in the radial or polar direction, as depicted in figure 1.3.4. Note that the orientation of these unit vectors changes with position in the xy plane, whereas the orientation of the Cartesian unit vectors \mathbf{e}_x and \mathbf{e}_y is fixed.

In terms of the local unit vectors \mathbf{e}_r and \mathbf{e}_θ , the position vector is given by

$$\mathbf{x} = r \mathbf{e}_r, \quad (1.3.33)$$

and the velocity vector \mathbf{v} is given by

$$\mathbf{v} = v_r \mathbf{e}_r + v_\theta \mathbf{e}_\theta. \quad (1.3.34)$$

The coefficients v_r and v_θ are the plane polar components of the velocity.

Relation to Cartesian vector components

Using elementary trigonometry, we derive the following relations between the Cartesian and plane polar unit vectors,

$$\mathbf{e}_r = \cos \theta \mathbf{e}_x + \sin \theta \mathbf{e}_y, \quad \mathbf{e}_\theta = -\sin \theta \mathbf{e}_x + \cos \theta \mathbf{e}_y, \quad (1.3.35)$$

and the inverse relations

$$\mathbf{e}_x = \cos \theta \mathbf{e}_r - \sin \theta \mathbf{e}_\theta, \quad \mathbf{e}_y = \sin \theta \mathbf{e}_r + \cos \theta \mathbf{e}_\theta. \quad (1.3.36)$$

The corresponding relations for the components of the velocity are

$$v_r = \cos \theta v_x + \sin \theta v_y, \quad v_\theta = -\sin \theta v_x + \cos \theta v_y, \quad (1.3.37)$$

and

$$v_x = \cos \theta v_r - \sin \theta v_\theta, \quad v_y = \sin \theta v_r + \cos \theta v_\theta. \quad (1.3.38)$$

Rates of change

The counterparts of expressions (1.3.4) for the plane polar coordinates are

$$r = R(t), \quad \theta = \Theta(t). \quad (1.3.39)$$

The rate of change of the unit vectors following the motion of a molecule is given by the relations

$$\frac{d\mathbf{e}_r}{dt} = \frac{d\Theta}{dt} \mathbf{e}_\theta, \quad \frac{d\mathbf{e}_\theta}{dt} = -\frac{d\Theta}{dt} \mathbf{e}_r. \quad (1.3.40)$$

Substituting the first of (1.3.39) into the right-hand side of (1.3.33), taking the time derivative of both sides of the resulting equation, identifying the left-hand side with the velocity, expanding out the derivatives of the products on the right-hand side, using the first of relations (1.3.40) to eliminate the time derivatives of the radial unit vector, and then comparing the result with expressions (1.3.34), we derive the counterparts of equations (1.3.7),

$$v_r = \frac{dR}{dt}, \quad v_\theta = R \frac{d\Theta}{dt}. \quad (1.3.41)$$

Problems

Problem 1.3.1 Spherical polar coordinates.

Derive the inverse of the transformation rules shown in equations (1.3.27); that is, express the Cartesian components in terms of the spherical polar components of the velocity.

Problem 1.3.2 Acceleration.

The acceleration vector, denoted by \mathbf{a} , is defined as the rate of change of the velocity vector,

$$\mathbf{a} = \frac{d\mathbf{v}}{dt} = \frac{d^2\mathbf{X}}{dt^2}. \quad (1.3.42)$$

By definition then, the Cartesian components of the acceleration are given by

$$a_x = \frac{d^2X}{dt^2}, \quad a_y = \frac{d^2Y}{dt^2}, \quad a_z = \frac{d^2Z}{dt^2}. \quad (1.3.43)$$

(a) Show that the cylindrical polar components of the acceleration are given by

$$\begin{aligned}
 a_x &= \frac{d^2 X}{dt^2}, & a_\sigma &= \frac{d^2 \Sigma}{dt^2} - \Sigma \left(\frac{d\Phi}{dt} \right)^2, \\
 a_\varphi &= 2 \frac{d\Sigma}{dt} \frac{d\Phi}{dt} + \Sigma \frac{d^2 \Phi}{dt^2}.
 \end{aligned}
 \tag{1.3.44}$$

(b) Show that the spherical polar components of the acceleration are given by

$$\begin{aligned}
 a_r &= \frac{d^2 R}{dt^2} - R \left(\frac{d\Phi}{dt} \right)^2 \sin^2 \theta - R \left(\frac{d\Theta}{dt} \right)^2, \\
 a_\theta &= R \frac{d^2 \Theta}{dt^2} + 2 \frac{dR}{dt} \frac{d\Theta}{dt} - R \left(\frac{d\Phi}{dt} \right)^2 \sin \theta \cos \theta, \\
 a_\varphi &= R \frac{d^2 \Phi}{dt^2} \sin \theta + 2 \frac{dR}{dt} \frac{d\Phi}{dt} \sin \theta + 2 R \frac{d\Theta}{dt} \frac{d\Phi}{dt} \cos \theta.
 \end{aligned}
 \tag{1.3.45}$$

(c) Show that the plane polar components of the acceleration are given by

$$\begin{aligned}
 a_r &= \frac{d^2 R}{dt^2} - R \left(\frac{d\Theta}{dt} \right)^2, \\
 a_\theta &= 2 \frac{dR}{dt} \frac{d\Theta}{dt} + R \frac{d^2 \theta}{dt^2} = \frac{1}{R} \frac{d}{dt} \left(R^2 \frac{d\Theta}{dt} \right).
 \end{aligned}
 \tag{1.3.46}$$

1.4 Fluid velocity and streamlines

Having prepared the ground for describing the motion of the molecules in quantitative terms, we turn to considering the motion of fluid parcels consisting of large collections of molecules.

Consider a homogeneous fluid consisting of identical molecules, and label the N molecules comprising a fluid parcel using the index i , where $i = 1, 2, \dots, N$. Let $v_x^{(i)}$, $v_y^{(i)}$, and $v_z^{(i)}$ be the Cartesian components

of the velocity of the i th molecule at a particular time instant. The corresponding components of the mean velocity are defined as

$$\langle v_x \rangle = \frac{1}{N} \sum_{i=1}^N v_x^{(i)}, \quad \langle v_y \rangle = \frac{1}{N} \sum_{i=1}^N v_y^{(i)}, \quad \langle v_z \rangle = \frac{1}{N} \sum_{i=1}^N v_z^{(i)}, \quad (1.4.1)$$

where the pointed brackets on the left-hand sides denote averages over all molecules. In compact notation, equations (1.4.1) combine into the vector form

$$\langle \mathbf{v} \rangle = \frac{1}{N} \sum_{i=1}^N \mathbf{v}^{(i)}. \quad (1.4.2)$$

Assume now that, at a particular time t , the fluid parcel under consideration is centered at the point \mathbf{x} . As the size of the parcel becomes smaller, the parcel tends to occupy an infinitesimal volume in space containing the point \mathbf{x} . In this limit, the components of the parcel velocity defined in equations (1.4.1) reduce to the corresponding components of the *fluid velocity*, denoted by u_x , u_y , and u_z , forming the ordered triplet

$$\mathbf{u} = (u_x, u_y, u_z). \quad (1.4.3)$$

Since different choices for the designated parcel center \mathbf{x} at different times t produce different fluid velocities, the components of the velocity vector \mathbf{u} are functions of the components of the position vector $\mathbf{x} = (x, y, z)$ and time t . To signify this dependence, we append to u_x , u_y , and u_z a set of parentheses enclosing the four independent variables, writing

$$u_x(x, y, z, t), \quad u_y(x, y, z, t), \quad u_z(x, y, z, t). \quad (1.4.4)$$

In compact notation,

$$u_x(\mathbf{x}, t), \quad u_y(\mathbf{x}, t), \quad u_z(\mathbf{x}, t), \quad (1.4.5)$$

and in full vector notation,

$$\mathbf{u}(\mathbf{x}, t). \quad (1.4.6)$$

As an example, the Cartesian components of one particular velocity field are given by

$$\begin{aligned}
 u_x(x, y, z, t) &= a(y^2 + z^2) + (b + ct)x^3y z + ce^{dxt}, \\
 u_y(x, y, z, t) &= a(z^2 + x^2) + (b + ct)xy^3z + ce^{dyt}, \\
 u_z(x, y, z, t) &= a(x^2 + y^2) + (b + ct)xy z^3 + ce^{dzt},
 \end{aligned}
 \tag{1.4.7}$$

where a, b, c and d are four constants. Velocity has dimensions of length per time L/T , and the position vector has dimensions of length L . In order for both sides of equations (1.4.7) to have the same units, the constant a must have dimensions of inverse length-time, $1/(LT)$.

If a flow is steady or time-independent, the components of the velocity do not depend on time, and we omit t from the list of arguments in (1.4.4)-(1.4.6), writing $\mathbf{u}(\mathbf{x})$.

If the fluid translates as a rigid body in a certain direction possibly with a time-dependent velocity, we omit \mathbf{x} in the list of arguments, writing $\mathbf{u}(t)$.

1.4.1 Two-dimensional flow

When the z component of the fluid velocity vanishes while the x and y components depend on the x and y but not on the z coordinate, we obtain a two-dimensional flow in the xy plane. The velocity vector at any point in this two-dimensional flow also lies in the xy plane.

1.4.2 Swirling flow

Consider the system of cylindrical polar coordinates depicted in figure 1.3.2. The cylindrical polar components of the velocity, u_σ and u_φ , are related to the Cartesian components by equations (1.3.17), with v replaced throughout by the fluid velocity u . If the velocity vector points in the direction of the meridional angle φ at every point in the flow, that is, u_x and u_σ vanish whereas u_φ is non-zero and independent of φ , then we obtain a *swirling flow*.

1.4.3 Axisymmetric flow

In contrast, if the meridional component of the velocity u_φ vanishes at every point in the flow, whereas u_x and u_σ are non-zero but independent of φ , then we obtain an axially symmetric or *axisymmetric flow*. The

velocity vector of an axisymmetric flow lies in a meridional plane; that is, in a plane that passes through the x axis.

Superposing a swirling flow and an axisymmetric flow, we obtain a three-dimensional flow described as axisymmetric flow with swirling motion. All three velocity components u_x , u_σ , and u_φ in such a flow are generally non-zero but independent of the meridional angle φ .

1.4.4 Streamlines and stagnation points

Consider a flow at a certain time instant, and draw velocity vectors at a large number of points distributed in the domain of flow. The collection of these vectors defines a vector field called the velocity field. Starting at a certain point in the flow, we may draw a line that is tangential to the velocity vector at each point, as illustrated in figure 1.4.1. This generally curved three-dimensional line is called a *streamline*, and a collection of streamlines composes a *streamline pattern*.

Two or more streamlines may meet at a point called a *stagnation point*, as illustrated in figure 1.4.1. Since the velocity is unique value at each point in a flow, all velocity components must necessarily vanish at a stagnation point. A streamline is a closed line, extends to infinity, crosses a moving boundary, or terminates at a stagnation point.

Problems

Problem 1.4.1 *Dimensions of coefficients.*

Deduce the dimensions of the coefficients b , c , d on the right-hand sides of equations (1.4.7).

Problem 1.4.2 *Streamline patterns.*

Sketch streamline patterns of (a) a two-dimensional flow, (b) a swirling flow, (c) an axisymmetric flow, and (d) an axisymmetric flow with swirling motion.

1.5 Point particles and their trajectories

As the size of a fluid parcel tends to zero, the parcel reduces to an abstract entity called a *point particle*. By definition, the rate of change

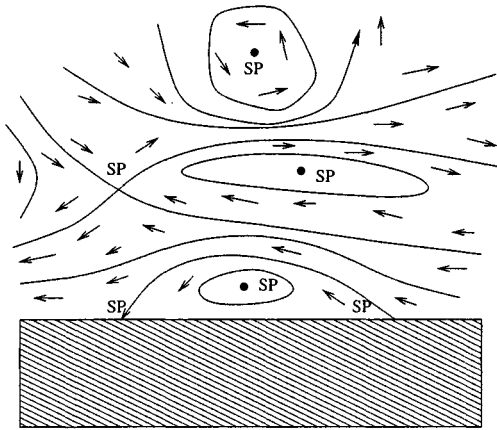


Figure 1.4.1 Illustration of a velocity vector field and associated streamline pattern in a two-dimensional flow, involving stagnation points denoted as “SP”. Stagnation points may occur in the interior of a flow or at the boundaries.

of the position of a point particle is equal to the velocity of the fluid evaluated at the instantaneous position of the point particle.

If, during an infinitesimal period of time dt , the x coordinate of a point particle located at the position $\mathbf{x} = \mathbf{X}$ has changed by the infinitesimal distance dX , then $u_x = dX/dt$, where the velocity u_x is evaluated at $\mathbf{x} = \mathbf{X}$ at the current time t . Writing the counterparts of this equation for the y and z components, we obtain

$$\begin{aligned} \frac{dX}{dt} &= u_x(X(t), Y(t), Z(t), t), \\ \frac{dY}{dt} &= u_y(X(t), Y(t), Z(t), t), \\ \frac{dZ}{dt} &= u_z(X(t), Y(t), Z(t), t), \end{aligned} \tag{1.5.1}$$

where the first set of parentheses on the right-hand sides enclose the four scalar arguments of the velocity.

A conceptual difficulty casts a shadow of ambiguity on the definition of the fluid velocity based on relations (1.5.1). In the limit as the size of a fluid parcel tends to zero, the number of molecules residing inside

the parcel also tends to zero, and the pointed-bracket averages defined in equations (1.4.1) become ill-defined. Consider, for example, a spherical particle of radius ϵ . As ϵ tends to zero, a graph of the average molecular velocity $\langle v_x \rangle$ plotted against ϵ shows strong fluctuations that are manifestations of random molecular motions.

To circumvent this difficulty, we adopt the *continuum mechanics approximation*: as the size of a fluid parcel tends to zero, the limit of the average molecular velocity is computed before the discrete nature of the fluid becomes apparent. In the context of continuum mechanics, a point particle is large enough to contain a large number of molecules whose average velocity is well-defined, but small enough so that its volume is infinitesimal; that is, the ratio of the volume of a point particle to the volume of the fluid to which the point particle belongs is equal to zero. Two consequences of this idealization are:

- A *finite* fluid parcel is comprised of an *infinite* number of point particles.
- The product of the infinite number of point particles and the infinitesimal volume of each point particle is finite and non-zero, and equal to the parcel volume.

1.5.1 Point particle motion and path lines

Since a point particle moves with the local fluid velocity, its coordinates generally change in time according to equations (1.5.1) even if the flow is steady: point particles remain stationary only if the velocity vanishes and the fluid is in a macroscopic state of rest.

Mathematically, equations (1.5.1) comprise a system of three first-order ordinary differential equations, concisely called ODEs. The solution of this system subject to an initial condition that specifies the position of a point particle at a certain time – for example, at a designated origin of time – provides us with the trajectory of a point particle called a *path line*.

If the flow is steady, the system of ODEs is *autonomous*, meaning that there is no explicit time dependence on the right-hand side, whereas if the flow is unsteady, the system is *non-autonomous*. The right-hand side of a non-autonomous system depends on time implicitly through the arguments of the dependent variables, in this case $X(t)$, $Y(t)$, and $Z(t)$, as well as explicitly through the unsteadiness of the flow.

Assume, for example, that the Cartesian velocity components of a certain steady unidirectional flow are given by

$$u_x = a y^2 + b y + c, \quad u_y = 0, \quad u_z = 0, \quad (1.5.2)$$

where a , b , and c are three constants with appropriate dimensions. In this case, the fluid moves along the x axis with velocity that depends on the y coordinate alone. The trajectories of the point particles are straight lines described by the autonomous system of ODEs

$$\frac{dX}{dt} = a Y^2 + b Y + c, \quad \frac{dY}{dt} = 0, \quad \frac{dZ}{dt} = 0. \quad (1.5.3)$$

The solution of these equations is readily found to be

$$\begin{aligned} X(t) &= X(t=0) + (a Y^2 + b Y + c) t, \\ Y(t) &= Y(t=0), \quad Z(t) = Z(t=0), \end{aligned} \quad (1.5.4)$$

where $X(0)$, $Y(0)$, and $Z(0)$ are the coordinates of a point particle at the initial instant, $t = 0$.

In general, however, the solution of the system (1.5.1) may not be found by analytical methods, and the use of numerical methods will be imperative.

1.5.2 Explicit Euler method

A simple algorithm for generating the trajectory of a point particle emerges by considering the change in the position of the point particle over a small time interval Δt , and replacing the differential equations (1.5.1) with the algebraic equations

$$\begin{aligned} \frac{X(t + \Delta t) - X(t)}{\Delta t} &= u_x(X(t), Y(t), Z(t), t), \\ \frac{Y(t + \Delta t) - Y(t)}{\Delta t} &= u_y(X(t), Y(t), Z(t), t), \\ \frac{Z(t + \Delta t) - Z(t)}{\Delta t} &= u_z(X(t), Y(t), Z(t), t). \end{aligned} \quad (1.5.5)$$

To obtain these equations, we have replaced the time derivatives on the left-hand sides of equations (1.5.1) with *forward finite differences*, which is a consistent approximation: since, by definition, the first derivative dX/dt is equal to the limit of the ratio $[X(t + \Delta t) - X(t)]/\Delta t$ as Δt tends to zero, we expect that, as long as Δt is sufficiently small, the error introduced by replacing a derivative with a forward finite difference will also be reasonably small.

In fact, analysis shows that the magnitude of the error associated with the approximate forms (1.5.5) is comparable to the magnitude of Δt . For example if Δt is equal to 0.1 in some units, then the error associated with the preceding approximation will be on the order of 0.1 multiplied by a constant whose value is on the order of unity; that is, a constant whose absolute value ranges between 0.5 and 5 in corresponding units.

In vector notation, the so-called discrete form of the differential system (1.5.1) expressed by the algebraic system (1.5.5) takes the form

$$\frac{\mathbf{X}(t + \Delta t) - \mathbf{X}(t)}{\Delta t} = \mathbf{u}(\mathbf{X}(t), t) + O(\Delta t), \quad (1.5.6)$$

where the term $O(\Delta t)$ on the right-hand side signifies the order of the error due to the finite-difference approximation.

Solving the first of equations (1.5.5) for $X(t + \Delta t)$, the second equation for $Y(t + \Delta t)$, and the third equation for $Z(t + \Delta t)$, we obtain

$$X(t + \Delta t) = X(t) + \Delta t u_x(X(t), Y(t), Z(t), t),$$

$$Y(t + \Delta t) = Y(t) + \Delta t u_y(X(t), Y(t), Z(t), t),$$

$$Z(t + \Delta t) = Z(t) + \Delta t u_z(X(t), Y(t), Z(t), t). \quad (1.5.7)$$

In physical terms, equations (1.5.7) state that the position of a point particle at time $t + \Delta t$ is equal to the position at the previous time t plus a small displacement that is equal to the distance travelled over the small time interval Δt . The velocity of travel has been assumed to be constant and equal to the point particle or fluid velocity at the beginning of the time step corresponding to time t .

Algorithm

Equations (1.5.7) provide us with a basis for computing the trajectory of a point particle according to the following algorithm:

1. Specify the initial time; for example, set $t = 0$.
2. Select the size of the time step Δt .
3. Specify the initial coordinates $X(0)$, $Y(0)$, and $Z(0)$.
4. Evaluate the velocities $u_x(X(t), Y(t), Z(t), t)$, $u_y(X(t), Y(t), Z(t), t)$, and $u_z(X(t), Y(t), Z(t), t)$ on the right-hand side of equations (1.5.7).
5. Evaluate the right-hand sides of (1.5.7) to obtain the coordinates of the point particle $X(t + \Delta t)$, $Y(t + \Delta t)$, and $Z(t + \Delta t)$.
6. Reset the time to $t + \Delta t$.
7. Stop if desired, or return to execute steps 4-6.

The procedure just described is the *explicit Euler* method for solving a system of ordinary differential equations. The qualifier *explicit* emphasizes that the new position of the point particle is computed in terms of the old position at a single stage by means of multiplications.

Numerical error

It was mentioned earlier that the finite-difference approximation of the derivative $d\mathbf{X}/dt$ introduces an error that is comparable to the magnitude of Δt , as shown in equations (1.5.6). Accordingly, the error in the position of the point particle after it has travelled for the time interval Δt , will be on the order of Δt^2 . Based on the value of this exponent of Δt , we say that the explicit Euler method carries a *stepwise error* of second order with respect to the size of the time step.

If N_{steps} steps are executed from time $t = 0$ to time $t = t_{final}$, the stepwise error will accumulate to an amount that is comparable to the product $N_{steps} \times \Delta t^2$. But since, by definition, $N_{steps} \times \Delta t = t_{final}$, the cumulative error will be on the order of $t_{final} \times \Delta t$. This expression shows that the cumulative error is of first order with respect to the size of the time step. Unless Δt is sufficiently small, this level of error is not tolerated in scientific computing.

1.5.3 Explicit modified Euler method

To reduce the magnitude of the error, we implement a simple modification of the explicit Euler method. The new algorithm involves the following steps:

1. Set the initial time; for example, set $t = 0$.
2. Select the size of the time step Δt .
3. Specify the initial coordinates $X(0)$, $Y(0)$, and $Z(0)$.
4. Evaluate the velocities $u_x(X(t), Y(t), Z(t), t)$, $u_y(X(t), Y(t), Z(t), t)$, and $u_z(X(t), Y(t), Z(t), t)$ on the right-hand side of equations (1.5.7), and save them for future use.
5. Evaluate the right-hand sides of (1.5.7) to obtain the predicted coordinates of the point particle at time $t + \Delta t$, denoted by X^{pred} , Y^{pred} , and Z^{pred} .
6. Evaluate the following velocities at the predicted position, at time $t + \Delta t$,

$$\begin{aligned} u_x^{pred}(X^{pred}, Y^{pred}, Z^{pred}, t + \Delta t), \\ u_y^{pred}(X^{pred}, Y^{pred}, Z^{pred}, t + \Delta t), \\ u_z^{pred}(X^{pred}, Y^{pred}, Z^{pred}, t + \Delta t). \end{aligned} \quad (1.5.8)$$

7. Compute the mean of the initial and predicted velocities

$$\begin{aligned} u_x^M &= \frac{1}{2} [u_x(X(t), Y(t), Z(t), t) + u_x^{pred}], \\ u_y^M &= \frac{1}{2} [u_y(X(t), Y(t), Z(t), t) + u_y^{pred}], \\ u_z^M &= \frac{1}{2} [u_z(X(t), Y(t), Z(t), t) + u_z^{pred}]. \end{aligned} \quad (1.5.9)$$

8. Compute the coordinates of the point particle at time $t + \Delta t$, by returning to the position at time t and traveling with the mean velocity computed at step 7, using the formulae

$$\begin{aligned} X(t + \Delta t) &= X(t) + \Delta t u_x^M, \\ Y(t + \Delta t) &= Y(t) + \Delta t u_y^M, \\ Z(t + \Delta t) &= Z(t) + \Delta t u_z^M. \end{aligned} \quad (1.5.10)$$

9. Reset the time to $t + \Delta t$.
10. Stop if desired, or return to execute steps 4-9.

The procedure just described is the *explicit modified Euler* method. The algorithm is a special member of the inclusive family of *second-order Runge-Kutta* algorithms for solving systems of ordinary differential equations.

An error analysis shows that each time step introduces a numerical error in the position of the point particle that is comparable to the cubic power of time step Δt^3 . The cumulative error is on the order of $t_{final} \times \Delta t^2$, which is much smaller than that incurred by the explicit Euler method.

1.5.4 Streaklines

A streakline emerges by connecting the instantaneous positions of point particles that have been released into the flow from a stationary or moving point at previous times. Alternatively, the point particles may have been residing in the flow at all times, but they were colored or tagged as they passed through the tip of a stationary or moving probe. If the flow is steady and the probe is stationary, a streakline is also a streamline.

To compute a streakline, we solve the differential equations describing the motion of the point particles after they have entered the flow or passed through the coloring probe, using the methods described earlier for particle paths. Since the motion of the point particles is independent of their relative position, the trajectory of each point particle may be computed individually and independently, as though each point particle moved in isolation.

1.5.5 Streamlines

By definition, a streamline is tangential to the instantaneous velocity vector field at every point. If the flow is steady, a streamline is also a path line.

If the flow is unsteady, an *instantaneous streamline* is the path described by a point particle that moves as though the instantaneous velocity field were kept frozen at subsequent times.

Problems

Problem 1.5.1 *Streamlines by analytical integration.*

Consider a steady two-dimensional flow with velocity components

$$u_x = a x + b y, \quad u_y = b x - a y. \quad (1.5.11)$$

Deduce the dimensions of the constants a and b , and derive analytical expressions for the position of a point particle, similar to those shown in (1.5.4).

Problem 1.5.2 *Point particle motion in polar coordinates.*

(a) In the cylindrical polar coordinates depicted in figure 1.3.2, the position of a point particle is described by the functions $x = X(t)$, $\sigma = \Sigma(t)$, and $\varphi = \Phi(t)$. Using the transformation rules given in Section 1.3, derive the differential equations

$$\begin{aligned} \frac{dX}{dt} &= u_x(X(t), \Sigma(t), \Phi(t), t), & \frac{d\Sigma}{dt} &= u_\sigma(X(t), \Sigma(t), \Phi(t), t), \\ \frac{d\Phi}{dt} &= \frac{u_\varphi(X(t), \Sigma(t), \Phi(t), t)}{\Sigma(t)}. \end{aligned} \quad (1.5.12)$$

(b) In the spherical polar coordinates depicted in figure 1.3.3, the position of a point particle is described by the functions $r = R(t)$, $\theta = \Theta(t)$, and $\varphi = \Phi(t)$. Using the transformation rules given in Section 1.3, derive the differential equations

$$\begin{aligned} \frac{dR}{dt} &= u_r(X(t), \Theta(t), \Phi(t), t), & \frac{d\Theta}{dt} &= \frac{u_\theta(X(t), \Theta(t), \Phi(t), t)}{R(t)}, \\ \frac{d\Phi}{dt} &= \frac{u_\varphi(X(t), \Theta(t), \Phi(t), t)}{R(t) \sin \Theta(t)}. \end{aligned} \quad (1.5.13)$$

(c) In the plane polar coordinates depicted in figure 1.3.4, the position of a point particle is described by the functions $r = R(t)$ and $\theta = \Theta(t)$. Using the transformation rules given in Section 1.3, derive the differential equations

$$\frac{dR}{dt} = u_r(R(t), \Theta(t), t), \quad \frac{d\Theta}{dt} = \frac{u_\theta(R(t), \Theta(t), t)}{R(t)}. \quad (1.5.14)$$

Computer problem

Problem c.1.5.1 Streamlines by numerical integration.

Directory *04_various/strmll* of *FDLIB* includes the main program *strmll* that generates streamlines emanating from a specified collection of points in the domain of a two-dimensional flow, computed by the explicit modified Euler method.

(a) Run the program for three velocity fields of your choice implemented in the program, generate and discuss the structure of the streamlines patterns.

(b) Enhance the program with a new flow of your choice, generate and discuss the corresponding streamline pattern.

1.6 Material surfaces and elementary motions

An infinite collection of point particles distributed over a surface that resides within a fluid or over the boundaries defines a *material surface*. A cylindrical material surface in a two-dimensional flow can be identified by its trace in the xy plane, and an axisymmetric material surface in an axisymmetric flow can be identified by its trace in a meridional plane corresponding to a certain meridional angle φ .

Any patch on the surface of the ocean is a material surface with a distinct identity. Under most conditions, if a material patch lies at the boundary of a fluid at a certain time, it will remain at the boundary of the fluid at all times; that is, the point particles comprising the patch will not be able to penetrate the fluid.

1.6.1 Material parcels

A closed material surface is the boundary of a *material parcel* consisting of a fixed mass of fluid with a permanent identity. Under most conditions, if a material surface is located at the boundary of a material parcel at a certain time, it will remain at the boundary of the parcel at all times. To analyze the evolution of a material parcel and visualize its motion, we compute the trajectories of the point particles that lie on its boundary using analytical or numerical methods.

1.6.2 Fluid parcel rotation

Consider a two-dimensional flow in the xy plane with velocity components

$$u_x = -\Omega y, \quad u_y = \Omega x, \quad (1.6.1)$$

where Ω is a constant with units of inverse time. In vector-matrix notation, equations (1.6.1) are collected into the form

$$\begin{bmatrix} u_x & u_y \end{bmatrix} = \begin{bmatrix} x & y \end{bmatrix} \cdot \begin{bmatrix} 0 & \Omega \\ -\Omega & 0 \end{bmatrix}. \quad (1.6.2)$$

According to our discussion in Section 1.5, the trajectory of a point particle with Cartesian coordinates $(X(t), Y(t))$, is governed by the differential equations

$$\frac{dX}{dt} = -\Omega Y, \quad \frac{dY}{dt} = \Omega X, \quad (1.6.3)$$

subject to a specified initial condition $X_{t=0} \equiv X(t=0)$ and $Y_{t=0} \equiv Y(t=0)$. The solution is readily found to be

$$\begin{aligned} X(t) &= \cos(\Omega t) X_{t=0} - \sin(\Omega t) Y_{t=0}, \\ Y(t) &= \sin(\Omega t) X_{t=0} + \cos(\Omega t) Y_{t=0}. \end{aligned} \quad (1.6.4)$$

In vector-matrix notation,

$$\begin{bmatrix} X(t) \\ Y(t) \end{bmatrix} = \begin{bmatrix} \cos(\Omega t) & -\sin(\Omega t) \\ \sin(\Omega t) & \cos(\Omega t) \end{bmatrix} \cdot \begin{bmatrix} X_{t=0} \\ Y_{t=0} \end{bmatrix}. \quad (1.6.5)$$

To deduce the nature of the motion, we refer to plane polar coordinates and find that the distance of a point particle from the origin, denoted by $R(t) \equiv \sqrt{X(t)^2 + Y(t)^2}$ remains constant in time and equal to the initial distance $R(t=0)$, whereas the polar angle θ defined by the equation $\tan \theta = Y(t)/X(t)$ increases linearly in time at the rate $d\theta/dt = \Omega$. That is, $\theta = \theta_0 + \Omega t$, where θ_0 is the polar angle at $t=0$.

These results suggest that a circular material line centered at the origin rotates around the origin as a rigid body with angular velocity Ω , maintaining its circular shape. Accordingly, the velocity field associated with (1.6.1) expresses rigid-body rotation around the origin in the xy plane.

1.6.3 Fluid parcel deformation

Consider now a different type of two-dimensional flow in the xy plane with velocity components

$$u_x = G x, \quad u_y = -G y, \quad (1.6.6)$$

where G is a constant with dimensions of inverse time. In vector-matrix notation,

$$\begin{bmatrix} u_x & u_y \end{bmatrix} = \begin{bmatrix} x & y \end{bmatrix} \cdot \begin{bmatrix} G & 0 \\ 0 & -G \end{bmatrix}. \quad (1.6.7)$$

In this case, the trajectory of a point particle is governed by the differential equations

$$\frac{dX}{dt} = G X, \quad \frac{dY}{dt} = -G Y, \quad (1.6.8)$$

subject to a specified initial condition. Note that equations (1.6.8) are decoupled, in the sense that the first equation contains only X and the second equation contains only Y . The solution is readily found to be

$$X(t) = e^{Gt} X_{t=0}, \quad Y(t) = e^{-Gt} Y_{t=0}. \quad (1.6.9)$$

In vector-matrix notation,

$$\begin{bmatrix} X(t) \\ Y(t) \end{bmatrix} = \begin{bmatrix} e^{Gt} & 0 \\ 0 & e^{-Gt} \end{bmatrix} \cdot \begin{bmatrix} X_{t=0} \\ Y_{t=0} \end{bmatrix}. \quad (1.6.10)$$

The evolution of a circular material line centered at the origin is illustrated in figure 1.6.1 for a positive value of G . As soon as the motion begins, the circular contour deforms into an ellipse with the major and minor axis oriented in the x or y direction. Accordingly, the velocity field associated with the flow (1.6.7) describes pure deformation occurring at an exponential rate; and the constant G is the *rate of deformation*. More detailed consideration reveals that the area enclosed by the deforming circle remains constant in time: the deformation conserves the area of the parcel enclosed by the deforming circle during the motion.

1.6.4 Fluid parcel expansion

As a third case study, we consider a two-dimensional flow in the xy plane with velocity components

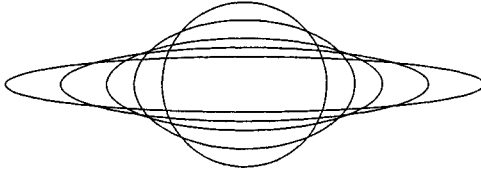


Figure 1.6.1 Deformation of a circular material line under the influence of a two-dimensional elongational flow.

$$u_x = \frac{1}{2} \alpha x, \quad u_y = \frac{1}{2} \alpha y, \quad (1.6.11)$$

where α is a constant with dimensions of inverse time. In vector-matrix notation,

$$\begin{bmatrix} u_x & u_y \end{bmatrix} = \begin{bmatrix} x & y \end{bmatrix} \cdot \begin{bmatrix} \frac{1}{2} \alpha & 0 \\ 0 & \frac{1}{2} \alpha \end{bmatrix}. \quad (1.6.12)$$

The trajectory of a point particle in this flow is governed by the decoupled differential equations

$$\frac{dX}{dt} = \frac{1}{2} \alpha X, \quad \frac{dY}{dt} = \frac{1}{2} \alpha Y, \quad (1.6.13)$$

subject to a specified initial condition. The solution is found by elementary methods to be

$$X(t) = \exp\left(\frac{1}{2} \alpha t\right) X_{t=0}, \quad Y(t) = \exp\left(\frac{1}{2} \alpha t\right) Y_{t=0}. \quad (1.6.14)$$

In vector-matrix notation,

$$\begin{bmatrix} X(t) \\ Y(t) \end{bmatrix} = \begin{bmatrix} \exp\left(\frac{1}{2} \alpha t\right) & 0 \\ 0 & \exp\left(\frac{1}{2} \alpha t\right) \end{bmatrix} \cdot \begin{bmatrix} X_{t=0} \\ Y_{t=0} \end{bmatrix}. \quad (1.6.15)$$

Based on these expressions, we deduce that a circular material line centered at the origin expands at an exponential rate, while maintaining its circular shape. Accordingly, the velocity field associated with equations (1.6.11) expresses *isotropic expansion*. If $a(t)$ is the radius of the circular material line at time t , and $a(t=0)$ is the radius at the origin of time, then

$$a(t) = a(t=0) \exp\left(\frac{1}{2} \alpha t\right). \quad (1.6.16)$$

Raising both sides of equation (1.6.16) to the second power, and multiplying the result by π , we find that the ratio of the areas enclosed by the circular material lines is given by

$$\frac{\pi a^2(t)}{\pi a^2(t=0)} = \exp(\alpha t). \quad (1.6.17)$$

Accordingly, the constant α is the *rate of areal expansion*.

1.6.5 Superposition of rotation, deformation, and expansion

For future convenience, we relabel the Cartesian coordinates from (x, y) to (x', y') . Superposing the three types of flow discussed in the preceding sections, we obtain a compound velocity field with components

$$\begin{bmatrix} u_{x'} & u_{y'} \end{bmatrix} = \begin{bmatrix} x' & y' \end{bmatrix} \cdot \left(\begin{bmatrix} 0 & \Omega \\ -\Omega & 0 \end{bmatrix} + \begin{bmatrix} G & 0 \\ 0 & -G \end{bmatrix} + \begin{bmatrix} \frac{1}{2}\alpha & 0 \\ 0 & \frac{1}{2}\alpha \end{bmatrix} \right). \quad (1.6.18)$$

The three matrices on the right-hand side of (1.6.18) express, respectively, fluid parcel rotation, pure deformation, and isotropic expansion. Summing corresponding elements, we obtain the synthesized vector form

$$\mathbf{u}' = \mathbf{x}' \cdot \mathbf{A}, \quad (1.6.19)$$

where $\mathbf{u}' = (u_{x'}, u_{y'})$, $\mathbf{x}' = (x', y')$, and the matrix \mathbf{A} is defined as

$$\mathbf{A} = \begin{bmatrix} G + \frac{1}{2}\alpha & \Omega \\ -\Omega & -G + \frac{1}{2}\alpha \end{bmatrix}. \quad (1.6.20)$$

Because the velocity field (1.6.19) depends linearly on the position vector, the associated flow is *linear*. Varying the relative magnitudes of the three parameters Ω , G , and α allows us to alter the character of the flow by forming hybrid forms of its three constituents.

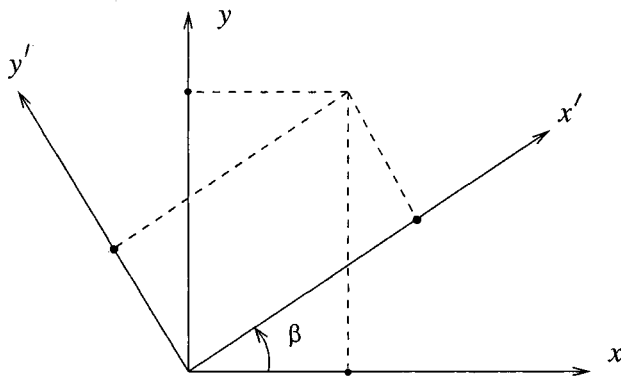


Figure 1.6.2 A system of Cartesian axes (x', y') arising by rotating the (x, y) axes by the angle β .

1.6.6 Rotated coordinates

To this end, we observe that, although fluid parcel rotation, deformation, and expansion have been deduced with reference to the $x'y'$ system of Cartesian coordinates, as discussed previously in this section, expressing the position and velocity vectors in a different system of coordinates should leave the physical nature of the motion unchanged. Motivated by this observation, we set out to generalize the velocity field described by equation (1.6.19) in a way that extends its physical interpretation.

Consider a two-dimensional Cartesian system $x'y'$ that has been rotated with respect to the xy system by the angle β , as shown in figure 1.6.2. Note that the angle β is positive when the system $x'y'$ arises from the counter-clockwise rotation of xy , and negative otherwise. A point in the $x'y'$ or xy plane may be identified by its primed coordinates (x', y') , or un-primed coordinates (x, y) . Using elementary trigonometry, we find that the two sets of coordinates are related by

$$x = x' \cos \beta - y' \sin \beta, \quad y = x' \sin \beta + y' \cos \beta. \quad (1.6.21)$$

In vector-matrix notation,

$$\begin{bmatrix} x & y \end{bmatrix} = \begin{bmatrix} x' & y' \end{bmatrix} \cdot \begin{bmatrix} \cos \beta & \sin \beta \\ -\sin \beta & \cos \beta \end{bmatrix}. \quad (1.6.22)$$

To simplify the notation, we introduce the *rotation matrix*

$$\mathbf{R} \equiv \begin{bmatrix} \cos \beta & \sin \beta \\ -\sin \beta & \cos \beta \end{bmatrix}, \quad (1.6.23)$$

and express (1.6.22) in the form

$$\mathbf{x} = \mathbf{x}' \cdot \mathbf{R}, \quad (1.6.24)$$

where $\mathbf{x}' = (x', y')$ and $\mathbf{x} = (x, y)$.

The rotation matrix \mathbf{R} has two important properties. First, its determinant is equal to 1. To explain the second property, we introduce the transpose of \mathbf{R} , which arises by interchanging the off-diagonal elements R_{12} and R_{21} to form the new matrix

$$\mathbf{R}^T = \begin{bmatrix} \cos \beta & -\sin \beta \\ \sin \beta & \cos \beta \end{bmatrix}. \quad (1.6.25)$$

Using the rules of matrix multiplication, we find

$$\mathbf{R} \cdot \mathbf{R}^T = \mathbf{I}, \quad \mathbf{R}^T \cdot \mathbf{R} = \mathbf{I}, \quad (1.6.26)$$

where \mathbf{I} is the unit or identity matrix defined as

$$\mathbf{I} = \begin{bmatrix} 1 & 0 \\ 0 & 1 \end{bmatrix}. \quad (1.6.27)$$

Now, the inverse of an arbitrary square matrix \mathbf{A} is defined as another matrix \mathbf{A}^{-1} with the properties $\mathbf{A} \cdot \mathbf{A}^{-1} = \mathbf{I}$ and $\mathbf{A}^{-1} \cdot \mathbf{A} = \mathbf{I}$. If \mathbf{A}^{-1} is equal to \mathbf{A}^T , where the superscript T denotes the transpose, then the matrix \mathbf{A} is called *orthogonal*. In light of this definition, equations (1.6.26) ensure that the rotation matrix \mathbf{R} is orthogonal.

Working in a similar fashion, we find that the components of the velocity vector in the xy and $x'y'$ system of coordinates are related by an equation that is analogous to (1.6.24),

$$\mathbf{u} = \mathbf{u}' \cdot \mathbf{R}, \quad (1.6.28)$$

where $\mathbf{u}' = (u_{x'}, u_{y'})$ and $\mathbf{u} = (u_x, u_y)$.

Having completed the necessary preparations, we multiply both sides of equation (1.6.19) by the matrix \mathbf{R} , and exploit the first of the orthogonality properties (1.6.26) to obtain the equivalent form

$$\mathbf{u}' \cdot \mathbf{R} = \mathbf{x}' \cdot \mathbf{A} \cdot \mathbf{R} = \mathbf{x}' \cdot \mathbf{I} \cdot \mathbf{A} \cdot \mathbf{R} = \mathbf{x}' \cdot \mathbf{R} \cdot \mathbf{R}^T \mathbf{A} \cdot \mathbf{R}. \quad (1.6.29)$$

Using equations (1.6.24) and (1.6.28), we rewrite equation (1.6.29) in the form

$$\mathbf{u} = \mathbf{x} \cdot \mathbf{B}, \quad (1.6.30)$$

where we have introduced the new matrix

$$\mathbf{B} \equiv \mathbf{R}^T \cdot \mathbf{A} \cdot \mathbf{R}. \quad (1.6.31)$$

Substituting (1.6.20), (1.6.23), and (1.6.25) into the right-hand side of (1.6.31), and using the trigonometric identities $\cos(2\beta) = \cos^2 \beta - \sin^2 \beta$ and $\sin(2\beta) = 2 \sin \beta \cos \beta$, we derive the explicit form

$$\mathbf{B} = \begin{bmatrix} G \cos(2\beta) + \frac{1}{2} \alpha & -G \sin(2\beta) + \Omega \\ -G \sin(2\beta) - \Omega & -G \cos(2\beta) + \frac{1}{2} \alpha \end{bmatrix}. \quad (1.6.32)$$

Note that, when $\beta = 0$ or π , the matrix \mathbf{B} reduces to the matrix \mathbf{A} given in equation (1.6.20). The four elements of the matrix \mathbf{B} contain the three flow parameters Ω , G , and α , and the rotation angle β .

1.6.7 Flow decomposition

In practice, we are interested in the inverse problem: given the four elements of the matrix \mathbf{B} , obtained by laboratory measurements or numerical computation, we want to evaluate the four parameters Ω , G , and α , and β , and thereby deduce, respectively, the rate of rotation, the rate of deformation, the rate of expansion, and the direction of deformation.

To be more specific, we consider a *linear* flow with velocity components

$$\begin{bmatrix} u_x & u_y \end{bmatrix} = \begin{bmatrix} x & y \end{bmatrix} \cdot \begin{bmatrix} a & b \\ c & d \end{bmatrix}, \quad (1.6.33)$$

where a , b , c , and d are four constants with dimensions of inverse time. Setting the components of the matrix on the right-hand side of (1.6.33) equal to the corresponding components of the matrix \mathbf{B} on the right-hand side of (1.6.32), we obtain a nonlinear system of four trigonometric equations for the four unknowns Ω , G , α , and β . The solution can be found most readily according to the following steps.

First, we decompose the matrix shown on the right-hand side of (1.6.33) into three constituents, as follows:

$$\mathbf{B} = \begin{bmatrix} a & b \\ c & d \end{bmatrix} = \frac{1}{2} \begin{bmatrix} 0 & b-c \\ c-b & 0 \end{bmatrix} + \frac{1}{2} \begin{bmatrix} a-d & b+c \\ c+b & d-a \end{bmatrix} + \frac{1}{2} \begin{bmatrix} a+d & 0 \\ 0 & a+d \end{bmatrix}. \quad (1.6.34)$$

The first matrix on the right-hand side of (1.6.34) is antisymmetric or skew-symmetric; that is, the 12 component is equal to the negative of the 21 component. The second matrix is symmetric and its trace, defined as the sum of the diagonal elements, is equal to zero. The third matrix is diagonal and isotropic, meaning that the two diagonal elements are identical.

With reference to the first matrix, we set

$$\Omega = \frac{b-c}{2}. \quad (1.6.35)$$

With reference to the third matrix, we set

$$\alpha = a+d. \quad (1.6.36)$$

To compute the remaining unknowns G and β , we consider the second matrix on the right-hand side of (1.6.34), defined as

$$\mathbf{E} = \frac{1}{2} \begin{bmatrix} a-d & b+c \\ c+b & d-a \end{bmatrix}. \quad (1.6.37)$$

An eigenvalue λ of \mathbf{E} and the corresponding eigenvector $\mathbf{f} = \begin{bmatrix} f_x \\ f_y \end{bmatrix}$ satisfy the equation

$$\mathbf{E} \cdot \mathbf{f} = \lambda \mathbf{f}, \quad (1.6.38)$$

or

$$(\mathbf{E} - \lambda \mathbf{I}) \cdot \mathbf{f} = \mathbf{0}. \quad (1.6.39)$$

The eigenvalues of \mathbf{E} are found by setting the determinant of the matrix $\mathbf{E} - \lambda \mathbf{I}$ equal to zero, obtaining the quadratic equation

$$\left[\frac{1}{2}(a-d) - \lambda \right] \left[\frac{1}{2}(d-a) - \lambda \right] - \frac{1}{4}(b+c)^2 = 0, \quad (1.6.40)$$

whose roots are found to be

$$\lambda = \pm \frac{1}{2} \sqrt{(a-d)^2 + (b+c)^2}. \quad (1.6.41)$$

The corresponding eigenvectors are found by solving the homogeneous system (1.6.39). Having found the eigenvalues and eigenvectors of the matrix \mathbf{E} , we recover G and β by setting

$$G = \lambda, \quad (1.6.42)$$

with the plus or minus sign selected on the right-hand side of (1.6.41), and then identify β with the angle subtended between the corresponding eigenvector \mathbf{f} and the x axis; that is, we compute the angle β from the equation $\tan \beta = f_y/f_x$.

As an example, consider a two-dimensional velocity field with components

$$u_x(x, y, t) = w(t) (2x - y), \quad u_y(x, y, t) = w(t) (-3x + 3y), \quad (1.6.43)$$

where $w(t)$ is a function of time. The four time-dependent constants a, b, c and d introduced in equation (1.6.33) are given by

$$a = 2w(t), \quad b = -3w(t), \quad c = -w(t), \quad d = 3w(t). \quad (1.6.44)$$

Carrying out the decomposition shown in equation (1.6.34), we find

$$\begin{aligned} \mathbf{B} &= w(t) \begin{bmatrix} 2 & -3 \\ -1 & 3 \end{bmatrix} \\ &= w(t) \frac{1}{2} \begin{bmatrix} 0 & -2 \\ 2 & 0 \end{bmatrix} + w(t) \frac{1}{2} \begin{bmatrix} -1 & -4 \\ -4 & 1 \end{bmatrix} + w(t) \frac{1}{2} \begin{bmatrix} 5 & 0 \\ 0 & 5 \end{bmatrix}. \end{aligned} \quad (1.6.45)$$

Using equations (1.6.35) and (1.6.36), we find that the rate of rotation is given by $\Omega = -w(t)$, and the rate of expansion is given by $\alpha = 5w(t)$. The symmetric matrix \mathbf{E} defined in equation (1.6.37) is given by the second term on the right-hand side of (1.6.45),

$$\mathbf{E} = w(t) \frac{1}{2} \begin{bmatrix} -1 & -4 \\ -4 & 1 \end{bmatrix}. \quad (1.6.46)$$

The eigenvalues of \mathbf{E} are found by setting the determinant of the matrix

$$\mathbf{E} - \lambda \mathbf{I} = \begin{bmatrix} -\frac{1}{2} w(t) - \lambda & -2w(t) \\ -2w(t) & \frac{1}{2} w(t) - \lambda \end{bmatrix} \quad (1.6.47)$$

equal to zero. The roots of the resulting quadratic equation are given by

$$\lambda = \pm \frac{\sqrt{17}}{2} w(t). \quad (1.6.48)$$

Either one of these values may be identified with the rate of extension G , as indicated by equation (1.6.42).

Substituting expressions (1.6.48) into the system (1.6.39), we find

$$\begin{bmatrix} -\frac{1}{2} (1 \pm \sqrt{17}) & -2 \\ -2 & -\frac{1}{2} (-1 \pm \sqrt{17}) \end{bmatrix} \cdot \begin{bmatrix} f_x \\ f_y \end{bmatrix} = \begin{bmatrix} 0 \\ 0 \end{bmatrix}. \quad (1.6.49)$$

The two scalar equations comprising system (1.6.49) are, in fact, identical. Using the first equation, we find

$$\frac{f_y}{f_x} = -\frac{1 \pm \sqrt{17}}{4}. \quad (1.6.50)$$

Executing the instructions given in the paragraph following equation (1.6.41), we finally set $\tan \beta = f_y/f_x$, and find

$$\beta = -\arctan \frac{1 \pm \sqrt{17}}{4}. \quad (1.6.51)$$

Problems

Problem 1.6.1 *Material lines.*

A collection of point particles distributed over a line in a three-dimensional flow defines a *material line*. Explain why, if the flow is steady, a material line that lies on a streamline at a certain time will remain on the streamline at all times.

Problem 1.6.2 *Rotation of coordinates.*

Derive two equations that relate the old coordinates (x', y') to the new coordinates (x, y) , and then express them in vector form similar to that shown in equation (1.6.22).

Problem 1.6.3 *Flow decomposition.*

Carry out the decomposition of a two-dimensional flow with velocity components $u_x(x, y, t) = w(t)(2x + 3y)$ and $u_y(x, y, t) = w(t)(-x - 2y)$, where $w(t)$ is a function of time.

1.7 Interpolation

In practice, the components of the fluid velocity are hardly ever given in explicit form, as was done in equations (1.4.7) and (1.5.2). Instead, they are either measured in the laboratory with velocity probes, or computed by numerical methods at *data points* located in the domain of flow. The velocity at an arbitrary point is then obtained by a numerical procedure called *function interpolation*.

Typically, but not always, the data points are located at the nodes of a grid defined by the intersections of planar or curved surfaces in three dimensions, and straight or curved lines in two dimensions. A Cartesian grid is defined by the intersections of planes that are normal to the x , y , and z axis in three dimensions, or by the intersections of lines that are normal to the x and y axes in two dimensions. A one-dimensional, a two-dimensional, and a three-dimensional Cartesian grid with evenly spaced grid-lines are illustrated in figure 1.7.1.

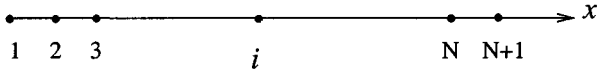
1.7.1 Interpolation in one dimension

As a prelude to computing the components of the velocity at an arbitrary point in a flow from specified grid values, we consider interpolating a function $f(x)$ of one independent variable x .

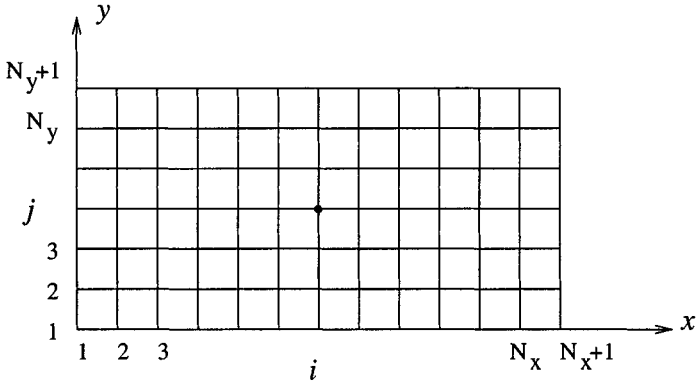
Let us assume that we are given the values of the function $f(x)$ at the $N + 1$ nodes of a one-dimensional grid located at x_i , where $i = 1, 2, \dots, N + 1$, and $x_1 < x_2 < \dots < x_{N+1}$, as shown in figure 1.7.1(a). Effectively, we are provided with a three-column table of $N + 1$ entries listing i, x_i , and $f(x_i)$; for simplicity, we denote $f(x_i)$ by f_i . Our goal is to compute the value of the function $f(x)$ at a point x that does not necessarily coincide with a node.

A set of $N + 1$ nodes define N intervals, where the i th interval starts at the i th node and ends at the $i + 1$ node. Suppose that the point x lies within the k th interval subtended between the nodes x_k and x_{k+1} . A simple way of finding the value of k is by computing the products

(a)



(b)



(c)

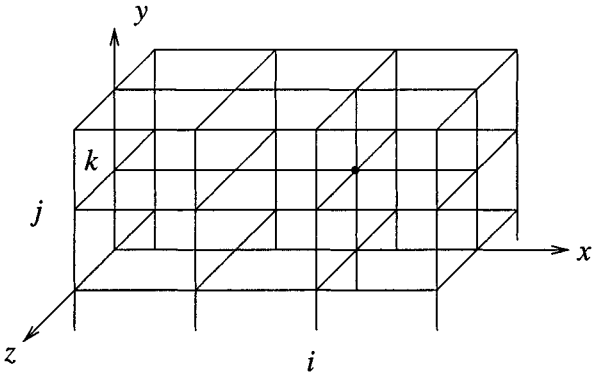


Figure 1.7.1 Illustration of (a) a one-dimensional, (b) a two-dimensional, and (c) a three-dimensional Cartesian grid with evenly spaced grid-lines.

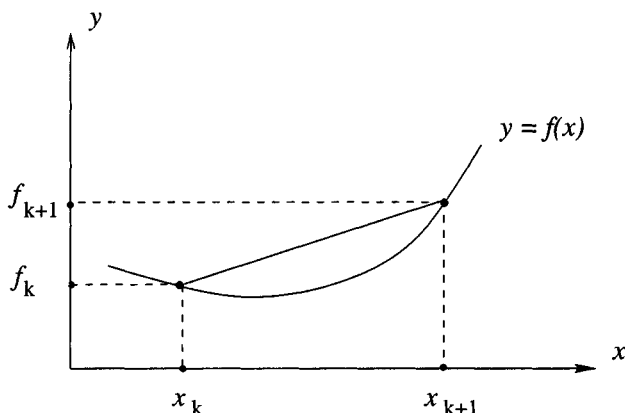


Figure 1.7.2 Local approximation of a function with a linear interpolating function represented by the straight line.

$p_i = (x - x_i)(x - x_{i+1})$ for all values of i . The appropriate value of k is the unique value of i for which p_i is negative.

There are better and faster methods of finding the label of the host interval k . For example, in the method of logarithmic search, we first examine whether the point x lies on the left or on the right of the midpoint of the interpolation domain (x_1, x_{N+1}) . Having found the host half-interval, we repeat the process until the host sub-interval has been reduced to the k th interval.

Linear interpolation

One way to compute the value $f(x)$ is by approximating the graph of the function $f(x)$ over the interval (x_k, x_{k+1}) with a straight line, and requiring that the straight line pass through the two data points corresponding to the doublets (x_k, f_k) and (x_{k+1}, f_{k+1}) , as illustrated in figure 1.7.2.

In mathematical terms, we approximate the function $f(x)$ over the interval (x_k, x_{k+1}) with a linear function expressed by the first-degree polynomial

$$P_1^{(k)}(x) = a^{(k)}(x - x_k) + b^{(k)}, \quad (1.7.1)$$

where the coefficient $a^{(k)}$ is the slope. Note that we have expressed this polynomial in terms of the shifted monomial $x - x_k$ rather than

the unshifted monomial x in order to facilitate forthcoming algebraic manipulations.

To compute the constants $a^{(k)}$ and $b^{(k)}$, we require the *interpolation conditions*

$$\begin{aligned} P_1^{(k)}(x_k) &= b^{(k)} = f_k, \\ P_1^{(k)}(x_{k+1}) &= a^{(k)}(x_{k+1} - x_k) + b^{(k)} = f_{k+1}, \end{aligned} \quad (1.7.2)$$

ensuring that the graph of the polynomial passes through the data points labelled k and $k+1$. Solving the system of the two linear equations (1.7.2) for the two monomial coefficients, we find

$$a^{(k)} = \frac{f_{k+1} - f_k}{x_{k+1} - x_k}, \quad b^{(k)} = f_k. \quad (1.7.3)$$

To evaluate the linear polynomial $P_1^{(k)}(x)$, we first compute the coefficients $a^{(k)}$ and $b^{(k)}$ using equations (1.7.3), and then evaluate the right-hand side of (1.7.1) for a desired value of x that lies between x_k and x_{k+1} . The result will be a reasonable approximation to the unknown value $f(x)$.

Quadratic interpolation

Interpolation based on the straight-line approximation overlooks the curvature of the graph of the function $f(x)$. For better accuracy, we approximate the graph of the interpolated function $f(x)$ over the interval (x_k, x_{k+1}) with a parabola, as depicted in figure 1.7.3.

In mathematical terms, we approximate the function $f(x)$ over this interval with a quadratic function expressed by the second-degree polynomial

$$P_2^{(k)}(x) = a^{(k)}(x - x_k)^2 + b^{(k)}(x - x_k) + c^{(k)}. \quad (1.7.4)$$

As previously, we have expressed the polynomial in terms of the shifted monomial $x - x_k$ instead of the unshifted monomial x in order to simplify the forthcoming algebraic manipulations.

To compute the three constants $a^{(k)}$, $b^{(k)}$, and $c^{(k)}$, we require three equations. First, we demand that the parabola pass through the two data points (x_k, f_k) and (x_{k+1}, f_{k+1}) , and obtain the interpolation conditions

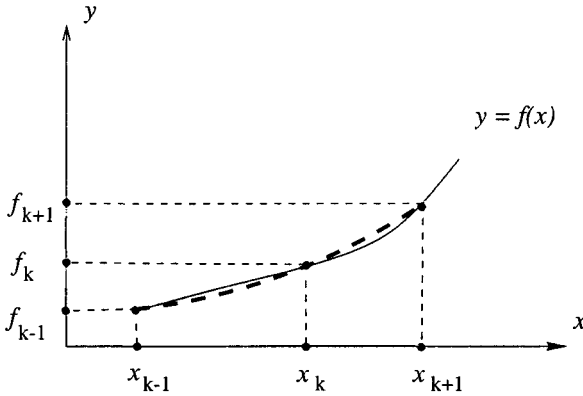


Figure 1.7.3 Local approximation of a function with a parabolic interpolating function represented by the thick dashed line.

$$P_2^{(k)}(x_k) = c^{(k)} = f_k,$$

$$P_2^{(k)}(x_{k+1}) = a^{(k)}(x_{k+1} - x_k)^2 + b^{(k)}(x_{k+1} - x_k) + c^{(k)} = f_{k+1}. \quad (1.7.5)$$

One more data point is required, and we may choose either the backward point (x_{k-1}, f_{k-1}) , or the forward point (x_{k+2}, f_{k+2}) . The backward choice provides us with the condition

$$P_2^{(k)}(x_{k-1}) = a^{(k)}(x_{k-1} - x_k)^2 + b^{(k)}(x_{k-1} - x_k) + c^{(k)} = f_{k-1}. \quad (1.7.6)$$

With the choice expressed by equations (1.7.5) and (1.7.6), the coefficients of the binomial are found to be

$$a^{(k)} = \frac{\frac{f_{k+1} - f_k}{h_k} - \frac{f_k - f_{k-1}}{h_{k-1}}}{h_k + h_{k-1}}, \quad b^{(k)} = \frac{h_{k-1} \frac{f_{k+1} - f_k}{h_k} + h_k \frac{f_k - f_{k-1}}{h_{k-1}}}{h_k + h_{k-1}},$$

$$c^{(k)} = f_k, \quad (1.7.7)$$

where

$$h_{k-1} = x_k - x_{k-1}, \quad h_k = x_{k+1} - x_k, \quad (1.7.8)$$

are the lengths of the backward and forward intervals.

When the data points are spaced evenly, $h_{k-1} = h_k = h$, we obtain the simplified expressions

$$a^{(k)} = \frac{f_{k+1} - 2f_k + f_{k-1}}{2h^2}, \quad b^{(k)} = \frac{f_{k+1} - f_{k-1}}{2h}, \quad c^{(k)} = f_k. \quad (1.7.9)$$

To evaluate $P_2^{(k)}(x)$, we first compute the coefficients $a^{(k)}$, $b^{(k)}$ and $c^{(k)}$ using the preceding equations, and then evaluate the right-hand side of (1.7.4). The result will be an improved approximation to $f(x)$.

1.7.2 Interpolation in two dimensions

Consider now a function f of two independent variables x and y . For the present purposes, a function of two variables is an engine that receives the pair of numbers x and y and produces the new number $f(x, y)$.

Assume that we are given the values of the function $f(x, y)$ at the nodes of a two-dimensional grid defined by the intersections of the x -level lines x_i , where $i = 1, 2, \dots, N_x + 1$, and the y -level lines y_j , where $j = 1, 2, \dots, N_y + 1$, as shown in figure 1.7.1(b). A grid-node is defined by the values of the indices i and j forming the ordered integer doublet (i, j) , as illustrated in figure 1.7.1(b). The value of the function $f(x, y)$ at the (i, j) node is equal to $f(x_i, y_j)$. Our goal is to compute the value of f at a point (x, y) that is not necessarily a node.

Suppose that the value of x lies inside the k_x th x -interval confined between the x_{k_x} and x_{k_x+1} x -level lines, and the value of y lies inside the k_y th y -interval confined between the y_{k_y} and y_{k_y+1} y -level lines, as shown in figure 1.7.4. The values of k_x and k_y may be found by the methods discussed in Section 1.7.1 for one-dimensional interpolation.

Bilinear interpolation

An approximation to $f(x, y)$ may be obtained by replacing the unknown function $f(x, y)$ with the function $P_{BL}^{k_x, k_y}(x, y)$ defined over the rectangular domain that is confined between the x -level lines $x = x_{k_x}$, $x = x_{k_x+1}$, and the y -level lines $y = y_{k_y}$, and $y = y_{k_y+1}$. The bilinear function $P_{BL}^{k_x, k_y}(x, y)$ is endowed with the following properties:

1. For a fixed value of x , call it x_0 , the function $P_{BL}^{k_x, k_y}(x_0, y)$ varies linearly with respect to y .

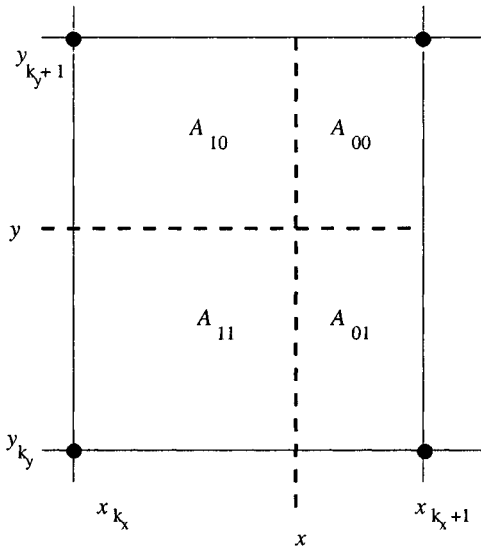


Figure 1.7.4 Bilinear interpolation of a scalar function through a rectangular grid.

2. For a fixed value of y , call it y_0 , the function $P_{BL}^{k_x, k_y}(x, y_0)$ varies linearly with respect to x .
3. The following four *interpolation conditions* ensuring that the bilinear function reproduces the neighboring grid values are met:

$$\begin{aligned}
 P_{BL}^{k_x, k_y}(x_{k_x}, y_{k_y}) &= f(x_{k_x}, y_{k_y}), \\
 P_{BL}^{k_x, k_y}(x_{k_x}, y_{k_y+1}) &= f(x_{k_x}, y_{k_y+1}), \\
 P_{BL}^{k_x, k_y}(x_{k_x+1}, y_{k_y}) &= f(x_{k_x+1}, y_{k_y}), \\
 P_{BL}^{k_x, k_y}(x_{k_x+1}, y_{k_y+1}) &= f(x_{k_x+1}, y_{k_y+1}).
 \end{aligned} \tag{1.7.10}$$

The first and second of the above properties require that the bilinear function have the functional form

$$P_{BL}^{k_x, k_y}(x, y) = (a_x^{k_x, k_y} x + b_x^{k_x, k_y}) (a_y^{k_x, k_y} y + b_y^{k_x, k_y}). \tag{1.7.11}$$

To evaluate the four constants $a_x^{k_x, k_y}$, $b_x^{k_x, k_y}$, $a_y^{k_x, k_y}$, and $b_y^{k_x, k_y}$, we use the four interpolation conditions (1.7.10), finding

$$\begin{aligned}
P_{BL}^{k_x, k_y}(x, y) &= w_{00}^{k_x, k_y}(x, y) f(x_{k_x}, y_{k_y}) + w_{10}^{k_x, k_y}(x, y) f(x_{k_x+1}, y_{k_y}) \\
&\quad + w_{01}^{k_x, k_y}(x, y) f(x_{k_x}, y_{k_y+1}) + w_{11}^{k_x, k_y}(x, y) f(x_{k_x+1}, y_{k_y+1}),
\end{aligned} \tag{1.7.12}$$

where we have introduced the position-dependent *interpolation weights*

$$\begin{aligned}
w_{00}^{k_x, k_y}(x, y) &= \frac{A_{00}}{A}, & w_{01}^{k_x, k_y}(x, y) &= \frac{A_{10}}{A}, \\
w_{10}^{k_x, k_y}(x, y) &= \frac{A_{01}}{A}, & w_{11}^{k_x, k_y}(x, y) &= \frac{A_{11}}{A}.
\end{aligned} \tag{1.7.13}$$

The numerators A_{00} , A_{10} , A_{01} , and A_{11} are the areas of the four sub-rectangles depicted in figure 1.7.4, given by

$$\begin{aligned}
A_{00} &= (x_{k_x+1} - x)(y_{k_y+1} - y), & A_{10} &= (x - x_{k_x})(y_{k_y+1} - y), \\
A_{01} &= (x_{k_x+1} - x)(y - y_{k_y}), & A_{11} &= (x - x_{k_x})(y - y_{k_y}),
\end{aligned} \tag{1.7.14}$$

The denominator A is the area of the interpolation rectangle, given by

$$A = (x_{k_x+1} - x_{k_x})(y_{k_y+1} - y_{k_y}). \tag{1.7.15}$$

It is reassuring to observe that the sum of the four interpolation weights given in (1.7.13) is equal to unity independent of the values of x and y ,

$$w_{00}(x, y) + w_{10}(x, y) + w_{01}(x, y) + w_{11}(x, y) = 1. \tag{1.7.16}$$

This property guarantees that, if the four grid values

$$f(x_{k_x}, y_{k_y}), \quad f(x_{k_x}, y_{k_y+1}), \quad f(x_{k_x+1}, y_{k_y}), \quad f(x_{k_x+1}, y_{k_y+1})$$

are the same, equal to a , then bilinear interpolation based on (1.7.12) produces

$$P_{BL}^{k_x, k_y}(x, y) = a (w_{00} + w_{10} + w_{01} + w_{11}) = a, \tag{1.7.17}$$

as required.

1.7.3 Interpolation of the velocity in a two-dimensional flow

Returning to fluid mechanics, we consider a two-dimensional flow in the xy plane, and specify the values of the x and y velocity components u_x and u_y at the nodes of a two-dimensional Cartesian grid. To obtain the corresponding values at an arbitrary point (x, y) , we employ bilinear interpolation, finding

$$u_x(x, y) = w_{00}^{k_x, k_y}(x, y) u_x(x_{k_x}, y_{k_y}) + w_{10}^{k_x, k_y}(x, y) u_x(x_{k_x+1}, y_{k_y}) \\ + w_{01}^{k_x, k_y}(x, y) u_x(x_{k_x}, y_{k_y+1}) + w_{11}^{k_x, k_y}(x, y) u_x(x_{k_x+1}, y_{k_y+1}), \quad (1.7.18)$$

and

$$u_y(x, y) = w_{00}^{k_x, k_y}(x, y) u_y(x_{k_x}, y_{k_y}) + w_{10}^{k_x, k_y}(x, y) u_y(x_{k_x+1}, y_{k_y}) \\ + w_{01}^{k_x, k_y}(x, y) u_y(x_{k_x}, y_{k_y+1}) + w_{11}^{k_x, k_y}(x, y) u_y(x_{k_x+1}, y_{k_y+1}). \quad (1.7.19)$$

Our ability to interpolate the velocity components at any point in a flow from specified grid values allows us to generate particle paths and streamlines without having available explicit expressions for the velocity in analytical form. In practice, the grid values are computed by solving the equations governing the motion of the fluid using a variety of numerical methods, as will be discussed later in this text.

Problems

Problem 1.7.1 Quadratic interpolation.

Solve the linear system of three equations (1.7.5) and (1.7.6) to derive formulas (1.7.7). *Hint:* Compute first the coefficient $c^{(k)}$ using the first of equations (1.7.5).

Problem 1.7.2 Forward-point parabolic interpolation.

Consider the parabolic interpolation of a function of one variable $f(x)$, as discussed in the text. Forward interpolation uses the interpolation condition

$$P_2^{(k)}(x_{k+2}) = a^{(k)}(x_{k+2} - x_k)^2 + b^{(k)}(x_{k+2} - x_k) + c^{(k)} = f_{k+2}, \quad (1.7.20)$$

in place of (1.7.6). Derive expressions for the coefficients $a^{(k)}$, $b^{(k)}$, and $c^{(k)}$ in terms of the grid values f_k , f_{k+1} , and f_{k+2} , and the interval sizes h_k and h_{k+1} . Then derive simplified expressions when h_k and h_{k+1} are equal to h .

Problem 1.7.3 *Trilinear interpolation.*

Consider a function of three variables $f(x, y, z)$. Extend the method of bilinear interpolation of a function of two variables discussed in the text, to the method of trilinear interpolation that generates the value of f at an arbitrary point (x, y, z) using the values of f at the nodes of a three-dimensional Cartesian grid. The interpolation formula should be the counterpart of (1.7.12) with properly defined interpolation weights.

Computer problems

Problem c.1.7.1 *Bilinear interpolation.*

Directory *02_grids/rec_2d* of *FDLIB* contains a program that interpolates the x and y components of the velocity and draws the velocity vector field over a rectangular domain confined between $a_x < x < b_x$ and $a_y < y < b_y$. The interpolation is based on specified values of the velocity at the nodes of a uniform $N_x \times N_y$ Cartesian grid, as shown in figure 1.7.5.

(a) Run the program for a velocity field of your choice offered in the main, confirm that the interpolated values are identical to the specified grid values, and prepare a plot of the velocity vector field similar to that displayed in figure 1.7.5.

(b) Enhance the menu with a new flow of your choice; plot and discuss the structure of the velocity field.

Problem c.1.7.2 *Streamlines by interpolation.*

Directory *02_grids/rec_2d_strml* of *FDLIB* contains a program that generates streamlines originating from specified points in a rectangular domain of a two-dimensional flow. The velocity components are computed by bilinear interpolation based on specified grid values.

(a) Run the program for a velocity field of your choice offered in the main menu, generate, plot, and discuss the streamline pattern.

(b) Enhance the main menu with a new flow of your choice, plot and discuss the streamline pattern.

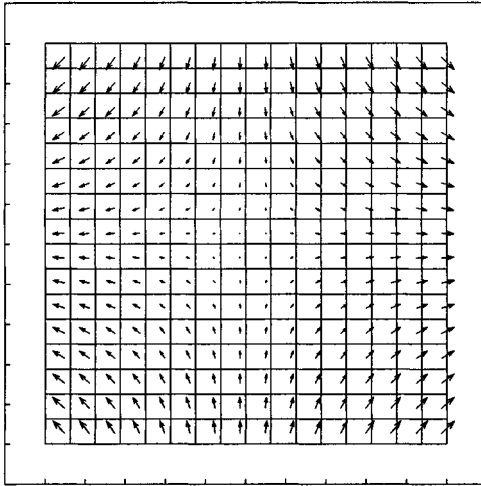


Figure 1.7.5 Bilinear interpolation of a velocity vector field through a Cartesian grid in a two-dimensional flow.

Chapter 2

Fluid Motion: More on Kinematics

- 2.1 Fundamental modes of fluid parcel motion
- 2.2 Fluid parcel expansion
- 2.3 Fluid parcel rotation and vorticity
- 2.4 Fluid parcel deformation
- 2.5 Numerical differentiation
- 2.6 Areal and volumetric flow rate
- 2.7 Mass flow rate, mass conservation, and the continuity equation
- 2.8 Properties of point particles
- 2.9 Incompressible fluids and stream functions
- 2.10 Kinematic conditions at boundaries

We continue the study of kinematics by considering, in more detail, the behavior of fluid parcels, by deriving expressions for the volumetric and mass flow rate across surfaces drawn in a fluid, and by developing numerical methods for evaluating kinematical variables defined in terms of derivatives or integrals of the velocity. Conservation of mass required by thermodynamics, and physical conditions imposed at boundaries introduce mathematical constraints that motivate the description of a flow in terms of ancillary functions that expedite analysis and numerical computation.

2.1 Fundamental modes of fluid parcel motion

In Chapter 1, we pointed out that the nature of the motion of a small fluid parcel is determined by the relative motion of point particles residing within the parcel and over its boundary. If, for example, the velocity of all point particles is nearly the same, that is, variations in the point particle velocity are small compared to the average velocity, then

the parcel exhibits rigid-body translation. Significant variations in the point particle velocity generate more general types of motion including local rotation, deformation, and isotropic expansion.

To study the relative motion of point particles in the vicinity of a certain point $\mathbf{x}_0 = (x_0, y_0, z_0)$, we consider differences in corresponding components of the velocity evaluated at a point $\mathbf{x} = (x, y, z)$ that lies close to \mathbf{x}_0 , and at the chosen point \mathbf{x}_0 . If the differences are small compared to the distance between the points \mathbf{x} and \mathbf{x}_0 , both measured in proper units, the relative motion is negligible. If the differences are substantial, the relative motion is significant and needs to be properly analyzed.

2.1.1 Function linearization

To prepare the ground for this analysis, we consider a scalar function of three independent variables that receives a triplet of numbers (x, y, z) and produces the number $f(x, y, z)$. If the function f is locally well behaved, and the point \mathbf{x} lies near the point \mathbf{x}_0 , then the value $f(x, y, z)$ is expected to be close to the value $f(x_0, y_0, z_0)$. Stated differently, in the limit as all three scalar differences $x - x_0$, $y - y_0$, and $z - z_0$ tend to vanish, meaning that \mathbf{x} tends to \mathbf{x}_0 , the difference in the function values $f(x, y, z) - f(x_0, y_0, z_0)$ will also tend to vanish.

Now, the variable point \mathbf{x} may approach the fixed point \mathbf{x}_0 from many different directions. Selecting the direction that is parallel to the x axis, we set $\mathbf{x} = (x, y_0, z_0)$, and consider the limit of the difference $f(x, y_0, z_0) - f(x_0, y_0, z_0)$ as $x - x_0$ tends to zero. Because the function f has been assumed to be well behaved, the ratio of the differences

$$\frac{f(x, y_0, z_0) - f(x_0, y_0, z_0)}{x - x_0} \quad (2.1.1)$$

tends to a finite number defined as the first partial derivative of the function f with respect to the variable x evaluated at the point \mathbf{x}_0 , denoted by $(\partial f / \partial x)(\mathbf{x}_0)$. Elementary calculus ensures that the partial derivative may be computed using the usual rules of differentiation of a function of one variable with respect to x , regarding the other independent variables as constant. For example, if $f = xyz$, then $\partial f / \partial x = yz$, and $(\partial f / \partial x)(\mathbf{x}_0) = y_0 z_0$,

Setting the fraction shown in (2.1.1) equal to $(\partial f / \partial x)(\mathbf{x}_0)$, and solving the resulting equation for $f(x, y_0, z_0)$, we find

$$f(x, y_0, z_0) \simeq f(x_0, y_0, z_0) + (x - x_0) \frac{\partial f}{\partial x}(\mathbf{x}_0). \quad (2.1.2)$$

It is important to bear in mind that this equation is exact only in the limit as $\Delta x = x - x_0$ tends to zero. For small but non-infinitesimal values of Δx , the difference between the left- and right-hand side is on the order of Δx^2 , which, however, is small compared to Δx . For example, if Δx is equal to 0.01 in some units, then Δx^2 is equal to 0.0001 in corresponding units.

The point \mathbf{x} may also approach the point \mathbf{x}_0 along the y or z axis, yielding the counterparts of (2.1.2),

$$f(x_0, y, z_0) \simeq f(x_0, y_0, z_0) + (y - y_0) \frac{\partial f}{\partial y}(\mathbf{x}_0), \quad (2.1.3)$$

and

$$f(x_0, y_0, z) \simeq f(x_0, y_0, z_0) + (z - z_0) \frac{\partial f}{\partial z}(\mathbf{x}_0). \quad (2.1.4)$$

Combining the arguments that led us to equations (2.1.2)-(2.1.4), we let the point \mathbf{x} approach the point \mathbf{x}_0 from an arbitrary direction, and derive the approximation

$$\begin{aligned} f(x, y, z) \simeq & f(x_0, y_0, z_0) + (x - x_0) \frac{\partial f}{\partial x}(\mathbf{x}_0) + (y - y_0) \frac{\partial f}{\partial y}(\mathbf{x}_0) \\ & + (z - z_0) \frac{\partial f}{\partial z}(\mathbf{x}_0). \end{aligned} \quad (2.1.5)$$

We pause to emphasize that relation (2.1.5) is exact only in the limit as all three differences $\Delta x = x - x_0$, $\Delta y = y - y_0$, and $\Delta z = z - z_0$ tend to zero. For small but non-infinitesimal values of any of these differences, the left-hand side of (2.1.5) differs from the right-hand side by an amount that is generally on the order of the maximum of Δx^2 , Δy^2 or Δz^2 .

Equation (2.1.5) can be made exact for any value of Δx , Δy , or Δz , by adding to the right-hand side a term called the *remainder*. Clearly, as all three differences Δx , Δy , and Δz tend to zero, the remainder must vanish. Elementary calculus shows that when Δx , Δy , and Δz are sufficiently small, the remainder may be expressed as an infinite series involving products of powers of Δx , Δy , and Δz , called the Taylor series of the function f about the point \mathbf{x}_0 .

The process of deriving (2.1.5) is called *linearization* of the function f about the point \mathbf{x}_0 . The linearized form (2.1.5) states that, in the

immediate vicinity of a point \mathbf{x}_0 , any regular function resembles a linear function of the shifted monomials Δx , Δy , and Δz . If all three first partial derivatives vanish at the point \mathbf{x}_0 , then f behaves like a quadratic function; this, however, is an exception.

Gradient of a scalar function

To economize our notation, we introduce the gradient of the function f , denoted by ∇f defined as the vector of the three partial derivatives,

$$\nabla f \equiv \mathbf{e}_x \frac{\partial f}{\partial x} + \mathbf{e}_y \frac{\partial f}{\partial y} + \mathbf{e}_z \frac{\partial f}{\partial z}, \quad (2.1.6)$$

where \mathbf{e}_x , \mathbf{e}_y , and \mathbf{e}_z are the unit vectors along the x , y , and z axes. The symbol ∇ is a vector operator called the *del* or *gradient* operator, defined as

$$\nabla = \mathbf{e}_x \frac{\partial}{\partial x} + \mathbf{e}_y \frac{\partial}{\partial y} + \mathbf{e}_z \frac{\partial}{\partial z}. \quad (2.1.7)$$

Unlike a regular vector, ∇ may not stand alone but must operate on a scalar function of position from the left to acquire a meaningful interpretation.

Inner vector product

As a second preliminary, we introduce the inner product of two three-dimensional vectors $\mathbf{f} = (f_x, f_y, f_z)$ and $\mathbf{g} = (g_x, g_y, g_z)$ defined as the scalar

$$\mathbf{f} \cdot \mathbf{g} = f_x g_x + f_y g_y + f_z g_z. \quad (2.1.8)$$

In index notation,

$$\mathbf{f} \cdot \mathbf{g} \equiv f_i g_i, \quad (2.1.9)$$

where summation of the repeated index i is implied over x , y , and z , as required by Einstein's repeated-index summation convention: if an index appears twice in a product, then summation of that index is implied over its range.

It can be shown using elementary trigonometry that the inner product defined in (2.1.8) is equal to the product of (a) the length of the first vector \mathbf{f} , (b) the length of the second vector \mathbf{g} , and (c) the cosine of the angle subtended between the two vectors. If the angle is equal to $\pi/2$, that is, the two vectors are orthogonal, the cosine of the angle is equal to

zero, and the inner product vanishes. If the angle is equal to zero, that is, the two vectors are parallel, the inner product is equal to the product of the lengths of the two vectors. If both \mathbf{f} and \mathbf{g} are unit vectors, that is, their lengths are equal to one unit of length, then the inner product is equal to the cosine of the subtended angle.

Linearized expansion in compact form

Subject to the preceding definitions, equation (2.1.5) may be written in the compact vector form

$$f(\mathbf{x}) \simeq f(\mathbf{x}_0) + (\mathbf{x} - \mathbf{x}_0) \cdot (\nabla f)_{\mathbf{x}_0}, \quad (2.1.10)$$

where the subscript \mathbf{x}_0 denotes that the gradient ∇f is evaluated at the point \mathbf{x}_0 . The second term on the right-hand side of (2.1.10) is the inner product of (a) the relative position vector $\mathbf{x} - \mathbf{x}_0$, and (b) the gradient vector ∇f .

2.1.2 Velocity gradient tensor

To derive the linearized form of the velocity field in the vicinity of the point \mathbf{x}_0 , we identify the function f with the x , y , or z component of the velocity, u_x , u_y , or u_z , and obtain

$$\begin{aligned} u_x(\mathbf{x}) &\simeq u_x(\mathbf{x}_0) + (x - x_0) \frac{\partial u_x}{\partial x}(\mathbf{x}_0) + (y - y_0) \frac{\partial u_x}{\partial y}(\mathbf{x}_0) + (z - z_0) \frac{\partial u_x}{\partial z}(\mathbf{x}_0), \\ u_y(\mathbf{x}) &\simeq u_y(\mathbf{x}_0) + (x - x_0) \frac{\partial u_y}{\partial x}(\mathbf{x}_0) + (y - y_0) \frac{\partial u_y}{\partial y}(\mathbf{x}_0) + (z - z_0) \frac{\partial u_y}{\partial z}(\mathbf{x}_0), \\ u_z(\mathbf{x}) &\simeq u_z(\mathbf{x}_0) + (x - x_0) \frac{\partial u_z}{\partial x}(\mathbf{x}_0) + (y - y_0) \frac{\partial u_z}{\partial y}(\mathbf{x}_0) + (z - z_0) \frac{\partial u_z}{\partial z}(\mathbf{x}_0). \end{aligned} \quad (2.1.11)$$

Collecting these equations into the unified vector form, we obtain

$$\mathbf{u}(\mathbf{x}) \simeq \mathbf{u}(\mathbf{x}_0) + (\mathbf{x} - \mathbf{x}_0) \cdot \mathbf{A}(\mathbf{x}_0), \quad (2.1.12)$$

where \mathbf{A} is a 3×3 matrix called the *velocity gradient tensor*, defined as

$$\mathbf{A} = \begin{bmatrix} \frac{\partial u_x}{\partial x} & \frac{\partial u_y}{\partial x} & \frac{\partial u_z}{\partial x} \\ \frac{\partial u_x}{\partial y} & \frac{\partial u_y}{\partial y} & \frac{\partial u_z}{\partial y} \\ \frac{\partial u_x}{\partial z} & \frac{\partial u_y}{\partial z} & \frac{\partial u_z}{\partial z} \end{bmatrix}. \quad (2.1.13)$$

The notation $\mathbf{A}(\mathbf{x}_0)$ in (2.1.12) emphasizes that the nine components of the velocity gradient tensor are evaluated at the chosen point \mathbf{x}_0 around which linearization has taken place.

As an example, the velocity gradient corresponding to the velocity field expressed by equations (1.4.7) is given by the matrix \mathbf{A} defined as

$$\left[\begin{array}{ccc} (b+ct)3x^2yz + cdt e^{dt} x^2 & 2ax + (b+ct)y^3z & 2ax + (b+ct)yz^3 \\ 2ay + (b+ct)x^3z & (b+ct)3y^2xz + cdt e^{dt} y^2 & 2ay + (b+ct)xz^3 \\ 2az + (b+ct)x^3y & 2az + (b+ct)xy^3 & (b+ct)3z^2xy + cdt e^{dt} z^2 \end{array} \right]. \quad (2.1.14)$$

Placing the point \mathbf{x}_0 at the location $(x_0, y_0, z_0) = (1, 0, 0)$, we obtain

$$\mathbf{A}(\mathbf{x}_0) = \left[\begin{array}{ccc} cdt e^{dt} & 2a & 2a \\ 0 & cdt & 0 \\ 0 & 0 & cdt \end{array} \right]. \quad (2.1.15)$$

Thus, in the vicinity of the point $(1, 0, 0)$, the flow expressed by equations (1.4.7) may be approximated with a linear flow expressed by

$$\begin{aligned} u_x(x, y, z) &\simeq u_x(1, 0, 0) + cdt e^{dt} (x - 1), \\ u_y(x, y, z) &\simeq u_y(1, 0, 0) + 2a(x - 1) + cdt y, \\ u_z(x, y, z) &\simeq u_z(1, 0, 0) + 2a(x - 1) + cdt z. \end{aligned} \quad (2.1.16)$$

The right-hand sides of equations (2.1.16) are linear functions of the spatial coordinates x , y , and z .

Tensorial nature of a matrix

The velocity gradient tensor is a matrix containing the three first partial derivatives of the three components of the velocity with respect to x , y , and z , a total of nine scalar elements. Why have we called this matrix a tensor?

A tensor is a matrix whose elements are physical entities evaluated with reference to a chosen system of Cartesian or polar coordinates. If the coordinate system is changed, for example, by translation or rotation, then the elements of the matrix will also change to reflect the new directions. This change is analogous to that undergone by the components of the position or velocity vector, occurring by referring to a new system of coordinates, as discussed in Section 1.5.

Now, if the elements of the matrix corresponding to the new system are related to the elements corresponding to the old system by certain

rules discussed in texts of matrix calculus, then the matrix is called a tensor. Establishing whether or not a matrix is a tensor is important in deriving physical laws relating matrices with different physical interpretations.

2.1.3 Relative motion of point particles

According to equation (2.1.12), the motion of a point particle that is close to the point \mathbf{x}_0 is governed by the equation

$$\frac{d\mathbf{X}}{dt} = \mathbf{u}(\mathbf{x}) \simeq \mathbf{u}(\mathbf{x}_0) + (\mathbf{X} - \mathbf{x}_0) \cdot \mathbf{A}(\mathbf{x}_0), \quad (2.1.17)$$

where \mathbf{X} is the position of the point particle, and \mathbf{u} is the point-particle velocity, equal to the local and instantaneous fluid velocity. The first term on the right-hand side of (2.1.17) states that a point particle located at \mathbf{X} translates with the velocity of the point particle located at \mathbf{x}_0 . The second term expresses the *relative motion* with respect to the point particle located at \mathbf{x}_0 . Different velocity gradient tensors $\mathbf{A}(\mathbf{x}_0)$ represent different types of relative motion; our goal is to establish the nature of this motion in terms of the components of $\mathbf{A}(\mathbf{x}_0)$.

2.1.4 Rotation, deformation, and expansion in two-dimensional flow

To begin, we consider a two-dimensional flow in the xy plane, and introduce the 2×2 velocity gradient tensor

$$\mathbf{A} = \begin{bmatrix} \frac{\partial u_x}{\partial x} & \frac{\partial u_y}{\partial x} \\ \frac{\partial u_x}{\partial y} & \frac{\partial u_y}{\partial y} \end{bmatrix}. \quad (2.1.18)$$

In Section 1.6, we studied the velocity field associated with the linear flow expressed by equation (1.6.33). Comparing equations (2.1.12) and (2.1.18) with equation (1.6.33), we set

$$a = \frac{\partial u_x}{\partial x}, \quad b = \frac{\partial u_y}{\partial x}, \quad c = \frac{\partial u_x}{\partial y}, \quad d = \frac{\partial u_y}{\partial y}, \quad (2.1.19)$$

where all partial derivatives are evaluated at \mathbf{x}_0 .

To study the properties of the linearized flow, we carry out the decomposition shown in equation (1.6.34), setting

$$\mathbf{A} = \mathbf{\Xi} + \mathbf{E} + \alpha \frac{1}{2} \begin{bmatrix} 1 & 0 \\ 0 & 1 \end{bmatrix}, \quad (2.1.20)$$

where

$$\mathbf{\Xi} \equiv \frac{1}{2} \begin{bmatrix} 0 & \frac{\partial u_y}{\partial x} - \frac{\partial u_x}{\partial y} \\ \frac{\partial u_x}{\partial y} - \frac{\partial u_y}{\partial x} & 0 \end{bmatrix} \quad (2.1.21)$$

is a skew-symmetric matrix with zero trace called the *vorticity tensor*,

$$\mathbf{E} \equiv \frac{1}{2} \begin{bmatrix} \frac{\partial u_x}{\partial x} - \frac{\partial u_y}{\partial y} & \frac{\partial u_y}{\partial x} + \frac{\partial u_x}{\partial y} \\ \frac{\partial u_x}{\partial y} + \frac{\partial u_y}{\partial x} & \frac{\partial u_y}{\partial y} - \frac{\partial u_x}{\partial x} \end{bmatrix} \quad (2.1.22)$$

is a symmetric matrix with zero trace called the *rate of deformation tensor*, and the scalar

$$\alpha = \frac{\partial u_x}{\partial x} + \frac{\partial u_y}{\partial y} \quad (2.1.23)$$

is the areal rate of expansion.

Expansion

The results of Section 1.6 suggest that a fluid parcel centered at the point \mathbf{x}_0 expands isotropically with an areal rate of expansion that is equal to the right-hand side of (2.1.23) evaluated at \mathbf{x}_0 , as illustrated in figure 2.1.1.

Rotation

Referring to equation (1.6.35), we find that a fluid parcel centered at the point \mathbf{x}_0 rotates in the xy plane around the point \mathbf{x}_0 , with angular velocity

$$\Omega = \frac{1}{2} \left(\frac{\partial u_y}{\partial x} - \frac{\partial u_x}{\partial y} \right), \quad (2.1.24)$$

where the right-hand side is evaluated at \mathbf{x}_0 , as shown in figure 2.1.1. When Ω is positive, the parcel rotates in the counter-clockwise direction, whereas when Ω is negative, the parcel rotates in the clockwise direction.

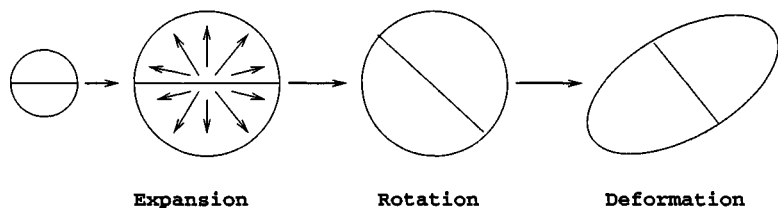


Figure 2.1.1 Expansion, rotation, and deformation of a small discoidal fluid parcel in a two-dimensional flow, occurring during an infinitesimal period of time.

Deformation

The discussion in Section 1.6 suggests that the flow associated with the rate of deformation tensor \mathbf{E} expresses pure deformation, as illustrated in figure 2.1.1. To compute the rate of deformation G , we search for the eigenvalues of \mathbf{E} . Denoting $E_{xx} \equiv E_{11}$, and similarly for the other components, and taking into account that, by definition, $E_{xx} + E_{yy} = 0$, and $E_{xy} = E_{yx}$, we find

$$G = \pm \sqrt{E_{xx}^2 + E_{xy}^2}. \quad (2.1.25)$$

The corresponding eigenvectors define the *principal directions of the rate of strain*. It can be shown that, because \mathbf{E} is symmetric, the two eigenvectors are mutually orthogonal.

Each one of the two eigenvalues of the rate of strain tensor expresses the rate of deformation of a circular fluid parcel centered at the point \mathbf{x}_0 , in the direction of the respective eigenvector. A theorem of matrix calculus requires that the sum of the eigenvalues be equal to the sum of the diagonal elements of \mathbf{E} , which is equal to zero. Because of this property, the deformation conserves the area of the parcel during the motion.

2.1.5 Three-dimensional flow

Extending the preceding analysis to three-dimensional flow, we decompose the velocity gradient tensor into three parts, as

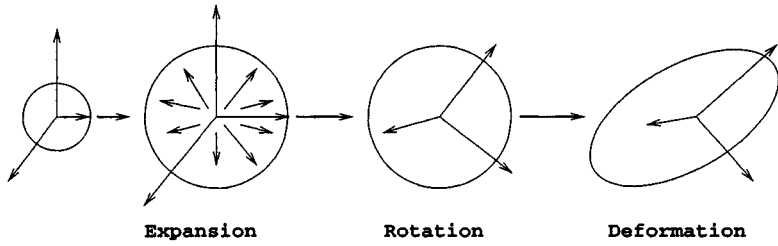


Figure 2.1.2 Expansion, rotation, and deformation of a small spherical fluid parcel in a three-dimensional flow, occurring during an infinitesimal period of time.

$$\mathbf{A} = \Xi + \mathbf{E} + \alpha \frac{1}{3} \begin{bmatrix} 1 & 0 & 0 \\ 0 & 1 & 0 \\ 0 & 0 & 1 \end{bmatrix}, \quad (2.1.26)$$

where

$$\Xi \equiv \frac{1}{2} \begin{bmatrix} 0 & \frac{\partial u_y}{\partial x} - \frac{\partial u_x}{\partial y} & \frac{\partial u_z}{\partial x} - \frac{\partial u_x}{\partial z} \\ \frac{\partial u_x}{\partial y} - \frac{\partial u_y}{\partial x} & 0 & \frac{\partial u_z}{\partial y} - \frac{\partial u_y}{\partial z} \\ \frac{\partial u_x}{\partial z} - \frac{\partial u_z}{\partial x} & \frac{\partial u_y}{\partial z} - \frac{\partial u_z}{\partial y} & 0 \end{bmatrix} \quad (2.1.27)$$

is the skew-symmetric vorticity tensor,

$$\mathbf{E} \equiv \begin{bmatrix} \frac{\partial u_x}{\partial x} - \frac{1}{3}\alpha & \frac{1}{2}(\frac{\partial u_y}{\partial x} + \frac{\partial u_x}{\partial y}) & \frac{1}{2}(\frac{\partial u_z}{\partial x} + \frac{\partial u_x}{\partial z}) \\ \frac{1}{2}(\frac{\partial u_x}{\partial y} + \frac{\partial u_y}{\partial x}) & \frac{\partial u_y}{\partial y} - \frac{1}{3}\alpha & \frac{1}{2}(\frac{\partial u_z}{\partial y} + \frac{\partial u_y}{\partial z}) \\ \frac{1}{2}(\frac{\partial u_x}{\partial z} + \frac{\partial u_z}{\partial x}) & \frac{1}{2}(\frac{\partial u_y}{\partial z} + \frac{\partial u_z}{\partial y}) & \frac{\partial u_z}{\partial z} - \frac{1}{3}\alpha \end{bmatrix} \quad (2.1.28)$$

is the symmetric and traceless rate of deformation tensor, and the scalar coefficient

$$\alpha \equiv \frac{\partial u_x}{\partial x} + \frac{\partial u_y}{\partial y} + \frac{\partial u_z}{\partial z} \quad (2.1.29)$$

is the volumetric rate of expansion.

The three terms on the right-hand side of (2.1.26) express, respectively, isotropic expansion, rotation, and pure deformation, as illustrated in figure 2.1.2. Because of the fundamental significance of these motions in fluid mechanics, these terms will be given individual attention in the next three sections.

Problems

Problem 2.1.1 *Inner vector product.*

Prove the interpretation of the inner vector product described after equation (2.1.9).

Problem 2.1.2 *Decomposition of a linearized flow.*

Linearize the velocity described by equations (1.5.2) around the origin of the y axis, and decompose the velocity gradient tensor of the linearized flow into the three modes shown on the right-hand side of (2.1.26).

Problem 2.1.3 *Decomposition of a linearized flow.*

Decompose the velocity gradient tensor of the linearized flow expressed by equations (2.1.16) into the three modes shown on the right-hand side of (2.1.26).

Problem 2.1.4 *Gradient in cylindrical polar coordinates.*

In the cylindrical polar coordinates depicted in figure 1.3.2, the gradient of a scalar function f is defined by its cylindrical polar components F_x , F_σ , and F_φ , as

$$\nabla f = F_x \mathbf{e}_x + F_\sigma \mathbf{e}_\sigma + F_\varphi \mathbf{e}_\varphi. \quad (2.1.30)$$

Using the transformation rules shown in equations (1.3.17), we find

$$F_\sigma = \cos \varphi \frac{\partial f}{\partial y} + \sin \varphi \frac{\partial f}{\partial z}, \quad F_\varphi = -\sin \varphi \frac{\partial f}{\partial y} + \cos \varphi \frac{\partial f}{\partial z}. \quad (2.1.31)$$

To express the derivatives with respect to y and z in terms of derivatives with respect to polar cylindrical coordinates, we use the chain rule of differentiation along with the coordinate transformation rules (1.3.11) and (1.3.12), and find

$$\begin{aligned} \left(\frac{\partial f}{\partial y}\right)_{x,z} &= \left(\frac{\partial f}{\partial x}\right)_{\sigma,\varphi} \left(\frac{\partial x}{\partial y}\right)_{x,z} + \left(\frac{\partial f}{\partial \sigma}\right)_{x,\varphi} \left(\frac{\partial \sigma}{\partial y}\right)_{x,z} + \left(\frac{\partial f}{\partial \varphi}\right)_{x,\sigma} \left(\frac{\partial \varphi}{\partial y}\right)_{x,z} \\ &= \cos \varphi \left(\frac{\partial f}{\partial \sigma}\right)_{x,\varphi} - \frac{\sin \varphi}{\sigma} \left(\frac{\partial f}{\partial \varphi}\right)_{x,\sigma}, \end{aligned} \quad (2.1.32)$$

and

$$\begin{aligned} \left(\frac{\partial f}{\partial z}\right)_{x,y} &= \left(\frac{\partial f}{\partial x}\right)_{\sigma,\varphi} \left(\frac{\partial x}{\partial z}\right)_{x,y} + \left(\frac{\partial f}{\partial \sigma}\right)_{x,\varphi} \left(\frac{\partial \sigma}{\partial z}\right)_{x,y} + \left(\frac{\partial f}{\partial \varphi}\right)_{x,\sigma} \left(\frac{\partial \varphi}{\partial z}\right)_{x,y} \\ &= \sin \varphi \left(\frac{\partial f}{\partial \sigma}\right)_{x,\varphi} + \frac{\cos \varphi}{\sigma} \left(\frac{\partial f}{\partial \varphi}\right)_{x,\sigma}. \end{aligned} \quad (2.1.33)$$

Substitute relations (2.1.32) and (2.1.33) into the right-hand sides of relations (2.1.31), and thus derive the relations

$$F_x = \frac{\partial f}{\partial x}, \quad F_\sigma = \frac{\partial f}{\partial \sigma}, \quad F_\varphi = \frac{1}{\sigma} \frac{\partial f}{\partial \varphi}. \quad (2.1.34)$$

Equations (2.1.34) illustrate that the polar components of the gradient are equal to the partial derivatives with respect to the corresponding variable, multiplied by an appropriate scaling factor.

Problem 2.1.5 *Gradient in spherical polar coordinates.*

In the spherical polar coordinates depicted in figure 1.3.3, the gradient of a scalar function f is defined by its spherical polar components F_r , F_θ , and F_φ , as

$$\nabla f = F_r \mathbf{e}_r + F_\theta \mathbf{e}_\theta + F_\varphi \mathbf{e}_\varphi. \quad (2.1.35)$$

Working as in problem 2.1.4, show that

$$F_r = \frac{\partial f}{\partial r}, \quad F_\theta = \frac{1}{r} \frac{\partial f}{\partial \theta}, \quad F_\varphi = \frac{1}{r \sin \theta} \frac{\partial f}{\partial \varphi}. \quad (2.1.36)$$

Note that the expression for F_φ is consistent with that given in the third of relations (2.1.34), subject to the substitution $\sigma = r \sin \theta$.

Problem 2.1.6 *Gradient in plane polar coordinates.*

In the plane polar coordinates depicted in figure 1.3.4, the gradient of a scalar function f is defined by its plane polar components F_r and F_θ , as

$$\nabla f = F_r \mathbf{e}_r + F_\theta \mathbf{e}_\theta. \quad (2.1.37)$$

Working as in problem 2.1.4, show that

$$F_r = \frac{\partial f}{\partial r}, \quad F_\theta = \frac{1}{r} \frac{\partial f}{\partial \theta}. \quad (2.1.38)$$

2.2 Fluid parcel expansion

Consider the velocity field associated with the third term on the right-hand side of (2.1.26), given by

$$\mathbf{u}^{Expansion}(\mathbf{x}) = \alpha(\mathbf{x}_0) \frac{1}{3} (\mathbf{x} - \mathbf{x}_0) \cdot \begin{bmatrix} 1 & 0 & 0 \\ 0 & 1 & 0 \\ 0 & 0 & 1 \end{bmatrix}. \quad (2.2.1)$$

Under the influence of this field, a spherical fluid parcel centered at the point \mathbf{x}_0 expands when the coefficient $\alpha(\mathbf{x}_0)$ is positive, or contracts when the coefficient $\alpha(\mathbf{x}_0)$ is negative, always maintaining the spherical shape.

To see this more clearly, we consider the motion of a point particle that lies at the surface of the spherical parcel. Using (2.2.1), we find that the radius of the parcel $a(t)$, is given by

$$a(t) = a(t=0) \exp\left(\frac{1}{3}\alpha t\right). \quad (2.2.2)$$

Raising both sides of equation (2.2.2) to the third power, and multiplying the result by the factor $4\pi/3$, we find that the ratio of the instantaneous to the initial parcel volume is given by

$$\frac{\frac{4\pi}{3}a^3(t)}{\frac{4\pi}{3}a^3(t=0)} = \exp(\alpha t). \quad (2.2.3)$$

This result explains why the constant α is called the *rate of volumetric expansion*.

2.2.1 Divergence of the velocity field

The rate of expansion defined in equation (2.1.29) may be expressed in compact form that simplifies the notation. Taking the inner product of the del operator defined in (2.1.7) and the velocity, we find

$$\nabla \cdot \mathbf{u} \equiv \frac{\partial u_x}{\partial x} + \frac{\partial u_y}{\partial y} + \frac{\partial u_z}{\partial z}. \quad (2.2.4)$$

In index notation,

$$\nabla \cdot \mathbf{u} \equiv \frac{\partial u_i}{\partial x_i}, \quad (2.2.5)$$

where summation of the repeated index i is implied over x , y , and z . In the case of two-dimensional flow in the xy plane, the derivative with respect to z does not appear.

Accordingly, we write

$$\alpha = \nabla \cdot \mathbf{u}. \quad (2.2.6)$$

The right-hand side of (2.2.6) is defined as the *divergence of the velocity*.

2.2.2 Solenoidal velocity fields

We have found that the rate of volumetric expansion at a point in a three-dimensional flow, or the areal rate of expansion at a point in a two-dimensional flow, is equal to the divergence of the velocity evaluated at that point. If the divergence of the velocity vanishes at every point in the flow, with the physical consequence that no fluid parcel undergoes expansion but only translation, rotation, and deformation, then the velocity field is called *solenoidal*.

Problem

Problem 2.2.1 Rate of expansion.

Derive the rate of expansion of the flow described by equations (1.4.7), and then evaluate it at the point $\mathbf{x}_0 = (1, 0, 1)$.

2.3 Fluid parcel rotation and vorticity

Consider the velocity field associated with the first term on the right-hand side of (2.1.26), given by

$$\mathbf{u}^{Rotation}(x, y, z) = (\mathbf{x} - \mathbf{x}_0) \cdot \Xi(\mathbf{x}_0), \quad (2.3.1)$$

where Ξ is the vorticity tensor defined in equation (2.1.27).

An areal fluid parcel in a two-dimensional flow occurring in the xy plane may only rotate around the z axis. In contrast, a three-dimensional fluid parcel in a three-dimensional flow may rotate around any arbitrary axis that passes through the designated center of rotation \mathbf{x}_0 and points in an arbitrary direction. The direction, magnitude, and sense of the rotation define the angular velocity vector $\boldsymbol{\Omega}$ whose components may be

deduced from the three upper triangular or three lower triangular entries of the vorticity tensor shown on the left-hand side of (2.1.27), and are given by

$$\begin{aligned}\Omega_x &= \frac{1}{2} \left(\frac{\partial u_z}{\partial y} - \frac{\partial u_y}{\partial z} \right), & \Omega_y &= \frac{1}{2} \left(\frac{\partial u_z}{\partial x} - \frac{\partial u_x}{\partial z} \right), \\ \Omega_z &= \frac{1}{2} \left(\frac{\partial u_y}{\partial x} - \frac{\partial u_x}{\partial y} \right),\end{aligned}\tag{2.3.2}$$

where the right-hand sides are evaluated at the designated parcel center \mathbf{x}_0 . As we look down into the vector $\boldsymbol{\Omega}$ from the tip of its arrow, the fluid rotates in the clockwise direction.

Equation (2.3.1) may be recast into a compact form in terms of the angular velocity vector, as

$$\mathbf{u}^{\text{Rotation}}(x, y, z) = (\mathbf{x} - \mathbf{x}_0) \cdot \begin{bmatrix} 0 & \Omega_z & \Omega_y \\ -\Omega_z & 0 & \Omega_x \\ -\Omega_y & -\Omega_x & 0 \end{bmatrix},\tag{2.3.3}$$

where $\boldsymbol{\Omega}$ derives from the velocity by means of (2.3.2).

The three components of the angular velocity vector arise by combining selected partial derivatives of the components of the velocity in a particular fashion. Stated differently, the angular velocity vector field arises from the velocity field by operating on it with a differential operator, just as the rate of expansion arises from the velocity field by operating on it with the divergence operator ($\nabla \cdot$), as discussed in Section 2.2.

2.3.1 Outer vector product

To identify the differential operator that generates the angular velocity field from the velocity field according to equations (2.3.2), we introduce the outer vector product.

Consider a vector $\mathbf{f} = (f_x, f_y, f_z)$, and another vector $\mathbf{g} = (g_x, g_y, g_z)$; the outer product of the first vector with the second vector, stated in this particular order, is a new vector denoted by $\mathbf{f} \times \mathbf{g}$, defined as

$$\begin{aligned}\mathbf{f} \times \mathbf{g} &= (f_y g_z - f_z g_y) \mathbf{e}_x + (f_z g_x - f_x g_z) \mathbf{e}_y \\ &\quad + (f_x g_y - f_y g_x) \mathbf{e}_z,\end{aligned}\tag{2.3.4}$$

where \mathbf{e}_x , \mathbf{e}_y , and \mathbf{e}_z are the unit vectors along the x , y , and z axis.

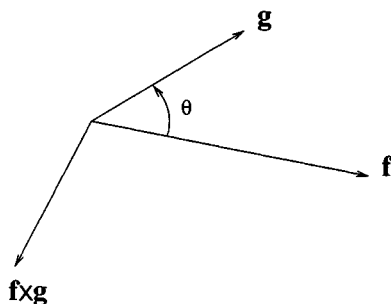


Figure 2.3.1 The outer product of two vectors \mathbf{f} and \mathbf{g} is a new vector perpendicular to their plane.

It can be shown that the vector $\mathbf{f} \times \mathbf{g}$ is normal to the plane defined by \mathbf{f} and \mathbf{g} , as illustrated in figure 2.3.1, and its magnitude is equal to the product of (a) the length of the vector \mathbf{f} , (b) the length of the vector \mathbf{g} , and (c) the absolute value of the sine of the angle θ subtended between the two vectors. The orientation of $\mathbf{f} \times \mathbf{g}$ is chosen such that, as we look down at the plane defined by \mathbf{f} and \mathbf{g} towards the negative direction of $\mathbf{f} \times \mathbf{g}$, the angle θ measured in the counterclockwise direction from \mathbf{f} is less than 180° . If θ is equal to 0 or π , that is, if the two vectors are parallel or anti-parallel, then the sine of the angle is equal to zero, and the outer product vanishes. The directions indicated by the three vectors \mathbf{f} , \mathbf{g} , and $\mathbf{f} \times \mathbf{g}$, arranged in this particular order, form a right-handed system of axes. This is another way of saying that $\mathbf{f} \times \mathbf{g}$ arises from \mathbf{f} and \mathbf{g} according to the right-hand rule.

Using the definition of the cross product, we recast equation (2.3.3) into the form

$$\mathbf{u}^{\text{Rotation}}(x, y, z) = \boldsymbol{\Omega} \times (\mathbf{x} - \mathbf{x}_0), \quad (2.3.5)$$

which is the classical definition of *rigid-body rotation* around the point \mathbf{x}_0 with angular velocity $\boldsymbol{\Omega}$, in agreement with the previously stated physical interpretation.

2.3.2 Curl and vorticity

Taking the outer product of the del operator and the velocity field, we obtain the curl of the velocity defined as the vorticity,

$$\begin{aligned}\omega &\equiv \nabla \times \mathbf{u} \\ &= \left(\frac{\partial u_z}{\partial y} - \frac{\partial u_y}{\partial z}\right) \mathbf{e}_x + \left(\frac{\partial u_x}{\partial z} - \frac{\partial u_z}{\partial x}\right) \mathbf{e}_y + \left(\frac{\partial u_y}{\partial x} - \frac{\partial u_x}{\partial y}\right) \mathbf{e}_z.\end{aligned}\quad (2.3.6)$$

Comparing equation (2.3.6) with equations (2.3.2), we find

$$\boldsymbol{\Omega} = \frac{1}{2} \boldsymbol{\omega}, \quad (2.3.7)$$

which shows that the angular velocity vector is equal to half the vorticity vector, or half the curl of the velocity.

2.3.3 Irrotational flow

If the curl of a velocity field vanishes at every point in a flow, with the consequence that no spherical fluid parcel undergoes rotation, then the velocity field is called *irrotational*. The properties and computation of irrotational flow will be discussed in Chapter 3, and then again in Chapter 12 in the context of aerodynamics.

2.3.4 The alternating tensor

The long expression on the right-hand side of equation (2.3.4) defining the outer vector product is cumbersome. To simplify the notation, we introduce the three-index alternating tensor ϵ_{ijk} , defined as follows:

1. If $i = j$, or $j = k$, or $k = i$, then $\epsilon_{ijk} = 0$. For example, $\epsilon_{xxy} = \epsilon_{zyz} = \epsilon_{zyy} = 0$.
2. If i, j , and k are all different, then $\epsilon_{ijk} = \pm 1$. The plus sign applies when the triplet ijk is a cyclic permutation of xyz , and the minus sign applies otherwise. For example, $\epsilon_{xyz} = \epsilon_{zxy} = \epsilon_{yzx} = 1$, but $\epsilon_{xzy} = -1$.

Two important properties of the alternating tensor stemming from its definition are

$$\epsilon_{ijk} \epsilon_{ljk} = 2 \delta_{il}, \quad (2.3.8)$$

where summation of the repeated indices j and k is implied on the left-hand side, and

$$\epsilon_{ijk} \epsilon_{lmk} = \delta_{il} \delta_{jm} - \delta_{im} \delta_{jl}, \quad (2.3.9)$$

where summation of the repeated index k is implied on the left-hand side. Kronecker's delta δ_{ij} represents the identity matrix: $\delta_{ij} = 1$ if $i = j$, or 0 if $i \neq j$. Additional properties of the alternating tensor are listed in problem 2.3.2.

In terms of the alternating tensor, the i th component of the outer product $\mathbf{f} \times \mathbf{g}$ defined in equation (2.3.4) is given by

$$(\mathbf{f} \times \mathbf{g})_i = \epsilon_{ijk} f_j g_k, \quad (2.3.10)$$

where summation of the two repeated indices j and k is implied on the right-hand side.

Using the definition (2.3.6), we find that the i th component of the vorticity is given by

$$\omega_i = \epsilon_{ijk} \frac{\partial u_k}{\partial x_j}. \quad (2.3.11)$$

A straightforward manipulation of (2.3.11) provides us with an expression for the vorticity vector in terms of the vorticity tensor

$$\begin{aligned} \omega_i &= \frac{1}{2} \left(\epsilon_{ijk} \frac{\partial u_k}{\partial x_j} + \epsilon_{ijk} \frac{\partial u_k}{\partial x_j} \right) = \frac{1}{2} \left(\epsilon_{ijk} \frac{\partial u_k}{\partial x_j} - \epsilon_{ikj} \frac{\partial u_k}{\partial x_j} \right) \\ &= \frac{1}{2} \left(\epsilon_{ijk} \frac{\partial u_k}{\partial x_j} - \epsilon_{ijk} \frac{\partial u_j}{\partial x_k} \right) = \epsilon_{ijk} \frac{1}{2} \left(\frac{\partial u_k}{\partial x_j} - \frac{\partial u_j}{\partial x_k} \right) = \epsilon_{ijk} \Xi_{jk}. \end{aligned} \quad (2.3.12)$$

The converse relationship is (problem 2.3.3)

$$\Xi_{ij} = \frac{1}{2} \epsilon_{ijk} \omega_k. \quad (2.3.13)$$

2.3.5 Two-dimensional flow

Consider a two-dimensional flow in the xy plane. Inspection of the right-hand side of (2.3.6) shows that the x and y components of the vorticity vanish, and the vorticity vector is parallel to the z axis and thus perpendicular to the plane of the flow,

$$\boldsymbol{\omega} = \omega_z \mathbf{e}_z, \quad (2.3.14)$$

where \mathbf{e}_z is the unit vector along the z axis. The scalar ω_z is the strength of the vorticity, defined as

$$\omega_z = \frac{\partial u_y}{\partial x} - \frac{\partial u_x}{\partial y}. \quad (2.3.15)$$

Using the transformation rules discussed in Section 1.1, we find that, in the plane polar coordinates depicted in figure 1.1.4, the strength of the vorticity is given by

$$\omega_z = \frac{1}{r} \left(\frac{\partial(r u_\theta)}{\partial r} - \frac{\partial u_r}{\partial \theta} \right). \quad (2.3.16)$$

2.3.6 Axisymmetric flow

Consider next an axisymmetric flow without swirling motion, and refer to the polar cylindrical coordinates (x, σ, φ) depicted in figure 1.1.2, and to the spherical polar coordinates (r, θ, φ) depicted in figure 1.1.3. A fluid patch that lies in a meridional plane over which φ is constant, is able to rotate only around an axis that is perpendicular to this plane and thus points in the direction of increasing or decreasing angle φ . This observation suggests that the vorticity vector takes the form

$$\boldsymbol{\omega} = \omega_\varphi \mathbf{e}_\varphi, \quad (2.3.17)$$

where \mathbf{e}_φ is the unit vector pointing in the meridional direction, and ω_φ is the strength of the vorticity given by

$$\omega_\varphi = \frac{\partial u_\sigma}{\partial x} - \frac{\partial u_x}{\partial \sigma} = \frac{1}{r} \left(\frac{\partial(r u_\theta)}{\partial r} - \frac{\partial u_r}{\partial \theta} \right). \quad (2.3.18)$$

Note that the expression in spherical polar coordinates given on the right-hand side of (2.3.18) is identical to that in plane polar coordinates given in (2.3.16).

Problems

Problem 2.3.1 *Properties of the outer vector product.*

(a) With the outer vector product defined in equation (2.3.4), show that

$$\mathbf{f} \times \mathbf{g} = -\mathbf{g} \times \mathbf{f}. \quad (2.3.19)$$

(b) The outer vector product of two vectors \mathbf{f} and \mathbf{g} may be identified with the determinant of a matrix,

$$\mathbf{f} \times \mathbf{g} = \text{Det} \left(\begin{bmatrix} \mathbf{e}_x & \mathbf{e}_y & \mathbf{e}_z \\ f_x & f_y & f_z \\ g_x & g_y & g_z \end{bmatrix} \right). \quad (2.3.20)$$

Show that this rule is consistent with the definition of the curl in (2.3.6).

Problem 2.3.2 *Properties of Kronecker's delta and alternating tensor.*

Prove the properties:

$$\delta_{ii} = 3, \quad \epsilon_{ljk} \delta_{jk} = 0, \quad a_j \delta_{jk} = a_k, \quad A_{lj} \delta_{jk} = A_{lk}, \quad (2.3.21)$$

where δ_{ij} is Kronecker's delta representing the 3×3 identity matrix, summation is implied over a repeated index, \mathbf{a} is an arbitrary vector and \mathbf{A} is an arbitrary matrix.

Problem 2.3.3 *Relation between the vorticity tensor and vector.*

Prove relation (2.3.13). *Hint:* Express the vorticity in terms of the velocity as shown in (2.3.11), and then use property (2.3.9).

Problem 2.3.4 *Solenoidal nature of the vorticity field.*

Show that $\nabla \cdot \boldsymbol{\omega} = 0$; that is, the vorticity field is solenoidal.

2.4 Fluid parcel deformation

Consider the velocity field associated with the second term on the right-hand side of (2.1.26), given by

$$\mathbf{u}^{\text{Deformation}}(x, y, z) = (\mathbf{x} - \mathbf{x}_0) \cdot \mathbf{E}(\mathbf{x}_0), \quad (2.4.1)$$

where \mathbf{E} is the symmetric rate of deformation tensor defined in equation (2.1.28).

To develop insights into the nature of the motion described by (2.4.1), we consider a special case where $\mathbf{E}(\mathbf{x}_0)$ is diagonal, given by

$$\mathbf{E}(\mathbf{x}_0) = \begin{bmatrix} \frac{\partial u_x}{\partial x} - \frac{1}{3}\alpha & 0 & 0 \\ 0 & \frac{\partial u_y}{\partial y} - \frac{1}{3}\alpha & 0 \\ 0 & 0 & \frac{\partial u_z}{\partial z} - \frac{1}{3}\alpha \end{bmatrix}, \quad (2.4.2)$$

with the understanding that the right-hand side is evaluated at the point \mathbf{x}_0 . The matrix (2.4.2) has three real eigenvalues that are equal to the diagonal elements; the corresponding eigenvectors point along the x , y , or z axes.

Cursory inspection reveals that, under the action of the flow described by (2.4.1) and (2.4.2), a spherical fluid parcel centered at the point \mathbf{x}_0 deforms to obtain an ellipsoidal shape while preserving its volume, as illustrated in figure 2.1.2. The three eigenvalues of the rate of deformation tensor express the rate of deformation in the three principal directions corresponding to the eigenvectors. If an eigenvalue is negative, then the parcel is compressed in the corresponding direction to obtain an oblate shape.

More generally, the rate of deformation tensor has three real eigenvalues, λ_1, λ_2 , and λ_3 , that are found by setting the determinant of the matrix

$$\mathbf{E} - \lambda \mathbf{I} = \begin{bmatrix} E_{xx} - \lambda & E_{xy} & E_{xz} \\ E_{yx} & E_{yy} - \lambda & E_{yz} \\ E_{zx} & E_{zy} & E_{zz} - \lambda \end{bmatrix}, \quad (2.4.3)$$

equal to zero, and then computing the roots of the emerging cubic equation for λ , as will be discussed later in this section. It can be shown that, because \mathbf{E} is symmetric, all three eigenvalues are real, and each eigenvalue has a distinct corresponding eigenvector. Moreover, the three eigenvectors are mutually orthogonal, pointing in the *principal directions of the rate of strain*.

Under the action of the flow (2.4.1), a spherical fluid parcel centered at the point \mathbf{x}_0 deforms to obtain an ellipsoidal shape whose axes are generally inclined with respect to the x , y , and z axes. The three axes of the ellipsoid are parallel to the eigenvectors of \mathbf{E} , and the respective rates of deformation are equal to the corresponding eigenvalues. A theorem of matrix calculus states that the sum of the eigenvalues is equal to the

sum of the diagonal elements of \mathbf{E} , which is equal to zero. Because of this property, the deformation conserves the parcel volume.

2.4.1 Computation of the rate of strain

Setting the determinant of the matrix (2.4.3) equal to zero, we obtain the cubic equation

$$\lambda^3 + a\lambda^2 + b\lambda + c = 0, \quad (2.4.4)$$

where

$$\begin{aligned} a &= -\text{Trace}(\mathbf{E}) = -(E_{xx} + E_{yy} + E_{zz}), \\ b &= (E_{yy}E_{zz} - E_{yz}E_{zy}) + (E_{xx}E_{zz} - E_{xz}E_{zx}) + (E_{xx}E_{yy} - E_{xy}E_{yx}), \\ c &= -\text{Det}(\mathbf{E}), \end{aligned} \quad (2.4.5)$$

and Det stands for the determinant. Using Cardano's formulae, we find that the three roots of (2.4.4), are given by

$$\begin{aligned} \lambda_1 &= -\frac{a}{3} + d \cos \frac{\chi}{3}, & \lambda_2 &= -\frac{a}{3} - d \cos \frac{\chi - \pi}{3}, \\ \lambda_3 &= -\frac{a}{3} - d \cos \frac{\chi + \pi}{3}, \end{aligned} \quad (2.4.6)$$

where

$$\begin{aligned} d &= 2\sqrt{\frac{|p|}{3}}, & \chi &= \arccos\left(-\frac{1}{2\left(\frac{|p|}{3}\right)^{3/2}}\right), \\ p &= b - \frac{1}{3}a^2, & q &= c + \frac{2}{27}a^3 - \frac{1}{3}ab. \end{aligned} \quad (2.4.7)$$

In the present case, because $a = 0$, we obtain the simplified expressions

$$\lambda_1 = d \cos \frac{\chi}{3}, \quad \lambda_2 = -d \cos \frac{\chi - \pi}{3}, \quad \lambda_3 = -d \cos \frac{\chi + \pi}{3}, \quad (2.4.8)$$

where

$$d = 2\sqrt{\frac{|b|}{3}}, \quad \chi = \arccos\left(-\frac{c}{2\left(\frac{|b|}{3}\right)^{3/2}}\right). \quad (2.4.9)$$

Once the eigenvalues have been found, the eigenvectors are computed by solving a homogeneous system of three equations for three unknowns. For example, the eigenvector $\mathbf{e}^{(1)} = (e_x^{(1)}, e_y^{(1)}, e_z^{(1)})$ corresponding to the eigenvalue λ_1 is found by solving the homogeneous system

$$(\mathbf{E} - \lambda_1 \mathbf{I}) \cdot \mathbf{e}^{(1)} = \mathbf{0}, \quad (2.4.10)$$

which can be restated as

$$\begin{aligned} (E_{xx} - \lambda_1) e_x^{(1)} + E_{xy} e_y^{(1)} &= -E_{xz} e_z^{(1)}, \\ E_{yx} e_x^{(1)} + (E_{yy} - \lambda_1) e_y^{(1)} &= -E_{yz} e_z^{(1)}, \\ E_{zx} e_x^{(1)} + E_{zy} e_y^{(1)} &= -(E_{zz} - \lambda_1) e_z^{(1)}. \end{aligned} \quad (2.4.11)$$

To solve the system (2.4.11), we assign an arbitrary value to $e_z^{(1)}$ on the right-hand sides, and solve the first two equations for $e_x^{(1)}$, and $e_y^{(1)}$ using, for example, Cramer's rule. The solution is guaranteed to also satisfy the third equation. A solution will not exist when the eigenvector is perpendicular to the z axis, in which case $e_z^{(1)}$ is equal to zero. If this occurs, we simply transfer to the right-hand side the term involving $e_x^{(1)}$ or $e_y^{(1)}$, and solve for the other two components.

Problem

Problem 2.4.1 *Properties of eigenvalues.*

(a) Confirm that the sum of the three eigenvalues given in (2.4.6) is equal to the trace of \mathbf{E} .

(b) Confirm that the product of the three eigenvalues given in (2.4.6) is equal to the determinant of \mathbf{E} .

(c) Confirm that, when \mathbf{E} is diagonal, formulae (2.4.6) identify the eigenvalues with the diagonal elements.

Computer problem

Problem c.2.4.1 *Eigenvalues and eigenvectors.*

Directory `01_num_meth/05_eigen` of *FDLIB* contains program *eigen33* that computes the eigenvalues of a 3×3 matrix. Use the program to compute the eigenvalues and eigenvectors of the rate of deformation tensor corresponding to the linearized flow (2.1.16) for $a = 1s^{-1}$ and $cdt = 2s^{-1}$.

2.5 Numerical differentiation

We have mentioned on an earlier occasion that, in practice, the components of the velocity field are hardly ever given in analytical form by means of analytical expressions. Instead, their values are either measured in the laboratory with probes, or computed by numerical methods at data points or grid nodes located in the domain of flow. The partial derivatives of the velocity are then recovered by a numerical procedure called numerical differentiation.

2.5.1 Numerical differentiation in one dimension

As a prelude to computing the partial derivatives of the components of the velocity from specified grid values, we consider computing the first derivative of a function f of one independent variable x from specified grid values. Assume that we are given the values of the function $f(x)$ at $N + 1$ nodes of a one-dimensional grid with nodes located at x_i , $i = 1, 2, \dots, N + 1$, where $x_1 < x_2 < \dots < x_{N+1}$, as shown in figure 1.7.1(a). Our goal is to compute the derivative df/dx at a point x that lies within the k th interval subtended between the nodes x_k and x_{k+1} .

First-order differentiation

A reasonable way of computing df/dx involves approximating the graph of the function $f(x)$ over the interval (x_k, x_{k+1}) with a straight line, as shown in figure 1.7.2, and then approximating df/dx with the slope. Using equations (1.7.1) and (1.7.3), we derive the finite-difference approximation

$$\frac{df}{dx}(x) \simeq \frac{f_{k+1} - f_k}{x_{k+1} - x_k}. \quad (2.5.1)$$

Identifying now the evaluation point x with the grid point x_k , we obtain the *forward-difference* approximation

$$\frac{df}{dx}(x_k) \simeq \frac{f_{k+1} - f_k}{x_{k+1} - x_k}. \quad (2.5.2)$$

Using, instead, the straight-line approximation for the $k - 1$ interval, we obtain the *backward-difference* approximation

$$\frac{df}{dx}(x_k) \simeq \frac{f_k - f_{k-1}}{x_k - x_{k-1}}. \quad (2.5.3)$$

Formulae (2.5.2) and (2.5.3) carry a comparable amount of error due to the straight-line approximation.

To evaluate $\frac{df}{dx}(x_1)$, we use the forward difference; to evaluate $\frac{df}{dx}(x_{N+1})$ we use the backward difference; to evaluate $\frac{df}{dx}(x_i)$ at an interior grid point, $i = 2, 3, \dots, N$ we use either the forward or the backward difference approximation, whichever is more convenient or appropriate.

Second-order differentiation

Numerical differentiation based on linear interpolation discussed in the preceding subsection neglects the curvature of the graph of the function $f(x)$. To improve the accuracy, we approximate the graph of $f(x)$ over the interval (x_k, x_{k+1}) with a parabola, as depicted in figure 1.7.3, and then approximate the slope of the function, df/dx , with the slope of the parabola. Differentiating once the right-hand side of (1.7.4), we derive the second-order finite-difference approximation

$$\frac{df}{dx}(x) \simeq 2 a^{(k)} (x - x_k) + b^{(k)}, \quad (2.5.4)$$

where the coefficients $a^{(k)}$ and $b^{(k)}$ are given in (1.7.7).

Identifying the evaluation point x with the grid point x_k , we obtain the *centered-difference* approximation

$$\frac{df}{dx}(x_k) \simeq b^{(k)}. \quad (2.5.5)$$

When the grid points are spaced evenly, $x_k - x_{k-1} = x_{k+1} - x_k = h$, where h is the grid spacing, we obtain the simple form

$$\frac{df}{dx}(x_k) \simeq \frac{f_{k+1} - f_{k-1}}{2 h}. \quad (2.5.6)$$

The parabolic approximation allows us to also obtain an estimate for the second derivative $d^2 f/dx^2$. Differentiating the right-hand side of (1.7.4) twice with respect to x , we derive the finite-difference approximation

$$\frac{d^2 f}{dx^2}(x) \simeq 2 a^{(k)}, \quad (2.5.7)$$

where the coefficient $a^{(k)}$ is given in (1.7.7). When the grid points are distributed evenly with spacing h , we obtain the simpler form

$$\frac{d^2 f}{dx^2}(x) \simeq \frac{f_{k+1} - 2f_k + f_{k-1}}{h^2}. \quad (2.5.8)$$

2.5.2 Numerical differentiation in two dimensions

Consider now the computation of the first partial derivatives of a function $f(x, y)$ of two independent variables x and y , $\partial f/\partial x$ and $\partial f/\partial y$, given the values of the function at the nodes of a two-dimensional grid defined by the intersections of the x -level lines x_i , $i = 1, 2, \dots, N_x + 1$, and y -level lines y_j , $j = 1, 2, \dots, N_y + 1$, as illustrated in figure 1.7.2.

Suppose that x lies within the k_x th x -interval confined between the x_{k_x} and x_{k_x+1} x -level lines, and y lies within the k_y th y -interval confined between the y_{k_y} and y_{k_y+1} y -level lines.

First-order differentiation

Using the method of bilinear interpolation discussed in Section 1.7, we approximate the first partial derivatives of the function $f(x, y)$ with the partial derivatives of the bilinear function defined in equation (1.7.12). Considering the derivative with respect to x , we obtain the forward-difference approximation

$$\begin{aligned} \left(\frac{\partial f}{\partial x}\right)(x, y) &\simeq \left(\frac{\partial P_{BL}^{k_x, k_y}}{\partial x}\right)(x, y) \\ &= \frac{\partial w_{00}^{k_x, k_y}}{\partial x}(x, y) f(x_{k_x}, y_{k_y}) + \frac{\partial w_{10}^{k_x, k_y}}{\partial x}(x, y) f(x_{k_x+1}, y_{k_y}) \\ &+ \frac{\partial w_{01}^{k_x, k_y}}{\partial x}(x, y) f(x_{k_x}, y_{k_y+1}) + \frac{\partial w_{11}^{k_x, k_y}}{\partial x}(x, y) f(x_{k_x+1}, y_{k_y+1}). \end{aligned} \quad (2.5.9)$$

Using expressions (1.7.13) and (1.7.14), we find

$$\begin{aligned} \left(\frac{\partial f}{\partial x}\right)(x, y) &= -\frac{y_{k_y+1} - y}{A} f(x_{k_x}, y_{k_y}) + \frac{y_{k_y+1} - y}{A} f(x_{k_x+1}, y_{k_y}) \\ &- \frac{y - y_{k_y}}{A} f(x_{k_x}, y_{k_y+1}) + \frac{y - y_{k_y}}{A} f(x_{k_x+1}, y_{k_y+1}). \end{aligned} \quad (2.5.10)$$

Recalling that $A = (x_{k_x+1} - x_{k_x})(y_{k_y+1} - y_{k_y})$, as given in (1.7.15), we derive the first-order forward difference approximation for the southwestern grid point,

$$\left(\frac{\partial f}{\partial x}\right)(x_{k_x}, y_{k_y}) \simeq \frac{f(x_{k_x+1}, y_{k_y}) - f(x_{k_x}, y_{k_y})}{x_{k_x+1} - x_{k_x}}. \quad (2.5.11)$$

A similar approximation of the y derivative yields

$$\left(\frac{\partial f}{\partial y}\right)(x_{k_x}, y_{k_y}) \simeq \frac{f(x_{k_x}, y_{k_y+1}) - f(x_{k_x}, y_{k_y})}{y_{k_y+1} - y_{k_y}}. \quad (2.5.12)$$

Second-order differentiation

Second-order centered-difference formulae for evaluating the first partial derivative of a function at a grid point may be derived on the basis of the one-dimensional formula (2.5.5). Using the expression for the coefficient $b^{(k)}$ given in equations (1.7.7), we obtain

$$\left(\frac{\partial f}{\partial x}\right)(x_{k_x}, y_{k_y}) = \frac{(x_{k_x} - x_{k_x-1}) \frac{f_{k_x+1, k_y} - f_{k_x, k_y}}{x_{k_x+1} - x_{k_x}} + (x_{k_x+1} - x_{k_x}) \frac{f_{k_x, k_y} - f_{k_x-1, k_y}}{x_{k_x} - x_{k_x-1}}}{x_{k_x+1} - x_{k_x-1}} \quad (2.5.13)$$

The corresponding expression for the derivative with respect to y is

$$\left(\frac{\partial f}{\partial y}\right)(x_{k_x}, y_{k_y}) = \frac{(y_{k_y} - y_{k_y-1}) \frac{f_{k_x, k_y+1} - f_{k_x, k_y}}{y_{k_y+1} - y_{k_y}} + (y_{k_y+1} - y_{k_y}) \frac{f_{k_x, k_y} - f_{k_x, k_y-1}}{y_{k_y} - y_{k_y-1}}}{y_{k_y+1} - y_{k_y-1}}. \quad (2.5.14)$$

When the grid lines are spaced evenly, $x_{k_x} - x_{k_x-1} = x_{k_x+1} - x_{k_x} = h_x$, and $y_{k_y} - y_{k_y-1} = y_{k_y+1} - y_{k_y} = h_y$, we obtain the simpler forms

$$\left(\frac{\partial f}{\partial x}\right)(x_{k_x}, y_{k_y}) = \frac{f_{k_x+1, k_y} - f_{k_x-1, k_y}}{2 h_x}, \quad (2.5.15)$$

and

$$\left(\frac{\partial f}{\partial y}\right)(x_{k_x}, y_{k_y}) = \frac{f_{k_x, k_y+1} - f_{k_x, k_y-1}}{2 h_y}. \quad (2.5.16)$$

2.5.3 Numerical computation of the velocity gradient and related functions

The formulae derived previously in this section may be used to obtain approximations to the elements of the velocity gradient tensor, rate of deformation tensor, vorticity tensor, vorticity vector, and rate of expansion, from specified values of the velocity at grid points. For illustration, we consider a two-dimensional flow and refer to a uniform grid with constant x and y grid spacings equal to h_x and h_y .

Using the second-order centered-difference approximations (2.5.15) and (2.5.16), we find that the rate of expansion can be approximated with the finite difference formula

$$(\nabla \cdot \mathbf{u})(x_{k_x}, y_{k_y}) = \frac{(u_x)_{k_x+1, k_y} - (u_x)_{k_x-1, k_y}}{2 h_x} + \frac{(u_y)_{k_x, k_y+1} - (u_y)_{k_x, k_y-1}}{2 h_y}. \quad (2.5.17)$$

The corresponding finite-difference approximation for the strength of the vorticity is

$$\omega_z(x_{k_x}, y_{k_y}) = \frac{(u_y)_{k_x+1, k_y} - (u_y)_{k_x-1, k_y}}{2 h_x} - \frac{(u_x)_{k_x, k_y+1} - (u_x)_{k_x, k_y-1}}{2 h_y}. \quad (2.5.18)$$

Similar finite-difference approximations may be derived for the elements of the rate of deformation tensor, and subsequently used to obtain approximations to its eigenvalues and eigenvectors.

Problem

Problem 2.5.1 Numerical differentiation.

Use formula (2.5.8) to evaluate the second derivative of the exponential function $f(x) = e^x$ at $x = 0$ in terms of the values of $f(x)$ at $x = -h, 0, h$, for $h = 0.16, 0.08, 0.04, 0.02$, and 0.01 . Then compute the error defined as the difference between the numerical and the exact value, plot it against h on a linear-log scale, and discuss the slope of the graph.

Computer problem

Problem c.2.5.1 Numerical differentiation of a two-dimensional flow.

Directory *02_grids/rec_2d* of *FDLIB* contains a program that computes by interpolation: (a) the strength of the vorticity, (b) the rate of deformation tensor, and (c) the eigenvalues and eigenvectors of the rate of deformation tensor, over a rectangular domain of flow confined between $a_x < x < b_x$ and $a_y < y < b_y$. The input data specify the components of the velocity at the nodes of a uniform $N_x \times N_y$ Cartesian grid, as shown in figure 1.7.1(b).

(a) Run the program for two velocity fields offered in the main, prepare and discuss plots of the strength of the vorticity, eigenvalues, and eigenvectors of the rate of strain tensor.

(b) Enhance the menu with a new flow of your choice, and repeat part (a).

2.6 Areal and volumetric flow rate

Consider a two-dimensional flow in the xy plane, and draw a line that resides completely in the fluid. At any instant, point particles cross the line, thereby generating a net, positive or negative, areal flow rate towards a designated direction. Our goal is to quantify this flow rate in terms of the shape of the line and the fluid velocity.

2.6.1 Unit tangent and unit normal vectors

Consider first an open line beginning at the point A and ending at the point B , as shown in figure 2.6.1(a). As a preliminary, we introduce the *unit tangent vector*, denoted by $\mathbf{t} = (t_x, t_y)$, defined as the vector that is tangential to the line at a point, and whose magnitude is equal to one unit of length; by definition, $t_x^2 + t_y^2 = 1$. The direction of \mathbf{t} is chosen such that, if we start traveling along the line from point A in the direction of \mathbf{t} , we will finally end up at point B .

Next, we introduce the *unit normal vector*, denoted by $\mathbf{n} = (n_x, n_y)$, defined as the vector that is perpendicular to the line at every point, and whose magnitude is equal to one unit of length; by definition, $n_x^2 + n_y^2 = 1$. The orientation of \mathbf{n} is such that the tangent vector \mathbf{t} arises by rotating \mathbf{n} around the z axis in the counterclockwise direction by an angle equal to $\pi/2$.

2.6 Areal and volumetric flow rate

Computer problem

Problem c.2.5.1 *Numerical differentiation of a two-dimensional flow.*

Directory `02_grids/rec_2d` of *FDLIB* contains a program that computes by interpolation: (a) the strength of the vorticity, (b) the rate of deformation tensor, and (c) the eigenvalues and eigenvectors of the rate of deformation tensor, over a rectangular domain of flow confined between $a_x < x < b_x$ and $a_y < y < b_y$. The input data specify the components of the velocity at the nodes of a uniform $N_x \times N_y$ Cartesian grid, as shown in figure 1.7.1(b).

(a) Run the program for two velocity fields offered in the main, prepare and discuss plots of the strength of the vorticity, eigenvalues, and eigenvectors of the rate of strain tensor.

(b) Enhance the menu with a new flow of your choice, and repeat part (a).

2.6 Areal and volumetric flow rate

Consider a two-dimensional flow in the xy plane, and draw a line that resides completely in the fluid. At any instant, point particles cross the line, thereby generating a net, positive or negative, areal flow rate towards a designated direction. Our goal is to quantify this flow rate in terms of the shape of the line and the fluid velocity.

2.6.1 Unit tangent and unit normal vectors

Consider first an open line beginning at the point A and ending at the point B , as shown in figure 2.6.1(a). As a preliminary, we introduce the *unit tangent vector*, denoted by $\mathbf{t} = (t_x, t_y)$, defined as the vector that is tangential to the line at a point, and whose magnitude is equal to one unit of length; by definition, $t_x^2 + t_y^2 = 1$. The direction of \mathbf{t} is chosen such that, if we start traveling along the line from point A in the direction of \mathbf{t} , we will finally end up at point B .

Next, we introduce the *unit normal vector*, denoted by $\mathbf{n} = (n_x, n_y)$, defined as the vector that is perpendicular to the line at every point, and whose magnitude is equal to one unit of length; by definition, $n_x^2 + n_y^2 = 1$. The orientation of \mathbf{n} is such that the tangent vector \mathbf{t} arises by rotating \mathbf{n} around the z axis in the counterclockwise direction by an angle equal to $\pi/2$.

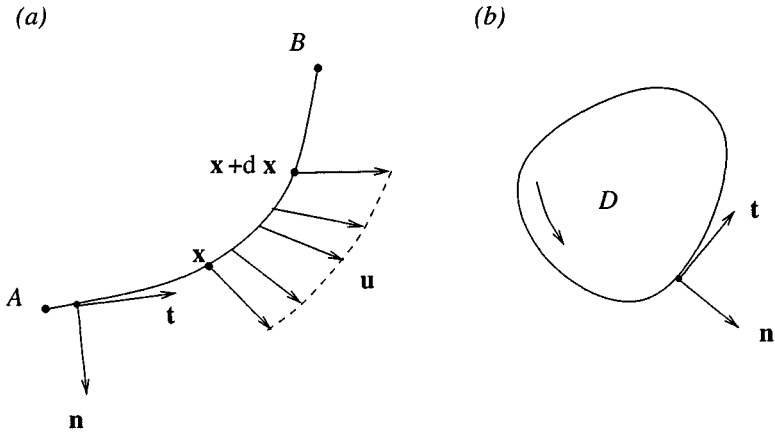


Figure 2.6.1 (a) An open line with end-points A and B , used to define the local areal flow rate and flux in a two-dimensional flow. When the end-points A and B coincide, we obtain the closed line shown in (b).

Consider now an infinitesimal section of the line beginning at the point \mathbf{x} and ending at the point $\mathbf{x} + d\mathbf{x}$, where the differential displacement $d\mathbf{x} = (dx, dy)$ is parallel to, and points in the direction of \mathbf{t} . The components of the unit tangent and unit normal vector are given by

$$t_x = \frac{dx}{dl}, \quad t_y = \frac{dy}{dl}, \quad (2.6.1)$$

and

$$n_x = \frac{dy}{dl}, \quad n_y = -\frac{dx}{dl}, \quad (2.6.2)$$

where

$$dl = \sqrt{dx^2 + dy^2} = \sqrt{1 + \left(\frac{dy}{dx}\right)^2} |dx| \quad (2.6.3)$$

is the differential arc length of the infinitesimal section of the line.

2.6.2 Normal and tangential velocity

Consider next a group of adjacent point particles which, at a certain time, are deployed over the infinitesimal arc length dl . During an infinitesimal period of time dt , the point particles move to a new position,

thus allowing other point particles located behind or in front of them to cross the line into the other side. To compute the net area of fluid that has crossed the infinitesimal arc length dl , we resolve the velocity of the point particles into a normal and a tangential component, writing

$$\mathbf{u} = u_n \mathbf{n} + u_t \mathbf{t}. \quad (2.6.4)$$

The normal and tangential velocities u_n and u_t may be computed readily in terms of the inner vector product defined in equation (2.1.8).

First, we note that, because \mathbf{t} and \mathbf{n} are mutually orthogonal, their inner product vanishes,

$$\mathbf{t} \cdot \mathbf{n} = \mathbf{n} \cdot \mathbf{t} = 0. \quad (2.6.5)$$

To confirm this, simply substitute (2.6.1) and (2.6.2) into the right-hand side of (2.1.8).

Second, we recall that the magnitudes of \mathbf{n} and \mathbf{t} are equal to unity,

$$\mathbf{n} \cdot \mathbf{n} = 1, \quad \mathbf{t} \cdot \mathbf{t} = 1. \quad (2.6.6)$$

To confirm this, we substitute (2.6.1) or (2.6.2) into the right-hand side of (2.1.8), and use (2.6.3).

Third, we take the inner product of the unit normal vector with both sides of (2.6.4), and use (2.6.5) and (2.6.6) to find

$$u_n = \mathbf{u} \cdot \mathbf{n} = u_x n_x + u_y n_y. \quad (2.6.7)$$

Finally, we take the inner product of the unit tangent vector with both sides of (2.6.4), and use (2.6.5) and (2.6.6) to find

$$u_t = \mathbf{u} \cdot \mathbf{t} = u_x t_x + u_y t_y. \quad (2.6.8)$$

2.6.3 Local areal flow rate and flux

The local areal flow rate across the infinitesimal section dl , defined as the area of fluid that crosses this section during an infinitesimal period of time, denoted by da/dt , is given by

$$\frac{da}{dt} = u_n dl, \quad (2.6.9)$$

Why have we selected the normal component of the velocity on the right-hand side of (2.6.9)? The answer becomes evident by observing that, if the normal component vanishes, then the particles move tangentially to the line, in which case fluid does not cross the line.

The corresponding local *areal flux*, denoted by q , is defined as the ratio of the local areal flow rate da/dt to the infinitesimal length of the line across which transport takes place. Equation (2.6.9) shows that

$$q \equiv \frac{da}{dt dl} = u_n, \quad (2.6.10)$$

that is, the local areal flux is equal to the normal component of the fluid velocity.

Substituting (2.6.7) into (2.6.9), and using (2.6.2), we find

$$\begin{aligned} \frac{da}{dt} &= u_n dl = q dl \\ &= (u_x n_x + u_y n_y) dl = u_x dy - u_y dx, \end{aligned} \quad (2.6.11)$$

which allows us to evaluate the local areal flow rate in terms of the components of the velocity.

2.6.4 Areal flow rate across a line

To compute the areal flow rate across the open line depicted in figure 2.6.1(a), denoted by Q , we subdivide the line into an infinite collection of infinitesimal sections with differential length dl , and add all contributions. In mathematical terms, we integrate the local areal flux along the line with respect to arc length, finding

$$\begin{aligned} Q &= \int_A^B q dl = \int_A^B \frac{da}{dt dl} dl = \int_A^B \frac{da}{dt} = \int_A^B (u_x n_x + u_y n_y) dl \\ &= \int_A^B u_n dl = \int_A^B (u_x dy - u_y dx). \end{aligned} \quad (2.6.12)$$

The expression on the right-hand side of (2.6.12) allows us to evaluate Q in terms of the geometry of the line and the two components of the velocity. This integral representation is also applicable for the closed line depicted in figure 2.6.1(b); in this case, the last point B simply coincides with the first point A , yielding a closed integral.

2.6.5 Analytical integration

If the line has a simple shape, and the components of the velocity are known functions of position with simple forms, we may be able to compute the integrals in (2.6.12) by analytical methods.

Consider, for example, a line that has the shape of a section of a circle of radius R centered at the point \mathbf{x}_c , with end-points corresponding to the polar angles θ_A and θ_B . In this case, $x = x_c + R \cos \theta$ and $y = y_c + R \sin \theta$. Differentiating these equations with respect to θ , we find $dx = -R \sin \theta d\theta$ and $dy = R \cos \theta d\theta$. Substituting these expressions into the last integral in (2.6.12), we obtain

$$Q = R \int_{\theta_A}^{\theta_B} (u_x \cos \theta + u_y \sin \theta) d\theta. \quad (2.6.13)$$

If the velocity components are available explicitly in terms of the angle θ , then they may be substituted into (2.6.13) to yield an integral representation with respect to θ . For example, if $u_x = \alpha \cos \theta / (2\pi r)$ and $u_y = \alpha \sin \theta / (2\pi r)$, where α is a constant and r is the distance from the origin,

$$Q = R \frac{\alpha}{2\pi R} \int_{\theta_A}^{\theta_B} d\theta = \frac{\alpha}{2\pi} (\theta_B - \theta_A). \quad (2.6.14)$$

If the circular segment forms a complete circle, and the integration is done in the counterclockwise direction from $\theta_A = \theta_0$ to $\theta_B = 2\pi - \theta_0$, where θ_0 is an arbitrary angle, then $Q = \alpha$ independent of the radius R .

2.6.6 Numerical integration

Under most conditions, we will not be able to compute the line integrals in (2.6.12) exactly by analytical methods, and we must resort to numerical approximations. To perform a numerical computation, we mark the location of the line with $N + 1$ sequential nodes denoted by \mathbf{x}_i , where $i = 1, 2, \dots, N + 1$, as depicted in figure 2.6.2. The first node coincides with the first point, A , and the last node coincides with the last point, B . If the line is closed, the nodes numbered 1 and $N + 1$ coincide.

Next, we approximate the shape of the line between two successive nodes numbered i and $i + 1$ with a straight segment passing through these nodes, denoted by E_i , where E stands for "element". There are a

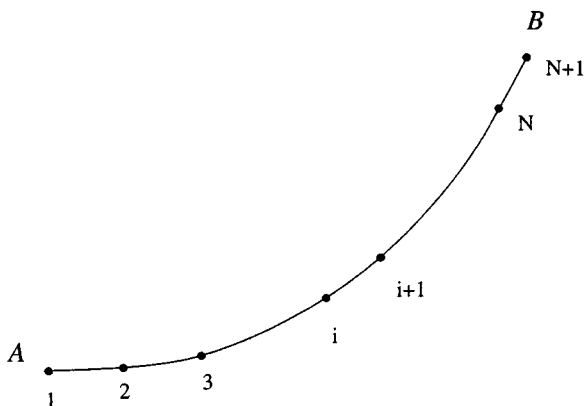


Figure 2.6.2 An array of points deployed along a section of a line in the xy plane, used to compute the areal flow rate by numerical methods.

total of N elements whose union forms a polygonal line, called a *polyline*, beginning at the first point A and ending at the last point B .

The key step in developing a numerical approximation is the replacement of the line integrals in (2.6.12) with the sum of integrals over the elements, and the approximation of the velocity components over each element with the average of the values at the element end-points. With these simplifications, the last integral in (2.6.12) takes the form

$$Q = \sum_{i=1}^N \left[\frac{u_x(\mathbf{x}_i) + u_x(\mathbf{x}_{i+1})}{2} (y_{i+1} - y_i) - \frac{u_y(\mathbf{x}_i) + u_y(\mathbf{x}_{i+1})}{2} (x_{i+1} - x_i) \right]. \quad (2.6.15)$$

Writing out the sum, and rearranging, we find the equivalent expression

$$\begin{aligned} Q &= \frac{1}{2} [u_x(\mathbf{x}_1)(y_2 - y_1) - u_y(\mathbf{x}_1)(x_2 - x_1)] \\ &+ \frac{1}{2} \sum_{i=2}^N [u_x(\mathbf{x}_i)(y_{i+1} - y_{i-1}) - u_y(\mathbf{x}_i)(x_{i+1} - x_{i-1})] \\ &+ \frac{1}{2} [u_x(\mathbf{x}_{N+1})(y_{N+1} - y_N) - u_y(\mathbf{x}_{N+1})(x_{N+1} - x_N)]. \end{aligned} \quad (2.6.16)$$

If the line is closed, in which case nodes 1 and $N + 1$ coincide, the first and last contributions on the right-hand side of (2.6.16) combine to yield the simpler form

$$Q = \frac{1}{2} \sum_{i=1}^N [u_x(\mathbf{x}_i)(y_{i+1} - y_{i-1}) - u_y(\mathbf{x}_i)(x_{i+1} - x_{i-1})], \quad (2.6.17)$$

where the wrapped point numbered 0 coincides with the penultimate point numbered N .

The computation of the right-hand sides of (2.6.16) and (2.6.17) requires knowledge of the velocity components at the nodes; these are either given explicitly or computed by interpolation from grid values, as discussed in Section 1.7.

2.6.7 The Gauss divergence theorem in two dimensions

Consider a closed loop in the xy plane, denoted by C , and a vector function of position $\mathbf{h} = (h_x, h_y)$, where $h_x(x, y)$ and $h_y(x, y)$ are two scalar functions. The normal component of \mathbf{h} along C is given by the inner product

$$h_n \equiv \mathbf{h} \cdot \mathbf{n} = h_x n_x + h_y n_y. \quad (2.6.18)$$

The divergence of \mathbf{h} is a scalar function of position given by

$$\nabla \cdot \mathbf{h} = \frac{\partial h_x}{\partial x} + \frac{\partial h_y}{\partial y}. \quad (2.6.19)$$

The Gauss divergence theorem states that the line integral of h_n along C is equal to the integral of the divergence of \mathbf{h} over the area D enclosed by C ,

$$\oint_C \mathbf{h} \cdot \mathbf{n} \, dl = \int_D \nabla \cdot \mathbf{h} \, dx \, dy, \quad (2.6.20)$$

where \mathbf{n} is the unit vector normal to C pointing outward.

Consider now the areal flow rate across a closed loop. Applying (2.6.20) with $\mathbf{h} = \mathbf{u}$, we find that the flow rate across this loop is equal to the areal integral of the divergence of the velocity over D ,

$$Q = \oint_C \mathbf{u} \cdot \mathbf{n} \, dl = \int_D \nabla \cdot \mathbf{u} \, dx \, dy, \quad (2.6.21)$$

where the unit normal vector points outward, as shown in figure 2.6.1(b). The right-hand side of (2.6.21) allows us to compute the instantaneous flow rate across a closed loop in terms of the integral of the rate of expansion over the enclosed area.

Incompressible fluids

It is clear from expression (2.6.21) that, if the velocity field is solenoidal, that is, the divergence of the velocity $\nabla \cdot \mathbf{u}$ vanishes at every point, then the areal flow rate across any closed loop is equal to zero. In physical terms, the fluid parcels deform and rotate but do not expand, and the amount of fluid entering the area enclosed by a stationary closed loop is equal to the amount of fluid exiting the loop during any period of time.

2.6.8 Three-dimensional flow

The preceding discussion for two-dimensional flow may be extended in a straightforward fashion to three-dimensional flow. To carry out this extension, we replace the line integrals along open or closed loops with surface integrals over open or closed surfaces.

Working in this manner, we find, for example, that the flow rate Q across an open or closed surface H is given by the surface integral

$$Q = \int_H \mathbf{u} \cdot \mathbf{n} \, dS. \quad (2.6.22)$$

The unit normal vector \mathbf{n} and the differential area of a surface element dS are depicted in figure 2.6.3.

The Gauss divergence theorem in three dimensions

Consider a closed surface denoted by H , and a vector function of position $\mathbf{h} = (h_x, h_y, h_z)$. The normal component of \mathbf{h} over H is given by the inner product

$$h_n \equiv \mathbf{h} \cdot \mathbf{n} = h_x n_x + h_y n_y + h_z n_z, \quad (2.6.23)$$

and the divergence of \mathbf{h} is given by

$$\nabla \cdot \mathbf{h} = \frac{\partial h_x}{\partial x} + \frac{\partial h_y}{\partial y} + \frac{\partial h_z}{\partial z}. \quad (2.6.24)$$

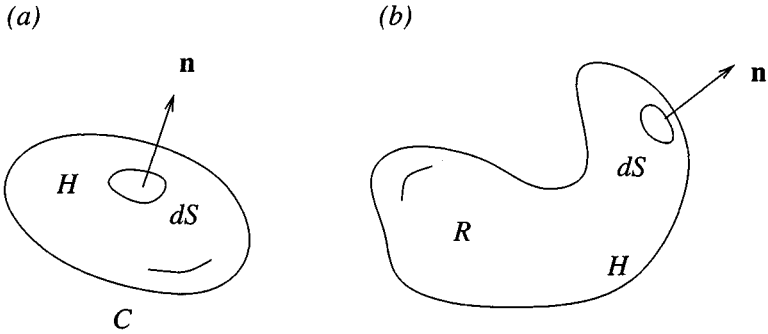


Figure 2.6.3 Illustration of (a) an open surface in a three-dimensional flow bounded by the closed line C , and (b) a closed surface enclosing the volume R , used to define the areal flow rate and establish the Gauss divergence theorem.

The Gauss divergence theorem states that the surface integral of h_n over H is equal to the integral of $\nabla \cdot \mathbf{h}$ over the volume R enclosed by H ,

$$\int_H \mathbf{h} \cdot \mathbf{n} \, dS = \int_R \nabla \cdot \mathbf{h} \, dV, \quad (2.6.25)$$

where \mathbf{n} is the unit vector normal to H pointing outward, and $dV = dx \, dy \, dz$ is the differential volume expressed in Cartesian coordinates.

Consider now the flow rate across the closed surface H , given in (2.6.22). Applying (2.6.25) with $\mathbf{h} = \mathbf{u}$, we find

$$Q = \int_R \nabla \cdot \mathbf{u} \, dV. \quad (2.6.26)$$

This expression shows that, if the velocity field is solenoidal, the volumetric flow rate across any closed surface enclosing fluid alone is required to vanish.

2.6.9 Axisymmetric flow

Next, we consider a meridional plane of an axisymmetric flow, and draw a line beginning at the point A and ending at the point B , as illustrated in figure 2.6.4. The flow rate across the axisymmetric surface that arises by rotating the line around the x axis is given by

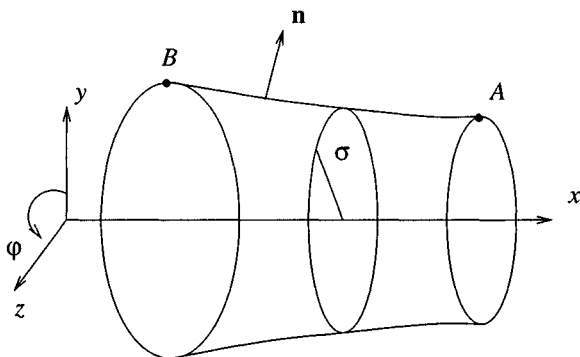


Figure 2.6.4 An axisymmetric surface whose trace in a meridional plane is an open line beginning at the point A and ending at the point B .

$$Q = \int_A^B (u_x n_x + u_\sigma n_\sigma) 2\pi\sigma dl = \int_A^B 2\pi\sigma (u_x d\sigma - u_\sigma dx), \quad (2.6.27)$$

where dl is the differential arc length along the generating line. Expression (2.6.27) arises by adding the fluxes across all elementary axisymmetric surfaces confined between two parallel planes that are perpendicular to the x axis and are separated by the infinitesimal distance dx corresponding to the arc length dl , taking into consideration that the surface area of an elementary surface centered at a ring of radius σ is equal to $2\pi\sigma dl$.

Computer problem

Problem c.2.6.1 *Flow rate across an ellipse.*

Consider a closed loop in the xy plane having the shape of a horizontal ellipse centered at the point \mathbf{x}_c , with major and minor semi-axes equal to a and b . The elliptical shape is described in parametric form by the equations $x = x_c + a \cos \chi$ and $y = y_c + b \sin \chi$, where χ is the native parameter of the ellipse ranging between 0 and 2π . The velocity components are given by $u_x = \alpha \cos \theta / (2\pi r)$ and $u_y = \alpha \sin \theta / (2\pi r)$, where α is a constant, and (r, θ) are plane polar coordinates in the xy plane with origin at the center of the ellipse.

Write a program that computes the flow rate across the ellipse using a numerical method based on equation (2.6.17). Perform computations for two ellipses with aspect ratios of your choice, in each case for $N = 8, 16, 32,$ and $64,$ and discuss your results.

2.7 Mass flow rate, mass conservation, and the continuity equation

In Section 1.5, we defined a point particle as an idealized entity arising in the limit as the size of a small fluid parcel becomes decreasingly small and eventually infinitesimal. In this limit, the ratio between the mass of the parcel and the volume of the parcel tends to a non-zero and non-infinite value defined as the fluid density ρ .

To signify that the density is a function of position and time, we write $\rho(x, y, z, t)$ or $\rho(\mathbf{x}, t)$, with the understanding that the density at a particular point in a flow is equal to the density of the point particle that happens to be at that point at the current time.

2.7.1 Mass flux and mass flow rate

Consider a two-dimensional flow in the xy plane, and draw a line beginning at the point A and ending at the point B , as illustrated in figure 2.6.1(a). At any instant, point particles cross this line, thereby generating a net mass flow rate toward a specified direction. Our goal is to quantify this flow rate in terms of the shape of the line and the distribution of the velocity and density in the flow.

Repeating the analysis of Section 2.6, we find that the mass flux across an infinitesimal section of a line is given by the following counterpart of equation (2.6.10),

$$q_m = \rho u_n, \quad (2.7.1)$$

where u_n is the component of the velocity normal to the line. The mass flow rate across a line beginning at the point A and ending at the point B is given by the following counterpart of equation (2.6.12),

$$Q_m = \int_A^B q_m dl = \int_A^B \rho \mathbf{u} \cdot \mathbf{n} dl = \int_A^B \rho (u_x dy - u_y dx). \quad (2.7.2)$$

The integrals in (2.7.2) may be computed by analytical or numerical methods, as discussed in Section 2.6.

2.7.2 Mass flow rate across a closed line

Correspondingly, the mass flow rate outward from a closed line may be expressed in terms of a closed line integral, as

$$Q_m = \oint q_m dl = \oint \rho \mathbf{u} \cdot \mathbf{n} dl = \oint \rho (u_x dy - u_y dx), \quad (2.7.3)$$

where the unit normal vector \mathbf{n} points into the exterior of the area enclosed by the line, as depicted in figure 2.6.1(b).

The Gauss divergence theorem expressed by equation (2.6.20) states that the line integral in (2.7.3) is equal to the following integral of the divergence of the velocity multiplied by the fluid density over the area D enclosed by the line,

$$Q_m = \int_D \nabla \cdot (\rho \mathbf{u}) dx dy, \quad (2.7.4)$$

where

$$\nabla \cdot (\rho \mathbf{u}) = \frac{\partial(\rho u_x)}{\partial x} + \frac{\partial(\rho u_y)}{\partial y}. \quad (2.7.5)$$

For future reference, we expand the derivatives of the products on the left-hand side of (2.7.5) using the rules of product differentiation, finding

$$\nabla \cdot \rho \mathbf{u} = \frac{\partial \rho}{\partial x} u_x + \frac{\partial u_x}{\partial x} \rho + \frac{\partial \rho}{\partial y} u_y + \frac{\partial u_y}{\partial y} \rho = \mathbf{u} \cdot (\nabla \rho) + \rho \nabla \cdot \mathbf{u}. \quad (2.7.6)$$

We have introduced the vector of the first partial derivatives of the density,

$$\nabla \rho = \left(\frac{\partial \rho}{\partial x}, \frac{\partial \rho}{\partial y} \right), \quad (2.7.7)$$

defined as the gradient of the density.

2.7.3 Mass conservation

The first thermodynamic principle requires that the rate of change of the mass residing within an area D that is enclosed by a stationary

closed line be equal to the mass flow rate inward across the line, or equivalently, to the negative of the mass flow rate outward across the line. If the outward mass flow rate is positive, then the rate of the change of mass enclosed by the line is negative reflecting a reduction in time. In terms of the areal mass flow rate defined in equation (2.7.3) and expressed in the form of an areal integral in equation (2.7.4),

$$\frac{d}{dt} \int_D \rho \, dx \, dy = -Q_m = - \int_D \nabla \cdot (\rho \mathbf{u}) \, dx \, dy. \quad (2.7.8)$$

Since the area D is fixed in space, we can interchange the order of time differentiation and space integration on the left-hand side of (2.7.8), and then combine the two integrals to find

$$\int_D \left[\frac{\partial \rho}{\partial t} + \nabla \cdot (\rho \mathbf{u}) \right] \, dx \, dy = 0. \quad (2.7.9)$$

Moreover, since the shape of the area D is arbitrary, the integrand on the right-hand side of (2.7.9) must vanish, yielding a partial differential equation expressing mass conservation,

$$\frac{\partial \rho}{\partial t} + \nabla \cdot (\rho \mathbf{u}) = 0, \quad (2.7.10)$$

called the *continuity equation*. This nomenclature is meant to emphasize that, in the absence of sources or sinks, mass neither appears nor disappears in the flow, and the fluid must move in a continuous fashion.

Combining equations (2.7.6) and (2.7.10), we derive an alternative form of the continuity equation,

$$\frac{\partial \rho}{\partial t} + \mathbf{u} \cdot \nabla \rho + \rho \nabla \cdot \mathbf{u} = 0, \quad (2.7.11)$$

involving the density gradient and the rate of expansion.

2.7.4 Three-dimensional flow

The preceding discussion for two-dimensional flow may be generalized in a straightforward fashion to three-dimensional flow. To carry out this extension, we replace the line integrals with surface integrals over a closed or open surface. The mass flow rate Q_m across an open or closed surface R depicted in figure 2.6.3 is given by the surface integral

$$Q_m = \int \int_R \rho \mathbf{u} \cdot \mathbf{n} dS. \quad (2.7.12)$$

If the surface is closed and the unit normal vector points outward, as shown in figure 2.6.3(b), we may use the divergence theorem to recast the surface integral on the right-hand side of (2.7.12) into an integral of the rate of expansion over the volume R enclosed by the surface,

$$Q_m = \int \int \int_R \nabla \cdot (\rho \mathbf{u}) dV. \quad (2.7.13)$$

The continuity equation expressed by (2.7.10) or (2.7.11) stands true, with the understanding that $\nabla \rho$ is the three-dimensional density gradient with components

$$\nabla \rho = \left(\frac{\partial \rho}{\partial x}, \frac{\partial \rho}{\partial y}, \frac{\partial \rho}{\partial z} \right). \quad (2.7.14)$$

2.7.5 Evolution equation for the density

The continuity equation may be regarded as an evolution equation for the density, determined by the velocity. To see this, we recast equation (2.7.10) into the form

$$\frac{\partial \rho}{\partial t} = -\nabla \cdot (\rho \mathbf{u}). \quad (2.7.15)$$

Evaluating the right-hand side of (2.7.15) at a certain point in terms of the instantaneous velocity and density, we obtain an expression for the current and local temporal rate of change of the density.

Consider, for example, the change in density occurring during a small time interval Δt following the present time t . Evaluating both sides of equation (2.7.15) at the point \mathbf{x} , and approximating the right-hand side with a first-order forward finite difference, we find

$$\frac{\rho(\mathbf{x}, t + \Delta t) - \rho(\mathbf{x}, t)}{\Delta t} = -[\nabla \cdot (\rho \mathbf{u})](\mathbf{x}, t), \quad (2.7.16)$$

where the right-hand side is evaluated at (\mathbf{x}, t) . Solving for $\rho(\mathbf{x}, t + \Delta t)$, we obtain

$$\rho(\mathbf{x}, t + \Delta t) = \rho(\mathbf{x}, t) - \Delta t [\nabla \cdot (\rho \mathbf{u})](\mathbf{x}, t), \quad (2.7.17)$$

which provides us with an explicit expression for $\rho(\mathbf{x}, t + \Delta t)$ in terms of values at the previous time t .

Finite-difference method

In practice, equation (2.7.15) is typically solved using a numerical method. Consider an idealized one-dimensional flow along the x axis representing, for example, flow along a conduit with a known axial velocity $u(x, t)$. The one-dimensional version of the continuity equation (2.7.15) reads

$$\frac{\partial \rho}{\partial t} = -\frac{\partial(\rho u)}{\partial x}. \quad (2.7.18)$$

The solution is to be found over an interval that is confined within $a < x < b$, subject to: (a) an initial condition that specifies the density distribution at the designated origin of time, $\rho(x, t = 0)$, and (b) a boundary condition that specifies the density at the left end of the domain of flow, $x = a$.

To compute a numerical solution, we divide the domain $a < x < b$ into N intervals demarkated by the $N + 1$ nodes x_i , $i = 1, 2, \dots, N + 1$, as depicted in figure 1.7.1(a). The first node coincides with the left end-point a , and the last node coincides with the right end-point b . Our goal is to generate the values of ρ at the nodes, at a sequence of time intervals separated by the time interval Δt .

To simplify the notation, we denote the density at the i th node at the k th time level corresponding to time $t_k = k \Delta t$, by ρ_i^k . Evaluating both sides of (2.7.18) at the i th node at the k th time level, and approximating the time derivative on the left-hand side with a first-order forward difference and the spatial derivative on the right-hand side with a first-order backward difference, we derive the finite-difference approximation

$$\frac{\rho_i^{k+1} - \rho_i^k}{\Delta t} = -\frac{(\rho u)_i^k - (\rho u)_{i-1}^k}{x_i - x_{i-1}}. \quad (2.7.19)$$

Solving for ρ_i^{k+1} , we obtain

$$\rho_i^{k+1} = \rho_i^k - \frac{\Delta t}{x_i - x_{i-1}} [(\rho u)_i^k - (\rho u)_{i-1}^k]. \quad (2.7.20)$$

The numerical method involves the following steps:

1. Specify the initial values ρ_i^0 for $i = 1, 2, \dots, N + 1$.
2. Use equation (2.7.20) to compute ρ_i^1 for $i = 2, 3, \dots, N + 1$.
3. Use the left-end boundary condition to set the value of ρ_1^1 .

4. Stop, or return to step 2 and repeat.

Problems

Problem 2.7.1 *Convection under constant velocity.*

(a) Show that when a fluid translates as a rigid body, that is, the fluid velocity \mathbf{u} has the constant but possibly time-dependent value $\mathbf{U}(t)$, the continuity equation (2.7.10) simplifies to the linear convection equation

$$\frac{\partial \rho}{\partial t} + \mathbf{U} \cdot \nabla \rho = 0. \quad (2.7.21)$$

(b) Consider a steady flow where \mathbf{U} is independent of time. In this case, if $\rho_0(\mathbf{x})$ is the density field at $t = 0$, then

$$\rho(\mathbf{x}, t) = \rho_0(\mathbf{x} - \mathbf{U} t) \quad (2.7.22)$$

will be the density field at any subsequent time t . To confirm this, we define the auxiliary variables $w_x \equiv x - U_x t$, $w_y \equiv y - U_y t$, and $w_z \equiv z - U_z t$, and use the chain rule to write

$$\begin{aligned} \frac{\partial \rho}{\partial t} &= \frac{\partial \rho_0}{\partial w_x} \frac{\partial w_x}{\partial t} + \frac{\partial \rho_0}{\partial w_y} \frac{\partial w_y}{\partial t} + \frac{\partial \rho_0}{\partial w_z} \frac{\partial w_z}{\partial t} \\ &= \frac{\partial \rho_0}{\partial w_x} (-U_x) + \frac{\partial \rho_0}{\partial w_y} (-U_y) + \frac{\partial \rho_0}{\partial w_z} (-U_z). \end{aligned} \quad (2.7.23)$$

Continuing in this manner, complete the proof.

(c) The results of part (b) suggest that the density at the point $\mathbf{x} = \mathbf{x}_0 - \mathbf{U} t$ at time t is equal to the density at the point \mathbf{x}_0 at $t = 0$. In physical terms, the density is “convected” by the uniform flow.

Consider the one-dimensional flow discussed in the text with u being a constant, and sketch a profile for the density distribution along the x axis at the initial time $t = 0$ and at a subsequent time.

Problem 2.7.2 *Steady state.*

Consider a steady one-dimensional flow with a specified velocity $u(x)$, and derive an expression for the density distribution at steady state. Discuss the behavior of the density when the velocity vanishes at a point.

Computer problem

Problem c.2.7.1 *Finite-difference method.*

Consider a steady, one-dimensional, periodic flow along the x axis with velocity $u(x) = U(1 + \epsilon \cos(2\pi x/L))$, where U is a constant velocity, ϵ is a specified dimensionless constant, and L is the period. Write a computer program that uses the numerical method discussed in the text to compute the evolution of the density over one spatial period L , subject to a uniform initial distribution. Run the program for $\epsilon = 0.0, 0.2, 0.4,$ and 0.8 , prepare graphs of the density distribution at different times, and discuss the behavior of the solution at long times.

2.8 Properties of point particles

The physical properties of a homogeneous fluid parcel consisting of a single chemical species are determined by, and can be quantified in terms of, the number of molecules, the kinetic energy, the potential energy, and the thermal energy of the molecules that comprise the parcel. Each one of these physical properties is *extensive*, in the sense that the larger the parcel volume, the larger the magnitude of the physical property. As the size of a parcel tends to zero, the ratio between the value of an extensive property and the parcel volume tends to a limit that may be regarded as an *intensive* physical property of the point particle emerging from the parcel immediately before the molecular nature of the fluid becomes apparent.

For example, we have already seen that, as the volume of a parcel tends to zero, the ratio of the mass of the parcel to the volume of the parcel tends to a finite limit defined as the fluid density, ρ . Similarly, the ratio of the number of molecules residing within the parcel to the volume of the parcel tends to the molecular number density, and the ratio of the potential energy of the molecules to the volume of the parcel tends to the specific potential energy.

2.8.1 The material derivative

To prepare the ground for establishing evolution laws governing the motion and physical state of a fluid, we seek corresponding laws determining the rate of change of physical and kinematical properties of

point particles moving with the local fluid velocity. Kinematical properties include the velocity and its first time derivative defined as the point particle acceleration, the vorticity, and the rate of strain.

A key concept is the material derivative, defined as the rate of change of a physical or kinematical property following a point particle. Our first objective is to derive an expression for the material derivative in terms of Eulerian derivatives; that is, partial derivatives with respect to time and spatial coordinates.

Consider the material derivative of the density of a point particle which, at a certain time t_0 , is located at the point \mathbf{x}_0 . In three-dimensional flow, the density is a function of four independent variables: the three Cartesian coordinates (x, y, z) determining position in space, and time t . We begin by linearizing the density field $\rho(x, y, z, t)$ around the hyperpoint (x_0, y_0, z_0, t_0) , as discussed in Section 2.1. Adding time-dependence to equation (2.1.5), and identifying the generic function f with the density, we obtain

$$\begin{aligned} \rho(x, y, z, t) &= \rho(x_0, y_0, z_0, t_0) + (t - t_0) \frac{\partial \rho}{\partial t}(\mathbf{x}_0, t_0) \\ &+ (x - x_0) \frac{\partial \rho}{\partial x}(\mathbf{x}_0, t_0) + (y - y_0) \frac{\partial \rho}{\partial y}(\mathbf{x}_0, t_0) + (z - z_0) \frac{\partial \rho}{\partial z}(\mathbf{x}_0, t_0). \end{aligned} \quad (2.8.1)$$

Next, we bring the first term on the right-hand side, $\rho(x_0, y_0, z_0, t_0)$, to the left-hand side, and divide both sides of the resulting equation by the time lapse $t - t_0$, to find

$$\begin{aligned} \frac{\rho(x, y, z, t) - \rho(x_0, y_0, z_0, t_0)}{t - t_0} &= \frac{\partial \rho}{\partial t}(\mathbf{x}_0, t_0) + \frac{x - x_0}{t - t_0} \frac{\partial \rho}{\partial x}(\mathbf{x}_0, t_0) \\ &+ \frac{y - y_0}{t - t_0} \frac{\partial \rho}{\partial y}(\mathbf{x}_0, t_0) + \frac{z - z_0}{t - t_0} \frac{\partial \rho}{\partial z}(\mathbf{x}_0, t_0). \end{aligned} \quad (2.8.2)$$

The second key step involves the judicious choice of the point \mathbf{x} . This point is selected so that, if a point particle is located at the position \mathbf{x}_0 at time t_0 , then the same point particle will be located at the position \mathbf{x} at the later time t . By definition then, the left-hand side of (2.8.2) reduces to the material derivative. Moreover, since the point particle moves with the fluid velocity, the three fractions on the right-hand side

of (2.8.2) reduce to the three components of the fluid velocity u_x , u_y , and u_z . Denoting the material derivative by $\frac{D}{Dt}$, we write

$$\frac{D\rho}{Dt}(\mathbf{x}_0, t_0) = \left[\frac{\partial\rho}{\partial t} + u_x \frac{\partial\rho}{\partial x} + u_y \frac{\partial\rho}{\partial y} + u_z \frac{\partial\rho}{\partial z} \right](\mathbf{x}_0, t_0). \quad (2.8.3)$$

Equation (2.8.3) allows us to compute the material derivative of the density in terms of Eulerian derivatives; that is, in terms of partial derivatives of the density with respect to time and spatial coordinates. In numerical practice, the partial derivatives are computed using finite-difference approximations, as discussed in Section 2.5.

In terms of the density gradient defined in (2.7.14), equation (2.8.3) takes the simpler form

$$\frac{D\rho}{Dt} = \frac{\partial\rho}{\partial t} + \mathbf{u} \cdot \nabla\rho, \quad (2.8.4)$$

where both sides are evaluated at the arbitrarily chosen point \mathbf{x}_0 at the arbitrary time t_0 .

The continuity equation

Comparing equation (2.8.4) with equation (2.7.11), we find that, in terms of the material derivative of the density, the continuity equation takes the form

$$\frac{D\rho}{Dt} + \rho \nabla \cdot \mathbf{u} = 0, \quad (2.8.5)$$

which illustrates that the rate of change of the density of a point particle is determined by the local rate of expansion. The inverse interpretation, however, is physically more appropriate: the structure of the velocity field is determined, in part, by the rate of change of the density of all point particles, as will be discussed in the next section.

2.8.2 Point particle acceleration

The acceleration of a point particle, denoted by \mathbf{a} , is defined as the rate of change of the point particle velocity. Invoking the definition of the material derivative, we find that the x component of \mathbf{a} is equal to material derivative of the x component of the point particle velocity, which is equal to the local fluid velocity; thus, $a_x = Du_x/Dt$; similar arguments reveal that $a_y = Du_y/Dt$ and $a_z = Du_z/Dt$.

Replacing ρ in equation (2.8.4) with u_x, u_y , or u_z , we find that the three Cartesian components of the point particle acceleration are given by

$$\begin{aligned} a_x &\equiv \frac{Du_x}{Dt} = \frac{\partial u_x}{\partial t} + \mathbf{u} \cdot \nabla u_x = \frac{\partial u_x}{\partial t} + u_x \frac{\partial u_x}{\partial x} + u_y \frac{\partial u_x}{\partial y} + u_z \frac{\partial u_x}{\partial z}, \\ a_y &\equiv \frac{Du_y}{Dt} = \frac{\partial u_y}{\partial t} + \mathbf{u} \cdot \nabla u_y = \frac{\partial u_y}{\partial t} + u_x \frac{\partial u_y}{\partial x} + u_y \frac{\partial u_y}{\partial y} + u_z \frac{\partial u_y}{\partial z}, \\ a_z &\equiv \frac{Du_z}{Dt} = \frac{\partial u_z}{\partial t} + \mathbf{u} \cdot \nabla u_z = \frac{\partial u_z}{\partial t} + u_x \frac{\partial u_z}{\partial x} + u_y \frac{\partial u_z}{\partial y} + u_z \frac{\partial u_z}{\partial z}. \end{aligned} \quad (2.8.6)$$

The three scalar equations (2.8.6) may be conveniently collected into the compact vector form

$$\frac{D\mathbf{u}}{Dt} = \frac{\partial \mathbf{u}}{\partial t} + \mathbf{u} \cdot \mathbf{A} = \frac{\partial \mathbf{u}}{\partial t} + \mathbf{u} \cdot \nabla \mathbf{u}, \quad (2.8.7)$$

where $\mathbf{A} = \nabla \mathbf{u}$ is the velocity gradient tensor defined in equation (2.1.13), with components $A_{ij} = \partial u_j / \partial x_i$. In index notation, the j th component of (2.8.7) takes the form $Du_j/Dt = \partial u_j / \partial t + u_i \partial u_j / \partial x_i$, where summation is implied over the repeated index i .

Cylindrical polar coordinates

In the system of cylindrical polar coordinates defined in figure 1.3.2, the point particle acceleration is expressed in terms of its cylindrical polar components a_x , a_σ , and a_φ , as

$$\mathbf{a} = a_x \mathbf{e}_x + a_\sigma \mathbf{e}_\sigma + a_\varphi \mathbf{e}_\varphi. \quad (2.8.8)$$

Using the transformation rules shown in equations (1.3.17), we find

$$a_\sigma = \cos \varphi a_y + \sin \varphi a_z, \quad a_\varphi = -\sin \varphi a_y + \cos \varphi a_z. \quad (2.8.9)$$

Substituting the right-hand sides of the second and third of relations (2.8.6) into the right-hand sides of equations (2.8.9), and using the chain rule of differentiation to convert derivatives with respect to x, y , and z

to derivatives with respect to x, σ , and φ in the resulting equations and in the first of (2.8.6), we obtain

$$\begin{aligned} a_x &= \frac{\partial u_x}{\partial t} + u_x \frac{\partial u_x}{\partial x} + u_\sigma \frac{\partial u_x}{\partial \sigma} + \frac{u_\varphi}{\sigma} \frac{\partial u_x}{\partial \varphi}, \\ a_\sigma &= \frac{\partial u_\sigma}{\partial t} + u_x \frac{\partial u_\sigma}{\partial x} + u_\sigma \frac{\partial u_\sigma}{\partial \sigma} + \frac{u_\varphi}{\sigma} \frac{\partial u_\sigma}{\partial \varphi} - \frac{u_\varphi^2}{\sigma}, \\ a_\varphi &= \frac{\partial u_\varphi}{\partial t} + u_x \frac{\partial u_\varphi}{\partial x} + u_\sigma \frac{\partial u_\varphi}{\partial \sigma} + \frac{u_\varphi}{\sigma} \frac{\partial u_\varphi}{\partial \varphi} + \frac{u_\sigma u_\varphi}{\sigma}. \end{aligned} \quad (2.8.10)$$

Using the expression for the gradient of a function in cylindrical polar coordinates defined in equations (2.1.30) and (2.1.34), we recast equations (2.8.10) into the more compact form

$$\begin{aligned} a_x &= \frac{\partial u_x}{\partial t} + \mathbf{u} \cdot \nabla u_x = \frac{Du_x}{Dt}, \\ a_\sigma &= \frac{\partial u_\sigma}{\partial t} + \mathbf{u} \cdot \nabla u_\sigma - \frac{u_\varphi^2}{\sigma} = \frac{Du_\sigma}{Dt} - \frac{u_\varphi^2}{\sigma}, \\ a_\varphi &= \frac{\partial u_\varphi}{\partial t} + \mathbf{u} \cdot \nabla u_\varphi + \frac{u_\sigma u_\varphi}{\sigma} = \frac{Du_\varphi}{Dt} + \frac{u_\sigma u_\varphi}{\sigma}. \end{aligned} \quad (2.8.11)$$

These expressions illustrate that the polar cylindrical components of the acceleration are *not* simply equal to the material derivative of the corresponding polar components of the velocity.

Spherical polar coordinates

In the system of spherical polar coordinates depicted in figure 1.3.3, the point particle acceleration is expressed in terms of its spherical polar components a_r , a_θ , and a_φ , as

$$\mathbf{a} = a_r \mathbf{e}_r + a_\theta \mathbf{e}_\theta + a_\varphi \mathbf{e}_\varphi. \quad (2.8.12)$$

Working as previously for the cylindrical polar coordinates, we find the somewhat more involved expressions

$$\begin{aligned}
a_r &= \frac{\partial u_r}{\partial t} + u_r \frac{\partial u_r}{\partial r} + \frac{u_\theta}{r} \frac{\partial u_r}{\partial \theta} + \frac{u_\varphi}{r \sin \theta} \frac{\partial u_r}{\partial \varphi} - \frac{u_\theta^2 + u_\varphi^2}{r} \\
&= \frac{Du_r}{Dt} - \frac{u_\theta^2 + u_\varphi^2}{r}, \\
a_\theta &= \frac{\partial u_\theta}{\partial t} + u_r \frac{\partial u_\theta}{\partial r} + \frac{u_\theta}{r} \frac{\partial u_\theta}{\partial \theta} + \frac{u_\varphi}{r \sin \theta} \frac{\partial u_\theta}{\partial \varphi} + \frac{u_r u_\theta}{r} - \frac{u_\varphi^2 \cot \theta}{r} \\
&= \frac{Du_\theta}{Dt} + \frac{u_r u_\theta}{r} - \frac{u_\varphi^2 \cot \theta}{r}, \\
a_\varphi &= \frac{\partial u_\varphi}{\partial t} + u_r \frac{\partial u_\varphi}{\partial r} + \frac{u_\theta}{r} \frac{\partial u_\varphi}{\partial \theta} + \frac{u_\varphi}{r \sin \theta} \frac{\partial u_\varphi}{\partial \varphi} + \frac{u_r u_\varphi}{r} + \frac{u_\theta u_\varphi}{r} \cot \theta \\
&= \frac{Du_\varphi}{Dt} + \frac{u_r u_\varphi}{r} + \frac{u_\theta u_\varphi}{r} \cot \theta.
\end{aligned} \tag{2.8.13}$$

Plane polar coordinates

In the system of plane polar coordinates depicted in figure 1.3.4, the point particle acceleration is expressed in terms of its plane polar components a_r and a_θ , as

$$\mathbf{a} = a_r \mathbf{e}_r + a_\theta \mathbf{e}_\theta. \tag{2.8.14}$$

Working in the familiar way, we find

$$\begin{aligned}
a_r &= \frac{\partial u_r}{\partial t} + u_r \frac{\partial u_r}{\partial r} + \frac{u_\theta}{r} \frac{\partial u_r}{\partial \theta} - \frac{u_\theta^2}{r} = \frac{Du_r}{Dt} - \frac{u_\theta^2}{r}, \\
a_\theta &= \frac{\partial u_\theta}{\partial t} + u_r \frac{\partial u_\theta}{\partial r} + \frac{u_\theta}{r} \frac{\partial u_\theta}{\partial \theta} + \frac{u_r u_\theta}{r} = \frac{Du_\theta}{Dt} + \frac{u_r u_\theta}{r}.
\end{aligned} \tag{2.8.15}$$

2.8.3 Point particle acceleration at a point with zero vorticity

If the components of the vorticity vector vanish at a point in the flow, then the velocity gradient tensor at that point is symmetric. Consequently, selected partial derivatives of the velocity must be such that the three terms enclosed by the parentheses on the right-hand side of (2.3.6) are equal to zero, yielding

$$\frac{\partial u_z}{\partial y} = \frac{\partial u_y}{\partial z}, \quad \frac{\partial u_x}{\partial z} = \frac{\partial u_z}{\partial x}, \quad \frac{\partial u_y}{\partial x} = \frac{\partial u_x}{\partial y}. \quad (2.8.16)$$

The sum of the last three terms on the right-hand side of the first of equations (2.8.6) may then be written as

$$\begin{aligned} u_x \frac{\partial u_x}{\partial x} + u_y \frac{\partial u_y}{\partial x} + u_z \frac{\partial u_z}{\partial x} &= \frac{1}{2} \frac{\partial u_x^2}{\partial x} + \frac{1}{2} \frac{\partial u_y^2}{\partial x} + \frac{1}{2} \frac{\partial u_z^2}{\partial x} \\ &= \frac{1}{2} \frac{\partial (u_x^2 + u_y^2 + u_z^2)}{\partial x}. \end{aligned} \quad (2.8.17)$$

Working in a similar manner with the y and z components, and collecting the derived expressions into a vector form, we obtain

$$\mathbf{u} \cdot \nabla \mathbf{u} = \frac{1}{2} \nabla u^2, \quad (2.8.18)$$

where $u^2 \equiv u_x^2 + u_y^2 + u_z^2$ is the square of the magnitude of the velocity, and $\nabla u^2 = (\partial u^2 / \partial x, \partial u^2 / \partial y, \partial u^2 / \partial z)$ is its gradient. The point particle acceleration may then be expressed in the alternative form

$$\mathbf{a} \equiv \frac{D\mathbf{u}}{Dt} = \frac{\partial \mathbf{u}}{\partial t} + \frac{1}{2} \nabla u^2. \quad (2.8.19)$$

If the flow is steady, the first term on the right-hand side of (2.8.19) vanishes, and the point particle acceleration is equal to the gradient of half the square of the magnitude of the local velocity, which is a measure of the local kinetic energy of the fluid: the acceleration points in the direction of maximum change of kinetic energy indicated by the gradient.

In Chapter 6, we shall see that the simplified expression (2.8.19) serves as a point of departure for the theoretical analysis and numerical computation of irrotational flows.

Problems

Problem 2.8.1 *Properties of the material derivative.*

Consider two scalar physical or kinematical fluid properties such as the density or a component of the velocity, denoted, respectively, by f and g . Prove that the following usual rule of product differentiation applies,

$$\frac{D(fg)}{Dt} = g \frac{Df}{Dt} + f \frac{Dg}{Dt}. \quad (2.8.20)$$

Problem 2.8.2 *Mass and momentum of a small fluid parcel.*

(a) Consider a small fluid parcel with volume δV_p and density ρ . By requiring mass conservation and using the continuity equation (2.8.5), show that

$$\frac{1}{\delta V_p} \frac{D(\delta V_p)}{Dt} = \nabla \cdot \mathbf{u}, \quad (2.8.21)$$

which reinforces our interpretation of the divergence of the velocity as the rate of volumetric expansion.

(b) The linear momentum of a fluid parcel is defined as the product of the mass of the parcel $\delta m_p = \rho \delta V_p$ and velocity \mathbf{u} . By requiring mass conservation, show that the rate of change of the linear momentum can be expressed in terms of the point particle acceleration in the form

$$\frac{D(\delta m_p \mathbf{u})}{Dt} = \frac{D\mathbf{u}}{Dt} \rho \delta V_p. \quad (2.8.22)$$

Problem 2.8.3 *Point particle acceleration in rotational flow.*

Show that the counterpart of equation (2.8.18) at a point where the vorticity does not necessarily vanish, is

$$\mathbf{u} \cdot \nabla \mathbf{u} = \frac{1}{2} \nabla u^2 - \mathbf{u} \times \boldsymbol{\omega}. \quad (2.8.23)$$

How does this expression simplify at a point where the velocity and vorticity point in the same direction?

Problem 2.8.4 *Point particle motion in one-dimensional flow.*

Consider an idealized one-dimensional flow along the x axis with velocity $u(x, t)$ satisfying the inviscid Burgers equation

$$\frac{\partial u}{\partial t} + u \frac{\partial u}{\partial x} = 0. \quad (2.8.24)$$

Explain why point particles in this flow travel with a time-independent velocity that is equal to the velocity assigned at the initial instant; different point particles may travel with different velocities.

2.9 Incompressible fluids and stream functions

If the volume of a fluid parcel is preserved as the parcel is convected in a flow, then the fluid residing within the parcel is incompressible. In contrast, if the volume of the parcel changes in time, then the fluid residing within the parcel is compressible. Conservation of mass requires that the mass of the fluid be conserved irrespective of whether the fluid is compressible or incompressible.

Since both the mass and volume of an incompressible fluid parcel are conserved during the motion, the density of the point particles comprising the parcel must remain constant in time. Using the definition of the material derivative, we derive the mathematical statement of incompressibility

$$\frac{D\rho}{Dt} = 0, \quad (2.9.1)$$

It is important to bear in mind that the density of an incompressible fluid is not necessarily uniform throughout the domain of flow. Different point particles may have different densities, but the density of each individual point particle must be conserved during the motion.

Using equation (2.9.1), we find that the continuity equation (2.8.5) for an incompressible fluid simplifies to

$$\nabla \cdot \mathbf{u} = 0, \quad (2.9.2)$$

stating that the velocity field is *solenoidal*, and the rate of expansion α defined in equation (2.2.6) is equal to zero: an incompressible fluid parcel undergoes translation, rotation, and isochoric deformation, but not expansion. “Isochoric” is composed from the Greek words $\iota\sigma\omicron\varsigma$ which means equal, and the word $\chi\omega\rho\omicron\varsigma$ which means volume or space.

It is furthermore important to bear in mind that the stipulation (2.9.1) is the defining property of an incompressible fluid, and the simplified form of the continuity equation (2.9.2) is a mere consequence of mass conservation.

2.9.1 Mathematical consequences of incompressibility

Equation (2.9.2) states that the x , y , and z components of the velocity of an incompressible fluid may not be prescribed arbitrarily, but must be such that the differential constraint imposed on them by the requirement that the velocity field be solenoidal is satisfied throughout the domain of

flow at all times. In contrast, the three components of the velocity of a compressible fluid may be arbitrary; the density of the point particles will then be adjusted to ensure mass conservation, as dictated by the continuity equation.

A second consequence of incompressibility is that, because the evolution of the density is governed by the kinematic constraint (2.9.1), an equation of state relating pressure to density and temperature is not required. The significance of this consequence will be discussed in Chapters 4 and 8 in the context of dynamics.

2.9.2 Stream function for two-dimensional flow

The continuity equation for two-dimensional flow in the xy plane, equation (2.9.2), takes the form

$$\frac{\partial u_x}{\partial x} + \frac{\partial u_y}{\partial y} = 0. \quad (2.9.3)$$

In computing the velocity field of an incompressible fluid using analytical or numerical methods, it is convenient to have this constraint fulfilled at the outset, so that we can concentrate on satisfying boundary conditions and other restrictions that arise by balancing forces and torques, as will be discussed in later chapters.

To achieve this, we express the two components of the velocity in terms of a scalar function ψ called the *stream function*, as

$$u_x = \frac{\partial \psi}{\partial y}, \quad u_y = -\frac{\partial \psi}{\partial x}. \quad (2.9.4)$$

If the two velocity components derive from ψ by means of equations (2.9.4), then the satisfaction of the incompressibility constraint (2.9.3) is guaranteed. To see this, we substitute (2.9.4) into (2.9.3) and find

$$\frac{\partial^2 \psi}{\partial x \partial y} - \frac{\partial^2 \psi}{\partial y \partial x} = 0. \quad (2.9.5)$$

Since the order of partial differentiation with respect to the two independent spatial variables x and y is immaterial, the equality is satisfied.

Consider, for example, a two-dimensional flow with velocity components $u_x = Gx$ and $u_y = -Gy$, where G is a constant. Substituting these expressions into (2.9.3) we confirm that the fluid is incompressible. The stream function corresponding to this flow is given by $\psi = Gxy + c$, where c is an unspecified constant.

Uniqueness of the stream function

The example discussed in the last paragraph illustrates that the stream function of a specified two-dimensional flow is not unique. Cursorily inspection of equation (2.9.4) shows that an arbitrary constant may be added to a particular stream function to yield another perfectly acceptable stream function expressing the same flow. This ambiguity, however, is neither essential nor alarming. In performing analytical or numerical computation, the arbitrary constant simply provides us with one degree of freedom that we may use to simplify numerical and algebraic manipulations.

Physical interpretation

Consider the areal flow rate Q across a line that begins at the point A and ends at the point B , as illustrated in figure 2.6.1(a). Substituting expressions (2.9.4) into the right-hand side of equation (2.6.12), we find

$$Q = \int_A^B \left(\frac{\partial\psi}{\partial y} dy + \frac{\partial\psi}{\partial x} dx \right) = \int_A^B d\psi = \psi_B - \psi_A, \quad (2.9.6)$$

where ψ_A and ψ_B are the values of the stream function at points A and B . Equation (2.9.6) shows that the difference in the values of the stream function between two points is equal to the areal flow rate across a line that begins at the first point and ends at the second point. Because the fluid is incompressible, the flow rate is independent of the actual shape of the line, provided that the line begins and ends at the specified points.

Vorticity

The strength of the vorticity in two-dimensional flow was given in equation (2.3.15) in terms of derivatives of the velocity. Substituting expressions (2.9.4) into the right-hand side, we find

$$\omega_z = -\left(\frac{\partial^2\psi}{\partial x^2} + \frac{\partial^2\psi}{\partial y^2} \right) \equiv -\nabla^2\psi, \quad (2.9.7)$$

where $\nabla^2 \equiv \partial^2/\partial x^2 + \partial^2/\partial y^2$ is the Laplacian operator, to be discussed further in Section 3.2. Thus, the strength of the vorticity is equal to the negative of the Laplacian of the stream function. If the stream function satisfies Laplace's equation $\partial^2\psi/\partial x^2 + \partial^2\psi/\partial y^2 = 0$, in which case the stream function is called harmonic, then the velocity field is solenoidal and the flow is irrotational.

Plane polar coordinates

Departing from equations (2.9.4) and (2.3.15), and using the rules of coordinate transformation, we find that, in plane polar coordinates (r, θ) , the velocity components and strength of the vorticity are given by

$$\begin{aligned} u_r &= \frac{1}{r} \frac{\partial \psi}{\partial \theta}, & u_\theta &= -\frac{\partial \psi}{\partial r}, \\ \omega_z &= -\left[\frac{1}{r} \frac{\partial}{\partial r} \left(r \frac{\partial \psi}{\partial r} \right) + \frac{1}{r^2} \frac{\partial^2 \psi}{\partial \theta^2} \right] \equiv -\nabla^2 \psi. \end{aligned} \quad (2.9.8)$$

The expression enclosed by the square brackets in the expression for the vorticity is the Laplacian of the stream function expressed in plane polar coordinates.

2.9.3 Stream function for axisymmetric flow

Consider now an axisymmetric flow without swirling motion. Expressing all dependent and independent variables in (2.9.2) in cylindrical polar coordinates, and carrying out a fair amount of algebra using the chain rule, we find that the continuity equation takes the form of the following constraint on the axial and radial components of the velocity,

$$\frac{\partial u_x}{\partial x} + \frac{1}{\sigma} \frac{\partial (\sigma u_\sigma)}{\partial \sigma} = 0. \quad (2.9.9)$$

To ensure the satisfaction of this equation, we express the axial and radial components of the velocity in terms of the axisymmetric stream function ψ , also called the Stokes stream function, defined by the equations

$$u_x = \frac{1}{\sigma} \frac{\partial \psi}{\partial \sigma}, \quad u_\sigma = -\frac{1}{\sigma} \frac{\partial \psi}{\partial x}. \quad (2.9.10)$$

Straightforward algebra shows that the velocity components given in (2.9.10) satisfy the continuity equation (2.9.9) for any choice of ψ .

Consider, for example, an axisymmetric flow with velocity components $u_x = G x$ and $u_\sigma = -\frac{1}{2} G \sigma$, where G is a constant. Substituting these expressions into (2.9.9), we readily confirm that the left-hand side vanishes and the fluid is incompressible. The corresponding stream function is given by $\psi = \frac{1}{2} G x \sigma^2 + c$, where c is an unspecified constant.

Physical interpretation

Working as previously for two-dimensional flow, we find that the volumetric flow rate Q across an axisymmetric surface whose trace in a meridional plane starts at the point A and ends at the point B , as illustrated in figure 2.6.4, is equal to $\psi_B - \psi_A$ (problem 2.9.2). This result is consistent with the dimensions of the axisymmetric stream function, evident from equations (2.9.10), velocity multiplied by length squared; in contrast, the two-dimensional stream function has units of velocity multiplied by length.

Vorticity

The strength of the vorticity in an axisymmetric flow was given in equation (2.3.18) in terms of derivatives of the cylindrical polar components of the velocity. Using expressions (2.9.10), we find

$$\omega_\varphi = -\frac{1}{\sigma} E^2 \psi = -\frac{1}{\sigma} \left(\frac{\partial^2 \psi}{\partial x^2} + \frac{\partial^2 \psi}{\partial \sigma^2} - \frac{1}{\sigma} \frac{\partial \psi}{\partial \sigma} \right), \quad (2.9.11)$$

where E^2 is a second-order differential operator defined as

$$E^2 \equiv \frac{\partial^2}{\partial x^2} + \frac{\partial^2}{\partial \sigma^2} - \frac{1}{\sigma} \frac{\partial}{\partial \sigma}. \quad (2.9.12)$$

If the stream function is such that the right-hand side of (2.9.11) vanishes throughout the domain of flow, then the flow is irrotational.

Spherical polar coordinates

Departing from equations (2.9.10) and (2.3.18), and using the rules of coordinate transformation, we find that, in spherical polar coordinates (r, θ, φ) , the velocity components are given by

$$u_r = \frac{1}{r^2 \sin \theta} \frac{\partial \psi}{\partial \theta}, \quad u_\theta = -\frac{1}{r \sin \theta} \frac{\partial \psi}{\partial r}, \quad (2.9.13)$$

and the strength of the vorticity is given by

$$\omega_\varphi = -\frac{1}{r \sin \theta} E^2 \psi, \quad (2.9.14)$$

where E^2 is the second-order differential operator defined in (2.9.12); in spherical polar coordinates,

$$\begin{aligned} E^2 &\equiv \frac{\partial^2}{\partial r^2} + \frac{\sin \theta}{r^2} \frac{\partial}{\partial \theta} \left(\frac{1}{\sin \theta} \frac{\partial}{\partial \theta} \right) \\ &= \frac{\partial^2}{\partial r^2} + \frac{1}{r^2} \frac{\partial^2}{\partial \theta^2} - \frac{\cot \theta}{r^2} \frac{\partial}{\partial \theta}. \end{aligned} \quad (2.9.15)$$

Problems

Problem 2.9.1 *Stream function of two-dimensional flow.*

Derive the Cartesian components of the velocity and the strength of the vorticity, and discuss the nature of the flow corresponding to the stream functions (a) $\psi = \frac{1}{2} a y^2$, and (b) $\psi = \frac{1}{2} a (x^2 - y^2)$, where a is a constant.

Problem 2.9.2 *Stream function of axisymmetric flow.*

Substitute expressions (2.9.10) into the right-hand side of (2.6.27) and perform the integration to show that $Q = \psi_B - \psi_A$, as stated in the text.

2.10 Kinematic conditions at boundaries

In practice, a flow always occurs in a domain that is bounded by stationary or moving surfaces with a variety of constitutions and physical properties. Examples include the flow in an internal combustion engine generated by the motion of an engine piston, the flow induced by the motion of an aircraft or ground vehicle, the flow induced by the sedimentation of an aerosol particle in the atmosphere, the flow induced by a small bubble rising in a carbonated beverage, and the flow induced by the motion of an elephant running through the savannah to escape a mouse.

In the context of flow kinematics, flow boundaries are classified into four main categories as follows:

1. *Impermeable solid boundaries.* Examples include the surface of a rigid or flexible solid body, such as a vibrating radio antenna or a swimming microorganism.

2. *Permeable solid boundaries.* Examples include the surface of a porous medium, such as a rock bed or a biological tissue composed of cells with gaps in the intervening spaces.
3. *Sharp interfaces* between immiscible fluids. Examples include the free surface of the ocean, and the interface between oil and vinegar in salad dressing.
4. *Diffuse interfaces* between miscible fluids. Examples include the fuzzy edge of a river discharging into the ocean, and the ambiguous edge of a smoke ring rising in still air.

2.10.1 The no-penetration boundary condition

By definition, a point particle moving with the fluid velocity may not cross an impermeable solid boundary or a sharp interface between two immiscible fluids, but is required to lie on one side at all times. As a consequence, the velocity of a point particle that lies on a stationary or moving impermeable boundary or a sharp interface must be compatible with, but not necessarily equal to, the velocity of the boundary or interface. To ensure this compatibility, we require the *no-penetration boundary condition*.

The no-penetration condition at an impermeable boundary

Consider a flow that is bounded by an impermeable solid boundary. The no-penetration condition requires that the component of the fluid velocity normal to the boundary be equal to the component of the boundary velocity normal to its instantaneous shape; the tangential component of the velocity can be arbitrary. If, in particular, the boundary is stationary, the normal component of the fluid velocity must vanish.

To derive the mathematical statement of the no-penetration condition, we introduce the unit vector normal to the boundary at a point, denoted by \mathbf{n} , and the velocity of the boundary \mathbf{v}^B , where the orientation of \mathbf{n} is left unspecified. If the boundary is stationary, the boundary velocity \mathbf{v}^B vanishes, and if the boundary translates as a rigid body, \mathbf{v}^B is constant. If the boundary rotates or exhibit some type of deformation, then \mathbf{v}^B is a function of position, as will be discussed later in this section. In all cases, the no-penetration boundary condition requires

$$\mathbf{u} \cdot \mathbf{n} = \mathbf{v}^B \cdot \mathbf{n}, \quad (2.10.1)$$

where both sides are evaluated at a point on the boundary.

Rigid-body motion

Consider an impermeable rigid boundary translating with velocity \mathbf{U}^B , and rotating around a specified center of rotation \mathbf{x}_R with angular velocity $\boldsymbol{\Omega}^B$. The angular velocity vector $\boldsymbol{\Omega}^B$ passes through the center of rotation \mathbf{x}_R , and its magnitude and orientation express the speed and direction of rotation. As we look down at the angular velocity vector from above, the body rotates in the counterclockwise direction.

In terms of the velocity of translation and angular velocity of rotation, the velocity at a point \mathbf{x} that lies on the boundary is given by the expression

$$\mathbf{v}^B = \mathbf{U}^B + \boldsymbol{\Omega}^B \times (\mathbf{x} - \mathbf{x}_R), \quad (2.10.2)$$

where \times denotes the outer vector product defined in equation (2.3.4). In component form,

$$\begin{aligned} \mathbf{v}^B &= \mathbf{e}_x [U_x^B + \Omega_y^B (z - z_R) - \Omega_z^B (y - y_R)] \\ &+ \mathbf{e}_y [U_y^B + \Omega_z^B (x - x_R) - \Omega_x^B (z - z_R)] \\ &+ \mathbf{e}_z [U_z^B + \Omega_x^B (y - y_R) - \Omega_y^B (x - x_R)], \end{aligned} \quad (2.10.3)$$

where \mathbf{e}_x , \mathbf{e}_y , and \mathbf{e}_z are the unit vectors parallel to the x , y , or z axis.

In the case of two-dimensional flow in the xy plane, the z component of the velocity vanishes, $U_z^B = 0$, and the angular velocity vector is parallel to the z axis, $\Omega_x^B = 0$, $\Omega_y^B = 0$, yielding the simplified form

$$\mathbf{v}^B = \mathbf{e}_x [U_x^B - \Omega_z^B (y - y_R)] + \mathbf{e}_y [U_y^B + \Omega_z^B (x - x_R)]. \quad (2.10.4)$$

The no-penetration boundary condition arises by substituting expression (2.10.3) or (2.10.4) into the right-hand side of (2.10.1), respectively, for three-dimensional or two-dimensional flow. If the boundary is stationary, $\mathbf{v}^B = \mathbf{0}$ we obtain the simple form

$$\mathbf{u} \cdot \mathbf{n} = 0. \quad (2.10.5)$$

The no-penetration condition in terms of the stream function

Consider an incompressible fluid in two-dimensional flow, and express the velocity in terms of the stream function ψ defined in equations (2.9.4). The no-penetration condition (2.10.1) requires

$$u_x n_x + u_y n_y = \frac{\partial \psi}{\partial y} n_x - \frac{\partial \psi}{\partial x} n_y = \mathbf{v}^B \cdot \mathbf{n}. \quad (2.10.6)$$

To this end, we use expressions (2.6.2) for the components of the normal vector in terms of differential displacements along the boundary, and obtain

$$\frac{\partial \psi}{\partial y} \frac{dy}{dl} + \frac{\partial \psi}{\partial x} \frac{dx}{dl} = \frac{d\psi}{dl} = \mathbf{v}^B \cdot \mathbf{n}, \quad (2.10.7)$$

where dl is the differential of the arc length measured along the boundary from an arbitrary origin.

If the boundary is stationary, the right-hand side of (2.10.7) vanishes, leaving the condition $d\psi/dl = 0$: the stream function over a stationary impermeable boundary is constant, and the no-penetration condition takes the form

$$\psi = \psi_0, \quad (2.10.8)$$

where ψ_0 is a constant that is either assigned arbitrarily or computed as part of the solution.

Similar arguments reveal that the stream function is also constant over a stationary boundary in axisymmetric flow (problem 2.10.2(b)).

2.10.2 The no-penetration condition at a sharp interface

Consider now the no-penetration condition over a stationary or moving sharp interface separating two immiscible fluids. Physical arguments require that the normal component of the fluid velocity on one side of the interface be equal to the normal component of the velocity on the other side. To derive the mathematical statement of this condition, we introduce the velocity on one side of the interface, denoted by $\mathbf{u}^{(1)}$, and the velocity on the other side of the interface, denoted by $\mathbf{u}^{(2)}$, and require

$$\mathbf{u}^{(1)} \cdot \mathbf{n} = \mathbf{u}^{(2)} \cdot \mathbf{n}, \quad (2.10.9)$$

where both sides of (2.10.9) are evaluated at a point on the interface, and the direction of the unit normal vector \mathbf{n} is left unspecified.

Problems

Problem 2.10.1 *Shifting the center of rotation.*

The center of rotation of a rigid body may be placed at any arbitrary point. Suppose that we choose the point \mathbf{x}'_R instead of the point \mathbf{x}_R discussed in the text. The counterpart of equation (2.10.2) is

$$\mathbf{v}^B = \mathbf{U}'^B + \boldsymbol{\Omega}'^B \times (\mathbf{x} - \mathbf{x}'_R). \quad (2.10.10)$$

By setting the right-hand side of (2.10.10) equal to the right-hand side of (2.10.2), derive expressions for \mathbf{U}'^B and $\boldsymbol{\Omega}'^B$ in terms of \mathbf{U}^B and $\boldsymbol{\Omega}^B$, and vice versa.

Problem 2.10.2 *Stream functions.*

(a) Use the no-penetration boundary condition to derive an expression for the stream function over a translating but non-rotating two-dimensional impermeable boundary.

(b) Show that the no-penetration condition over a stationary boundary in axisymmetric flow takes the form expressed by (2.10.8).

Chapter 3

Flow Computation based on Kinematics

- 3.1 Flow classification based on kinematics**
- 3.2 Irrotational flows and the velocity potential**
- 3.3 Finite-difference methods**
- 3.4 Linear solvers**
- 3.5 Two-dimensional point sources and point-source dipoles**
- 3.6 Three-dimensional point sources and point-source dipoles**
- 3.7 Point vortices and line vortices**

Flows are classified according to the vorticity distribution as *irrotational* flows wherein the vorticity vanishes throughout the domain of flow, *vortex* flows characterized by the presence of compact regions of concentrated vorticity in an otherwise irrotational fluid, and *rotational* flows wherein the vorticity is significant throughout the domain of flow. In this chapter, we discuss the kinematical structure and mathematical description of the simplest class of irrotational flows. Specifically, we develop finite-difference methods for computing the velocity field from knowledge of the velocity distribution over the boundaries, and derive a class of elementary irrotational flows that serve as building blocks for generating desired solutions. Complementary building blocks associated with elementary vortex flows will provide us with additional degrees of freedom and will allow us to address more general configurations pertinent to a broader class of flow conditions.

3.1 Flow classification based on kinematics

In Chapters 1 and 2, we have discussed general kinematical features of a flow with special reference to the motion of fluid parcels and in-

finitesimal point particles. Further progress can be made in two ways: we may either study flows on a case-by-case basis and then attempt generalization by critical comparison; or we may establish a taxonomy, that is, classify flows into general categories according to some sensible criteria. The second approach is desirable from the fundamental standpoint of the physical scientist as well as from the practical standpoint of the computational scientist or engineer.

On the basis of kinematics alone, flows are classified into three main categories including: (a) irrotational flows, (b) flows containing compact regions of intense vorticity, called vortices, embedded in an otherwise perfectly or nearly irrotational fluid, and (c) rotational flows with distributed vorticity.

3.1.1 Irrotational flows

The first category includes flows wherein the vorticity vector vanishes, and thus the magnitude of the vorticity is equal to zero, throughout the domain of flow. According to our discussion in Chapter 2, a small spherical fluid parcel in a three-dimensional irrotational flow, or a discoidal fluid parcel in a two-dimensional irrotational flow, translates and deforms but does not rotate.

A perfectly irrotational flow is a mathematical idealization; in practice, a small amount of vorticity is almost always present, and a real-life nominally irrotational flow is nearly but not perfectly irrotational. An example of a nearly irrotational flow is high-speed flow past a slender airfoil under conditions of no-stall, as will be discussed in Chapter 12 in the context of aerodynamics.

3.1.2 Vortex flows

The second category includes flows that contain well-defined compact regions wherein the magnitude of the vorticity is significant, embedded in an otherwise irrotational fluid. These vortical regions may not be neglected without introducing serious discrepancies and error, or without compromising the physics of the flow under consideration. In practice, regions where the vorticity is significant appear in the form of narrow layers, thin filaments, and compact structures including wakes behind bluff bodies, tornados and swirls. An example of a vortex flow familiar to the aircraft traveler is the flow associated with a high-speed jet emerging from a turbine engine.

3.1.3 Rotational flows

The third category includes flows wherein the vorticity is significant throughout the domain of flow. The distinction between vortex flows and rotational flows is somewhat vague, and there are flows that may be classified in either category. We shall see in subsequent chapters, however, that vortex flows may be analyzed and computed using a special class of numerical methods, called vortex methods for flow simulation, and the availability of these methods provides us with a distinguishing, albeit somewhat artificial criterion.

3.1.4 Flows in nature and technology

Flows in nature and technology are typically rotational; examples include the flow due to a small particle settling in the atmosphere, the flow through a turbine engine, and blood flow in the heart and through blood vessels and capillaries. High-speed flows tend to develop regions of concentrated vorticity and are typically classified as vortex flows. High-speed turbulent flows, in particular, contain random collections of rapidly evolving vortices called eddies or coherent structures, embedded in a low- or moderate-vorticity background fluid.

Irrotational flows are simplified models of vortex flows that emerge by neglecting the regions of concentrated vorticity, or else by shifting the actual boundaries of the flow to the edges of the vortex regions, thereby placing them outside the domain of flow.

A considerable amount of physical insight and experience is necessary in order to predict whether a flow will develop to become a nearly irrotational flow, a rotational flow, or a vortex flow. Insights may be gained by studying model problems that are amenable to analytical and simple numerical methods, and also by analyzing the laws governing the generation and evolution of the vorticity field, to be discussed in future chapters.

3.1.5 Flow computation

The difficulty of computing flows increases in the following ascending order: irrotational flows, vortex flows, and rotational flows; exceptions to this general rule arise in special cases.

Our discussion of analytical and computational methods for flow computation begins in this chapter by considering the most amenable class

of irrotational flows. In the context of kinematics, the problem to be solved can be stated as follows: given the boundary geometry and the velocity distribution over the boundaries, compute the structure of a steady irrotational flow or the evolution of an unsteady irrotational flow from a specified initial state.

3.2 Irrotational flows and the velocity potential

The vorticity of a three-dimensional flow was defined in equation (2.3.6) as the curl of the velocity. The scalar strength of the vorticity of a two-dimensional flow was defined in equation (2.3.15), and the scalar strength of the vorticity of an axisymmetric flow was defined in equation (2.3.18). If the flow is irrotational, the structure of the velocity field must be such that the right-hand sides of these equations vanish.

3.2.1 Two-dimensional flow

Consider a two-dimensional irrotational flow in the xy plane. Setting the left-hand side of equation (2.3.15) equal to zero, we obtain a constraint on selected partial derivatives of the velocity,

$$\frac{\partial u_y}{\partial x} = \frac{\partial u_x}{\partial y}. \quad (3.2.1)$$

To compute a two-dimensional irrotational flow, we may either choose to compute the two velocity components individually subject to constraints imposed by the continuity equation and by the boundary conditions, while ensuring that (3.2.1) is fulfilled at every point in the flow, or we may choose to satisfy (3.2.1) at the outset and then concentrate on fulfilling the rest of the requirements. It should not be surprising that the second approach is much more expedient and has become the standard choice.

The velocity potential

The key idea is to introduce a new scalar function ϕ called the *velocity potential*, such that the two velocity components derive from ϕ by the relations

$$u_x = \frac{\partial \phi}{\partial x}, \quad u_y = \frac{\partial \phi}{\partial y}. \quad (3.2.2)$$

In vector notation, equations (3.2.2) are expressed by the compact form

$$\mathbf{u} = \nabla\phi, \quad (3.2.3)$$

where $\nabla\phi = (\partial\phi/\partial x, \partial\phi/\partial y)$ is the two-dimensional gradient of the potential. The velocity, and thus the potential ϕ , is a function of position (x, y, z) and, in the case of unsteady flow, time t . Inspection of (3.2.2) reveals that the velocity potential has dimensions of velocity multiplied by length, which amounts to length squared divided by time.

It is straightforward to verify that, if the velocity components derive from ϕ in terms of equations (3.2.2), then the irrotationality constraint (3.2.1) is automatically satisfied: substituting expressions (3.2.2) into (3.2.1), we find

$$\frac{\partial^2\phi}{\partial x\partial y} = \frac{\partial^2\phi}{\partial y\partial x}. \quad (3.2.4)$$

Since the order of partial differentiation with respect to two independent spatial variables x and y may be interchanged, relation (3.2.1) is satisfied. Accordingly, an irrotational flow is also called a *potential flow* and vice-versa.

It is important to observe that the velocity potential of a certain irrotational flow is not defined uniquely. Given a particular potential, an arbitrary constant may be added to it to produce another perfectly acceptable potential. This ambiguity, however, is neither essential nor alarming. In performing analytical or numerical computation, the arbitrary constant is determined by requiring a proper constraint, as will be discussed in subsequent sections.

Given the velocity field of an irrotational flow, we may derive the corresponding potential by integrating the system of differential equations (3.2.2), where the left-hand sides are treated as knowns. Consider, for example, unidirectional streaming flow with velocity components given by

$$u_x = V_x, \quad u_y = V_y, \quad (3.2.5)$$

where V_x and V_y are two constant velocities. Integrating the first of equations (3.2.2), we find that the potential must take the form $\phi = x V_x + f(y)$, where $f(y)$ is an unknown function of y . Differentiating both sides of this equation with respect to y , and using the second of equations (3.2.2), we find $df/dy = V_y$, which may be integrated to give $f(y) = y V_y + c$, where c is an arbitrary constant. Combining these expressions, we find that the velocity potential corresponding to (3.2.5) is given by

$$\phi = x V_x + y V_y + c. \quad (3.2.6)$$

In agreement with our previous observation, the velocity potential is defined uniquely only up to the arbitrary constant c .

Computation of the potential based on kinematics

The automatic satisfaction of (3.2.1) by use of the velocity potential is helpful, but we still require one equation, or a system of equations, that will allow us to compute the potential. Normally, these equations would have to be derived by considering the forces and torques exerted on the surface and over the volume of small fluid parcels, as will be discussed in subsequent chapters with reference to the more general class of rotational flows. Fortunately, in the case of irrotational flow, this is not necessary: *Given the boundary distribution of the velocity, an irrotational flow may be computed exclusively on the basis of kinematics.*

3.2.2 Incompressible fluids and the harmonic potential

If the fluid is incompressible, conservation of mass requires that the velocity field be solenoidal, which means that the velocity components must satisfy the constraint expressed by the continuity equation (2.9.2) presented explicitly in (2.9.3) for two-dimensional flow. Substituting expressions (3.2.2) into (2.9.3), we find

$$\frac{\partial^2 \phi}{\partial x^2} + \frac{\partial^2 \phi}{\partial y^2} = 0, \quad (3.2.7)$$

which is *Laplace's equation* in two dimensions. It is convenient to define the two-dimensional Laplacian operator, $\nabla^2 \equiv \partial^2/\partial x^2 + \partial^2/\partial y^2$, and recast (3.2.7) into the more compact form

$$\nabla^2 \phi = 0. \quad (3.2.8)$$

A function that satisfies Laplace's equation (3.2.7) or (3.2.8) is called *harmonic*.

It is instructive to derive Laplace's equation working in vector notation. Substituting (3.2.3) into (2.9.2), we find

$$\nabla \cdot \mathbf{u} = \nabla \cdot (\nabla \phi) \equiv \nabla^2 \phi = 0, \quad (3.2.9)$$

which identifies the Laplacian operator with the divergence of the gradient, $\nabla^2 = \nabla \cdot \nabla$.

Laplace's equation (3.2.8) is a statement of mass conservation for an incompressible fluid. Although time does not appear explicitly in this equation, the velocity field, and thus the velocity potential, will be time-dependent when the flow is unsteady. The absence of explicit time dependence classifies the irrotational flow of an incompressible fluid as a *quasi-steady flow*, meaning that the instantaneous structure of the flow depends on the instantaneous boundary geometry and boundary conditions, and is independent of the motion at previous times. Thus, if all boundaries are stationary at a particular time, the fluid will also be stationary at that time, independent of the history of fluid and boundary motion.

Laplace's equation arises in a broad range of contexts within and beyond fluid mechanics. For example, it governs the steady-state distribution of temperature in a conductive material such as a fin or a cooling plate.

3.2.3 Three-dimensional flow

The foregoing analysis may be extended in a straightforward manner to three-dimensional flow. The velocity components of a three-dimensional flow derive from the velocity potential by the equations

$$u_x = \frac{\partial \phi}{\partial x}, \quad u_y = \frac{\partial \phi}{\partial y}, \quad u_z = \frac{\partial \phi}{\partial z}. \quad (3.2.10)$$

The velocity components, and thus the potential ϕ , are functions of position (x, y, z) and, if the flow is unsteady, time t .

If the fluid is incompressible, the velocity potential is a harmonic function; that is, it satisfies the counterpart of Laplace's equation (3.2.9) for three-dimensional flow,

$$\nabla \cdot \mathbf{u} = \nabla \cdot (\nabla \phi) \equiv \nabla^2 \phi \equiv \frac{\partial^2 \phi}{\partial x^2} + \frac{\partial^2 \phi}{\partial y^2} + \frac{\partial^2 \phi}{\partial z^2} = 0, \quad (3.2.11)$$

where $\nabla^2 \equiv \partial^2/\partial x^2 + \partial^2/\partial y^2 + \partial^2/\partial z^2$ is the Laplacian operator in three dimensions. A function that satisfies Laplace's equation is called harmonic.

3.2.4 Boundary conditions

Viewed from a mathematical standpoint, Laplace's equation in two or three dimensions is a second-order partial differential equation that is classified as *elliptic*. One implication of this classification is that, in order to compute the solution, we must have available one scalar boundary condition for ϕ , one of its *first* partial derivatives, or a combination thereof, along each boundary.

Impermeable boundaries

Over an *impermeable* solid boundary, we require the no-penetration condition discussed in Section 2.10. If the boundary is stationary, we require the condition $\mathbf{u} \cdot \mathbf{n} = 0$, where \mathbf{n} is the unit vector normal to the boundary pointing either into or outward from the domain of flow. Using equations (3.2.2), we find that, in the case of two-dimensional flow,

$$n_x \frac{\partial \phi}{\partial x} + n_y \frac{\partial \phi}{\partial y} = 0. \quad (3.2.12)$$

This is a boundary condition for the normal component of the gradient of the potential, which is equal to the derivative with respect to distance normal to the boundary, called a *Neumann* boundary condition. Because the right-hand side of (3.2.12) is equal to zero, this boundary condition is *homogeneous*.

Permeable boundaries

Over a *permeable* boundary, we may specify the tangential component of the velocity and leave the normal component unspecified. To implement this condition in the case of two-dimensional flow, we introduce the unit vector tangential to the boundary, denoted by \mathbf{t} , whose components are given in equations (2.6.1). The tangential component of the velocity in the direction of \mathbf{t} is given by the inner product

$$u_t \equiv \mathbf{u} \cdot \mathbf{t} = t_x \frac{\partial \phi}{\partial x} + t_y \frac{\partial \phi}{\partial y} = \frac{dx}{dl} \frac{\partial \phi}{\partial x} + \frac{dy}{dl} \frac{\partial \phi}{\partial y} = \frac{\partial \phi}{\partial l}, \quad (3.2.13)$$

where l is the arc length measured in the direction of \mathbf{t} .

If the distribution of ϕ over the boundary is known, the right-hand side of (3.2.13) may be computed by differentiating the potential with respect to arc length using analytical or numerical methods. This observation suggests that, instead of specifying the tangential component of

the velocity, we may alternatively specify the boundary distribution of the potential. A boundary condition for the distribution of the potential is a *Dirichlet* boundary condition.

A word of caution is in order here: if the flow is bounded by a number of disconnected boundaries, replacing the boundary condition for the tangential velocity with a boundary condition for the distribution of the potential is permissible only over one boundary, otherwise inconsistencies may arise.

3.2.5 Cylindrical polar coordinates

Consider a three-dimensional irrotational flow, and introduce the cylindrical polar coordinates (x, σ, φ) depicted in figure 1.3.2. Using expressions (2.1.34), we find that the cylindrical polar components of the velocity are given by

$$u_x = \frac{\partial \phi}{\partial x}, \quad u_\sigma = \frac{\partial \phi}{\partial \sigma}, \quad u_\varphi = \frac{1}{\sigma} \frac{\partial \phi}{\partial \varphi}. \quad (3.2.14)$$

Laplace's equation for the harmonic potential reads

$$\nabla^2 \phi \equiv \frac{\partial^2 \phi}{\partial x^2} + \frac{1}{\sigma} \frac{\partial}{\partial \sigma} \left(\sigma \frac{\partial \phi}{\partial \sigma} \right) + \frac{1}{\sigma^2} \frac{\partial^2 \phi}{\partial \varphi^2} = 0. \quad (3.2.15)$$

If the flow is axisymmetric, the velocity potential is a function of x and σ but not of φ , as required for u_φ to vanish.

3.2.6 Spherical polar coordinates

Consider now a three-dimensional irrotational flow, and introduce the spherical coordinates (r, θ, φ) depicted in figure 1.3.3. Using relations (2.1.36), we find that the spherical polar components of the velocity are given by

$$u_r = \frac{\partial \phi}{\partial r}, \quad u_\theta = \frac{1}{r} \frac{\partial \phi}{\partial \theta}, \quad u_\varphi = \frac{1}{r \sin \theta} \frac{\partial \phi}{\partial \varphi}. \quad (3.2.16)$$

Laplace's equation for the harmonic potential takes the form

$$\nabla^2 \phi \equiv \frac{1}{r^2} \frac{\partial}{\partial r} \left(r^2 \frac{\partial \phi}{\partial r} \right) + \frac{1}{r^2 \sin \theta} \frac{\partial}{\partial \theta} \left(\sin \theta \frac{\partial \phi}{\partial \theta} \right) + \frac{1}{r^2 \sin^2 \theta} \frac{\partial^2 \phi}{\partial \varphi^2} = 0. \quad (3.2.17)$$

If the flow is axisymmetric, the velocity potential is a function of r and θ but not of φ , as required for u_φ to vanish.

3.2.7 Plane polar coordinates

Consider finally a two-dimensional irrotational flow, and introduce the plane polar coordinates (r, θ) depicted in figure 1.3.4. Using relations (2.1.38), we find that the plane polar components of the velocity are given by

$$u_r = \frac{\partial \phi}{\partial r}, \quad u_\theta = \frac{1}{r} \frac{\partial \phi}{\partial \theta}. \quad (3.2.18)$$

Laplace's equation for the harmonic potential takes the form

$$\nabla^2 \phi \equiv \frac{1}{r} \frac{\partial}{\partial r} \left(r \frac{\partial \phi}{\partial r} \right) + \frac{1}{r^2} \frac{\partial^2 \phi}{\partial \theta^2} = 0. \quad (3.2.19)$$

Problems

Problem 3.2.1 *Deriving the velocity potential.*

(a) Consider a two-dimensional flow with velocity components given by

$$u_x = V \cos(kx) e^{-ky}, \quad u_y = -V \sin(kx) e^{-ky}, \quad (3.2.20)$$

where V and k are two constants. Confirm that this flow is irrotational, derive the corresponding velocity potential, and investigate whether or not the potential is harmonic and explain why. Sketch the streamline pattern, and discuss the structure of this flow and the physical interpretation of the constant k .

(b) Consider a three-dimensional flow with velocity components

$$\begin{aligned} u_x &= \frac{V k_x}{\sqrt{k_x^2 + k_y^2}} \cos(k_x x) \sin(k_y y) e^{-z\sqrt{k_x^2 + k_y^2}}, \\ u_y &= \frac{V k_y}{\sqrt{k_x^2 + k_y^2}} \sin(k_x x) \sin(k_y y) e^{-z\sqrt{k_x^2 + k_y^2}}, \\ u_z &= -V \sin(k_x x) \cos(k_y y) e^{-z\sqrt{k_x^2 + k_y^2}}, \end{aligned} \quad (3.2.21)$$

where V, k_x , and k_y , are three constants. This is the three-dimensional version of the two-dimensional flow discussed in (a). Confirm that this flow is irrotational, derive the corresponding velocity potential, and investigate whether or not the potential is harmonic and explain why. Discuss the structure of this flow and the physical interpretation of the constants k_x and k_y .

(c) Explain why it is not possible to find a velocity potential for *simple shear flow* along the x axis varying along the y axis, whose velocity components are given by $u_x = ky, u_y = 0$, and $u_z = 0$, where k is a constant with dimensions of inverse time called the shear rate.

Problem 3.2.2 *Irrotational flow in cylindrical polar coordinates.*

Verify by direct substitution that the potential

$$\phi = U x \left(1 + \frac{1}{2} \frac{a^3}{(x^2 + \sigma^2)^{3/2}} \right), \quad (3.2.22)$$

where U and a are constants, satisfies Laplace's equation (3.2.15), and discuss the structure of the axisymmetric flow represented by this potential.

Problem 3.2.3 *Irrotational flow in spherical polar coordinates.*

Verify by direct substitution that the potential

$$\phi = U r \cos \theta \left(1 + \frac{1}{2} \frac{a^3}{r^3} \right), \quad (3.2.23)$$

where U and a are constants, satisfies Laplace's equation (3.2.17), and discuss the structure of the axisymmetric flow represented by this potential.

Problem 3.2.4 *Irrotational flow in plane polar coordinates.*

Verify by direct substitution that the potential

$$\phi = U r \cos \theta \left(1 + \frac{a^2}{r^2} \right) + \frac{\kappa}{2\pi} \theta, \quad (3.2.24)$$

where κ, U and a are constants, satisfies Laplace's equation (3.2.19), and discuss the structure of the two-dimensional flow represented by this potential.

3.3 Finite-difference methods

In practice, Laplace's equation for the harmonic potential is typically solved using numerical methods, with the finite-difference method being a common choice. To illustrate the implementation of the method, we consider two-dimensional potential flow in the xy plane within a rectangular domain confined between

$$a_x < x < b_x, \quad a_y < y < b_y, \quad (3.3.1)$$

as illustrated in figure 3.3.1. The left, bottom, and right walls are impermeable, whereas the top wall is exposed to an external flow.

3.3.1 Boundary conditions

Before attempting to compute the solution, we must decide on the required boundary conditions. Over the left wall, the unit vector normal to the wall pointing into the flow is given by $\mathbf{n} = (1, 0)$. Accordingly, the no-penetration condition (3.2.12) provides us with the Neumann boundary condition

$$\frac{\partial \phi}{\partial x} = 0 \quad \text{at} \quad x = a_x. \quad (3.3.2)$$

Over the bottom wall, the unit vector normal to the wall pointing into the flow is given by $\mathbf{n} = (0, 1)$. Accordingly, the no-penetration condition (3.2.12) provides us with the Neumann boundary condition

$$\frac{\partial \phi}{\partial y} = 0 \quad \text{at} \quad y = a_y. \quad (3.3.3)$$

Over the right wall, the unit vector normal to the wall pointing into the flow is given by $\mathbf{n} = (-1, 0)$. Accordingly, the no-penetration condition (3.2.12) provides us with the Neumann boundary condition

$$\frac{\partial \phi}{\partial x} = 0 \quad \text{at} \quad x = b_x. \quad (3.3.4)$$

Over the top wall, we *stipulate* that the tangential component of the velocity is constant and equal to V ; this is just one choice that we adopt for the purpose of illustration; other choices reflect different flow conditions. Since the top wall is parallel to the x axis, the unit tangent vector over it is given by $\mathbf{t} = (1, 0)$. Accordingly, expression (3.2.13) provides us with the Neumann boundary condition

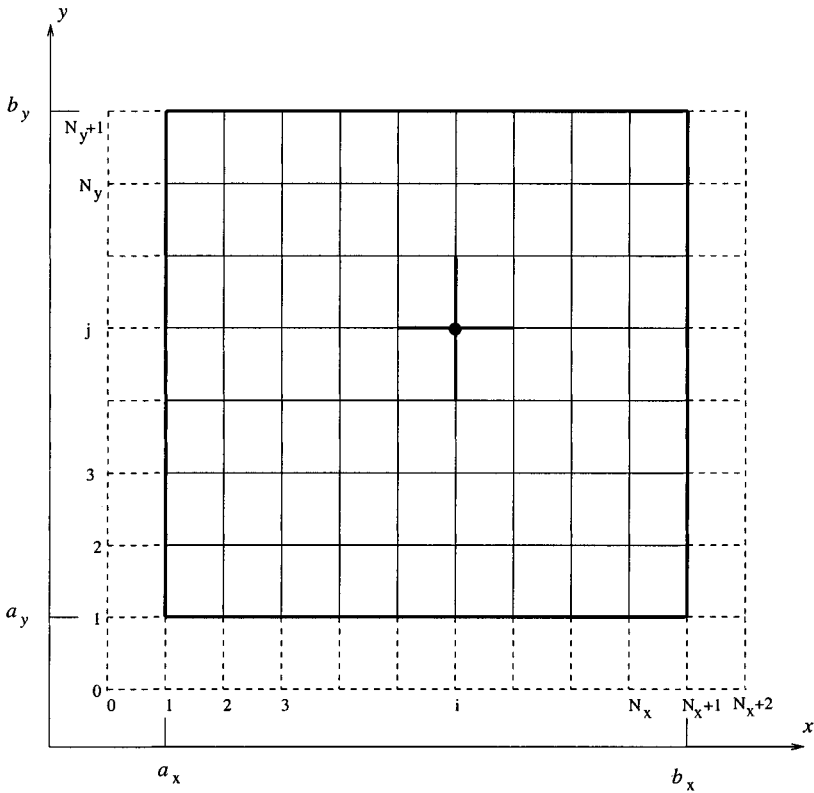


Figure 3.3.1 A Cartesian grid used to compute the harmonic potential of an irrotational flow in a rectangular domain. The solution is found by solving Laplace's equation using a finite-difference method.

$$u_t \equiv \mathbf{u} \cdot \mathbf{t} = \frac{\partial \phi}{\partial x} = V \quad \text{at} \quad y = b_y. \quad (3.3.5)$$

Straightforward integration of (3.3.5) with respect to x shows that this condition is equivalent to the Dirichlet boundary condition

$$\phi = Vx + c \quad \text{at} \quad y = b_y, \quad (3.3.6)$$

where c is an arbitrary constant that may be set equal to zero without any consequences on the structure of the flow.

The problem formulation is now complete, and we proceed to compute the solution. Our task is to solve Laplace's equation (3.2.7) subject to the four boundary conditions expressed by equations (3.3.2)-(3.3.4), and (3.3.6).

3.3.2 Finite-difference grid

We begin implementing the finite-difference method by dividing the x interval (a_x, b_x) into N_x evenly spaced sub-intervals separated by the spacing $\Delta x = (b_x - a_x)/N_x$, and draw vertical grid lines at $x = x_i$, where

$$x_i = a_x + (i - 1) \Delta x, \quad (3.3.7)$$

for $i = 1, 2, \dots, N_x + 1$, as shown in figure 3.3.1.

Similarly, we divide the y interval (a_y, b_y) into N_y evenly spaced sub-intervals separated by the spacing $\Delta y = (b_y - a_y)/N_y$, and draw horizontal grid lines at $y = y_j$, where

$$y_j = a_y + (j - 1) \Delta y, \quad (3.3.8)$$

for $j = 1, 2, \dots, N_y + 1$, as shown in figure 3.3.1.

The intersections of the vertical and horizontal grid lines define *grid-points* or *nodes*. For convenience, we denote the value of the harmonic potential ϕ at the (i, j) node as

$$\phi_{i,j} \equiv \phi(x_i, y_j). \quad (3.3.9)$$

The Dirichlet boundary condition (3.3.6) provides us with the values

$$\phi_{i, N_y + 1} = V x_i. \quad (3.3.10)$$

where we have set $c = 0$. Our objective is to compute the remaining unknown values $\phi_{i,j}$ at the grid-points $i = 1, 2, \dots, N_x + 1$ and $j = 1, 2, \dots, N_y$; a total of $N_u = (N_x + 1)N_y$ unknowns.

3.3.3 Finite-difference discretization

To build a system of equations for the unknowns, we require the satisfaction of Laplace's equation (3.2.7) at the (i, j) grid-point, and approximate the second partial derivatives with finite differences. Using formula (2.5.8), we introduce the approximations

$$\left(\frac{\partial^2 \phi}{\partial x^2}\right)_{i,j} \simeq \frac{\phi_{i+1,j} - 2\phi_{i,j} + \phi_{i-1,j}}{\Delta x^2}, \quad (3.3.11)$$

and

$$\left(\frac{\partial^2 \phi}{\partial y^2}\right)_{i,j} \simeq \frac{\phi_{i,j+1} - 2\phi_{i,j} + \phi_{i,j-1}}{\Delta y^2}, \quad (3.3.12)$$

and transform the *differential* equation (3.2.7) to the *algebraic* equation

$$\frac{\phi_{i+1,j} - 2\phi_{i,j} + \phi_{i-1,j}}{\Delta x^2} + \frac{\phi_{i,j+1} - 2\phi_{i,j} + \phi_{i,j-1}}{\Delta y^2} = 0. \quad (3.3.13)$$

Rearranging the left-hand side, we obtain

$$\phi_{i+1,j} - 2(1 + \beta)\phi_{i,j} + \phi_{i-1,j} + \beta\phi_{i,j+1} + \beta\phi_{i,j-1} = 0, \quad (3.3.14)$$

where we have defined the square of the grid-spacing ratio,

$$\beta \equiv \left(\frac{\Delta x}{\Delta y}\right)^2. \quad (3.3.15)$$

We can apply equation (3.3.13), or its equivalent (3.3.14), at the *interior* grid-points $i = 2, 3, \dots, N_x$ and $j = 2, 3, \dots, N_y$, and thus obtain $N_{fde} = (N_x - 1)(N_y - 1)$ finite-difference equations. But if we apply this equation at a boundary grid-point, we will find that one grid point involved in the finite-difference approximation lies in the exterior of the flow domain, and is thus not defined. We must somehow generate a number of

$$N_u - N_{fde} = (N_x + 1)N_y - (N_x - 1)(N_y - 1) = N_x + 2N_y - 1 \quad (3.3.16)$$

additional equations.

The missing equations must originate from the Neumann boundary conditions on the left, bottom, and right walls where the no-penetration condition is required. One way to implement these boundary conditions with an error that is comparable to that of the finite-difference approximations (3.3.11) and (3.3.12), is to extend the domain of solution beyond the physical boundaries of the flow, and introduce the *fictitious* or *phantom* grid lines located at

$$x = x_0 = a_x - \Delta x, \quad y = y_0 = a_y - \Delta y,$$

$$x = x_{N_x+2} = b_x + \Delta x. \quad (3.3.17)$$

Having introduced these extensions, we may use the second-order finite difference approximation (2.5.6) to recast the Neumann boundary conditions into the discrete form

$$\frac{\phi_{2,j} - \phi_{0,j}}{2 \Delta x} = 0 \quad (3.3.18)$$

for $j = 1, \dots, N_y$, corresponding to the left wall,

$$\frac{\phi_{i,2} - \phi_{i,0}}{2 \Delta y} = 0 \quad (3.3.19)$$

for $i = 1, \dots, N_x + 1$, corresponding to the bottom wall, and

$$\frac{\phi_{N_x+2,j} - \phi_{N_x,j}}{2 \Delta x} = 0 \quad (3.3.20)$$

for $j = 1, \dots, N_y$ corresponding to the right wall.

Algebraic balance

To this end, we pause to count the number of unknowns and ensure that it match the number of available equations. First, we note that the difference equation (3.3.13) or (3.3.14) may now be applied at the interior *and* boundary nodes for $i = 1, 2, \dots, N_x + 1$ and $j = 1, 2, \dots, N_y$, to yield $(N_x + 1)N_y$ equations. Adding to these equations the $N_x + 2N_y + 1$ boundary conditions (3.3.18) - (3.3.20), we obtain $(N_x + 1)(N_y + 1) + 2N_y$ equations. The total number of equations matches the number of unknowns including the values of ϕ at the $(N_x + 1)N_y$ interior and boundary nodes, and the values of ϕ at the $2N_y + N_x + 1$ phantom nodes.

3.3.4 Compilation into a linear system of equations

To formalize the method, we collect the interior and boundary unknowns into a long vector \mathbf{w} consisting of row-blocks, beginning from the bottom,

$$\mathbf{w} = \begin{bmatrix} \phi_{1,1}, \phi_{2,1}, \dots, \phi_{N_x+1,1}, \\ \phi_{1,2}, \phi_{2,2}, \dots, \phi_{N_x+1,2}, \\ \dots, \\ \phi_{1,N_y-1}, \phi_{2,N_y-1}, \dots, \phi_{N_x+1,N_y-1}, \\ \phi_{1,N_y}, \phi_{2,N_y}, \dots, \phi_{N_x+1,N_y} \end{bmatrix}. \quad (3.3.21)$$

Next, we apply the finite-difference equation (3.3.14) successively at the boundary and interior nodes. Without loss of generality, we choose to scan the grid points row-by-row starting from the bottom; a column-by-column compilation would also be acceptable.

Considering first the southwestern corner node $(1, 1)$, we obtain the finite-difference equation

$$\phi_{2,1} - 2(1 + \beta)\phi_{1,1} + \phi_{0,1} + \beta\phi_{1,2} + \beta\phi_{1,0} = 0. \quad (3.3.22)$$

Boundary condition (3.3.18) for $j = 1$ requires $\phi_{2,1} = \phi_{0,1}$, and boundary condition (3.3.17) for $j = 1$ requires $\phi_{1,2} = \phi_{1,0}$. Using these equations to eliminate $\phi_{0,1}$ and $\phi_{1,0}$ in favor of $\phi_{2,1}$ and $\phi_{1,2}$ on the right-hand side of (3.3.22), we find

$$2\phi_{2,1} - 2(1 + \beta)\phi_{1,1} + 2\beta\phi_{1,2} = 0. \quad (3.3.23)$$

For future reference, we express this equation in the form of the inner product of a vector $\mathbf{a}^{(1,1)}$ and the vector of unknowns \mathbf{w} defined in equation (3.3.21), as

$$\mathbf{a}^{(1,1)} \cdot \mathbf{w} = 0, \quad (3.3.24)$$

where we have introduced the vector

$$\mathbf{a}^{(1,1)} = \begin{bmatrix} -2(1 + \beta), 2, 0, \dots, 0, \\ 2\beta, 0, 0, \dots, 0, \\ \dots, \\ 0, 0, \dots, 0 \end{bmatrix}. \quad (3.3.25)$$

Each one of the N_y blocks on the right-hand side of (3.3.25) has $N_x + 1$ entries.

Considering next the boundary node (2, 1), we obtain

$$\phi_{3,1} - 2(1 + \beta)\phi_{2,1} + \phi_{1,1} + \beta\phi_{2,2} + \beta\phi_{2,0} = 0. \quad (3.3.26)$$

Boundary condition (3.3.19) applied for $i = 2$ requires $\phi_{2,2} = \phi_{2,0}$. Using this equation to eliminate $\phi_{2,0}$ in favor of $\phi_{2,2}$ on the right-hand side of (3.3.26), we find

$$\phi_{3,1} - 2(1 + \beta)\phi_{2,1} + \phi_{1,1} + 2\beta\phi_{2,2} = 0. \quad (3.3.27)$$

For future reference, we express this equation in the form of the inner product

$$\mathbf{a}^{(2,1)} \cdot \mathbf{w} = 0, \quad (3.3.28)$$

where we have introduced the vector

$$\mathbf{a}^{(2,1)} = \begin{bmatrix} 1, -2(1 + \beta), 1, 0, \dots, 0, \\ 0, 2\beta, 0, 0, \dots, 0, \\ \dots, \\ 0, 0, \dots, 0 \end{bmatrix}. \quad (3.3.29)$$

Each one of the N_y blocks on the right-hand side of (3.3.29) has $N_x + 1$ entries.

Continuing in this fashion, we build the rest of the vectors $\mathbf{a}^{(i,j)}$ for $i = 1, 2, \dots, N_x + 1$ and $j = 1, 2, \dots, N_y - 1$, until we reach the row corresponding to $j = N_y$. In simplifying the finite-difference equations for this row, we take into consideration not only the Neumann boundary conditions (3.3.18) and (3.3.20) for the side walls, but also the Dirichlet condition (3.3.10) for the top wall. For example, considering the north-western node (1, N_y), we obtain the difference equation

$$-2(1 + \beta)\phi_{1,N_y} + 2\phi_{2,N_y} + \beta\phi_{1,N_y-1} = -\beta V x_1, \quad (3.3.30)$$

which may be expressed in the form of the inner product

$$\mathbf{a}^{(1,N_y)} \cdot \mathbf{w} = -\beta V x_1, \quad (3.3.31)$$

where we have introduced the vector

$$\mathbf{a}^{(1, N_y)} = [\begin{array}{l} 0, 0, 0, \dots, 0, \\ \dots, \\ 0, 0, 0, \dots, 0, \\ \beta, 0, 0, \dots, 0, \\ -2(1 + \beta), 2, 0, \dots, 0 \end{array}]. \tag{3.32}$$

Finally, we collect equations (3.3.24), (3.3.28), (3.3.31) and their counterparts for the rest of the interior and boundary nodes into a large system of equations,

$$\mathbf{A} \cdot \mathbf{w} = \mathbf{b}. \tag{3.33}$$

The first row of the matrix \mathbf{A} is the vector $\mathbf{a}^{(1,1)}$ defined in (3.3.25); the second row is the vector $\mathbf{a}^{(2,1)}$ defined in (3.3.29); subsequent rows have similar identities. The vector \mathbf{b} on the right-hand side of (3.3.33) is given by

$$\mathbf{b} = [\begin{array}{l} 0, 0, 0, \dots, 0, \\ \dots, \\ 0, 0, 0, \dots, 0, \\ -\beta V x_1, -\beta V x_2, \dots, -\beta V x_{N_x+1} \end{array}]. \tag{3.34}$$

Upon inspection, we find that the matrix \mathbf{A} has the *block tridiagonal* form

$$\mathbf{A} = \left[\begin{array}{ccccccc} \mathbf{T} & \mathbf{D} & \mathbf{0} & \dots & \dots & \dots & \mathbf{0} \\ \mathbf{D} & \mathbf{T} & \mathbf{D} & \mathbf{0} & \dots & \dots & \mathbf{0} \\ \mathbf{0} & \mathbf{D} & \mathbf{T} & \mathbf{D} & \mathbf{0} & \dots & \mathbf{0} \\ \dots & \dots & \dots & \dots & \dots & \dots & \dots \\ \mathbf{0} & \mathbf{0} & \dots & \mathbf{D} & \mathbf{T} & \mathbf{D} & \mathbf{0} \\ \mathbf{0} & \mathbf{0} & \dots & \mathbf{0} & \mathbf{D} & \mathbf{T} & \mathbf{D} \\ \mathbf{0} & \mathbf{0} & \mathbf{0} & \dots & \mathbf{0} & \mathbf{D} & \mathbf{T} \end{array} \right], \tag{3.35}$$

composed of N_y vertical and N_y horizontal partitions, subject to the following definitions:

- \mathbf{T} is a tridiagonal matrix with dimensions $(N_x + 1) \times (N_x + 1)$, defined as

$$\begin{bmatrix} -2(1+\beta) & 2 & 0 & 0 & \dots & 0 & 0 \\ 1 & -2(1+\beta) & 1 & 0 & \dots & 0 & 0 \\ 0 & 1 & -2(1+\beta) & 1 & \dots & 0 & 0 \\ \dots & \dots & \dots & \dots & \dots & \dots & \dots \\ 0 & 0 & \dots & \dots & 1 & -2(1+\beta) & 1 \\ 0 & 0 & \dots & \dots & 0 & 2 & -2(1+\beta) \end{bmatrix}. \quad (3.3.36)$$

Note that the super- and sub-diagonal elements of \mathbf{T} are equal to unity, except for the elements in the first the last row that are equal to 2.

- \mathbf{D} is a diagonal matrix with dimensions $(N_x+1) \times (N_x+1)$, defined as

$$\begin{bmatrix} \beta & 0 & 0 & 0 & \dots & 0 & 0 \\ 0 & \beta & 0 & 0 & \dots & 0 & 0 \\ 0 & 0 & \beta & 0 & \dots & 0 & 0 \\ \dots & \dots & \dots & \dots & \dots & \dots & \dots \\ 0 & 0 & \dots & \dots & 0 & \beta & 0 \\ 0 & 0 & \dots & \dots & 0 & 0 & \beta \end{bmatrix}. \quad (3.3.37)$$

Cursory inspection reveals that all elements of the matrix \mathbf{A} are equal to zero, except for the elements along five diagonals. Because of the dominant presence of zeros, the matrix \mathbf{A} is classified as *sparse*.

We have formulated the problem in terms of the linear system of equations (3.3.33) for the vector \mathbf{w} defined in (3.3.21). Our next task is to solve this system using a numerical method. Figure 3.3.2 displays the velocity vector field generated by solving system (3.3.33) using the method of Gauss elimination discussed in Section 3.4, and then computing the components of the velocity at the nodes by taking partial derivatives of the potential using finite-difference methods.

Problems

Problem 3.3.1 *Explicit form of the linear system.*

Write out the explicit form of the linear system (3.3.33) for the discretization level $N_x = 2$ and $N_y = 2$.

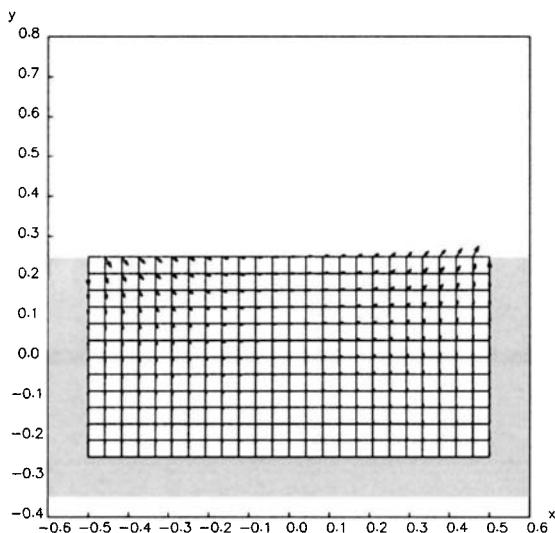


Figure 3.3.2 Velocity vector field of two-dimensional potential flow in a rectangular cavity computed by the finite-difference method discussed in the text.

Problem 3.3.2 *Neumann boundary conditions all around.*

Derive the counterpart of the linear system (3.3.33) when the no-penetration condition is required over all four walls. Specifically, write out the components of the unknown vector \mathbf{w} , constant vector \mathbf{b} , and coefficient matrix \mathbf{A} in a form that is analogous to that displayed in (3.3.35). Then confirm that the sum of the elements in each row of the matrix \mathbf{A} is equal to zero and, based on this result, explain why the matrix \mathbf{A} is singular, that is, its determinant is equal to zero.

3.4 Linear solvers

In Section 3.3, we reduced the problem of solving Laplace's equation for the harmonic potential in a rectangular domain, representing the domain of a two-dimensional flow, to the problem of solving a linear system of equations (3.3.33) for the value of the potential at the nodes of a finite-difference grid. The reduction was done by replacing Laplace's differential equation with an algebraic equation obtained using a finite-difference method. In this section, we discuss numerical methods for

solving the derived system of linear equations. Since numerical solutions of linear systems are required in broad range of applications, we discuss the algorithms within a somewhat more generalized framework.

Consider a system of N linear algebraic equations for the N unknown scalars w_1, w_2, \dots, w_N ,

$$\begin{aligned} A_{1,1} w_1 + A_{1,2} w_2 + \dots + A_{1,N-1} w_{N-1} + A_{1,N} w_N &= b_1, \\ A_{2,1} w_1 + A_{2,2} w_2 + \dots + A_{2,N-1} w_{N-1} + A_{2,N} w_N &= b_2, \\ \dots, \\ A_{N,1} w_1 + A_{N,2} w_2 + \dots + A_{N,N-1} w_{N-1} + A_{N,N} w_N &= b_N, \end{aligned} \quad (3.4.1)$$

where $A_{i,j}$, for $i = 1, 2, \dots, N$ and $j = 1, 2, \dots, N$ are given coefficients, and b_i are given constants. In matrix notation, the system (3.4.1) takes the compact form

$$\mathbf{A} \cdot \mathbf{w} = \mathbf{b}, \quad (3.4.2)$$

where \mathbf{A} is the $N \times N$ coefficient matrix

$$\mathbf{A} = \begin{bmatrix} A_{1,1} & A_{1,2} & \dots & A_{1,N-1} & A_{1,N} \\ A_{2,1} & A_{2,2} & \dots & A_{2,N-1} & A_{2,N} \\ \dots & & & & \\ A_{N-1,1} & A_{N-1,2} & \dots & A_{N-1,N-1} & A_{N-1,N} \\ A_{N,1} & A_{N,2} & \dots & A_{N,N-1} & A_{N,N} \end{bmatrix}, \quad (3.4.3)$$

and \mathbf{b} is the N -dimensional vector

$$\mathbf{b} = \begin{bmatrix} b_1 \\ b_2 \\ \dots \\ b_{N-1} \\ b_N \end{bmatrix}. \quad (3.4.4)$$

The most general method of solving system (3.4.2) is by the method of Gauss elimination.

3.4.1 Gauss elimination

The basic idea is to solve the first equation of (3.4.1) for the first unknown x_1 , and use the expression for x_1 thus obtained to eliminate x_1 from all subsequent equations. We then retain the first equation as is,

and replace all subsequent equations with their descendants that do not contain x_1 .

At the second stage, we solve the second equation for the second unknown x_2 , and use the expression for x_2 thus obtained to eliminate x_2 from all subsequent equations. We then retain the first and second equations, and replace all subsequent equations with their descendants that do not contain x_1 or x_2 . Continuing in this manner, we arrive at the last equation, which contains only the last unknown x_N .

Having completed the elimination, we compute the unknowns by the method of *backward substitution*. First, we solve the last equation for x_N , which thus becomes a known. Second, we solve the penultimate equation for x_{N-1} which also becomes a known. Continuing in the backward direction, we scan the reduced system until we have evaluated all unknowns.

Pivoting

Immediately before the m th equation has been solved for the m th unknown, where $m = 1, 2, \dots, N - 1$, the linear system has the form

$$\begin{bmatrix} A_{1,1}^{(m)} & A_{1,2}^{(m)} & \dots & \dots & \dots & A_{1,N}^{(m)} \\ 0 & A_{2,2}^{(m)} & \dots & \dots & \dots & A_{2,N}^{(m)} \\ 0 & 0 & \dots & \dots & \dots & \dots \\ 0 & 0 & A_{m-1,m-1}^{(m)} & A_{m-1,m}^{(m)} & \dots & A_{m-1,N}^{(m)} \\ 0 & \dots & 0 & A_{m,m}^{(m)} & \dots & A_{m,N}^{(m)} \\ 0 & \dots & 0 & \dots & \dots & \dots \\ 0 & \dots & 0 & A_{N,m}^{(m)} & \dots & A_{N,N}^{(m)} \end{bmatrix} \begin{bmatrix} x_1 \\ x_2 \\ x_3 \\ \dots \\ x_{N-1} \\ x_N \end{bmatrix} = \begin{bmatrix} b_1^{(m)} \\ b_2^{(m)} \\ b_3^{(m)} \\ \dots \\ b_{N-1}^{(m)} \\ b_N^{(m)} \end{bmatrix}, \quad (3.4.5)$$

where $A_{i,j}^{(m)}$ are intermediate coefficients and $b_i^{(m)}$ are intermediate right-hand sides. The first equation of (3.4.5) is identical to the first equation of (3.4.1) for any value of m ; subsequent equations are different, except at the first step corresponding to $m = 1$.

A difficulty arises when the diagonal element $A_{m,m}^{(m)}$ is nearly or precisely equal to zero, for then, we may no longer solve the m th equation for x_m , as required. The failure of the method, however, does *not* imply that the system does not have a solution. To circumvent this difficulty, we simply rearrange the equations or relabel the unknowns so as to bring the m th unknown to the m th equation, using the method of *pivoting*. If there is no way we can make this happen, then the matrix \mathbf{A} is singular, and the linear system has either no solution or an infinite number of solutions.

In the method of *row pivoting*, potential difficulties are bypassed by switching the m th equation in the system (3.4.5) with the subsequent k th equation, where $k > m$; the value k is chosen so that $|A_{k,m}^{(m)}|$ is the maximum value of the elements in the m th column below the diagonal, $A_{i,m}^{(m)}$, for $i \geq m$. If it happens that $A_{i,m}^{(m)} = 0$ for all $i \geq m$, then the system under consideration does not have a unique solution: the matrix \mathbf{A} is singular.

3.4.2 A menagerie of other methods

In practice, the size of the system (3.3.33) can be on the order of $10^4 \times 10^4$ or higher, corresponding to discretization levels N_x and N_y on the order of 10^2 . For such large systems, the method of Gauss elimination requires a prohibitively long computational time. The practical need to solve systems of large size has motivated the development of a host of powerful methods for general or specific applications.

For sparse systems of large size, an iterative solution is appropriate. The main idea is to split the coefficient matrix \mathbf{A} into two matrices, writing

$$\mathbf{A} = \mathbf{A}' - \mathbf{A}'', \quad (3.4.6)$$

and then recast the system (3.4.2) into the form

$$\mathbf{A}' \cdot \mathbf{x} = \mathbf{A}'' \cdot \mathbf{x} + \mathbf{b}. \quad (3.4.7)$$

The procedure involves guessing the solution \mathbf{x} , computing the right-hand side of (3.4.7), and solving for \mathbf{x} on the left-hand side. The advantage of this approach is that, if the splitting (3.4.6) is done craftily, solving (3.4.7) is much easier to do than solving (3.4.2) for \mathbf{x} on the left-hand side. The computation is then repeated until the value of \mathbf{x} used to compute the right-hand side of (3.4.7) is virtually identical to that arising by solving the linear system (3.4.7). The iterative methods of *Jacobi* and *Gauss-Siedel* fall into this category of methods.

A different class of iterative methods search for the solution vector \mathbf{x} by making steps in the N -dimensional space toward craftily designed or even optimal directions. For example, directory *01_num_meth/03_lin_eq* of *FDLIB* contains programs that solve a linear system of equations using the method of *conjugate* or *biconjugate gradients* which fall into the category of directional-search methods.

Computer problems

Problem c.3.4.1 Gauss elimination.

Directory *01_num_meth/03_lin_eq* of *FDLIB* includes the program *gel.f* that solves a system of linear equations using the method of Gauss elimination with row pivoting. Use the program to solve a system of your choice, and verify the accuracy of the solution.

Problem c.3.4.2 Irrotational flow in a cavity.

Directory *07_ptf/cvt_2d* of *FDLIB* includes a code that computes potential flow in a rectangular cavity using the finite-difference method discussed in Section 3.3.

(a) Run the code for a cavity with length to depth ratio equal to unity, and discretization level as high as you can afford. Prepare a velocity-vector plot, and discuss the structure of the flow.

(b) Repeat (a) for a cavity with length to depth ratio equal to 2.0, and discuss the dependence of the structure of the flow on the cavity aspect ratio.

3.5 Two-dimensional point sources and point-source dipoles

Laplace's equation for the harmonic velocity potential, equation (3.2.8) for two-dimensional flow or equation (3.2.11) for three-dimensional flow, has the distinctive property of being *linear*. This means that if ϕ_1 and ϕ_2 are two harmonic potentials representing two elementary flows, a linear combination of them,

$$\phi = a \phi_1 + b \phi_2, \quad (3.5.1)$$

where a and b are two constants, will also be a harmonic potential representing a hybrid flow.

3.5.1 Function superposition and fundamental solutions

The linearity of Laplace's equation allows us to generate a desired solution in exact or approximate fashion by the method of *superposition*. The key idea is to introduce a family of harmonic potentials playing the role of *basis functions*, also called *fundamental solutions*, and then use

them as building blocks to generate further solutions. For example, if ϕ_1 and ϕ_2 are two such fundamental solutions, then a desired solution may be assumed in the form of the right-hand side of equation (3.5.1), and the two constants a and b may be adjusted to satisfy the boundary conditions.

There are various families of fundamental solutions appropriate, for example, for flows in infinite or semi-infinite domains, and for singly-, doubly-, or triply-periodic flows. The most general class of fundamental solutions consists of the *fundamental singularities* of potential flow.

3.5.2 Two-dimensional point source

Imagine that an incompressible fluid is being discharged into an infinite pool through an infinite perforated cylinder, thereby generating a radial flow in the xy plane outward from the point of inlet. In plane polar coordinates centered at the point of discharge $\mathbf{x}_0 = (x_0, y_0)$, the radial and polar components of the velocity at the point $\mathbf{x} = (x, y)$ are given by

$$u_r(x, y) = \frac{m}{2\pi} \frac{1}{r}, \quad u_\theta(x, y) = 0, \quad (3.5.2)$$

where $r = \sqrt{(x - x_0)^2 + (y - y_0)^2}$ is the distance of the field point \mathbf{x} from the point of discharge \mathbf{x}_0 , and m is a constant expressing the rate of areal discharge; the units of m are velocity multiplied by length. The flow described by equations (3.5.2) is attributed to a *two-dimensional point source*, and the rate of areal discharge m is the strength of the point source. If m is negative, we obtain a point source with negative strength described as a *point sink*.

The radial velocity of the flow due to a point source was chosen to decay as the inverse of the distance from the point of discharge, r , for the following reason. Since the fluid is incompressible, the flow rate Q across any circular loop or radius R centered at the point of discharge must be independent of the loop radius. To verify that the velocity field (3.5.2) satisfies this restriction, we use expression (2.6.13) and find

$$Q = R \int_0^{2\pi} u_r d\theta = R \int_0^{2\pi} \frac{m}{2\pi} \frac{1}{r} d\theta = R \frac{m}{2\pi} \frac{1}{R} \int_0^{2\pi} d\theta = m, \quad (3.5.3)$$

as required. If we had set for example, $u_r = m/(2\pi r^k)$, where the exponent k is not equal to unity, then the restriction of constant areal flow rate associated with an incompressible fluid would not be satisfied.

Singular behavior of the point source

As the distance from the point source r tends to zero, the right-hand side of the radial velocity in (3.5.2) tends to infinity. This singular behavior is a manifestation of the idealized nature of the flow due to a point source, and explains why the point source is classified as a *singularity*.

In practice, the flow expressed by (3.5.2) is valid only for $r > b$, where b is the radius of the cylinder discharging the fluid. Extending the domain of flow all the way up to the center of the cylinder located at \mathbf{x}_0 , we allow for the occurrence of a mathematical singularity.

Velocity potential

The velocity potential of a two-dimensional point source, denoted by ϕ^{2D-PS} , is related to the velocity components according to equations (3.2.18),

$$\frac{\partial \phi^{2D-PS}}{\partial r} = \frac{m}{2\pi} \frac{1}{r}, \quad \frac{\partial \phi^{2D-PS}}{\partial \theta} = 0. \quad (3.5.4)$$

Integrating the first of these equations, and using the second equation to evaluate the constant of integration, we find

$$\begin{aligned} \phi^{2D-PS} &= \frac{m}{2\pi} \ln r = \frac{m}{2\pi} \ln \sqrt{(x - x_0)^2 + (y - y_0)^2} \\ &= \frac{m}{4\pi} \ln[(x - x_0)^2 + (y - y_0)^2]. \end{aligned} \quad (3.5.5)$$

Straightforward differentiation confirms that ϕ^{2D-PS} satisfies Laplace's equation in two dimensions at every point except at the singular point \mathbf{x}_0 where the potential and its derivatives are not defined.

Cartesian components of the velocity

To derive the Cartesian components of the velocity, we take the partial derivatives of ϕ^{2D-PS} with respect to x or y , and find

$$\begin{aligned} u_x^{2D-PS} &= \frac{\partial \phi^{2D-PS}}{\partial x} = \frac{m}{2\pi} \frac{x - x_0}{(x - x_0)^2 + (y - y_0)^2}, \\ u_y^{2D-PS} &= \frac{\partial \phi^{2D-PS}}{\partial y} = \frac{m}{2\pi} \frac{y - y_0}{(x - x_0)^2 + (y - y_0)^2}. \end{aligned} \quad (3.5.6)$$

The streamlines of the flow due to a point source are radial straight lines emanating from the singular point \mathbf{x}_0 .

Point source embedded in uniform flow

As an application, consider the superposition of (a) a uniform flow along the x axis with velocity V_x , and (b) the flow due to a point source with strength m situated at the origin, at $x_0 = 0$ and $y_0 = 0$. Using the potential (3.2.6) for uniform flow with the constant c set equal to zero, and the potential (3.5.5) for the point source, we find that the potential of the composite flow is given by

$$\phi = x V_x + \frac{m}{4\pi} \ln(x^2 + y^2). \quad (3.5.7)$$

The associated Cartesian components of the velocity are given by

$$\begin{aligned} u_x &= V_x + \frac{m}{2\pi} \frac{x}{x^2 + y^2} = V_x \left[1 + \frac{m}{2\pi a V_x} \frac{\frac{x}{a}}{\left(\frac{x}{a}\right)^2 + \left(\frac{y}{a}\right)^2} \right], \\ u_y &= \frac{m}{2\pi} \frac{y}{x^2 + y^2} = V_x \frac{m}{2\pi a V_x} \frac{\frac{y}{a}}{\left(\frac{x}{a}\right)^2 + \left(\frac{y}{a}\right)^2}, \end{aligned} \quad (3.5.8)$$

where a is an arbitrary length.

To study the structure of the flow, we recast equations (3.5.8) into the dimensionless forms

$$\hat{u}_x = 1 + \beta \frac{\hat{x}}{\hat{x}^2 + \hat{y}^2}, \quad \hat{u}_y = \beta \frac{\hat{y}}{\hat{x}^2 + \hat{y}^2}, \quad (3.5.9)$$

where we have defined the dimensionless variables

$$\hat{x} = \frac{x}{a}, \quad \hat{y} = \frac{y}{a}, \quad \hat{u}_x = \frac{u_x}{V_x}, \quad \hat{u}_y = \frac{u_y}{V_x}, \quad (3.5.10)$$

and we have introduced the dimensionless parameter

$$\beta = \frac{m}{2\pi a V_x}, \quad (3.5.11)$$

expressing the strength of the point source relative to the magnitude of the incident flow. Equations (3.5.9) reveal that the structure of the flow is determined by the value of the parameter β .

Figure 3.5.1 illustrates the streamline pattern for $\beta = 0.25$, revealing that the potential (3.5.7) describes uniform flow along the x axis past a

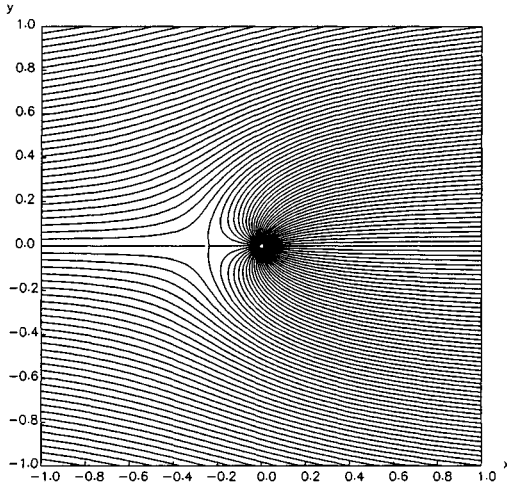


Figure 3.5.1 Streamline pattern of the flow due to the superposition of (a) the flow due to a two-dimensional point source, and (b) streaming (uniform) flow along the x axis.

semi-infinite body whose surface may be identified with the two streamlines emanating from the stagnation point on the x axis. Using the first of equations (3.5.9), we find that the x component of the velocity on the x axis vanishes when $\hat{x} = b$, where $0 = 1 + \beta/b$, or $b = -\beta$. Thus, the larger the value of β expressing the strength of the point source, the farther the stagnation point is located from the origin.

3.5.3 Two-dimensional point-source dipole

Consider next the flow due to the superposition of a point source with strength m located at the point $(x_0 + a, y_0)$, and a point sink with strength $-m$ located at the point $(x_0 - a, y_0)$, as illustrated in figure 3.5.2(a), where a is a specified distance. Using expression (3.5.5), we find that the harmonic potential induced by these two singularities is given by

$$\begin{aligned} \phi &= \frac{m}{4\pi} \ln\{[x - (x_0 + a)]^2 + (y - y_0)^2\} - \frac{m}{4\pi} \ln\{[x - (x_0 - a)]^2 + (y - y_0)^2\} \\ &= \frac{m}{4\pi} \ln \frac{[x - (x_0 + a)]^2 + (y - y_0)^2}{[x - (x_0 - a)]^2 + (y - y_0)^2}. \end{aligned} \quad (3.5.12)$$

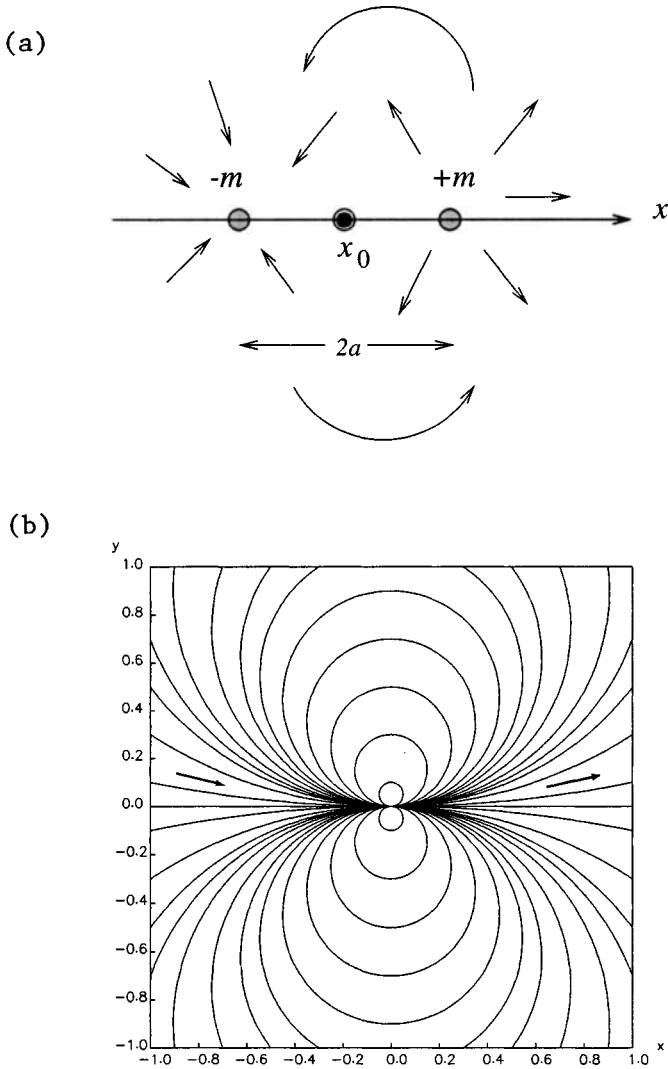


Figure 3.5.2 (a) A point source and a point sink merge to yield a point-source dipole. (b) Streamline pattern due to a two-dimensional dipole pointing along the x axis.

The Cartesian components of the velocity are given by

$$u_x = \frac{\partial \phi}{\partial x} = \frac{m}{2\pi} \left[\frac{x - (x_0 + a)}{[x - (x_0 + a)]^2 + (y - y_0)^2} - \frac{x - (x_0 - a)}{[x - (x_0 - a)]^2 + (y - y_0)^2} \right],$$

$$u_y = \frac{\partial \phi}{\partial y} = \frac{m}{2\pi} \left[\frac{y - y_0}{[x - (x_0 + a)]^2 + (y - y_0)^2} - \frac{y - y_0}{[x - (x_0 - a)]^2 + (y - y_0)^2} \right].$$
(3.5.13)

Let us now hold the position of the field point (x, y) fixed, and reduce the distance between the two singularities; that is, let a tend to zero. In this limit, the flow due to the point sink tends to cancel the flow due to the point source. But if the strength m increases as the inverse of the distance between the two singularities, $2a$, then a nontrivial flow, called the flow due to a *point-source dipole*, will arise in the limit.

To derive the flow due to a point-source dipole, we recast the expression on the right-hand side of (3.5.12) into the form

$$\phi = \frac{m}{4\pi} \left[\ln \left(1 - a \frac{2(x - x_0) - a}{(x - x_0)^2 + (y - y_0)^2} \right) - \ln \left(1 + a \frac{2(x - x_0) + a}{(x - x_0)^2 + (y - y_0)^2} \right) \right]$$

$$= \frac{m}{4\pi} [\ln(1 - \epsilon_1) - \ln(1 + \epsilon_2)],$$
(3.5.14)

where we have introduced the dimensionless numbers

$$\epsilon_1 \equiv a \frac{2(x - x_0) - a}{(x - x_0)^2 + (y - y_0)^2}, \quad \epsilon_2 \equiv a \frac{2(x - x_0) + a}{(x - x_0)^2 + (y - y_0)^2}.$$
(3.5.15)

As the distance a becomes smaller than the distance between the points \mathbf{x} and \mathbf{x}_0 , both ϵ_1 and ϵ_2 tend to zero.

Now, a Taylor series expansion of the logarithmic function $\ln w$ about the point $w = 1$ provides us with the approximations

$$\ln(1 - \epsilon_1) = -\epsilon_1 + \dots, \quad \ln(1 + \epsilon_2) = \epsilon_2 + \dots, \quad (3.5.16)$$

Introducing these expressions into the right-hand side of (3.5.14), and neglecting the terms represented by the dots, we obtain the velocity potential due to a point-source dipole located at the point (x_0, y_0) and oriented in the x direction,

$$\phi^{2D-PSD-x} = -\frac{m}{4\pi}(\epsilon_1 + \epsilon_2) = -\frac{d_x}{2\pi} \frac{x - x_0}{(x - x_0)^2 + (y - y_0)^2}, \quad (3.5.17)$$

where we have introduced the strength of the dipole

$$d_x \equiv 2ma. \quad (3.5.18)$$

It is instructive to note that the potential due to a point-source dipole oriented along the x axis arises by differentiating the potential due to a point source with respect to its x coordinate x_0 : comparing (3.5.5), (3.5.17) and (3.5.18), we find

$$\phi^{2D-PSD-x} = 2a \frac{\partial \phi^{2D-PS}}{\partial x_0}. \quad (3.5.19)$$

This property classifies the dipole as a *derivative singularity* descending from the point source.

The components of the velocity associated with a dipole oriented along the x axis are given by

$$\begin{aligned} u_x^{2D-PSD-x} &= \frac{\partial \phi^{2D-PSD-x}}{\partial x} = 2a \frac{\partial^2 \phi^{2D-PS}}{\partial x \partial x_0} = -2a \frac{\partial^2 \phi^{2D-PS}}{\partial x^2} \\ &= \frac{d_x}{2\pi} \left[-\frac{1}{(x - x_0)^2 + (y - y_0)^2} + \frac{2(x - x_0)^2}{[(x - x_0)^2 + (y - y_0)^2]^2} \right], \end{aligned} \quad (3.5.20)$$

and

$$\begin{aligned} u_y^{2D-PSD-x} &= \frac{\partial \phi^{2D-PSD-x}}{\partial y} = 2a \frac{\partial^2 \phi^{2D-PS}}{\partial y \partial x_0} = -2a \frac{\partial^2 \phi^{2D-PS}}{\partial x \partial y} \\ &= \frac{d_x}{2\pi} \frac{2(x - x_0)(y - y_0)}{[(x - x_0)^2 + (y - y_0)^2]^2}. \end{aligned} \quad (3.5.21)$$

The associated streamline pattern is shown in figure 3.5.2(b).

Working in a similar fashion, we derive the flow due to a point-source dipole with strength d_y oriented along the y axis. The associated harmonic potential is given by

$$\phi^{2D-PSD-y} = 2a \frac{\partial \phi^{2D-PS}}{\partial y_0} = -\frac{d_y}{2\pi} \frac{y - y_0}{(x - x_0)^2 + (y - y_0)^2}, \quad (3.5.22)$$

where $d_y = 2ma$. The corresponding velocity components are given by

$$\begin{aligned} u_x^{2D-PSD-y} &= \frac{\partial \phi^{2D-PSD-y}}{\partial x} = 2a \frac{\partial^2 \phi^{2D-PS}}{\partial x \partial y_0} = -2a \frac{\partial^2 \phi^{2D-PS}}{\partial x \partial y} \\ &= \frac{d_y}{2\pi} \frac{2(x - x_0)(y - y_0)}{[(x - x_0)^2 + (y - y_0)^2]^2}, \end{aligned} \quad (3.5.23)$$

and

$$\begin{aligned} u_y^{2D-PSD-y} &= \frac{\partial \phi^{2D-PSD-y}}{\partial y} = 2a \frac{\partial^2 \phi^{2D-PS}}{\partial y \partial y_0} = -2a \frac{\partial^2 \phi^{2D-PS}}{\partial y^2} \\ &= \frac{d_y}{2\pi} \left[-\frac{1}{(x - x_0)^2 + (y - y_0)^2} + \frac{2(y - y_0)^2}{[(x - x_0)^2 + (y - y_0)^2]^2} \right]. \end{aligned} \quad (3.5.24)$$

The associated streamline pattern is found by rotating the pattern shown in figure 3.5.2(b) by 90° around the location of the dipole.

3.5.4 Flow past a circular cylinder

As an application, we consider the superposition of (a) uniform flow along the x axis with velocity V_x , and (b) the flow due to a point-source dipole located at the origin and oriented along the x axis. Using the potential (3.2.6) with $c = 0$ for the uniform flow, and the potential (3.5.17) with $x_0 = 0$ and $y_0 = 0$ for dipole, we find that the potential of the composite flow is given by

$$\begin{aligned} \phi(x, y) &= V_x x - \frac{d_x}{2\pi} \frac{x}{x^2 + y^2} = V_x x \left(1 - \frac{d_x}{2\pi V_x r^2} \right) \\ &= V_x \left(r - \frac{d_x}{2\pi V_x r} \right) \cos \theta, \end{aligned} \quad (3.5.25)$$

where $r = \sqrt{x^2 + y^2}$ is the distance of the field point (x, y) from the center of the cylinder, and θ is the polar angle measured around the center of the cylinder, defined such that $x = r \cos \theta$.

Now, using the expression for the radial component of the velocity u_r in terms of the potential, given in the first of equations (3.2.18), we find

$$u_r = \frac{\partial \phi}{\partial r} = V_x \left(1 + \frac{d_x}{2\pi V_x} \frac{1}{r^2} \right) \cos \theta. \quad (3.5.26)$$

The sum inside the parentheses on the right-hand side of (3.5.26) vanishes at the radial distance $r = \sqrt{-d_x/(2\pi V_x)}$. Conversely, if the strength of the dipole has the value

$$d_x = -2\pi V_x a^2, \quad (3.5.27)$$

then the radial velocity will vanish at the radial distance $r = a$.

It is evident then that the potential (3.5.25) with d_x evaluated from expression (3.5.27) describes uniform flow with velocity V_x past a circular cylinder of radius a centered at the origin, with the no-penetration condition satisfied over the cylinder. Substituting (3.5.27) into (3.5.25), we derive the explicit solution

$$\phi = V_x \left(r + \frac{a^2}{r} \right) \cos \theta. \quad (3.5.28)$$

The corresponding Cartesian components of the velocity are given by

$$u_x = V_x \left[1 + \frac{a^2}{r^4} - \frac{2x^2 a^2}{r^4} \right], \quad u_y = -V_x \frac{2xy a^2}{r^2}, \quad (3.5.29)$$

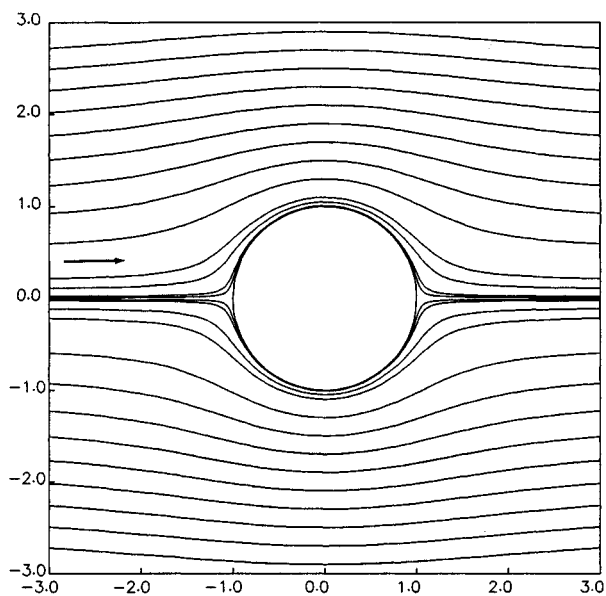
and the associated streamline pattern is shown in figure 3.5.3(a).

3.5.5 Point sources and point-source dipoles in the presence of boundaries

When the domain of flow is bounded by impermeable surfaces, the flow due to a point source or point-source dipole must be enhanced with a complementary flow whose purpose is to satisfy the no-penetration boundary condition. For simple boundary geometries, the complementary flow may be identified with the flow generated by singularities located at image positions; two examples will be given at the remainder of this section.

Directory *07_ptf/lgf_2d* of *FDLIB* contains a collection of subroutines that evaluate the harmonic potential and associated velocity field for several boundary geometries.

(a)



(b)

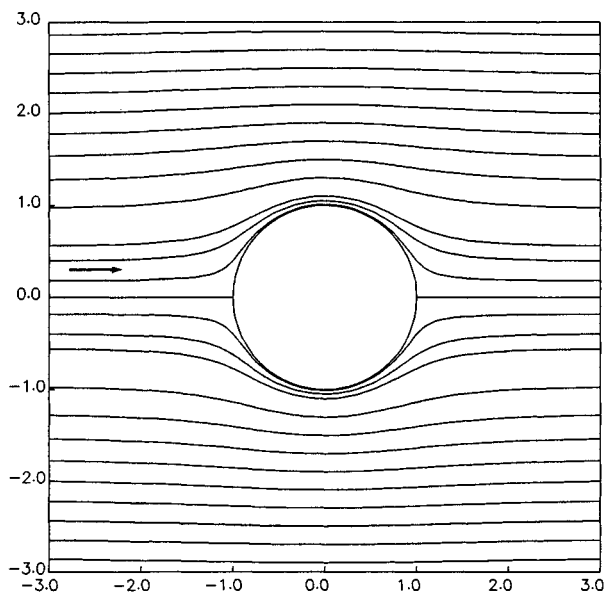


Figure 3.5.3 Streamline pattern of (a) uniform flow past a circular cylinder with vanishing circulation around the cylinder, (b) uniform flow past a sphere.

Point source above a plane

In the case of a point source placed above a plane wall located at $y = w$, the complementary flow is generated by the reflection of the point source with respect to the wall. If a primary point source with strength m is located at the point (x_0, y_0) , then an image point source with equal strength is located at the point $(x_0, 2w - y_0)$. The streamline pattern is depicted in figure 3.5.4(a).

Point source outside a circular cylinder

In the case of a point source placed outside a circular cylinder of radius a centered at the point (x_c, y_c) , the complementary flow is generated by two image point sources. The first image point source is located at the inverse point of the primary point source with respect to the cylinder; if a primary point source with strength m is located at (x_0, y_0) , then an image point source with the same strength is located at the point

$$x_0^I = x_c + (x_0 - x_c) \frac{a^2}{d^2}, \quad y_0^I = y_c + (y_0 - y_c) \frac{a^2}{d^2}, \quad (3.5.30)$$

where $d = \sqrt{(x_0 - x_c)^2 + (y_0 - y_c)^2}$ is the distance of the primary point source from the center of the cylinder. The second image point source is located at the center of the cylinder, and its strength is equal to $-m$. Note that the sum of the strengths of the image singularities vanishes, thereby ensuring that fluid does not cross the surface of the cylinder. The streamline pattern of the induced flow is shown in figure 3.5.4(b).

Problems**Problem 3.5.1** *Oblique streaming flow past a circular cylinder.*

Derive an expression for the harmonic potential and Cartesian components of the velocity of oblique streaming flow with uniform velocity $u_x = V_x$, $u_y = V_y$ past a circular cylinder of radius a centered at the origin.

Problem 3.5.2 *Flow due to a point-source dipole.*

Combining equations (3.5.17) and (3.5.22), we find that the harmonic potential due to a potential dipole with vectorial strength $\mathbf{d} \equiv (d_x, d_y)$ is given by

$$\phi = \mathbf{d} \cdot \Phi^{2D-PSD}, \quad (3.5.31)$$

where the vector function Φ^{2D-PSD} is defined as

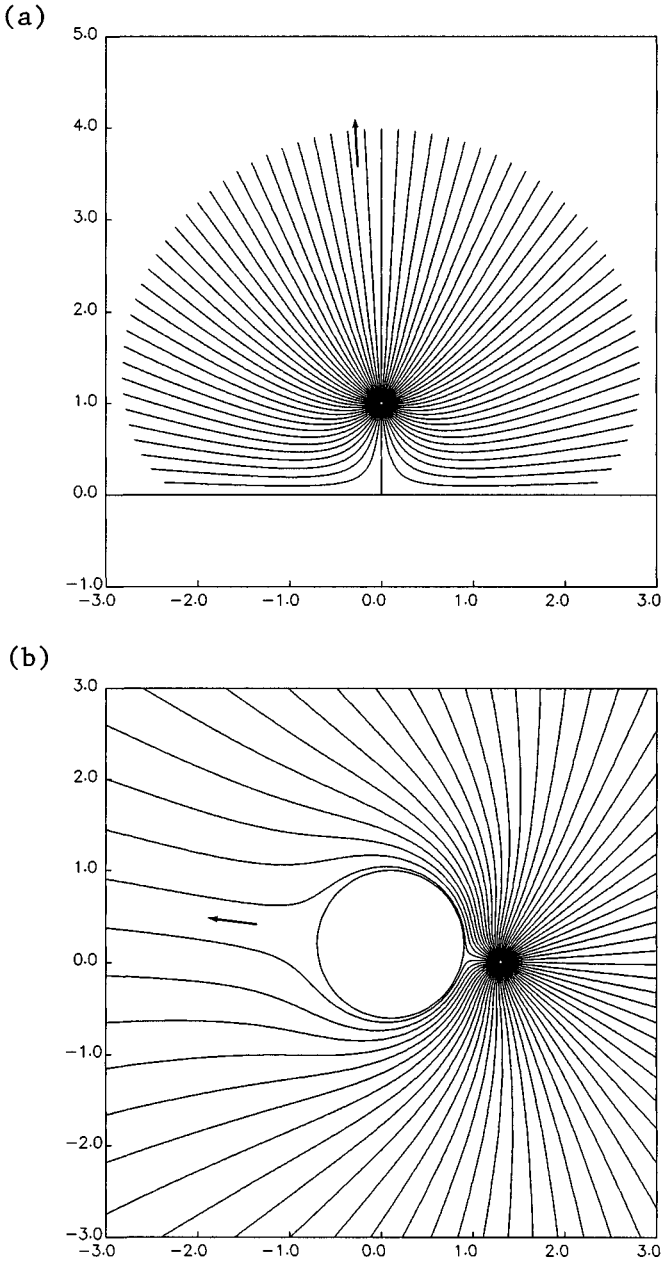


Figure 3.5.4 Streamline pattern of the flow due to a two-dimensional point source (a) above a plane wall, (b) in front of a circular cylinder, and (c) between two parallel walls.

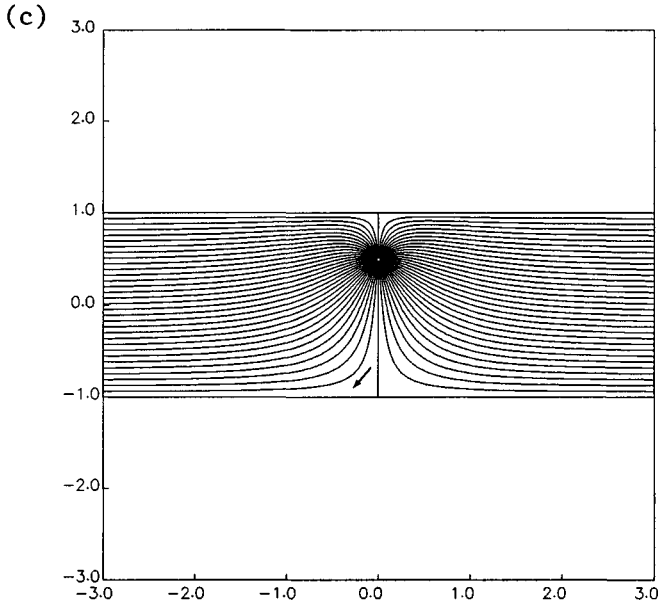


Figure 3.5.4 *Continued.*

$$\Phi^{2D-PSD} \equiv -\frac{1}{2\pi} \begin{bmatrix} \frac{x-x_0}{(x-x_0)^2+(y-y_0)^2} \\ \frac{y-y_0}{(x-x_0)^2+(y-y_0)^2} \end{bmatrix}. \quad (3.5.32)$$

The velocity field may be expressed in the corresponding form

$$\mathbf{u} = -\mathbf{d} \cdot \mathbf{U}^{2D-PSD}, \quad (3.5.33)$$

where \mathbf{U}^{2D-PSD} is a 2×2 matrix function of position.

Using expressions (3.5.20), (3.5.21), (3.5.23), and (3.5.24), derive the explicit form of the matrix \mathbf{U}^{2D-PSD} .

Problem 3.5.3 *Stream functions.*

Derive an expression for the stream function associated with (a) a two-dimensional point source, and (b) a two-dimensional point-source dipole pointing in the x or y direction.

Computer problem

Problem c.3.5.1 *Point source in a semi-infinite rectangular strip.*

Directory *04_various/strmll* of *FDLIB* contains a program that generates streamline patterns of the flow induced by a point source for several boundary geometries. Three examples are illustrated in figure 3.5.4. Run the program to generate the streamline pattern of the flow due to a point source in a semi-infinite rectangular strip.

3.6 Three-dimensional point sources and point-source dipoles

The fundamental solutions described in Section 3.5 for two-dimensional potential flow may be extended in a straightforward fashion to three-dimensional flow.

3.6.1 Three-dimensional point source

The harmonic potential due to a three-dimensional point source of strength m located at the point $\mathbf{x}_0 = (x_0, y_0, z_0)$ is given by

$$\phi^{3D-PS} = -\frac{m}{4\pi} \frac{1}{r}, \quad (3.6.1)$$

where $r = \sqrt{(x - x_0)^2 + (y - y_0)^2 + (z - z_0)^2}$ is the distance of the field point \mathbf{x} from the location of the point source \mathbf{x}_0 . The corresponding Cartesian components of the velocity are given by

$$\begin{aligned} u_x^{3D-PS} &= \frac{m}{4\pi} \frac{x - x_0}{r^3}, \\ u_y^{3D-PS} &= \frac{m}{4\pi} \frac{y - y_0}{r^3}, \\ u_z^{3D-PS} &= \frac{m}{4\pi} \frac{z - z_0}{r^3}. \end{aligned} \quad (3.6.2)$$

The streamlines are radial straight lines emanating from the singular point \mathbf{x}_0 .

3.6.2 Three-dimensional point-source dipole

The harmonic potential due to a three-dimensional point-source dipole oriented along the x , y , or z axis is given, respectively, by

$$\begin{aligned}\phi^{3D-PSD-x} &= -\frac{d_x}{4\pi} \frac{x - x_0}{r^3}, \\ \phi^{3D-PSD-y} &= -\frac{d_y}{4\pi} \frac{y - y_0}{r^3}, \\ \phi^{3D-PSD-z} &= -\frac{d_z}{4\pi} \frac{z - z_0}{r^3},\end{aligned}\tag{3.6.3}$$

where d_x , d_y , and d_z are the directional strengths of the dipole.

The corresponding velocity components are found by straightforward differentiation. For a dipole oriented along the x axis,

$$\begin{aligned}u_x^{3D-PSD-x} &= \frac{\partial \phi^{3D-PSD-x}}{\partial x} = \frac{d_x}{4\pi} \left[-\frac{1}{r^3} + \frac{3(x - x_0)^2}{r^5} \right], \\ u_y^{3D-PSD-x} &= \frac{\partial \phi^{3D-PSD-x}}{\partial y} = \frac{d_x}{4\pi} \frac{3(x - x_0)(y - y_0)}{r^5}, \\ u_z^{3D-PSD-x} &= \frac{\partial \phi^{3D-PSD-x}}{\partial z} = \frac{d_x}{4\pi} \frac{3(x - x_0)(z - z_0)}{r^5}.\end{aligned}\tag{3.6.4}$$

The streamline pattern in the xy plane is qualitatively similar, but not identical, to that shown in figure 3.5.2(b) for two-dimensional flow.

For a dipole oriented along the y axis,

$$\begin{aligned}u_x^{3D-PSD-y} &= \frac{\partial \phi^{3D-PSD-y}}{\partial x} = \frac{d_y}{4\pi} \frac{3(y - y_0)(x - x_0)}{r^5}, \\ u_y^{3D-PSD-y} &= \frac{\partial \phi^{3D-PSD-y}}{\partial y} = \frac{d_y}{4\pi} \left[-\frac{1}{r^3} + \frac{3(y - y_0)^2}{r^5} \right], \\ u_z^{3D-PSD-y} &= \frac{\partial \phi^{3D-PSD-y}}{\partial z} = \frac{d_y}{4\pi} \frac{3(y - y_0)(z - z_0)}{r^5}.\end{aligned}\tag{3.6.5}$$

For a dipole oriented along the z axis,

$$\begin{aligned} u_x^{3D-PSD-z} &= \frac{\partial \phi^{3D-PSD-z}}{\partial x} = \frac{d_z}{4\pi} \frac{3(z-z_0)(x-x_0)}{r^5}, \\ u_y^{3D-PSD-z} &= \frac{\partial \phi^{3D-PSD-z}}{\partial y} = \frac{d_z}{4\pi} \frac{3(z-z_0)(y-y_0)}{r^5}, \\ u_z^{3D-PSD-z} &= \frac{\partial \phi^{3D-PSD-z}}{\partial z} = \frac{d_z}{4\pi} \left[-\frac{1}{r^3} + \frac{3(z-z_0)^2}{r^5} \right]. \end{aligned} \quad (3.6.6)$$

Expressions (3.6.4)-(3.6.6) may be placed into a compact vector-matrix form, as discussed in problem 3.6.1.

3.6.3 Flow past a sphere

As an application, we consider the superposition of (a) uniform flow along the x axis with velocity V_x , and (b) the flow due to a three-dimensional point-source dipole located at the origin, $x_0 = 0$, $y_0 = 0$, and $z_0 = 0$, pointing along the x axis. Using expression (3.2.6) with $c = 0$ for the uniform flow, and expression (3.6.1) for the point-source dipole, we find that the potential of the composite flow is given by

$$\begin{aligned} \phi &= x V_x - \frac{d_x}{4\pi} \frac{x}{r^3} = V_x x \left(1 - \frac{d_x}{4\pi V_x} \frac{1}{r^3} \right) \\ &= V_x \left(r - \frac{d_x}{4\pi V_x} \frac{1}{r^2} \right) \cos \theta, \end{aligned} \quad (3.6.7)$$

where $r = \sqrt{x^2 + y^2 + z^2}$ is the distance from the origin, and θ is the azimuthal angle defined such that $x = r \cos \theta$.

Using the first of equations (3.2.16), we find that the radial component of the velocity is given by

$$u_r = \frac{\partial \phi}{\partial r} = V_x \left(1 + \frac{d_x}{2\pi V_x} \frac{1}{r^3} \right) \cos \theta. \quad (3.6.8)$$

The sum within the parentheses on the right-hand side of (3.6.8) vanishes at the radial distance $r = [-d_x/(2\pi V_x)]^{1/3}$. Conversely, if the strength of the dipole has the value

$$d_x = -2\pi V_x a^3, \quad (3.6.9)$$

then the radial velocity will vanish at the radial distance $r = a$. These observations suggest that the potential (3.6.7) with d_x evaluated from expression (3.6.9) describes uniform flow along the x axis with velocity V_x past a stationary sphere of radius a centered at the origin. Substituting (3.6.9) into (3.6.7), we obtain an explicit expression for the potential,

$$\phi = V_x \left(r + \frac{1}{2} \frac{a^3}{r^2} \right) \cos \theta. \quad (3.6.10)$$

The corresponding Cartesian components of the velocity are given by

$$\begin{aligned} u_x &= V_x \left[1 + \frac{a^3}{2} \left(\frac{1}{r^3} - \frac{3x^2}{r^5} \right) \right], \\ u_y &= -V_x \frac{a^3}{2} \frac{3xy}{r^5}, \quad u_z = -V_x \frac{a^3}{2} \frac{3xz}{r^5}. \end{aligned} \quad (3.6.11)$$

The streamline pattern in a meridional plane is shown in figure 3.5.3(b).

3.6.4 Point sources and point-source dipoles in the presence of boundaries

To account for the presence of boundaries, we introduce a complementary flow in order to satisfy the no-penetration boundary condition, as discussed in Section 3.5.5 for two-dimensional flow. For simple boundary geometries, the complementary flow may be identified with the flow produced by singularities located at image positions.

Directory *07_ptf/lgf_3d* of *FDLIB* contains a collection of subroutines that evaluate the velocity field for several boundary geometries. Figure 3.6.1(a) illustrates the streamline pattern of the flow due to a point source located above a plane wall, and figure 3.6.1(b) illustrates the streamline pattern of the flow due to a point source located in front of a sphere. In the first case, the complementary flow is due to a reflected point source.

Problems

Problem 3.6.1 *Flow due to a three-dimensional point-source dipole.*

Repeat problem 3.5.2 for the three-dimensional point-source dipole. The result should be expressed in terms of a three-component vector function Φ^{3D-PSD} and a 3×3 matrix function \mathbf{U}^{3D-PSD} .

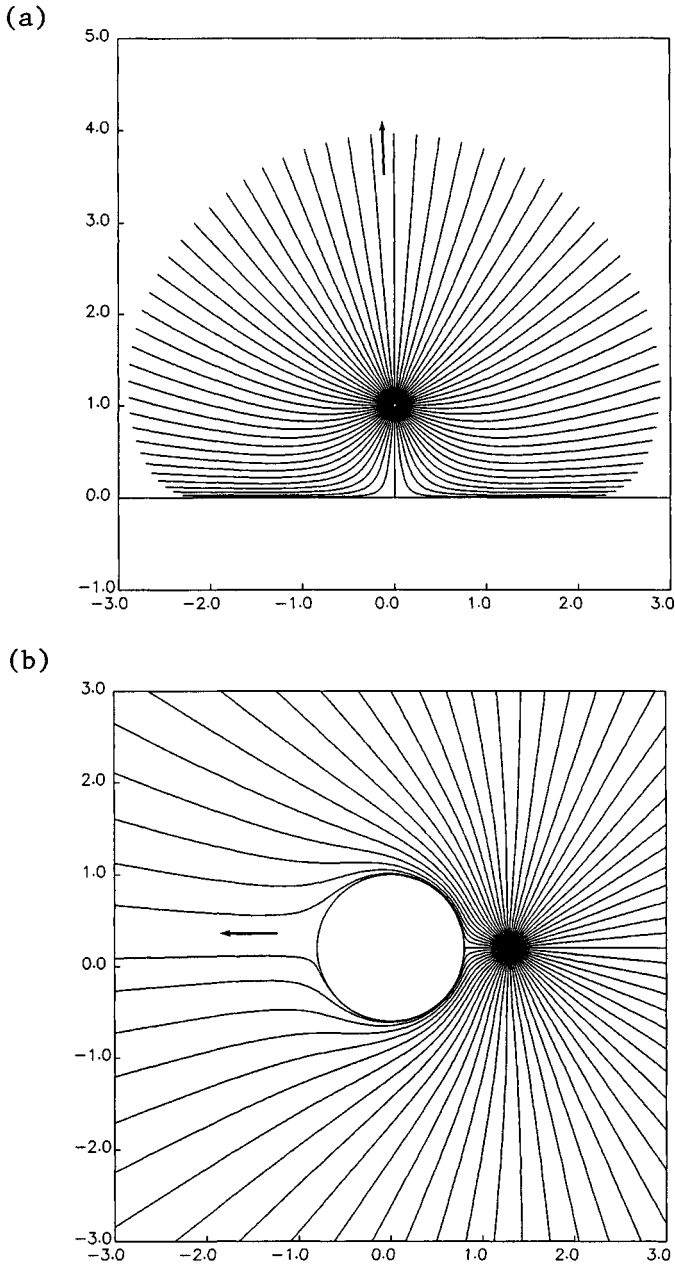


Figure 3.6.1 Streamline pattern in a meridional plane of the flow due to a three-dimensional point source (a) above a plane wall, and (b) in front of a sphere.

Problem 3.6.2 *Stream functions.*

Consider a system of cylindrical polar coordinates with origin at the location of a three-dimensional point source or point-source dipole, and derive expressions for the axisymmetric stream function.

3.7 Point vortices and line vortices

Consider a long circular cylinder parallel to the z axis immersed in an infinite fluid, rotating around its axis at constant angular velocity, thereby generating a two-dimensional swirling flow. In plane polar coordinates with origin at the center of the cylinder located at $\mathbf{x}_0 = (x_0, y_0)$, the radial and polar components of the velocity are given by

$$u_r(x, y) = 0, \quad u_\theta(x, y) = \frac{\kappa}{2\pi} \frac{1}{r}, \quad (3.7.1)$$

where $r = \sqrt{(x - x_0)^2 + (y - y_0)^2}$ is the distance of the point where the velocity is evaluated, $\mathbf{x} = (x, y)$, from the center of the cylinder, and κ is a constant with units of velocity multiplied by length. The magnitude and sign of κ express, respectively, the strength of the flow and the direction of rotation. If κ is positive, point particles in the flow rotate in the counter-clockwise direction around the cylinder; if κ is negative, point particles rotate in the clockwise direction.

Note that the magnitude of the polar component of the velocity u_θ decays like $1/r$. In contrast, if the fluid rotated as a rigid body around the point \mathbf{x}_0 with angular velocity Ω , then u_θ would be increasing linearly with respect to radial distance r , as $u_\theta = \Omega r$. Clearly, the velocity field (3.7.1) represents a flow that is different than rigid-body rotation.

3.7.1 Point vortex singularity

The flow described by equations (3.7.1) is physically meaningful only in the exterior of the cylinder. Neglecting the surface of the cylinder and extending the domain of flow all the way up to the center of the cylinder, we obtain a singular flow described as the flow due to a *point vortex* with strength κ , as illustrated in figure 3.7.1(a). The singularity occurs because, as the distance from the point vortex, r , tends to zero, the magnitude of the velocity tends to become infinite.

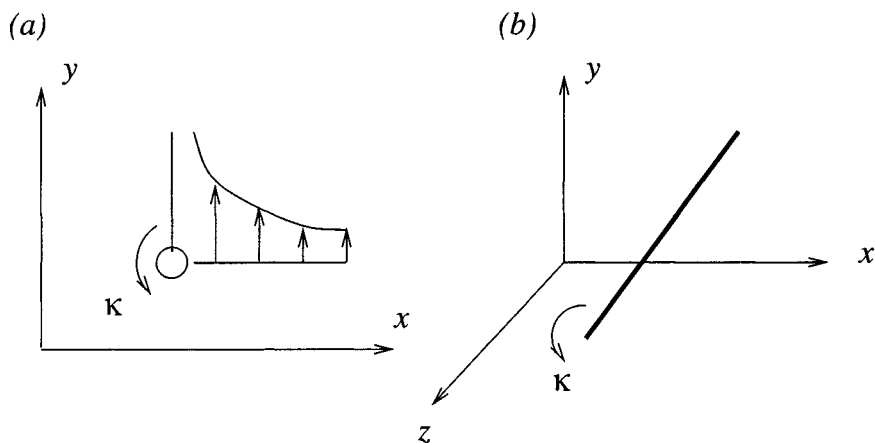


Figure 3.7.1 (a) Two-dimensional, and (b) three-dimensional perspective of a point vortex with positive strength representing a rectilinear line vortex parallel to the z axis.

3.7.2 Vorticity and circulatory motion

To confirm that the flow due to a point vortex is irrotational, we substitute expressions (3.7.1) into equation (2.3.16), and find that the strength of the vorticity vanishes at every point in the flow, except at the location of the point vortex \mathbf{x}_0 where a singularity appears. This behavior is responsible for classifying the point vortex as a singularity of two-dimensional irrotational flow.

A seemingly paradoxical behavior has arisen: because the flow is irrotational at every point except at the location of the point vortex, small circular fluid parcels not containing the point vortex translate and deform but do not rotate around their center, and yet the fluid exhibits a net circulatory motion. These two features, however, are not inconsistent, and their apparent but not essential contradiction serves to underscore that *global circulatory motion does not necessarily imply a rotational flow*.

3.7.3 The potential of irrotational circulatory flow

The occurrence of circulation has an important implication on the description of the flow in terms of the velocity potential. To see this, we

use equations (3.2.18) to find that the potential due to a point vortex, denoted by ϕ^{PV} , satisfies the equations

$$\frac{\partial \phi^{PV}}{\partial r} = 0, \quad \frac{1}{r} \frac{\partial \phi^{PV}}{\partial \theta} = \frac{\kappa}{2\pi} \frac{1}{r}, \quad (3.7.2)$$

which may be integrated to yield

$$\phi^{PV} = \frac{\kappa}{2\pi} \theta, \quad (3.7.3)$$

where θ is the polar angle measured around the point vortex from an arbitrary orientation. An arbitrary but irrelevant constant may be added to the right-hand side of (3.7.3).

As we move around the point vortex on a circular path in the counterclockwise direction, the potential increases in proportion to the angle θ according to equation (3.7.3). But then, as we approach the point of departure, because θ has increased by 2π , the potential undergoes a jump with respect to the initial value, equal to κ . We can continue traveling around the point vortex for one more turn, only to find that each time we perform a complete rotation, the potential undergoes a jump equal to κ . This observation illustrates that the potential associated with a point vortex is multi-valued. Moreover, since our point of departure is arbitrary, the potential is multi-valued at every point in the flow.

We have discovered, by example, that circulatory motion is associated with a multi-valued potential, and vice versa. In practice, a multi-valued potential is too ambiguous to handle by analytical or numerical methods. To circumvent this difficulty, we may proceed in two ways. In the first approach, we decompose the potential into an “easy to handle” multi-valued part and a “harder to get” complementary single-valued part; we specify the former, and obtain the latter by analytical or numerical computation. The implementation of this method will be discussed in Chapter 12 in the context of aerodynamics. In the second approach, we introduce an artificial boundary residing in the fluid, called a branch cut, and work under the assumption that the potential on either side of this boundary has two different values. If the flow does not exhibit a net circulatory motion, the two values are identical.

3.7.4 Flow past a circular cylinder with non-zero circulation

To illustrate the usefulness of the point vortex singularity, we reconsider the problem of uniform flow past a cylinder discussed in Section

3.5. Equation (3.5.28) provides us with the single-value harmonic potential in the absence of circulatory motion around the cylinder. To allow for circulatory motion, we add to the right-hand side of (3.5.28) the potential due to a point vortex situated at the center of cylinder given in equation (3.7.3), obtaining

$$\phi = V_x \left(r + \frac{a^2}{r} \right) \cos \theta + \frac{\kappa}{2\pi} \theta. \quad (3.7.4)$$

The corresponding Cartesian components of the velocity are given by

$$\begin{aligned} u_x &= V_x \left[1 + \frac{a^2}{r^2} - \frac{2x^2 a^2}{r^4} \right] - \frac{\kappa}{2\pi} \frac{y}{r^2}, \\ u_y &= -V_x \frac{2xy a^2}{r^4} + \frac{\kappa}{2\pi} \frac{x}{r^2}. \end{aligned} \quad (3.7.5)$$

The radial component of the velocity $u_r = \partial\phi/\partial r$ vanishes at the surface of the cylinder located at $r = a$, and the no-penetration condition is fulfilled, as required.

A simple rearrangement of (3.7.4) provides us with the dimensionless form

$$\phi = V_x a \left[\cos \theta \left(\hat{r} + \frac{1}{\hat{r}} \right) - 2\beta \theta \right], \quad (3.7.6)$$

where $\hat{r} = r/a$ is the dimensionless radial distance, with the value of unity $\hat{r} = 1$ corresponding to the surface of the cylinder, and

$$\beta \equiv -\frac{\kappa}{4\pi V_x a} \quad (3.7.7)$$

is the dimensionless circulation number. When $\beta = 0$, the circulation vanishes. Expression (3.7.6) reveals that the structure of the flow is determined by the value of the dimensionless parameter β .

The tangential component of the velocity on the surface of the cylinder is given by

$$u_\theta(r = a) = -2 V_x \sin \theta + \frac{\kappa}{2\pi a} = -2 V_x (\sin \theta + \beta). \quad (3.7.8)$$

The magnitude of $u_\theta(r = a)$ vanishes when $\theta = \arcsin(-\beta)$, and this suggests that stagnation points occur on the surface on the cylinder when $-1 \leq \beta \leq 1$. As β is raised from zero to unity, the stagnation points at $\theta = 0$ and π move towards, and then merge at the lowest point on the surface of the cylinder located at $\theta = -\pi/2$. When β exceeds the

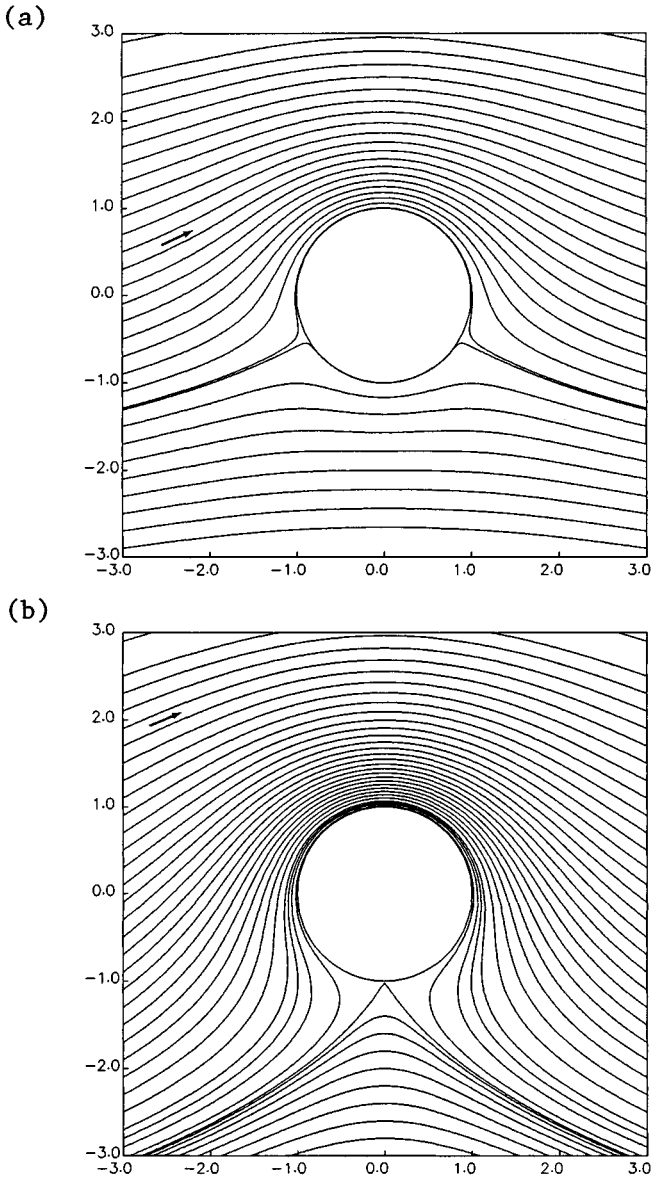


Figure 3.7.2 Streamline pattern of uniform flow past a circular cylinder with different degrees of circulation around the cylinder determined by the dimensionless parameter β defined in equation (3.7.7); (a) $\beta = 0.5$, (b) 1.0, and (c) 1.2. The streamline pattern for $\beta=0$ is shown in figure 3.5.3(a).

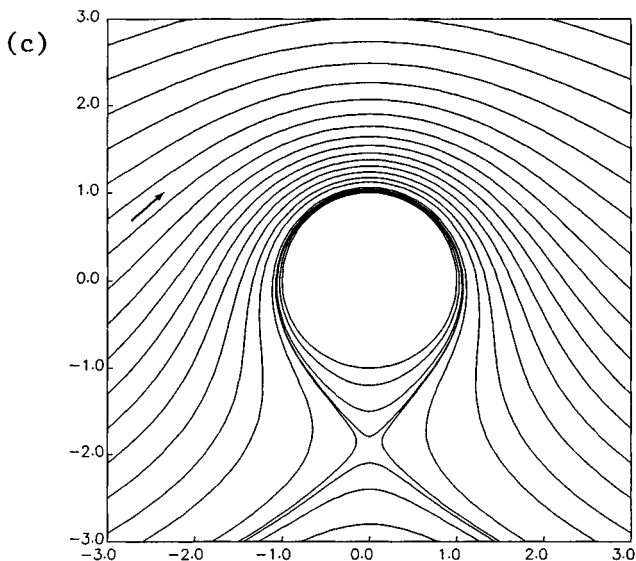


Figure 3.7.2 *Continued.*

value of unity, the merged stagnation point moves off the surface of the cylinder and into the flow. Streamline patterns for $\beta = 0.5, 1.0,$ and 1.2 illustrating this transition are shown in figure 3.7.2.

3.7.5 Circulation

Having discussed the occurrence of circulation around a cylinder placed in a uniform flow, we proceed to extend the concept of circulation to more general flow configurations.

Consider a two-dimensional flow in the xy plane, and draw a simple closed loop within it. If the loop encloses fluid alone and no boundaries, then it is called *reducible*, whereas if the loop encloses fluid and one or more boundaries, then it is called *irreducible*. The distinguishing feature of a reducible loop is that it can be shrunk to a point without crossing flow boundaries. A reducible and two irreducible loops are depicted in figure 3.7.3.

Select now a point on a reducible or irreducible loop, and introduce the unit tangent vector $\mathbf{t} = (t_x, t_y)$ pointing in the counterclockwise direction, as shown in figure 3.7.3. The inner product of the velocity and the unit tangent vector is given by the right-hand side of (2.6.8). The cir-

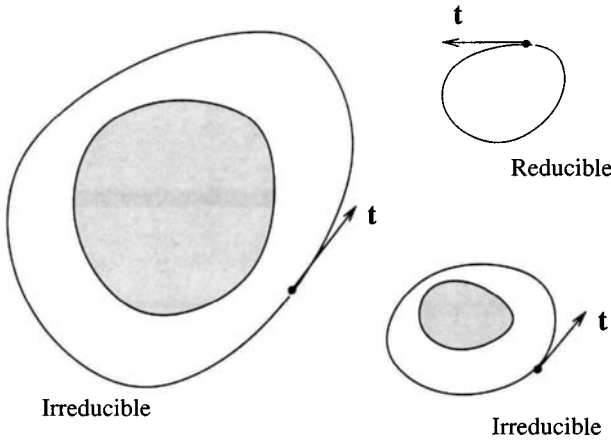


Figure 3.7.3 Examples of a reducible loop and two irreducible loops in a two-dimensional flow. The shaded areas represent flow boundaries.

circulation around the loop is defined as the line integral of the tangential component of the velocity with respect to arc length around the closed loop, l ,

$$C \equiv \oint_L u_t dl = \oint_L \mathbf{u} \cdot \mathbf{t} dl, \quad (3.7.9)$$

where L denotes the loop, and $dl = \sqrt{dx^2 + dy^2}$ is the differential arc length around the loop.

Reducible loops

Stokes's circulation theorem, to be discussed in Section 11.1, states that *if a loop is reducible*, and if no point vortices reside within the area enclosed by the loop, then the circulation around the loop is equal to the strength of the vorticity integrated over the area of fluid D enclosed by the loop,

$$C = \int_D \omega_z dx dy. \quad (3.7.10)$$

In this case, the right-hand sides of (3.7.9) and (3.7.10) are equal.

One consequence of the Stokes circulation theorem is that, because the strength of the vorticity in an irrotational flow vanishes at every point,

the circulation around any reducible loop drawn in an irrotational flow is equal to zero. The important implications of this statement will be discussed in Chapter 11 in the context of vortex dynamics.

Reducible loops enclosing point vortices

If a reducible loop encloses a collection of N point vortices with strengths $\kappa_1, \kappa_2, \dots, \kappa_N$, then the circulation around the loop is equal to the sum of the strengths of the point vortices,

$$C = \sum_{i=1}^N \kappa_i. \quad (3.7.11)$$

If some of the point vortices have positive strength and others have negative strength, so that the net sum of the strengths is equal to zero, then the circulation around the loop vanishes.

As an example, we consider uniform flow past a circular cylinder described by the potential shown in equation (3.7.4). According to the preceding discussion, the circulation around any loop that encloses the cylinder should be equal to κ . To confirm this, we compute the circulation around a loop of radius R centered at the cylinder, and find

$$\begin{aligned} C &\equiv \oint u_t \, dl = \oint u_\theta \, R \, d\theta = R \oint \frac{1}{r} \frac{\partial \phi}{\partial \theta} \, d\theta \\ &= R \frac{1}{R} \oint \frac{\kappa}{2\pi} \, d\theta = \kappa, \end{aligned} \quad (3.7.12)$$

as expected.

Irreducible loops

If a loop encloses one or more flow boundaries, then the circulation around the loop may have any value. In practice, this value is set internally during the start up period when the flow develops from the state of rest. The amount circulation established around a moving body is of great significance in aerodynamics, as will be discussed in Chapter 12.

3.7.6 Line vortices in three-dimensional flow

Viewed from a three-dimensional perspective, a point vortex in the xy plane appears like a straight line vortex, also called a *rectilinear* line

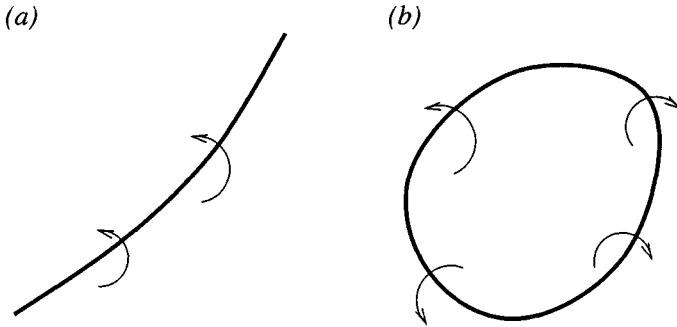


Figure 3.7.4 Illustration of (a) an infinite, and (b) a closed line vortex in three-dimensional flow.

vortex parallel to the z axis, as shown in figure 3.7.1(b). Deforming this rectilinear line vortex, or merging its two ends to form a closed loop, we obtain a curved three-dimensional line vortex in a three-dimensional flow. An example familiar to smokers is a closed line vortex with a circular or wobbly shape, called a line vortex ring.

A line vortex may be infinite, as illustrated in figure 3.7.4(a), or closed, as illustrated in figure 3.7.4(b), but may not end suddenly in the interior of the fluid. In real life, of course, a fluid is always bounded, and an infinite line vortex must inevitably end at the boundaries of the flow. The analysis and computation of the flow associated with, and induced by three-dimensional line vortices defines an important field of fluid dynamics with important applications in turbulent motion and aerodynamics, as will be discussed in Chapters 11 and 12.

Problems

Problem 3.7.1 *Stream function of a point vortex.*

Derive the stream function associated with a point vortex.

Problem 3.7.2 *Circulation around a loop.*

Consider a closed loop that performs two turns around a point vortex with strength κ . Explain why the circulation around this loop is equal to 2κ .

Problem 3.7.3 *Point-vortex doublet.*

Just as the point-source dipole arises from a point source/sink doublet, as discussed in Section 3.5, a point-vortex doublet arises from a point vortex with positive strength and a point vortex with negative strength of equal magnitude, in the limit as the distance between the two point vortices vanishes while their strength increases by the inverse proportion.

The harmonic potential associated with a point-vortex doublet oriented along the x or y axis is given, respectively, by

$$\phi^{PVD-x}(x, y) = \lambda_x \frac{\partial \theta^{PV}}{\partial x_0}, \quad \phi^{PVD-y}(x, y) = \lambda_y \frac{\partial \theta^{PV}}{\partial y_0}, \quad (3.7.13)$$

where λ_x and λ_y are the components of the vectorial strength of the point-vortex dipole in the x and y direction.

Carry out the differentiations on the right-hand sides of (3.7.13), and compare the resulting expressions with those shown in equations (3.5.17) and (3.5.22) for the two-dimensional point-source dipole. On the basis of this comparison, establish a relationship between the flow due to a point-vortex doublet and the flow due to a point-source dipole.

Problem 3.7.4 *Loops in three-dimensional flow.*

(a) Consider a three-dimensional flow extending to infinity and bounded internally by a toroidal boundary having the shape of a doughnut. Show that this flow contains irreducible loops that may not be shrunk to a point without crossing the boundaries.

(b) Invent another three-dimensional flow containing irreducible loops.

Chapter 4

Forces and stresses

- 4.1 Body forces and surface forces
- 4.2 Traction and the stress tensor
- 4.3 Traction jump across a fluid interface
- 4.4 Stresses in a fluid at rest
- 4.5 Viscous and Newtonian fluids
- 4.6 Simple non-Newtonian fluids
- 4.7 Stresses in polar coordinates
- 4.8 Boundary condition on the tangential velocity
- 4.9 Wall stresses in Newtonian fluids

In previous chapters, we have discussed the kinematic structure of a flow, but made no reference to the external action that is necessary for establishing the flow or to the physical mechanism that is responsible for sustaining the motion. Consideration of these issues requires an understanding of the hydrodynamic forces developing in a fluid as a result of the motion. In this chapter, we discuss the physical origin of these forces and introduce constitutive equations relating the stresses developing at the surface of infinitesimal fluid parcels to the parcel deformation. In subsequent chapters, we shall use these constitutive equations to build an integrated theoretical framework that will allow us to compute the structure of a steady flow and the evolution of an unsteady flow from a specified initial state.

4.1 Body forces and surface forces

Two types of forces are exerted on any piece of material: homogeneous forces acting on its volume, and surface forces acting on its boundaries. Establishing the origin of these forces is the subject of molecular physics. A brief overview for fluids suffices for the purposes of our discussion.

4.1.1 Body forces

A parcel of fluid, like any material, is subject to forces mediated by an ambient gravitational, electrical, or electromagnetic field; the last two types of forces arise only when the fluid is electrically charged, or else contains molecules or particles of a polarized material. Under the influence of these fields, the molecules residing within the parcel are acted upon individually and *independently* by a force that may be constant or vary with position in the fluid. The sum of the forces exerted on the individual molecules amounts to a net *body force* that is proportional to the number of molecules residing within the parcel, and thus to the parcel volume.

Consider, for example, the force $d\mathbf{F}_p$ exerted on a small fluid parcel with volume dV_p , density ρ , and mass $dm_p = \rho dV_p$, due to the gravitational field. By definition, the gravitational force is given by

$$d\mathbf{F}_p = \mathbf{g} \rho dV_p, \quad (4.1.1)$$

where \mathbf{g} is the acceleration of gravity. The right-hand side of (4.1.1) has units of acceleration multiplied by mass which amounts to force. One distinguishing feature of the body force due to gravity is that it is independent of the molecular motion: a certain mass of fluid weighs the same independent of whether the fluid is stationary or flows.

4.1.2 Surface forces

A different kind of force arises at the surfaces of fluid parcels and at the boundaries of a fluid. This surface force is responsible, for example, for the force exerted on the surface of a bubble rising through an ambient liquid due to buoyancy. More generally, a surface force is defined on any surface drawn within the bulk of a fluid or over its boundary.

Understanding the physical origin of the surface forces requires consideration of molecular motions and necessitates a distinction between gases and liquids. One key idea is the equivalence between local hydrodynamic force and rate of exchange of momentum between adjacent fluid layers due to molecular excursions.

To understand the origin of surface forces developing in a gas, we draw a surface in its interior, and consider the momentum of the molecules crossing the surface from either side. The momentum normal to the surface is responsible for a normal force. If the molecules move with different

average velocities on either side of the surface, where the average velocity can be identified with the velocity of the fluid at the location where a molecule last underwent a collision with one of its peers, then the net transport of tangential momentum due to this difference is responsible for a tangential surface force necessary to accelerate or decelerate the molecules. The effective force field due to the tangential surface force slows down fast-moving molecules as they move towards regions of slower moving fluid.

The physical origin of surface forces developing in a liquid is somewhat different. The molecules of a liquid perform oscillatory motions around a mean position with an amplitude that is determined by their distance from the closely packed neighbors. Occasional excursions into vacant spots are responsible for momentum transport which may be attributed to the action of a surface force.

4.2 Traction and the stress tensor

Consider a small surface with area dS centered at the point $\mathbf{x} = (x, y, z)$, drawn within a stationary or moving fluid, as illustrated in figure 4.2.1(a). The designated outer side of the surface is indicated by the direction of the unit vector normal to the surface at the point \mathbf{x} , denoted as \mathbf{n} . According to our discussion in Section 4.1, a body of fluid whose instantaneous boundary includes the small surface under consideration experiences a surface force denoted as $d\mathbf{F}^S$. This surface force may point in any direction, that is, it may have a component normal to the surface, and a component tangential to the surface.

The ratio between the surface force $d\mathbf{F}^S$ and the area of the surface dS is the *average stress* exerted on the surface. As the surface area dS becomes infinitesimal, the average stress tends to a limit defined as the traction exerted on the infinitesimal surface, denoted as \mathbf{f} . Thus, by definition, the traction is given by the relation

$$\mathbf{f} \equiv \frac{d\mathbf{F}^S}{dS}. \quad (4.2.1)$$

The three scalar components of the traction have units of force per area which amounts to stress. Rearranging equation (4.2.1), we obtain an expression for the surface force exerted on an infinitesimal surface in terms of the traction,

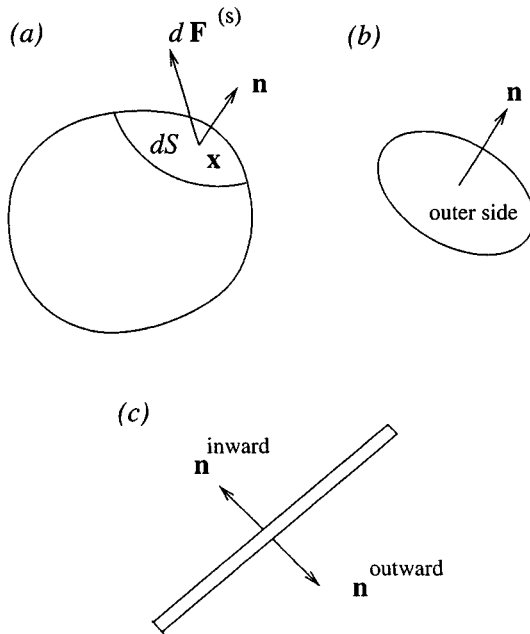


Figure 4.2.1 Illustration of (a) a small section of the surface of a fluid parcel used to define the hydrodynamic traction exerted on the parcel; (b) a thin layer of a fluid with a designated outer side; and (c) a thin layer of a fluid adjacent to a boundary used to define the hydrodynamic force exerted on the boundary.

$$d\mathbf{F}^S = \mathbf{f} dS. \quad (4.2.2)$$

It is clear from the definition (4.2.1) that the traction is physically significant only when (a) the location, and (b) the side of the infinitesimal surface upon which the traction is exerted are specified, respectively, in terms of the coordinates of the center-point \mathbf{x} and the orientation of the unit normal vector \mathbf{n} . This requirement is signified by writing

$$\mathbf{f}(\mathbf{x}, \mathbf{n}), \quad (4.2.3)$$

where the parentheses enclose the arguments of the three scalar components of the traction. If the flow is unsteady, or the position or orientation of the surface change in time, time should be added to the list of arguments on the right-hand side of (4.2.3).

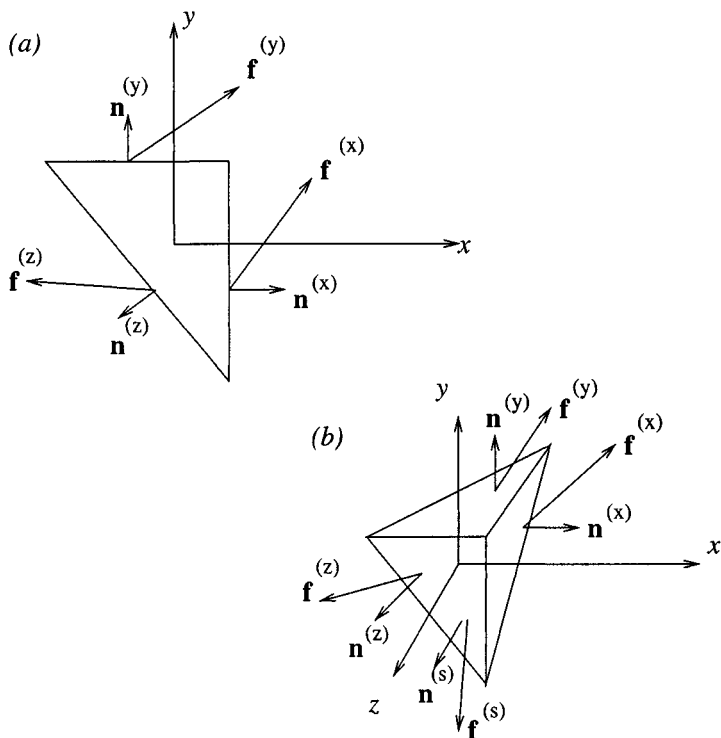


Figure 4.2.2 (a) A triangular fluid parcel in a two-dimensional flow, and (b) a polyhedral fluid parcel in a three-dimensional fluid, used as devices for computing the traction exerted on an arbitrary surface in terms of the unit vector normal to the surface and the stress tensor.

4.2.1 The stress tensor

Consider the traction exerted on a small surface that is perpendicular to the x , y or z axis, where the normal vector points in the positive directions of these axes, denoted, respectively, by

$$\mathbf{f}^{(x)} = (f_x^{(x)}, f_y^{(x)}, f_z^{(x)}), \quad \mathbf{f}^{(y)} = (f_x^{(y)}, f_y^{(y)}, f_z^{(y)}),$$

$$\mathbf{f}^{(z)} = (f_x^{(z)}, f_y^{(z)}, f_z^{(z)}), \tag{4.2.4}$$

as depicted in figure 4.2.2. Stacking these vectors on top of one another

in a particular order, we obtain the stress tensor

$$\sigma \equiv \begin{bmatrix} f_x^{(x)} & f_y^{(x)} & f_z^{(x)} \\ f_x^{(y)} & f_y^{(y)} & f_z^{(y)} \\ f_x^{(z)} & f_y^{(z)} & f_z^{(z)} \end{bmatrix}. \quad (4.2.5)$$

Introducing the standard two-index notation for the components of the stress tensor, we write

$$\sigma_{ij} \equiv f_j^{(i)}. \quad (4.2.6)$$

The first index of σ_{ij} indicates the component of the normal vector of the infinitesimal surface upon which the traction is exerted; the second index indicates the component of the corresponding traction. With the convention expressed by (4.2.6), the stress tensor takes the form

$$\sigma = \begin{bmatrix} \sigma_{xx} & \sigma_{xy} & \sigma_{xz} \\ \sigma_{yx} & \sigma_{yy} & \sigma_{yz} \\ \sigma_{zx} & \sigma_{zy} & \sigma_{zz} \end{bmatrix}. \quad (4.2.7)$$

In the case of two-dimensional flow in the xy plane, the stresses are placed in the 2×2 stress tensor

$$\sigma = \begin{bmatrix} \sigma_{xx} & \sigma_{xy} \\ \sigma_{yx} & \sigma_{yy} \end{bmatrix}. \quad (4.2.8)$$

We shall see later in this chapter that, with the exception of σ_{zz} , the omitted components involving the subscript z are equal to zero.

4.2.2 Traction in terms of the stress tensor

We shall demonstrate now that the dependence of the traction on the position vector and on the normal vector, displayed symbolically in (4.2.3), may be decoupled in a simple fashion yielding

$$\mathbf{f}(\mathbf{x}, \mathbf{n}) = \mathbf{n} \cdot \sigma(\mathbf{x}). \quad (4.2.9)$$

In index notation,

$$f_j(\mathbf{x}, \mathbf{n}) = n_i \sigma_{ij} = n_x \sigma_{xj} + n_y \sigma_{yj} + n_z \sigma_{zj}, \quad (4.2.10)$$

where the index j is free to vary over x , y , and z , and summation of the repeated index i is implied in the middle expression of (4.2.10).

An important consequence of (4.2.9) is that, if the nine components of the stress tensor are known at a point, then the traction exerted on *any* infinitesimal surface centered at that point may be evaluated in terms of the unit normal vector, merely by carrying out a vector-matrix multiplication.

To confirm that expression (4.2.9) is consistent with the foregoing definitions, we choose $\mathbf{n} = (1, 0, 0)$ and carry out the vector-matrix multiplication on the right-hand side of (4.2.10) to find $\mathbf{f} = \mathbf{f}^{(x)}$, as required. Working in a similar fashion with $\mathbf{n} = (0, 1, 0)$ and $\mathbf{n} = (0, 0, 1)$, we find $\mathbf{f} = \mathbf{f}^{(y)}$ and $\mathbf{f} = \mathbf{f}^{(z)}$, as required. It remains to show that (4.2.9) holds true for more general orientations of the unit normal vector \mathbf{n} . For simplicity, we work out the proof for two-dimensional flow in the xy plane, with reference to the 2×2 stress tensor defined in (4.2.8).

We begin by considering a small area of fluid enclosed by an infinitesimal triangle with two sides perpendicular to the x and y axis, as depicted in figure 4.2.2(a). Newton's second law of motion requires that the rate of change of momentum of the fluid enclosed by the triangle be balanced by the forces exerted on it, including the body force and the surface force associated with the traction exerted on the three sides.

Now, the momentum of the parcel and the body force exerted on the parcel are both proportional to the area of the triangle, $\frac{1}{2}\Delta x\Delta y$. The surface force exerted on the vertical side is equal to $\mathbf{f}^{(x)}\Delta y$, the surface force exerted on the horizontal side is equal to $\mathbf{f}^{(y)}\Delta x$, and the surface force exerted on the slanted side is equal to $\mathbf{f}^{(s)}\Delta l$, where $\Delta l = \sqrt{\Delta x^2 + \Delta y^2}$. In the limit as Δx and Δy tend to zero, the fluid momentum and body force become negligible compared to the surface forces exerted on the sides, and the sum of the three surface forces should vanish. Setting the x and y components of the sum equal to zero, we find

$$\begin{aligned} f_x^{(s)} \Delta l + \sigma_{xx} \Delta y + \sigma_{yx} \Delta x &= 0, \\ f_y^{(s)} \Delta l + \sigma_{xy} \Delta y + \sigma_{yy} \Delta x &= 0. \end{aligned} \tag{4.2.11}$$

Considering now the unit vector normal to the slanted side of the triangle pointing outward, denoted by $\mathbf{n}^{(s)}$, we use elementary trigonometry to write

$$n_x^{(s)} = -\frac{\Delta y}{\Delta l}, \quad n_y^{(s)} = -\frac{\Delta x}{\Delta l}. \tag{4.2.12}$$

Combining equations (4.2.11) and (4.2.12), we find

$$\begin{aligned}
 f_x^{(s)} &= n_x^{(s)} \sigma_{xx} + n_y^{(s)} \sigma_{yx}, \\
 f_y^{(s)} &= n_x^{(s)} \sigma_{xy} + n_y^{(s)} \sigma_{yy},
 \end{aligned}
 \tag{4.2.13}$$

which are the x and y components of (4.2.9).

An analogous proof can be worked out for three-dimensional flow, by considering the forces exerted on the polyhedral fluid parcel illustrated in figure 4.2.2(b) (problem 4.2.1).

4.2.3 Traction on either side of a fluid surface

Consider now a thin layer of fluid with a designated outer side indicated by the direction of the unit normal vector \mathbf{n} , and an opposing inner side indicated by the direction of the normal vector $\mathbf{n}^{inner} = -\mathbf{n}$, as illustrated in figure 4.2.1(b). Balancing the rate of change of momentum of the fluid that resides within the layer with the forces exerted on it, and repeating the preceding arguments on the insignificance of the fluid momentum and body forces compared to the surface forces, we derive the force balance equation

$$\mathbf{f}^{outer} + \mathbf{f}^{inner} = \mathbf{0},
 \tag{4.2.14}$$

which is a statement of Newton's law of action and reaction: the force exerted on one body by another is equal in magnitude and opposite in direction to that exerted on the second body by the first.

It is reassuring to confirm that expression (4.2.9) is consistent with the physical law expressed by (4.2.14). Substituting the former into the latter, we obtain

$$\mathbf{n} \cdot \boldsymbol{\sigma} + \mathbf{n}^{inner} \cdot \boldsymbol{\sigma} = \mathbf{0},
 \tag{4.2.15}$$

which holds true in view of the definition $\mathbf{n}^{inner} = -\mathbf{n}$. More generally, a prerequisite for the satisfaction of (4.2.14) is the property

$$\mathbf{f}(\mathbf{x}, -\mathbf{n}) = -\mathbf{f}(\mathbf{x}, \mathbf{n}),
 \tag{4.2.16}$$

which is clearly shared by the right-hand side of (4.2.9)

4.2.4 Traction exerted on a boundary

Consider next a small fluid surface at the boundary of a flow. The outer side of the surface is indicated by the unit normal vector $\mathbf{n}^{outward}$ pointing into the boundary, as illustrated in figure 4.2.1(c). Newton's law of action and reaction requires that the traction exerted on the fluid surface should balance the traction exerted by the fluid on the boundary, denoted by \mathbf{f}^B . Thus,

$$\mathbf{f}^B + \mathbf{n}^{outward} \cdot \sigma = 0. \quad (4.2.17)$$

In terms of the inward unit normal vector pointing into the fluid, denoted by $\mathbf{n}^{inward} = -\mathbf{n}^{outward}$, we obtain

$$\mathbf{f}^B = \mathbf{n}^{inward} \cdot \sigma, \quad (4.2.18)$$

Expression (4.2.18) allows us to compute the traction exerted on a boundary in terms of the stress tensor evaluated at the boundary.

4.2.5 Symmetry of the stress tensor

A fundamental law of mechanics originating from Newton's second law of motion requires that the rate of change of angular momentum of a fluid parcel be balanced by the torque exerted on it, including the torque due to body forces and the torque due to surface forces. The torque with respect to the point \mathbf{x}_0 due to a force \mathbf{F} applied at the point \mathbf{x} is defined by the outer vector product

$$\mathbf{T} \equiv (\mathbf{x} - \mathbf{x}_0) \times \mathbf{F}. \quad (4.2.19)$$

Applying this law for a rectangular fluid parcel whose sides are parallel to the x , y , and z , axes, we find, that, in the absence of a body force that induces a torque, the tangential component of the traction in the j th direction exerted on the side that is perpendicular to the i th axis must be equal to the tangential component of the traction in the i th direction exerted on the side that is perpendicular to the j th axis, otherwise an imbalanced asymmetry will arise (problem 4.2.2). Thus,

$$f_j^{(i)} = f_i^{(j)}, \quad (4.2.20)$$

which states that the stress tensor is symmetric,

$$\sigma_{ij} = \sigma_{ji}. \quad (4.2.21)$$

It is important to emphasize that the stress tensor is symmetric only in the absence of an externally induced torque; that is, in the absence of an external force field causing point particles to spin around an axis. In the remainder of this book, we shall tacitly assume that this restriction is satisfied.

Problems

Problem 4.2.1 *Traction in three-dimensional flow.*

Prove expression (4.2.9) for three-dimensional flow. *Hint:* Perform a force balance over the polyhedral volume depicted in figure 4.2.2(b).

Problem 4.2.2 *Symmetry of the stress tensor.*

Prove the symmetry of the tensor for two-dimensional flow in the absence of an externally induced torque.

4.3 Traction jump across a fluid interface

Equation (4.2.14) states that the traction exerted on one side of a surface drawn in a fluid is equal in magnitude and opposite in direction to that exerted on the other side. To derive this relation, we performed a force balance over a thin fluid layer centered at the surface, considering the force exerted along the edges infinitesimal. If the fluid residing within the layer is homogeneous, then the edge force scales with the layer thickness and is negligible indeed compared to the surface force exerted on the sides.

If, however, the thin layer is centered at an interface between two different fluids instead of a regular surface residing in a homogeneous fluid, differences in the magnitude of molecular forces on either side of the layer generate an edge force that does not scale with the layer thickness. This edge force may be expressed in terms of the interfacial tension γ , defined as the force per unit length exerted around the edge of a section of an interface.

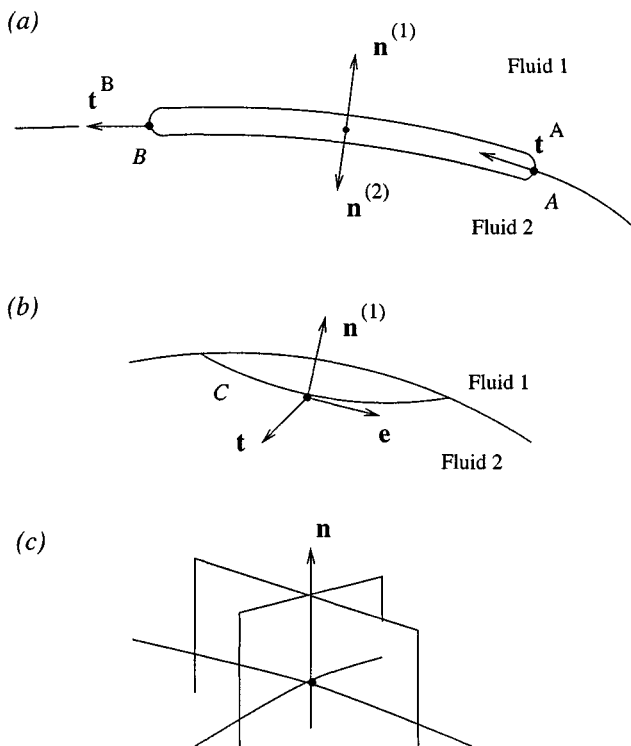


Figure 4.3.1 Forces exerted on a thin fluid layer centered at (a) a two-dimensional, or (b) a three-dimensional interface, including the hydrodynamic force due to the fluid stresses, and the force due to the surface tension. (c) The mean curvature of a three-dimensional surface is equal to the average of the directional curvatures in two perpendicular planes containing the normal vector.

The interfacial tension pulls the interfacial layer in a direction that is tangential to the interface and normal to the edges. The magnitude of the tension depends on the local temperature and molecular constitution of the interface as determined, for example, by the concentration of a surface-active substance residing over interface, called a surfactant. The higher the temperature or the concentration of a surfactant, the lower the surface tension. Surfactants are often added to liquids to lower the surface tension and achieve a desired effect: a dish or laundry detergent is a common household surfactant used to lower the strength of the forces anchoring particles to a soiled surface.

4.3.1 Two-dimensional interfaces

Consider a small section of a two-dimensional interface with length Δl , as illustrated in figure 4.3.1(a). Surface tension pulls the layer from the two edges in directions that are tangential to the interface at the two end-points A and B . Balancing the surface force due to the stress tensor and the edge forces, we obtain

$$[\mathbf{n}^{(1)} \cdot \boldsymbol{\sigma}^{(1)}] \Delta l + [\mathbf{n}^{(2)} \cdot \boldsymbol{\sigma}^{(2)}] \Delta l - \gamma^A \mathbf{t}^A + \gamma^B \mathbf{t}^B = \mathbf{0}, \quad (4.3.1)$$

where the unit normal vector $\mathbf{n}^{(1)}$ points into the fluid labelled 1, and the unit normal vector $\mathbf{n}^{(2)} = -\mathbf{n}^{(1)}$ points into the fluid labelled 2. Expressing the second normal vector in terms of the first one, and rearranging the resulting expression, we find

$$\mathbf{n}^{(1)} \cdot (\boldsymbol{\sigma}^{(1)} - \boldsymbol{\sigma}^{(2)}) = -\frac{\gamma^B \mathbf{t}^B - \gamma^A \mathbf{t}^A}{\Delta l}. \quad (4.3.2)$$

If the surface tension is uniform, $\gamma^B = \gamma^A$, and if the interface is flat, in which case $\mathbf{t}^B = \mathbf{t}^A$ and the vectorial difference $\mathbf{t}^B - \mathbf{t}^A$ is equal to zero, the right-hand side of (4.3.2) vanishes. Equation (4.3.2) then requires that the traction be continuous across the interface.

More generally, in the limit as the length of the segment Δl tends to zero, the right-hand side of (4.3.2) tends to the derivative of the product $\gamma \mathbf{t}$ with respect to arc length l measured in the direction of the tangent vector \mathbf{t} from an arbitrary origin,

$$\mathbf{n}^{(1)} \cdot (\boldsymbol{\sigma}^{(1)} - \boldsymbol{\sigma}^{(2)}) = -\frac{d(\gamma \mathbf{t})}{dl}. \quad (4.3.3)$$

Expanding out the derivative of the product on the right-hand side of (4.3.3), we find

$$\mathbf{n}^{(1)} \cdot (\boldsymbol{\sigma}^{(1)} - \boldsymbol{\sigma}^{(2)}) = -\gamma \frac{d\mathbf{t}}{dl} - \frac{d\gamma}{dl} \mathbf{t}. \quad (4.3.4)$$

The second term on the right-hand side of (4.3.4) contributes a traction discontinuity that is tangential to the interface, known as the *Marangoni traction*. If the surface tension is constant, the Marangoni traction does not appear.

To interpret the first term on the right-hand side of (4.3.4), we consider the difference between the two nearly equal tangent vectors \mathbf{t}^B

and \mathbf{t}^A . In the limit as Δl tends to zero, the difference between these vectors tends to a new vector directed normal to the interface. More precisely, in this limit,

$$\frac{\mathbf{t}^B - \mathbf{t}^A}{\Delta l} \rightarrow \frac{d\mathbf{t}}{dl} = -\kappa \mathbf{n}^{(1)}, \quad (4.3.5)$$

where κ is the positive or negative curvature of the interface. By definition, $\kappa = 1/R$, where R is the positive or negative radius of curvature of the interface. Substituting (4.3.5) into (4.3.4), and rearranging, we find

$$\Delta \mathbf{f} \equiv \mathbf{n}^{(1)} \cdot (\sigma^{(1)} - \sigma^{(2)}) = \gamma \kappa \mathbf{n}^{(1)} - \frac{d\gamma}{dl} \mathbf{t}. \quad (4.3.6)$$

The first term on the right-hand side of (4.3.6) contributes a traction discontinuity normal to the interface. If either the curvature of the interface or the surface tension vanishes, the normal stress is continuous across the interface.

As an example, we consider the jump in traction across the interface depicted in figure 4.3.2. The origin of the Cartesian axes has been set at a point on the interface, the x axis has been positioned tangentially to the interface, and the y axis has been positioned normal to the interface pointing into fluid labelled 1. At the origin of the Cartesian axes, the components of the unit normal vector $\mathbf{n}^{(1)}$ are given by $n_x^{(1)} = 0$ and $n_y^{(1)} = 1$, and the jump in traction is given by

$$\Delta \mathbf{f} = (\sigma_{yx}^{(1)} - \sigma_{yx}^{(2)}) \mathbf{e}_x + (\sigma_{yy}^{(1)} - \sigma_{yy}^{(2)}) \mathbf{e}_y, \quad (4.3.7)$$

where \mathbf{e}_x and \mathbf{e}_y are, respectively, the unit vectors parallel to the x and y axes. Observing that, at the origin, $\mathbf{t} = \mathbf{e}_x$ and $\mathbf{n}^{(1)} = \mathbf{e}_y$, and comparing the right-hand sides of (4.3.7) and (4.3.6), we derive an expression for the jump in the shear stress,

$$\sigma_{yx}^{(1)} - \sigma_{yx}^{(2)} = -\frac{d\gamma}{dl}, \quad (4.3.8)$$

and another expression for the jump in the normal stress,

$$\sigma_{yy}^{(1)} - \sigma_{yy}^{(2)} = \gamma \kappa. \quad (4.3.9)$$

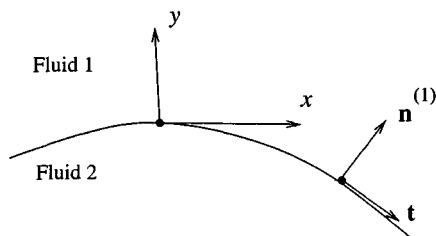


Figure 4.3.2 A local coordinate system with the x axis tangential to a two-dimensional interface at a point, used to evaluate the jump in traction across the interface.

4.3.2 Three-dimensional interfaces

To derive the counterpart of the interfacial condition (4.3.6) for a three-dimensional interface, we consider a thin fluid layer straddling a three-dimensional interface, as illustrated in figure 4.3.1(b). Let $\mathbf{n}^{(1)}$ be the unit vector normal to the interface pointing into fluid 1, and \mathbf{e} be the unit vector tangential to the layer edge. The surface tension pulls the layer in the direction of the unit vector \mathbf{t} that is tangential to the interface and normal to both $\mathbf{n}^{(1)}$ and \mathbf{e} . Recalling the geometrical interpretation of the outer vector product discussed in Section 2.3, we write

$$\mathbf{t} = \mathbf{e} \times \mathbf{n}. \quad (4.3.10)$$

Next, we balance the surface force due to the fluid stress and the edge force due to the surface tension, and find

$$[\mathbf{n}^{(1)} \cdot \boldsymbol{\sigma}^{(1)}] \Delta S + [\mathbf{n}^{(2)} \cdot \boldsymbol{\sigma}^{(2)}] \Delta S + \oint_C \gamma \mathbf{t} \, dl = 0, \quad (4.3.11)$$

where ΔS is the surface area of the layer, and l is the arc length around the layer edge C . Equation (4.3.11) is the three-dimensional counterpart of (4.3.1). Putting $\mathbf{n}^{(2)} = -\mathbf{n}^{(1)}$ and rearranging, we find

$$\mathbf{n}^{(1)} \cdot (\boldsymbol{\sigma}^{(1)} - \boldsymbol{\sigma}^{(2)}) = -\frac{1}{\Delta S} \oint_C \gamma \mathbf{t} \, dl. \quad (4.3.12)$$

It can be shown that, in the limit as ΔS tends to zero and the loop C shrinks to a point, equation (4.3.12) reduces to

$$\Delta \mathbf{f} \equiv \mathbf{n}^{(1)} \cdot (\sigma^{(1)} - \sigma^{(2)}) = \gamma 2 \kappa_m \mathbf{n}^{(1)} - \frac{\partial \gamma}{\partial l'} \mathbf{t}', \quad (4.3.13)$$

where:

- κ_m is the mean curvature of the interface.
- \mathbf{t}' is the unit vector tangent to the interface pointing in the direction along which the surface tension changes most rapidly.
- l' is the arc length measured in the direction of \mathbf{t}' .
- $\partial \gamma / \partial l'$ is the corresponding maximum rate of change of the surface tension with respect to arc length.

The first term on the right-hand side of (4.3.13) expresses a discontinuity in the normal direction; the second term expresses a discontinuity in the tangential direction identified as the Marangoni traction.

Mean curvature

To compute the mean curvature of a three-dimensional interface, we consider the traces of the interface in two orthogonal planes that are normal to the interface at a point and thus contain the normal vector, as depicted in figure 4.3.1(c). If κ_1 and κ_2 are the curvatures of the two traces at that point, computed using formula (4.3.5) with the x and y axes residing in the two planes, then the mean curvature of the interface is given by

$$\kappa_m = \frac{1}{2} (\kappa_1 + \kappa_2). \quad (4.3.14)$$

A theorem due to Euler states that the mean value is independent of the orientation of the two planes, provided that the planes are mutually orthogonal. There is a particular orientation corresponding to maximum directional curvature κ_1 , and a conjugate orthogonal orientation corresponding to minimum directional curvature κ_2 ; these are the principal curvatures of the interface at the chosen point. The computation of the mean curvature will be discussed further in chapter 5 in the context of hydrostatics.

Problems

Problem 4.3.1 *Curvature of an ellipse.*

A circle of radius a centered at the origin is described in parametric form by the equations $x = a \cos \theta$ and $y = a \sin \theta$, where θ is the polar angle varying between 0 and 2π . The components of the unit tangent vector pointing in the counter-clockwise direction are given by

$$t_x = \frac{dx}{dl}, \quad t_y = \frac{dy}{dl}, \quad (4.3.15)$$

where $dl = \sqrt{dx^2 + dy^2}$ is the differential arc length measured in the counter-clockwise direction. Using the parametric representation, we find

$$dx = -a \sin \theta d\theta, \quad dy = a \cos \theta d\theta, \quad dl = a d\theta, \quad (4.3.16)$$

yielding

$$t_x = -\sin \theta, \quad t_y = \cos \theta. \quad (4.3.17)$$

Based on these formulas, we compute

$$\frac{dt_x}{dl} = \frac{d(-\sin \theta)}{d(a\theta)} = -\frac{1}{a} \cos \theta, \quad \frac{dt_y}{dl} = \frac{d(\cos \theta)}{d(a\theta)} = -\frac{1}{a} \sin \theta. \quad (4.3.18)$$

Collecting the component equations (4.3.18), we derive the vector form

$$\frac{d\mathbf{t}}{dl} = -\frac{1}{a} \mathbf{n}^{(1)}, \quad (4.3.19)$$

where $\mathbf{n}^{(1)} = (\cos \theta, \sin \theta)$ is the unit vector normal to the circle pointing into the exterior. Comparing (4.3.20) with (4.3.5), we deduce that $\kappa = 1/a$, thereby confirming that the curvature of the circle is equal to the inverse of its radius.

Consider a horizontal ellipse centered at the origin, described in parametric form by the equations $x = a \cos \chi$ and $y = b \sin \chi$, where χ is the natural parameter of the ellipse varying between 0 and 2π , and a, b are the ellipse semi-axes. Repeat the preceding analysis to derive an expression for the curvature in terms of a, b , and χ . Confirm that, as b tends to a , the curvature of the ellipse reduces to that of a circle.

Problem 4.3.2 *Mean curvature.*

(a) Based on formula (4.3.14) and its accompanying interpretation discussed in the text, show that the mean curvature of a sphere of radius a is equal to $\kappa_m = 1/a$, whereas the mean curvature of a circular cylinder of radius a is equal to $\kappa_m = 1/(2a)$.

(b) The sphere and the circular cylinder are two examples of shapes with constant mean curvature. Discuss one additional example.

Problem 4.3.3 *Jump in traction in local coordinates.*

Derive the counterparts of equations (4.3.8) and (4.3.9) for a three-dimensional interface.

Computer problems

Problem c.4.3.1 *Computation of the curvature.*

Consider a line in the xy plane described by a set of $N + 1$ marker points with coordinates (x_i, y_i) , $i = 1, 2, \dots, N + 1$. An approximation to the components of the tangent vector at the i th point is provided by the central-difference formulas

$$t_x^{(i)} = \frac{x_{i+1} - x_{i-1}}{\Delta l^{(i)}}, \quad t_y^{(i)} = \frac{y_{i+1} - y_{i-1}}{\Delta l^{(i)}}, \quad (4.3.20)$$

where

$$\Delta l^{(i)} = [(x_{i+1} - x_{i-1})^2 + (y_{i+1} - y_{i-1})^2]^{1/2}. \quad (4.3.21)$$

The derivatives of the components of the tangent vector with respect to arc length may be approximated with the corresponding formulas

$$\frac{dt_x^{(i)}}{dl} = \frac{t_x^{(i+1)} - t_x^{(i-1)}}{\Delta l^{(i)}}, \quad \frac{dt_y^{(i)}}{dl} = \frac{t_y^{(i+1)} - t_y^{(i-1)}}{\Delta l^{(i)}}. \quad (4.3.22)$$

The components of the outward normal vector at the marker points are given by

$$[n_x^{(1)}]^{(i)} = t_y^{(i)}, \quad [n_y^{(1)}]^{(i)} = -t_x^{(i)}. \quad (4.3.23)$$

Write a computer program that reads or generates the coordinates of a set of marker points, computes the right-hand sides of (4.3.20)-(4.3.23), and then evaluates the curvature at the marker points from the expression

$$\kappa = -\frac{d\mathbf{t}}{dl} \cdot \mathbf{n}^{(1)}, \quad (4.3.24)$$

which arises by taking the inner product of the unit normal vector and the middle and right-hand side of (4.3.5).

Perform a series of computations with marker points distributed evenly along a circle, and compare the numerically computed curvatures with the exact curvature derived in problem 4.3.1.

Problem c.4.3.2 *Motion induced by curvature.*

Interfaces move under the influence of surface tension in a variety of modes. In a simplified model, point particles distributed along a two-dimensional interface move normal to the interface with velocity that is proportional to the local curvature. If $\mathbf{X}^{(i)}$ is the position of the i th marker point, then the motion of the marker point is described by the vectorial differential equation

$$\frac{d\mathbf{X}^{(i)}}{dt} = \kappa [\mathbf{n}^{(1)}]^{(i)}, \quad (4.3.25)$$

where t stands for time, $\mathbf{n}^{(1)}$ is the outward normal vector, and κ is the curvature.

Write a program that computes the motion of marker points distributed over an interface using the finite-difference approximations discussed in problem c.4.3.1, and the modified Euler method for integrating in time the differential equations (4.3.25). Run the program to compute the evolution of marker points distributed along a circle or an ellipse with axes ratio equal to 2.0, and discuss the nature of the motion.

4.4 Stresses in a fluid at rest

If a fluid does not appear to execute macroscopic motion as seen by a stationary observer, that is, the observable velocity vanishes, then the molecules are in a state of dynamic equilibrium determined by the physical conditions prevailing in their immediate environment.

Consider a cubic fluid parcel with its six faces perpendicular to the x , y , or z axis, as illustrated in figure 4.4.1. In the absence of net fluid motion, the traction exerted on the sides that are perpendicular to the x axis must be directed normal to this side, otherwise, an unresolved tangential component pointing in a physically indeterminate direction will arise. In the notation of Section 4.2,

$$f_x^{(x)} \neq 0, \quad f_y^{(x)} = 0, \quad f_z^{(x)} = 0. \quad (4.4.1)$$

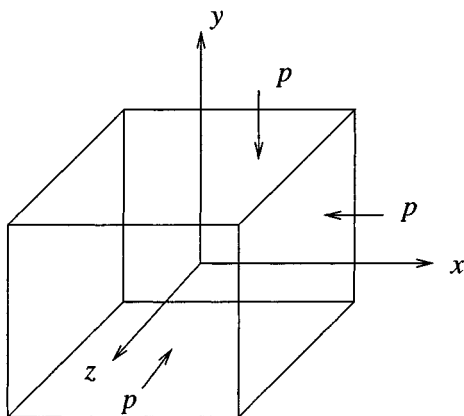


Figure 4.4.1 The traction exerted on the three sides of a cubic parcel of a stationary fluid has only a normal component that is defined in terms of the thermodynamic pressure.

Similar arguments suggest that the tractions exerted on the sides that are perpendicular to the y or z axes must be directed normal to these sides, requiring that

$$f_x^{(y)} = 0, \quad f_y^{(y)} \neq 0, \quad f_z^{(y)} = 0, \quad (4.4.2)$$

and

$$f_x^{(z)} = 0, \quad f_y^{(z)} = 0, \quad f_z^{(z)} \neq 0. \quad (4.4.3)$$

If the size of the cubic parcel is infinitesimal, the fluid residing inside the parcel is perfectly or nearly homogeneous, and the nonvanishing components of the tractions $f_x^{(x)}$, $f_y^{(y)}$, and $f_z^{(z)}$ must be identical. By definition, the common value of these normal components is equal to the negative of the pressure p ,

$$f_x^{(x)} = f_y^{(y)} = f_z^{(z)} \equiv -p. \quad (4.4.4)$$

Thus, in hydrostatics, the stress tensor introduced in equation (4.2.7) is defined exclusively in terms of the pressure, and is given by

$$\sigma = \begin{bmatrix} -p & 0 & 0 \\ 0 & -p & 0 \\ 0 & 0 & -p \end{bmatrix} = -p \begin{bmatrix} 1 & 0 & 0 \\ 0 & 1 & 0 \\ 0 & 0 & 1 \end{bmatrix}. \quad (4.4.5)$$

In compact form

$$\sigma = -p \mathbf{I}, \quad (4.4.6)$$

where \mathbf{I} is the unit or identity matrix shown on the right-hand side of (4.4.5).

4.4.1 Traction on a surface

As an application, we use expression (4.4.6) to evaluate the traction exerted on a surface drawn in a stationary fluid. Using formula (4.2.9), we find

$$\mathbf{f}(\mathbf{x}, \mathbf{n}) = \mathbf{n} \cdot (-p \mathbf{I}) = -p \mathbf{n} \cdot \mathbf{I} = -p \mathbf{n}. \quad (4.4.7)$$

The last equality arises from the identity $\mathbf{n} \cdot \mathbf{I} = \mathbf{n}$. Equation (4.4.7) shows that the traction exerted on a surface in hydrostatics is directed normal to the surface; the tangential component vanishes.

4.4.2 Traction on a flow boundary

As a second application, we use (4.4.6) to evaluate the traction exerted on a boundary confining the fluid. Using formula (4.2.18), we find

$$\mathbf{f}^B = \mathbf{n}^{inward} \cdot (-p \mathbf{I}) = -p \mathbf{n}^{inward} \cdot \mathbf{I} = -p \mathbf{n}^{inward}. \quad (4.4.8)$$

The last equality arises from the identity $\mathbf{n}^{inward} \cdot \mathbf{I} = \mathbf{n}^{inward}$. Thus, the traction exerted on a fluid boundary in hydrostatics is directed normal to the boundary; the tangential component vanishes.

4.4.3 Thermodynamics

The hydrostatic pressure distribution established in a fluid at rest cannot be computed working exclusively in the context of fluid mechanics. Additional information concerning the relationship between the density and the pressure for the particular fluid under consideration is required, and must be provided by thermodynamics.

For example, molecular thermodynamics states that the pressure of a small parcel of gas is determined by (a) the number of molecules residing within the parcel expressed by the local density ρ , (b) the kinetic energy of the molecules expressed by the absolute temperature T , and (c) the nature and intensity of the intermolecular forces expressed by an intermolecular potential. In the case of an ideal gas, intermolecular

forces are negligible, and the pressure derives from the density and the temperature in terms of the ideal gas law

$$p = \frac{\rho RT}{M}, \quad (4.4.9)$$

where:

- M is the grammo-molecular mass, defined as the mass of one mole which is comprised of a collection of N_A molecules, where $N_A = 6.022 \times 10^{26}$ is Avogadro's number. The grammo-molecular weight of an element is equal to the atomic weight of the element listed in the periodic table, expressed in grams.
- R is the ideal gas constant, equal to $R = 8.314 \times 10^3 \text{ kg m}^2/(\text{sec}^2 \text{ kmole K})$.
- T is Kelvin's absolute temperature, equal to the Celsius centigrade temperature reduced by 273 units.

Liquids, on the other hand, are nearly incompressible, and thermodynamics allows us to compute their pressure under the assumption that the density is a function of temperature alone, independent of pressure.

The computation of the hydrostatic pressure distribution in gases and liquids will be discussed in more detail in Chapter 5.

4.4.4 Jump in the hydrostatic pressure across an interface

Equations (4.3.6) and (4.3.13) provide us with expressions for the jump in the traction across a two- or three-dimensional interface. If the two fluids on either side of the interface are stationary, then the corresponding stress tensors are given by (4.4.6) with the superscript 1 or 2 included to signify the choice of fluid, and the jump in the traction is given by

$$\begin{aligned} \Delta \mathbf{f} &\equiv \mathbf{n}^{(1)} \cdot (\boldsymbol{\sigma}^{(1)} - \boldsymbol{\sigma}^{(2)}) = \mathbf{n}^{(1)} \cdot [-p^{(1)}\mathbf{I} - (-p^{(2)}\mathbf{I})] \\ &= (p^{(2)} - p^{(1)}) \mathbf{n}^{(1)}. \end{aligned} \quad (4.4.10)$$

Assuming that the surface tension is uniform, we compare the right-hand side of (4.4.10) to the right-hand side of the force equilibrium equation (4.3.6) for a two-dimensional interface, finding

$$p^{(2)} - p^{(1)} = \gamma \kappa, \quad (4.4.11)$$

Working in a similar fashion for a three-dimensional interface using (4.3.13), we find

$$p^{(2)} - p^{(1)} = \gamma 2 \kappa_m, \quad (4.4.12)$$

where κ_m is the mean curvature.

We have found that the jump in pressure across a two- or three-dimensional interface is equal to the product of the surface tension and, respectively, the curvature or twice the mean curvature of the interface.

As an application, we compute the jump in pressure across a spherical interface of radius a , representing the surface of a liquid drop or bubble. Designating the outer fluid as fluid 1 and the inner fluid as fluid 2, we find that the mean curvature of the interface is equal to $\kappa_m = 1/a$. Consequently, the pressure jump is given by $p^{(2)} - p^{(1)} = 2 \gamma/a$.

Problems

Problem 4.4.1 *Jump in pressure across a two-dimensional interface.*

Derive an expression for the jump in pressure across a circular interface of radius a representing the trace of a cylindrical thread in the xy plane.

Problem 4.4.2 *Curvature of a soap film.*

Explain why the mean curvature of a thin soap film confined between two adjacent interfaces attached to a wire frame, must vanish.

4.5 Viscous and Newtonian fluids

In the absence of macroscopically observable fluid motion, the traction exerted on a specified side of a small fluid surface is given by equation (4.4.7) in terms of the pressure. If the fluid exhibits macroscopic motion, this equation is modified in two ways: first, the normal component of the traction is enhanced with a new contribution that depends on the physical properties of the fluid and the character of the local motion; second, a tangential component is established.

To understand how these new contributions arise, we consider the tractions developing in two complementary types of flow: an extensional flow where the fluid is stretched and elongates, and a channel flow where the fluid is sheared due to boundary motion.

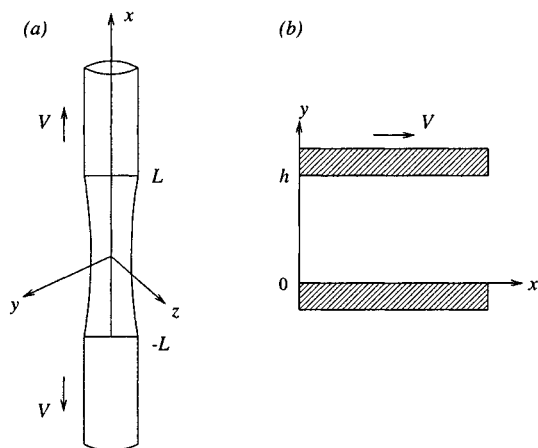


Figure 4.5.1 (a) Extension of a liquid bridge subtended between two coaxial cylinders that are pulled apart along their axes; (b) shear flow in a two-dimensional channel confined between two parallel plates; the motion is due to the in-plane translation of the upper plate.

4.5.1 Extension of a thread

In one experiment, a thread of a liquid is suspended between two rods forming an axisymmetric bridge, and the rods are pulled apart with velocity V thereby extending the thread, as illustrated in figure 4.5.1(a). A force is required to pull the rods apart and thus overcome the normal component of the hydrodynamic traction, $f_x^{(x)}$, imparted by the fluid to the tips of the rods. The faster the rods are pulled apart, the higher the magnitude of the traction; the greater the distance between the rods, the lower the magnitude of the traction.

For most common fluids, a linear relationship exists between the traction, the velocity of the rods, and the inverse of their distance, in the form

$$f_x^{(x)} = -p + 2 \mu^{ext} \frac{V}{L}, \quad (4.5.1)$$

where p is the pressure discussed in Section 4.4 in the context of hydrostatics, V is the velocity of the rods, L is half the distance between the rods, and μ^{ext} is a physical constant called the *extensional viscosity* of the liquid comprising the thread.

4.5.2 Shearing of a layer

In a second experiment, a fluid is placed in a channel that is confined between two parallel plates. The upper plate translates in the x direction parallel to itself with constant velocity V , while the lower plate is held stationary, as depicted in figure 4.5.1(b). A force in the x direction must be exerted on the upper plate to balance the tangential component of the traction $f_x^{(y)}$ developing due to the fluid motion. The higher the velocity of the translating plate, the larger the magnitude of the traction; the greater the distance between the two plates, the lower the magnitude of the traction.

For most common fluids, a linear relationship exists between the traction, the velocity of the moving plate, and the inverse of the distance between the plates, h ,

$$f_x^{(y)} = \mu^{sh} \frac{V}{h}, \quad (4.5.2)$$

where μ^{sh} is a physical constant associated with the fluid, called the *shear viscosity*.

4.5.3 Simple fluids

We have established that stresses develop in a fluid as a result of the motion. To proceed further, we consider the tractions developing on the surface of a small fluid parcel, and argue the following properties characterizing a simple fluid:

- If the parcel translates or rotates as a rigid body, tractions do not develop over its surface.
- Tractions develop only when the parcel deforms.
- The distribution of traction over the parcel surface at a particular instant in time depends only on the type and rate of deformation that the parcel is undergoing at that particular time.

To this end, we recall the results of our analysis of kinematics in Chapter 2: a small spherical fluid parcel in a flow deforms to obtain an ellipsoidal shape whose axes are parallel to the three eigenvectors of the rate of deformation tensor defined in equation (2.1.28); the rates of deformation are equal to the corresponding eigenvalues.

With the above properties as a point of departure, we proceed to relate the stress tensor to the physical properties of the fluid and to the structure of the velocity field by means of a *constitutive equation*.

4.5.4 Incompressible Newtonian fluids

The constitutive equation for an incompressible Newtonian fluid takes the form

$$\boldsymbol{\sigma} = -p \mathbf{I} + \mu \mathbf{2 E}, \quad (4.5.3)$$

where p is the pressure, the coefficient μ is the fluid viscosity, sometimes called the dynamic viscosity, and \mathbf{E} is the rate of deformation tensor defined in equation (2.1.28). Note that the Newtonian constitutive relation respects the symmetry of the stress tensor discussed at the end of Section 4.2.

Explicitly, the components of the stress tensor are given by the matrix equation

$$\begin{bmatrix} \sigma_{xx} & \sigma_{xy} & \sigma_{xz} \\ \sigma_{yx} & \sigma_{yy} & \sigma_{yz} \\ \sigma_{zx} & \sigma_{zy} & \sigma_{zz} \end{bmatrix} = \begin{bmatrix} -p + 2\mu \frac{\partial u_x}{\partial x} & \mu \left(\frac{\partial u_y}{\partial x} + \frac{\partial u_x}{\partial y} \right) & \mu \left(\frac{\partial u_z}{\partial x} + \frac{\partial u_x}{\partial z} \right) \\ \mu \left(\frac{\partial u_x}{\partial y} + \frac{\partial u_y}{\partial x} \right) & -p + 2\mu \frac{\partial u_y}{\partial y} & \mu \left(\frac{\partial u_z}{\partial y} + \frac{\partial u_y}{\partial z} \right) \\ \mu \left(\frac{\partial u_x}{\partial z} + \frac{\partial u_z}{\partial x} \right) & \mu \left(\frac{\partial u_y}{\partial z} + \frac{\partial u_z}{\partial y} \right) & -p + 2\mu \frac{\partial u_z}{\partial z} \end{bmatrix}. \quad (4.5.4)$$

In the absence of flow, we recover the hydrostatic stress tensor defined in equation (4.4.6), involving the pressure.

Unidirectional shear flow

As an example, we consider the flow of a Newtonian fluid in a two-dimensional channel confined between two parallel plane walls, where the motion is generated by the translation of the upper plate, as depicted in figure 4.5.1(b). Physical intuition suggests that, at low and moderate velocities, the fluid will translate only in the x direction with a position-dependent velocity u_x varying in the y direction; to signify this dependence, we write $u_x(y)$.

Using equation (2.1.22), we find that the rate of deformation tensor for this two-dimensional flow is given by

$$\mathbf{E} = \frac{1}{2} \begin{bmatrix} 0 & \frac{du_x}{dy} \\ \frac{du_x}{dy} & 0 \end{bmatrix}. \quad (4.5.5)$$

Substituting (4.5.5) into the right-hand side of (4.5.3), we obtain the stress tensor

$$\sigma = \begin{bmatrix} -p & \mu \frac{du_x}{dy} \\ \mu \frac{du_x}{dy} & -p \end{bmatrix}. \quad (4.5.6)$$

The x component of the traction exerted on a fluid surface that is perpendicular to the y axis, identified as the shear stress, is given by

$$f_x^{(y)} = \sigma_{yx} = \mu \frac{du_x}{dy}. \quad (4.5.7)$$

Physically, this traction is attributed to the friction experienced by adjacent fluid layers as they slide over one another with slightly different velocities.

4.5.5 Viscosity

Strictly speaking, the viscosity of a fluid is a proportionality coefficient relating the stress tensor to the rate of deformation tensor, as depicted in equation (4.5.3). It is reassuring, however, to know that this mathematical definition, established by phenomenological observation, has a firm physical foundation. Thus, the viscosity is a genuine physical constant dependent on the local physical conditions including temperature. The following table summarizes the viscosities of water and air at three temperatures; cp stands for *centipoise* which is one hundredth of the viscosity unit *poise* defined as $1 \text{ g}/(\text{cm sec})$.

Viscosity, μ

<i>Temperature</i> $^{\circ}C$	<i>Water</i> $cp \equiv 10^{-2} \text{ g}/(\text{cm sec})$	<i>Air</i> cp
20	1.002	0.0181
40	0.653	0.0191
80	0.355	0.0209

As the temperature is raised, the viscosity of liquids is reduced, whereas the viscosity of gases increases. This dichotomy is a reflection of the different physical mechanisms that are responsible for the development of stresses in these two fundamental classes of fluids. In the case of liquids, the viscosity is due to occasional molecular excursions from a mean position into neighboring empty sites. In the cases of gases, the viscosity is due to relentless molecular excursions from regions of high velocity to regions of low velocity in the course of random motions due to thermal fluctuations.

Viscosity of gases

To demonstrate the relation between molecular and macroscopic fluid motion, we consider a gas undergoing unidirectional shear flow, and derive an expression for the viscosity in terms of molecular properties. In the simplest kinetic theory, the molecules are modeled as rigid spheres moving with the local fluid velocity defined in Section 1.4, and with a randomly fluctuating component. The average magnitude of the fluctuating component is

$$\bar{v} = \sqrt{\frac{8 k_B T}{\pi M}}, \quad (4.5.8)$$

where k_B is Boltzmann's constant, T is the absolute temperature, and M is the molecular weight. In the course of the random motion, two molecules occasionally collide after having travelled an average distance equal to the *mean free path*, λ .

Consider a macroscopically stationary gas with vanishing fluid velocity. Using principles of statistical mechanics, we find that the number of molecules crossing a unit surface area per unit time as a result of the fluctuating motion, denoted by Z , is proportional to (a) the number of molecules per unit volume defined as the number density n , and (b) the average magnitude of the fluctuating velocity \bar{v} . It can be shown, in particular, that

$$Z = \frac{1}{4} n \bar{v}, \quad (4.5.9)$$

A molecule crossing the unit surface at a particular instant has collided with another molecule at an average distance a above or below the surface. Using principles of statistical mechanics, we find

$$a = \frac{2}{3} \lambda, \quad (4.5.10)$$

where λ is the mean free path. Relations (4.5.9) and (4.5.10) have been derived taking into consideration that, since the molecules move randomly in all directions, only one component of the velocity brings them toward the unit surface under consideration.

Relations (4.5.8)-(4.5.10) also hold true when the fluid exhibits a macroscopic motion, provided that the molecular velocity is computed relative to the average velocity at the position where a molecule last underwent a collision.

Figure 4.5.2 shows a schematic illustration of the instantaneous distribution of molecules in a gas undergoing unidirectional shear flow. Without loss of generality, we have assumed that the fluid velocity increases in the positive direction of the y axis. In the course of the motion, molecules cross a horizontal plane corresponding to a certain value of y , drawn with the heavy horizontal line, from either side. Because the x velocity of molecules crossing from above is higher than the x velocity of molecules crossing from below, x momentum is transferred toward the negative direction of the y axis. The rate of transfer of x momentum across a surface that is perpendicular to the y axis amounts to the hydrodynamic traction $f_x^{(y)}$.

Now, the rate of momentum transport defined in the preceding paragraph can be quantified by setting

$$f_x^{(y)} = -M (Z^- u_x^- - Z^+ u_x^+), \quad (4.5.11)$$

where u_x is the fluid velocity, and the superscripts $+$ and $-$ indicate that the underlying variable is evaluated at a distance equal to a above or below the transport surface. Effectively, the collection of molecules crossing the y plane during a unit length of time are represented by model molecules with the following properties: (a) the model molecules last underwent a collision a distance a above or below the y plane, and (b) the model molecules move with an average velocity that is equal to the local fluid velocity evaluated at the position of last collision.

Because the flow is unidirectional, the average fluid velocity normal to a horizontal plane vanishes, and the number of molecules crossings the y plane from either side per unit length of time are equal. Combining equations (4.5.9)-(4.5.11), we find

$$f_x^{(y)} = M \frac{1}{4} n \bar{v} \left(\frac{u_x^+ - u_x^-}{2a} \right) \frac{4}{3} \lambda. \quad (4.5.12)$$

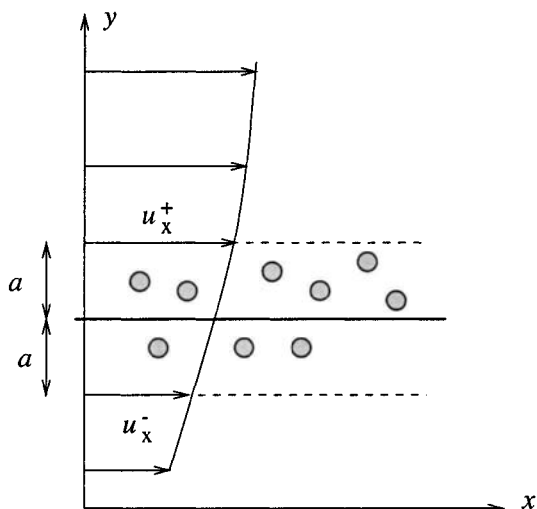


Figure 4.5.2 A molecular model of the shear flow of a gas used to derive the expression for the viscosity in terms of molecular properties, shown in equation (4.5.14).

Since a is small compared to the macroscopic length scale of the shear flow, we may approximate the fraction enclosed by the parentheses on the right-hand side of (4.5.12) with a derivative, obtaining

$$f_x^{(y)} = \frac{1}{3} n M \bar{v} \lambda \frac{du_x}{dy}. \quad (4.5.13)$$

Comparing equations (4.5.13) and (4.5.7), we now obtain an expression for the fluid viscosity,

$$\mu = \frac{1}{3} n M \bar{v} \lambda. \quad (4.5.14)$$

We have derived the Newtonian constitutive equation from molecular considerations and, in addition, we have obtained a prediction for the viscosity of a gas in terms of molecular properties.

4.5.6 Ideal fluids

If the viscosity of a fluid vanishes, the fluid is considered *frictionless* and is called *ideal*. The stress tensor in an ideal fluid is given by the simplified version of (4.5.3)

$$\sigma = -p \mathbf{I}. \quad (4.5.15)$$

It is important to bear in mind that absence of viscosity is a mathematical idealization adopted only to facilitate the analysis. In the real world, absence of viscosity should be interpreted as insignificance of hydrodynamic stresses associated with the fluid viscosity. The formal requirement for viscous stresses to be negligible will be discussed in Chapter 6.

Problems

Problem 4.5.1 *Flow in a channel.*

Consider steady unidirectional flow in a channel due to the translation of the upper wall, as depicted in figure 4.5.1(b).

(a) Perform a force balance over a rectangular fluid layer confined between two y levels to show that, when the pressure is uniform, the shear stress $f_x^{(y)}$ must be independent of y .

(b) Having established that $f_x^{(y)}$ is constant, solve the first-order differential equation (4.5.7) for u_x in terms of y subject to the boundary conditions $u_x(y = 0) = 0$ and $u_x(y = h) = V$, and evaluate $f_x^{(y)}$ in terms of μ , V , and the channel width h .

Problem 4.5.2 *Extensional flows.*

(a) Consider a two-dimensional extensional flow in the xy plane with velocity components $u_x = kx$ and $u_y = -ky$, where k is a constant with dimensions of inverse time called the rate of extension. The corresponding pressure is constant. Confirm that the fluid is incompressible, sketch the streamline pattern, and evaluate the stress tensor.

(b) Repeat (a) for axisymmetric extensional flow whose Cartesian velocity components are given by $u_x = kx$, $u_y = -\frac{1}{2}ky$, and $u_z = -\frac{1}{2}kz$.

(c) The axisymmetric extensional flow describes the motion inside the thread illustrated in figure 4.5.1(a). Assuming that the fluid is Newtonian, compute the force necessary to pull the rods away with velocity V in terms of the half-length of the thread L , the fluid viscosity μ , and the cross-sectional area of the rods A .

4.6 Simple non-Newtonian fluids

The Newtonian constitutive equation for an incompressible fluid, shown in equation (4.5.3), describes the stresses developing in a fluid consisting of small molecules. Fluids containing or consisting of macromolecules, such as polymeric solutions and melts, and fluids containing suspended rigid or deformable particles, such as pastes, bubbly liquids, and blood, exhibit more complicated behavior that is described by more involved constitutive equations.

To derive constitutive equations for non-Newtonian fluids, we consider the motion of a fluid parcel and seek to establish a relation between the instantaneous tractions exerted on the parcel surface and the history of the parcel deformation. In the simplest class of materials, the tractions depend only on the *instantaneous* rate by which the parcel is deforming, expressed by the rate of deformation tensor \mathbf{E} . The distinguishing feature of a non-Newtonian fluid is that the relation between the stress tensor σ and the rate of deformation tensor \mathbf{E} is nonlinear.

4.6.1 Unidirectional shear flow

In the case of unidirectional shear flow, the Newtonian shear stress (4.5.7) can be generalized by allowing the viscosity to be a function of the shear rate du_x/dy . If the viscosity is reduced as the shear rate is raised, the fluid is called *shear-thinning* or *pseudo-plastic*; whereas if the viscosity is increased as the shear rate is raised, the fluid is called *shear-thickening* or *dilatant*.

Physically, the dependence of the viscosity on the shear rate is attributed to changes in the configuration of molecules, changes in the shape and relative position of particles suspended in the fluid, or to the spontaneous formation of internal microstructure due to intermolecular force fields and particle interactions.

4.6.2 Power-law fluids

The shear stress developing in a certain class of fluids in unidirectional shear flow is described by the *Ostwald-de Waele model*. In this model, the viscosity is proportional to the magnitude of the shear rate raised to a power,

$$\mu = \mu_0 \left| \frac{du_x}{dy} \right|^{n-1}, \quad (4.6.1)$$

where μ_0 is a constant, and n is the *power-law exponent*. When $n = 1$, we obtain a Newtonian fluid with viscosity μ_0 ; $n < 1$ corresponds to shear-thinning fluids, and $n > 1$ corresponds to shear-thickening fluids.

Substituting (4.6.1) into (4.5.7), we derive an expression for the shear stress

$$f_x^{(y)} = \sigma_{yx} = \mu_0 \left| \frac{du_x}{dy} \right|^{n-1} \frac{du_x}{dy}. \quad (4.6.2)$$

Consider now flow in a channel generated by the translation of the upper wall with velocity V , as illustrated in figure 4.5.1(b). Performing a force balance over a rectangular fluid layer, as discussed in problem 4.5.1, we find that, if the pressure is uniform, the shear stress is independent of y , and the right-hand side of (4.6.2) is constant.

Now, the fluid velocity at the upper wall located at $y = h$ is equal to the wall velocity V , and the velocity at the lower wall located at $y = 0$ is required to vanish. Integrating equation $du_x/dy = c$, where c is the constant shear rate, and using the aforementioned boundary conditions, we find a linear velocity profile with shear rate $du_x/dy = V/h$ irrespective of the value of n .

Although the velocity profile is linear for any value of n , the magnitude of the shear stress is a function of n , as shown in equation (4.6.2). This distinction emphasizes that the kinematic appearance of a flow does not necessarily reflect the magnitude of the stresses developing in the fluid. Two flows that are kinematically identical may support different stresses.

4.6.3 Yield-stress fluids

A certain class of heterogeneous fluids, including pastes and concentrated suspensions of fine particles, called *Bingham plastics*, flow only when the shear stress established due to the motion lies above a certain threshold. An idealized constitutive equation between stress and shear rate for this class of materials is

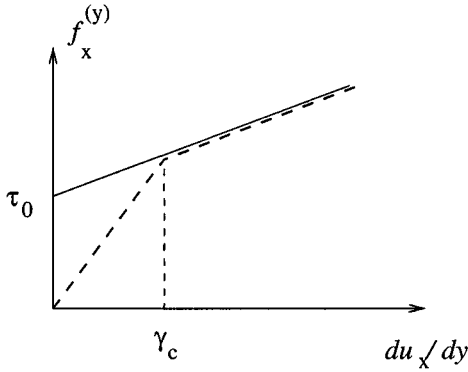


Figure 4.6.1 Rheological response of a Bingham plastic showing a yield-stress behavior in unidirectional flow.

$$\frac{du_x}{dy} = 0 \quad \text{if} \quad |\sigma_{yx}| < \tau_0,$$

$$f_x^{(y)} = \sigma_{yx} = \tau_0 + \mu \frac{du_x}{dy} \quad \text{if} \quad |\sigma_{yx}| > \tau_0, \quad (4.6.3)$$

where the constant τ_0 is called the *yield stress*, and μ is the viscosity. The relation between the shear stress and the shear rate is represented by the solid line in figure 4.6.1.

Consider the familiar flow in a channel confined between two parallel-sided walls generated by imparting to the upper wall a force F_x parallel to the x axis. If the fluid is a Bingham plastic whose rheological behavior is described by equations (4.6.3), a shear flow across the whole of the channel will be established only when the externally imposed force F per unit length of the channel L , counteracting the shear stress, $\sigma_{yx} = F/L$, is greater than the yield stress τ_0 .

Assuming that this occurs, we treat σ_{yx} as a constant, solve the second of equations (4.6.3) for du_x/dy , and then integrate with respect to y subject to the boundary condition $u_x(y=0) = 0$ to obtain the linear velocity

$$u_x = y \frac{\frac{F}{L} - \tau_0}{\mu}. \quad (4.6.4)$$

The velocity of the upper wall is given by

$$u_x(y = h) = h \frac{\frac{F}{L} - \tau_0}{\mu} = V. \quad (4.6.5)$$

Equation (4.6.5) allows to estimate the values of the physical constants μ and τ_0 from laboratory observation.

Problem

Problem 4.6.1 *Yield-stress fluids.*

The relation between the shear stress and the shear rate for a class of yield-stress fluids is described by the long-dashed line in figure 4.6.1, where the constant γ_c is the critical shear rate. State the equations describing this rheological behavior, and compute the shear stress established in a channel with parallel-sided walls, where the upper wall translates with velocity V , while the lower wall is held stationary.

4.7 Stresses in polar coordinates

We have discussed tractions and stresses in Cartesian coordinates. In practice, it may be more convenient to work in cylindrical, spherical, or plane polar coordinates with the benefit of reduced algebraic manipulations. In this section, we define the components of the stress tensor in these polar coordinates, and relate them to the pressure and to the corresponding components of the rate of deformation tensor using the constitutive equation for incompressible Newtonian fluids.

4.7.1 Cylindrical polar coordinates

Consider the system of cylindrical polar coordinates (x, σ, φ) depicted in figure 4.7.1. The traction $\mathbf{f}^{(x)}$ exerted on a small surface that is perpendicular to the x axis, acting on the side facing the positive direction of the x axis, may be resolved into its cylindrical polar components as

$$\mathbf{f}^{(x)} = f_x^{(x)} \mathbf{e}_x + f_\sigma^{(x)} \mathbf{e}_\sigma + f_\varphi^{(x)} \mathbf{e}_\varphi, \quad (4.7.1)$$

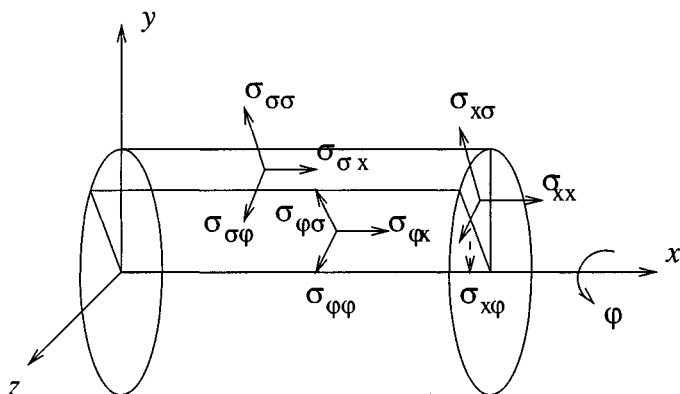


Figure 4.7.1 Components of the stress tensor in cylindrical polar coordinates.

where \mathbf{e}_x , \mathbf{e}_σ , and \mathbf{e}_φ are unit vectors pointing, respectively, in the axial, radial, and meridional directions. Recall that the orientation of \mathbf{e}_x is constant, whereas the orientation of \mathbf{e}_σ and \mathbf{e}_φ changes with position in the flow.

The traction $\mathbf{f}^{(\sigma)}$ exerted on a small surface that is perpendicular to the vectorial distance from the x axis, and is thus parallel to the axial and meridional directions at the designated center of the surface, may be resolved into corresponding components as

$$\mathbf{f}^{(\sigma)} = f_x^{(\sigma)} \mathbf{e}_x + f_\sigma^{(\sigma)} \mathbf{e}_\sigma + f_\varphi^{(\sigma)} \mathbf{e}_\varphi. \quad (4.7.2)$$

Thirdly, the traction $\mathbf{f}^{(\varphi)}$ exerted on a small surface that is normal to the meridional direction, may be resolved as

$$\mathbf{f}^{(\varphi)} = f_x^{(\varphi)} \mathbf{e}_x + f_\sigma^{(\varphi)} \mathbf{e}_\sigma + f_\varphi^{(\varphi)} \mathbf{e}_\varphi. \quad (4.7.3)$$

Stacking the coefficients of the unit vectors on the right-hand sides of (4.7.1)-(4.7.3) on top of one another in a particular order, we obtain the stress tensor in cylindrical polar coordinates,

$$\sigma \equiv \begin{bmatrix} f_x^{(x)} & f_\sigma^{(x)} & f_\varphi^{(x)} \\ f_x^{(\sigma)} & f_\sigma^{(\sigma)} & f_\varphi^{(\sigma)} \\ f_x^{(\varphi)} & f_\sigma^{(\varphi)} & f_\varphi^{(\varphi)} \end{bmatrix}. \quad (4.7.4)$$

To simplify the nomenclature, we introduce the standard two-index notation, writing

$$\sigma_{\alpha\beta} \equiv f_\beta^{(\alpha)}, \quad (4.7.5)$$

where Greek indices stand for x , σ , or φ . With the convention expressed by (4.7.5), the stress tensor is given by

$$\sigma = \begin{bmatrix} \sigma_{xx} & \sigma_{x\sigma} & \sigma_{x\varphi} \\ \sigma_{\sigma x} & \sigma_{\sigma\sigma} & \sigma_{\sigma\varphi} \\ \sigma_{\varphi x} & \sigma_{\varphi\sigma} & \sigma_{\varphi\varphi} \end{bmatrix}. \quad (4.7.6)$$

The stress components for an incompressible Newtonian fluid derive from the constitutive equation (4.5.3) as

$$\begin{aligned} \sigma_{xx} &= -p + 2\mu \frac{\partial u_x}{\partial x}, \\ \sigma_{x\sigma} &= \sigma_{\sigma x} = \mu \left[\frac{\partial u_x}{\partial \sigma} + \frac{\partial u_\sigma}{\partial x} \right], \\ \sigma_{x\varphi} &= \sigma_{\varphi x} = \mu \left[\frac{\partial u_\varphi}{\partial x} + \frac{1}{\sigma} \frac{\partial u_x}{\partial \varphi} \right], \\ \sigma_{\sigma\sigma} &= -p + 2\mu \frac{\partial u_\sigma}{\partial \sigma}, \\ \sigma_{\sigma\varphi} &= \sigma_{\varphi\sigma} = \mu \left[\sigma \frac{\partial}{\partial \sigma} \left(\frac{u_\varphi}{\sigma} \right) + \frac{1}{\sigma} \frac{\partial u_\sigma}{\partial \varphi} \right], \\ \sigma_{\varphi\varphi} &= -p + 2\mu \left[\frac{1}{\sigma} \frac{\partial u_\varphi}{\partial \varphi} + \frac{1}{\sigma} u_\sigma \right]. \end{aligned} \quad (4.7.7)$$

Note that the stress tensor remains symmetric in the cylindrical polar coordinates.

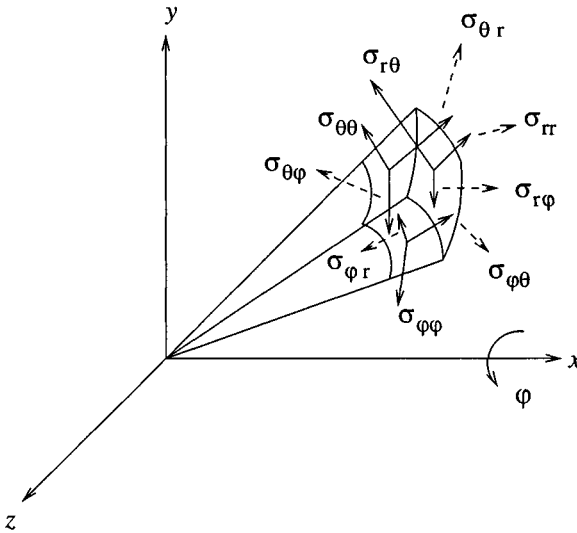


Figure 4.7.2 Components of the stress tensor in spherical polar coordinates.

4.7.2 Spherical polar coordinates

Consider the system of spherical polar coordinates (r, θ, φ) depicted in figure 4.7.2. The traction $\mathbf{f}^{(r)}$ exerted on a small surface that is normal to the vectorial distance from the origin, acting on the side of the surface facing away from the origin, may be resolved into its spherical polar components as

$$\mathbf{f}^{(r)} = f_r^{(r)} \mathbf{e}_r + f_\theta^{(r)} \mathbf{e}_\theta + f_\varphi^{(r)} \mathbf{e}_\varphi, \quad (4.7.8)$$

where \mathbf{e}_r , \mathbf{e}_θ , and \mathbf{e}_φ are the unit vectors pointing in the radial, azimuthal, and meridional directions.

The traction $\mathbf{f}^{(\theta)}$ exerted on a small surface that is perpendicular to the azimuthal direction corresponding to the angle θ , and is thus parallel to the radial and meridional directions, may be resolved in the corresponding form

$$\mathbf{f}^{(\theta)} = f_r^{(\theta)} \mathbf{e}_r + f_\theta^{(\theta)} \mathbf{e}_\theta + f_\varphi^{(\theta)} \mathbf{e}_\varphi. \quad (4.7.9)$$

Thirdly, the traction $\mathbf{f}^{(\varphi)}$ exerted on a small surface that is normal to the meridional direction, and is thus parallel to the radial and azimuthal directions, may be resolved as

$$\mathbf{f}^{(\varphi)} = f_r^{(\varphi)} \mathbf{e}_r + f_\theta^{(\varphi)} \mathbf{e}_\theta + f_\varphi^{(\varphi)} \mathbf{e}_\varphi. \quad (4.7.10)$$

Stacking the coefficients of the unit vectors on the right-hand sides of (4.7.8)-(4.7.10) on top of one another in a particular order, we obtain the stress tensor in spherical polar coordinates

$$\sigma \equiv \begin{bmatrix} f_r^{(r)} & f_\theta^{(r)} & f_\varphi^{(r)} \\ f_r^{(\theta)} & f_\theta^{(\theta)} & f_\varphi^{(\theta)} \\ f_r^{(\varphi)} & f_\theta^{(\varphi)} & f_\varphi^{(\varphi)} \end{bmatrix}. \quad (4.7.11)$$

To simplify the nomenclature, we introduce the standard two-index notation, writing of the stress tensor, writing

$$\sigma_{\alpha\beta} \equiv f_\beta^{(\alpha)}, \quad (4.7.12)$$

where Greek indices stand for r , θ , or φ . With the convention expressed by (4.7.12), the stress tensor is given by

$$\sigma = \begin{bmatrix} \sigma_{rr} & \sigma_{r\theta} & \sigma_{r\varphi} \\ \sigma_{\theta r} & \sigma_{\theta\theta} & \sigma_{\theta\varphi} \\ \sigma_{\varphi r} & \sigma_{\varphi\theta} & \sigma_{\varphi\varphi} \end{bmatrix}. \quad (4.7.13)$$

The stress components for an incompressible Newtonian fluid derive from (4.5.3) as

$$\begin{aligned} \sigma_{rr} &= -p + 2\mu \frac{\partial u_r}{\partial r}, \\ \sigma_{r\theta} &= \sigma_{\theta r} = \mu \left[r \frac{\partial}{\partial r} \left(\frac{u_\theta}{r} \right) + \frac{1}{r} \frac{\partial u_r}{\partial \theta} \right], \\ \sigma_{r\varphi} &= \sigma_{\varphi r} = \mu \left[\frac{1}{r \sin \theta} \frac{\partial u_r}{\partial \varphi} + r \frac{\partial}{\partial r} \left(\frac{u_\varphi}{r} \right) \right], \\ \sigma_{\theta\theta} &= -p + 2\mu \left[\frac{1}{r} \frac{\partial u_\theta}{\partial \theta} + \frac{u_r}{r} \right], \\ \sigma_{\theta\varphi} &= \sigma_{\varphi\theta} = \mu \left[\frac{\sin \theta}{r} \frac{\partial}{\partial \theta} \left(\frac{u_\varphi}{\sin \theta} \right) + \frac{1}{r \sin \theta} \frac{\partial u_\theta}{\partial \varphi} \right], \\ \sigma_{\varphi\varphi} &= -p + \mu \frac{2}{r \sin \theta} \left(\frac{\partial u_\varphi}{\partial \varphi} + u_r \sin \theta + u_\theta \cos \theta \right). \end{aligned} \quad (4.7.14)$$

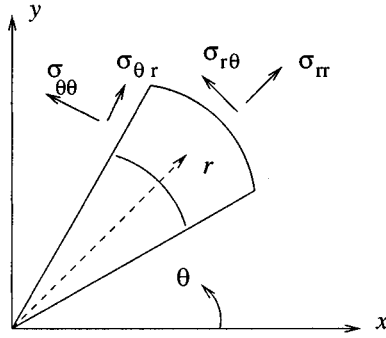


Figure 4.7.3 Components of the stress tensor in plane polar coordinates.

Note that the stress tensor remains symmetric in the spherical polar coordinates.

4.7.3 Plane polar coordinates

Consider finally a two-dimensional flow in the xy plane and refer to the plane polar coordinates (r, θ) depicted in figure 4.7.3. The traction $\mathbf{f}^{(r)}$ exerted on a small segment that is normal to the distance from the origin, acting on the side facing away from the origin, may be resolved into its plane polar components as

$$\mathbf{f}^{(r)} = f_r^{(r)} \mathbf{e}_r + f_\theta^{(r)} \mathbf{e}_\theta, \quad (4.7.15)$$

where \mathbf{e}_r and \mathbf{e}_θ are the unit vectors pointing in the radial and polar directions.

The traction $\mathbf{f}^{(\theta)}$ exerted on a small surface that is normal to the direction of the polar angle θ , and is thus parallel to the distance from the origin, may be resolved as

$$\mathbf{f}^{(\theta)} = f_r^{(\theta)} \mathbf{e}_r + f_\theta^{(\theta)} \mathbf{e}_\theta. \quad (4.7.16)$$

Stacking the coefficients of the unit vectors on the right-hand sides of (4.7.15)-(4.7.16) on top of one another in a particular order, we obtain the stress tensor in plane polar coordinates

$$\sigma \equiv \begin{bmatrix} f_r^{(r)} & f_\theta^{(r)} \\ f_r^{(\theta)} & f_\theta^{(\theta)} \end{bmatrix}, \quad (4.7.17)$$

To simplify the nomenclature, we introduce the usual two-index notation, writing

$$\sigma_{\alpha\beta} \equiv f_\beta^{(\alpha)}, \quad (4.7.18)$$

where Greek indices stand for r or θ . With the convention expressed by (4.7.18), the stress tensor is given by

$$\sigma = \begin{bmatrix} \sigma_{rr} & \sigma_{r\theta} \\ \sigma_{\theta r} & \sigma_{\theta\theta} \end{bmatrix}. \quad (4.7.19)$$

The stress components for an incompressible Newtonian fluid derive from the constitutive equation (4.5.3) as

$$\begin{aligned} \sigma_{rr} &= -p + 2\mu \frac{\partial u_r}{\partial r}, \\ \sigma_{r\theta} = \sigma_{\theta r} &= \mu \left[r \frac{\partial}{\partial r} \left(\frac{u_\theta}{r} \right) + \frac{1}{r} \frac{\partial u_r}{\partial \theta} \right], \\ \sigma_{\theta\theta} &= -p + 2\mu \left[\frac{1}{r} \frac{\partial u_\theta}{\partial \theta} + \frac{1}{r} u_r \right]. \end{aligned} \quad (4.7.20)$$

Note that the stress tensor remains symmetric in the plane polar coordinates.

4.8 Boundary condition on the tangential velocity

In Section 2.10, we discussed the no-penetration boundary condition over impermeable solid boundaries and interfaces between immiscible fluids, involving the normal component of the fluid velocity. Viscous fluids, that is, *all* real fluids obey an additional boundary condition concerning the tangential component of the velocity.

Under most conditions, the vast majority of fluids satisfy the *no-slip* boundary condition which requires that (a) the tangential component of the fluid velocity over a solid boundary be equal to the tangential component of the boundary velocity, and (b) the tangential component of the fluid velocity be continuous across an interface between two immiscible fluids. Combined with the no-slip condition, the no-penetration condition requires that the fluid velocity be equal to the velocity of an impermeable solid boundary, and continuous across an interface.

The physical origin of the no-slip boundary condition over a solid surface has not been established with certainty. One theory argues that the molecules of a fluid next to a solid surface are adsorbed onto the surface for a short period of time, and are then desorbed and ejected into the fluid. This process slows down the fluid and renders the tangential component of the fluid velocity equal to the corresponding component of the boundary velocity. Another theory argues that the true boundary condition is the condition of vanishing shear stress, and the no-slip boundary condition arises due to microscopic boundary roughness; thus, a perfectly smooth boundary would allow the fluid to slip.

In practice, the no-slip boundary condition has been confirmed in the overwhelming majority of applications, and is the standard choice in mainstream fluid dynamics. Exceptions to the no-slip boundary condition are found in the flow of rarified gases, in the flow of polymeric melts at high pressure, and in the flow near a three-phase contact line where a solid meets two liquids or a gas and a liquid. Another exception occurs for a certain class of interfaces consisting of dual or multiple molecular layers that may exhibit relative motion yielding a discontinuous velocity. Finally, the no-slip boundary condition is sometimes relaxed in numerical simulations to prevent the occurrence of singularities stemming from excessive idealization; one example is the development of infinite force on a plate scraping fluid off a surface.

Problem

Problem 4.8.1 *Flow in a channel with slip.*

Consider steady unidirectional flow in a channel with parallel walls driven by the translation of the upper wall along the x axis with velocity V , as illustrated in figure 4.5.1(b); the lower wall is stationary. The fluid is allowed to slip over the lower wall so that the slip velocity $u_x(y = 0)$

is related to the wall shear stress by

$$u_x(y=0) = l \sigma_{yx}(y=0) = l \left(\frac{\partial u_x}{\partial y} \right)_{y=0}, \quad (4.8.1)$$

where l is a constant called the *slip coefficient*. When $l = 0$, the slip velocity vanishes and the no-slip boundary condition prevails.

In previous sections, we saw that, when the pressure is uniform, the shear stress σ_{yx} is constant and independent of y . Assuming that the no-slip condition applies at the upper wall, derive an expression for σ_{yx} and for the velocity profile in terms of V , h , μ , and l .

4.9 Wall stresses in Newtonian fluids

Combining the no-slip boundary condition discussed in Section 4.8 with the no-penetration boundary condition discussed in Section 2.10, we may derive remarkably simple expressions for the Newtonian traction exerted on a solid surface, amenable to simple physical interpretation.

Consider flow above a stationary flat solid surface located at $y = 0$, as illustrated in figure 4.9.1. The no-slip boundary condition requires that the tangential components of the velocity, and thus their derivatives with respect to x and z , vanish over the surface,

$$\frac{\partial u_x}{\partial x} = 0, \quad \frac{\partial u_z}{\partial x} = 0, \quad \frac{\partial u_x}{\partial z} = 0, \quad \frac{\partial u_z}{\partial z} = 0, \quad (4.9.1)$$

where the partial derivatives are evaluated at $y = 0$. The no-penetration condition requires that the normal component of the velocity, and thus its derivatives with respect to x and z , also vanish over the surface,

$$\frac{\partial u_y}{\partial x} = 0, \quad \frac{\partial u_y}{\partial z} = 0, \quad (4.9.2)$$

where the partial derivatives are evaluated at $y = 0$.

4.9.1 Shear stress

The two components of the Newtonian shear stress exerted on the surface are given by

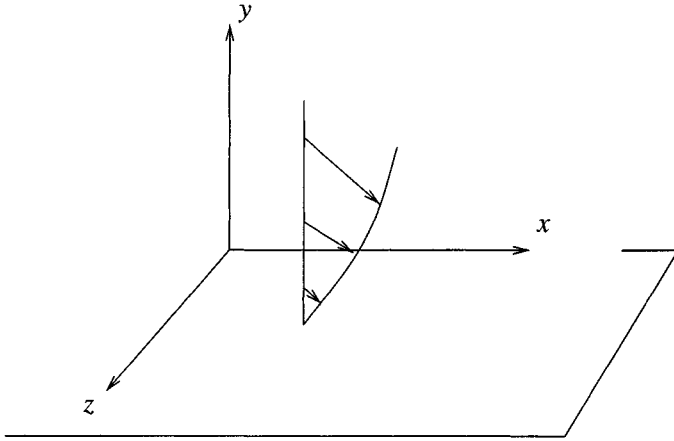


Figure 4.9.1 Flow over a plane wall where the no-slip boundary condition is required. The wall shear stress is proportional to the slope of the velocity with respect to distance normal to the wall; the normal stress is equal to the negative of the pressure.

$$\sigma_{yx} = \mu \left(\frac{\partial u_x}{\partial y} + \frac{\partial u_y}{\partial x} \right), \quad \sigma_{yz} = \mu \left(\frac{\partial u_z}{\partial y} + \frac{\partial u_y}{\partial z} \right), \quad (4.9.3)$$

evaluated at $y = 0$. Using (4.9.2) to simplify (4.9.3), we find

$$\sigma_{yx} = \mu \frac{\partial u_x}{\partial y}, \quad \sigma_{yz} = \mu \frac{\partial u_z}{\partial y}, \quad (4.9.4)$$

evaluated at $y = 0$.

Equations (4.9.4) show that the wall shear stress is simply equal to the slope of the tangential velocity with respect to distance in the normal direction, multiplied by the fluid viscosity.

4.9.2 Normal stress

The Newtonian normal stress exerted on the solid surface is given by

$$\sigma_{yy} = -p + 2\mu \frac{\partial u_y}{\partial y}, \quad (4.9.5)$$

evaluated at $y = 0$, where p is the pressure. Since the fluid has been assumed incompressible, we may use the continuity equation (2.9.2) to write

$$\frac{\partial u_y}{\partial y} = -\frac{\partial u_x}{\partial x} - \frac{\partial u_z}{\partial z}, \quad (4.9.6)$$

evaluated at $y = 0$, and then invoke the first and fourth of equations (4.9.1) to find $\partial u_y / \partial y = 0$. Expression (4.9.5) thus simplifies to

$$\sigma_{yy} = -p, \quad (4.9.7)$$

which shows that the normal stress at a solid surface is equal to the negative of the pressure.

4.9.3 Generalization

The results displayed in equations (4.9.4) and (4.9.7) remain valid even when the surface translates with a constant or time-dependent velocity. Moreover, these results also apply when the surface is curved, provided only that the y axis is defined to be normal to the surface at the position when the shear or normal stress is evaluated.

Problem

Problem 4.9.1 *Vorticity at a no-slip surface.*

Show that the component of the vorticity vector normal to an impermeable surface vanishes. *Hint:* Use the second and third of equations (4.9.1).

Chapter 5

Hydrostatics

- 5.1 Equilibrium of pressure and body forces**
- 5.2 Force exerted on immersed surfaces**
- 5.3 Archimedes' principle**
- 5.4 Shapes of two-dimensional interfaces**
- 5.5 A semi-infinite interface attached to an inclined plate**
- 5.6 Meniscus between two parallel plates**
- 5.7 A two-dimensional drop on a horizontal plate**
- 5.8 Axisymmetric shapes**

The simplest state of a fluid is the state of rest: the macroscopically observed velocity vanishes, and the forces developing in the fluid are described in terms of the pressure field established in response to a body force. The subject of hydrostatics encompasses two main topics: the computation of forces exerted on immersed surfaces and submerged bodies, and the study of the shapes of interfaces separating two stationary, translating, or rotating fluids. The problem statement and mathematical formulation in both cases is straightforward, but deriving solutions for all but the simplest configurations requires the use of numerical methods for solving algebraic, ordinary, and partial differential equations.

5.1 Equilibrium of pressure and body forces

Consider a parcel of a stationary fluid, as illustrated in figure 5.1.1(a). Newton's second law of motion requires that, in the absence of a macroscopically observable flow, the sum of the forces exerted on the parcel should balance to zero. In Chapter 4, we saw that two kinds of forces are exerted on the parcel: a body force due to the gravitational or some other force field mediated by long-range molecular interactions, and a surface force associated with the hydrodynamic traction.

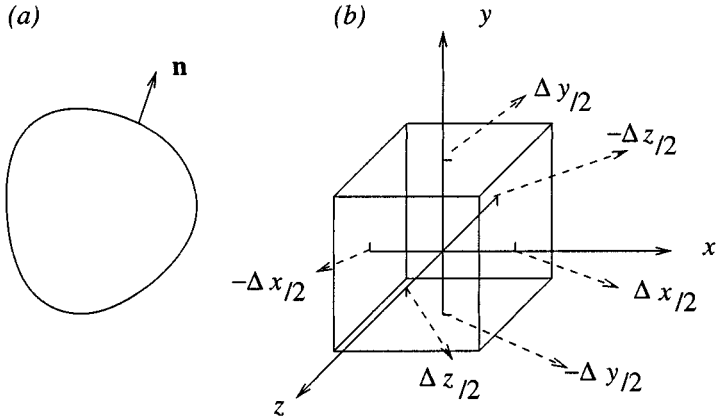


Figure 5.1.1 (a) Schematic illustration of a parcel of a stationary fluid with the unit normal vector pointing outward. (b) A parcel with the shape of a rectangular parallelepiped serving as a control volume for deriving the differential equations of hydrostatics.

5.1.1 Body force

The body force due to gravity may be expressed as an integral over the volume of the parcel involving the generally position-dependent density ρ , in the form

$$\mathbf{F}^B = \int_{Parcel} \rho \mathbf{g} dV, \quad (5.1.1)$$

where $\mathbf{g} = (g_x, g_y, g_z)$ is the vectorial acceleration of gravity. On the surface of the earth, the magnitude of \mathbf{g} has the approximate value $|\mathbf{g}| \equiv g = 9.80665 \text{ m/sec}^2$.

5.1.2 Surface force

The surface force may be expressed in terms of the traction \mathbf{f} exerted on the surface of the parcel in the corresponding form

$$\mathbf{F}^S = \int_{Parcel} \mathbf{f} dS. \quad (5.1.2)$$

In the absence of observable fluid motion, the traction is due to the pressure alone pushing the surface of the parcel toward the interior. If \mathbf{n}

is the unit vector normal to the surface of the parcel pointing outward, as illustrated in figure 5.1.1(a), then

$$\mathbf{f} = -p \mathbf{n}. \quad (5.1.3)$$

The minus sign on the right-hand side accounts for the opposite orientations of the normal vector and of the normal traction due to the pressure. Substituting (5.1.3) into (5.1.2), we derive an expression for the surface force in terms of the pressure,

$$\mathbf{F}^S = - \int_{Parcel} p \mathbf{n} dS. \quad (5.1.4)$$

5.1.3 Force equilibrium

Setting the sum of the body force given in (5.1.1) and the surface force given in (5.1.4) equal to zero, we obtain the vectorial equilibrium condition

$$\int_{Parcel} \rho \mathbf{g} dV - \int_{Parcel} p \mathbf{n} dS = \mathbf{0}, \quad (5.1.5)$$

whose three scalar components are

$$\begin{aligned} \int_{Parcel} \rho g_x dV &= \int_{Parcel} p n_x dS, \\ \int_{Parcel} \rho g_y dV &= \int_{Parcel} p n_y dS, \\ \int_{Parcel} \rho g_z dV &= \int_{Parcel} p n_z dS. \end{aligned} \quad (5.1.6)$$

5.1.4 Equilibrium of an infinitesimal parcel

Consider now a small fluid parcel with the shape of a rectangular parallelepiped centered at the origin, as illustrated in figure 5.1.1(b). The six flat sides of the parcel are perpendicular to the x , y , or z axis, the lengths of the three sides are, respectively, equal to Δx , Δy , and Δz , and the volume of the parcel is equal to $\Delta V = \Delta x \Delta y \Delta z$.

Because the size of the parcel is small, variations in the density over the volume of the parcel can be neglected, and the volume integrals on the left-hand side of equations (5.1.6) may be approximated with the products

$$\rho_0 g_x \Delta V, \quad \rho_0 g_y \Delta V, \quad \rho_0 g_z \Delta V, \quad (5.1.7)$$

where ρ_0 is the density of the fluid evaluated at the center of the parcel, located at the origin.

Consider the surface integral on the left-hand side of the first of equations (5.1.6). The x component of the normal vector vanishes on all sides, except on the two sides that are perpendicular to the x axis, located at $x = \frac{1}{2}\Delta x$, and $x = -\frac{1}{2}\Delta x$, designated as the first and second side. On the first side $n_x = 1$, and on the second side $n_x = -1$. Because the size of the parcel is small, variations in pressure over each side may be neglected, and the pressure over a side may be approximated with the value at the side center. Subject to this approximation, the surface integrals on the right-hand side of the first of equations (5.1.6) over the first and second side are, respectively, equal to

$$\begin{aligned} p(x = \frac{1}{2}\Delta x, y = 0, z = 0) \Delta y \Delta z, \\ -p(x = -\frac{1}{2}\Delta x, y = 0, z = 0) \Delta y \Delta z, \end{aligned} \quad (5.1.8)$$

where the parentheses enclose arguments. Adding these two contributions, we obtain

$$[p(x = \frac{1}{2}\Delta x, y = 0, z = 0) - p(x = -\frac{1}{2}\Delta x, y = 0, z = 0)] \Delta y \Delta z. \quad (5.1.9)$$

Next, we observe that, in the limit as Δx tends to zero, the ratio of the differences

$$\begin{aligned} & \frac{p(x = \frac{1}{2}\Delta x, y = 0, z = 0) - p(x = -\frac{1}{2}\Delta x, y = 0, z = 0)}{\frac{1}{2}\Delta x - (-\frac{1}{2}\Delta x)} \\ = & \frac{p(x = \frac{1}{2}\Delta x, y = 0, z = 0) - p(x = -\frac{1}{2}\Delta x, y = 0, z = 0)}{\Delta x} \end{aligned} \quad (5.1.10)$$

tends to the partial derivative $\partial p/\partial x$ evaluated at the origin, and the difference (5.1.9) reduces to

$$\frac{\partial p}{\partial x}(x=0, y=0, z=0) \Delta x \Delta y \Delta z = \frac{\partial p}{\partial x}(x=0, y=0, z=0) \Delta V. \quad (5.1.11)$$

Substituting (5.1.11) along with the first of the approximate forms (5.1.7) into the x component of the force balance (5.1.6), and simplifying by eliminating ΔV on both sides, we obtain the differential equation

$$\rho g_x = \frac{\partial p}{\partial x}, \quad (5.1.12)$$

where the density and the partial derivative of the pressure are evaluated at the origin. Since, however, the location of the origin is arbitrary, equation (5.1.12) is valid at every point in the fluid.

Working in a similar fashion with the second and third of the hydrostatic equilibrium equations (5.1.6), we obtain the corresponding differential equations

$$\rho g_y = \frac{\partial p}{\partial y}, \quad \rho g_z = \frac{\partial p}{\partial z}. \quad (5.1.13)$$

The three scalar equations (5.1.12) and (5.1.13) may be collected into the compact vector form

$$\rho \mathbf{g} = \nabla p, \quad (5.1.14)$$

where $\nabla p = (\partial p/\partial x, \partial p/\partial y, \partial p/\partial z)$ is the gradient of the pressure. In physical terms, the differential equation (5.1.14) expresses a balance between gravitational and pressure force in hydrostatics.

Equation (5.1.14) provides us with a basis for computing the distribution of pressure and density in a fluid, subject to additional conditions concerning the physical properties of the fluid, as required by thermodynamics. Specifically, given the density field, or a relation between the density and the pressure, equation (5.1.14) allows us to compute the corresponding pressure and vice versa. To this end, we make a distinction between compressible gases and incompressible liquids.

5.1.5 Gases in hydrostatics

The density of a gas is related to the pressure by means of an equation of state provided by thermodynamics. For an ideal gas,

$$\rho = \frac{M p}{R T}, \quad (5.1.15)$$

where M is the gramo-molecular weight, and R is the ideal-gas constant, as discussed in Section 4.4. Substituting (5.1.15) into (5.1.14), and rearranging, we obtain a vectorial equation involving the pressure and temperature,

$$\frac{M}{R T} \mathbf{g} = \frac{1}{p} \nabla p. \quad (5.1.16)$$

For example, the x component of equation (5.1.16) reads

$$\frac{M g_x}{R T} = \frac{1}{p} \frac{\partial p}{\partial x} = \frac{\partial \ln p}{\partial x}. \quad (5.1.17)$$

Assuming now that the temperature of the fluid is uniform, we integrate (5.1.17) with respect to x and find

$$\ln p = \frac{M g_x}{R T} x + f_x(y, z), \quad (5.1.18)$$

where $f_x(y, z)$ is an unknown function. Working in a similar fashion with the y and z components of (5.1.16), always under the assumption that the temperature is uniform, we find

$$\ln p = \frac{M g_y}{R T} y + f_y(x, z), \quad \ln p = \frac{M g_z}{R T} z + f_z(x, y). \quad (5.1.19)$$

Comparing the last three equations, we obtain the pressure distribution

$$\ln p = \frac{M}{R T} (g_x x + g_y y + g_z z) + \ln c, \quad (5.1.20)$$

where c is a positive, possibly time-dependent, constant with units of pressure, determined by requiring an appropriate boundary condition.

Expressing the term in the parentheses on the right-hand side of (5.1.20) in terms of the inner product of the gravity vector and the position vector, and transferring the last term to the left-hand side, we obtain the compact form

$$\ln \frac{p}{c} = \frac{M}{R T} \mathbf{g} \cdot \mathbf{x}, \quad (5.1.21)$$

which describes the pressure distribution in an ideal gas with uniform temperature.

Pressure distribution in the atmosphere

As an application, we consider the pressure distribution in the atmosphere, regarded as an ideal gas with molecular weight $M = 28.97$ kg/kmole, at temperature 25° C corresponding to the absolute temperature $T = 298$ K. In Cartesian coordinates with origin at sea level, the y axis pointing upward, and the x and z axes horizontal, the components of the acceleration of gravity vector are given by $g_x = 0$, $g_y = -g$, and $g_z = 0$, where $g = 9.80665$ m/sec². Equation (5.1.21) simplifies to

$$\ln \frac{p}{c} = -\frac{Mg}{RT} y, \quad (5.1.22)$$

where $c = P_0$ is the pressure at sea level. Solving for p , we find the exponentially decaying field

$$p = P_0 \exp\left(-\frac{Mg}{RT} y\right). \quad (5.1.23)$$

Taking $P_0 = 1.0$ atm = 1.0133×10^5 Pascal = 1.0133×10^5 kg m⁻¹ sec⁻², we find that the pressure at the elevation of $y = 1000$ m is equal to

$$p = 1.0 \exp\left(-\frac{28.97 \times 9.80665}{8.314 \times 10^3 \times 298} 1000\right) \text{ atm} = 0.892 \text{ atm}. \quad (5.1.24)$$

The corresponding density distribution is found by substituting the pressure distribution (5.1.23) into the right-hand side of the equation of state (5.1.15).

5.1.6 Liquids in hydrostatics

Liquids at low and moderate pressures are nearly incompressible: the density is a physical constant dependent primarily on temperature. Working as in the case of gases, but treating the density as a constant, we find that the pressure distribution is given by the counterpart of equation (5.1.21)

$$\begin{aligned} p &= \rho (g_x x + g_y y + g_z z) + c \\ &= \rho \mathbf{g} \cdot \mathbf{x} + c, \end{aligned} \quad (5.1.25)$$

where c is a constant with units of pressure determined by requiring an appropriate boundary condition.

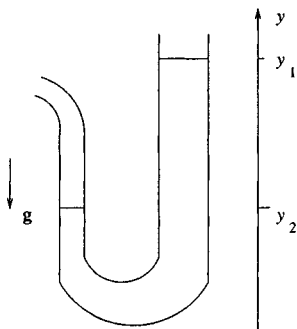


Figure 5.1.2 Illustration of a U-tube manometer. The pressure distribution in the fluid is described by the equations of hydrostatics even when the fluid has a convoluted shape, as long as it remains continuous and it is not interrupted.

Pressure distribution in a pool

As an example, we consider the pressure distribution in a liquid pool with a horizontal surface. In Cartesian coordinates with the y axis perpendicular to the surface of the pool pointing in the vertical direction upward, and the x and z axes horizontal, the components of the acceleration of gravity vector are given by $g_x = 0$, $g_y = -g$, and $g_z = 0$, where g is the magnitude of the acceleration of gravity. In this case, equation (5.1.25) simplifies to

$$p = -\rho g y + c. \quad (5.1.26)$$

Setting the origin of the y axis at the pool surface where the liquid pressure is equal to the atmospheric pressure P_{Atm} , we find that the constant c is equal to P_{Atm} .

Manometer

The pressure distribution given in (5.1.25) is also valid even when the liquid occupies a convoluted domain, provided only that the liquid remains continuous and it is not interrupted. In practice, this property is exploited for computing the pressure difference across the two ends of a tube in terms of the difference in the levels of a liquid column placed within the tube. A simple device that serves this purpose is the U-tube manometer illustrated in figure 5.1.2.

The pressure distribution in the liquid inside the U-tube manometer is given by equation (5.1.26). Applying this equation at the two ends of the liquid located at $y = y_1$ and y_2 , and subtracting the resulting expressions, we find

$$\Delta p \equiv p(y_1) - p(y_2) = \rho g (y_2 - y_1). \quad (5.1.27)$$

If the tube is exposed to the atmosphere at the first end, $p(y_1) = P_{Atm}$, then $p(y_2) = P_{Atm} + \rho g h$ where $h \equiv y_1 - y_2$ is the readily measurable rise of the liquid column in the manometer.

Problems

Problem 5.1.1 *Hydrostatic pressure distribution.*

(a) Derive the pressure distribution in an incompressible liquid given in equation (5.1.25).

(b) Derive the pressure distribution in an ideal gas occupying the semi-infinite region $y > 0$, when the temperature decreases exponentially as $T = T_0 - \Delta T (1 - e^{-\alpha y})$, where T_0 , ΔT , and α are three specified constants. The gravity vector points in the negative direction of the y axis.

Problem 5.1.2 *Function of an aircraft altimeter.*

The temperature in the lower part of the troposphere, extending 10 km above the surface of the earth, decreases at a nearly linear rate as $T = T_0 - \alpha y$, where T_0 is the temperature at the surface of the earth corresponding to $y = 0$, and α is the lapse rate; in North America, $\alpha = 6.5$ K/km.

(a) Assuming that the atmosphere behaves like an ideal gas, derive the pressure distribution

$$p = P_0 \left(1 - \frac{\beta}{T_0} y\right)^\beta, \quad (5.1.28)$$

where P_0 is the pressure at sea level, and evaluate the dimensionless exponent

$$\beta \equiv \frac{Mg}{R\alpha}. \quad (5.1.29)$$

(b) Show that, as α tends to zero, in which case the temperature distribution tends to become constant, the pressure distribution (5.1.28) reduces to that shown in (5.1.23).

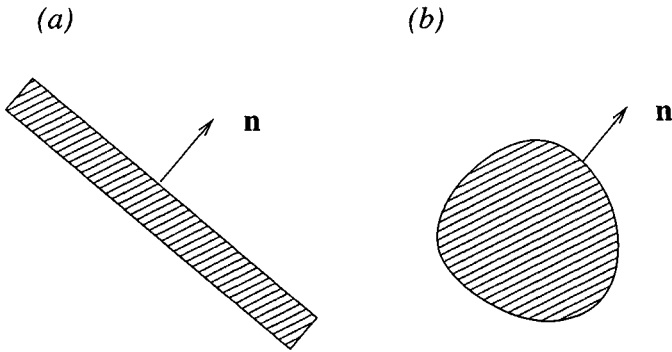


Figure 5.2.1 Illustration of a surface that (a) contains or (b) is immersed in a stationary fluid.

Solving (5.1.28) for the elevation y , we find

$$y = \frac{T_0}{\beta} \left[1 - \left(\frac{P}{P_0} \right)^{1/\beta} \right]. \quad (5.1.30)$$

This equation is used for calibrating aircraft altimeters, that is, for translating pressure measured with a barometer into altitude.

Problem 5.1.3 *How many molecules within a volume of gas?*

How many molecules are there within 1 cubic centimeter (1 milliliter) of gas under atmospheric pressure and temperature 25°C ?

5.2 Force exerted on immersed surfaces

To compute the hydrostatic surface force exerted on a surface that either contains or is immersed in a stationary fluid, as illustrated in figure 5.2.1(a, b), we repeat the arguments that led us to equation (5.1.4), and find

$$\mathbf{F}^S = - \int p \mathbf{n} \, dS, \quad (5.2.1)$$

where \mathbf{n} is the unit vector normal to the surface pointing into the fluid, and the integration is performed over the surface. To evaluate the right-hand side of (5.2.1), we must first compute the pressure distribution within the fluid as discussed in Section 5.1, and then compute the integral by analytical or numerical methods.

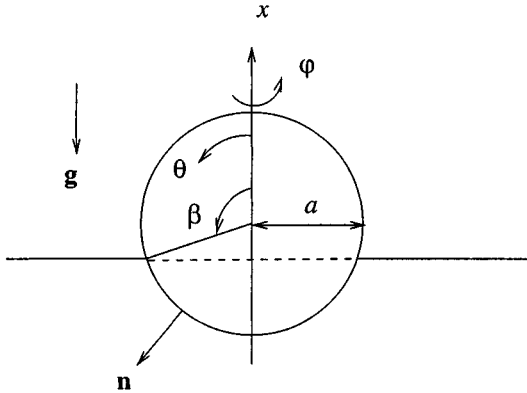


Figure 5.2.2 A sphere floating on the surface of a liquid at floating angle β . The dashed line represents the contact line.

5.2.1 Force on a floating sphere

As an example, we consider the force exerted on a sphere of radius a floating on the surface of a liquid, as depicted in figure 5.2.2. In spherical polar coordinates with origin at the center of the sphere and the x axis pointing upward, the circular contact line where the surface of the liquid meets the sphere is located at $\theta = \beta$. Symmetry requires that the horizontal components of the surface force exerted on the sphere vanish. The vertical component of the surface force is given by

$$F_x^S = - \int p n_x dS, \quad (5.2.2)$$

where $n_x = \cos \theta$ is the x component of the unit normal vector.

The pressure distribution is given in equation (5.1.25) with $g_x = -g$, $g_y = 0$, and $g_z = 0$, yielding $p = -\rho g x + c$. To compute the constant c , we require that the pressure at the contact line be equal to the atmospheric pressure, $p(x = a \cos \beta) = P_{Atm}$, and find $P_{Atm} = -\rho g a \cos \beta + c$, which may be rearranged to give $c = \rho g a \cos \beta + P_{Atm}$. Writing $x = a \cos \theta$, we find that the pressure distribution is given by

$$p = -\rho g a (\cos \theta - \cos \beta) + P_{Atm}. \quad (5.2.3)$$

Substituting now (5.2.3) into the integral on the right-hand side of (5.2.2), we find that the force exerted on the sphere by the liquid is given by

$$F_x^S = \int [\rho g a (\cos \theta - \cos \beta) - P_{Atm}] \cos \theta dS. \quad (5.2.4)$$

To evaluate this integral, we note that the differential of the surface area of the sphere may be expressed in the form $dS = (\sigma d\varphi)(a d\theta)$, where $\sigma = a \sin \theta$ is the distance of a point on the surface of the sphere from the x axis, and φ is the meridional angle. Substituting this expression into the right-hand side of (5.2.4), and integrating with respect to φ , we find

$$F_x^S = 2\pi a^2 \int_{\beta}^{\pi} [\rho g a (\cos \theta - \cos \beta) - P_{Atm}] \cos \theta \sin \theta d\theta. \quad (5.2.5)$$

Next, we set $\sin \theta d\theta = -d \cos \theta$, and carry out the integration on the right-hand side to find

$$F_x^S = \pi a^2 [\rho g a \frac{1}{3} (2 + 3 \cos \beta - \cos^3 \beta) + P_{Atm} (1 - \cos^2 \beta)]. \quad (5.2.6)$$

Working in a similar fashion, we find that the x component of the force due to the atmospheric pressure exerted on the non-immersed part of the sphere, subtended between $\theta = 0$ and β , is given by

$$\begin{aligned} F_x^{Atm} &= -2\pi a^2 \int_0^{\beta} P_{Atm} \cos \theta \sin \theta d\theta \\ &= -\pi a^2 P_{Atm} (1 - \cos^2 \beta). \end{aligned} \quad (5.2.7)$$

Adding the two contributions (5.2.6) and (5.2.7), we obtain the *buoyancy force* exerted on the sphere, given by

$$F_x^{BNC} \equiv F_x^S + F_x^{Atm} = \rho g [a^3 \frac{\pi}{3} (2 + 3 \cos \beta - \cos^3 \beta)]. \quad (5.2.8)$$

It can be shown by elementary trigonometry that the term enclosed by the square brackets on the right-hand side of (5.2.8) is equal to the immersed volume of the sphere, that is, the volume of the sphere lying underneath the surface of the liquid, which is equal to the volume of the fluid displaced by the sphere. When the sphere is completely immersed, corresponding to $\beta = 0$, the term enclosed by the parantheses on the right-hand side of (5.2.8) is equal to 4, and the term enclosed by the square brackets is equal to the volume of the sphere, $4\pi a^3/3$.

Equation (5.2.8) states that the hydrostatic force exerted on a floating sphere is equal in magnitude and opposite in direction to the weight of the fluid displaced by the sphere. In Section 5.3, we shall see that this is a more general result applicable to arbitrarily shaped floating or immersed bodies.

Computation of the floating angle

The floating angle β is determined by the weight of the sphere: the heavier the sphere, the smaller the angle. There is a critical weight where β becomes equal to zero and the sphere is completely submerged. To compute the floating angle corresponding to a certain weight W , we set W equal to the buoyancy force given in (5.2.8), and rearrange to obtain a cubic equation for $\cos \beta$,

$$\cos^3 \beta - 3 \cos \beta + 2(2s - 1) = 0, \quad (5.2.9)$$

where

$$s \equiv \frac{W}{\rho g \frac{4\pi a^3}{3}} \quad (5.2.10)$$

is a dimensionless constant. We note that the fraction in the denominator of (5.2.10) is equal to the volume of the sphere, and this suggests that, if the sphere is made of a homogeneous material of density ρ_B , then $s = \rho_B/\rho$ is the density ratio. A neutrally buoyant sphere corresponds to $s = 1$, in which case $\cos \beta = 1$ and $\beta = 0$ satisfies equation (5.2.9), as expected.

Newton's method

A variety of numerical methods are available for solving the nonlinear algebraic equation (5.2.9). In practice, Newton's method strikes the optimal balance between conceptual simplicity and numerical efficiency, and is a standard choice.

To formalize Newton's method in general terms, we define the variable $q \equiv \cos \beta$, and express (5.2.9) in the generic form

$$f(q) = 0, \quad (5.2.11)$$

where, in the case of the floating sphere,

$$f(q) \equiv q^3 - 3q + 2(2s - 1). \quad (5.2.12)$$

The graph of the function $f(q)$ for $s = 0.25$ is shown in figure 5.2.3. The requisite value of q is located at the crossing of the graph of $f(q)$ and the q axis, denoted by Q , satisfying $f(Q) = 0$.

To implement Newton's method, we make an initial guess for the desired root Q , denoted by $q^{(0)}$, and then generate a sequence of improvements working as follows. Near the point $q^{(0)}$, the function $f(q)$ may be approximated with a linear function that arises by expanding $f(q)$ in a Taylor series about $q^{(0)}$, and discarding all nonlinear terms to obtain the approximate form

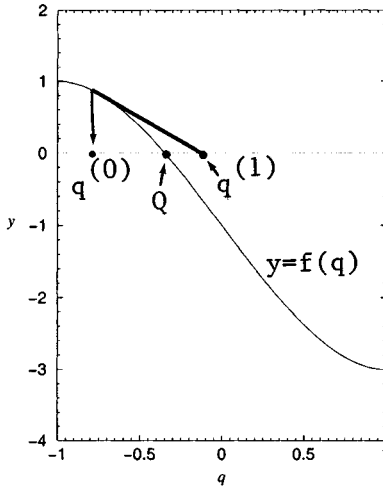


Figure 5.2.2 Graph of the function $f(q)$ defined in equation (5.2.12) whose root Q is required. To compute the root using Newton's method, we make an initial guess for Q , called $q^{(0)}$, and then improve it moving along the tangent to the graph toward the q axis.

$$f(q) \simeq f(q^{(0)}) + \left(\frac{\partial f}{\partial q}\right)_{q=q^{(0)}} (q - q^{(0)}). \quad (5.2.13)$$

The graph of this linear function is drawn with the straight line in figure 5.2.2. Setting $f(q) = 0$, solving for the q that is located within the parentheses on the right-hand side of (5.2.13), and denoting the solution by $q^{(1)}$, we obtain the improved value

$$q^{(1)} = q^{(0)} - \left(\frac{f(q)}{\frac{\partial f}{\partial q}(q)}\right)_{q=q^{(0)}}. \quad (5.2.14)$$

In the case of the floating sphere, $(\partial f / \partial q)(q) = 3q^2 - 3$. The process is then repeated yielding a sequence of successive approximations based on the recursive formula

$$q^{(k+1)} = q^{(k)} - \left(\frac{f(q)}{\frac{\partial f}{\partial q}(q)}\right)_{q=q^{(k)}}, \quad (5.2.15)$$

for $k = 0, 1, \dots$. Erroneously replacing the minus sign with a plus sign on the right-hand side of (5.2.15) is a common source of frustration.

An error analysis shows that, as long as the initial guess $q^{(0)}$ is sufficiently close to the root Q , the sequence defined by (5.2.15) converges to Q , and the rate of convergence behaves as follows:

- If the graph of the function $f(q)$ is not horizontal at the root, that is, $(df/dq)_{q=Q} \neq 0$, then the rate of convergence is quadratic, meaning that

$$q^{(k+1)} - Q \simeq \delta (q^{(k)} - Q)^2, \quad (5.2.16)$$

where $\delta = f''(Q)/[2f'(Q)]$ is an *a priori* unknown constant.

Equation (5.2.16) states that the magnitude of the error in the current iteration, expressed by the left-hand side, is roughly equal to the square of the magnitude of the error in the previous iteration, multiplied by a constant. Consequently, if the initial error $q^{(0)} - Q$ is sufficiently small, the magnitude of the error $q^{(k)} - Q$ will keep decreasing during the iterations, no matter how large the value of the coefficient δ , as long as the initial guess is close to the root for (5.2.16) to be valid.

- If the graph of the function $f(q)$ is horizontal at the root, in which case $(df/dq)_{q=Q} = 0$ and the root is multiple, the rate of convergence is linear, meaning that

$$q^{(k+1)} - Q \simeq \frac{m-1}{m} (q^{(k)} - Q), \quad (5.2.17)$$

where m is the multiplicity of the root; for a double root, $m = 2$.

Equation (5.2.17) states that the magnitude of the error in the current iteration is roughly equal to that in the previous iteration multiplied by the positive coefficient $(m-1)/m$ which is less than unity for any value of $m > 1$. Consequently, the error $|q^{(k)} - Q|$ will keep decreasing during the iterations as long as the initial guess is close to the root for (5.2.17) to be valid.

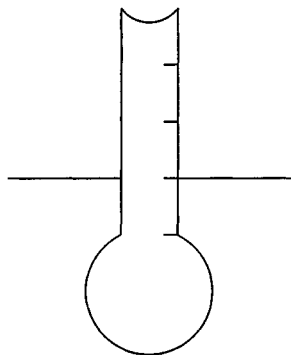


Figure 5.2.3 A pycnometer is used to measure the specific gravity of a liquid, that is, the ratio between the density of the liquid and the density of water.

Problem

Problem 5.2.1 *Pycnometer.*

A pycnometer is an antiquated device used for measuring the specific gravity of a liquid, defined as the ratio of the density of the liquid and the density of water. This is done by reading the level of the free-surface on a scale printed on a vertical tube attached to a spherical flask floating on the liquid, as illustrated in figure 5.2.4. Pycnometer derives from the Greek word $\piυκνoτ\eta\tau\alpha$ which means density. Derive an equation that allows us to calibrate a pycnometer on the basis of the known density of water.

Computer problem

Problem c.5.2.1 *Floating sphere.*

(a) Directory `00_num_men/04_nl_eq` of *FDLIB* includes the program `non_lin1.f` that implements Newton's method for solving one nonlinear equation. Use the program to solve equation (5.2.9), and plot the floating angle β against the dimensionless parameter s defined in equation (5.2.10). Discuss the rate of convergence of the iterations in light of equations (5.2.16) and (5.2.17).

(b) Directory *00_num_men/04_nl_eq* of *FDLIB* includes the program *cubic.f* that computes the three roots of a cubic equation using Cardano's formulae. Use the program to solve equation (5.2.9), and plot the floating angle β against the dimensionless parameter s .

5.3 Archimedes' principle

Consider the force exerted on a body with arbitrary shape immersed in a stationary fluid. Using equation (5.2.1), we find that the surface force exerted on the body is given by

$$\mathbf{F}^S = - \int_{Body} p \mathbf{n} dS, \quad (5.3.1)$$

where \mathbf{n} is the unit vector normal to the body pointing into the fluid. It would appear that the computation of the integral on the right-hand side of (5.3.1) requires detailed knowledge of the geometry of the body; this is true when the fluid is incompressible. When, however, the fluid is incompressible, the integral may be evaluated in a generic fashion yielding a remarkably simple expression for the force in terms of the body volume and fluid density.

Substituting the pressure distribution for an incompressible fluid given in (5.1.25) into the right-hand side of (5.3.1), we find

$$\mathbf{F}^S = - \int_{Body} [\rho (g_x x + g_y y + g_z z) + P_0] \mathbf{n} dS. \quad (5.3.2)$$

A key observation in evaluating the integral is that the integrand is the product of the unit normal vector and a scalar function that is *linear* with respect to the components of the position vector.

To see how the evaluation of the integral can be simplified, we consider a body having the shape of a rectangular parallelepiped, as illustrated in figure 5.1.1(b). The six flat sides of the body are perpendicular to the x , y , or z axis, the lengths of the edges are equal to Δx , Δy , and Δz , and the volume of the body is equal to $V_B = \Delta x \Delta y \Delta z$. The unit normal vector is constant over each one of the six sides; for example, over the side that is perpendicular to the x axis and faces the positive direction of the x axis, $\mathbf{n} = (1, 0, 0)$. Taking into consideration this and similar simplifications, we evaluate the integral on the right-hand side of (5.3.2) without any approximation, and find

$$\mathbf{F}^S = -\rho V_B \mathbf{g}, \quad (5.3.3)$$

which expresses Archimedes's principle: the force exerted on an immersed body by the ambient fluid is equal in magnitude and opposite in direction to the weight of the fluid displaced by the body.

To compute the integral on the right-hand side of (5.3.2) over an arbitrarily shaped body, we subdivide the volume of the body into small rectangular parallelepipeds, and approximate the surface of the body with the collection of the faces of the parallelepipeds that are wetted by the fluid. Because of cancellations, the sum of the integrals over the faces of all elementary parallelepipeds is equal to the sum of the integrals of the faces that are wetted by the fluid. Summing the contributions, we find that the force exerted on the body is given by (5.3.3) independent of the shape of the body: Archimedes's principles stands true for arbitrarily shaped bodies.

5.3.1 The Gauss divergence theorem

Formula (5.3.3) may be derived in a more rigorous fashion using the Gauss divergence theorem in three dimensions stated in equation (2.6.25). Selecting $h_x = f$, $h_y = 0$, and $h_z = 0$ to form the vector function $\mathbf{h} = (f, 0, 0)$, where f is a scalar function of position, we obtain

$$\int_H f n_x dS = \int_R \frac{\partial f}{\partial x} dV. \quad (5.3.4)$$

The complementary selections $\mathbf{h} = (0, f, 0)$ and $\mathbf{h} = (0, 0, f)$ yield the corresponding identities

$$\int_H f n_y dS = \int_R \frac{\partial f}{\partial y} dV, \quad \int_H f n_z dS = \int_R \frac{\partial f}{\partial z} dV. \quad (5.3.5)$$

Relations (5.3.4) and (5.3.5) may be collected into the vector identity

$$\int_H f \mathbf{n} dS = \int_R \nabla f dV, \quad (5.3.6)$$

where $\nabla f = (\partial f/\partial x, \partial f/\partial y, \partial f/\partial z)$ is the gradient of f .

Comparing now (5.3.6) with (5.3.2), we set

$$f \equiv \rho (g_x x + g_y y + g_z z) + P_0, \quad (5.3.7)$$

compute

$$\nabla f = \rho (g_x, g_y, g_z) = \rho \mathbf{g}, \quad (5.3.8)$$

and find that the surface force is given by

$$\begin{aligned} \mathbf{F}^S &= - \int_{Body} [\rho(g_x x + g_y y + g_z z) + P_0] \mathbf{n} \, dS \\ &= -\rho \mathbf{g} \int_{Body} dV = -\rho \mathbf{g} V_B, \end{aligned} \quad (5.3.9)$$

which reproduces and confirms equation (5.3.3).

5.3.2 Net force on a submerged body

If a body of volume V_B consists of a homogeneous material with density ρ_B , then the mass of the body is equal to $m_B = \rho_B V_B$, and its weight is equal to

$$\mathbf{W} = \rho_B V_B \mathbf{g}, \quad (5.3.10)$$

where \mathbf{g} is the acceleration of gravity. Adding the weight of the body to the buoyancy force given in (5.3.3), we find that the net force exerted on an immersed body is given by

$$\mathbf{F} = \mathbf{F}^S + \mathbf{W} = (\rho_B - \rho) V_B \mathbf{g}. \quad (5.3.11)$$

The density of a neutrally buoyant body is equal to the density of the ambient fluid, and the right-hand side of (5.3.11) vanishes yielding a zero net force.

Consideration of the moments of the traction exerted on the body reveals that the buoyancy force passes through the center of mass of the fluid displaced by the body, whereas the weight of the body passes through the center of mass of the body. If the former lies above the latter, then the body is in a state of stable equilibrium and will remain stationary; otherwise, it will spontaneously rotate to reach a stable configuration.

Problem

Problem 5.3.1 *Applications of the Gauss divergence theorem.*

(a) Apply (5.3.6) for a constant function f and discuss your result.

(b) The center of gravity of a homogeneous body with uniform density is defined in terms of a volume integral as

$$\mathbf{x}_c = \frac{1}{V_B} \int_{Body} \mathbf{x} dV. \quad (5.3.12)$$

Show that an equivalent expression in terms of a surface integral is

$$\mathbf{x}_c = \frac{1}{2V_B} \int_{Body} (x^2 + y^2 + z^2) \mathbf{n} dS. \quad (5.3.13)$$

5.4 Shapes of two-dimensional interfaces

Consider two superposed stationary incompressible fluids separated by an infinite horizontal interface located at $y = y_I$, as illustrated in figure 5.4.1. The upper fluid is designated as fluid 1, and the lower fluid is designated as fluid 2. Using the general expression for the pressure distribution in an incompressible liquid given in equation (5.1.25), we find that the pressure distributions in the two fluids are given by

$$p^{(1)}(y) = -\rho_1 g y + c_1, \quad p^{(2)}(y) = -\rho_2 g y + c_2. \quad (5.4.1)$$

The two constants c_1 and c_2 are related by the condition for the jump in the traction across an interface with constant surface tension stated in equation (4.4.11). Since in this case the curvature of the interface vanishes, $\kappa = 0$, condition (4.4.11) requires that the pressure be continuous across the interface,

$$p^{(1)}(y = y_I) = p^{(2)}(y = y_I). \quad (5.4.2)$$

Substituting the pressure distributions (5.4.1) into (5.4.2), we find

$$-\rho_1 g y_I + c_1 = -\rho_2 g y_I + c_2, \quad (5.4.3)$$

which may be rearranged to give

$$c_2 = c_1 + (\rho_2 - \rho_1) g y_I. \quad (5.4.4)$$

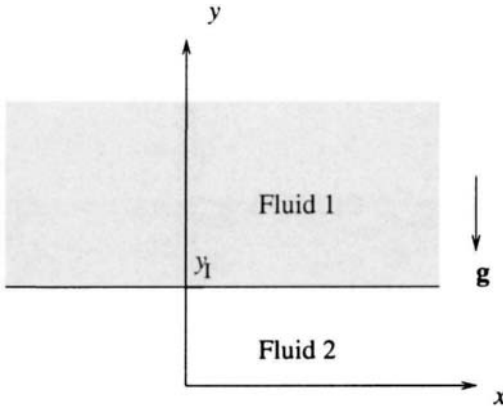


Figure 5.4.1 An infinite horizontal interface separating two stationary fluids.

One of the two constants c_1 or c_2 is determined by requiring an appropriate boundary condition far from the interface, and the second follows from (5.4.4). For example, if the pressure on the upper side of the interface is equal to the atmospheric pressure P_{Atm} , then $c_1 = P_{Atm} + \rho_1 g y_1$ and $c_2 = P_{Atm} + \rho_2 g y_1$.

5.4.1 Static contact angle

In practice, the flat interface depicted in figure 5.4.1 terminates at a side wall, as illustrated in figure 5.4.2. Further examples of terminated interfaces are depicted in figure 5.5.1 illustrating a semi-infinite interface ending at an inclined plate, in figure 5.6.1 illustrating a finite interface confined between two parallel flat plates, and in figure 5.7.1 illustrating the finite interface enclosing a drop attached to a horizontal plane.

The line where the two fluids meet at a solid surface is called the *contact line*. In the case of two-dimensional or axisymmetric interfaces, the contact line is represented by the *contact point*, which is the trace of the contact line in the xy or a meridional plane, identified by a filled circle in figures 5.5.1, 5.6.1, and 5.7.1.

The angle subtended between (a) the line that is normal to the contact line and tangential to the solid surface, and (b) the line that is normal to the contact line and tangential to the interface, measured on

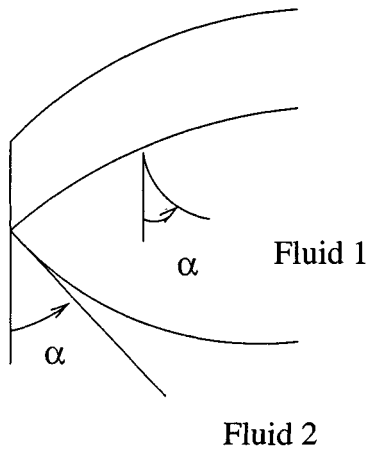


Figure 5.4.2 An interface ending at a contact line; α is the contact angle measured on the side of fluid numbered 2.

the side of fluid labelled 2, as illustrated in figure 5.4.2, is called the *static contact angle*. The static contact angle is a physical constant determined by the prevailing physical conditions and physical properties of the solid and fluids. If fluid 1 wets the solid better than fluid 2 does, then the contact angle is smaller than $\pi/2$; whereas if fluid 2 wets the solid better than fluid 1 does, the contact angle is larger than $\pi/2$ but less than the maximum possible value of π .

If the side-wall illustrated in figure 5.4.2 is vertical, and the static contact angle is equal to $\pi/2$, the interface will remain flat all the way up to the contact line. Under more general conditions, the interface will assume a curved shape with nonzero curvature established to satisfy the physical requirement on the contact angle.

5.4.2 The Laplace-Young equation

To derive the equation governing the shape of a curved interface, we substitute the pressure distributions (5.4.1) into the interfacial condition (4.4.11), and find

$$-\rho_2 g y_I + c_2 + \rho_1 g y_I - c_1 = \gamma \kappa. \quad (5.4.5)$$

Rearranging, we obtain the Laplace-Young equation governing the shape of a two-dimensional interface in hydrostatics,

$$\kappa = -\frac{\Delta\rho g}{\gamma}y_I + B, \quad (5.4.6)$$

where $\Delta\rho \equiv \rho_2 - \rho_1$, and $B \equiv (c_2 - c_1)/\gamma$ is a constant with dimensions of inverse length determined by requiring an appropriate boundary condition or global constraint. Implicit in (5.4.6) is the assumption that the acceleration of gravity points toward the negative direction of the y axis; for different orientations, straightforward modifications are necessary.

Assuming that the fluids are stably stratified, that is, $\rho_2 > \rho_1$ or $\Delta\rho > 0$, we introduce the *capillary length* defined as

$$l = \left(\frac{\gamma}{\Delta\rho g}\right)^{1/2}, \quad (5.4.7)$$

and recast equation (5.4.6) into the simpler form

$$\kappa = -\frac{y_I}{l^2} + B. \quad (5.4.8)$$

For an air-water interface at 20° Celsius, $\gamma = 73$ dynes/cm = 73×10^{-3} kg/sec², $\rho_1 = 0.0$ kg/m³, $\rho_2 = 1000.0$ kg/m³, yielding a capillary length of 2.72 mm.

The Laplace-Young equation (5.4.8) requires that the curvature of an interface be a linear function of the elevation from a reference state. An obvious solution arises by assuming that y_I is constant, and then setting $B = y_I/l^2$ to find $\kappa = 0$. The flat shape of the interface computed in this manner, however, will not necessarily conform with the boundary condition on the static contact angle, and the obvious solution will not generally be admissible: the shape of the interface must be found so that both (5.4.8) and the boundary condition on the contact angle are satisfied.

Problem

Problem 5.4.1 *Laplace-Young equation in three dimensions.*

Show that the counterpart of equation (5.4.8) for a three-dimensional interface is

$$2\kappa_m = -\frac{y_I}{l^2} + B, \quad (5.4.9)$$

where κ_m is the mean curvature.

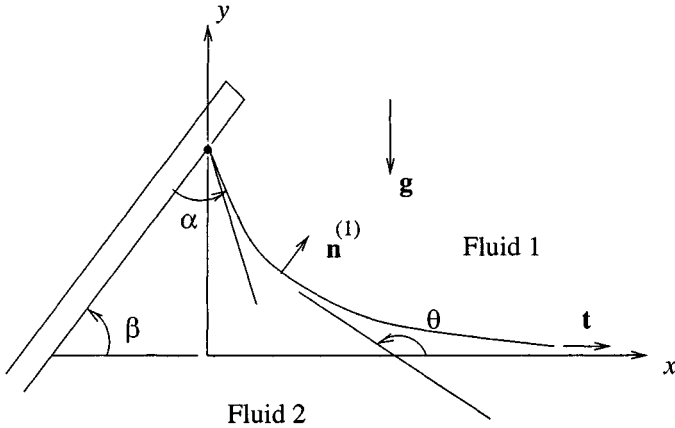


Figure 5.5.1 A semi-infinite interface attached to an inclined plate. Far from the plate, the interface becomes horizontal.

5.5 A semi-infinite interface attached to an inclined plate

We begin the study of two-dimensional interfacial shapes by considering a semi-infinite interface attached to a flat plate that is inclined at an angle β with respect to the horizontal, as illustrated in figure 5.5.1. Far from the plate, as x tends to infinity, the interface tends to become horizontal. The contact angle subtended between the inclined plate and the tangent to the interface at the contact point is required to have the prescribed value α .

It will be convenient to set the origin of the y axis at the position of the flat interface far from the plate, and describe the interface by the equation

$$y_I = f(x). \quad (5.5.1)$$

As x tends to infinity, the function $f(x)$ tends to zero yielding a flat interface. Since the curvature of the interface vanishes far from the plate, the constant B on the right-hand side of the Laplace-Young equation (5.4.8) must be equal to zero, yielding the simpler form

$$\kappa = -\frac{f}{l^2}. \quad (5.5.2)$$

Our first task is to derive an expression for the curvature in terms of the function $f(x)$.

5.5.1 Curvature

Taking the inner product of equation (4.3.5) and the unit normal vector $\mathbf{n}^{(1)}$, we find

$$\kappa = -\mathbf{n}^{(1)} \cdot \frac{d\mathbf{t}}{dl} = -\frac{dx}{dl} \mathbf{n}^{(1)} \cdot \frac{d\mathbf{t}}{dx}. \quad (5.5.3)$$

When the interface does not turn upon itself but has the monotonic shape depicted in figure 5.5.1, we may write

$$\begin{aligned} \mathbf{n}^{(1)} &= \frac{1}{(1+f'^2)^{1/2}} (-f', 1), \\ \mathbf{t} &= \frac{1}{(1+f'^2)^{1/2}} (1, f'), \quad \frac{dl}{dx} = (1+f'^2)^{1/2}, \end{aligned} \quad (5.5.4)$$

where a prime denotes a derivative with respect to x . Substituting expressions (5.5.4) into the right-hand side of (5.5.3), and simplifying, we obtain the desired expression for the curvature,

$$\kappa = -\frac{f''}{(1+f'^2)^{3/2}} = \frac{1}{f'} \frac{d}{dx} \frac{1}{(1+f'^2)^{1/2}}. \quad (5.5.5)$$

It will be useful to introduce the slope angle θ shown in figure 5.5.1, defined by the equation

$$\tan \theta = f' \quad (5.5.6)$$

and note that the fraction on the right-hand side of (5.5.5) is equal to $|\cos \theta|$. The curvature of the interface is then given by the alternative expression

$$\kappa = \frac{1}{f'} \frac{d|\cos \theta|}{dx}. \quad (5.5.7)$$

5.5.2 Governing equation

Combining (5.5.5), (5.5.7), and the Laplace-Young equation (5.5.2), we derive a differential equation governing the shape of the interface,

$$\frac{d}{dx} \left(\frac{1}{(1+f'^2)^{1/2}} \right) = \frac{d|\cos\theta|}{dx} = -\frac{f f'}{l^2} = -\frac{1}{2} \frac{(f^2)'}{l^2}. \quad (5.5.8)$$

Integrating once with respect to x , we obtain

$$\frac{1}{(1+f'^2)^{1/2}} = |\cos\theta| = -\frac{1}{2} \frac{f^2}{l^2} + C, \quad (5.5.9)$$

where C is an integration constant. Demanding that, as x tends to infinity, θ tends to π and f tends to vanish, we find $C = 1$.

5.5.3 Capillary rise

At the contact line located at $x = 0$, the slope angle θ defined in equation (5.5.6) takes the value

$$\theta_{CL} = \alpha + \beta. \quad (5.5.10)$$

Evaluating (5.5.9) at $x = 0$, setting $C = 1$, and rearranging, we obtain an expression for the positive or negative capillary rise $h \equiv f(0)$,

$$\frac{h^2}{2l^2} = 1 - |\cos(\alpha + \beta)|, \quad (5.5.11)$$

which shows that the maximum possible value of $|h|$ occurs when $\alpha + \beta$ is a multiple of $\pi/2$, and the maximum value is equal to $\sqrt{2}l$.

5.5.4 Numerical formulation

To compute the shape of the interface, we set the left-hand side of (5.5.9) equal to the right-hand side with $C = 1$, and rearrange to obtain the first-order ordinary differential equation

$$\frac{df}{dx} = \pm \left(\frac{4}{(2 - \hat{f}^2)^2} - 1 \right)^{1/2} = \pm \hat{f} \frac{(4 - \hat{f}^2)^{1/2}}{2 - \hat{f}^2}, \quad (5.5.12)$$

where we have introduced the dimensionless function $\hat{f} \equiv f/l$. The plus or minus sign on the right-hand side must be selected according to the expected interface shape.

The preceding analysis assumes that the interface has a monotonic shape, and this requires that θ_{CL} lie in the range $(\pi/2, 3\pi/2)$. Outside

this range, the capillary rise is given by equation (5.5.11), but with the minus sign replaced by a plus sign on the right-hand side.

When the shape of the interface is non-monotonic, which means that the interface becomes vertical at a point, the function $f(x)$ is multi-valued, and the integration of (5.5.12) requires special attention. To bypass this subtlety, we regard x along the interface as a function of the independent variable f , and recast (5.5.12) into the form

$$\frac{dx}{df} = \pm \frac{2 - \hat{f}^2}{\hat{f} (4 - \hat{f}^2)^{1/2}}. \quad (5.5.13)$$

The solution of (5.5.13) is to be found for $|f| < |h|$, where $|h|$ is the capillary rise computed from equation (5.5.11).

5.5.5 Numerical method

A numerical solution of (5.5.13) may be computed according to the following steps:

1. Compute the angle θ_{CL} from equation (5.5.10).
2. Compute the capillary rise h using the formulae:

$$h = \begin{cases} +2^{1/2}l (1 + |\cos(\theta_{CL})|)^{1/2} & \text{if } 0 < \theta_{CL} < \pi/2 \\ +2^{1/2}l (1 - |\cos(\theta_{CL})|)^{1/2} & \text{if } \pi/2 < \theta_{CL} < \pi \\ -2^{1/2}l (1 - |\cos(\theta_{CL})|)^{1/2} & \text{if } \pi < \theta_{CL} < 3\pi/2 \\ -2^{1/2}l (1 + |\cos(\theta_{CL})|)^{1/2} & \text{if } 3\pi/2 < \theta_{CL} < 2\pi \end{cases} \quad (5.5.14)$$

3. Integrate the differential equation (5.5.13) from $f = h$ to 0 with initial condition $x(f = h) = 0$ using, for example, the explicit Euler method or the explicit modified Euler method discussed in Section 1.5. If h is negative, use a negative spatial step.

To implement the explicit Euler method, we select a small positive or negative integration step $\Delta f = h/N$, where N defines the level of numerical discretization, evaluate equation (5.5.13) at the point f , and approximate the derivative on the left-hand side with the finite difference $[x(f + \Delta f) - x(f)]/\Delta f$. Rearranging, we obtain

$$x(f + \Delta f) = x(f) + \Delta f \frac{2 - \hat{f}^2}{\hat{f} (4 - \hat{f}^2)^{1/2}}. \quad (5.5.15)$$

The repetitive application of this formula, starting from $f = h$ where $x = 0$, generates a sequence of points distributed over the interface.

To implement the explicit modified Euler method, we replace formula (5.5.15) with the slightly more involved formula

$$x(f + \Delta f) = x(f) + \Delta f \frac{1}{2} \left(\frac{2 - \hat{f}^2}{\hat{f} (4 - \hat{f}^2)^{1/2}} + \frac{2 - \hat{f}^{tmp^2}}{\hat{f}^{tmp} (4 - \hat{f}^{tmp^2})^{1/2}} \right), \quad (5.5.16)$$

where $f^{tmp} = f + \Delta f$.

Computer problem

Problem c.5.5.1 *Semi-infinite interface.*

Directory *05_hydrostat/men_2d_plate* of *FDLIB* includes the main program *men_2d_plate* that computes the shape of the semi-infinite interface discussed in the text. Run the program to generate a family of shapes corresponding to a fixed value of the plate inclination angle β and various contact angles α , and another family of shapes corresponding to a fixed value of the contact angle and various plate inclination angles. Discuss the behavior of the capillary rise in each case.

5.6 A meniscus between two parallel plates

Consider an interface subtended between two parallel vertical plates that are separated by the distance $2b$, as illustrated in figure 5.6.1. The two contact points are at the same elevation, and the interface is symmetric with respect to the mid-plane located at $x = 0$.

It will be convenient to set the origin of the Cartesian axes on the interface midway between the plates, and describe the position of the interface by the equation $y_I = f(x)$. Outside and far from the plates, the interface assumes a horizontal shape located at $y_I = -h$, where h is the positive or negative capillary rise of the meniscus midway between the plates. Our objective is to compute h along with the unknown shape of the meniscus by solving the Laplace-Young equation (5.4.8). We begin by making several preliminary observations:

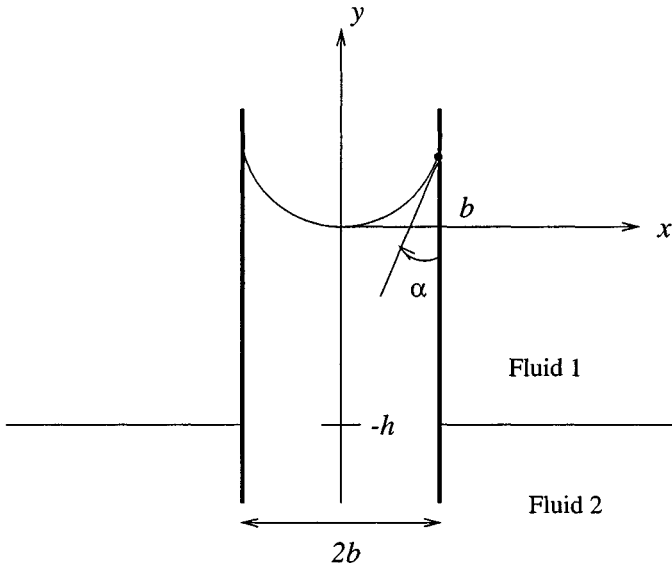


Figure 5.6.1 Illustration of a two-dimensional meniscus subtended between two parallel vertical plates, for contact angle α less than $\pi/2$. When α is greater than $\pi/2$, the meniscus submerges and the capillary rise h is negative.

1. The choice of Cartesian axes requires that $y_I = 0$ at $x = 0$; equation (5.4.8) then gives

$$\kappa(0) = B. \quad (5.6.1)$$

Because the interface is symmetric with respect to $x = 0$, $df/dx = 0$ at $x = 0$, equation (5.5.5) gives

$$\kappa(0) = -f''(0). \quad (5.6.2)$$

Combining equations (5.6.1) and (5.6.2), we find

$$B = -f''(0). \quad (5.6.3)$$

2. Evaluating (5.4.8) at a point outside and far from the plates where the curvature of the interface tends to vanish and $y_I \rightarrow -h$, we obtain

$$B = -\frac{h}{l^2}. \quad (5.6.4)$$

Combining equations (5.6.2) - (5.6.4), we find

$$h = -l^2 \kappa(0) = l^2 f''(0), \quad (5.6.5)$$

which shows that the capillary rise may be computed from knowledge of the curvature of the interface at the mid-point.

Proceeding now with the mathematical formulation, we substitute the first expression for the curvature shown in (5.5.5) and the value of B shown in (5.6.4) into the Laplace-Young equation (5.4.8), and rearrange to derive a second-order ordinary differential equation involving the capillary rise h as an unknown parameter,

$$f'' = \frac{1}{l^2} (f + h) (1 + f'^2)^{3/2}. \quad (5.6.6)$$

The solution is to be found over the interval $0 < x < b$, subject to the boundary conditions

$$f(0) = 0, \quad f'(0) = 0, \quad f'(b) = \cot \alpha. \quad (5.6.7)$$

The third condition specifies the prescribed value of the contact angle. If $\alpha = \pi/2$, all three boundary (5.6.7) are homogeneous, and the obvious solution $h = 0$ and $f = 0$ describes a flat non-elevated and non-submerged interface.

5.6.1 Canonical form

To compute the solution under more general conditions, we recast the second-order differential equation (5.6.6) involving the unspecified parameter h into the canonical form of a system of three first-order differential equations. The word canonical derives from the Greek work *κανονικός* which means *normal*; in real life, normal is not necessarily desirable. This is done by introducing the three new variables

$$q_1 = f, \quad q_2 \equiv f', \quad q_3 \equiv h, \quad (5.6.8)$$

where $q_2' = f''$. Subject to these definitions, equation (5.6.6) is resolved into the three first-order component equations,

$$\begin{aligned}\frac{dq_1}{dx} &= q_2, \\ \frac{dq_2}{dx} &= \frac{1}{l^2} (q_1 + q_3) (1 + q_2^2)^{3/2}, \\ \frac{dq_3}{dx} &= 0.\end{aligned}\tag{5.6.9}$$

The third equation simply states that $q_3 \equiv h$ is a constant. In terms of the new variables, the boundary conditions (5.6.7) become

$$q_1(0) = 0, \quad q_2(0) = 0, \quad q_2(b) = \cot \alpha.\tag{5.6.10}$$

If the value of $q_3(0) = h$ were known, we would be able to integrate the system (5.6.9) from $x = 0$ to b using, for example, the explicit Euler or the modified Euler method discussed in Sections 1.5 and 5.5.

Explicit Euler method

To implement the explicit Euler method, we recast the system (5.6.9) into the general symbolic form

$$\begin{aligned}\frac{dq_1}{dx} &= f_1(q_1, q_2, q_3, x), \\ \frac{dq_2}{dx} &= f_2(q_1, q_2, q_3, x), \\ \frac{dq_3}{dx} &= f_3(q_1, q_2, q_3, x),\end{aligned}\tag{5.6.11}$$

where, in the present case,

$$\begin{aligned}f_1(q_1, q_2, q_3, x) &\equiv q_2, \\ f_2(q_1, q_2, q_3, x) &\equiv \frac{1}{l^2} (q_1 + q_3) (1 + q_2^2)^{3/2}, \\ f_3(q_1, q_2, q_3, x) &\equiv 0.\end{aligned}\tag{5.6.12}$$

Next, we evaluate equations (5.6.11) at a point x , select a small spatial step Δx , and approximate the derivatives on the left-hand sides with finite differences writing, for example, $dq_1/dx = (q_1(x + \Delta x) - q_1(x))/\Delta x$. Solving for $q_1(x + \Delta x)$, and repeating for the second and third equation, we find

$$\begin{aligned} q_1(x + \Delta x) &= q_1(x) + \Delta x f_1(q_1(x), q_2(x), q_3(x), x), \\ q_2(x + \Delta x) &= q_2(x) + \Delta x f_2(q_1(x), q_2(x), q_3(x), x), \\ q_3(x + \Delta x) &= q_3(x) + \Delta x f_3(q_1(x), q_2(x), q_3(x), x). \end{aligned} \quad (5.6.13)$$

In vector notation,

$$\mathbf{q}(x + \Delta x) = \mathbf{q}(x) + \Delta x \mathbf{f}(\mathbf{q}(x), x), \quad (5.6.14)$$

where we have defined the solution vector $\mathbf{q} \equiv (q_1, q_2, q_3)$ and the corresponding phase-space velocity vector $\mathbf{f} \equiv (f_1, f_2, f_3)$. The repetitive application of formula (5.6.14), starting from $x = 0$, allows us to generate a sequence of points distributed over the meniscus.

Explicit modified Euler method

To implement the explicit modified Euler method, we replace formula (5.6.14) with the union of a predictor and a corrector formula,

$$\begin{aligned} \mathbf{q}^{tmp} &= \mathbf{q}(x) + \Delta x \mathbf{f}(\mathbf{q}(x), x), \\ \mathbf{q}(x + \Delta x) &= \mathbf{q}(x) + \Delta x \frac{1}{2} [\mathbf{f}(\mathbf{q}(x), x) + \mathbf{f}(\mathbf{q}^{tmp}, x + \Delta x)], \end{aligned} \quad (5.6.15)$$

where the superscript *tmp* denotes a preliminary value computed by the explicit Euler method. The first equation generates a provisional value, and the second equation advances the solution using the initial and the provisional value.

5.6.2 The shooting method

Because, however, the value of h is unknown, the starting vector $\mathbf{q}(0)$ is not available, and the solution of (5.6.9) must be computed using an iterative method. The shooting method prescribes the obvious: guess the value of $q_3(0) = h$, compute the solution of (5.6.9), and then check whether the third condition in (5.6.10) is fulfilled; if not, repeat the computation with an improved guess.

To improve the guess in a systematic fashion that guarantees rapid convergence, we note that the value of $q_2(b)$ computed by solving equations (5.6.9) is a function of the guessed value $q_3(0) = h$; to signify this dependence, we extend the list of arguments of q_2 , writing $q_2(b; h)$. The third of the boundary conditions (5.6.10) requires $q_2(b; h) - \cot \alpha = 0$, which means that h is a root of the *objective function*

$$Q(h) \equiv q_2(b; h) - \cot \alpha. \quad (5.6.16)$$

The problem has been reduced to computing the solution of the algebraic equation

$$Q(h) = 0, \quad (5.6.17)$$

where the left-hand side is evaluated by integrating equations (5.6.9) with a specified value of h .

5.6.3 The secant method

The secant method provides us with a simple algorithm for solving the nonlinear algebraic equation (5.6.16) according to the following steps:

1. Select a value for h that approximates the root, called $h^{(1)}$, and compute $Q(h^{(1)})$ by solving (5.6.9).

A reasonable approximation may be obtained by assuming that the meniscus has a circular shape of radius R , which is positive when the interface is concave upward and negative when the interface is concave downward. Using elementary trigonometry, we find that the prescribed boundary condition on the contact angle will be satisfied when $\cos \alpha = b/R$, which may be rearranged to yield the approximation $\kappa \simeq -1/R = -\cos \alpha/b$. Combining equations (5.6.2) and (5.6.5), we obtain the desired educated guess

$$h \simeq \cos \alpha \frac{l^2}{b}. \quad (5.6.18)$$

Equation (5.6.18) reveals that the maximum possible value of $|h|$ is equal to l^2/b .

2. Select another value for h called $h^{(2)}$, and compute $Q(h^{(2)})$ by solving (5.6.9).

3. Approximate the graph of the function $Q(h)$ with a straight line passing through the points computed in steps 1 and 2. The slope of the approximating straight line is

$$s^{(2)} = \frac{Q(h^{(2)}) - Q(h^{(1)})}{h^{(2)} - h^{(1)}}. \quad (5.6.19)$$

4. Identify the improved value $h^{(3)}$ with the root of the linear function describing the approximating straight line. Elementary algebra shows that the root is given by

$$h^{(3)} = h^{(2)} - \frac{Q(h^{(2)})}{s^{(2)}}. \quad (5.6.20)$$

5. Repeat the computation with the pairs $h^{(2)}$ and $h^{(3)}$.

Computer problem

Problem c.5.6.1 Meniscus between plates.

Directory `05_hydrostat/men_2d` of *FDLIB* includes the main program `men_2d` that computes the shape of a meniscus subtended between two parallel plates. Run the program to generate a family of shapes corresponding to a fixed value of the plate separation and various contact angles, and another family of shapes corresponding to a fixed value of the contact angle and various plate separations. Discuss the behavior of the capillary rise in each case.

5.7 A two-dimensional drop on a horizontal plane

Consider now a two-dimensional drop of a fluid labelled 2 resting above, or hanging below, a horizontal plate while surrounded by a stationary ambient fluid labelled 1, as illustrated in figure 5.7.1. The resting drop shown in frame (a) is called a *sessile* drop, and the hanging drop shown in frame (b) is called a *pendant* drop. Our objective is to compute the shape of the interface for a specified value of the contact angle α and drop area A_D .

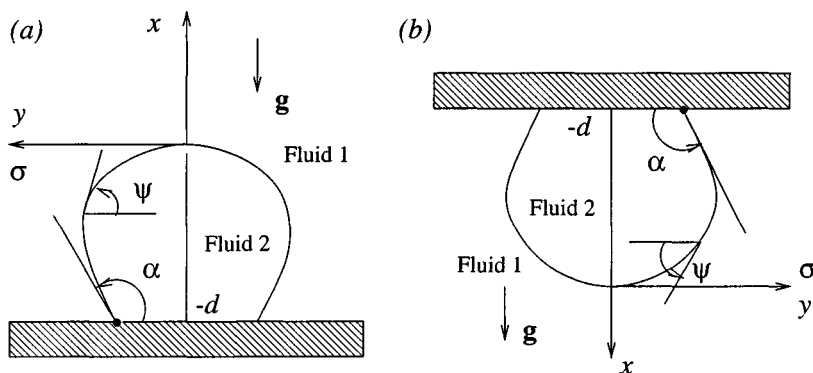


Figure 5.7.1 Illustration of a two-dimensional or axisymmetric drop resting on, or hanging below a horizontal plate called, respectively, a sessile or a pendant drop.

It will be convenient to introduce Cartesian axes with origin at the extreme point of the interface, and the x axis pointing normal to the interface and into the ambient fluid, as depicted in figure 5.7.1(a, b), respectively, for the sessile or pendant drop.

5.7.1 Parametric representation

One difference between the problem presently considered and the ones discussed in preceding sections, is that, in the present case, neither the range of x nor the range of y is known over the span of the interface. To circumvent this difficulty, we describe the shape of the interface in parametric form in terms of the slope angle ψ defined in figure 5.7.1, increasing from 0 at the origin to α at the contact point.

Our objective is to compute the two scalar functions of ψ such that the x and y coordinates of a point at the interface are described by the functions

$$x = X(\psi), \quad y = Y(\psi), \quad (5.7.1)$$

for $0 < \psi < \alpha$. To compute $X(\psi)$ and $Y(\psi)$, we require two ordinary differential equations and a suitable number of boundary conditions or global constraints.

5.7.2 Parametric equations

The first differential equation is the definition of the chosen parameter ψ in terms of the interface slope,

$$\cot \psi = -\frac{dY}{dX}. \quad (5.7.2)$$

One important benefit of the adopted parametrization is that the boundary condition for the contact angle at the contact point is satisfied automatically and may be removed from further discussion.

The second differential equation must arise from the Laplace-Young equation determining the jump in pressure across the interface. Working as in Section 5.4, we find

$$\kappa = -s_1 \frac{\Delta\rho g}{\gamma} X + B, \quad (5.7.3)$$

where $\Delta\rho = \rho_2 - \rho_1$; the coefficient s_1 is equal to 1 for a sessile drop or -1 for a pendant drop, reflecting the orientation of the gravity with respect to the positive direction of the x axis. To simplify the notation, we introduce the capillary length

$$l = \left(\frac{\gamma}{|\Delta\rho| g}\right)^{1/2}, \quad (5.7.4)$$

and recast (5.7.3) into the simpler form

$$\kappa = -s_1 s_2 \frac{X}{l^2} + B, \quad (5.7.5)$$

where the coefficient s_2 is equal to 1 when $\rho_2 > \rho_1$, or -1 when $\rho_2 < \rho_1$. Evaluating equation (5.7.5) at the origin, we find that the constant B is equal to the unknown curvature of the interface at the plane of symmetry located at $y = 0$.

Considering now equation (5.5.5), we set $f' = dY/dX$, and use (5.7.2) to find

$$\begin{aligned} \kappa &= -\frac{1}{\cot \psi} \frac{d}{dX} \left(\frac{1}{(1 + \cot^2 \psi)^{1/2}} \right) \\ &= -\frac{1}{\cot \psi} \frac{d \sin \psi}{dX} = -\sin \psi \frac{d\psi}{dX}. \end{aligned} \quad (5.7.6)$$

Substituting the right-hand side of (5.7.6) into the left-hand side of (5.7.5), we obtain

$$\sin \psi \frac{d\psi}{dX} = s_1 s_2 \frac{X}{l^2} - B, \quad (5.7.7)$$

which may be rearranged to give the desired parametric dependence

$$\frac{dX}{d\psi} = \frac{\sin \psi}{\Phi}, \quad (5.7.8)$$

where

$$\Phi \equiv s_1 s_2 \frac{X}{l^2} - B. \quad (5.7.9)$$

To derive a corresponding parametric dependence for Y , we recast (5.7.2) into the form

$$\frac{dY}{d\psi} = -\cot \psi \frac{dX}{d\psi}. \quad (5.7.10)$$

Substituting (5.7.8) into (5.7.10), we find

$$\frac{dY}{d\psi} = -\frac{\cos \psi}{\Phi}. \quad (5.7.11)$$

Equations (5.7.8) and (5.7.11) provide us with the requisite system of two first-order differential equations involving the unspecified parameter B , to be solved subject to (a) the boundary conditions

$$X(0) = 0, \quad Y(0) = 0, \quad (5.7.12)$$

and (b) the constraint on the drop area A_D ,

$$2 \int_{-d}^0 Y dx = A_D, \quad (5.7.13)$$

where $x = -d$ describes the position of the plane.

5.7.3 The shooting method

Because the value of the constant B is *a priori* unknown, the solution must be found using an iterative method. The shooting method, combined with the secant method for improving the guess, provides us with an efficient algorithm. The numerical procedure involves the following steps:

1. Guess a value for B .

Since B is equal to the unknown curvature of the interface at the mid-plane located at $y = 0$, a reasonable guess can be obtained by assuming that the interface has the shape of a section of a circle, and then computing the radius of the circle a according to the specified values of the contact angle and drop area. Using elementary trigonometry, we find

$$a = \left(\frac{2 A_D}{2 \alpha - \sin(2\alpha)} \right)^{1/2}. \quad (5.7.14)$$

2. Integrate the system of equations (5.7.8) and (5.7.11) using, for example, the explicit Euler method or the explicit modified Euler method discussed in Section 5.6.
3. Compute the integral on the right-hand side of (5.7.13) using the trapezoidal rule, and then evaluate the objective function

$$Q \equiv 2 \int_{-d}^0 y \, dx - A_D. \quad (5.7.15)$$

4. Improve the value of B with the goal of driving the objective function Q to zero using, for example, the secant method discussed in Section 5.6.

Problems

Problem 5.7.1 *Two-dimensional drop on a horizontal plane.*

Derive formula (5.7.14).

Problem 5.7.2 *Two-dimensional drop on an inclined plane.*

Formulate the problem of a pendant or sessile two-dimensional drop attached to an inclined plane.

Computer problem

Problem c.5.7.1 *Two-dimensional drop by numerical computation.*

Subdirectory *05_hydrostat/drop_2d* of *FDLIB* includes the main program *drop_2d* that computes the shape of a sessile or pendant two-dimensional drop using the shooting method discussed in the text. Run

the program to generate a family of shapes corresponding to a fixed value of the drop area and various contact angles, and another family of shapes corresponding to a fixed value of the contact angle and various drop areas. Discuss the computed interfacial shapes.

5.8 Axisymmetric shapes

To compute the shape of axisymmetric interfaces, we work as in the case of two-dimensional interfaces discussed in the preceding sections. Additional considerations include certain subtleties in the computation of the mean curvature, and a more pronounced sensitivity of the numerical methods to the parameters of the computation. In this section, we illustrate the new features by discussing the axisymmetric versions of the two-dimensional problems considered in Sections 5.6 and 5.7.

5.8.1 A meniscus in a vertical capillary

Consider an axisymmetric meniscus inside a vertical cylindrical tube of radius a , as illustrated in figure 5.8.1, which is the counterpart of the two-dimensional meniscus depicted in figure 5.6.1. In the cylindrical polar coordinates depicted in figure 5.8.1, the interface is located at

$$x_I = f(\sigma). \quad (5.8.1)$$

Outside the tube, the interface assumes a horizontal shape with vanishing curvature located at $x = -h$.

Laplace-Young equation

Working as in Section 5.4 but with the interfacial condition (4.4.12) in place of (4.4.11), we derive the three-dimensional version of the Laplace-Young equation (5.4.6), given by

$$2 \kappa_m = -\frac{\Delta\rho g}{\gamma} x_I + B, \quad (5.8.2)$$

where κ_m is the interface mean curvature. The constant B is defined immediately after equation (5.4.6), and is given in terms of the capillary rise in equation (5.6.4).

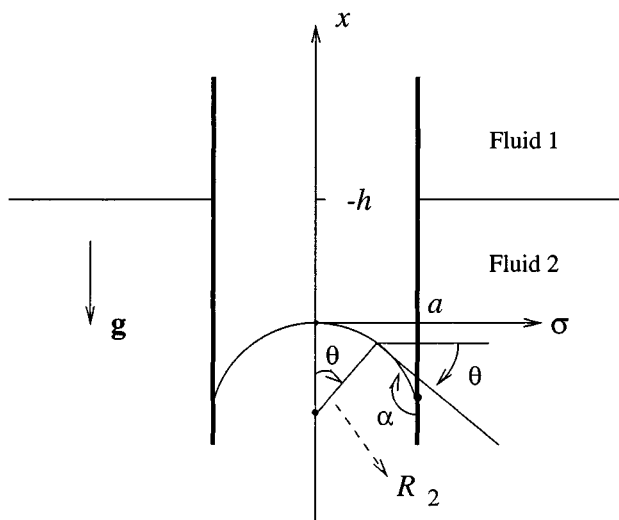


Figure 5.8.1 Schematic illustration of an axisymmetric meniscus inside a vertical circular tube, for contact angle α greater than $\pi/2$.

Mean curvature

The mean curvature is the average of the two principal curvatures: one is the curvature of the trace of the interface in the σx plane, denoted by κ_1 , and the second is the curvature of the trace of the interface in the orthogonal plane, denoted by κ_2 . Working as in Section 5.5, we find that the first principal curvature is given by the following counterpart of equation (5.5.5),

$$\kappa_1 = -\frac{f''}{(1+f'^2)^{3/2}} = \frac{1}{f'} \frac{d}{d\sigma} \frac{1}{(1+f'^2)^{1/2}}, \quad (5.8.3)$$

where a prime denotes a derivative with respect to σ .

It can be shown that the radius of curvature of the second principal curvature, denoted by R_2 , is equal to the signed distance between (a) the point where the curvature is evaluated, and (b) the intersection of the normal to the interface and the x axis, as illustrated in figure 5.8.1,

$$R_2 = -\frac{\sigma}{\sin \theta} = -\sigma \frac{(1+f'^2)^{1/2}}{f'}, \quad \kappa_2 = \frac{1}{R_2}, \quad (5.8.4)$$

where θ is the interface slope angle defined in figure 5.8.1, $f' = \tan \theta$. For the submerged meniscus depicted in figure 5.8.1, θ is negative and R_2 is positive.

Combining expressions (5.8.3) and (5.8.4), we find

$$\begin{aligned}
 2 \kappa_m &= \kappa_1 + \kappa_2 = \frac{1}{f'} \frac{d}{d\sigma} \left[\frac{1}{(1 + f'^2)^{1/2}} \right] - \frac{\sin \theta}{\sigma} \\
 &= \frac{1}{\tan \theta} \frac{d}{d\sigma} \left[\frac{1}{(1 + \tan^2 \theta)^{1/2}} \right] - \frac{\sin \theta}{\sigma} \\
 &= \frac{1}{\tan \theta} \frac{d \cos \theta}{d\sigma} - \frac{\sin \theta}{\sigma} \\
 &= -\cos \theta \frac{d\theta}{d\sigma} - \frac{\sin \theta}{\sigma}.
 \end{aligned} \tag{5.8.5}$$

Parametric representation

It is expedient to describe the shape of the interface in parametric form in terms of the slope angle θ varying from 0 at the center of the tube to $\pi/2 - \alpha$ at the inner wall of the tube, where α is the contact angle. The axial and radial position of a point at the interface is described, respectively, by the functions

$$x = X(\theta), \quad \sigma = \Sigma(\theta). \tag{5.8.6}$$

Substituting the right-hand side of (5.8.5) into the left-hand side of the Laplace-Young equation (5.8.2), and rearranging, we find

$$\frac{d\Sigma}{d\theta} = \frac{\cos \theta}{\Phi}, \tag{5.8.7}$$

where we have defined

$$\Phi \equiv \frac{X + h}{l^2} - \frac{\sin \theta}{\Sigma}. \tag{5.8.8}$$

Equation (5.8.7) governs the parametric representation of the radial position σ in terms of the slope angle θ . To derive a corresponding equation for the axial position X , we combine the definition $f' = \tan \theta = dX/d\Sigma$ with (5.8.7), and obtain

$$\frac{dX}{d\theta} = \frac{\sin \theta}{\Phi}. \quad (5.8.9)$$

The boundary conditions require

$$\Sigma = 0 \quad \text{and} \quad X = 0 \quad \text{at} \quad \theta = 0, \quad (5.8.10)$$

and

$$\Sigma = a \quad \text{at} \quad \theta = \pi/2 - \alpha. \quad (5.8.11)$$

An apparent difficulty arises when we attempt to evaluate the function Φ defined in equation (5.8.8) at $\theta = 0$ corresponding to $\Sigma = 0$: the second fraction on the right-hand side is undefined. Using, however, the l'Hôpital rule, we find that, as θ tends to zero, this ratio reduces to $d\theta/d\Sigma$. Substituting this asymptotic limit into (5.8.8) and the result into (5.8.7) and (5.8.9), we find the regularized initial conditions

$$\left(\frac{d\Sigma}{d\theta}\right)_{\theta=0} = 2 \frac{l^2}{h}, \quad \left(\frac{dX}{d\theta}\right)_{\theta=0} = 0, \quad (5.8.12)$$

which are used to start up the integration.

Solution by iteration

Since the value of the capillary rise h is *a priori* unknown, the solution must be found by iteration. The shooting method involves the following steps: guess the value of h , compute the solution of (5.8.7) and (5.8.9) subject to the initial conditions (5.8.10), and check whether (5.8.11) is satisfied. If not, improve the guess using, for example, the secant method discussed in Section 5.6. A reasonable initial guess emerges by assuming that the meniscus has a spherical shape that is consistent with the prescribed contact angle; using elementary trigonometry, we find

$$h \simeq 2 \cos \alpha \frac{l^2}{a}. \quad (5.8.13)$$

5.8.2 Drop on a plane

Consider next an axisymmetric drop of a fluid labelled 2, resting above or hanging below a horizontal plane while surrounded by an ambient fluid labelled 1, as illustrated in figure 5.7.1. We wish to compute the shape of the interface for a specified value of the contact angle α and drop volume V_D .

Working as in the case of the two-dimensional drop discussed in Section 5.7, we describe the interface in parametric form in terms of the slope angle ψ defined in figure 5.7.1, as

$$x = X(\psi), \quad \sigma = \Sigma(\psi), \quad (5.8.14)$$

where

$$\cot \psi = -\frac{d\Sigma}{dX}. \quad (5.8.15)$$

The counterparts of equations (5.7.8) and (5.7.11) are

$$\frac{dX}{d\psi} = \frac{\sin \psi}{\Phi}, \quad \frac{d\Sigma}{d\psi} = -\frac{\cos \psi}{\Phi}, \quad (5.8.16)$$

where

$$\Phi \equiv \frac{\sin \psi}{\Sigma} + s_1 s_2 \frac{X}{l^2} - B. \quad (5.8.17)$$

The boundary conditions are

$$X(0) = 0, \quad \Sigma(0) = 0, \quad (5.8.18)$$

and the constraint on the drop volume V_D takes the form

$$\int_{-d}^0 \pi \Sigma^2 dx = V_D, \quad (5.8.19)$$

where $x = -d$ describes the position of the plane. At the axis of symmetry located at $\sigma = 0$, equations (5.8.16) are replaced by the regularized forms

$$\left(\frac{d\Sigma}{d\psi}\right)_{\psi=0} = \frac{2}{B}, \quad \left(\frac{dX}{d\psi}\right)_{\psi=0} = 0. \quad (5.8.20)$$

The solution of the parametric equations (5.8.16) can be found using the shooting method discussed in Section 5.7 for the corresponding problem in two dimensions. In the present case, the constant B is equal to twice the mean curvature of the interface at the x axis. A reasonable guess for B arises by assuming that the interface has the shape of a section of a sphere, and computing the radius of the sphere a to satisfy the constraints on the contact angle and drop volume. Using elementary trigonometry, we find

$$a = \left(\frac{3V_D/\pi}{2 + \cos^3 \alpha - 3 \cos \alpha} \right)^{1/3}, \quad (5.8.21)$$

and then set $B = 2/a$.

Problem

Problem 5.8.1 *Drop on a plane.*

(a) Derive the regularized expressions (5.8.20) departing from equations (5.8.16) and (5.8.17).

(b) Derive formula (5.8.21).

Computer problems

Problem c.5.8.1 *Axisymmetric meniscus.*

Directory *05_hydrostat/men_ax* of *FDLIB* includes the main program *men_ax* that computes the shape of a meniscus. Run the program to generate a family of shapes corresponding to a fixed value of the tube radius and various contact angles, and another family of shapes corresponding to a fixed value of the contact angle and various tube radii. Discuss the behavior of the capillary rise in each case.

Problem c.5.8.2 *Axisymmetric drop.*

Directory *05_hydrostat/drop_ax* of *FDLIB* includes the main program *drop_ax* that computes the shape of a sessile or pendant axisymmetric drop using the shooting method. Run the program to generate a family of shapes corresponding to a fixed value of the drop volume and various contact angles, and another family of shapes corresponding to a fixed value of the contact angle and various drop volumes. Discuss the computed interfacial shapes.

Chapter 6

Equation of motion and vorticity transport

- 6.1 Newton's second law for the motion of a parcel
- 6.2 Integral momentum balance
- 6.3 Cauchy's equation of motion
- 6.4 Euler's and Bernoulli's equations
- 6.5 The Navier-Stokes equation
- 6.6 Vorticity transport
- 6.7 Dynamic similitude, the Reynolds number and dimensionless numbers in fluid dynamics

Fluid flow is established in response to an external action mediated by boundary motion, by the application of a surface force, or by the presence of a body force. The evolution of a transient flow and the structure of a steady flow established after an initial start-up period are governed by two fundamental principles of thermodynamics and classical mechanics: mass conservation, and Newton's second law for the motion of fluid parcels. The implementation of Newton's law in fluid mechanics leads to Cauchy's equation of motion, which provides us with an expression for the point particle acceleration in terms of the stresses, and to the vorticity transport equation governing the point particle rate of rotation. The derivation and interpretation of these equations in general and specific forms, and their solution for simple flow configurations will be the theme of our discussion.

6.1 Newton's second law for the motion of a parcel

Consider a fluid parcel in motion, as illustrated in figure 5.1.1(a). Newton's second law of motion requires that the rate of change of the linear momentum of the parcel, denoted by \mathbf{M}_p , be equal to the sum of

the forces exerted on the parcel, including the body force due to gravity given in equation (5.1.1), and the surface force given in equation (5.1.2). Expressing these forces in terms of surface and volume integrals, we obtain

$$\frac{d \mathbf{M}_p}{dt} = \mathbf{F}^S + \mathbf{F}^B = \int_{Parcel} \mathbf{f} dS + \int_{Parcel} \rho \mathbf{g} dV, \quad (6.1.1)$$

where \mathbf{f} is the hydrodynamic traction exerted on the parcel surface. Expressing further the traction in terms of the stress tensor, as shown in equation (4.2.9), we find

$$\frac{d \mathbf{M}_p}{dt} = \int_{Parcel} \mathbf{n} \cdot \boldsymbol{\sigma} dS + \int_{Parcel} \rho \mathbf{g} dV, \quad (6.1.2)$$

where the unit normal vector \mathbf{n} points into the parcel exterior. Our next task is to relate the rate of change of the parcel momentum to the fluid density and velocity.

6.1.1 Rate of change of linear momentum

An expression for the linear momentum arises by subdividing the parcel into elementary subparcels of volume dV_p and mass $dm_p = \rho dV$, and then summing the contributions by integration, obtaining

$$\mathbf{M}_p = \int_{Parcel} \mathbf{u} dm_p = \int_{Parcel} \mathbf{u} \rho dV, \quad (6.1.3)$$

where \mathbf{u} is the fluid velocity. The rate of change of linear momentum is given by

$$\frac{d \mathbf{M}_p}{dt} = \frac{d}{dt} \int_{Parcel} \mathbf{u} dm_p = \frac{d}{dt} \int_{Parcel} \mathbf{u} \rho dV. \quad (6.1.4)$$

Now, because the integration is over the volume of the parcel which is not stationary but changes in time, interchanging the time differentiation and the volume integration on the right-hand side of (6.1.4) is permissible only if the time derivative is replaced by the material derivative D/Dt under the integral sign. Thus,

$$\frac{d \mathbf{M}_p}{dt} = \int_{Parcel} \frac{D(\mathbf{u} dm_p)}{Dt} = \int_{Parcel} \left[\frac{D \mathbf{u}}{Dt} dm_p + \frac{D dm_p}{Dt} \mathbf{u} \right]. \quad (6.1.5)$$

Conservation of mass requires that the material derivative of the elementary mass dm_p vanish, yielding the simplified expression

$$\frac{d \mathbf{M}_p}{dt} = \int_{Parcel} \frac{D \mathbf{u}}{Dt} dm_p = \int_{Parcel} \frac{D \mathbf{u}}{Dt} \rho dV. \quad (6.1.6)$$

6.1.2 Equation of parcel motion

Substituting the right-hand side of (6.1.6) into the left-hand side of (6.1.2), we obtain the desired equation of fluid parcel motion,

$$\int_{Parcel} \frac{D \mathbf{u}}{Dt} \rho dV = \int_{Parcel} \mathbf{n} \cdot \boldsymbol{\sigma} dS + \int_{Parcel} \rho \mathbf{g} dV, \quad (6.1.7)$$

involving the point particle acceleration, the stress tensor, and the body force. Explicitly, the x , y , and z components of (6.1.7) are given by

$$\begin{aligned} \int_{Parcel} \frac{Du_x}{Dt} \rho dV &= \int_{Parcel} (n_x \sigma_{xx} + n_y \sigma_{yx} + n_z \sigma_{zx}) dS \\ &\quad + \int_{Parcel} \rho g_x dV, \\ \int_{Parcel} \frac{Du_y}{Dt} \rho dV &= \int_{Parcel} (n_x \sigma_{xy} + n_y \sigma_{yy} + n_z \sigma_{zy}) dS \\ &\quad + \int_{Parcel} \rho g_y dV, \\ \int_{Parcel} \frac{Du_z}{Dt} \rho dV &= \int_{Parcel} (n_x \sigma_{xz} + n_y \sigma_{yz} + n_z \sigma_{zz}) dS \\ &\quad + \int_{Parcel} \rho g_z dV. \end{aligned} \quad (6.1.8)$$

Equations (6.1.8) are valid irrespective of whether the fluid is compressible or incompressible.

6.1.3 Two-dimensional flow

The counterpart of equation (6.1.7) for two-dimensional flow in the xy plane is

$$\int_{Parcel} \frac{D \mathbf{u}}{Dt} \rho dA = \int_{Parcel} \mathbf{n} \cdot \boldsymbol{\sigma} dl + \int_{Parcel} \rho \mathbf{g} dA, \quad (6.1.9)$$

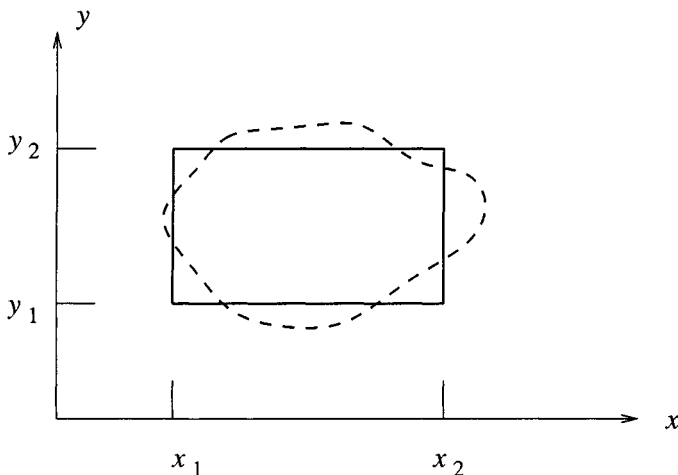


Figure 6.1.1 Illustration of a fluid parcel with an instantaneous rectangular shape, drawn with the solid line, in two-dimensional flow. The fact that the parcel generally deforms to obtain a warped shape, drawn with the dashed line, does not prevent us from applying Newton's law of motion in its integral form over the instantaneous parcel shape.

where dA is the differential of the surface area, and dl is the differential of the arc length along the contour of a parcel in the xy plane. Explicitly, the x and y components of (6.1.9) are given by

$$\int_{Parcel} \frac{Du_x}{Dt} \rho dA = \int_{Parcel} (n_x \sigma_{xx} + n_y \sigma_{yx}) dl + \int_{Parcel} \rho g_x dA,$$

$$\int_{Parcel} \frac{Du_y}{Dt} \rho dA = \int_{Parcel} (n_x \sigma_{xy} + n_y \sigma_{yy}) dl + \int_{Parcel} \rho g_y dA. \quad (6.1.10)$$

We note again that these equations are valid irrespective of whether the fluid is compressible or incompressible.

Motion of a rectangular parcel

As an application, we consider the motion of a fluid parcel with an *instantaneous* rectangular shape whose sides are parallel to the x or y axes, as depicted in figure 6.1.1. It is important to note that the parcel

will remain rectangular only if the fluid exhibits rigid-body motion; under more general conditions, the parcel will deform to obtain a warped shape drawn with the dashed line in figure 6.1.1. The fact that the parcel will generally deform, however, does not prevent us from evaluating the integrals in (6.1.10) over the instantaneous rectangular shape.

For simplicity, we assume that the density of the fluid is uniform, and the acceleration of gravity is constant. Taking into consideration that the unit normal vector is parallel to the x or y axis over each side, we find that equations (6.1.10) assume the simpler forms

$$\begin{aligned} \int_{x_1}^{x_2} \int_{y_1}^{y_2} \left(\frac{Du_x}{Dt} - g_x \right) \rho \, dy \, dx &= \int_{y_1}^{y_2} [(\sigma_{xx})_{x=x_2} - (\sigma_{xx})_{x=x_1}] \, dy \\ &+ \int_{x_1}^{x_2} [(\sigma_{yx})_{y=y_2} - (\sigma_{yx})_{y=y_1}] \, dx, \end{aligned} \quad (6.1.11)$$

and

$$\begin{aligned} \int_{x_1}^{x_2} \int_{y_1}^{y_2} \left(\frac{Du_y}{Dt} - g_y \right) \rho \, dy \, dx &= \int_{y_1}^{y_2} [(\sigma_{xy})_{x=x_2} - (\sigma_{xy})_{x=x_1}] \, dy \\ &+ \int_{x_1}^{x_2} [(\sigma_{yy})_{y=y_2} - (\sigma_{yy})_{y=y_1}] \, dx. \end{aligned} \quad (6.1.12)$$

The first integral on the right-hand side of (6.1.11) involves normal stresses exerted on the vertical sides, and the second integral involves shear stresses exerted on the horizontal sides; the converse is true for (6.1.12).

Steady unidirectional flow

In the case of steady unidirectional flow along the x axis, the point particles move along the x axis with constant velocity and vanishing acceleration, $D\mathbf{u}/Dt = 0$. The left-hand side of the equation of motion (6.1.9) vanishes, yielding a balance between the hydrodynamic and body force,

$$\int_{Parcel} \mathbf{n} \cdot \boldsymbol{\sigma} \, dl + \int_{Parcel} \rho \mathbf{g} \, dA = \mathbf{0}. \quad (6.1.13)$$

Restricting our attention to Newtonian fluids and using the constitutive equation (4.5.4), we find the following:

- In the absence of axial and transverse stretching, $\partial u_x / \partial x = 0$ and $\partial u_y / \partial y = 0$, the normal stresses σ_{xx} and σ_{yy} are equal to the negative of the pressure p , $\sigma_{xx} = \sigma_{yy} = -p$.

- The shear stresses $\sigma_{xy} = \sigma_{yx}$ are independent of streamwise position x , but may depend on the lateral position y .

Subject to these simplifications, the balance equations (6.1.11) and (6.1.12) reduce to

$$\int_{y_1}^{y_2} [p_{x=x_2} - p_{x=x_1}] dy - [(\sigma_{yx})_{y=y_2} - (\sigma_{yx})_{y=y_1}] \Delta x = \rho g_x \Delta x \Delta y,$$

$$\int_{x_1}^{x_2} [p_{y=y_2} - p_{y=y_1}] dx = \rho g_y \Delta x \Delta y, \quad (6.1.14)$$

where $\Delta x \equiv x_2 - x_1$ and $\Delta y = y_2 - y_1$. The second of equations (6.1.14) is clearly satisfied when

$$\frac{p_{x,y=y_2} - p_{x,y=y_1}}{\Delta y} = \rho g_y. \quad (6.1.15)$$

reflecting the hydrostatic pressure variation. The first of equations (6.1.14) is satisfied when

$$\frac{p_{x=x_2,y} - p_{x=x_1,y}}{\Delta x} = \rho g_x - G,$$

$$\frac{(\sigma_{yx})_{x,y=y_2} - (\sigma_{yx})_{x,y=y_1}}{\Delta y} = -G, \quad (6.1.16)$$

where G is a free parameter called the *modified pressure gradient*. Physically, G is determined by the physical mechanism driving the flow:

1. When $G = 0$, the first of equations (6.1.16) shows that the pressure variation in the x direction is hydrostatic, and the second of equations (6.1.16) shows that the shear stress σ_{yx} is constant, independent of y . This is the case of *shear-driven flow*.
2. When the streamwise pressure drop vanishes, $p_{x=x_2,y} = p_{x=x_1,y}$, the first of equations (6.1.16) requires that $G = \rho g_x$, and the second of equations (6.1.16) shows that the difference in the shear stress $(\sigma_{yx})_{x,y=y_2} - (\sigma_{yx})_{x,y=y_1}$ is equal to $-\rho g_x \Delta y$. This is the case of *gravity-driven flow*.
3. When the flow is horizontal, $g_x = 0$, the first of equations (6.1.16) shows that G is the negative of the streamwise pressure gradient, and the second of equation (6.1.16) shows that the difference in the shear stress $(\sigma_{yx})_{x,y=y_2} - (\sigma_{yx})_{x,y=y_1}$ is equal to $-G \Delta y$. This is the case of *pressure-driven flow*.

Problem

Problem 6.1.1 *Body force in terms of a surface integral.*

Show that the body force expressed by the second integral on the right-hand side of (6.1.7) may be expressed as a surface integral in the form

$$\int_{\text{Parcel}} \rho (\mathbf{g} \cdot \mathbf{x}) \mathbf{n} dS \quad (6.1.17)$$

Hint: Use the Gauss divergence theorem (2.6.25).

6.2 Integral momentum balance

Consider the integrand of the rate of the change of momentum on the left-hand side of equation (6.1.7). Using the rules of product differentiation and the continuity equation (2.8.5), we write

$$\rho \frac{D \mathbf{u}}{Dt} = \frac{D(\rho \mathbf{u})}{Dt} - \mathbf{u} \frac{D\rho}{Dt} = \frac{D(\rho \mathbf{u})}{Dt} + (\rho \mathbf{u}) (\nabla \cdot \mathbf{u}), \quad (6.2.1)$$

where $\nabla \cdot \mathbf{u} \equiv \partial u_x / \partial x + \partial u_y / \partial y + \partial u_z / \partial z$ is the divergence of the velocity. If the fluid is incompressible, the second term on the right-hand side of (6.2.1) is absent.

The x component of the vectorial expression (6.2.1) may be manipulated to give

$$\begin{aligned} \rho \frac{D u_x}{Dt} &= \frac{D(\rho u_x)}{Dt} + (\rho u_x) (\nabla \cdot \mathbf{u}) \\ &= \frac{\partial(\rho u_x)}{\partial t} + \mathbf{u} \cdot \nabla(\rho u_x) + (\rho u_x) (\nabla \cdot \mathbf{u}) \\ &= \frac{\partial(\rho u_x)}{\partial t} + u_x \frac{\partial(\rho u_x)}{\partial x} + u_y \frac{\partial(\rho u_x)}{\partial y} + u_z \frac{\partial(\rho u_x)}{\partial z} \\ &\quad + (\rho u_x) (\nabla \cdot \mathbf{u}), \end{aligned} \quad (6.2.2)$$

where the time derivative $\partial/\partial t$ is taken keeping the spatial position fixed. Combining the last four terms on the right-hand side of (6.2.2), we find

$$\rho \frac{D u_x}{Dt} = \frac{\partial(\rho u_x)}{\partial t} + \frac{\partial(\rho u_x u_x)}{\partial x} + \frac{\partial(\rho u_y u_x)}{\partial y} + \frac{\partial(\rho u_z u_x)}{\partial z}. \quad (6.2.3)$$

Working in a similar fashion with the y and z components of (6.2.1), we derive the corresponding expressions

$$\rho \frac{D u_y}{Dt} = \frac{\partial(\rho u_y)}{\partial t} + \frac{\partial(\rho u_x u_y)}{\partial x} + \frac{\partial(\rho u_y u_y)}{\partial y} + \frac{\partial(\rho u_z u_y)}{\partial z}, \quad (6.2.4)$$

and

$$\rho \frac{D u_z}{Dt} = \frac{\partial(\rho u_z)}{\partial t} + \frac{\partial(\rho u_x u_z)}{\partial x} + \frac{\partial(\rho u_y u_z)}{\partial y} + \frac{\partial(\rho u_z u_z)}{\partial z}. \quad (6.2.5)$$

6.2.1 Momentum tensor

To collect equations (6.2.3) - (6.2.5) into a unified form, we introduce the momentum tensor M_{ij} , defined as

$$M_{ij} \equiv \rho u_i u_j, \quad (6.2.6)$$

where the indices i and j range over x , y , and z or, correspondingly, 1, 2, and 3. It is evident from the definition (6.2.6) that the tensor \mathbf{M} is symmetric, $M_{ij} = M_{ji}$.

Moreover, we introduce the divergence of the momentum tensor defined as a vector whose i th component is given by

$$\frac{\partial M_{ji}}{\partial x_j} = \frac{\partial M_{ij}}{\partial x_j}, \quad (6.2.7)$$

where summation of the repeated index j is implied. For example, the x component of the divergence of \mathbf{M} is given by

$$\frac{\partial M_{jx}}{\partial x_j} = \frac{\partial M_{xx}}{\partial x} + \frac{\partial M_{yx}}{\partial y} + \frac{\partial M_{zx}}{\partial z}. \quad (6.2.8)$$

Subject to these definitions, equations (6.2.3) - (6.2.5) are expressed by the collective form

$$\rho \frac{D u_i}{Dt} = \frac{\partial(\rho u_i)}{\partial t} + \frac{\partial M_{ji}}{\partial x_j}, \quad (6.2.9)$$

where $i = x, y,$ or z . The corresponding vector form is

$$\rho \frac{D \mathbf{u}}{Dt} = \frac{\partial(\rho \mathbf{u})}{\partial t} + \nabla \cdot \mathbf{M}. \quad (6.2.10)$$

The right-hand sides of equations (6.2.9) and (6.2.10) involve Eulerian derivatives, that is, derivatives with respect to time and spatial coordinates.

6.2.2 Integral momentum balance

Substituting now (6.2.10) into the left-hand side of the equation of parcel motion (6.1.7), we derive the alternative form

$$\int_{Parcel} \left(\frac{\partial(\rho \mathbf{u})}{\partial t} + \nabla \cdot \mathbf{M} \right) dV = \int_{Parcel} \mathbf{n} \cdot \boldsymbol{\sigma} dS + \int_{Parcel} \rho \mathbf{g} dV, \quad (6.2.11)$$

To this end, we use the Gauss divergence theorem stated in equation (2.6.25) to convert the volume integral of the divergence of the momentum tensor into a surface integral over the parcel volume, obtaining

$$\int_{Parcel} \frac{\partial(\rho \mathbf{u})}{\partial t} dV + \int_{Parcel} \mathbf{n} \cdot \mathbf{M} dS = \int_{Parcel} \mathbf{n} \cdot \boldsymbol{\sigma} dS + \int_{Parcel} \rho \mathbf{g} dV, \quad (6.2.12)$$

where the unit normal vector \mathbf{n} points outward from the parcel. In index notation,

$$\int_{Parcel} \frac{\partial(\rho u_i)}{\partial t} dV + \int_{Parcel} n_j M_{ji} dS = \int_{Parcel} n_j \sigma_{ji} dS + \int_{Parcel} \rho g_i dV, \quad (6.2.13)$$

where summation is implied over the repeated index j .

6.2.3 Control volumes

It is important to remember that equation (6.2.13) has originated from Newton's second law for the motion of a fluid parcel. In the process of expressing the material derivative in terms of Eulerian derivatives taken with respect to time and position in space, however, the parcel

has lost its significance as a material body of fluid, and has become relevant only insofar as to define the volume that it occupies in space.

To signify the new interpretation, we rewrite (6.2.13) in identical form, except that the domain of integration is now called a control volume, denoted by CV . Using the definition of the momentum tensor shown in (6.2.6), we express the integral momentum balance in the form

$$\int_{CV} \frac{\partial(\rho u_i)}{\partial t} dV + \int_{CV} (n_j u_j) \rho u_i dS = \int_{CV} n_j \sigma_{ji} dS + \int_{CV} \rho g_i dV. \quad (6.2.14)$$

The four integrals on the left- and right-hand side of (6.2.14) have the following interpretation:

1. The first integral is the rate of change of the i th component of momentum of the fluid residing inside the control volume. At steady state, this term vanishes.
2. The scalar $n_j u_j$ of the second integrand on the left-hand side of (6.2.14) is the component of the fluid velocity normal to the boundary of the control volume; accordingly, the corresponding integral expresses the rate of *convective* transport of the i th component of the fluid momentum across the boundary of the control volume.
3. The first integral on the right-hand side of (6.2.14) is the i th component of the *surface force* exerted on the boundary of the control volume.
4. The second integral on the right-hand side of (6.2.14) is the i th component of the *body force* exerted on the control volume.

We proceed now to discuss a particular application illustrating the usefulness of the integral momentum balance in engineering analysis.

6.2.4 Flow through a sudden enlargement ¹

Consider steady flow in a duct through the sudden enlargement, as illustrated in figure 6.2.1, and identify the control volume with the section of the duct confined between the vertical planes labelled 1 and 2.

¹This example, and the one discussed in problem 6.2.1 was borrowed from the pioneering text by Bird, Stewart, and Lightfoot cited in the bibliography, where a collection of engineering problems are solved by use of integral mass, momentum, and energy balances.

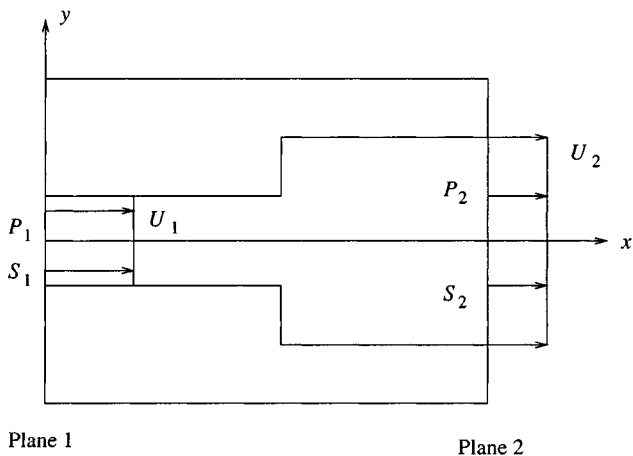


Figure 6.2.1 Simplified model of flow in a duct through a sudden enlargement. An integral momentum balance allows us to compute the pressure rise $P_2 - P_1$ as a function of the inlet and outlet cross-sectional areas S_1 and S_2 .

Assuming that the density of the fluid is uniform and the velocity profile is flat at the inlet and outlet, neglecting the shear stress at the walls, approximating the normal stress at the inlet and outlet with the negative of the pressure, assuming that the pressure at the washer-shaped area is equal to the inlet pressure, and neglecting the effects of gravity, we find that the integral momentum balance (6.2.14) at steady state simplifies to

$$\rho U_2^2 S_2 - \rho U_1^2 S_1 = -P_2 S_2 + P_1 S_1 + P_1 (S_2 - S_1), \quad (6.2.15)$$

where S_1 and S_2 are the cross-sectional areas of the inlet and outlet. The three terms on the right-hand side of (6.2.15) are approximations to the first integral on the right-hand side of (6.2.14) for the outlet, washer-shaped area, and inlet. Mass conservation requires $U_1 S_1 = U_2 S_2$; solving this equation for U_1 , and substituting the result into (6.2.15), we find an expression for the pressure drop

$$P_2 - P_1 = \left(\frac{S_2}{S_1} - 1 \right) \rho U_2^2, \quad (6.2.16)$$

which predicts a rise in pressure in agreement with laboratory observation.

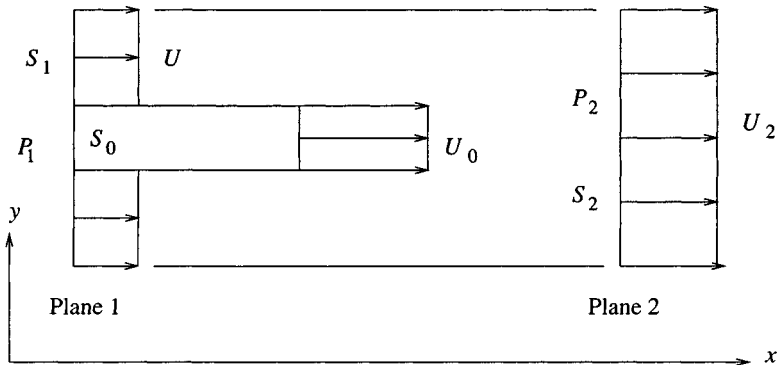


Figure 6.2.2 Schematic illustration of an ejector pump. The pressure rise $P_2 - P_1$ may be estimated by performing an integral momentum balance.

Problem

Problem 6.2.1 *Operation of an ejector pump.*

Figure 6.2.2 shows a schematic illustration of an ejector pump. At plane 1, two fluid streams merge; one with uniform velocity U_1 over a cross-sectional area S_1 , and the second with uniform velocity U_0 over a cross sectional area S_0 . At plane 2, the velocity profile is uniform over the cross-sectional area $S_2 = S_0 + S_1$. The pressure is assumed to be uniform over the cross-section of the inlet and outlet, respectively, equal to P_1 and P_2 , and the fluid density is assumed to be uniform throughout the flow.

Derive an expression for the rise in pressure $P_2 - P_1$ in terms of ρ, U_0, U_1, S_0 , and S_1 , similar to that shown in equation (6.2.16).

6.3 Cauchy's equation of motion

Equation (6.1.7) contains two volume integrals and one surface integral over the boundary of a fluid parcel. If we managed to convert the surface integral into a volume integral, we would be able to collect all integrands into one common expression. Since the volume of the parcel is arbitrary, the unified integrand would have to vanish, providing us with a differential equation.

6.3.1 Hydrodynamic volume force

Transforming the surface integral of the traction into a volume integral can be done using, once again, the Gauss divergence theorem stated in equation (2.6.25). Identifying the vector \mathbf{h} with each one of the three columns of the stress tensor, we obtain

$$\int_{\text{Parcel}} \mathbf{n} \cdot \boldsymbol{\sigma} dS = \int_{\text{Parcel}} \nabla \cdot \boldsymbol{\sigma} dV. \quad (6.3.1)$$

In index notation,

$$\int_{\text{Parcel}} n_j \sigma_{ji} dS = \int_{\text{Parcel}} \frac{\partial \sigma_{ji}}{\partial x_j} dV, \quad (6.3.2)$$

where summation of the repeated index j is implied; the index i is free to vary over x, y , or z .

The divergence of the stress tensor $\nabla \cdot \boldsymbol{\sigma}$ under the integral sign on the right-hand side of (6.3.1) or (6.3.2) is a vector denoted by

$$\boldsymbol{\Sigma} \equiv \nabla \cdot \boldsymbol{\sigma}, \quad (6.3.3)$$

with Cartesian components

$$\begin{aligned} \Sigma_x &= \frac{\partial \sigma_{xx}}{\partial x} + \frac{\partial \sigma_{yx}}{\partial y} + \frac{\partial \sigma_{zx}}{\partial z}, \\ \Sigma_y &= \frac{\partial \sigma_{xy}}{\partial x} + \frac{\partial \sigma_{yy}}{\partial y} + \frac{\partial \sigma_{zy}}{\partial z}, \\ \Sigma_z &= \frac{\partial \sigma_{xz}}{\partial x} + \frac{\partial \sigma_{yz}}{\partial y} + \frac{\partial \sigma_{zz}}{\partial z}. \end{aligned} \quad (6.3.4)$$

Physically, $\boldsymbol{\Sigma}$ is the hydrodynamic force per unit volume of fluid; in contrast, the traction \mathbf{f} is the hydrodynamic force per unit surface area.

6.3.2 Force on an infinitesimal parcel

To confirm identity (6.3.2), we consider a small fluid parcel with the shape of a rectangular parallelepiped centered at the origin, as illustrated in figure 5.1.1(b). The six flat sides of the parcel are perpendicular to the x, y , or z axis, the lengths of the three edges are, respectively,

equal to Δx , Δy , and Δz , and the volume of the parcel is equal to $\Delta V = \Delta x \Delta y \Delta z$.

Consider the surface integral on the left-hand side of equation (6.3.2). Over the sides that are perpendicular to the x axis, located at $x = \frac{\Delta x}{2}$, and $x = -\frac{\Delta x}{2}$, designated as the first and second side, the unit normal vector is parallel to the x axis; over the first side $n_x = 1$, and over the second side $n_x = -1$. Because the size of the parcel is small, the stresses over each side may be approximated with the corresponding values at the side center. Subject to this approximation, the surface integral on the left-hand side over the first and second side take the forms

$$\begin{aligned} & \sigma_{xi}(x = \frac{\Delta x}{2}, y = 0, z = 0) \Delta y \Delta z, \\ & -\sigma_{xi}(x = -\frac{\Delta x}{2}, y = 0, z = 0) \Delta y \Delta z, \end{aligned} \quad (6.3.5)$$

where the parentheses enclose the coordinates of the evaluation point. Adding the two contributions, and factoring out the common product $\Delta y \Delta z$, we obtain

$$[\sigma_{xi}(x = \frac{\Delta x}{2}, y = 0, z = 0) - \sigma_{xi}(x = -\frac{\Delta x}{2}, y = 0, z = 0)] \Delta y \Delta z. \quad (6.3.6)$$

Next, we observe that, in the limit as Δx tends to zero, the ratio of the differences

$$\begin{aligned} & \frac{\sigma_{xi}(x = \frac{\Delta x}{2}, y = 0, z = 0) - \sigma_{xi}(x = -\frac{\Delta x}{2}, y = 0, z = 0)}{\frac{\Delta x}{2} - (-\frac{\Delta x}{2})} \\ & = \frac{\sigma_{xi}(x = \frac{\Delta x}{2}, y = 0, z = 0) - \sigma_{xi}(x = -\frac{\Delta x}{2}, y = 0, z = 0)}{\Delta x} \end{aligned} \quad (6.3.7)$$

tends to the partial derivative $\partial \sigma_{xi} / \partial x$ evaluated at the origin. Correspondingly, the difference (6.3.6) reduces to

$$\frac{\partial \sigma_{xi}}{\partial x} \Delta x \Delta y \Delta z = \frac{\partial \sigma_{xi}}{\partial x} \Delta V, \quad (6.3.8)$$

where the derivatives are evaluated at the origin.

Working in a similar fashion with pairs of sides that are perpendicular to the y or z axis, and summing the contributions, we find that the left-hand side of (6.3.2) takes the approximate form

$$\left(\frac{\partial \sigma_{xi}}{\partial x} + \frac{\partial \sigma_{yi}}{\partial y} + \frac{\partial \sigma_{zi}}{\partial z} \right) \Delta V, \quad (6.3.9)$$

where the quantity enclosed by the parentheses is evaluated at the origin. Expression (6.3.9) is an approximation to the volume integral on the right-hand side of (6.3.2), confirming the identity.

6.3.3 The equation of motion

Substituting now (6.3.1) into (6.1.7), consolidating the integrals, and arguing that, because the volume of integration is arbitrary, the composite integrand must vanish, we obtain Cauchy's differential equation

$$\rho \frac{D \mathbf{u}}{Dt} = \nabla \cdot \boldsymbol{\sigma} + \rho \mathbf{g} \quad (6.3.10)$$

governing the motion of a compressible or incompressible fluid. In index notation,

$$\rho \frac{D u_i}{Dt} = \frac{\partial \sigma_{ji}}{\partial x_j} + \rho g_i, \quad (6.3.11)$$

where summation of the repeated index j is implied, and the index i is free to vary over x, y , or z .

Using equations (2.8.7) and (6.2.10), we derive two equivalent forms of (6.3.10) involving Eulerian derivatives,

$$\rho \left(\frac{\partial \mathbf{u}}{\partial t} + \mathbf{u} \cdot \nabla \mathbf{u} \right) = \nabla \cdot \boldsymbol{\sigma} + \rho \mathbf{g}, \quad (6.3.12)$$

and

$$\frac{\partial (\rho \mathbf{u})}{\partial t} + \nabla \cdot (\rho \mathbf{u} \mathbf{u}) = \nabla \cdot \boldsymbol{\sigma} + \rho \mathbf{g}. \quad (6.3.13)$$

Explicitly, the three scalar components of (6.3.12) are given by

$$\begin{aligned} \rho \left(\frac{\partial u_x}{\partial t} + u_x \frac{\partial u_x}{\partial x} + u_y \frac{\partial u_x}{\partial y} + u_z \frac{\partial u_x}{\partial z} \right) &= \frac{\partial \sigma_{xx}}{\partial x} + \frac{\partial \sigma_{yx}}{\partial y} + \frac{\partial \sigma_{zx}}{\partial z} + \rho g_x, \\ \rho \left(\frac{\partial u_y}{\partial t} + u_x \frac{\partial u_y}{\partial x} + u_y \frac{\partial u_y}{\partial y} + u_z \frac{\partial u_y}{\partial z} \right) &= \frac{\partial \sigma_{xy}}{\partial x} + \frac{\partial \sigma_{yy}}{\partial y} + \frac{\partial \sigma_{zy}}{\partial z} + \rho g_y, \\ \rho \left(\frac{\partial u_z}{\partial t} + u_x \frac{\partial u_z}{\partial x} + u_y \frac{\partial u_z}{\partial y} + u_z \frac{\partial u_z}{\partial z} \right) &= \frac{\partial \sigma_{xz}}{\partial x} + \frac{\partial \sigma_{yz}}{\partial y} + \frac{\partial \sigma_{zz}}{\partial z} + \rho g_z. \end{aligned} \quad (6.3.14)$$

The terms enclosed by the parentheses on the left-hand sides are the Cartesian components of the point particle acceleration; the right-hand sides include the Cartesian components of the volume force due to the hydrodynamic stresses and the components of the body force.

We emphasize again that equations (6.3.10) - (6.3.13) are valid for both compressible and incompressible fluids.

6.3.4 Evolution equations

Given the instantaneous velocity and stress fields, we may evaluate the the right-hand sides of (6.3.10) and (6.3.12), as well as the second term on the left-hand side of (6.3.12), and thereby compute the rates of change $D\mathbf{u}/Dt$ and $\partial\mathbf{u}/\partial t$. This observation suggests that the equation of motion (6.3.10) is, in fact, an evolution equation for the point particle velocity, and equation (6.3.12) is an evolution equation for the velocity at a fixed point in the flow.

A similar evolution equation for the density was derived in Chapter 2 on the basis of the continuity equation, as shown in (2.7.15). The evolution equations for the density and velocity originate from fundamental physical laws: mass conservation is required by thermodynamics, and Newton's second law of motion expresses a fundamental law of classical mechanics.

6.3.5 Cylindrical polar coordinates

In the cylindrical polar coordinates illustrated in figure 1.3.2, the hydrodynamic volume force defined in equation (6.3.3) is expressed by

$$\Sigma = \Sigma_x \mathbf{e}_x + \Sigma_\sigma \mathbf{e}_\sigma + \Sigma_\varphi \mathbf{e}_\varphi. \quad (6.3.15)$$

Using the rules of coordinate transformation and the chain rule of differentiation, we find

$$\begin{aligned} \Sigma_x &= \frac{\partial\sigma_{xx}}{\partial x} + \frac{1}{\sigma} \frac{\partial(\sigma\sigma_{\sigma x})}{\partial\sigma} + \frac{1}{\sigma} \frac{\partial\sigma_{\varphi x}}{\partial\varphi}, \\ \Sigma_\sigma &= \frac{\partial\sigma_{x\sigma}}{\partial x} + \frac{1}{\sigma} \frac{\partial(\sigma\sigma_{\sigma\sigma})}{\partial\sigma} + \frac{1}{\sigma} \frac{\partial\sigma_{\varphi\sigma}}{\partial\varphi} - \frac{1}{\sigma} \sigma_{\varphi\varphi}, \\ \Sigma_\varphi &= \frac{\partial\sigma_{x\varphi}}{\partial x} + \frac{1}{\sigma^2} \frac{\partial(\sigma^2\sigma_{\varphi\sigma})}{\partial\sigma} + \frac{1}{\sigma} \frac{\partial\sigma_{\varphi\varphi}}{\partial\varphi}. \end{aligned} \quad (6.3.16)$$

The cylindrical polar components of the equation of motion are

$$\rho a_x = \Sigma_x + \rho g_x, \quad \rho a_\sigma = \Sigma_\sigma + \rho g_\sigma, \quad \rho a_\varphi = \Sigma_\varphi + \rho g_\varphi, \quad (6.3.17)$$

where a_x , a_σ , and a_φ are the cylindrical polar components of the point particle acceleration given in equations (2.8.10).

Using the alternative expressions (2.8.11), we find

$$\begin{aligned} \rho \frac{Du_x}{Dt} &= \Sigma_x + \rho g_x, \\ \rho \frac{Du_\sigma}{Dt} &= \rho \frac{u_\varphi^2}{\sigma} + \Sigma_\sigma + \rho g_\sigma, \\ \rho \frac{Du_\varphi}{Dt} &= -\rho \frac{u_\sigma u_\varphi}{\sigma} + \Sigma_\varphi + \rho g_\varphi. \end{aligned} \quad (6.3.18)$$

Centrifugal force

The first term on the right-hand side of the second of equations (6.3.18), $\rho u_\varphi^2/\sigma$, is the centrifugal force familiar from classical mechanics. This term expresses an effective volume force in the σ direction due to fluid motion in the meridional φ direction. The centrifugal force arises, for example, in the flow generated by the rotation of a circular cylinder about its axis in a viscous liquid, as will be discussed in Section 7.5.

Coriolis force

The negative of the first term on the right-hand side of the third of equations (6.3.18), $\rho u_\sigma u_\varphi/\sigma$, is the *Coriolis force*. This term expresses an effective force in the φ direction when flow occurs in both the σ and φ directions. The Coriolis force arises, for example, in the flow due to a spinning circular disk immersed in a tank of fluid.

6.3.6 Spherical polar coordinates

In the spherical polar coordinates depicted in figure 1.3.3, the hydrodynamic volume force defined in equation (6.3.3) is expressed by

$$\Sigma = \Sigma_r \mathbf{e}_r + \Sigma_\theta \mathbf{e}_\theta + \Sigma_\varphi \mathbf{e}_\varphi. \quad (6.3.19)$$

Using the rules of coordinate transformation and the chain rule of differentiation, we find

$$\begin{aligned}\Sigma_r &= \frac{1}{r^2} \frac{\partial(r^2 \sigma_{rr})}{\partial r} + \frac{1}{r \sin \theta} \frac{\partial(\sigma_{r\theta} \sin \theta)}{\partial \theta} + \frac{1}{r \sin \theta} \frac{\partial \sigma_{\varphi r}}{\partial \varphi} - \frac{\sigma_{\theta\theta} + \sigma_{\varphi\varphi}}{r}, \\ \Sigma_\theta &= \frac{1}{r^2} \frac{\partial(r^2 \sigma_{r\theta})}{\partial r} + \frac{1}{r \sin \theta} \frac{\partial(\sigma_{\theta\theta} \sin \theta)}{\partial \theta} + \frac{1}{r \sin \theta} \frac{\partial \sigma_{\varphi\theta}}{\partial \varphi} \\ &+ \frac{\sigma_{r\theta} - \sigma_{\varphi\varphi} \cot \theta}{r}, \\ \Sigma_\varphi &= \frac{1}{r^2} \frac{\partial(r^2 \sigma_{r\varphi})}{\partial r} + \frac{1}{r} \frac{\partial \sigma_{\theta\varphi}}{\partial \theta} + \frac{1}{r \sin \theta} \frac{\partial \sigma_{\varphi\varphi}}{\partial \varphi} + \frac{\sigma_{r\varphi} + 2 \sigma_{\theta\varphi} \cot \theta}{r}.\end{aligned}\tag{6.3.20}$$

The spherical polar components of the equation of motion are

$$\rho a_r = \Sigma_r + \rho g_r, \quad \rho a_\theta = \Sigma_\theta + \rho g_\theta, \quad \rho a_\varphi = \Sigma_\varphi + \rho g_\varphi,\tag{6.3.21}$$

where a_r, a_θ , and a_φ are the spherical polar components of the point particle acceleration given in equations (2.8.13).

6.3.7 Plane polar coordinates

In the plane polar coordinates depicted in figure 1.3.4, the hydrodynamic volume force defined in equation (6.3.3) is expressed by

$$\Sigma = \Sigma_r \mathbf{e}_r + \Sigma_\theta \mathbf{e}_\theta.\tag{6.3.22}$$

Using the coordinate transformation rules and the chain rule of differentiation, we find

$$\begin{aligned}\Sigma_r &= \frac{1}{r} \frac{\partial(r \sigma_{rr})}{\partial r} + \frac{1}{r} \frac{\partial \sigma_{\theta r}}{\partial \theta} - \frac{1}{r} \sigma_{\theta\theta}, \\ \Sigma_\theta &= \frac{1}{r^2} \frac{\partial(r^2 \sigma_{r\theta})}{\partial r} + \frac{1}{r} \frac{\partial \sigma_{\theta\theta}}{\partial \theta}.\end{aligned}\tag{6.3.23}$$

The plane polar components of the equation of motion are

$$\rho a_r = \Sigma_r + \rho g_r, \quad \rho a_\theta = \Sigma_\theta + \rho g_\theta,\tag{6.3.24}$$

where a_r and a_θ are the plane polar components of the point particle acceleration given in equations (2.8.15).

Alternative expressions are

$$\begin{aligned}\rho \frac{Du_r}{Dt} &= \rho \frac{u_\theta^2}{r} + \Sigma_r + \rho g_r, \\ \rho \frac{Du_\theta}{Dt} &= -\rho \frac{u_r u_\theta}{r} + \Sigma_\theta + \rho g_\theta,\end{aligned}\tag{6.3.25}$$

involving, respectively, the centrifugal force and the negative of the Coriolis force on the right-hand side.

6.3.8 Vortex force

Returning to equation (6.3.12), we replace the second term in the parentheses on the left-hand side with the right-hand side of (2.8.23), and find

$$\rho \left(\frac{\partial \mathbf{u}}{\partial t} + \frac{1}{2} \nabla u^2 + \boldsymbol{\omega} \times \mathbf{u} \right) = \nabla \cdot \boldsymbol{\sigma} + \rho \mathbf{g},\tag{6.3.26}$$

where

$$u^2 \equiv u_x^2 + u_y^2 + u_z^2\tag{6.3.27}$$

is the square of the magnitude of the velocity. The third term on the left-hand side of (6.3.26) is called the *vortex force*. This force appears when the vorticity vector is non-parallel to the velocity vector, otherwise their cross product will vanish. A flow wherein the vorticity vector is parallel to the velocity vector at every point, is called a *Beltrami flow*.

Problem

Problem 6.3.1 *Beltrami flow*.

Explain why a two-dimensional or an axisymmetric flow cannot be a Beltrami flow.

6.4 Euler's and Bernoulli's equations

Euler's equation derives from the equation of motion (6.3.10) by substituting in it the simplest possible constitutive equation for the stress

tensor corresponding to an ideal fluid, expressed by (4.5.15). Consideration of the individual components of the volume force Σ , given in (6.3.4), shows that

$$\Sigma \equiv \nabla \cdot \sigma = -\nabla p = -\frac{\partial p}{\partial x} \mathbf{e}_x - \frac{\partial p}{\partial y} \mathbf{e}_y - \frac{\partial p}{\partial z} \mathbf{e}_z. \quad (6.4.1)$$

The equation of motion (6.3.10) then reduces to the Euler equation

$$\rho \frac{D \mathbf{u}}{Dt} = -\nabla p + \rho \mathbf{g}. \quad (6.4.2)$$

The associated Eulerian form is

$$\rho \left(\frac{\partial \mathbf{u}}{\partial t} + \mathbf{u} \cdot \nabla \mathbf{u} \right) = -\nabla p + \rho \mathbf{g}. \quad (6.4.3)$$

Explicitly, the three Cartesian components of (6.4.3) are given by

$$\begin{aligned} \rho \left(\frac{\partial u_x}{\partial t} + u_x \frac{\partial u_x}{\partial x} + u_y \frac{\partial u_x}{\partial y} + u_z \frac{\partial u_x}{\partial z} \right) &= -\frac{\partial p}{\partial x} + \rho g_x, \\ \rho \left(\frac{\partial u_y}{\partial t} + u_x \frac{\partial u_y}{\partial x} + u_y \frac{\partial u_y}{\partial y} + u_z \frac{\partial u_y}{\partial z} \right) &= -\frac{\partial p}{\partial y} + \rho g_y, \\ \rho \left(\frac{\partial u_z}{\partial t} + u_x \frac{\partial u_z}{\partial x} + u_y \frac{\partial u_z}{\partial y} + u_z \frac{\partial u_z}{\partial z} \right) &= -\frac{\partial p}{\partial z} + \rho g_z. \end{aligned} \quad (6.4.4)$$

The cylindrical, spherical, and plane polar components of Euler's equation follow readily from equations (6.3.17), (6.3.21), and (6.3.24), by using the constitutive equations (4.7.7), (4.7.14), and (4.7.20) with vanishing fluid viscosity.

Using the expression for the point particle acceleration shown on the left-hand side of equation (6.3.26), we find an alternative form of Euler's equation in terms of the vortex force,

$$\rho \left(\frac{\partial \mathbf{u}}{\partial t} + \frac{1}{2} \nabla u^2 - \mathbf{u} \times \omega \right) = -\nabla p + \rho \mathbf{g}, \quad (6.4.5)$$

where $u^2 \equiv u_x^2 + u_y^2 + u_z^2$ is the square of the magnitude of the velocity.

6.4.1 Boundary conditions

Euler's equation is a first-order differential equation for the velocity and the pressure in the spatial variables. To compute a solution, we require one scalar boundary condition or two scalar jump conditions involving the velocity or pressure along each boundary:

- Over an impermeable surface, we require the no-penetration condition.
- Over a free surface, we require that the pressure be equal to the ambient pressure increased or decreased by an amount that is equal to the product of the surface tension and twice the local mean curvature.
- Over a fluid interface, we require a kinematic and a dynamic continuity or jump condition. The kinematic condition requires that the normal component of the fluid velocity remain continuous across the interface. The dynamic condition requires that the pressure undergo a discontinuity by an amount that is equal to the product of the surface tension and twice the local mean curvature.

6.4.2 Bernoulli's equation for irrotational flow

If the flow is irrotational, the third term on the left-hand side of (6.4.5) vanishes. Expressing the velocity in terms of the gradient of the velocity potential ϕ , as shown in equation (3.2.3) and more explicitly in equations (3.2.10), we find that Euler's equation (6.4.5) assumes the simplified form

$$\rho \left(\frac{\partial \nabla \phi}{\partial t} + \frac{1}{2} \nabla u^2 \right) = -\nabla p + \rho \mathbf{g}. \quad (6.4.6)$$

The order of time and space differentiation in the gradient of the potential may be freely switched in the first term on the left-hand side.

Assuming now that the density of the fluid is uniform, we express the acceleration of gravity as the gradient of the scalar $s \equiv \mathbf{g} \cdot \mathbf{x}$, writing

$$\mathbf{g} = \nabla s = \nabla(\mathbf{g} \cdot \mathbf{x}) = \nabla(g_x x + g_y y + g_z z). \quad (6.4.7)$$

Substituting this form into (6.4.6), and collecting all terms under the gradient, we find

$$\nabla \left(\frac{\partial \phi}{\partial t} + \frac{1}{2} u^2 + \frac{p}{\rho} - \mathbf{g} \cdot \mathbf{x} \right) = \mathbf{0}. \quad (6.4.8)$$

Since the spatial derivatives of the scalar quantity enclosed by the parentheses on the left-hand side vanish, this quantity must be spatially uniform but possibly time-dependent. On the basis of this argument, Euler's equation for irrotational flow reduces to Bernoulli's equation for the irrotational flow of a uniform-density fluid,

$$\frac{\partial \phi}{\partial t} + \frac{1}{2} u^2 + \frac{p}{\rho} - \mathbf{g} \cdot \mathbf{x} = c(t), \quad (6.4.9)$$

where $c(t)$ is an unspecified function of time.

Evolution of the potential

Bernoulli's equation (6.4.9) may be regarded as an evolution equation for the harmonic potential: given the instantaneous velocity and pressure, we may evaluate the second, third, and fourth terms on the left-hand side, compute the time derivative $\partial\phi/\partial t$, and advance the potential over a small period of elapsed time. The last term $c(t)$ causes the potential to increase or decrease uniformly at the same rate throughout the fluid. But since the velocity is computed by taking derivatives of the potential with respect to the spatial coordinates, this uniform change does not affect the distribution of the velocity in the fluid.

In problems involving a free surface with a prescribed pressure on one side, it is appropriate to convert the Eulerian time derivative $\partial\phi/\partial t$ on the left-hand side of (6.4.9) to the material derivative $D\phi/Dt$. Invoking the definition of the material derivative, and expressing the velocity as the gradient of the potential, as shown in equations (3.2.10), we find

$$\frac{D\phi}{Dt} = \frac{\partial\phi}{\partial t} + \mathbf{u} \cdot \nabla\phi = \frac{\partial\phi}{\partial t} + \mathbf{u} \cdot \mathbf{u} = \frac{\partial\phi}{\partial t} + u^2. \quad (6.4.10)$$

Combining equations (6.4.9) and (6.4.10), we find

$$\frac{D\phi}{Dt} = \frac{1}{2} u^2 - \frac{p}{\rho} + \mathbf{g} \cdot \mathbf{x} - c(t), \quad (6.4.11)$$

which provides us with the rate of change of the potential following a point particle.

Fluid sloshing in a tank

Consider, for example, the sloshing of a fluid in a container, as illustrated in figure 6.4.1. The pressure at the free surface on the side of the liquid, denoted by p_{FS} , is related to the ambient pressure P_{Atm} by the dynamic boundary condition

$$p_{FS} = P_{Atm} + \gamma 2 \kappa_m, \quad (6.4.12)$$

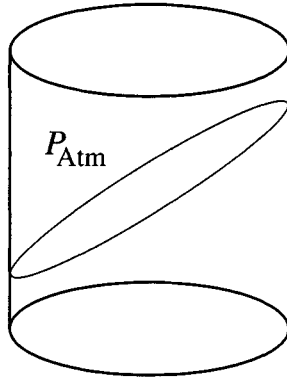


Figure 6.4.1 Irrotational motion due to the sloshing of a fluid in a container. Bernoulli's equation provides us with an evolution equation for the potential following the motion of point particles distributed over the free surface.

where γ is the surface tension, and κ_m is the mean curvature of the free surface. Applying equation (6.4.11) at a point on the free surface, and using (6.4.12), we find that the rate of change of the potential following a point particle is given by

$$\frac{D\phi}{Dt} = \frac{1}{2} u^2 - \frac{P_{Atm} + \gamma 2 \kappa_m}{\rho} + \mathbf{g} \cdot \mathbf{x} - c(t). \quad (6.4.13)$$

Integrating this equation in time, we obtain a boundary condition for the potential over the free surface.

6.4.3 Bernoulli's equation for steady irrotational flow

At steady state, the time derivative of the potential on the left-hand side of (6.4.9) vanishes, yielding the best-known version of Bernoulli's equation

$$\frac{1}{2} u^2 + \frac{p}{\rho} - \mathbf{g} \cdot \mathbf{x} = c(t). \quad (6.4.14)$$

The time-dependence of the constant $c(t)$ on the right-hand side accounts for a possible uniform change in the level of the pressure throughout the fluid.

The three terms on the right-hand side of the (6.4.14) express, respectively, the kinetic energy, the potential energy due to the pressure,

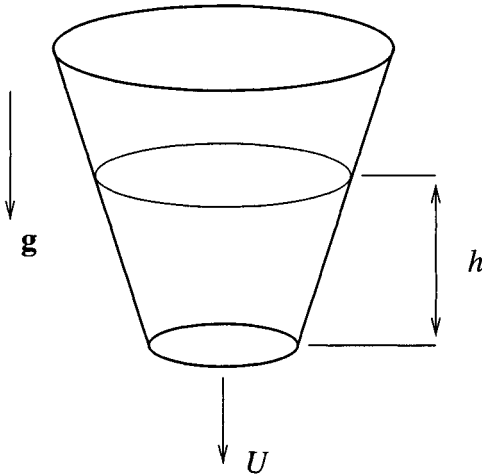


Figure 6.4.2 Illustration of gravity-driven drainage of a fluid from a tank. The exit velocity may be computed using Bernoulli's equation for irrotational flow, and is given by Toricelli's law.

and the potential energy due to the body force, all three per unit mass of fluid. Bernoulli's equation requires that the sum of the three energies be uniform throughout the domain of flow.

Toricelli's law

Bernoulli's equation allows us to carry out approximate engineering analyses of several classes of internal and external high-speed flows. Consider, for example, the gravity-driven drainage of a fluid from a tank, as illustrated in figure 6.4.2. If the rate of drainage is sufficiently slow, the flow may be assumed to be in a quasi-steady state; that is, the magnitude of the time derivative is small compared to the rest of the terms in the unsteady Bernoulli equation (6.4.9), and the steady version of Bernoulli's equation (6.4.14) can be employed.

To compute the velocity at the point of drainage, denoted by U , we evaluate the left-hand side of (6.4.14) first at the free surface and second at the point of drainage, and set the two expressions equal. Considering the velocity at the free surface negligible, and setting the pressure at the free surface and at the point of drainage equal to the ambient

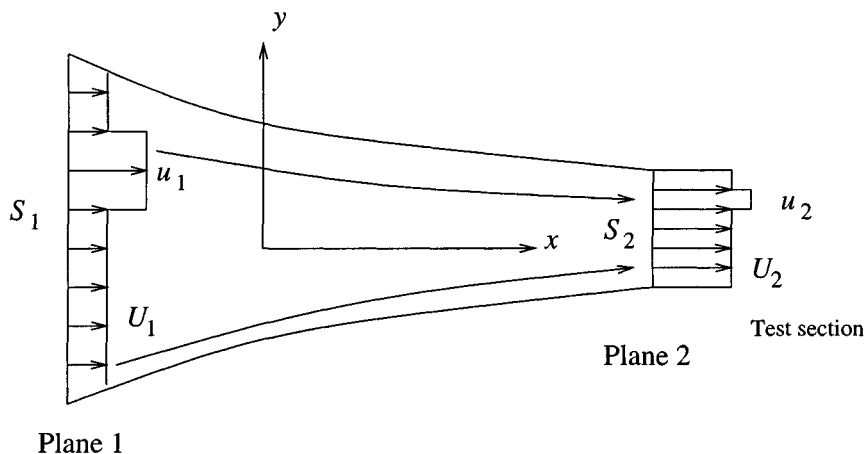


Figure 6.4.3 Flow in a wind or water tunnel with a contraction that dampens small perturbations.

atmospheric pressure, we derive Toricelli's law

$$U = \sqrt{2gh}, \quad (6.4.15)$$

also describing the velocity of a rigid body in free gravitational fall.

Decay of perturbations in a wind or water tunnel

Wind and water tunnels are used widely in studies of high-speed flows. To obtain a desirable uniform velocity profile, the tunnel is designed with a smooth contraction upstream from a test section where measurement or observation takes places, as illustrated in figure 6.4.3.

Consider a small perturbation of the otherwise flat upstream velocity profile at plane 1, as illustrated in figure 6.4.3. The pressure is assumed to be uniform over any cross-section along the contraction. Applying Bernoulli's equation (6.4.14) for the fluid outside or inside the perturbed region, and neglecting the effects of gravity, we find

$$\frac{1}{2} U_1^2 + \frac{P_1}{\rho} = \frac{1}{2} U_2^2 + \frac{P_2}{\rho}, \quad \frac{1}{2} u_1^2 + \frac{P_1}{\rho} = \frac{1}{2} u_2^2 + \frac{P_2}{\rho}. \quad (6.4.16)$$

Combining these equations to eliminate the pressure, and rearranging, we find

$$\frac{U_2 - u_2}{U_1 - u_1} = \frac{U_1 + u_1}{U_2 + u_2}. \quad (6.4.17)$$

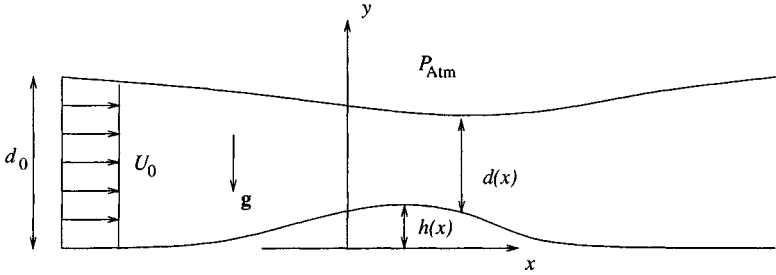


Figure 6.4.4 Irrotational free-surface flow of a horizontal stream over a hump.

Now, because the perturbation has been assumed small, the actual velocities u_1 and u_2 may be replaced with the unperturbed velocities U_1 and U_2 in the numerator and denominator of the fraction on the right-hand side of (6.4.17), yielding

$$\frac{U_2 - u_2}{U_1 - u_1} = \frac{U_1}{U_2}. \quad (6.4.18)$$

Combining the approximate mass balance $U_1 S_1 = U_2 S_2$ with equation (6.4.18), and rearranging, we obtain

$$\frac{(U_2 - u_2)/U_2}{(U_1 - u_1)/U_1} = \left(\frac{S_2}{S_1}\right)^2, \quad (6.4.19)$$

which shows that the relative amplitude of the perturbation decays like the square of the contraction ratio S_2/S_1 , confirming that the contraction aids in the establishment of a uniform velocity profile.

Flow of a horizontal stream over a hump

As a third example, we consider steady two-dimensional irrotational flow of a horizontal stream over a gently sloped hump, called the Venturi flume, as illustrated in figure 6.4.4. The free surface is located at $y = h(x) + d(x)$, where $h(x)$ is the height of the hump and $d(x)$ is the depth of the stream. As x tends to plus or minus infinity, $h(x)$ tends to zero. The profile of the streamwise velocity is assumed to be uniform across the stream; thus, $u_x = u(x)$.

Applying Bernoulli's equation (6.4.14) first at a point at the free surface located far upstream, and second at an arbitrary point at the free surface, neglecting the y component of the free-surface velocity and the pressure drop across the free surface due to surface tension, and noting that the gravitational acceleration vector is given by $\mathbf{g} = (0, -g)$, we find

$$\frac{1}{2} U_0^2 + \frac{P_{Atm}}{\rho} + g d_0 = \frac{1}{2} u^2(x) + \frac{P_{Atm}}{\rho} + g [h(x) + d(x)]. \tag{6.4.20}$$

where U_0 is the upstream velocity, and $d_0 \equiv d(x = -\infty)$ is the upstream depth. Combining now the mass conservation equation $U_0 d_0 = u(x) d(x)$ with equation (6.4.20) to eliminate $u(x)$, and rearranging the resulting expression, we derive a cubic equation for the reduced layer depth $\hat{d}(x) \equiv d(x)/d_0$,

$$\hat{d}^3(x) + \hat{d}^2(x) [\hat{h}(x) - 1 - \frac{1}{2} Fr^2] + \frac{1}{2} Fr^2 = 0, \tag{6.4.21}$$

where $\hat{h}(x) \equiv h(x)/d_0$ is the reduced height of the hump. We have introduced the dimensionless ratio

$$Fr \equiv \frac{U_0}{\sqrt{g d_0}}, \tag{6.4.22}$$

expressing the relative magnitude of inertial and gravitational forces, called the Froude number.

In practice, the Venturi flume is used to deduce the flow rate from measurements of the deflection of the free surface from the horizontal position. As the Froude number tends to zero, gravitational forces dominate, and equation (6.4.21) has the obvious solution $\hat{d}(x) = 1 - \hat{h}(x)$, which shows that the free surface tends to become flat. On the other hand, as the Froude number tends to infinity, inertial forces dominate, and equation (6.4.21) has the obvious solution $\hat{d}(x) = 1$, which shows that the depth of the stream remains constant, and the free surface follows the topography of the hump. Intermediate values of the Froude number yield free-surface profiles with a downward deflection (problem c.6.4.1).

6.4.4 Bernoulli's equation for steady rotational flow

Let us return to Euler's equation (6.4.5), and consider a rotational flow at steady state. The time derivative on the left-hand side vanishes, yielding

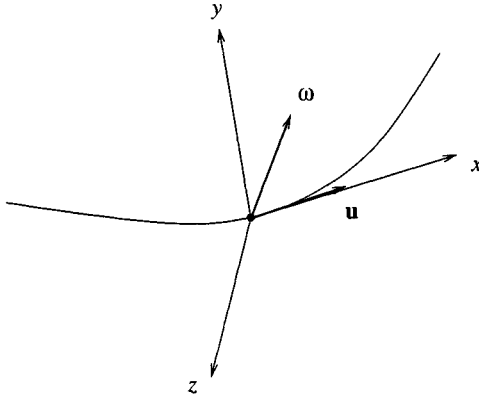


Figure 6.4.5 A system of Cartesian coordinates with the x axis tangential to a streamline, used to derive Bernoulli's equation for steady rotational flow, equation (6.4.26).

$$\frac{1}{2} \nabla u^2 - \mathbf{u} \times \boldsymbol{\omega} = -\frac{1}{\rho} \nabla p + \mathbf{g}, \quad (6.4.23)$$

where $u^2 \equiv u_x^2 + u_y^2 + u_z^2$ is the square of the magnitude of the velocity. The x component of equation (6.4.23) reads

$$\frac{1}{2} \frac{\partial u^2}{\partial x} - u_y \omega_z + u_z \omega_y = -\frac{1}{\rho} \frac{\partial p}{\partial x} + g_x. \quad (6.4.24)$$

Next, we place the origin of the Cartesian axes at a point in the fluid, identify the streamline that passes through that point, and orient the x axis tangentially to the streamline and thus parallel to the local velocity, as illustrated in figure 6.4.5. By construction then, the y and z components of the velocity vanish at the origin, and the second and third terms on the left-hand side of equation (6.4.24) are equal to zero. Taking advantage of these simplifications, we derive the reduced form

$$\frac{\partial}{\partial x} \left(\frac{1}{2} u^2 + \frac{1}{\rho} p - g_x x \right) = 0, \quad (6.4.25)$$

where the left-hand side is evaluated at the origin. Equation (6.4.25) states that the rate of change of the quantity enclosed by the parentheses on the left-hand side with respect to distance along the streamline should

vanish; thus, the quantity enclosed by the parentheses must remain constant along the streamline. An equivalent mathematical statement is

$$\frac{1}{2} u^2 + \frac{p}{\rho} - \mathbf{g} \cdot \mathbf{x} = f(x, y, z), \tag{6.4.26}$$

where the function $f(x, y, z)$ remains constant along a streamline. In two-dimensional or axisymmetric flow, the function $f(x, y, z)$ may be considered as a function of the stream function ψ which, by definition, is constant along a streamline.

Problems

Problem 6.4.1 *Flow through a sudden enlargement.*

Consider the flow through a sudden enlargement depicted in figure 6.2.1. Use Bernoulli’s equation to compute the rise in pressure $P_2 - P_1$, and compare your result to that shown in equation (6.2.16) obtained by an approximate integral momentum balance.

Problem 6.4.2 *Bernoulli’s equation for two-dimensional flow with uniform vorticity.*

The velocity field \mathbf{u} of a two-dimensional flow in the xy plane with uniform vorticity $\omega_z = \Omega$ may be decomposed into the velocity field of a simpler two-dimensional flow with uniform vorticity Ω , denoted by \mathbf{v} , and a potential flow expressed by the harmonic potential ϕ , so that $\mathbf{u} = \mathbf{v} + \nabla\phi$. Two examples of simpler flows are the simple shear flow with velocity $\mathbf{v} = (-\Omega y, 0)$, and a flow expressing rigid-body rotation with velocity $\mathbf{v} = \frac{\Omega}{2}(-y, x)$. Using this decomposition, derive Bernoulli’s equation

$$\frac{\partial\phi}{\partial t} + \frac{1}{2} u^2 + \frac{p}{\rho} - \mathbf{g} \cdot \mathbf{x} + \Omega \psi = c(t), \tag{6.4.27}$$

where ψ is the stream function and $u = |\mathbf{u}|$ is the magnitude of the velocity of the decomposed flow.

Problem 6.4.3 *Flow due to an unsteady point source or point vortex.*

(a) Discuss whether the flow due to a two- or three-dimensional point source with time-dependent strength satisfies the Euler equation for inviscid flow.

(b) Repeat (a) for a two-dimensional point vortex.

Problem 6.4.4 *Force on a sphere in accelerating potential flow .*

Consider unsteady irrotational flow past a sphere that is held stationary in an accelerating stream with velocity $V_x(t)$. The velocity potential and Cartesian components of the velocity are given by equations (3.6.10) and (3.6.11). Use Bernoulli's equation (6.4.9) to evaluate the pressure, and then compute the force exerted on the sphere by evaluating the surface integral

$$\mathbf{F} = - \int_{\text{Sphere}} p \mathbf{n} dS, \quad (6.4.28)$$

where \mathbf{n} is the unit vector normal to the sphere pointing into the fluid. Based on this result, evaluate the force exerted on a sphere held stationary in a non-accelerating steady flow, and discuss the physical relevance of the assumption of irrotational motion.

Computer problems

Problem c.6.4.1 *Flow over a hump.*

Consider the flow of a horizontal stream over a hump illustrated in figure 6.4.4. The height of the hump is described by the parabolic shape function $h(x) = h_0 [1 - (x/a)^2]$, for $-a \leq x \leq a$, where a is the half-length of the hump and h_0 is the maximum height. Substituting this profile into (6.4.21), we find

$$\hat{d}^3(x) + \hat{d}^2(x) \left[\frac{h_0}{d_0} (1 - \hat{x}^2) - 1 - \frac{1}{2} Fr^2 \right] + \frac{1}{2} Fr^2 = 0, \quad (6.4.29)$$

for $-1 \leq \hat{x} \leq 1$, where $\hat{x} \equiv x/a$ is the reduced distance from the midpoint. Compute and plot the reduced layer depth \hat{d} against \hat{x} for $h_0/d_0 = 0.01, 0.05, 0.10$ and $Fr = 0.01, 0.1, 10, 100$, and discuss the free-surface shapes.

6.5 The Navier-Stokes equation

The Navier-Stokes equation derives from the equation of motion (6.3.10) using the constitutive equation for the stress tensor for an incompressible Newtonian fluid, equation (4.5.3). If the viscosity of the fluid is uniform, the hydrodynamic volume force is given by

$$\Sigma \equiv \nabla \cdot \sigma = \nabla \cdot (-p \mathbf{I} + \mu 2 \mathbf{E}) = -\nabla p + \mu 2 \nabla \cdot \mathbf{E}, \quad (6.5.1)$$

where \mathbf{I} is the identity matrix.

Working in index notation, we find that the i th component of twice the divergence of the rate of deformation tensor \mathbf{E} on the right-hand side of (6.5.1) is given by

$$\begin{aligned} 2 \frac{\partial E_{ji}}{\partial x_j} &= 2 \frac{\partial}{\partial x_j} \left[\frac{1}{2} \left(\frac{\partial u_i}{\partial x_j} + \frac{\partial u_j}{\partial x_i} \right) \right] = \frac{\partial^2 u_i}{\partial x_j \partial x_j} + \frac{\partial^2 u_j}{\partial x_j \partial x_i} \\ &= \frac{\partial^2 u_i}{\partial x_j \partial x_j} + \frac{\partial}{\partial x_i} \left(\frac{\partial u_j}{\partial x_j} \right), \end{aligned} \tag{6.5.2}$$

where summation of the repeated index j is implied. The term enclosed by the parentheses on the right-hand side of (6.5.2) is equal to the divergence of the velocity; because the fluid has been assumed incompressible, this term is equal to zero. The first term on the right-hand side of (6.5.2) is the Laplacian of the i th component of the velocity,

$$\frac{\partial^2 u_i}{\partial x_j \partial x_j} = \frac{\partial^2 u_i}{\partial x^2} + \frac{\partial^2 u_i}{\partial y^2} + \frac{\partial^2 u_i}{\partial z^2} \equiv \nabla^2 u_i. \tag{6.5.3}$$

Using these results to simplify expression (6.5.1), we find that the hydrodynamic volume force is given by

$$\Sigma \equiv \nabla \cdot \sigma = -\nabla p + \mu \nabla^2 \mathbf{u}. \tag{6.5.4}$$

Correspondingly, the equation of motion (6.3.10) reduces to the Navier-Stokes equation

$$\rho \frac{D \mathbf{u}}{Dt} = -\nabla p + \mu \nabla^2 \mathbf{u} + \rho \mathbf{g}, \tag{6.5.5}$$

which is distinguished from Euler's equation (6.4.2) by the presence of the viscous force represented by the product of the viscosity and the Laplacian of the velocity on the right-hand side.

The associated Eulerian form is

$$\rho \left(\frac{\partial \mathbf{u}}{\partial t} + \mathbf{u} \cdot \nabla \mathbf{u} \right) = -\nabla p + \mu \nabla^2 \mathbf{u} + \rho \mathbf{g}, \tag{6.5.6}$$

whose three Cartesian components are:

$$\begin{aligned} \rho \left(\frac{\partial u_x}{\partial t} + u_x \frac{\partial u_x}{\partial x} + u_y \frac{\partial u_x}{\partial y} + u_z \frac{\partial u_x}{\partial z} \right) &= -\frac{\partial p}{\partial x} + \mu \left(\frac{\partial^2 u_x}{\partial x^2} + \frac{\partial^2 u_x}{\partial y^2} + \frac{\partial^2 u_x}{\partial z^2} \right) + \rho g_x, \\ \rho \left(\frac{\partial u_y}{\partial t} + u_x \frac{\partial u_y}{\partial x} + u_y \frac{\partial u_y}{\partial y} + u_z \frac{\partial u_y}{\partial z} \right) &= -\frac{\partial p}{\partial y} + \mu \left(\frac{\partial^2 u_y}{\partial x^2} + \frac{\partial^2 u_y}{\partial y^2} + \frac{\partial^2 u_y}{\partial z^2} \right) + \rho g_y, \\ \rho \left(\frac{\partial u_z}{\partial t} + u_x \frac{\partial u_z}{\partial x} + u_y \frac{\partial u_z}{\partial y} + u_z \frac{\partial u_z}{\partial z} \right) &= -\frac{\partial p}{\partial z} + \mu \left(\frac{\partial^2 u_z}{\partial x^2} + \frac{\partial^2 u_z}{\partial y^2} + \frac{\partial^2 u_z}{\partial z^2} \right) + \rho g_z. \end{aligned} \tag{6.5.7}$$

6.5.1 Pressure and viscous forces

The first term on the right-hand side of (6.5.6), equal to the negative of the pressure gradient, represents the pressure force. The second term, equal to the Laplacian of the velocity multiplied by the viscosity, is the viscous force.

Working in index notation under the assumption that the fluid is incompressible and thus the velocity field is solenoidal, $\nabla \cdot \mathbf{u} = 0$, we find that the Laplacian of the velocity is equal to the negative of the curl of the vorticity,

$$\nabla^2 \mathbf{u} = -\nabla \times \boldsymbol{\omega} \tag{6.5.8}$$

(problem 6.5.1). An important consequence of this identity is that, if the flow is irrotational, or if the vorticity is constant, or if the vorticity field is irrotational, then the viscous force vanishes even though the fluid may not be inviscid. In this case, the Navier-Stokes equation reduces to Euler's equation which may be integrated to yield Bernoulli's equation (6.4.9) for irrotational flow, or equation (6.4.26) for steady rotational flow.

A radially expanding or contracting bubble

An example of a viscous flow with non-zero viscous stresses but vanishing viscous forces is provided by the irrotational flow generated by

the radial expansion or contraction of a spherical bubble with time-dependent radius $a(t)$. The velocity may be represented in terms of a three-dimensional point source with time dependent strength $m(t)$ placed at the bubble center. In spherical polar coordinates with the origin at the bubble center, the velocity potential and radial component of the velocity are given, respectively, by

$$\phi(r, t) = -\frac{m(t)}{4\pi} \frac{1}{r}, \quad u_r(r, t) = \frac{\partial\phi}{\partial r} = \frac{m(t)}{4\pi} \frac{1}{r^2}, \quad (6.5.9)$$

where $m(t)$ is the strength of the point source. The no-penetration condition at the surface of the bubble requires $da/dt = u_r(r = a)$, which may be rearranged to give an expression for the strength of the point source in terms of the bubble radius,

$$m(t) = 4\pi a^2(t) \frac{da}{dt}. \quad (6.5.10)$$

Substituting (6.5.10) into equations (6.5.9), we find

$$\phi(r) = -a^2(t) \frac{da}{dt} \frac{1}{r} = -\frac{1}{3} \frac{da^3}{dt} \frac{1}{r}, \quad u_r(r) = \frac{\partial\phi}{\partial r} = \frac{1}{3} \frac{da^3}{dt} \frac{1}{r^2}. \quad (6.5.11)$$

Referring now to Bernoulli's equation (6.4.9) for unsteady irrotational flow, we compute the first and second terms on the left-hand side,

$$\frac{\partial\phi}{\partial t} = -\frac{1}{3} \frac{d^2a^3}{dt^2} \frac{1}{r}, \quad u^2 = u_r^2(r) = \frac{1}{9} \left(\frac{da^3}{dt}\right)^2 \frac{1}{r^4}. \quad (6.5.12)$$

Substituting these expressions into Bernoulli's equation (6.4.9), and solving for the pressure, we find

$$\frac{p(r)}{\rho} = \frac{1}{3} \frac{d^2a^3}{dt^2} \frac{1}{r} - \frac{1}{18} \left(\frac{da^3}{dt}\right)^2 \frac{1}{r^4} + c(t) + \mathbf{g} \cdot \mathbf{x}. \quad (6.5.13)$$

Far from the bubble, the first and second terms on the right-hand side of (6.5.13) vanish, and the pressure is given by the linear and possibly time-dependent distribution $p_\infty(\mathbf{x}, t) = \rho [c(t) + \mathbf{g} \cdot \mathbf{x}]$.

The normal stress σ_{rr} undergoes a jump across the surface of the bubble, as determined by the bubble radius and surface tension γ . Using the simplified version of the interfacial condition (4.3.13) for constant surface tension, we find

$$\sigma_{rr}(r = a) + p_B(t) = \gamma 2 \kappa_m = \gamma \frac{2}{a}, \quad (6.5.14)$$

where $p_B(t)$ is the pressure in the interior of the bubble, and $\kappa_m = 1/a$ is the mean curvature of the interface. Substituting the second of (6.5.11) into the Newtonian constitutive equation $\sigma_{rr} = -p + 2 \mu \partial u_r / \partial r$, and the result into (6.5.14), we find

$$p(r = a) = p_B(t) - 4 \mu \frac{da}{dt} \frac{1}{a} - \gamma \frac{2}{a}. \quad (6.5.15)$$

Finally, we apply (6.5.13) at the surface of the bubble, evaluate the pressure from (6.5.15), neglect hydrostatic variations over the diameter of the bubble, and rearrange the resulting expression to obtain the generalized Rayleigh equation

$$\rho a \frac{d^2 a}{dt^2} + \frac{3}{2} \rho \left(\frac{da}{dt} \right)^2 + 4 \mu \frac{da}{dt} \frac{1}{a} + \gamma \frac{2}{a} = p_B(t) - p_\infty(\mathbf{x}_B, t), \quad (6.5.16)$$

where \mathbf{x}_B is the location of the bubble center.

Equation (6.5.16) is a second-order nonlinear ordinary differential equation governing the evolution of the bubble radius. To compute the solution, we require the initial bubble radius, the initial rate of expansion da/dt , and also the bubble pressure and pressure at infinity. The bubble pressure may be further related to the bubble volume by means of an appropriate equation of state provided by thermodynamics.

6.5.2 Boundary conditions

The Navier-Stokes equation is a second-order differential equation for the velocity with respect to the spatial coordinates. To compute a solution, we require one scalar boundary condition for each component of the velocity or traction over each boundary:

- Over an impermeable solid surface, we require the no-penetration and no-slip boundary conditions.
- Over a free surface, we require that the normal component of the traction be equal to the ambient pressure increased or decreased by an amount that is equal to the product of the surface tension and twice the local mean curvature, and the tangential component vanish.

- Over a fluid interface, we require kinematic and dynamic continuity or jump conditions. The kinematic condition requires that all components of the velocity be continuous across an interface. The dynamic condition requires that the normal component of the traction undergo a discontinuity by an amount that is equal to the product of the surface tension and twice the local mean curvature, and the tangential component of the traction undergo a discontinuity that is determined by the Marangoni tractions due to variations in surface tension.

6.5.3 Cylindrical polar coordinates

The cylindrical polar components of the hydrodynamic volume force for a Newtonian fluid arise by substituting the constitutive relations (4.7.7) into expressions (6.3.16). After a fair amount of algebra, we find

$$\begin{aligned}\Sigma_x &= -\frac{\partial p}{\partial x} + \mu \left[\frac{\partial^2 u_x}{\partial x^2} + \frac{1}{\sigma} \frac{\partial}{\partial \sigma} \left(\sigma \frac{\partial u_x}{\partial \sigma} \right) + \frac{1}{\sigma^2} \frac{\partial^2 u_x}{\partial \varphi^2} \right], \\ \Sigma_\sigma &= -\frac{\partial p}{\partial \sigma} + \mu \left[\frac{\partial^2 u_\sigma}{\partial x^2} + \frac{\partial}{\partial \sigma} \left(\frac{1}{\sigma} \frac{\partial (\sigma u_\sigma)}{\partial \sigma} \right) + \frac{1}{\sigma^2} \frac{\partial^2 u_\sigma}{\partial \varphi^2} - \frac{2}{\sigma^2} \frac{\partial u_\varphi}{\partial \varphi} \right], \\ \Sigma_\varphi &= -\frac{1}{\sigma} \frac{\partial p}{\partial \varphi} + \mu \left[\frac{\partial^2 u_\varphi}{\partial x^2} + \frac{\partial}{\partial \sigma} \left(\frac{1}{\sigma} \frac{\partial (\sigma u_\varphi)}{\partial \sigma} \right) + \frac{1}{\sigma^2} \frac{\partial^2 u_\varphi}{\partial \varphi^2} + \frac{2}{\sigma^2} \frac{\partial u_\sigma}{\partial \varphi} \right].\end{aligned}\tag{6.5.17}$$

The cylindrical polar components of the Navier-Stokes equation arise by substituting these expressions into the right-hand sides of (6.3.17) or (6.3.18).

6.5.4 Spherical polar coordinates

The spherical polar components of the hydrodynamic volume force arise by substituting the constitutive relations (4.7.14) into expressions (6.3.20). After a fair amount of algebra, we find

$$\begin{aligned}\Sigma_r &= -\frac{\partial p}{\partial r} + \mu \left(\nabla^2 u_r - \frac{2}{r^2} u_r - \frac{2}{r^2} \frac{\partial u_\theta}{\partial \theta} - \frac{2}{r^2} u_\theta \cot \theta - \frac{2}{r^2 \sin \theta} \frac{\partial u_\varphi}{\partial \varphi} \right), \\ \Sigma_\theta &= -\frac{1}{r} \frac{\partial p}{\partial \theta} + \mu \left(\nabla^2 u_\theta + \frac{2}{r^2} \frac{\partial u_r}{\partial \theta} - \frac{u_\theta}{r^2 \sin^2 \theta} - \frac{2 \cos \theta}{r^2 \sin^2 \theta} \frac{\partial u_\varphi}{\partial \varphi} \right), \\ \Sigma_\varphi &= -\frac{1}{r \sin \theta} \frac{\partial p}{\partial \varphi} + \mu \left(\nabla^2 u_\varphi - \frac{u_\varphi}{r^2 \sin^2 \theta} + \frac{2}{r^2 \sin \theta} \frac{\partial u_r}{\partial \varphi} + \frac{2 \cos \theta}{r^2 \sin^2 \theta} \frac{\partial u_\theta}{\partial \varphi} \right).\end{aligned}\tag{6.5.18}$$

The Laplacian operator ∇^2 in spherical polar coordinates was defined in equation (3.2.17). The spherical polar components of the Navier-Stokes equation arise by substituting these expressions into the right-hand sides of (6.3.21).

6.5.5 Plane polar coordinates

The plane polar components of the hydrodynamic volume force arise by substituting the constitutive relations (4.7.20) into expressions (6.3.23). The result is

$$\begin{aligned}\Sigma_r &= -\frac{\partial p}{\partial r} + \mu \left[\frac{\partial}{\partial r} \left(\frac{1}{r} \frac{\partial(r u_r)}{\partial r} \right) + \frac{1}{r^2} \frac{\partial^2 u_r}{\partial \theta^2} - \frac{2}{r^2} \frac{\partial u_\theta}{\partial \varphi} \right], \\ \Sigma_\theta &= -\frac{1}{r} \frac{\partial p}{\partial \theta} + \mu \left[\frac{\partial}{\partial r} \left(\frac{1}{r} \frac{\partial(r u_\theta)}{\partial r} \right) + \frac{1}{r^2} \frac{\partial^2 u_\theta}{\partial \theta^2} + \frac{2}{r^2} \frac{\partial u_r}{\partial \theta} \right].\end{aligned}\tag{6.5.19}$$

The plane polar components of the Navier-Stokes equation arise by substituting these expressions into the right-hand sides of (6.3.25).

Problems

Problem 6.5.1 Viscous force.

Prove identity (6.5.8). *Hint:* Set the vorticity equal to the curl of the velocity; express the curl of the vorticity in index notation; and then use identity (2.3.9).

Problem 6.5.2 *Steady flow.*

Consider a flow at steady state. Explain why it is not generally permissible to specify an arbitrary solenoidal velocity field that satisfies the boundary conditions, and then compute the pressure by solving the Navier-Stokes equation (6.5.6). *Hint:* Consider the conditions subject to which the equation $\nabla p = \mathbf{F}$, where \mathbf{F} is a vector function, has a solution, and note that the curl of the gradient of a function vanishes, as shown in equation (6.6.10).

Problem 6.5.3 *Expansion of a bubble.*

Show that, when the right-hand side of (6.5.16) vanishes and viscous stresses and surface tension are insignificant, an exact solution to equation (6.5.16) is given by

$$\frac{a(t)}{a(t=0)} = \left[1 + \frac{5}{2} \frac{t}{a(t=0)} \left(\frac{da}{dt} \right)_{t=0} \right]^{2/5}. \quad (6.5.20)$$

6.6 Vorticity transport

In Section 6.3, we interpreted the equation of motion as an evolution equation determining the rate of change of the velocity of a point particle, or the rate of change of the fluid velocity at a fixed point in the flow. Descendant evolution equations governing the rate of change of the spatial derivatives of the velocity comprising the velocity gradient tensor and its symmetric and skew-symmetric components may be derived by straightforward differentiation.

Of particular interest is the evolution of the skew-symmetric part of the velocity gradient tensor related to the vorticity as shown in equation (2.3.13). The availability of an evolution equation for the vorticity allows us to study the rate of change of the angular velocity of a small fluid parcel as it translates and deforms while it is convected in a flow.

6.6.1 Two-dimensional flow

To begin, we consider the evolution of the strength of the vorticity ω_z in a two-dimensional flow, defined in terms of the velocity in equation (2.3.15). To derive an evolution equation for ω_z , we divide both sides of the equation of motion (6.3.12) by the density to remove it from

the left-hand side, and then take the y derivative of the x component of the resulting equation and subtract it from the x derivative of the corresponding y component. The result is

$$\begin{aligned} & \frac{\partial \omega_z}{\partial t} + \frac{\partial}{\partial x} (u_x \frac{\partial u_y}{\partial x} + u_y \frac{\partial u_y}{\partial y}) - \frac{\partial}{\partial y} (u_x \frac{\partial u_x}{\partial x} + u_y \frac{\partial u_x}{\partial y}) \\ &= \frac{\partial}{\partial x} \left(\frac{1}{\rho} \Sigma_y \right) - \frac{\partial}{\partial y} \left(\frac{1}{\rho} \Sigma_x \right). \end{aligned} \quad (6.6.1)$$

Expanding out the derivatives on the left-hand side, and using the continuity equation $\partial u_x / \partial x + \partial u_y / \partial y = 0$, we obtain the remarkably simpler form

$$\frac{D\omega_z}{Dt} \equiv \frac{\partial \omega_z}{\partial t} + u_x \frac{\partial \omega_z}{\partial x} + u_y \frac{\partial \omega_z}{\partial y} = \frac{\partial}{\partial x} \left(\frac{1}{\rho} \Sigma_y \right) - \frac{\partial}{\partial y} \left(\frac{1}{\rho} \Sigma_x \right). \quad (6.6.2)$$

The left-hand side of (6.6.2) expresses the material derivative of the vorticity which, according to equation (2.3.7), is equal to twice the rate of change of the angular velocity of a small fluid parcel.

Next, we expand out the derivatives on the right-hand side of (6.6.2), and express the hydrodynamic volume force in terms of the stresses using the two-dimensional counterparts of equations (6.3.4), and thus obtain the general form of the vorticity transport equation for an incompressible fluid,

$$\frac{D\omega_z}{Dt} = \frac{1}{\rho^2} \left(-\Sigma_y \frac{\partial \rho}{\partial x} + \Sigma_x \frac{\partial \rho}{\partial y} \right) + \frac{1}{\rho} \left[\frac{\partial^2 \sigma_{xy}}{\partial x^2} - \frac{\partial^2 \sigma_{xy}}{\partial y^2} + \frac{\partial^2 (\sigma_{yy} - \sigma_{xx})}{\partial x \partial y} \right]. \quad (6.6.3)$$

Baroclinic production of vorticity

The term enclosed by the first set of parentheses on the right-hand side of (6.6.3) expresses generation of vorticity due to density inhomogeneities, known as *baroclinic* production of vorticity. To illustrate the physical mechanism that is responsible for this term, we consider a vertical column of fluid whose density increases upward in the direction of the y axis, as depicted in figure 6.6.1; thus, $\partial \rho / \partial y > 0$. The x component of the hydrodynamic volume force Σ_x causes the column to accelerate in the positive direction of the x axis; because the density and hence the inertia of the fluid increases with height, the top will accelerate less than the bottom. As a result, the column will buckle backwards exhibiting counterclockwise rotation expressed by the second terms within the first set of parentheses on the right-hand side of (6.6.3).

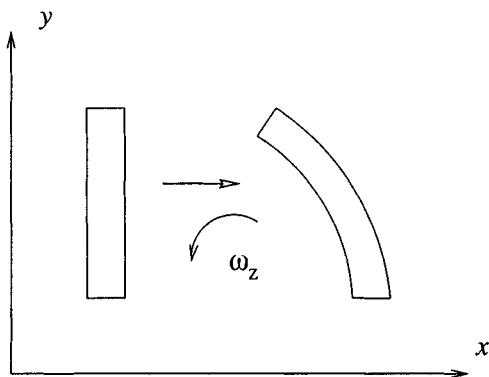


Figure 6.6.1 Vorticity is generated when a column of fluid that is heavier at the top buckles in acceleration under the influence of a volume force.

Inviscid fluids

If viscous forces are insignificant, the shear stresses vanish, the normal stresses are equal to the negative of the pressure, and the hydrodynamic volume force is equal to the negative of the pressure gradient. Consequently, the term enclosed by the square brackets on the right-hand side of (6.6.3) makes no contribution, and the term expressing baroclinic production obtains a simple form, yielding the vorticity transport equation

$$\rho^2 \frac{D\omega_z}{Dt} = \frac{\partial p}{\partial y} \frac{\partial \rho}{\partial x} - \frac{\partial p}{\partial x} \frac{\partial \rho}{\partial y} = (\nabla \rho \times \nabla p) \cdot \mathbf{e}_z, \quad (6.6.4)$$

where \mathbf{e}_z is the unit vector along the z axis which is perpendicular to the xy plane of the flow.

For a fluid with uniform density, equation (6.6.4) predicts

$$\frac{D\omega_z}{Dt} = 0, \quad (6.6.5)$$

showing that a small fluid parcel rotates at a constant angular velocity as it is convected by the flow. The physical origin of this remarkably simple result can be traced back to conservation of angular momentum in the absence of shear stresses imparting a torque.

Incompressible Newtonian fluids

Considering next the evolution of the vorticity in an incompressible Newtonian fluid with uniform density and viscosity, we substitute the constitutive equation for the stress tensor shown in equations (4.5.4) into the right-hand side of (6.6.3), and simplify the resulting expression by use of the continuity equation to derive the vorticity transport equation

$$\begin{aligned} \frac{D\omega_z}{Dt} &= \frac{\partial\omega_z}{\partial t} + u_x \frac{\partial\omega_z}{\partial x} + u_y \frac{\partial\omega_z}{\partial y} \\ &= \nu \left(\frac{\partial^2\omega_z}{\partial x^2} + \frac{\partial^2\omega_z}{\partial y^2} \right) \equiv \nu \nabla^2\omega_z, \end{aligned} \quad (6.6.6)$$

where $\nu \equiv \mu/\rho$ is a physical constant called the *kinematic viscosity*.

The following table displays the kinematic viscosities of water and air at three temperatures. Note that the kinematic viscosity of air is higher than that of water by two or three orders of magnitude. In contrast, the viscosity of water is higher than that of air by one or two orders of magnitude.

The right-hand side of (6.6.6) expresses diffusion of vorticity in the xy plane. Like temperature or concentration of a species, vorticity spreads out from regions of highly rotational flow, that is, regions where small spherical parcels exhibit intense rotation, to regions of weakly rotational or irrotational flow. The actual mechanism by which this occurs will be exemplified in subsequent chapters with reference to unsteady and boundary-layer flows.

Kinematic viscosity, ν

<i>Temperature</i> °C	<i>Water</i> $10^{-2} \text{cm}^2 \text{sec}$	<i>Air</i> $10^{-2} \text{cm}^2 \text{sec}$
20	1.004	15.05
40	0.658	18.86
80	0.365	20.88

6.6.2 Axisymmetric flow

Next, we consider an axisymmetric flow without swirling motion, and refer to the cylindrical polar coordinates (x, σ, φ) depicted in figure 6.6.2.

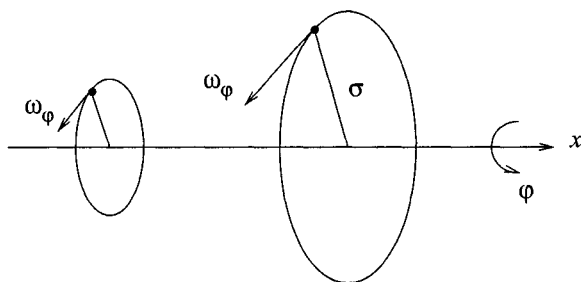


Figure 6.6.2 The vorticity of a point particle in axisymmetric flow increases as the particle moves farther away from the axis of symmetry, due to vortex stretching.

Working as previously for two-dimensional flow, we derive the counterpart of the vorticity transport equation (6.6.6) for an incompressible Newtonian fluid with uniform density and viscosity,

$$\frac{D}{Dt} \left(\frac{\omega_\varphi}{\sigma} \right) = \nu \frac{1}{\sigma^2} E^2 (\sigma \omega_\varphi). \quad (6.6.7)$$

The second-order linear differential operator E^2 on the right-hand side of (6.6.7), defined in equations (2.9.12) and (2.9.15), is the counterpart of the Laplacian operator for two-dimensional flow shown in (6.6.6).

Vortex stretching

If viscous forces are negligible, the right-hand side of (6.6.7) vanishes, and the resulting vorticity transport equation for inviscid flow takes the form

$$\frac{D}{Dt} \left(\frac{\omega_\varphi}{\sigma} \right) = 0. \quad (6.6.8)$$

This equation requires that the strength of the vorticity of a point particle, ω_φ , be proportional to the distance of the point particle from the axis of symmetry, σ , so that the ratio between them remains constant in time and equal to the initial value, as illustrated schematically in figure 6.6.2. This fundamental evolution law expresses a physical process known as vortex stretching. The significance of vortex stretching will be discussed in Chapter 11 in the framework of vortex flows.

6.6.3 Three-dimensional flow

Generalizing the preceding discussion, we set out to derive an evolution equation for the vorticity vector of a three-dimensional flow. For simplicity, we restrict our attention to incompressible Newtonian fluids and assume that the density and viscosity are uniform throughout the domain of flow. Our point of departure is the Navier-Stokes equation (6.4.2).

Using the expression for the point particle acceleration shown on the left-hand side of equation (6.3.26), we find the following alternative form of the Navier-Stokes equation in terms of the vortex force,

$$\rho \left(\frac{\partial \mathbf{u}}{\partial t} + \frac{1}{2} \nabla u^2 + \boldsymbol{\omega} \times \mathbf{u} \right) = -\nabla p + \mu \nabla^2 \mathbf{u} + \mathbf{g}, \quad (6.6.9)$$

where $u^2 \equiv u_x^2 + u_y^2 + u_z^2$ is the square of the magnitude of the velocity.

To derive an evolution equation for the vorticity, we take the curl of both sides of equation (6.6.9). A vector identity states that the curl of the gradient of a smooth scalar function of position f vanishes,

$$\nabla \times \nabla f = \mathbf{0}. \quad (6.6.10)$$

The proof follows readily working in index notation: the i th component of the left-hand side of (6.6.10) is given by

$$\epsilon_{ijk} \frac{\partial}{\partial x_j} \left(\frac{\partial f}{\partial x_k} \right) = \epsilon_{ijk} \frac{\partial^2 f}{\partial x_j \partial x_k} = -\epsilon_{ikj} \frac{\partial^2 f}{\partial x_k \partial x_j}. \quad (6.6.11)$$

The symmetry of the second derivative on the right-hand side of (6.6.11), combined with the inherent antisymmetry of the alternating tensor, requires that the right-hand side vanish.

Using identity (6.6.10), we find that the curl of the second term on the left-hand side of (6.6.9) and the curl of the first term on the right-hand side of (6.6.9) both vanish. Invoking the definition $\boldsymbol{\omega} = \nabla \times \mathbf{u}$, we obtain the vorticity transport equation for three-dimensional flow,

$$\frac{\partial \boldsymbol{\omega}}{\partial t} + \nabla \times (\boldsymbol{\omega} \times \mathbf{u}) = \nu \nabla^2 \boldsymbol{\omega}, \quad (6.6.12)$$

where $\nu \equiv \mu/\rho$ is the kinematic viscosity.

The second term on the left-hand side of (6.6.12) can be manipulated to acquire a physical interpretation. In index notation, the i th component of the vector expressed by this term is given by

$$\epsilon_{ijk} \frac{\partial}{\partial x_j} (\epsilon_{klm} \omega_l u_m) = \epsilon_{ijk} \epsilon_{klm} \frac{\partial(\omega_l u_m)}{\partial x_j} = \epsilon_{ijk} \epsilon_{lmk} \frac{\partial(\omega_l u_m)}{\partial x_j}. \quad (6.6.13)$$

Using property (2.3.9), we recast the right-hand side of (6.6.13) into the form

$$\begin{aligned} (\delta_{il} \delta_{jm} - \delta_{im} \delta_{jl}) \frac{\partial(\omega_l u_m)}{\partial x_j} &= \frac{\partial(\omega_i u_j)}{\partial x_j} - \frac{\partial(\omega_j u_i)}{\partial x_j} \\ &= u_j \frac{\partial \omega_i}{\partial x_j} + \omega_i \frac{\partial u_j}{\partial x_j} - u_i \frac{\partial \omega_j}{\partial x_j} - \omega_j \frac{\partial u_i}{\partial x_j}. \end{aligned} \quad (6.6.14)$$

An identity states that the divergence of the curl of a vector field vanishes; a consequence of this identity is that the vorticity field is solenoidal (problem 2.3.4). Because the fluid has been assumed incompressible, the velocity field is also solenoidal. Consequently, the second and third terms on the right-hand side of (6.6.14) vanish. Substituting the result back into equation (6.6.12), we find the desired vorticity transport equation

$$\frac{D\omega_i}{Dt} = \frac{\partial \omega_i}{\partial t} + u_j \frac{\partial \omega_i}{\partial x_j} = \omega_j \frac{\partial u_i}{\partial x_j} + \nu \nabla^2 \omega_i, \quad (6.6.15)$$

or in vector notation,

$$\frac{D\boldsymbol{\omega}}{Dt} = \frac{\partial \boldsymbol{\omega}}{\partial t} + \mathbf{u} \cdot \nabla \boldsymbol{\omega} = \boldsymbol{\omega} \cdot \nabla \mathbf{u} + \nu \nabla^2 \boldsymbol{\omega}. \quad (6.6.16)$$

The left-hand side of (6.6.15) or (6.6.16) is the material derivative of the vorticity, that is, the rate of change of the vorticity following the motion of point particles.

Vorticity rotation and stretching

To understand the nature of the first term on the right-hand side of (6.6.16), we consider a small material vector $d\mathbf{l}$, and label the first point as A , and the last point as B . Using a Taylor series expansion, we find that the difference in the velocity across the end-points is given by $\mathbf{u}^B - \mathbf{u}^A = d\mathbf{l} \cdot \nabla \mathbf{u}$. Comparing this expression with the first term on the right-hand side of (6.6.16), we find that the vorticity vector behaves like a material vector convected by the fluid: it rotates and stretches or compresses under the influence of the local flow.

In the case of two-dimensional flow, because the vorticity vector is normal to the plane of the flow, neither rotation nor stretching or compression can take place. In the case of axisymmetric flow, because the vorticity vector points in the meridional direction, rotation is prohibited, but stretching or compression can take place, as discussed in Section 6.6.2.

Persistence of irrotational motion in inviscid flow

One important consequence of (6.6.16) for inviscid fluids is that, if the vorticity of a point particle vanishes at the initial instant, it will vanish at all times. Thus, volumes of rotational fluid remain rotational, volumes of irrotational fluid remain irrotational, and the interface between them remains sharp and well-defined at all times.

Source of vorticity in viscous flow

In practice, a fluid flow is established from the state of rest; consequently, the initial vorticity distribution is equal to zero. Since the right-hand side of the vorticity transport equation (6.6.16) vanishes throughout the fluid, the initial rate of production of vorticity is equal to zero, and this seemingly suggests that the flow will remain irrotational at all times, which is known not to be true. The paradox is resolved by observing that vorticity, like heat, enters the fluid by diffusion across the boundaries. The precise mechanism by which this occurs will be discussed in Chapter 7.

Problems

Problem 6.6.1 *Reduction to two-dimensional flow.*

Show that the vorticity transport equation (6.6.16) reproduces the transport equation (6.6.6) for the strength of the vorticity ω_z of a two-dimensional flow.

Problem 6.6.2 *Convection of vorticity.*

Prove the identity

$$\omega_j \frac{\partial u_i}{\partial x_j} = \omega_j \frac{\partial u_j}{\partial x_i}, \quad (6.6.17)$$

which allows us to express the first term on the left-hand side of (6.6.16) in the alternative form $(\nabla \mathbf{u}) \cdot \boldsymbol{\omega}$. *Hint:* Begin with the identity $\boldsymbol{\omega} \times \boldsymbol{\omega} = \boldsymbol{\omega} \times \nabla \times \mathbf{u} = \mathbf{0}$, and then work in index notation using identity (2.3.9).

6.7 Dynamic similitude, the Reynolds number, and dimensionless numbers in fluid dynamics

Consider streaming flow along the x axis with velocity U_1 past a stationary body with designated size L_1 as illustrated in figure 6.7.1(a), and another streaming flow along the x axis with velocity U_2 past a second body that arises by shrinking or expanding the first body by a certain factor, as illustrated in figure 6.7.1(b). If the surface of the first body is described by the equation

$$f(x, y, z) = 0, \quad (6.7.1)$$

then, the surface of the second body is described by the equation

$$f\left(\frac{x}{\alpha}, \frac{y}{\alpha}, \frac{z}{\alpha}\right) = 0, \quad (6.7.2)$$

where

$$\alpha \equiv \frac{L_2}{L_1} \quad (6.7.3)$$

is a scaling factor.

For example, if the first body is a sphere with diameter L_1 centered at the the point (x_c, y_c, z_c) , then

$$f(x, y, z) = (x - x_c)^2 + (y - y_c)^2 + (z - z_c)^2 - \frac{L_1^2}{4}, \quad (6.7.4)$$

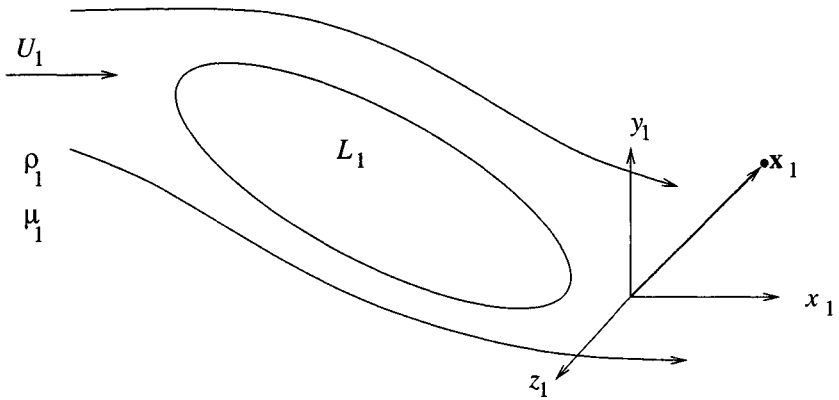
and

$$\begin{aligned} f\left(\frac{x}{\alpha}, \frac{y}{\alpha}, \frac{z}{\alpha}\right) &= \left(\frac{x}{\alpha} - x_c\right)^2 + \left(\frac{y}{\alpha} - y_c\right)^2 + \left(\frac{z}{\alpha} - z_c\right)^2 - \frac{L_1^2}{4} \\ &= \frac{1}{\alpha^2} [(x - \alpha x_c)^2 + (y - \alpha y_c)^2 + (z - \alpha z_c)^2 - \frac{L_2^2}{4}]. \end{aligned} \quad (6.7.5)$$

Setting the right-hand side of (6.7.5) equal to zero, we obtain the equation of a sphere with diameter L_2 centered at the point $(\alpha x_c, \alpha y_c, \alpha z_0)$.

Both fluids are assumed to be incompressible and Newtonian. Let ρ_1 and μ_1 be the density and viscosity of the first fluid, and ρ_2 and μ_2 be the density and viscosity of the second fluid.

(a)



(b)

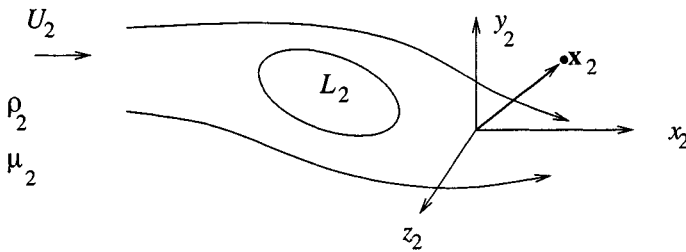


Figure 6.7.1 Flows in two similar domains. If the Reynolds numbers are equal, as shown in equation (6.7.6), the velocity and pressure field of the second flow may be deduced from those of the first flow by rescaling, and vice versa.

6.7.1 Similitude and the Reynolds number

We will show that, when the values of the four control and physical parameters characterizing the first flow, L_1, U_1, ρ_1 , and μ_1 , and the corresponding values of the control and physical parameters characterizing the second flow, L_2, U_2, ρ_2 , and μ_2 , are related by the equations

$$\frac{\rho_1 U_1 L_1}{\mu_1} = \frac{\rho_2 U_2 L_2}{\mu_2}, \quad (6.7.6)$$

then the structure of the second flow may be inferred from the structure of the first flow, and vice versa, by carrying out a simple computation described as *rescaling*, as will be explained in the following subsection.

The ratio on the left-hand side of (6.7.6) is defined as the Reynolds number of the first flow, and the the ratio on the right-hand side of (6.7.6) is defined as the Reynolds number of the second flow.

6.7.2 Rescaling

To deduce the structure of the second flow from the structure of the first flow, and vice versa, we introduce the dynamic pressure established due to the flow, defined as the pressure deviation from the hydrostatic distribution,

$$p_1^D \equiv p_1 - \rho_1 \mathbf{g} \cdot \mathbf{x}, \quad p_2^D \equiv p_2 - \rho_2 \mathbf{g} \cdot \mathbf{x}, \quad (6.7.7)$$

where the superscript D stands for “Dynamic” or, more accurately, “Hydrodynamic”. In the absence of an imposed flow, the pressure assumes its hydrostatic distribution, and the dynamic pressure vanishes throughout the fluid.

Consider an arbitrary point in the first flow, denoted by \mathbf{x}_1 , and a corresponding point in the second flow whose coordinates are given by

$$\mathbf{x}_2 = \alpha \mathbf{x}_1. \quad (6.7.8)$$

Equations (6.7.1) and (6.7.2) ensure that, if \mathbf{x}_1 lies at the surface of the body in the first flow, then \mathbf{x}_2 will lie at the surface of the body in the second flow. In Section 6.7.3, we will show that, when relation (6.7.6) is fulfilled, the velocity and dynamic pressure at the second point in the second flow are related to those at the first point in the first flow by the equations

$$\mathbf{u}_2(\mathbf{x}_2) = \delta \mathbf{u}_1(\mathbf{x}_2), \quad p_2^D(\mathbf{x}_2) = \beta \delta^2 p_1^D(\mathbf{x}_2), \quad (6.7.9)$$

where we have defined the ratio of the velocities of the incident flow, δ , the viscosity ratio λ , and the density ratio β ,

$$\delta \equiv \frac{U_2}{U_1}, \quad \lambda \equiv \frac{\mu_2}{\mu_1}, \quad \beta \equiv \frac{\rho_2}{\rho_1}. \quad (6.7.10)$$

The equality of the Reynolds numbers expressed by (6.7.6) requires $\beta \delta \alpha = \lambda$.

Relations (6.7.9) are also valid for unsteady flow, provided that the velocity field of the first flow at the designated origin of time is related to the velocity of the second flow by the first of equations (6.7.9), and the comparison is made at times t_1 and t_2 related by

$$t_2 = \frac{\delta t_1}{\alpha}. \quad (6.7.11)$$

6.7.3 Dimensional analysis

To prove relations (6.7.9), we consider the Navier-Stokes equation (6.5.6) and the continuity equation $\nabla \cdot \mathbf{u} = 0$ governing the structure and dynamics of the two flows with appropriate physical constants corresponding to the two fluids, subject to appropriate far-field and boundary conditions, and work as follows.

First flow

Considering the first flow, we introduce the dimensionless independent variables

$$\hat{x}_1 = \frac{x}{L_1}, \quad \hat{y}_1 = \frac{y}{L_1}, \quad \hat{z}_1 = \frac{z}{L_1}, \quad \hat{t}_1 = \frac{t U_1}{L_1}, \quad (6.7.12)$$

and the dimensionless dependent variables

$$\hat{u}_{x_1} = \frac{u_{x_1}}{U_1}, \quad \hat{u}_{y_1} = \frac{u_{y_1}}{U_1}, \quad \hat{u}_{z_1} = \frac{u_{z_1}}{U_1}, \quad \hat{p}_1^D = \frac{p_1^D}{\rho_1 U_1^2}. \quad (6.7.13)$$

Solving for the dimensional variables in terms of their dimensionless counterparts denoted by the hats, and substituting the result into the Navier-Stokes equation and into the continuity equation, we find

$$\frac{\partial \hat{\mathbf{u}}_1}{\partial \hat{t}_1} + \hat{\mathbf{u}}_1 \cdot \hat{\nabla}_1 \hat{\mathbf{u}}_1 = - \hat{\nabla}_1 \hat{p}_1^D + \frac{1}{Re_1} \hat{\nabla}_1^2 \hat{\mathbf{u}}_1, \quad (6.7.14)$$

and

$$\hat{\nabla}_1 \cdot \hat{\mathbf{u}}_1 = 0, \quad (6.7.15)$$

where $Re_1 \equiv \rho_1 U_1 L_1 / \mu_1$ is the Reynolds number of the first flow shown on the left-hand side of (6.7.6); we have introduced the dimensionless gradient $\hat{\nabla}_1 \equiv (\partial/\partial \hat{x}_1, \partial/\partial \hat{y}_1, \partial/\partial \hat{z}_1)$ and associated Laplacian operator

$$\hat{\nabla}_1^2 \equiv (\partial^2/\partial \hat{x}_1^2, \partial^2/\partial \hat{y}_1^2, \partial^2/\partial \hat{z}_1^2).$$

The far-field condition requires that, far from the body, the dimensionless velocity \hat{u}_{x_1} tends to unity, whereas \hat{u}_{y_1} and \hat{u}_{z_1} tend to vanish. The no-slip and no-penetration boundary conditions require that the velocity vanishes at points (x, y, z) that satisfy equation (6.7.1) or, equivalently, points $(\hat{x}_1, \hat{y}_1, \hat{z}_1)$ that satisfy

$$f(L_1 \hat{x}_1, L_1 \hat{y}_1, L_1 \hat{z}_1) = 0. \tag{6.7.16}$$

Second flow

Considering next the second flow, we introduce the dimensionless independent variables

$$\hat{x}_2 = \frac{x}{L_2}, \quad \hat{y}_2 = \frac{y}{L_2}, \quad \hat{z}_2 = \frac{z}{L_2}, \quad \hat{t}_2 = \frac{t U_2}{L_2}, \tag{6.7.17}$$

and the dimensionless dependent variables

$$\hat{u}_{x_2} = \frac{u_{x_2}}{U_2}, \quad \hat{u}_{y_2} = \frac{u_{y_2}}{U_2}, \quad \hat{u}_{z_2} = \frac{u_{z_2}}{U_2}, \quad \hat{p}_2^D = \frac{p_2^D}{\rho_2 U_2^2}. \tag{6.7.18}$$

Solving for the dimensional variables in terms of their dimensionless counterparts, and substituting the result into the Navier-Stokes equation and into the continuity equation, we find

$$\frac{\partial \hat{\mathbf{u}}_2}{\partial \hat{t}_2} + \hat{\mathbf{u}}_2 \cdot \hat{\nabla}_2 \hat{\mathbf{u}}_2 = - \hat{\nabla}_2 \hat{p}_2^D + \frac{1}{Re_2} \hat{\nabla}_2^2 \hat{\mathbf{u}}_2. \tag{6.7.19}$$

and

$$\hat{\nabla}_2 \cdot \hat{\mathbf{u}}_2 = 0, \tag{6.7.20}$$

where $Re_2 \equiv \rho_2 U_2 L_2 / \mu_2$ is the Reynolds number shown on the right-hand side of (6.7.6); we have introduced the dimensionless gradient $\hat{\nabla}_2 \equiv (\partial/\partial \hat{x}_2, \partial/\partial \hat{y}_2, \partial/\partial \hat{z}_2)$ and associated Laplacian operator

$$\hat{\nabla}_2^2 \equiv (\partial^2/\partial \hat{x}_2^2, \partial^2/\partial \hat{y}_2^2, \partial^2/\partial \hat{z}_2^2).$$

The far-field condition requires that, far from the body, the dimensionless velocity \hat{u}_{x_2} tends to unity, whereas \hat{u}_{y_2} and \hat{u}_{z_2} tend to vanish. The no-slip and no-penetration boundary conditions require that the velocity vanishes at points (x, y, z) that satisfy equation (6.7.2) or, equivalently, points $(\hat{x}_2, \hat{y}_2, \hat{z}_2)$ that satisfy

$$f(L_1 \hat{x}_2, L_1 \hat{y}_2, L_1 \hat{z}_2) = 0. \tag{6.7.21}$$

Comparison

To this end, we compare one by one the equations and boundary conditions governing the two flows in the dimensionless variables indicated by a hat, and deduce the following:

1. The Navier-Stokes equation (6.7.14) is identical to the Navier-Stokes equation (6.7.19) provided that the two Reynolds numbers are equal, as stated in (6.7.6).
2. The continuity equation (6.7.15) is identical to the continuity equation (6.7.20).
3. The far-field conditions are identical; both dimensionless velocities tend to $(1, 0, 0)$.
4. The boundary conditions on the first body described by (6.7.16) are identical to the boundary conditions on the second body described by (6.7.21).

These results suggest that, when the Reynolds numbers are equal, the values of the dimensionless dependent variables in the two flows at corresponding dimensionless times and corresponding dimensionless positions are equal. Setting, for example, $\hat{p}_1^D(\hat{\mathbf{x}}_1) = \hat{p}_2^D(\hat{\mathbf{x}}_2)$, and using the definitions (6.7.13) and (6.7.18), we find the second of relations (6.7.9) subject to (6.7.10).

6.7.4 Structure of a flow as a function of the Reynolds number

Generalizing the preceding discussion, we consider a flow in a domain with characteristic length scale L , identify an appropriate characteristic velocity U , and compute the Reynolds number

$$Re \equiv \frac{\rho L U}{\mu} = \frac{L U}{\nu}, \quad (6.7.22)$$

where $\nu \equiv \mu/\rho$ is the kinematic viscosity. We then introduce the dimensionless independent variables

$$\hat{x} = \frac{x}{L}, \quad \hat{y} = \frac{y}{L}, \quad \hat{z} = \frac{z}{L}, \quad \hat{t} = \frac{t U}{L}, \quad (6.7.23)$$

and the dimensionless dependent variables

$$\hat{u}_x = \frac{u_x}{U}, \quad \hat{u}_y = \frac{u_y}{U}, \quad \hat{u}_z = \frac{u_z}{U}, \quad \hat{p}^D = \frac{p^D}{\rho U^2}. \quad (6.7.24)$$

Solving for the dimensional variables in terms of their dimensionless counterparts, and substituting the result into the Navier-Stokes equation and into the continuity equation, we find

$$\frac{\partial \hat{\mathbf{u}}}{\partial \hat{t}} + \hat{\mathbf{u}} \cdot \hat{\nabla} \hat{\mathbf{u}} = -\hat{\nabla} \hat{p}^D + \frac{1}{Re} \hat{\nabla}^2 \hat{\mathbf{u}}, \quad (6.7.25)$$

and

$$\hat{\nabla} \cdot \hat{\mathbf{u}} = 0. \quad (6.7.26)$$

Our earlier analysis suggests that the structure of the flow depends on L , U , ρ and μ collectively through the dimensionless Reynolds number, in the sense of dynamic similitude expressed by equations (6.7.9) and (6.7.10).

Characteristic scales

The choice of characteristic velocity and length scale may be obvious in some cases but subtle in others. If all terms in the dimensionless Navier-Stokes equation (6.7.25) are of order unity, then the Reynolds number clearly expresses the relative importance of inertial forces, assumed to scale with $\rho U^2/L$, and viscous forces, assumed to scale with $\mu U/L^2$, so that their ratio is the Reynolds number defined in (6.7.22). If an alternative scaling for these forces is available on physical ground, then they should be used in place of a generic scaling that lacks physical insight.

Stokes flow

Inspecting the dimensionless Navier-Stokes equation (6.7.25), we note that, when the Reynolds number is small, viscous forces dominate and the left-hand side makes a negligible contribution. The dimensionless pressure gradient also appears to make a negligible contribution in this limit, but this is only a mathematical illusion: the dimensionless pressure arose from the arbitrary scaling shown in the last of equations (6.7.24), which may be contrasted with the physical scaling of the position vector and velocity in terms of the unambiguous length and velocity scales

L and U . As a consequence, the dimensionless pressure gradient may become singular as the Reynolds number tends to vanish, suggesting that an alternative scaling is required. To prevent this occurrence, we retain the dimensionless pressure gradient in the dimensionless form of the Navier-Stokes equation.

Reverting to dimensional variables, we find that the Navier-Stokes equation reduces to the Stokes equation

$$\mathbf{0} = -\nabla p + \mu \nabla^2 \mathbf{u} + \rho \mathbf{g}, \quad (6.7.27)$$

describing steady or unsteady creeping flows with negligible inertial forces. The analysis and computation of these flows will be the exclusive topic of our discussion in Chapter 9.

Flows at high Reynolds numbers

Inspecting (6.7.25), we find that when the Reynolds number is large, viscous forces are negligible and may be neglected throughout the domain of flow. This, however, is permissible only when the velocity does not change rapidly over small distances across fluid layers that are thin compared to the global size of the boundaries, otherwise the preceding scaling with respect to U and L may not be valid. Such thin layers typically occur along flow boundaries or interfaces between two adjacent streams of the same or different fluids. In Chapter 10, we shall demonstrate that viscous forces may be substantial or even dominant within these layers, even though the bulk of the flow may occur at high Reynolds numbers.

Laminar and turbulent flows

When the Reynolds number exceeds a certain threshold, an unsteady small-scale motion characterized by rapid fluctuations in the velocity and vorticity field is spontaneously established. This turbulent motion is superposed on a steady or unsteady slower-evolving macroscopic or large-scale flow. Flows below the critical Reynolds number are called laminar to indicate that the streamlines are smooth, and flows above this critical Reynolds number are called turbulent to indicate that the instantaneous streamlines are highly convoluted.

The transition from laminar to turbulent motion may occur by several mechanisms including the amplification of internal waves. The critical Reynolds number where transition occurs may be estimated theoretically

by carrying out a stability analysis, as will be discussed in Chapter 10. The dynamics of turbulent motion may be studied by several methods including statistical analysis, nonlinear dynamical systems theory, and vortex dynamics, as will be discussed in Chapter 10.

6.7.5 Dimensionless numbers in fluid mechanics

We have demonstrated that two geometrically related flows occurring at the same Reynolds numbers are similar, in the sense that one may be deduced from the other by rescaling. Arguments leading us to this conclusion have been made with reference to a flow that is bounded by a solid surface over which the no-slip and no-penetration boundary conditions are required. Moreover, a time-independent velocity was imposed in the far-field boundary condition in lieu of a driving mechanism.

If the driving mechanism is time-dependent, or if the flow is bounded by fluid interfaces and free surfaces, additional conditions for dynamic similitude requiring the equality of further dimensionless numbers are required. These dimensionless numbers enter the problem formulation either through the governing equations or through boundary and interfacial conditions.

Frequency parameter for a time-dependent flow

An externally imposed time-dependent flow with a time scale T is characterized by the dimensionless frequency parameter

$$\beta \equiv \frac{L^2}{T \nu}, \quad (6.7.28)$$

where ν is the kinematic viscosity. In the case of periodic flow with angular frequency ω due, for example, to an oscillating pressure gradient, T may be identified with the period $T = 2\pi/\omega$.

Froude number

The relative importance of inertial and gravitational forces in a flow bounded by a free surface, such as the flow due to the propagation of water waves in the ocean, is determined by the Froude number

$$Fr \equiv \frac{U}{\sqrt{gL}}, \quad (6.7.29)$$

where g is the acceleration of gravity. In the case of flow over a hump discussed in Section 6.4, the Froude number takes the specific form shown in equation (6.4.22).

Bond number

The relative importance of gravitational forces and surface tension in a fluid bounded by a free surface or interface is determined by the Bond number

$$Bo \equiv \frac{\rho g L^2}{\gamma}, \quad (6.7.30)$$

where γ is the surface tension (problem 6.7.3).

Weber number

The relative importance of inertial forces and surface tension in a fluid bounded by a free surface or interface is determined by the Weber number

$$We \equiv \frac{\rho U^2 L}{\gamma}. \quad (6.7.31)$$

For example, the Weber number determines the deformation and nature of the flow around a bubble rising or convected at high speed through an ambient liquid.

Problems

Problem 6.7.1 *Characteristic scales.*

Identify the characteristic velocity scale U , length scale L , and the Reynolds number of (a) simple shear flow past a stationary particle, (b) flow due to the settling of a particle in the atmosphere, and (c) flow due to a breaking wave in the ocean.

Problem 6.7.2 *Reynolds number.*

Compute the Reynolds number of (a) an ant crawling, (b) a person running, (c) a car moving at 100 km per hour, and (d) an elephant running across a plain at maximum speed.

Problem 6.7.3 *Bond number in hydrostatics.*

Explain how the Bond number emerges from the scaling of the Laplace-Young equation (5.4.6) in hydrostatics.

Chapter 7

Channel, tube, and film flows

- 7.1 Steady flow in a two-dimensional channel
- 7.2 Steady film flow down an inclined plane
- 7.3 Steady flow through a circular or annular tube
- 7.4 Steady flow through channels and tubes with various cross-sections
- 7.5 Steady swirling flow
- 7.6 Transient flow in a channel
- 7.7 Oscillatory flow in a channel
- 7.8 Transient and oscillatory flow in a circular tube

Having derived the equations governing the motion of an incompressible Newtonian fluid - by requiring mass conservation and Newton's second law for the motion of fluid parcels - and having established appropriate boundary and interfacial conditions, we proceed to derive analytical and semi-analytical solutions for a common class of steady and unsteady flows characterized by rectilinear or circular streamlines. The engineering significance of these flows, combined with their ability to demonstrate the salient mechanisms by which momentum and vorticity are distributed in a steady flow and transported in an unsteady flow, justify why these flows receive special attention.

7.1 Steady flow in a two-dimensional channel

Consider flow in a two-dimensional channel confined between two parallel walls that are inclined at an angle θ_0 with respect to the horizontal, and are separated by the distance $2h$, as illustrated in figure 7.1.1. In the inclined system of Cartesian coordinates depicted in this figure, where the x axis is parallel to the walls, the components of the gravity vector are given by $g_x = g \sin \theta_0$ and $g_y = -g \cos \theta_0$, where g is

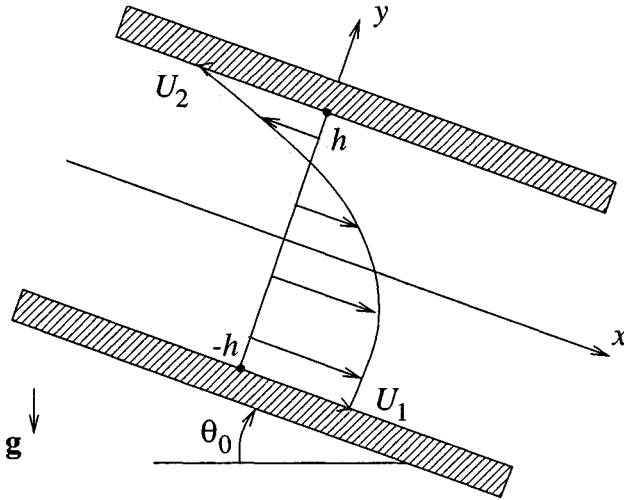


Figure 7.1.1 Steady flow a channel confined between two parallel walls.

the acceleration of gravity. The lower wall translates parallel to itself with constant velocity U_1 , and the upper wall translates parallel to itself with constant velocity U_2 . The motion of the fluid is governed by the Navier-Stokes equation (6.5.5) whose Cartesian components are shown in equations (6.5.7).

7.1.1 Assumption of unidirectional flow

Our analysis will be based on the fundamental assumption of steady unidirectional flow: the y and z velocity components vanish, $u_y = 0$ and $u_z = 0$, and the x component is independent of time, $\partial u_x / \partial t = 0$. This assumption precludes the occurrence of turbulent flow where an unsteady small-scale three-dimensional motion is established. The continuity equation for two-dimensional flow, $\partial u_x / \partial x + \partial u_y / \partial y = 0$, requires $\partial u_x / \partial x = 0$, which states that the flow is fully developed. Thus, the axial velocity u_x is only a function of position across the channel, y .

7.1.2 Velocity profile

Simplifying the x and y components of the equation of motion shown

in (6.5.7) by discarding terms that are identically equal to zero, we find

$$0 = -\frac{\partial p}{\partial x} + \mu \frac{d^2 u_x}{dy^2} + \rho g_x, \quad 0 = -\frac{\partial p}{\partial y} + \rho g_y. \quad (7.1.1)$$

The no-slip boundary condition at the two walls requires

$$u_x = U_1 \text{ at } y = -h, \quad u_x = U_2 \text{ at } y = h. \quad (7.1.2)$$

The second of equations (7.1.1) governs the pressure distribution in hydrostatics. It will be convenient to screen out the hydrostatic variation, by expressing the pressure in the form

$$p = P_0 - \chi x + \rho g_y y, \quad (7.1.3)$$

where P_0 is a constant and χ is the negative of the pressure gradient along the x axis. The first of equations (7.1.1) then takes the form

$$\frac{d^2 u_x}{dy^2} = -\frac{\chi + \rho g_x}{\mu}. \quad (7.1.4)$$

Integrating twice this second-order linear ordinary differential equation with respect to y , we find the parabolic profile

$$u_x(y) = -\frac{\chi + \rho g_x}{2\mu} y^2 + B y + A, \quad (7.1.5)$$

where A and B are two constants to be determined by requiring the no-slip boundary conditions (7.1.2). Solving for these constants, and substituting the results into (7.1.5), we derive the parabolic velocity profile

$$u_x(y) = U_1 + \frac{y+h}{2h} (U_2 - U_1) + \frac{\chi + \rho g_x}{2\mu} (h^2 - y^2). \quad (7.1.6)$$

It is instructive to identify three special cases of the most general flow expressed by (7.1.6):

1. When $\chi + \rho g_x = 0$, the last term on the right-hand side of (7.1.6) disappears, and the flow is driven by boundary motion in the *shear-driven mode*; this is the *plane Couette flow*.
2. When $U_1 = 0$ and $U_2 = 0$, and the channel is horizontal, $g_x = 0$, the flow is driven by an imposed pressure gradient along the x axis equal to the negative of χ , in the *pressure-driven mode*; this is the *Hagen flow*.

3. When $U_1 = 0$ and $U_2 = 0$, and also $\chi = 0$, which means that there is no pressure variation along the x axis, we obtain *gravity-driven flow*.

Subroutine *chan_2d* in directory *04_various/uni_flow* of *FDLIB* evaluates the velocity profile given in (7.1.6).

7.1.3 Shear stress

The shear stress σ_{xy} arises by differentiating the velocity profile (7.1.6) with respect to y , and is given by

$$\sigma_{xy} = \mu \frac{\partial u_x}{\partial y} = \mu \frac{U_2 - U_1}{2h} - (\chi + \rho g_x) y. \quad (7.1.7)$$

In gravity- and pressure-driven flow, the shear stress varies linearly across the channel; in plane Couette flow, the shear stress is constant determined by the velocities of, and distance between the two walls.

7.1.4 Flow rate

The flow rate along the x axis is found by integrating the velocity across the channel, obtaining

$$Q = \int_{-h}^h u_x(y) dy = \frac{1}{2} (U_1 + U_2) h + 2 \frac{\chi + \rho g_x}{3\mu} h^3. \quad (7.1.8)$$

As an example, consider a channel that is closed at two ends, so that the flow rate vanishes, $Q = 0$. Physically, the flow is driven by the translation of two moving belts identified with the lower and upper wall. Equation (7.1.8) shows that a pressure gradient will be established for the right-hand side to vanish.

7.1.5 Two-layer flow

Next, we consider the flow of two superimposed layers with generally different viscosities and densities, as illustrated in figure 7.1.2; the interface is located at $y = y_I$. The lower layer is labelled as fluid 1, and the upper layer is labelled as fluid 2.

Working as in the case of single-fluid flow, we derive the pressure distribution within each layer corresponding to (7.1.3),

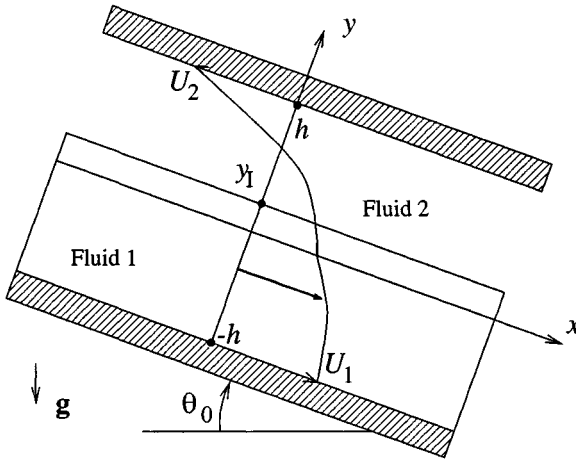


Figure 7.1.2 Steady two-layer flow in a channel confined between two parallel walls.

$$p^{(1)} = P_0 - \chi x + \rho_1 g_y (y - y_I),$$

$$p^{(2)} = P_0 - \chi x + \rho_2 g_y (y - y_I). \quad (7.1.9)$$

Note that the negative of the pressure gradient χ must be the same in the two fluids, otherwise the interfacial condition requiring continuity of normal stress, amounting to continuity of pressure, cannot be satisfied.

The velocity profile across each layer is governed by the counterparts of equation (7.1.4) for each fluid,

$$\frac{d^2 u_x^{(1)}}{dy^2} = -\frac{\chi + \rho_1 g_x}{\mu_1}, \quad \frac{d^2 u_x^{(2)}}{dy^2} = -\frac{\chi + \rho_2 g_x}{\mu_2}. \quad (7.1.10)$$

To facilitate forthcoming algebraic manipulations, we integrate equations (7.1.10) twice with respect to y , and express the solutions in the form

$$u_x^{(1)}(y) = -\frac{\chi + \rho_1 g_x}{2\mu_1} (y - y_I)^2 + \xi_1 (y - y_I) + u_I,$$

$$u_x^{(2)}(y) = -\frac{\chi + \rho_2 g_x}{\mu_2} (y - y_I)^2 + \xi_2 (y - y_I) + u_I, \quad (7.1.11)$$

where u_I is the common velocity of the two fluids at the location of the interface, and ξ_1, ξ_2 are the shear rates or slopes of the velocity on either side of the interface, defined as

$$\xi_1 \equiv \left(\frac{\partial u_x^{(1)}}{\partial y} \right)_{y=y_I}, \quad \xi_2 \equiv \left(\frac{\partial u_x^{(2)}}{\partial y} \right)_{y=y_I}. \quad (7.1.12)$$

To compute the three unknowns ξ_1, ξ_2 , and u_I , we require: (a) the no-slip boundary condition at the lower and upper wall $u_x^{(1)}(y = -h) = U_1$ and $u_x^{(2)}(y = h) = U_2$, and (b) a condition expressing continuity of shear stress across the interface,

$$\mu_1 \xi_1 = \mu_2 \xi_2. \quad (7.1.13)$$

After a fair amount of algebra, we find

$$u_I = \frac{1}{2} \frac{h_1 h_2}{\mu_1 \lambda + \delta} \left[(1 + \delta) \chi + \rho_1 g_x (1 + \beta \delta) \right] + \frac{\delta U_1 + \lambda U_2}{\delta + \lambda}, \quad (7.1.14)$$

and

$$\xi_1 = -\frac{\chi + \rho_1 g_x}{2 \mu_1} h_1 + \frac{u_I - U_1}{h_1}, \quad \xi_2 = \frac{\chi + \rho_2 g_x}{2 \mu_2} h_2 - \frac{u_I - U_2}{h_2}, \quad (7.1.15)$$

where $h_1 = h + y_I$ and $h_2 = h - y_I$ are the lower and upper layer thicknesses satisfying $h_1 + h_2 = 2h$. We have introduced the viscosity, density, and thickness ratio,

$$\lambda \equiv \frac{\mu_2}{\mu_1}, \quad \beta \equiv \frac{\rho_2}{\rho_1}, \quad \delta \equiv \frac{h_2}{h_1}. \quad (7.1.16)$$

Subroutine *chan_2d_2l* in directory *04_various/uni_flow* of *FDLIB* evaluates the interfacial velocity, shear rates, velocity profile across the two layers, and the corresponding flow rates.

7.1.6 Multi-layer flow

Generalizing the flow configuration, we consider the flow of an arbitrary number of N superimposed layers, as illustrated in figure 7.1.3. The bottom layer is labelled as fluid 1, and the top layer is labelled as fluid N . The $N - 1$ interfaces separating the layers are located at $y = y_I^{(i)}$, where $i = 1, 2, \dots, N - 1$.

The velocity profile across the i th layer is governed by the generalized version of equation (7.1.4)

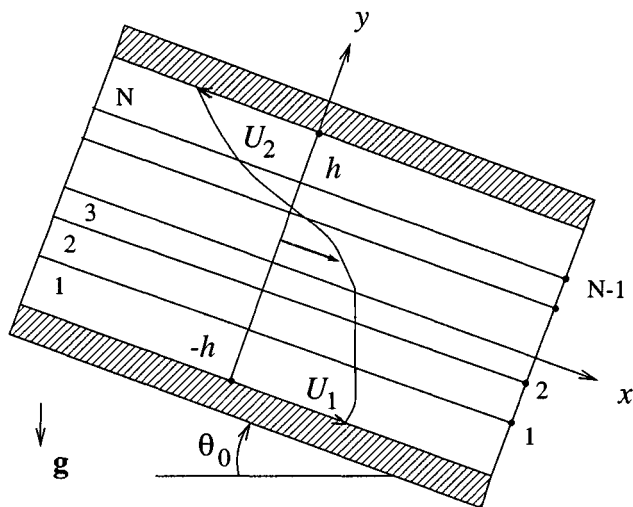


Figure 7.1.3 Steady multi-layer flow in a channel confined between two parallel walls. The numbers on the right are the interface labels.

$$\frac{d^2 u_x^{(i)}}{dy^2} = -\frac{\chi + \rho_i g_x}{\mu_i}, \quad (7.1.17)$$

where $i = 1, 2, \dots, N$. Integrating equation (7.1.17) twice with respect to y , we derive the parabolic profile

$$u_x^{(i)}(y) = -\frac{\chi + \rho_i g_x}{2\mu_i} y^2 + B^{(i)} y + A^{(i)}, \quad (7.1.18)$$

where $A^{(i)}$ and $B^{(i)}$ are unknown constants to be determined by requiring: (a) the no-slip boundary condition at the lower and upper wall, (b) continuity of velocity across the interfaces expressed by

$$u_x^{(i)}(y = y_I^{(i)}) = u_x^{(i+1)}(y = y_I^{(i)}), \quad (7.1.19)$$

for $i = 1, 2, \dots, N - 1$, and (c) continuity of shear stress across the interfaces expressed by

$$\mu_i \left(\frac{\partial u_x^{(i)}}{\partial y} \right)_{y=y_I^{(i)}} = \mu_{i+1} \left(\frac{\partial u_x^{(i+1)}}{\partial y} \right)_{y=y_I^{(i)}}, \quad (7.1.20)$$

for $i = 1, 2, \dots, N - 1$.

Substituting the profile (7.1.18) into (7.1.20), and solving for $B^{(i)}$, we derive a recursion relation for $B^{(i)}$,

$$B^{(i)} = \frac{\chi + \rho_i g_x}{\mu_i} y_I^{(i)} + \frac{\mu_{i+1}}{\mu_i} (B^{(i+1)} - \frac{\chi + \rho_{i+1} g_x}{\mu_{i+1}} y_I^{(i)}), \quad (7.1.21)$$

where $i = 1, 2, \dots, N - 1$.

To this end, we introduce the shear rate at the upper wall,

$$\alpha \equiv \left(\frac{\partial u_x^{(N)}}{\partial y} \right)_{y=h}. \quad (7.1.22)$$

Differentiating the profile (7.1.18) for $i = N$ with respect to y , and evaluating the derivative at $y = h$, we find

$$B^{(N)} = \alpha + \frac{\chi + \rho_N g_x}{\mu_N} h. \quad (7.1.23)$$

If we knew the value of α , we would be able to compute the coefficient $B^{(N)}$ from (7.1.23), and then evaluate the rest of the coefficients $B^{(i)}$ for $i = N - 1, \dots, 2, 1$, using the recursion relation (7.1.21). Once this has been accomplished, we could compute $A^{(1)}$ to satisfy the no-slip boundary condition at the bottom wall using the equation

$$u_x^{(1)}(y = -h) = -\frac{\chi + \rho_1 g_x}{2 \mu_1} h^2 - B^{(1)} h + A^{(1)} = U_1, \quad (7.1.24)$$

and then evaluate the rest of the coefficients $A^{(i)}$ by requiring continuity of velocity across each interface expressed by (7.1.19). In the end, the no-slip boundary condition at the upper wall would also be satisfied. Unfortunately, the value of α is not known *a priori*.

An expedient method of producing the value of α and simultaneously computing the unknown coefficients of the velocity profiles may be devised on the basis of the no-slip boundary condition at the upper wall. We begin by expressing this condition in the form

$$\begin{aligned} f(\alpha) &\equiv u_x^{(N)}(y = h) - U_2 \\ &= -\frac{\chi + \rho_N g_x}{2 \mu_N} h^2 + B^{(N)} h + A^{(N)} - U_2 = 0, \end{aligned} \quad (7.1.25)$$

Clearly, α is a root of the function $f(\alpha)$.

A key observation is that $f(\alpha)$ is a *linear* function of α , and may thus be expressed in the form

$$f(\alpha) = C \alpha + D, \quad (7.1.26)$$

where

$$C = f(1) - f(0), \quad D = f(0). \quad (7.1.27)$$

The linear dependence shown in equation (7.1.26) becomes evident by observing that, if we assign a certain value to α , we can use the procedure described in the paragraph following equation (7.1.23) to evaluate the coefficients of the velocity profiles across each layer, and then compute the left-hand side of (7.1.25) by linear algebraic manipulations.

Combining (7.1.26) and (7.1.27), we find that the required value of α satisfying $f(\alpha) = 0$ is given by

$$\alpha = -\frac{D}{C} = \frac{f(0)}{f(1) - f(0)}. \quad (7.1.28)$$

The solution procedure involves evaluating $f(0)$ and $f(1)$, and then using (7.1.28) to obtain α . The algorithm is implemented in subroutine *chan_2d_ml* in directory *04_various/uni_flow* of *FDLIB*.

Problems

Problem 7.1.1 *Reduction to single-layer flow.*

(a) Verify that, when $\lambda = 1$ and $\beta = 1$, expressions (7.1.14) and (7.1.15) are consistent with the velocity profile (7.1.6) for single-fluid flow.

(b) Confirm that, when the densities and viscosities of all layers are identical, the coefficients $A^{(i)}$ and $B^{(i)}$ are all equal to those corresponding to single-fluid flow.

Problem 7.1.2 *Integral momentum balance.*

Verify that the shear stress shown in (7.1.7) satisfies the integral momentum balance over the rectangular fluid parcel drawn with the solid line in figure 6.1.1.

Problem 7.1.3 *Power-law fluids.*

Derive the counterpart of the velocity profile (7.1.7) for a power-law fluid whose viscosity is a function of the shear rate, as shown in equation (4.6.1).

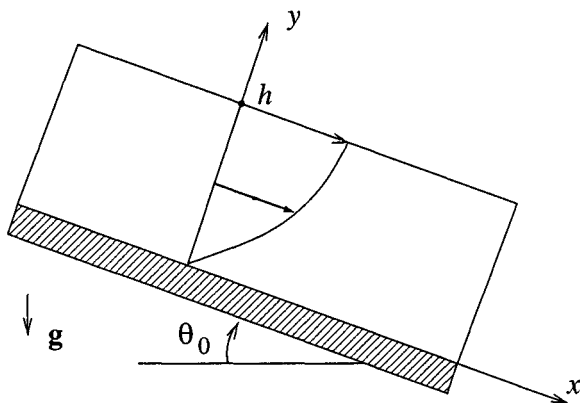


Figure 7.2.1 Gravity-driven flow of a film down an inclined plane.

Computer problem

Problem c.7.1.1 Multi-layer flow.

Use subroutine *chan_2d.ml* in directory *04_various/uni_flow* of *FDLIB* to compute and plot the velocity profile of a three-layer pressure-driven flow of your choice. Then investigate and discuss the effect of the viscosity of each layer on the velocity profile.

7.2 Steady film flow down an inclined plane

Gravity-driven flow of a liquid film down an inclined plane is encountered in a broad range of technological applications, including photographic and magnetic recording media coating.

Consider the flow of a film of thickness h down a plane wall that is inclined by the angle θ_0 with respect to the horizontal, as illustrated in figure 7.2.1. The no-slip boundary condition requires that the velocity vanish at the plane located at $y = 0$; the free-surface condition requires that the shear stress vanish at the free-surface located at $y = h$.

Under the assumption of unidirectional flow, the motion of the fluid is governed by the simplified equations of motion (7.1.1) subject to the

aforementioned boundary and free-surface conditions expressed by

$$u_x = 0 \text{ at } y = 0, \quad \frac{\partial u_x}{\partial y} = 0 \text{ at } y = h. \quad (7.2.1)$$

The pressure distribution is given by equation (7.1.3) with the pressure gradient χ set equal to zero, yielding $p(y) = P_0 + \rho g_y y$, where $g_y = -g \cos \theta_0$. Setting the pressure at the free surface equal to the ambient atmospheric pressure, we obtain $P_{Atm} = P_0 + \rho g_y h$ or $P_0 = P_{Atm} - \rho g_y h$, and then derive

$$p(y) = P_{Atm} + \rho g \cos \theta_0 (h - y). \quad (7.2.2)$$

Working as previously for channel flow, we obtain the Nusselt velocity profile

$$u_x(y) = \frac{\rho g_x}{2\mu} y (2h - y). \quad (7.2.3)$$

where $g_x = g \sin \theta_0$. This semi-parabolic profile is half the complete parabolic profile of pressure- or gravity-driven flow in a channel of width $2h$, where the free surface is located at the centerline. The shear stress varies linearly from a certain value at the wall to the required value of zero at the free surface.

The flow rate arises by integrating the velocity across the film, obtaining

$$Q \equiv \int_0^h u_x(y) dy = \frac{g \rho h^3}{3\mu} = \frac{2}{3} h u_x(h), \quad (7.2.4)$$

where $u_x(h)$ is the maximum velocity occurring at the free surface.

Subroutine *film_2d* in directory *04_various/uni_flow* of *FDLIB* evaluates the velocity profile and flow rate given in (7.2.3) and (7.2.4).

7.2.1 Multi-film flow

Consider next the gravity-driven flow of an arbitrary number of N superimposed films down an inclined plane, as illustrated in figure 7.2.2. In photographic film manufacturing, as many as thirteen films may flow down an inclined plane to be deposited onto a moving support.

In our notation, the bottom film is labelled as fluid 1, and the top layer is labelled as fluid N . The $N - 1$ interfaces separating the films are located at $y = y_I^{(i)}$, where $i = 1, 2, \dots, N - 1$; the free surface is located at $y = y_I^{(N)}$. The velocity profile across the i th film is governed by equation (7.1.17) with χ set equal to zero. Integrating (7.1.17) twice with respect to y , we derive the parabolic profile

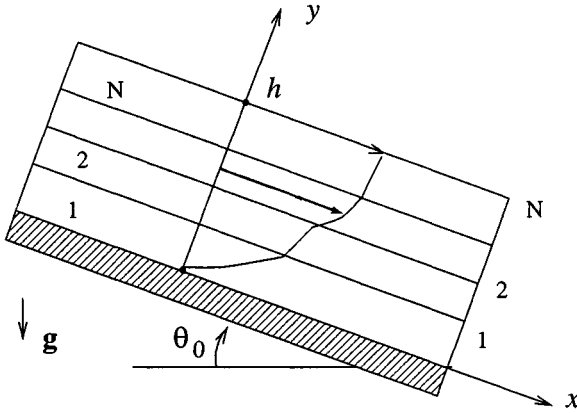


Figure 7.2.2 Gravity-driven multi-film flow down an inclined plane.

$$u_x^{(i)}(y) = -\frac{\rho_i g_x}{2\mu_i} y^2 + B^{(i)} y + A^{(i)}, \quad (7.2.5)$$

where $A^{(i)}$ and $B^{(i)}$ are unknown constants to be determined by requiring (a) the no-slip boundary condition at the plane, (b) continuity of velocity at the interfaces expressed by equation (7.1.18), (c) continuity of shear stress at the interfaces expressed by equation (7.1.19), and (d) the condition of zero shear stress at the free surface; with reference to equation (7.1.22), $\alpha = 0$.

Knowledge of the value of the shear stress at the free surface allows us to evaluate the coefficients $B^{(i)}$ and $A^{(i)}$, working as described in the paragraph following equation (7.1.22). The numerical method is implemented in subroutine *films_2d* located in directory *04_various/uni_flow* of *FDLIB*.

Wall shear stress

One interesting feature of the multi-film flow is that the wall shear stress and velocity profile across the first film that is adjacent to the wall, are independent of the viscosities of the rest of the films. To see this, we write the velocity profile (7.2.5) for $i = 1$, and require the no-slip boundary condition to find $A^{(1)} = 0$. To compute $B^{(1)}$, we perform a force balance over a section of the composite film confined between

the planes $x = x_1$ and x_2 . The balance requires that the force exerted by the shear stress at the wall and at the free surface counterbalance the horizontal component of the weight of the fluid residing within the control volume. We note that the shear stress at the free surface is equal to zero, and obtain

$$\sigma_{xy}^{(1)}(y=0) = \sum_{i=1}^N \rho_i g_x (y_I^{(i)} - y_I^{(i-1)}), \quad (7.2.6)$$

with the understanding that $y_I^{(0)} = 0$ and $y_I^{(N)} = h$. Using the profile (7.2.5) for $i = 1$, we find

$$\sigma_{xy}^{(1)}(y=0) = \mu_1 \left(\frac{\partial u_x^{(1)}}{\partial y} \right)_{y=0} = \mu_1 B^{(1)}. \quad (7.2.7)$$

Setting the right-hand side of (7.2.6) equal to the right-hand side of (7.2.7), solving for $B^{(1)}$, and substituting the result into the profile (7.2.5) for $i = 1$, proves the stated independence of the first velocity profile and wall shear stress on the viscosity of the overlying fluids.

Problems

Problem 7.2.1 Multi-film flow.

Confirm the independence of the wall shear stress on the viscosity of the films that are not adjacent to the wall on the basis of (a) the recursion relation (7.1.21) for gravity-driven flow, and (b) the free-surface condition expressed by (7.1.23) with $\alpha = 0$.

Problem 7.2.2 Power-law fluids.

Derive the counterpart of the velocity profile (7.2.3) for a power-law fluid whose viscosity is a function of the shear rate, as shown in equation (4.6.1).

Computer problem

Problem c.7.2.1 Multi-film flow.

Use subroutine *films_2d* in directory *04_various/uni_flow* of *FDLIB* to compute and plot the velocity profile of a three-film flow of your choice. Investigate and discuss the effect of the density of each film.

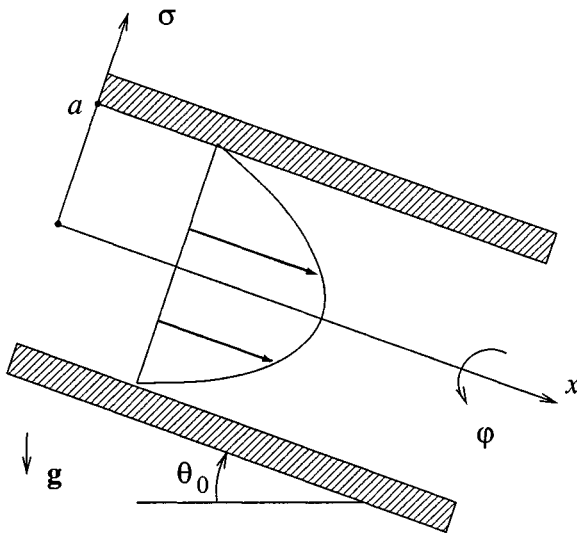


Figure 7.3.1 Illustration of steady unidirectional flow through a circular tube.

7.3 Steady flow through a circular or annular tube

The simplest conduit along which a fluid can be delivered is a cylindrical tube of radius a , as illustrated in figure 7.3.1. To derive the velocity profile, we introduce cylindrical polar coordinates with the x along the tube centerline. The assumption of unidirectional flow requires that the x component of the velocity is a function of distance σ from the centerline of the tube, signified by writing $u_x(\sigma)$, whereas the radial and meridional velocity components u_σ and u_ϕ vanish.

It will be convenient to screen out the hydrostatic pressure variation normal to the x axis, by expressing the pressure in the form

$$p = P_0 - \chi x + \rho (g_y y + g_z z), \quad (7.3.1)$$

where P_0 is a constant, and χ is the negative of the pressure gradient along the x axis. Consideration of the individual terms on the left-hand side of the x component of the equation of motion displayed in the first of equations (6.3.17), shows that the left-hand side vanishes. Using the

first of expressions (6.5.17), and rearranging, we derive the simplified equation of motion

$$\frac{1}{\sigma} \frac{d}{d\sigma} \left(\sigma \frac{du_x}{d\sigma} \right) = -\frac{\chi + \rho g_x}{\mu}, \quad (7.3.2)$$

which is the counterpart of equation (7.1.4) for two-dimensional channel flow. The solution is subject to the no-slip boundary condition $u_x = 0$ at $\sigma = a$, and a regularity condition requiring that u_x be finite at the centerline, $\sigma = 0$.

Two straightforward integrations of (7.3.2) with respect to σ provide us with the velocity profile

$$u_x(\sigma) = -\frac{\chi + \rho g_x}{4\mu} \sigma^2 + B \ln \sigma + A, \quad (7.3.3)$$

where A and B are two constants. For the velocity to be finite at the centerline, the constant B must be equal to zero. To evaluate the remaining constant A , we require the no-slip condition at the tube, and thus obtain the Poiseuille parabolic profile

$$u_x(\sigma) = \frac{\chi + \rho g_x}{4\mu} (a^2 - \sigma^2). \quad (7.3.4)$$

Maximum velocity occurs at the tube centerline, $\sigma = 0$. Subroutine *tube_crc* in directory *04_various/uni_flow* of *FDLIB* evaluates the velocity profile described by (7.3.4).

7.3.1 Shear stress and integral momentum balance

The shear stress $\sigma_{\sigma x}$ arises by differentiating the velocity profile (7.3.3) with respect to σ , and is found to be a linear function of distance from the centerline,

$$\sigma_{\sigma x} = \mu \frac{\partial u_x}{\partial \sigma} = -\frac{\chi + \rho g_x}{2} \sigma. \quad (7.3.5)$$

It is instructive to verify that this expression satisfies, and can be derived from, an integral momentum balance for a control volume that is confined between two parallel planes located at $x = x_1$ and $x = x_2$, and two cylindrical surfaces located at $\sigma = \sigma_1$ and $\sigma = \sigma_2$. Because the flow is steady, the rate of change of linear momentum of the fluid within the control volume should vanish. Balancing the normal force exerted on the planar sides, the shear force exerted at the cylindrical sides, and

the body force, and noting that the normal viscous stress vanishes and the normal stress over the planar sides is equal to the negative of the pressure, we find

$$2\pi \int_{\sigma_1}^{\sigma_2} [-p(x=x_2) + p(x=x_1)] \sigma d\sigma - \sigma_{\sigma x(\sigma=\sigma_1)} 2\pi \sigma_1 (x_2 - x_1) + \sigma_{\sigma x(\sigma=\sigma_2)} 2\pi \sigma_2 (x_2 - x_1) + \rho g_x \pi (\sigma_2^2 - \sigma_1^2) (x_2 - x_1) = 0. \quad (7.3.6)$$

Using (7.3.1) to express the pressure difference in terms of the pressure gradient χ , we find

$$\pi \chi (\sigma_2^2 - \sigma_1^2) (x_2 - x_1) - \sigma_{\sigma x(\sigma=\sigma_1)} 2\pi \sigma_1 (x_2 - x_1) + \sigma_{\sigma x(\sigma=\sigma_2)} 2\pi \sigma_2 (x_2 - x_1) + \rho g_x \pi (\sigma_2^2 - \sigma_1^2) (x_2 - x_1) = 0. \quad (7.3.7)$$

Setting $\sigma_1 = 0$ and solving for $\sigma_{\sigma x(\sigma=\sigma_2)}$, we derive expression (7.3.5) evaluated at $\sigma = \sigma_2$.

7.3.2 Flow rate

The flow rate along the tube arises by integrating the velocity over the cross-section, finding

$$\begin{aligned} Q &\equiv 2\pi \int_0^a u_x(\sigma) \sigma d\sigma = \frac{\chi + \rho g_x}{8\mu} \pi a^4 \\ &= \frac{1}{2} u_x(0) (\pi a^2), \end{aligned} \quad (7.3.8)$$

where $u_x(0)$ is the maximum velocity occurring at the centerline. The mean velocity, defined as the ratio of the flow rate to the tube cross-sectional area, $u_{Mean} \equiv Q/(\pi a^2)$, is equal to half the maximum velocity, $u_{Mean} = \frac{1}{2} u_x(0)$.

Equation (7.3.8) expresses *Poiseuille's law*, first established by laboratory observation. The data suggested that the flow rate through a circular tube subject to a constant pressure drop depends on the fourth power of the tube diameter.

7.3.3 Flow through an annular tube

The velocity profile of the flow through an annular tube confined between two coaxial cylinders with radii R_1 and R_2 , illustrated in figure

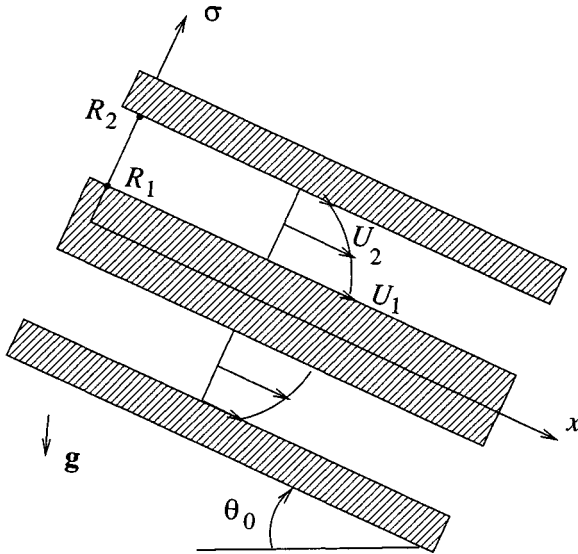


Figure 7.3.2 Steady flow through an annular tube with translating walls.

7.3.2, may be derived by a straightforward generalization of the preceding analysis. A new feature is that the two cylinders are allowed to translate parallel to themselves along the x axis with respective velocities equal to U_1 and U_2 .

Integrating (7.3.2) with respect to σ , we find that the axial component of the velocity is given by (7.3.3). To evaluate the constants A and B , we require the no-slip conditions $u_x(\sigma = R_1) = U_1$ and $u_x(\sigma = R_2) = U_2$, and derive the velocity profile

$$\begin{aligned}
 u_x(\sigma) = & U_2 + (U_1 - U_2) \frac{\ln \frac{R_2}{\sigma}}{\ln \frac{R_2}{R_1}} \\
 & + \frac{\chi + \rho g x}{4 \mu} [R_2^2 - \sigma^2 - (R_2^2 - R_1^2) \frac{\ln \frac{R_2}{\sigma}}{\ln \frac{R_2}{R_1}}]. \quad (7.3.9)
 \end{aligned}$$

The flow rate along the tube arises by integrating the velocity over the annular cross-section confined between the two concentric cylinders, obtaining

$$\begin{aligned}
Q &\equiv 2\pi \int_{R_1}^{R_2} u_x(\sigma) \sigma d\sigma \\
&= \pi (U_2 R_2^2 - U_1 R_1^2) - \frac{\pi}{2} (U_2 - U_1) \frac{R_2^2 - R_1^2}{\ln \frac{R_2}{R_1}} \\
&\quad + \pi \frac{\chi + \rho g_x}{8\mu} (R_2^2 - R_1^2) \left(R_2^2 + R_1^2 - \frac{R_2^2 - R_1^2}{\ln \frac{R_2}{R_1}} \right). \quad (7.3.10)
\end{aligned}$$

Subroutine *tube_ann* in directory *04_various/uni_flow* of *FDLIB* evaluates the velocity profile and the flow rate given in (7.3.9) and (7.3.10).

When the width of the annulus $R_2 - R_1$ is small compared to the inner tube radius R_1 , the curvature of the cylinders becomes insignificant, and equations (7.3.9) and (7.3.10) reduce to equations (7.1.6) and (7.1.8) with $R_2 - R_1 = 2h$ and $y = \sigma - \frac{1}{2}(R_1 + R_2)$ (problem 7.3.1).

7.3.4 Flow in a circular tube due to the translation of a sector

Earlier in this section, we considered pressure- and gravity-driven flow through a circular tube. Suppose now that the axial pressure gradient vanishes, the tube is horizontal, and the flow is driven by boundary motion. If the whole of the surface of the tube translates parallel to itself with constant velocity, then the fluid will also translate with the same uniform velocity in a plug-flow mode. If, however, only a sector of the tube confined between $-\alpha \leq \varphi \leq \alpha$ translates with velocity U , and the rest of the tube is stationary, as illustrated in figure 7.3.3(a), then a distributed velocity field will be established.

Assuming that the flow is unidirectional, we set the radial and meridional components of the velocity equal to zero, $u_\sigma = 0$ and $u_\varphi = 0$, and regard the axial component u_x as a function of distance from the tube centerline, σ , and meridional angle, φ . The no-slip boundary condition requires $u_x(\sigma = a, \varphi) = U$ for $-\alpha \leq \varphi \leq \alpha$, and $u_x(\sigma = a, \varphi) = 0$ otherwise.

Consideration of the individual terms on the left-hand side of the x component of the equation of motion, shown in the first of equations (6.3.17), reveals that the left-hand side vanishes. Using the first of expression (6.5.17), treating the pressure as a constant, and rearranging, we derive the simplified form

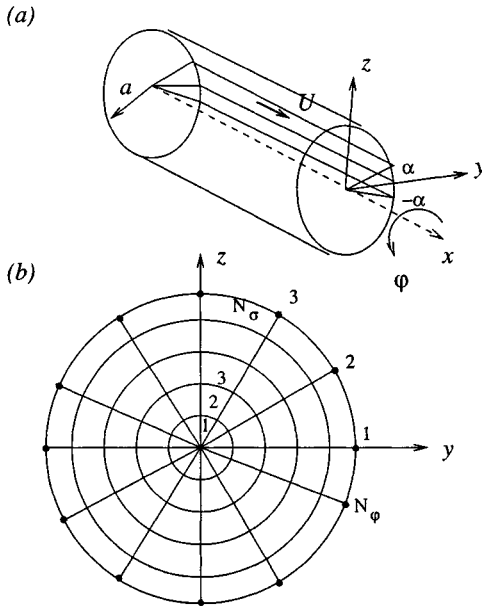


Figure 7.3.3 (a) Unidirectional flow through a circular tube due to the translation of a sector with semi-angle α . (b) Discretization of the tube cross-section for the purpose of computing the flow rate using the mid-point rule.

$$\nabla^2 u_x = \frac{1}{\sigma} \frac{\partial}{\partial \sigma} \left(\sigma \frac{\partial u_x}{\partial \sigma} \right) + \frac{1}{\sigma^2} \frac{\partial^2 u_x}{\partial \varphi^2} = 0, \quad (7.3.11)$$

where ∇^2 is the Laplacian operator in the yz plane expressed in cylindrical polar coordinates. Laplace's equation (7.3.11) is to be solved subject to the boundary conditions stated at the end of the last paragraph.

The solution may be found using a particular method for solving Laplace's equation in two dimensions in the interior or exterior of a circle subject to specified boundary conditions for the unknown function, expressed by the *Poisson integral* formula. For the problem under consideration, we find

$$u_x(\sigma, \varphi) = \frac{U}{\pi} \left[\arctan\left(\frac{a + \sigma}{a - \sigma} \tan \frac{\alpha - \varphi}{2}\right) + \arctan\left(\frac{a + \sigma}{a - \sigma} \tan \frac{\alpha + \varphi}{2}\right) \right]. \quad (7.3.12)$$

Inspection of the right-hand side confirms that, as the semi-angle of the translating sector α tends to π , the fluid tends to translate with uniform velocity in a plug-flow mode (problem 7.3.2). Subroutine *tube_crc_sec* in directory *04_various/uni_flow* of *FDLIB* evaluates the velocity profile given in (7.3.12).

Flow rate

The flow rate through the tube arises by integrating the velocity over the cross-section,

$$Q \equiv \int_0^{2\pi} \int_0^a u_x(\sigma, \varphi) \sigma \, d\sigma \, d\varphi. \quad (7.3.13)$$

The integral on the right-hand side is not known in analytical form. To obtain a numerical approximation, we divide the integration domain with respect to φ and σ into N_φ and N_σ evenly-spaced intervals of equal size $\Delta\varphi = 2\pi/N_\varphi$ and $\Delta\sigma = a/N_\sigma$, defining elemental cross-sectional areas, as shown in figure 7.3.3(b), and approximate the velocity over each elemental area with the value at the center. Replacing the double integral in (7.3.13) with a double sum, we obtain

$$Q = \Delta\varphi \Delta\sigma \sum_{i=1}^{N_\varphi} \sum_{j=1}^{N_\sigma} u_x(\sigma_j, \varphi_i) \sigma_j, \quad (7.3.14)$$

where

$$\varphi_i = \left(i - \frac{1}{2}\right) \Delta\varphi, \quad \sigma_j = \left(j - \frac{1}{2}\right) \Delta\sigma. \quad (7.3.15)$$

Equation (7.3.14) is an implementation of the mid-point rule for two-dimensional integration over a plane.

Problems

Problem 7.3.1 Reduction to channel flow.

Show that, when the width of the annulus $R_2 - R_1$ is small compared to the inner radius R_1 , equations (7.3.9) and (7.3.10) reduce to equations (7.1.6) and (7.1.8) for flow in a channel of width $2h = R_2 - R_1$, where $y = \sigma - \frac{1}{2}(R_1 + R_2)$.

Problem 7.3.2 *Flow in a tube due to a translating sector.*

Show that, as the translating sector semi-angle α tends to π , the right-hand side of (7.3.12) tends to the wall velocity U everywhere inside the tube.

Problem 7.2.3 *Axisymmetric film flow.*

A liquid film drains due to gravity downward along the surface of a vertical circular rod of radius a . Show that, in cylindrical polar coordinates with the x axis coaxial with the rod pointing upward, the velocity profile across the film is given by

$$u_x = \frac{g}{4\nu} [\sigma^2 - a^2 - 2(a+h)^2 \ln \frac{\sigma}{a}], \quad (7.3.16)$$

where h is the film thickness.

Computer problems

Problem c.7.3.1 *Flow in a circular tube due to the translation of a sector.*

Prepare and discuss a graph of the dimensionless mean velocity $\hat{u}_{Mean} = Q/(\pi a^2 U)$ against the reduced semi-angle α/π , using the numerical approximation implemented in (7.3.14). Your results should be accurate to the third significant figure.

Problem c.7.3.2 *Multi-layer tube flow.*

Subroutine `tube_crc_ml` in directory `04_various/uni_flow` of `FDLIB` computes the velocity profile of multi-layer pressure-driven tube flow. The algorithm is similar to that discussed in Section 7.2 for film flow. Note that the interfaces will remain concentric and cylindrical only in the absence of gravity, or when the fluid densities are identical; otherwise, hydrostatic pressure variations will cause non-axisymmetric displacements.

(a) Outline and explain the numerical procedure implemented in the code.

(b) Plot the velocity profile of a three-layer configuration of your choice.

(c) With reference to (b), investigate and discuss the effect of the layer viscosities on the velocity profile.

Problem c.7.3.3 *Multi-layer annular flow.*

Subroutine `tube_ann_ml` in directory `04_various/uni_flow` of `FDLIB` computes the velocity profile of a multi-layer annular flow. The algorithm

is similar to that discussed in Section 7.1 for multi-layer channel flow. Repeat the three parts of problem c.7.3.2.

7.4 Steady flow through channels and tubes with various cross-sections

Thus far, we have considered channel and tube flow where the streamwise velocity u_x is a function of lateral position, y , or distance from the tube centerline, σ . In this section, we consider flow in a channel or tube with arbitrary cross-section where the streamwise velocity is a function of the two spatial coordinates determining position over the cross-section, $u_x(y, z)$.

The assumption of unidirectional motion allows us to simplify the x , y , and z components of the equation of motion displayed in (6.5.7), obtaining

$$\begin{aligned} 0 &= -\frac{\partial p}{\partial x} + \mu \left(\frac{\partial^2 u_x}{\partial y^2} + \frac{\partial^2 u_x}{\partial z^2} \right) + \rho g_x, \\ 0 &= -\frac{\partial p}{\partial y} + \rho g_y, \\ 0 &= -\frac{\partial p}{\partial z}. \end{aligned} \tag{7.4.1}$$

Without loss of generality, we have assumed that the acceleration of gravity lies in the xy plane, that is, the z component vanishes.

The y and z components of system (7.4.1) are satisfied by the pressure distribution (7.1.3). To also satisfy the x component, we require that the streamwise velocity is a solution of the second-order partial differential equation

$$\nabla^2 u_x = \frac{\partial^2 u_x}{\partial y^2} + \frac{\partial^2 u_x}{\partial z^2} = -\frac{\chi + \rho g_x}{\mu}, \tag{7.4.2}$$

which is a Poisson equation with a constant right-hand side; $\nabla^2 \equiv \partial^2/\partial y^2 + \partial^2/\partial z^2$ is the Laplacian operator in the yz plane. The partial differential equation (7.4.2) is a generalization of the ordinary differential equations (7.1.4) and (7.3.2) for two-dimensional or axisymmetric flow. In the remainder of this section, we shall derive solutions to (7.4.2) for several boundary geometries.

7.4.1 Flow through an elliptical tube

First, we consider flow through a straight tube with an elliptical cross-section whose contour in the yz plane is described by the equation

$$f(y, z) = \frac{y^2}{a^2} + \frac{z^2}{b^2} - 1 = 0, \quad (7.4.3)$$

where a and b are the ellipse semi-axes, as illustrated in figure 7.4.1(a). The coordinates of a point on the elliptical contour may be identified by the value of a parameter η taking values in the range $[0, 2\pi)$, as

$$y = a \cos \eta, \quad z = b \sin \eta. \quad (7.4.4)$$

The no-slip boundary condition requires that $u_x(y, z) = 0$ for pairs (y, z) generated by (7.4.4), and thus satisfying $f(y, z) = 0$ according to (7.4.3).

Because $f(y, z)$ is a quadratic function of y and z , its Laplacian, defined after equation (7.4.2), is constant. Inspired by this observation, we express the velocity in the form $u_x(y, z) = c f(y, z)$ which guarantees the satisfaction of the aforementioned no-slip boundary condition, and adjust the value of the constant c to also satisfy the Poisson equation (7.4.2). The result is the velocity distribution

$$u_x(y, z) = \frac{\chi + \rho g_x}{2\mu} \frac{a^2 b^2}{a^2 + b^2} \left(1 - \frac{y^2}{a^2} - \frac{z^2}{b^2}\right). \quad (7.4.5)$$

Maximum velocity occurs at the tube centerline located at $y = 0$ and $z = 0$.

Flow rate

Taking advantage of the symmetry of the velocity profile with respect to the xy and xz planes, we express the axial flow rate as an integral of the velocity over the first quadrant, in the form

$$Q = \int \int_{\text{Ellipse}} u_x(y, z) dy dz = 4 \int_0^a \int_0^{z_{Max}} u_x(y, z) dz dy, \quad (7.4.6)$$

where z_{Max} is computed by solving equation (7.4.3) for z , yielding $z_{Max} = b\sqrt{1 - y^2/a^2}$. Substituting the velocity profile (7.4.5) into the integrand, and carrying out the integration with respect to z , we find

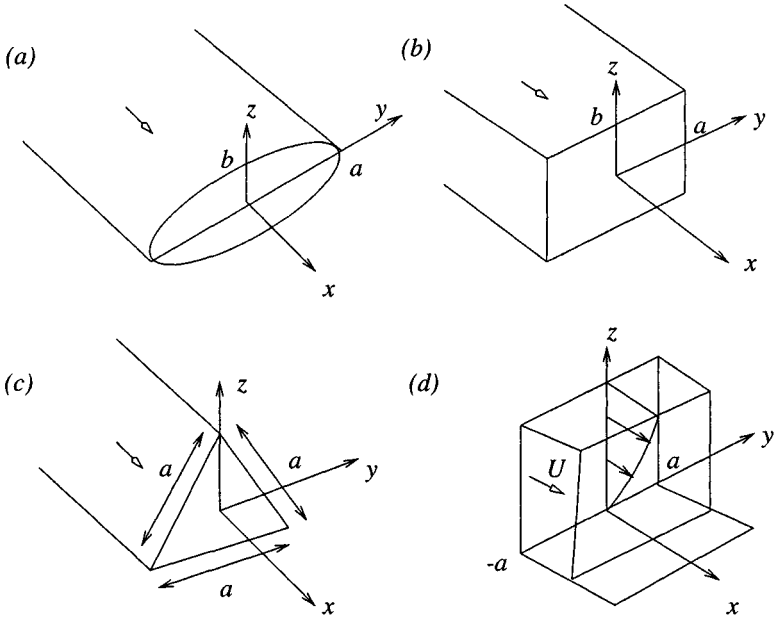


Figure 7.4.1 Steady flow through a tube with (a) elliptical, (b) rectangular, and (c) equilateral triangle cross-section. (d) Flow between two parallel plates moving over a plane wall regarded as a painted surface.

$$\begin{aligned}
 Q &= 2 \frac{\chi + \rho g x}{\mu} \frac{a^2 b^2}{a^2 + b^2} \int_0^a \left(1 - \frac{y^2}{a^2} - \frac{z^2 M_{ax}}{3 b^2}\right) z M_{ax} dy \\
 &= 4 \frac{\chi + \rho g x}{3\mu} \frac{a^2 b^3}{a^2 + b^2} \int_0^a \left(1 - \frac{y^2}{a^2}\right)^{3/2} dy \\
 &= 4 \frac{\chi + \rho g x}{3\mu} \frac{a^3 b^3}{a^2 + b^2} \int_0^1 (1 - \hat{y}^2)^{3/2} d\hat{y} \\
 &= 4 \frac{\chi + \rho g x}{3\mu} \frac{a^3 b^3}{a^2 + b^2} \int_0^{\pi/2} \cos^4 \xi d\xi,
 \end{aligned} \tag{7.4.7}$$

where we have set $\hat{y} \equiv y/a \equiv \sin \xi$. Reference to standard tables of integrals reveals that the last integral in (7.4.7) is equal to $3\pi/16$. The

final expression for the flow rate is

$$Q = \frac{\chi + \rho g_x}{4\mu} \pi \frac{a^3 b^3}{a^2 + b^2}. \quad (7.4.8)$$

As the second semi-axis b tends to become equal to the first semi-axis a , the cross-section of the tube tends to become circular, and the expressions for the velocity distribution and flow rate reduce to those shown in equations (7.3.4) and (7.3.8) for Poiseuille flow.

Subroutine *tube_ell* in directory *04_various/uni_flow* of *FDLIB* evaluates the velocity profile and the flow rate given in (7.4.5) and (7.4.8).

7.4.2 Flow through a rectangular tube

As a second case study, we consider flow through a tube whose cross-section is a rectangle with side-lengths equal to $2a$ and $2b$, as illustrated in figure 7.4.1(b). A standard method of solving the Poisson equation (7.4.2) involves expressing the velocity as the sum of a particular solution $u_x^P(y, z)$ that satisfies the Poisson equation (7.4.2) but not all boundary conditions, and a homogeneous solution $u_x^H(y, z)$ that satisfies Laplace's equation $\nabla^2 u_x^H = 0$ and boundary conditions that arise by requiring that the total velocity $u_x = u_x^P + u_x^H$ satisfies the no-slip boundary condition over the four walls.

A convenient choice of a particular solution is

$$u_x^P(y, z) = \frac{\chi + \rho g_x}{2\mu} (b^2 - z^2). \quad (7.4.9)$$

Requiring $u_x^P + u_x^H = 0$ along the four walls, we derive boundary conditions for the homogeneous solution,

$$u_x^H(y = \pm a, z) = -u_x^P(y = \pm a, z) = -\frac{\chi + \rho g_x}{2\mu} (b^2 - z^2), \quad (7.4.10)$$

and

$$u_x^H(y, z = \pm b) = -u_x^P(y, z = \pm b) = 0. \quad (7.4.11)$$

To compute the homogeneous solution, we express it in the form of a Fourier series with respect to z , setting

$$u_x^H(y, z) = \sum_{n=1}^{\infty} f_n(y) \cos(\alpha_n \frac{z}{b}), \quad (7.4.12)$$

where

$$\alpha_n = (n - \frac{1}{2}) \pi, \quad (7.4.13)$$

so that the expansion (7.4.12) satisfies the boundary conditions (7.4.11). The functions $f_n(y)$ will be computed so that the right-hand side of (7.4.12) satisfies Laplace's equation $\nabla^2 u_x^H = 0$, and respects the boundary conditions (7.4.10).

Taking the Laplacian of (7.4.12), we find

$$\nabla^2 u_x^H(y, z) = \sum_{n=1}^{\infty} \left[\frac{d^2 f_n(y)}{dy^2} - \frac{\alpha_n^2}{b^2} f_n(y) \right] \cos(\alpha_n \frac{z}{b}). \quad (7.4.14)$$

For the infinite sum on the right-hand side to vanish for any value of y and z , each term enclosed by the square brackets must be equal to zero, yielding

$$\frac{d^2 f_n(y)}{dy^2} - \frac{\alpha_n^2}{b^2} f_n(y) = 0. \quad (7.4.15)$$

The general solution of this equation is

$$f_n(y) = A_n \cosh(\alpha_n \frac{y}{b}) + B_n \sinh(\alpha_n \frac{y}{b}), \quad (7.4.16)$$

where A_n and B_n are constant coefficients. Discarding the hyperbolic sines to ensure that the functions $f_n(y)$ are even and the velocity profile is symmetric with respect to $y = 0$, and substituting the result into (7.4.12), we find

$$u_x^H(y, z) = \sum_{n=1}^{\infty} A_n \cosh(\alpha_n \frac{y}{b}) \cos(\alpha_n \frac{z}{b}). \quad (7.4.17)$$

To satisfy the remaining boundary conditions (7.4.10), we require

$$\sum_{n=1}^{\infty} A_n \cosh(\alpha_n \frac{a}{b}) \cos(\alpha_n \frac{z}{b}) = -\frac{\chi + \rho g x}{2\mu} (b^2 - z^2). \quad (7.4.18)$$

The left-hand side of (7.4.18) may be regarded as the Fourier series of the quadratic function with respect to z on the right-hand side.

The solution follows readily using the trigonometric identity

$$\int_{-b}^b \cos(\alpha_n \frac{z}{b}) \cos(\alpha_m \frac{z}{b}) dz = \begin{cases} b & \text{if } n = m \\ 0 & \text{if } n \neq m \end{cases}. \quad (7.4.19)$$

Multiplying both sides of (7.4.18) by $\cos(\alpha_m z/b)$, integrating with respect to z from $-b$ to b , using (7.4.19) to compute the integrals on the left-hand side, and then switching m to n , we find

$$\begin{aligned} A_n &= -\frac{\chi + \rho g_x}{2 \mu b \cosh(\alpha_n \frac{a}{b})} \int_{-b}^b \cos(\alpha_n \frac{z}{b}) (b^2 - z^2) dz \\ &= -\frac{\chi + \rho g_x}{2 \mu \cosh(\alpha_n \frac{a}{b})} b^2 \int_{-\alpha_n}^{\alpha_n} (1 - \frac{\eta^2}{\alpha_n^2}) \cos \eta d\eta \\ &= -\frac{\chi + \rho g_x}{2 \mu \cosh(\alpha_n \frac{a}{b})} \frac{4b^2}{\alpha_n^3} (-1)^n, \end{aligned} \quad (7.4.20)$$

where we have introduced the intermediate variable $\eta \equiv \alpha_m z/b$. Substituting expression (7.4.20) into (7.4.17), and adding to the homogeneous solution the particular solution expressed by (7.4.9), we obtain the velocity distribution in the form of an infinite series,

$$u_x(y, z) = \frac{\chi + \rho g_x}{2 \mu} b^2 \left[1 - \frac{z^2}{b^2} + 4 \sum_{n=1}^{\infty} \frac{(-1)^n \cosh(\alpha_n \frac{y}{b})}{\alpha_n^3 \cosh(\alpha_n \frac{a}{b})} \cos(\alpha_n \frac{z}{b}) \right]. \quad (7.4.21)$$

Flow rate

The flow rate arises by integrating the velocity over the tube cross-section,

$$Q \equiv \int_{-a}^a \int_{-b}^b u_x(y, z) dy dz. \quad (7.4.22)$$

Substituting the profile (7.4.21) into the integrand, and carrying out the integration, we find

$$Q = \frac{\chi + \rho g_x}{3 \mu} 4 a b^3 \left[1 - 6 \frac{b}{a} \sum_{n=1}^{\infty} \frac{1}{\alpha_n^5} \tanh(\alpha_n \frac{a}{b}) \right]. \quad (7.4.23)$$

Subroutine *chan_rec* in subdirectory *04_various/uni_flow* of *FDLIB* evaluates the velocity profile, the flow rate, and the maximum velocity occurring at the tube centerline.

7.4.3 Flow through a semi-infinite rectangular channel

As a third case study, we consider flow between two semi-infinite parallel plates sliding with velocity U over a stationary flat surface, as illustrated in figure 7.4.1(d). The motion of the plates generates a unidirectional flow along the x axis, which may be regarded as a model of the flow occurring between two hairs of an idealized two-dimensional brush moving over a painted surface.

In the absence of a pressure gradient and significant gravitational forces, the x component of the velocity satisfies Laplace's equation $\nabla^2 u_x = 0$, which arises from (7.4.2) by setting the right-hand side equal to zero. The no-slip boundary condition requires that the velocity vanishes over the flat surface located at $z = 0$, and has the constant value U over the sliding plates located at $y = \pm a$. Far from the painted surface, the fluid moves in a plug-flow mode with the plate velocity U .

To compute the solution, we use the method of Fourier expansions discussed earlier for flow through a tube with rectangular cross-section. Requiring that, as z tends to infinity, u_x tends to U , we obtain the counterpart of (7.4.17),

$$u_x(y, z) = U + \sum_{n=1}^{\infty} A_n \exp(-\alpha_n \frac{z}{a}) \cos(\alpha_n \frac{y}{a}), \quad (7.4.24)$$

where the coefficient α_n is defined in equation (7.4.13).

Expansion (7.4.24) satisfies the no-slip condition at the side walls. To also satisfy the no-slip condition at the painted surface, we require

$$u_x(y, z = 0) = U + \sum_{n=1}^{\infty} A_n \cos(\alpha_n \frac{y}{a}) = 0. \quad (7.4.25)$$

Using the counterpart of the trigonometric identity (7.4.19),

$$\int_{-a}^a \cos(\alpha_n \frac{y}{a}) \cos(\alpha_m \frac{y}{a}) dy = \begin{cases} a & \text{if } n = m \\ 0 & \text{if } n \neq m \end{cases}, \quad (7.4.26)$$

and working as previously for flow in a rectangular channel, we find

$$A_n = -\frac{U}{a} \int_{-a}^a \cos(\alpha_n \frac{y}{a}) dy = -\frac{2U}{\alpha_n} \sin \alpha_n = (-1)^n \frac{2U}{\alpha_n}. \quad (7.4.27)$$

Substituting this expression back into (7.4.24), we obtain the desired velocity distribution

$$u_x(y, z) = U \left[1 + 2 \sum_{n=1}^{\infty} \frac{(-1)^n}{\alpha_n} \exp(-\alpha_n \frac{z}{a}) \cos(\alpha_n \frac{y}{a}) \right]. \quad (7.4.28)$$

As the two plates travel over the stationary surface, they leave behind an amount of fluid at the flow rate

$$\begin{aligned} Q &= \int_0^{\infty} \int_{-a}^a [U - u_x(y, z)] dy dz \\ &= -2U \sum_{n=1}^{\infty} \frac{(-1)^n}{\alpha_n} \int_0^{\infty} \int_{-a}^a \exp(-\alpha_n \frac{z}{a}) \cos(\alpha_n \frac{y}{a}) dy dz \\ &= 4U a^2 \sum_{n=1}^{\infty} \frac{1}{\alpha_n^3} = 1.085 U a^2. \end{aligned} \quad (7.4.29)$$

Subroutine *chan_brush* in directory *04_various/uni_flow* of *FDLIB* evaluates the velocity field and flow rate given by (7.4.28) and (7.4.29).

Problems

Problem 7.4.1 Area of an ellipse.

Show that the area of an ellipse with semi-axes a and b is equal to πab .

Problem 7.4.2 Flow through a triangular tube.

Consider pressure- or gravity-driven flow through a tube whose cross-section is an equilateral triangle with side-length a , as illustrated in figure 7.4.1(c). The origin is located at the centroid of the triangle, and the y axis is parallel to the lower side.

(a) Confirm that the velocity distribution

$$u(y, z) = \frac{\chi + \rho g x}{36 \mu a} (2\sqrt{3}z + a)(\sqrt{3}z + 3y - a)(\sqrt{3}z - 3y - a) \quad (7.4.30)$$

satisfies the Poisson equation (7.4.2), and is consistent with the no-slip boundary condition along the three sides.

(b) Show that the flow rate is given by

$$Q = \frac{\sqrt{3}}{320} \frac{\chi + \rho g}{\mu} a^4. \quad (7.4.31)$$

(c) Compute the ratio of the flow rates through a circular tube and a triangular tube with the same cross-sectional areas, and discuss your results.

Computer problems

Problem c.7.4.1 Flow through an ellipse.

Using the parametrization (7.4.4), we find that the differential arc length along the contour of an ellipse is given by

$$\begin{aligned} dl &\equiv (dx^2 + dy^2)^{1/2} = (a^2 \sin^2 \eta + b^2 \cos^2 \eta)^{1/2} \\ &= [a^2 - (a^2 - b^2) \cos^2 \eta]^{1/2} = a (1 - k^2 \cos^2 \eta)^{1/2}, \end{aligned} \quad (7.4.32)$$

where $k^2 \equiv 1 - b^2/a^2$; for convenience, and without loss of generality, we have assumed $b \leq a$. The arc length of the ellipse is given by

$$\begin{aligned} L &= \oint dl = 4a \int_0^{\pi/2} (1 - k^2 \cos^2 \eta)^{1/2} d\eta \\ &= 4a \int_0^{\pi/2} (1 - k^2 \sin^2 \eta)^{1/2} d\eta. \end{aligned} \quad (7.4.33)$$

When $a = b$, whereupon $k^2 = 0$, we obtain the well-known result for the circle, $L = 2\pi a$.

The integral on the right-hand side of (7.4.33) is the *complete elliptic integral of the second kind*. In Section 11.5, we shall see that this integral may be evaluated using an efficient iterative method. As an alternative, we use the mid-point rule to approximate the integral with a sum,

$$L \simeq 4a \frac{\pi}{2N} \sum_{i=1}^N (1 - k^2 \sin^2 \eta_i)^{1/2}, \quad (7.4.34)$$

where N is a specified level of discretization, and $\eta_i = (i - \frac{1}{2})\frac{\pi}{2N}$.

(a) Prepare a graph of the reduced arc length L/a against the axes ratio b/a , where $0 < b/a < 1$. The value of N in (7.4.34) should be chosen large enough so that the arc length is computed accurate to the third decimal place.

(b) A gardener delivers water through a circular hose made of a flexible but inextensible material. By pinching the end of the hose, she is able to produce elliptical shapes of variable cross-section, while maintaining

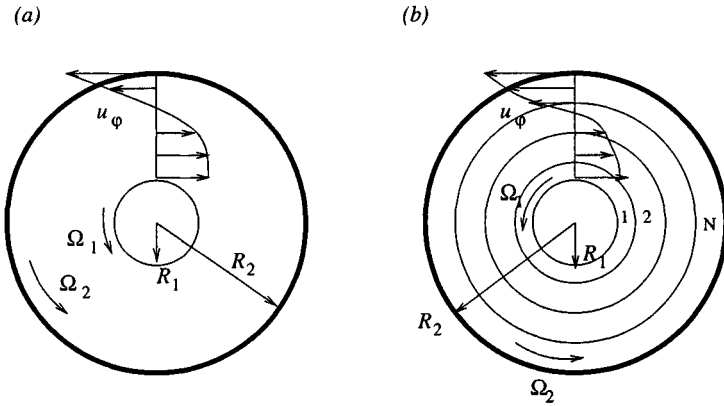


Figure 7.5.1 Swirling flow between two rotating concentric cylinders: (a) single-fluid flow, and (b) multi-layer flow.

the perimeter of the hose constant. Prepare a plot of the delivered flow rate versus the aspect ratio of the cross-section for a certain pressure gradient, and discuss your results.

7.5 Steady swirling flow

In previous sections, we have considered steady unidirectional flows with rectilinear streamlines. Because point particles travel on straight paths with constant velocity, inertial forces vanish and the flow is governed by the linear equation of motion expressing a balance between the pressure gradient, the viscous force, and the body force. In this section, we turn our attention to swirling flow with circular streamlines where centrifugal forces arise.

7.5.1 Flow between two concentric cylinders

Consider steady swirling flow between two infinite concentric cylinders with radii R_1 and R_2 rotating around their common axis with angular velocities Ω_1 and Ω_2 , as illustrated in figure 7.5.1(a). The established *circular Couette flow* is the counterpart of the plane Couette flow with rectilinear streamlines discussed in Section 7.1.

To compute the solution, we introduce cylindrical polar coordinates with the x axis coaxial with the cylinders, and assume that the axial and radial components of the velocity vanish, $u_x = 0$ and $u_\sigma = 0$, and the meridional component u_φ is independent of the meridional angle φ , $\partial u_\varphi / \partial \varphi = 0$. Thus, u_φ is only a function of distance from the x axis, σ , and $Du_\varphi / Dt = 0$, where D/Dt is the material derivative. The no-slip boundary condition at the surface of the cylinders requires

$$\begin{aligned} u_\varphi &= R_1 \Omega_1 & \text{at } \sigma = R_1, \\ u_\varphi &= R_2 \Omega_2 & \text{at } \sigma = R_2. \end{aligned} \quad (7.5.1)$$

In the case of steady swirling flow with circular streamlines, the cylindrical polar components of the equation of motion displayed in equations (6.3.18) obtain the simplified form

$$\begin{aligned} 0 &= -\frac{\partial p}{\partial x} + \rho g_x, \\ 0 &= \rho \frac{u_\varphi^2}{\sigma} - \frac{\partial p}{\partial \sigma} + \rho g_\sigma, \\ 0 &= -\frac{1}{\sigma} \frac{\partial p}{\partial \varphi} + \mu \frac{d}{d\sigma} \left(\frac{1}{\sigma} \frac{d(\sigma u_\varphi)}{d\sigma} \right) + \rho g_\varphi. \end{aligned} \quad (7.5.2)$$

To remove the hydrostatic pressure variation, we introduce the dynamic pressure defined by $p^D \equiv p - \rho(g_x x + g_y y + g_z z)$, and reduce the three differential equations (7.5.2) to the two ordinary differential equations

$$\frac{dp^D}{d\sigma} = \rho \frac{u_\varphi^2}{\sigma}, \quad \frac{d}{d\sigma} \left(\frac{1}{\sigma} \frac{d(\sigma u_\varphi)}{d\sigma} \right) = 0. \quad (7.5.3)$$

Straightforward integration of the second of equations (7.5.3) with respect to σ subject to the boundary conditions (7.5.1) provides us with the velocity profile

$$u_\varphi(\sigma) = \frac{\Omega_2 - \alpha \Omega_1}{1 - \alpha} \sigma - \frac{\Omega_2 - \Omega_1}{1 - \alpha} \frac{R_1^2}{\sigma}, \quad (7.5.4)$$

where

$$\alpha \equiv \left(\frac{R_1}{R_2} \right)^2 < 1. \quad (7.5.5)$$

The first term on the right-hand side of (7.5.4) expresses rigid-body rotation; the second term expresses swirling motion due to a point vortex situated at the cylinder axis. Subroutine *tube_ann_sw* in directory *04_various/uni_flow* of *FDLIB* evaluates the velocity profile given by (7.5.4). The pressure distribution follows by substituting (7.5.4) into the first of equations (7.5.3), and carrying out the integration with respect to σ .

Equation (7.5.4) confirms that when $\Omega_1 = \Omega_2 = \Omega$, or when the radius of the inner cylinder vanishes, $R_1 = 0$, the fluid rotates as a rigid body with angular velocity Ω . In this case, the pressure distribution is readily found to be

$$p^D = P_0 + \frac{1}{2} \rho \Omega^2 \sigma^2, \quad (7.5.6)$$

where P_0 is a constant. Thus, rigid body rotation is associated with a quadratic pressure distribution with respect to radial position, established to counteract the centrifugal force due to inertia.

As the clearance of the channel $R_2 - R_1$ tends to become small compared to the inner radius R_1 , we obtain plane Couette in a channel with parallel-sided walls studied in Section 7.1 (problem 7.5.1).

Problems

Problem 7.5.1 *Reduction to channel flow.*

Show that, when the width of the annulus $R_2 - R_1$ is small compared to the inner radius R_1 , equation (7.5.4) reduces to equation (7.1.6) for plane Couette flow in a channel with width $2h = R_2 - R_1$, where $y = \sigma - \frac{1}{2}(R_1 + R_2)$.

Problem 7.5.2 *Torque.*

Show that the torque exerted on either cylinder of a circular Couette flow device is given by

$$T \equiv 2 \pi \sigma \sigma_{\sigma\varphi} = -4 \pi \mu R_1^2 \frac{\Omega_2 - \Omega_1}{1 - \alpha}, \quad (7.5.7)$$

where the constant α is defined in (7.5.5).

Problem 7.5.3 *Free surface of a rotating liquid.*

A certain amount of liquid is placed in a horizontal cylindrical container that rotates as a rigid body with angular velocity Ω about the x

axis pointing against the direction of gravity. Using equation (7.5.6), we find that the pressure distribution in the liquid is given by

$$p = P_0 + \frac{1}{2} \rho \Omega^2 x^2 + \rho g x. \quad (7.5.8)$$

(a) Show that, when the surface tension is insignificant, the shape of the free surface is described by the equation

$$x = \frac{\Omega^2 \sigma^2}{2g} + c, \quad (7.5.9)$$

where c is a constant, and g is the acceleration of gravity.

(b) Derive a differential equation governing the shape of the free surface in the presence of surface tension.

Computer problem

Problem c.7.5.1 *Multi-layer annular flow.*

Subroutine *tube_ann_sw_ml* in directory *04_various/uni_flow* of *FDLIB* computes the velocity profile of multi-layer swirling annular flow, as illustrated in figure 7.5.1(b). The algorithm is similar to that discussed in Section 7.1 for multi-layer channel flow.

(a) Outline and explain the numerical procedure implemented in the code.

(b) Plot the velocity profile of a three-layer flow of your choice.

7.6 Transient flow in a channel

In the preceding sections, we have studied steady unidirectional flows with rectilinear or circular streamlines. In the remainder of this chapter, we turn our attention to the corresponding unsteady flows produced by sudden or oscillatory boundary motion, tilting, or application of a pressure gradient. Our analysis will continue to be based on the assumption of unidirectional motion with rectilinear or circular streamlines, but the velocity will be allowed to change in time.

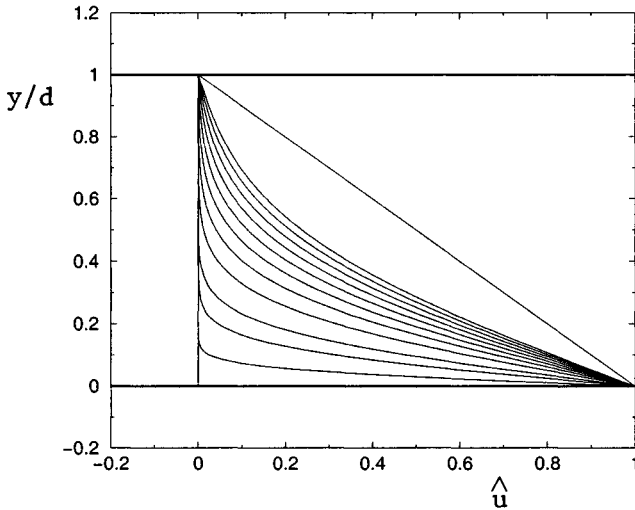


Figure 7.6.1 Transient Couette flow in a channel with parallel-sided walls due to the impulsive translation of the lower wall, at dimensionless times $\hat{t} \equiv t \nu/d^2 = 0.001, 0.005, 0.010, 0.020, 0.030, \dots, 0.14, 0.15$; the straight line is the linear profile established at long times.

7.6.1 Transient Couette flow

To begin, we consider flow in a two-dimensional channel with parallel walls separated by the distance d , where the lower wall is suddenly set in motion parallel to itself along the x axis with constant velocity U , while the upper wall is held stationary, as illustrated in figure 7.6.1

Working as in Section 7.1, we find that, in the absence of a pressure gradient along the x axis, the pressure assumes its hydrostatic distribution. The x component of the equation of motion provides us with a partial differential equation for the x component of the velocity,

$$\rho \frac{\partial u_x}{\partial t} = \mu \frac{\partial^2 u_x}{\partial y^2}, \quad (7.6.1)$$

which is to be solved subject to the initial condition

$$u_x = 0 \quad \text{for } 0 < y \leq d \text{ at } t = 0, \quad (7.6.2)$$

and to the no-slip boundary conditions

$$u_x(y = 0) = U, \quad u_x(y = d) = 0, \quad \text{for } t \geq 0. \quad (7.6.3)$$

At long times, we anticipate that the flow will reach a steady state with a linear velocity profile given by

$$u_x^{ss}(y) = U \left(1 - \frac{y}{d}\right), \quad (7.6.4)$$

as discussed in Section 7.1.

To compute the solution of (7.6.1), we consider the deviation of the transient velocity from the linear profile established at steady state, and expand it in a Fourier series with respect to y , obtaining

$$u_x(y, t) = u_x^{ss}(y) + \sum_{n=1}^{\infty} A_n(t) \sin \frac{n\pi y}{d}. \quad (7.6.5)$$

The arguments of the trigonometric functions on the right-hand side were designed to satisfy the boundary conditions (7.6.3) at all times. To compute the functions $A_n(t)$, we substitute expansion (7.6.5) into the governing equation (7.6.1), and carry out the time and space differentiation to find

$$\sum_{n=1}^{\infty} \left[\rho \frac{dA_n(t)}{dt} + \mu \left(\frac{n\pi}{d}\right)^2 A_n(t) \right] \sin \frac{n\pi y}{d} = 0. \quad (7.6.6)$$

To ensure the satisfaction of this equality for any value of y , we set the expression enclosed by the square brackets equal to zero, and thereby obtain a first-order linear differential equation for $A_n(t)$ whose solution is

$$A_n(t) = b_n \exp\left(-\frac{n^2\pi^2\nu}{d^2} t\right), \quad (7.6.7)$$

where $\nu = \mu/\rho$ is the kinematic viscosity, and b_n is a constant. Substituting expression (7.6.7) into (7.6.5), we find

$$u_x(y, t) = u_x^{ss}(y) + \sum_{n=1}^{\infty} b_n \exp\left(-\frac{n^2\pi^2\nu}{d^2} t\right) \sin \frac{n\pi y}{d}. \quad (7.6.8)$$

To compute the constants b_n , we require that (7.6.8) satisfies the initial condition (7.6.2),

$$u_x(y, t=0) = U \left(1 - \frac{y}{d}\right) + \sum_{n=1}^{\infty} b_n \sin \frac{n\pi y}{d} = 0. \quad (7.6.9)$$

The solution follows readily by use of the trigonometric identity

$$\int_0^d \sin \frac{n\pi y}{d} \sin \frac{m\pi y}{d} dy = \begin{cases} 0 & \text{if } n = 0 \text{ or } m = 0 \\ d/2 & \text{if } n = m \neq 0 \\ 0 & \text{if } n \neq m \end{cases} \quad (7.6.10)$$

Multiplying the middle and right-hand side of (7.6.9) with $\sin(m\pi y/d)$, integrating with respect to y from 0 to d , using identities (7.6.10), and then switching m to n , we find

$$b_n = -\frac{2U}{d} \int_0^d \left(1 - \frac{y}{d}\right) \sin \frac{n\pi y}{d} dy = -\frac{2U}{n\pi}. \quad (7.6.11)$$

The velocity profile (7.6.8) takes the final form

$$u_x(y, t) = U \left[1 - \frac{y}{d} - \frac{2}{\pi} \sum_{n=1}^{\infty} \frac{1}{n} \exp\left(-\frac{n^2\pi^2\nu}{d^2} t\right) \sin \frac{n\pi y}{d} \right]. \quad (7.6.12)$$

Subroutine *chan_2d.imp* in directory *04_various/uni_flow_u* of *FDLIB* evaluates the velocity given in (7.6.12). A sequence of developing profiles of the reduced velocity $\hat{u} \equiv u_x/U$ is shown in figure 7.6.1.

At long times, the summed terms on the right-hand side of (7.6.12) decay at an exponential rate, and the linear profile of the steady Couette flow expressed by the first two terms within the angular brackets on the right-hand side dominates. The elapsed time where steady flow has virtually been established, denoted by t_s , may be estimated by setting the magnitude of the argument of the exponential term on the right-hand side of (7.6.12) equal to unity for the lowest value of n , $n = 1$, obtaining

$$t_s \simeq \frac{d^2}{\pi^2\nu}. \quad (7.6.13)$$

Apart from the factor π^2 in the denominator, this estimate could have been deduced at the outset on the basis of dimensional analysis.

Diffusion of vorticity

The strength of the vorticity in unidirectional flow is given by $\omega_z = -\partial u_x/\partial y$. Differentiating both sides of (7.6.1) with respect to y , we find that the evolution of the vorticity is governed by equation (7.6.1), with u_x replaced by ω_z on both sides.

Figure 7.6.1 illustrates that, as soon as the lower wall begins translating, a thin layer of highly rotational fluid is established near the wall. The vorticity then diffuses away from the wall to occupy the whole of the channel. When steady state has been established, the vorticity has the uniform value U/d . This process exemplifies how vorticity enters a flow across a boundary during a period of transient motion.

7.6.2 Flow due to the impulsive motion of a plate

A more detailed analysis of the transient Couette flow at short times may be carried out by neglecting the presence of the upper wall, and concentrating on the behavior of the flow near the moving wall. This is done by setting $d = \infty$ in the initial condition (7.6.2) and boundary conditions (7.6.3). cursory inspection reveals that the Fourier-series solution (7.6.12) is no longer useful in this limit.

The absence of a length scale associated with a channel of infinite width suggests that the time and space dependencies must combine into a unified variable which can be nondimensionalized by the kinematic viscosity. Recalling that the kinematic viscosity has units of length squared divided by time, we introduce the dimensionless variable

$$\eta \equiv \frac{y}{\sqrt{\nu t}}, \quad (7.6.14)$$

ranging from zero to infinity, and express the velocity in the form

$$u_x(y, t) = U f(\eta), \quad (7.6.15)$$

where $f(\eta)$ is a function of a single variable. This functional form implies that the velocity, as seen by an observer who finds herself at the position $y = \sqrt{\nu t}$, and is thus traveling upward with velocity $dy/dt = \sqrt{\nu/(4t)}$, remains constant. The initial and boundary conditions are satisfied provided that the function $f(\eta)$ satisfies the boundary condition $f(\eta = 0) = 1$, and the far-field condition $f(\eta = \infty) = 0$.

Substituting (7.6.15) into (7.6.1), we find

$$\rho \frac{\partial u_x}{\partial t} = \rho U \frac{df}{d\eta} \frac{\partial \eta}{\partial t} = \mu U \frac{\partial^2 u_x}{\partial y^2} = \mu \frac{d}{d\eta} \left(\frac{\partial \eta}{\partial y} \frac{df}{d\eta} \right) \frac{\partial \eta}{\partial y}. \quad (7.6.16)$$

Carrying out the differentiations, we obtain the second-order *nonlinear* ordinary differential equation

$$\frac{d^2 f}{d\eta^2} = -\frac{1}{2} \eta \frac{df}{d\eta}. \quad (7.6.17)$$

To compute the solution, we recast (7.6.17) into the form

$$\frac{d}{d\eta} \left(\ln \frac{df}{d\eta} \right) = -\frac{1}{2} \eta. \quad (7.6.18)$$

which may be integrated to yield

$$\frac{df}{d\eta} = A \exp\left(-\frac{\eta^2}{4}\right), \quad (7.6.19)$$

where A is a constant. Carrying out a second integration, we find

$$\begin{aligned} f(\eta) &= A \int_0^\eta \exp\left(-\frac{q^2}{4}\right) dq + B \\ &= 2A \int_0^{\eta/2} \exp(-v^2) dv + B, \end{aligned} \quad (7.6.20)$$

where B is a new integration constant, q is a dummy variable of integration, and $v \equiv q/2$.

The integral on the right-hand side of (7.6.20) is not available in analytical form. As an alternative, we express it in terms of the *error function* defined as

$$\operatorname{erf}(z) \equiv \frac{2}{\sqrt{\pi}} \int_0^z \exp(-v^2) dz, \quad (7.6.21)$$

or in terms of the *complementary error function* defined as

$$\operatorname{erfc}(z) = 1 - \operatorname{erf}(z). \quad (7.6.22)$$

Graphs of these functions are shown in figure 7.6.2. As z tends to infinity, the error function tends to the asymptotic value of unity; correspondingly, the complementary error function tends to vanish.

The frequent occurrence of the error function in various branches of mathematical physics has motivated its tabulation and representation in terms of various approximations. Subroutine *error_f* in directory *01_num_meth/12_spec_fnc* of *FDLIB* evaluates the error function and the complementary error function using an accurate algebraic approximation.

Returning to (7.6.20), we express the right-hand side in terms of the error function, and require $f(\eta = 0) = 1$, and $f(\eta = \infty) = 0$ to obtain $A = -1/\sqrt{\pi}$ and $B = 1$, yielding the velocity profile

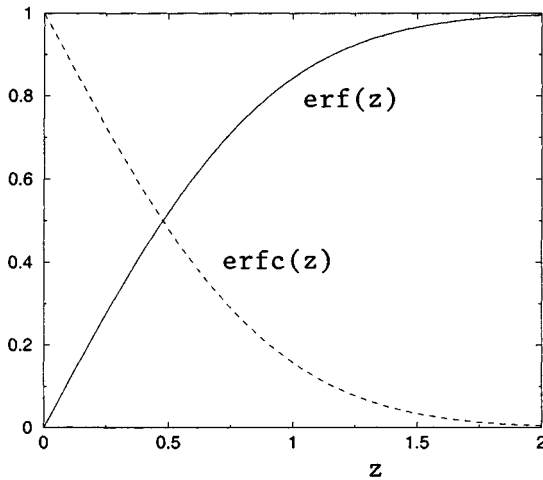


Figure 7.6.2 Graphs of the error function (solid line) and complementary error function (dashed line) defined in equations (7.6.20) and (7.6.21), computed using algebraic approximations.

$$u_x(y, t) = U f(\eta) = U \operatorname{erfc}\left(\frac{\eta}{2}\right). \quad (7.6.23)$$

The accompanying vorticity profile is given by

$$\omega_z(y, t) = -\frac{\partial u_x}{\partial y} = -U \frac{df}{d\eta} \frac{\partial \eta}{\partial y} = \frac{U}{\sqrt{\pi\nu t}} \exp\left(-\frac{y^2}{4\nu t}\right). \quad (7.6.24)$$

This expression illustrates explicitly the singular nature of the vorticity at the initial instant, and the spreading of the vorticity away from the moving wall due to viscous diffusion at later times.

The wall shear stress is given by

$$\sigma_{xy}(y = 0, t) = \mu \left(\frac{\partial u_x}{\partial y}\right)_{y=0} = -\frac{\mu U}{\sqrt{\pi\nu t}}. \quad (7.6.25)$$

This expression illustrates that an unphysical singularity occurs at the initial instant, as soon as the plate starts moving. In reality, a plate cannot start moving with constant velocity in an impulsive fashion; instead, its velocity must increase gradually from zero to the final value over a non-infinitesimal period of time, however small.

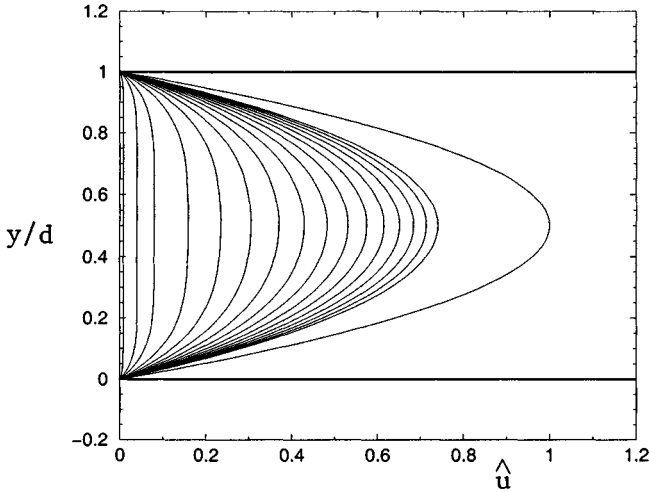


Figure 7.6.3 Transient pressure- or gravity-driven flow in a channel with parallel-sided walls separated by the distance d , due to the sudden application of a constant pressure gradient or sudden tilting, at dimensionless times $\hat{t} \equiv t\nu/d^2 = 0.001, 0.005, 0.010, 0.020, 0.030, \dots$. The parabolic line corresponds to the Hagen flow established at long times.

7.6.3 Transient pressure- or gravity-driven flow

As a second case study, we consider flow in a channel with stationary walls, where the motion is due to the sudden application of a constant pressure gradient or sudden tilting of the channel walls by a certain angle.

The x component of the equation of motion provides us with a partial differential equation for the x component of the velocity,

$$\rho \frac{\partial u_x}{\partial t} = \chi + \mu \frac{\partial^2 u_x}{\partial y^2} + \rho g_x. \quad (7.6.26)$$

The pressure field is given by equation (7.1.3), where the pressure gradient χ is a constant.

Working as in the case of transient Couette flow discussed previously in this section, and requiring that the velocity at the lower and upper wall vanishes at all times, we derive the transient velocity profile

$$u_x(y, t) = \frac{\chi + \rho g_x}{2\mu} [y(d - y) - \frac{8d^2}{\pi^3} \sum_{n=1,3,\dots}^{\infty} \frac{1}{n^3} \exp(-\frac{n^2\pi^2\nu}{d^2} t) \sin \frac{n\pi y}{d}]. \quad (7.6.27)$$

Subroutine *chan_2d_trans* in subdirectory *04_various/uni_flow_u* of *FDLIB* evaluates the profile at a specified time. A sequence of developing profiles of the dimensionless velocity $\hat{u} \equiv u_x/U$ is shown in figure 7.6.3, where U is the maximum velocity of the steady Hagen flow established at long times.

Problems

Problem 7.6.1 *Transient pressure-driven flow.*

Derive the transient velocity profile (7.6.27).

Problem 7.6.2 *Flow due to a constant shear stress.*

Show that the velocity field due to the application of a constant shear stress of magnitude τ on the planar boundary of a semi-infinite fluid occupying the upper half-space $y \geq 0$, is given by

$$u(y, t) = \frac{\tau}{\mu} \sqrt{\nu t} \left[\frac{2}{\sqrt{\pi}} \exp(-\frac{\eta^2}{4}) - \eta \operatorname{erfc}(\frac{\eta}{2}) \right], \quad (7.6.28)$$

where $\eta \equiv y/\sqrt{\nu t}$. Discuss the asymptotic behavior at long times.

7.7 Oscillatory flow in a channel

In Section 7.6, we discussed transient Couette flow and transient pressure- or gravity-driven flow. In all cases, vorticity enters the flow through the boundaries, and then diffuses to occupy the whole of the domain of flow. In this section, we consider the corresponding problems for oscillatory flow. The important new feature is that vorticity of alternating sign enters the flow across the boundaries, and cancellation by diffusion prevents the establishment of motion far from the boundaries.

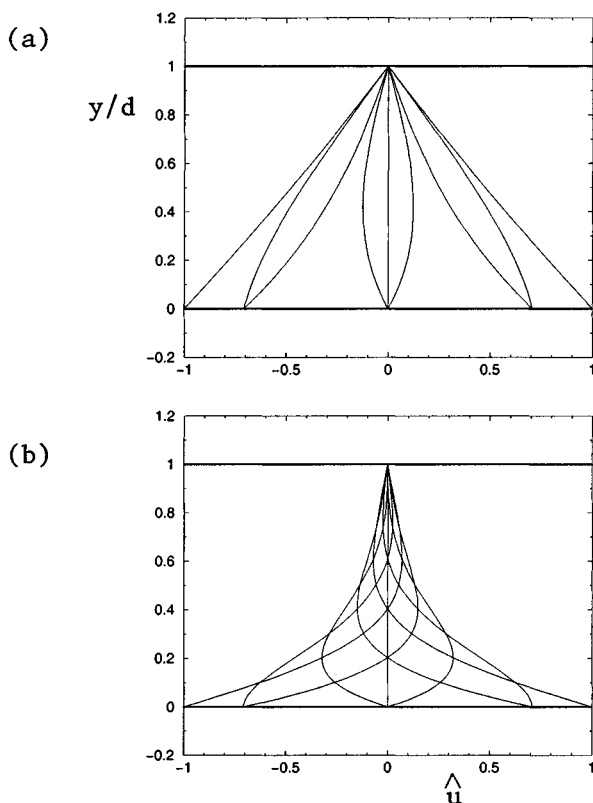


Figure 7.7.1 Velocity profiles of oscillatory Couette flow in a two-dimensional channel, at phase angles $\Omega t = 0, 0.25, 0.50, 0.75, 1.0, 1.25, 1.50, 1.75,$ and 2.0 , for Womersley number (a) $N_W = \sqrt{2}$, and (b) $\sqrt{30}$.

7.7.1 Oscillatory Couette flow

Suppose that the lower wall of a two-dimensional channel oscillates parallel to itself with velocity $U \cos(\Omega t)$, while the upper wall is stationary, thereby generating a time-periodic unidirectional flow, as illustrated in figure 7.7.1. The flow is governed by the unsteady diffusion equation (7.6.1), subject to the boundary conditions

$$u_x(y = 0) = U \cos(\Omega t), \quad u_x(y = d) = 0, \quad (7.7.1)$$

for $t \geq 0$.

Anticipating that the flow will be periodic in time, we express the velocity in the form

$$u_x(y, t) = U [f_c(y) \cos(\Omega t) + f_s(y) \sin(\Omega t)]. \quad (7.7.2)$$

To compute the functions $f_c(y)$ and $f_s(y)$, we substitute (7.7.2) into (7.6.1), carry out the time differentiation, collect the coefficients of the sines and cosines, and then set the compiled expressions equal to zero to obtain two linear coupled ordinary differential equations,

$$\frac{d^2 f_s}{dy^2} = -\frac{\Omega}{\nu} f_c, \quad \frac{d^2 f_c}{dy^2} = \frac{\Omega}{\nu} f_s, \quad (7.7.3)$$

where $\nu \equiv \mu/\rho$ is the kinematic viscosity.

To expedite the solution, we introduce the imaginary unit i , defined such that $i^2 = -1$, and the complex function

$$f(y) \equiv f_c(y) + i f_s(y). \quad (7.7.4)$$

Subject to this definition, the two equations in (7.7.3) combine into the single complex form

$$\frac{d^2 f}{dy^2} = -i \frac{\Omega}{\nu} f. \quad (7.7.5)$$

The real and imaginary parts of the complex equation (7.7.5) are equal, respectively, to the second and first of equations (7.7.3). Moreover, using the Euler decomposition $\exp(-i \Omega t) = \cos(\Omega t) - i \sin(\Omega t)$, we find that u_x is given by the real part of the complex function

$$w(y, t) \equiv U f(y) \exp(-i \Omega t). \quad (7.7.6)$$

The imaginary part of $w(y, t)$ also satisfies the governing equation (7.6.1).

The solution of (7.7.5) is readily found to be

$$f(y) = A \exp\left(y \sqrt{-i \frac{\Omega}{\nu}}\right) + B \exp\left(-y \sqrt{-i \frac{\Omega}{\nu}}\right), \quad (7.7.7)$$

where A and B are two complex constants, with the understanding that, if β is a positive or negative real number, then

$$\begin{aligned} \exp(\beta\sqrt{-i}) &= \exp\left[\frac{\beta}{\sqrt{2}}(-1+i)\right] = \exp\left(-\frac{\beta}{\sqrt{2}}\right) \exp\left(i\frac{\beta}{\sqrt{2}}\right) \\ &= \exp\left(-\frac{\beta}{\sqrt{2}}\right) \left[\cos\left(\frac{\beta}{\sqrt{2}}\right) + i \sin\left(\frac{\beta}{\sqrt{2}}\right)\right]. \end{aligned} \quad (7.7.8)$$

The no-slip boundary conditions (7.7.1) require $f(0) = 1$ and $f(d) = 0$. Using these equations to evaluate A and B , we find

$$A = \frac{\exp(-d\sqrt{-i\frac{\Omega}{\nu}})}{\exp(-d\sqrt{-i\frac{\Omega}{\nu}}) - \exp(d\sqrt{-i\frac{\Omega}{\nu}})} = \frac{1}{1 - \exp(2d\sqrt{-i\frac{\Omega}{\nu}})},$$

$$B = 1 - A. \quad (7.7.9)$$

Substituting these expressions into (7.7.6), and rearranging, we derive the complex function

$$f(y) = \frac{\exp(y\sqrt{-i\frac{\Omega}{\nu}}) - \exp[(2d-y)\sqrt{-i\frac{\Omega}{\nu}}]}{1 - \exp(2d\sqrt{-i\frac{\Omega}{\nu}})}, \quad (7.7.10)$$

whose real and imaginary parts provide us with the velocity according to equations (7.7.4) and (7.7.2). Subroutine *chan_2d_osc* in directory *04_various/uni_flow_u* of *FDLIB* evaluates the velocity profile for a specified angular frequency and reduced temporal phase angle Ωt .

The argument of the exponentials on the right-hand side of (7.7.10) suggests that the structure of the flow is determined by the reduced angular frequency expressed by the *Womersley number*

$$N_W \equiv d\sqrt{\frac{\Omega}{\nu}}. \quad (7.7.11)$$

Figure 7.7.1 illustrates profiles of the dimensionless velocity $\hat{u} \equiv u_x/U$ at $\Omega t = 0, 0.25, 0.50, 0.75, 1.0, 1.25, 1.50, 1.75,$ and 2.0 , for $N_W = \sqrt{2}$ and $\sqrt{30}$. When the Womersley number is small, the flow evolves in quasi-steady fashion, and the velocity profile is nearly linear at all times. As the Womersley number is raised, the motion is confined within a boundary layer close to the moving wall, and the rest of the fluid is virtually stationary.

7.7.2 Rayleigh's oscillating plate

To investigate the behavior at high frequencies or large channel widths, we consider the structure of the flow at large values of the Womersley number. In this limit, the second term in the numerator and the second term in the denominator on the right-hand side of (7.7.10) become exponentially small, leaving the simplified form

$$\begin{aligned} f(y) &= \exp\left(y \sqrt{-i \frac{\Omega}{\nu}}\right) \\ &= \exp\left(-y \sqrt{\frac{\Omega}{2\nu}}\right) \left[\cos\left(y \sqrt{\frac{\Omega}{2\nu}}\right) + i \sin\left(y \sqrt{\frac{\Omega}{2\nu}}\right)\right]. \end{aligned} \quad (7.7.12)$$

The associated velocity profile is given by

$$\begin{aligned} u_x(y, t) &= U \exp\left(-y \sqrt{\frac{\Omega}{2\nu}}\right) \\ &\quad \times \left[\cos(\Omega t) \cos\left(y \sqrt{\frac{\Omega}{2\nu}}\right) + \sin(\Omega t) \sin\left(y \sqrt{\frac{\Omega}{2\nu}}\right)\right] \\ &= U \exp\left(-y \sqrt{\frac{\Omega}{2\nu}}\right) \cos\left(\Omega t - y \sqrt{\frac{\Omega}{2\nu}}\right). \end{aligned} \quad (7.7.13)$$

Subroutine `plate_osc` in directory `04_various/uni_flow_u` of `FDLIB` evaluates this velocity profile at a specified time.

Expression (7.7.13) shows that the magnitude of the velocity decays at an exponential rate with respect to distance from the oscillating wall. The region where substantial fluid motion is established is identified as the *Stokes boundary layer*. A rough measure of the thickness of this boundary layer, denoted by δ , is the distance where the magnitude of the argument of the exponential on the right-hand side of (7.7.13) is equal to unity, yielding

$$\delta = \sqrt{\frac{2\nu}{\Omega}}. \quad (7.7.14)$$

Aside from the factor 2 in the numerator, this estimate could have been deduced at the outset on the basis of dimensional analysis.

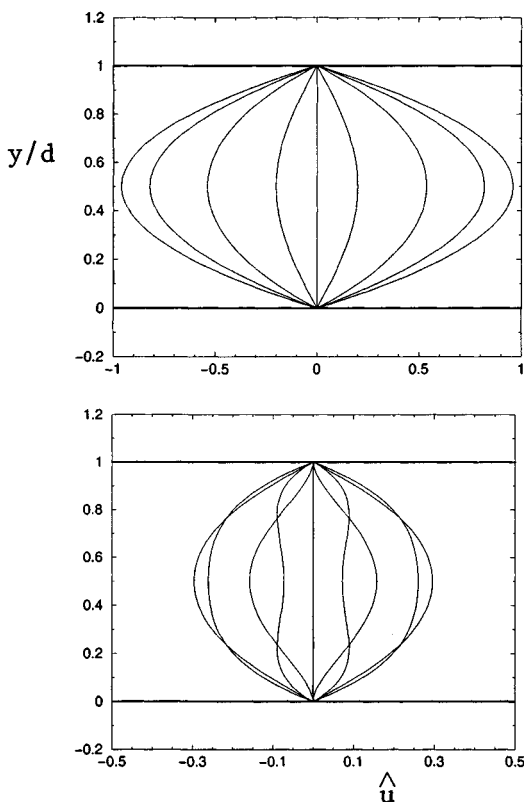


Figure 7.7.2 Velocity profiles of pulsating pressure-driven flow in a two-dimensional channel, at phase angles $\Omega t = 0, 0.25, 0.50, 0.75, 1.0, 1.25, 1.50, 1.75, 2.0$, for Womersley number (a) $N_W = \sqrt{2}$, and (b) $\sqrt{30}$.

7.7.3 Pulsating pressure-driven flow

As a last case study, we consider pulsating flow in a channel due to an oscillatory pressure gradient. The pressure field is given by equation (7.1.3), where $\chi = \bar{\chi} \sin(\Omega t)$. Thus, the pressure gradient varies harmonically in time with angular frequency Ω and amplitude $\bar{\chi}$.

Working as previously for oscillatory Couette flow, we express the velocity in the form

$$u_x(y, t) = -\frac{\bar{\chi}}{\rho \Omega} [f_c(y) \cos(\Omega t) + f_s(y) \sin(\Omega t)], \quad (7.7.15)$$

and introduce the complex function

$$f(y) = f_c(y) + i f_s(y), \quad (7.7.16)$$

which is required to satisfy the boundary conditions $f(0) = 0$ and $f(d) = 0$. The solution is found to be

$$f(y) = 1 - \frac{\cosh\left[\left(\frac{2y}{d} - 1\right) \frac{d}{2} \sqrt{\frac{-i\Omega}{\nu}}\right]}{\cosh\left(\frac{d}{2} \sqrt{\frac{-i\Omega}{\nu}}\right)}, \quad (7.7.17)$$

where the hyperbolic cosine of the complex argument on the right-hand side is computed by decomposing it into real exponentials, and using the definition $\cosh z \equiv [\exp(z) + \exp(-z)]/2$ in conjunction with (7.7.8). Subroutine *chan_2d_wom* in directory *04_various/uni_flow_u* of *FDLIB* evaluates the velocity profile using the preceding expressions.

Figure 7.7.2 presents two time sequences of profiles of the dimensionless velocity $\hat{u} \equiv u_x/U$ at a low and a moderate value of the Womersley number; U is the maximum velocity of the steady Hagen flow. At low frequencies, the motion is quasi-steady, and the velocity profile is nearly parabolic at all times. At high frequencies, the flow consists of a core oscillating in a plug-flow mode, and two Stokes boundary layers, one attached to each wall (problem 7.7.2). One interesting feature of the motion is that, under certain conditions, the amplitude of the velocity at the edges of the boundary layers may exceed that in the central core.

Problems

Problem 7.7.1 *Wall shear stress on an oscillating plate.*

(a) Derive the following expression for the shear stress exerted on an oscillating plate corresponding to the velocity profile (7.7.13),

$$\sigma_{xy}(y = 0, t) = U \sqrt{\mu \rho \Omega} \cos(\Omega t - \frac{3\pi}{4}). \quad (7.7.18)$$

(b) Expression (7.7.18) reveals that the wall shear stress lags behind the wall velocity by the phase $3\pi/4$, independent of the angular frequency. Does a similar independence arise in the case of channel flow where the velocity profile is given by (7.7.2), (7.7.4), and (7.7.10)?

Problem 7.7.2 *Womersley flow.*

Show that, at high values of the Womersley number, equation (7.7.17) assumes the approximate form

$$f(y) = 1 - \exp\left(y \sqrt{\frac{-i\Omega}{\nu}}\right) - \exp\left[(d-y) \sqrt{\frac{-i\Omega}{\nu}}\right], \quad (7.7.19)$$

thereby confirming the development of a plug-flow core and two Stokes boundary layers, one attached to each wall.

7.8 Transient and oscillatory flow in a circular tube

The study of transient and oscillatory channel flow undertaken in Sections 7.6 and 7.7 has revealed the physical mechanisms by which momentum is transmitted, and vorticity diffuses away from planar boundaries in an unsteady flow. In this section, we illustrate corresponding mechanisms for curved boundaries by studying unsteady unidirectional tube flow.

7.8.1 Transient Poiseuille flow

First, we consider transient flow in a cylindrical tube of radius a due to the sudden application of a pressure gradient or due to sudden tilting, and describe the motion in cylindrical polar coordinates with the x axis along the tube centerline. The axial component of the velocity is a function of distance from the x axis and time, $u_x(\sigma, t)$; the radial and meridional components vanish. The pressure field is given by equation (7.3.1), where the axial pressure gradient χ is a constant. The no-slip boundary condition requires that the velocity vanish at the surface of the tube at all times, $u_x(\sigma = a, t) = 0$.

Simplifying the x component of the equation of motion written in cylindrical polar coordinates, we obtain a partial differential equation for the axial velocity,

$$\rho \frac{\partial u_x}{\partial t} = \chi + \mu \left(\frac{\partial^2 u_x}{\partial \sigma^2} + \frac{1}{\sigma} \frac{\partial u_x}{\partial \sigma} \right) + \rho g_x. \quad (7.8.1)$$

At the initial instant, the fluid is quiescent. At long times, we anticipate that the flow will reach a steady state, and the velocity profile will assume

the parabolic form described by the Poiseuille solution (7.3.4), repeated here for ready reference,

$$u_x^{ss}(\sigma) = \frac{\chi + \rho g x}{4 \mu} (a^2 - \sigma^2). \quad (7.8.2)$$

To compute the solution of (7.8.1), we decompose the velocity into the Poiseuille profile and a transient profile that decays at long times,

$$u_x(\sigma, t) = u_x^{ss}(\sigma) + u_x^T(\sigma, t). \quad (7.8.3)$$

Substituting (7.8.3) into (7.8.1), we find that the transient component $u_x^T(\sigma, t)$ satisfies the homogeneous equation

$$\frac{\partial u_x^T}{\partial t} = \nu \left(\frac{\partial^2 u_x^T}{\partial \sigma^2} + \frac{1}{\sigma} \frac{\partial u_x^T}{\partial \sigma} \right), \quad (7.8.4)$$

where $\nu \equiv \mu/\rho$ is the kinematic viscosity.

Separation of variables

The solution of (7.8.4) may be found by the method of separation of variables based on the expansion

$$u_x^T(\sigma, t) = \sum_{n=1}^{\infty} c_n \phi_n(\sigma) \psi_n(t), \quad (7.8.5)$$

where c_n are constant coefficients, and $\phi_n(\sigma)$, $\psi_n(t)$ are unknown functions of their respective arguments. Substituting this expansion into (7.8.4), carrying out the differentiation, and rearranging, we obtain

$$\sum_{n=1}^{\infty} c_n \phi_n(\sigma) \psi_n(t) \left[\frac{1}{\psi_n} \frac{d\psi_n}{dt} - \frac{\nu}{\phi_n} \left(\frac{d^2 \phi_n}{d\sigma^2} + \frac{1}{\sigma} \frac{d\phi_n}{d\sigma} \right) \right] = 0. \quad (7.8.6)$$

For this equality to hold true for any value of σ and t , the expression enclosed by the square brackets on the right-hand side must vanish, yielding

$$\frac{1}{\psi_n} \frac{d\psi_n}{dt} = \frac{\nu}{\phi_n} \left(\frac{d^2 \phi_n}{d\sigma^2} + \frac{1}{\sigma} \frac{d\phi_n}{d\sigma} \right) = -\nu b_n^2, \quad (7.8.7)$$

where b_n^2 is a positive constant; the right-hand side of (7.8.7) was designed to facilitate forthcoming algebraic manipulations. Rearranging the two equalities inherent in (7.8.7), we derive two ordinary differential equations,

$$\frac{d\psi_n}{dt} = -\nu b_n^2 \psi_n, \quad \frac{d^2\phi_n}{d\sigma^2} + \frac{1}{\sigma} \frac{d\phi_n}{d\sigma} + b_n^2 \phi_n = 0. \quad (7.8.8)$$

The solution of the first equation is readily found to be

$$\psi_n(t) = \exp(-\nu b_n^2 t), \quad (7.8.9)$$

which reveals that the transient flow decays in an exponential fashion with respect to time.

Bessel functions

To find the solution of the second of equations (7.8.8), we introduce the Bessel function of the first kind $J_0(z)$ which, by definition, satisfies the zeroth-order Bessel equation

$$\begin{aligned} z \frac{d}{dz} \left(z \frac{dJ_0(z)}{dz} \right) + z^2 J_0(z) \\ = z^2 \frac{d^2 J_0(z)}{dz^2} + z \frac{dJ_0(z)}{dz} + z^2 J_0(z) = 0, \end{aligned} \quad (7.8.10)$$

and is also required to be finite for every value of the real variable z between, and including, zero and infinity.

The frequent occurrence of J_0 in various branches of mathematical physics has motivated its tabulation and representation in terms of infinite series and approximations. Subroutine *bess_J0* in directory *01_num_meth/12_spec_fnc* of *FDLIB* evaluates J_0 using an accurate algebraic approximation. The graph of $J_0(z)$ is shown with the solid line in figure 7.8.1.

Replacing z in Bessel's equation (7.8.10) with $b_n\sigma$, and simplifying, we find that the function

$$\phi_n(\sigma) = J_0(b_n\sigma) \quad (7.8.11)$$

satisfies the second of equations (7.8.8), and is thus the desired solution. To satisfy the no-slip boundary condition, we require

$$\phi_n(a) = J_0(b_n a) = 0, \quad (7.8.12)$$

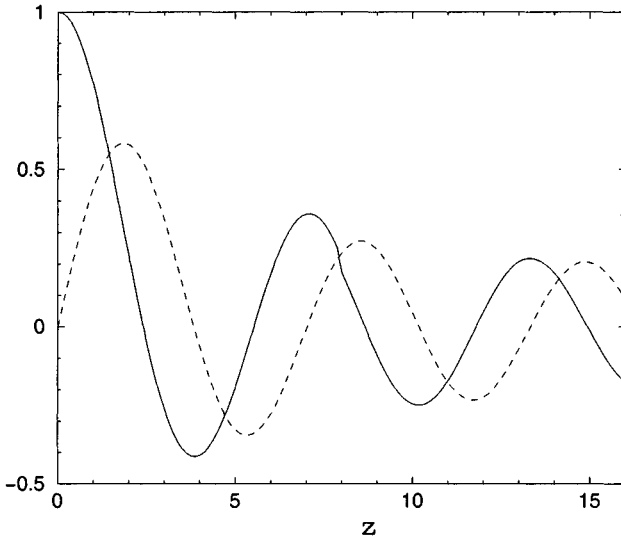


Figure 7.8.1 Graphs of the Bessel functions $J_0(z)$ and $J_1(z)$ drawn, respectively, with the solid and dashed line, arising in the computation of transient tube flow.

which shows that $b_n a$ is a root of $J_0(z)$, denoted by α_n . The first seven roots are known to be:

$$\begin{aligned} \alpha_1 = 2.4048, \quad \alpha_2 = 5.5201, \quad \alpha_3 = 8.6537, \quad \alpha_4 = 11.7915, \\ \alpha_5 = 14.9309, \quad \alpha_6 = 18.0711, \quad \alpha_7 = 21.2116. \end{aligned} \quad (7.8.13)$$

Accordingly, we set

$$b_n = \frac{\alpha_n}{a}. \quad (7.8.14)$$

Substituting (7.8.14) into (7.8.11) and (7.8.9), and the result into (7.8.5), we derive the expansion

$$u_x^T(\sigma, t) = \sum_{n=1}^{\infty} c_n J_0\left(\frac{\alpha_n \sigma}{a}\right) \exp\left(-\frac{\alpha_n^2 \nu t}{a^2}\right). \quad (7.8.15)$$

The representation (7.8.15) clearly satisfies the requirement that the transient flow decays at long times. To also satisfy the initial condition $u_x(\sigma, t = 0) = 0$, we evaluate the decomposition (7.8.3) at $t = 0$, and use (7.8.2) and (7.8.15) to obtain

$$\sum_{n=1}^{\infty} c_n J_0\left(\frac{\alpha_n \sigma}{a}\right) = -\frac{\chi + \rho g_x}{4\mu} (a^2 - \sigma^2). \quad (7.8.16)$$

The coefficients c_n must be such that this representation holds true for any value of σ .

Orthogonality of the zeroth order Bessel functions

To extract the coefficients c_n from (7.8.16), we use the following orthogonality property of the Bessel functions

$$\int_0^1 z J_0(\alpha_n z) J_0(\alpha_m z) dz = \begin{cases} \frac{1}{2} J_1^2(\alpha_n) & \text{if } n = m \\ 0 & \text{if } n \neq m \end{cases}, \quad (7.8.17)$$

where $J_1(z)$ is the Bessel function of the first kind. By definition, $J_1(z)$ satisfies the differential equation

$$z^2 \frac{d^2 J_1(z)}{dz^2} + z \frac{dJ_1(z)}{dz} + (z^2 - 1) J_1(z) = 0, \quad (7.8.18)$$

and is required to be finite for every value of z between, and including, zero and infinity. Subroutine *bess_J1* in directory *01_num.meth/12_spec.fnc* of *FDLIB* evaluates J_1 using an accurate algebraic approximation. The graph of $J_1(z)$ is shown with the dashed line in figure 7.8.2.

Replacing z in identity (7.8.17) with σ/a , and rearranging, we find

$$\int_0^a \sigma J_0\left(\frac{\alpha_n \sigma}{a}\right) J_0\left(\frac{\alpha_m \sigma}{a}\right) d\sigma = \begin{cases} \frac{1}{2} a^2 J_1^2(\alpha_n) & \text{if } n = m \\ 0 & \text{if } n \neq m \end{cases}. \quad (7.8.19)$$

Inspired by this identity, we multiply both sides of (7.8.16) by $\sigma J_0(\alpha_m \sigma/a)$, integrate with respect to σ from 0 to a , use the orthogonality property (7.8.19), and then switch m to n to find

$$\begin{aligned} c_n &= -\frac{\chi + \rho g_x}{2\mu a^2 J_1^2(\alpha_n)} \int_0^a J_0\left(\frac{\alpha_n \sigma}{a}\right) (a^2 - \sigma^2) \sigma d\sigma \\ &= -\frac{\chi + \rho g_x}{2\mu J_1^2(\alpha_n)} a^2 \int_0^1 J_0(\alpha_n v) (1 - v^2) v dv, \end{aligned} \quad (7.8.20)$$

where we have set $v \equiv \sigma/a$. To compute the last integral, we replace z in Bessel's equation (7.8.10) with $\alpha_n v$, and simplify to obtain

$$\alpha_n^2 v J_0(\alpha_n v) = -\frac{d}{dv} \left(v \frac{dJ_0(\alpha_n v)}{dv} \right). \quad (7.8.21)$$

Note that the left- and thus the right-hand side of (7.8.21) vanishes when $v = 0$ or 1. Integrating both sides of (7.8.21) with respect to v from 0 to 1, we find

$$\begin{aligned} & \alpha_n^2 \int_0^1 J_0(\alpha_n v) v \, dv \\ &= -\left[v \frac{dJ_0(\alpha_n v)}{dv} \right]_{v=1} + \left[v \frac{dJ_0(\alpha_n v)}{dv} \right]_{v=0} = \alpha_n J_1(\alpha_n), \end{aligned} \quad (7.8.22)$$

where the last expression was derived using the identity $dJ_0(z)/dz = -J_1(z)$. A similar computation yields

$$\begin{aligned} & \alpha_n^2 \int_0^1 J_0(\alpha_n v) v^3 \, dv = -\int_0^1 v^2 \frac{d}{dv} \left(v \frac{dJ_0(\alpha_n v)}{dv} \right) \, dv \\ &= -\left(v^3 \frac{dJ_0(\alpha_n v)}{dv} \right)_{v=1} + \left(v^3 \frac{dJ_0(\alpha_n v)}{dv} \right)_{v=0} + 2 \int_0^1 v^2 \frac{dJ_0(\alpha_n v)}{dv} \, dv \\ &= \alpha_n J_1(\alpha_n) + 2 \left[v^2 J_0(\alpha_n v) \right]_{v=1} - 2 \left[v^2 J_0(\alpha_n v) \right]_{v=0} \\ &- 4 \int_0^1 v J_0(\alpha_n v) \, dv = \left(\alpha_n - \frac{4}{\alpha_n} \right) J_1(\alpha_n). \end{aligned} \quad (7.8.23)$$

Substituting (7.8.22) and (7.8.23) into (7.8.20), we obtain the desired result

$$c_n = -\frac{\chi + \rho g_x}{\mu J_1(\alpha_n) \alpha_n^3} 2 a^2. \quad (7.8.24)$$

Finally, we substitute (7.8.24) into (7.8.15), and then into (7.8.3), and derive the velocity profile

$$u_x(\sigma, t) = \frac{\chi + \rho g_x}{4 \mu} \left[a^2 - \sigma^2 - 8 a^2 \sum_{n=1}^{\infty} \frac{1}{\alpha_n^3} \frac{J_0(\alpha_n \sigma/a)}{J_1(\alpha_n)} \exp\left(-\frac{\alpha_n^2 \nu t}{a^2}\right) \right]. \quad (7.8.25)$$

Subroutine *tube_crc_trans* in directory *04_various/uni_flow_u* of *FDLIB* evaluates the velocity described by (7.8.25). A time sequence of profiles is similar to that illustrated in figure 7.6.3 for channel flow.

7.8.2 Pulsating pressure-driven flow

Consider next pulsating flow in a circular tube due to an oscillatory pressure gradient. The no-slip boundary condition requires that the velocity vanish at all times over the tube wall. The pressure field is given by equation (7.3.1), where $\chi = \bar{\chi} \sin(\Omega t)$: the pressure gradient varies harmonically in time with angular frequency Ω and amplitude $\bar{\chi}$.

Working as in Section 7.7 for pulsating channel flow, we express the velocity in the form

$$u_x(\sigma, t) = -\frac{\bar{\chi}}{\rho\Omega} [f_c(\sigma) \cos(\Omega t) + f_s(\sigma) \sin(\Omega t)], \quad (7.8.26)$$

and introduce the complex function

$$f(\sigma) = f_c(\sigma) + i f_s(\sigma), \quad (7.8.27)$$

which is required to satisfy the boundary condition $f(a) = 0$. The solution is found to be

$$f(\sigma) = 1 - \frac{J_0(\sigma \sqrt{\frac{-i\Omega}{\nu}})}{J_0(a \sqrt{\frac{-i\Omega}{\nu}})}, \quad (7.8.28)$$

(problem 7.8.1), with the understanding that, if β is a positive real number, then

$$J_0(\beta\sqrt{-i}) = ber_0(\beta) + i bei_0(\beta), \quad (7.8.29)$$

where *ber*₀ and *bei*₀ are the zeroth order Kelvin functions. Subroutine *ber_bei_0* in directory *01_num_meth/12_spec_fnc* of *FDLIB* evaluates the Kelvin functions using functional approximations. Graphs of these functions are displayed in figure 7.8.2.

The functional form of the arguments of the Bessel functions on the right-hand side of (7.8.28) suggests that the structure of the flow is determined by the reduced angular frequency expressed by the *Womersley number*

$$N_W \equiv \frac{1}{2} a \sqrt{\frac{\Omega}{\nu}}, \quad (7.8.30)$$

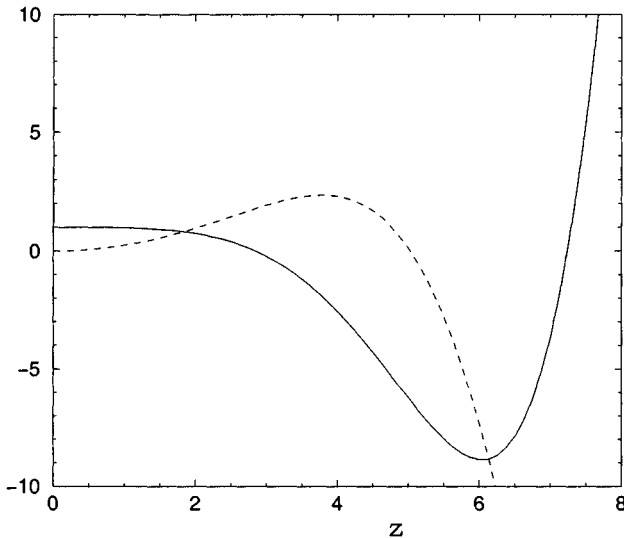


Figure 7.8.2 Graphs of the Kelvin functions $ber_0(z)$ and $bei_0(z)$ plotted, respectively, with the solid and dashed line, arising in the computation of oscillatory tube flow.

which is the counterpart of the Womersley number for channel flow defined in equation (7.7.11).

Subroutine *tube_crc_wom* in directory *04_various/uni_flow_u* of *FDLIB* evaluates the velocity profile using the expressions presented in this section. A time sequence of profiles is similar to that displayed in figure 7.7.3 for channel flow. At low frequencies, the flow is nearly quasi-steady and the velocity profile is nearly parabolic. At high frequencies, the flow consists of a central core oscillating in a plug-flow mode, and a Stokes boundary layer attached to the cylindrical wall. As in the case of channel flow, the amplitude of the velocity at the edge of the boundary layers may exceed that in the central core.

7.8.3 Bessel functions

We have seen that Bessel functions arise in the computation of flow in an axisymmetric domain. In concluding this section, we state an orthogonality property that is useful in evaluating the coefficients of Bessel expansions; an example is shown in (7.8.14).

First, we note that, by definition, the p th order Bessel function of the first kind $J_p(z)$, satisfies the p th order Bessel equation

$$\begin{aligned} z \frac{d}{dz} \left(z \frac{dJ_p(z)}{dz} \right) + (z^2 - p^2) J_p(z) \\ = z^2 \frac{d^2 J_p(z)}{dz^2} + z \frac{dJ_p(z)}{dz} + (z^2 - p^2) J_p(z) = 0, \end{aligned} \quad (7.8.31)$$

and is required to be finite for every value of z between, and including, zero and infinity. The particular cases $p = 0$ and 1 are shown in equations (7.8.10) and (7.8.18).

The orthogonality property of the Bessel functions is stated as follows: if α_n and α_m are two zeros of $J_p(z)$, then

$$\begin{aligned} \int_0^1 z J_p(\alpha_n z) J_p(\alpha_m z) dz \\ = \begin{cases} \frac{1}{2} J_{p+1}^2(\alpha_n) = \frac{1}{2} J_{p-1}^2(\alpha_n) = \frac{1}{2} J_p'^2(\alpha_n) & \text{if } n = m \\ 0 & \text{if } n \neq m \end{cases} \end{aligned} \quad (7.8.32)$$

It is illuminating to observe that the Bessel orthogonality property is analogous to the Fourier orthogonality property exhibited by trigonometric functions, as shown, for example, in equations (7.4.19).

Problems

Problem 7.8.1 *Pulsating pressure-driven flow.*

Derive the velocity profile given by (7.8.26) - (7.8.28).

Problem 7.8.2 *Transient swirling flow.*

(a) Show that the meridional velocity of an unsteady swirling flow with circular streamlines satisfies the linear partial differential equation

$$\frac{\partial u_\varphi}{\partial t} = \nu \left(\frac{\partial^2 u_\varphi}{\partial \sigma^2} + \frac{1}{\sigma} \frac{\partial u_\varphi}{\partial \sigma} - \frac{u_\varphi}{\sigma^2} \right), \quad (7.8.33)$$

where $\nu \equiv \mu/\rho$ is the kinematic viscosity.

(b) Consider transient flow in the interior of a hollow circular cylinder of radius a filled with a fluid. At the origin of time, the cylinder starts rotating suddenly around its axis with constant angular velocity Ω . Derive the following expression for the transient profile

$$u_{\varphi}(\sigma, t) = \Omega [\sigma + 2a \sum_{n=1}^{\infty} \frac{1}{\alpha_n} \frac{J_1(\alpha_n \sigma/a)}{J_0(\alpha_n)} \exp(-\frac{\alpha_n^2 \nu t}{a^2})], \quad (7.8.34)$$

where α_n are the positive zeros of the Bessel function J_1 . At long times, the summed terms on the right-hand side of (7.8.34) vanish, leaving a velocity field that expresses rigid-body rotation.

Computer problem

Problem c.7.8.1 *Transient swirling flow.*

Subroutine *tube_crc_sw* in directory *04_various/uni_flow_u* of *FDLIB* evaluates the velocity profile of transient swirling flow described by equation (7.8.34). Compute and plot profiles at a sequence of times, and discuss the consequences of truncating the infinite sum on the right-hand side.

Chapter 8

Finite-Difference Methods

- 8.1 Choice of governing equations**
- 8.2 Unidirectional flow;
velocity/pressure formulation**
- 8.3 Unidirectional flow;
velocity/vorticity formulation**
- 8.4 Unidirectional flow;
stream function/vorticity formulation**
- 8.5 Two-dimensional flow;
stream function/vorticity formulation**
- 8.6 Velocity/pressure formulation**
- 8.7 Operator splitting and solenoidal projection**

In previous chapters, we have discussed the equations governing the structure of a steady flow and the evolution of an unsteady flow, and derived selected solutions for simple flow configurations by analytical and numerical methods. To generate solutions for arbitrary boundary geometries and flow conditions, it is necessary to develop general-purpose numerical methods. In this chapter, we discuss the choice of governing equations and the implementation of finite-difference methods for incompressible Newtonian flow.

8.1 Choice of governing equations

General-purpose methods for computing the flow of an incompressible fluid may be classified into two categories distinguished by the choice of governing equations, as follows:

- In the first class of methods, the flow is described in terms of primary variables including the velocity and the pressure. The structure of the velocity and pressure field in a steady flow, and the evolution

of the velocity and pressure field in an unsteady flow, are computed by solving the Navier-Stokes equation and the continuity equation, subject to appropriate boundary conditions, initial conditions, and possibly supplementary constraints.

- In the second class of methods, the flow is computed on the basis of the vorticity transport equation. The numerical procedure involves two stages: compute the structure or evolution of the vorticity field using the vorticity transport equation discussed in Section 6.6, and obtain the simultaneous structure or evolution of the velocity field by inverting the equation defining the vorticity

$$\omega = \nabla \times \mathbf{u}, \quad (8.1.1)$$

subject to constraints imposed by the continuity equation and boundary conditions; by inverting (8.1.1), we mean solving for \mathbf{u} in terms of ω . Descendant methods are distinguished by the particular procedure used to recover the velocity field from the known vorticity distribution.

The strengths and weaknesses of the aforementioned two general classes of methods will become apparent as we describe their implementation. One appealing feature of the second class of methods based on the vorticity transport equation is the lack of need to solve for the pressure, which is desirable when boundary conditions for the pressure are not specified and must be derived. Disadvantages include the need to derive boundary conditions for the vorticity.

Problem

Problem 8.1.1 *Inversion of the vorticity.*

Show that, if \mathbf{u} is a velocity field corresponding to a certain vorticity field ω , then $\mathbf{u} + \nabla f$, where f is a smooth scalar function, corresponds to the same vorticity field. Explain why, for the velocity field to be solenoidal, $\nabla \cdot \mathbf{u} = 0$, the function f must be harmonic; that is, it must satisfy Laplace's equation $\nabla^2 f = 0$.

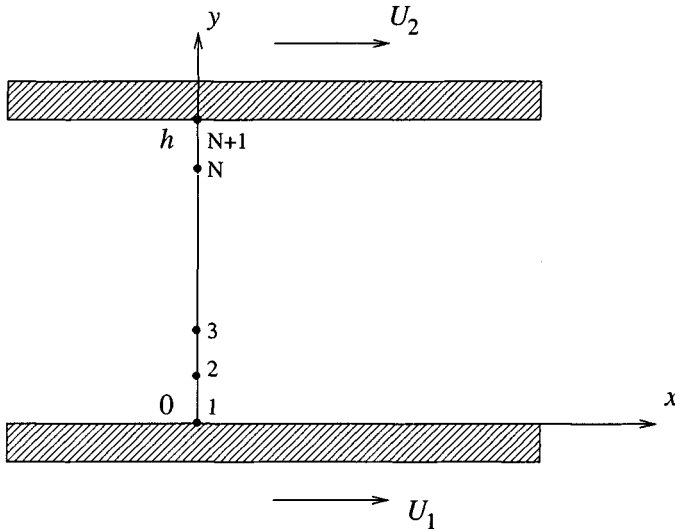


Figure 8.2.1 A one-dimensional finite-difference used to compute the velocity profile of unidirectional channel flow.

8.2 Unidirectional flow; velocity/pressure formulation

We begin developing finite-difference methods by considering the velocity-pressure formulation for unidirectional flow in a channel confined between two parallel walls located at $y = 0$ and $y = h$, as illustrated in figure 8.2.1. The lower and upper wall move parallel to themselves along the x axis with generally time-dependent velocities $U_1(t)$ and $U_2(t)$.

Channel flow may occur under two complementary sets of conditions reflecting the physical mechanism that drives the motion. In the first case, the flow rate along the channel $Q(t)$ is specified, and the stream-wise pressure gradient $\partial p(t)/\partial x$ is computed as part of the solution. In the second case, the pressure gradient is specified, and the flow rate is computed as part of the solution. In this section, we shall consider the case of flow due to a specified, possibly time-dependent, pressure gradient. In Section 8.4, we shall consider the complementary case of flow subject to a specified flow rate.

8.2.1 Governing equations

To set up the mathematical formulation, we consider the x component of the equation of motion which, in the case of unidirectional flow, simplifies to

$$\frac{\partial u_x}{\partial t} = -\frac{1}{\rho} \frac{\partial p}{\partial x} + \nu \frac{\partial^2 u_x}{\partial y^2} + g_x, \quad (8.2.1)$$

where ρ is the fluid density, ν is the kinematic viscosity, and g_x is the x component of the acceleration of gravity. Equation (8.2.1) is to be solved subject to a specified initial condition and to the possibly time-dependent velocity boundary conditions

$$u_x(y=0) = U_1(t), \quad u_x(y=h) = U_2(t), \quad (8.2.2)$$

requiring no-slip at the walls.

8.2.2 Explicit finite-difference method

To implement the finite-difference method, we divide the cross-section of the channel extending over $0 \leq y \leq h$ into N intervals defined by $N+1$ grid points, as shown in figure 8.2.1. For convenience, we denote the x component of the velocity at the i grid point as $u_i(t) \equiv u_x(y_i, t)$.

Next, we evaluate both sides of (8.2.1) at the i th *interior* grid point at time t , where $i = 2, 3, \dots, N$, and approximate the time derivative on the left-hand side with a first-order forward finite difference and the second derivative on the right-hand side with a second-order centered finite difference, to obtain the finite-difference equation, FDE,

$$\frac{u_i(t + \Delta t) - u_i(t)}{\Delta t} = -\frac{1}{\rho} \frac{\partial p}{\partial x}(t) + \nu \frac{u_{i+1}(t) - 2u_i(t) + u_{i-1}(t)}{\Delta y^2} + g_x. \quad (8.2.3)$$

Solving for $u_i(t + \Delta t)$ on the left-hand side, we find

$$u_i(t + \Delta t) = \alpha u_{i-1}(t) + (1 - 2\alpha) u_i(t) + \alpha u_{i+1}(t) - \frac{\Delta t}{\rho} \frac{\partial p}{\partial x}(t) + \Delta t g_x, \quad (8.2.4)$$

for $i = 2, 3, \dots, N$, where we have introduced the dimensionless ratio

$$\alpha \equiv \frac{\Delta t \nu}{\Delta y^2}, \quad (8.2.5)$$

called the *numerical diffusivity*. Equation (8.2.4) allows us to update the velocity at the interior grid points explicitly starting from the specified initial condition, and subject to the boundary conditions $u_1(t + \Delta t) = U_1(t + \Delta t)$ and $u_{N+1}(t + \Delta t) = U_2(t + \Delta t)$.

Numerical stability

Numerical experimentation reveals that the explicit method of updating the velocity based on equation (8.2.4) is free of oscillations only when the time step Δt is small enough so that the dimensionless numerical diffusivity α defined in (8.2.5) is less than 0.5. For larger time steps, the velocity profile develops unphysical oscillations of numerical nature that are unrelated to the physics of the problem under consideration. Accordingly, the explicit finite-difference method is only *conditionally stable*.

8.2.3 Implicit finite-difference method

To avoid the restriction on the time step required for numerical stability, we implement an implicit finite-difference method. This is done by evaluating both sides of (8.2.1) at the i th interior grid point at time $t + \Delta t$, where $i = 2, 3, \dots, N$, and then approximating the time derivative on the left-hand side with a first-order backward finite difference and the second derivative on the right-hand side with a second-order centered finite difference, obtaining

$$\begin{aligned} \frac{u_i(t + \Delta t) - u_i(t)}{\Delta t} &= -\frac{1}{\rho} \frac{\partial p}{\partial x}(t + \Delta t) \\ + \nu \frac{u_{i+1}(t + \Delta t) - 2u_i(t + \Delta t) + u_{i-1}(t + \Delta t)}{\Delta y^2} &+ g_x. \end{aligned} \quad (8.2.6)$$

Rearranging (8.2.6), we find

$$\begin{aligned} -\alpha u_{i-1}(t + \Delta t) + (1 + 2\alpha) u_i(t + \Delta t) - \alpha u_{i+1}(t + \Delta t) \\ = u_i(t) - \frac{\Delta t}{\rho} \frac{\partial p}{\partial x}(t + \Delta t) + \Delta t g_x, \end{aligned} \quad (8.2.7)$$

where α is the numerical diffusivity defined in equation (8.2.5). Equation (8.2.7) allows us to compute the velocity at the interior grid points at the

time level $t + \Delta t$ in an implicit fashion which involves solving simultaneously for all unknown grid values, subject to the boundary conditions $u_1(t + \Delta t) = U_1(t + \Delta t)$ and $u_{N+1}(t + \Delta t) = U_2(t + \Delta t)$.

To formalize the implicit algorithm, we write equation (8.2.7) for $i = 2, 3, \dots, N$, and use the boundary conditions stated at the end of the last paragraph to obtain a system of $N - 1$ linear equations for the velocity at the $N - 1$ interior grid points at time $t + \Delta t$,

$$\mathbf{A} \cdot \mathbf{u}(t + \Delta t) = \mathbf{u}(t) + \mathbf{b}. \quad (8.2.8)$$

We have introduced the tridiagonal coefficient matrix

$$\mathbf{A} = \begin{bmatrix} 1 + 2\alpha & -\alpha & 0 & 0 & 0 & \dots & 0 & 0 & 0 \\ -\alpha & 1 + 2\alpha & -\alpha & 0 & 0 & \dots & 0 & 0 & 0 \\ 0 & -\alpha & 1 + 2\alpha & -\alpha & 0 & \dots & 0 & 0 & 0 \\ \dots & \dots \\ 0 & 0 & 0 & 0 & 0 & \dots & -\alpha & 1 + 2\alpha & -\alpha \\ 0 & 0 & 0 & 0 & 0 & \dots & 0 & -\alpha & 1 + 2\alpha \end{bmatrix}, \quad (8.2.9)$$

the vector of unknown velocities

$$\mathbf{u}(t + \Delta t) = \begin{bmatrix} u_2(t + \Delta t) \\ u_3(t + \Delta t) \\ \vdots \\ u_{N-1}(t + \Delta t) \\ u_N(t + \Delta t) \end{bmatrix}, \quad (8.2.10)$$

and the known vectors

$$\mathbf{u}(t) = \begin{bmatrix} u_2(t) \\ u_3(t) \\ \vdots \\ u_{N-1}(t) \\ u_N(t) \end{bmatrix}, \quad \mathbf{b} = \begin{bmatrix} -\frac{\Delta t}{\rho} \frac{\partial p}{\partial x}(t + \Delta t) + \Delta t g_x + \alpha U_1(t + \Delta t) \\ -\frac{\Delta t}{\rho} \frac{\partial p}{\partial x}(t + \Delta t) + \Delta t g_x \\ \vdots \\ -\frac{\Delta t}{\rho} \frac{\partial p}{\partial x}(t + \Delta t) + \Delta t g_x \\ -\frac{\Delta t}{\rho} \frac{\partial p}{\partial x}(t + \Delta t) + \Delta t g_x + \alpha U_2(t + \Delta t) \end{bmatrix}. \quad (8.2.11)$$

The numerical method involves solving the linear system (8.2.8) at the time instant t to produce the velocity profile at the next time instant $t + \Delta t$, beginning from the specified initial state.

Numerical stability

Numerical experimentation reveals that the implicit method of updating the velocity based on equation (8.2.8) is free of numerical oscillations irrespective of the size of the time step Δt . Accordingly, the implicit finite-difference method is *unconditionally stable* and thus highly desirable.

8.2.4 Steady state

To obtain the velocity profile at steady state, we return to equation (8.2.8) and set $\mathbf{u}(t + \Delta t) = \mathbf{u}(t) = \mathbf{u}$ to find

$$(\mathbf{A} - \mathbf{I}) \cdot \mathbf{u} = \mathbf{b}, \quad (8.2.12)$$

where \mathbf{I} is the unit matrix. Dividing the individual equations contained in (8.2.12) by α , we obtain the simpler form

$$\mathbf{C} \cdot \mathbf{u} = \mathbf{d}, \quad (8.2.13)$$

involving the tridiagonal coefficient matrix

$$\mathbf{C} = \begin{bmatrix} 2 & -1 & 0 & 0 & 0 & \dots & 0 & 0 & 0 \\ -1 & 2 & -1 & 0 & 0 & \dots & 0 & 0 & 0 \\ 0 & -1 & 2 & -1 & 0 & \dots & 0 & 0 & 0 \\ \dots & \dots \\ 0 & 0 & 0 & 0 & 0 & \dots & -1 & 2 & -1 \\ 0 & 0 & 0 & 0 & 0 & \dots & 0 & -1 & 2 \end{bmatrix}, \quad (8.2.14)$$

the vector of unknown velocities at steady state

$$\mathbf{u} = \begin{bmatrix} u_2 \\ u_3 \\ \vdots \\ u_{N-1} \\ u_N \end{bmatrix}, \quad (8.2.15)$$

and the known vector

$$\mathbf{d} = \begin{bmatrix} -\frac{1}{\mu} \frac{\partial p}{\partial x} + \frac{\Delta y^2}{\nu} g_x + U_1 \\ -\frac{1}{\mu} \frac{\partial p}{\partial x} + \frac{\Delta x^2}{\nu} g_x \\ \vdots \\ -\frac{1}{\mu} \frac{\partial p}{\partial x} + \frac{\Delta y^2}{\nu} g_x \\ -\frac{1}{\mu} \frac{\partial p}{\partial x} + \frac{\Delta y^2}{\nu} g_x + U_2 \end{bmatrix}. \tag{8.2.16}$$

To compute the velocity profile at steady state, we merely solve the system of linear algebraic equations (8.2.13) using a numerical method.

8.2.5 Thomas algorithm

The tridiagonal form of the matrix \mathbf{A} displayed in (8.2.9), as well as of the matrix \mathbf{C} displayed in (8.2.14), allows us to compute the solution with great efficiency using the legendary Thomas algorithm. To formalize the numerical method in general terms, we consider the $K \times K$ linear system

$$\mathbf{D} \cdot \mathbf{x} = \mathbf{s} \tag{8.2.17}$$

for the unknown vector \mathbf{x} , where the vector \mathbf{s} is assumed to be known and the given matrix \mathbf{D} has the tridiagonal form

$$\mathbf{D} = \begin{bmatrix} a_1 & b_1 & 0 & 0 & 0 & \dots & 0 & 0 & 0 \\ c_2 & a_2 & b_2 & 0 & 0 & \dots & 0 & 0 & 0 \\ 0 & c_3 & a_3 & b_3 & 0 & \dots & 0 & 0 & 0 \\ \dots & \dots \\ 0 & 0 & 0 & 0 & 0 & \dots & c_{K-1} & a_{K-1} & b_{K-1} \\ 0 & 0 & 0 & 0 & 0 & \dots & 0 & c_K & a_K \end{bmatrix}. \tag{8.2.18}$$

Thomas's algorithm proceeds in two stages. At the first stage, the tridiagonal system (8.2.17) is transformed into the bidiagonal system

$$\mathbf{D}' \cdot \mathbf{x} = \mathbf{y} \tag{8.2.19}$$

involving the bidiagonal coefficient matrix

$$\mathbf{D}' = \begin{bmatrix} 1 & d_1 & 0 & 0 & 0 & \dots & 0 & 0 & 0 \\ 0 & 1 & d_2 & 0 & 0 & \dots & 0 & 0 & 0 \\ 0 & 0 & 1 & d_3 & 0 & \dots & 0 & 0 & 0 \\ \dots & \dots \\ 0 & 0 & 0 & 0 & 0 & \dots & 0 & 1 & d_{K-1} \\ 0 & 0 & 0 & 0 & 0 & \dots & 0 & 0 & 1 \end{bmatrix}. \quad (8.2.20)$$

At the second stage, the bidiagonal system (8.2.19) is solved by backward substitution, which involves solving the last equation for the last unknown x_K , and then moving upward to computing the rest of the unknowns in a sequential fashion. The combined algorithm is as follows:

Reduction to bidiagonal :

$$\begin{bmatrix} d_1 \\ y_1 \end{bmatrix} = \frac{1}{a_1} \begin{bmatrix} b_1 \\ s_1 \end{bmatrix}$$

Do $i = 1, K - 1$

$$\begin{bmatrix} d_{i+1} \\ y_{i+1} \end{bmatrix} = \frac{1}{a_{i+1} - c_{i+1}d_i} \begin{bmatrix} b_{i+1} \\ s_{i+1} - c_{i+1}y_i \end{bmatrix}$$

End Do

Backward substitution :

$$x_K = y_K$$

Do $i = K - 1, 1$ (step = -1)

$$x_i = y_i - d_i x_{i+1}$$

End Do

(8.2.21)

Thomas's algorithm is a special implementation of the inclusive method of Gauss elimination discussed earlier in Section 3.4 for general linear systems, designed to bypass unnecessary multiplications by zeros.

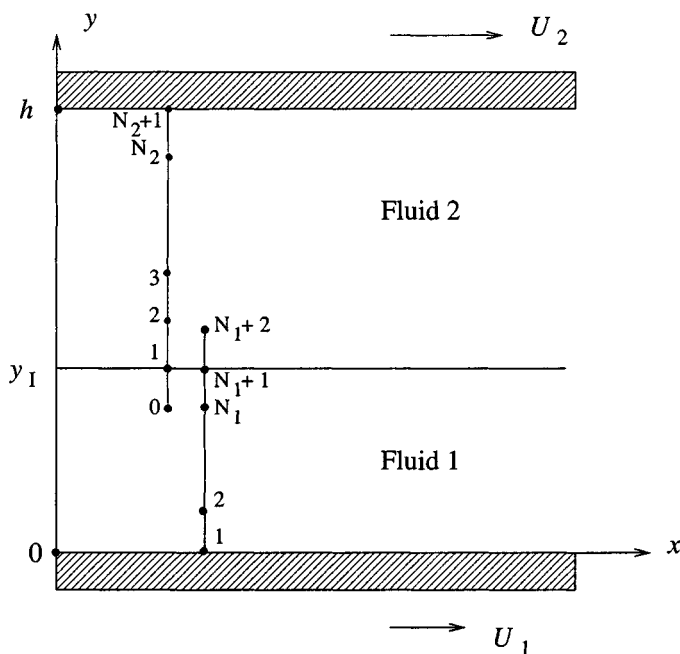


Figure 8.2.2 A composite finite-difference grid with extended or phantom nodes used to compute the velocity profile in unidirectional two-fluid channel flow.

8.2.6 Two-layer flow

A straightforward extension of the numerical methods described previously in this section allows us to compute the evolution of a two-layer channel flow, as illustrated in figure 8.2.2. Now, the channel is occupied by a lower layer labelled 1 and an upper layer labelled 2, and the two layers are separated by a flat interface located at $y = y_I$, where $y_I < h$. The thickness of the lower layer is denoted by $h_1 = y_I$, and the thickness of the upper layer is denoted by $h_2 = h - y_I$.

Interfacial conditions

At the interface, we require three conditions: continuity of velocity, continuity of shear stress, and continuity of normal stress. To satisfy the third condition, we require that the pressure gradient $\partial p / \partial x$ has the same value within both layers. Continuity of velocity and shear stress

require

$$u_x^{(1)}(y = y_I) = u_x^{(2)}(y = y_I), \quad (8.2.22)$$

and

$$\mu_1 \left(\frac{\partial u_x^{(1)}}{\partial y} \right)_{y=y_I} = \mu_2 \left(\frac{\partial u_x^{(2)}}{\partial y} \right)_{y=y_I}. \quad (8.2.23)$$

Using the equation of motion (8.2.1), we find that if (8.2.22) is true at the initial instant, it will also be true at all times provided that

$$-\frac{1}{\rho_1} \frac{\partial p}{\partial x} + \nu_1 \left(\frac{\partial^2 u_x^{(1)}}{\partial y^2} \right)_{y=y_I} = -\frac{1}{\rho_2} \frac{\partial p}{\partial x} + \nu_2 \left(\frac{\partial^2 u_x^{(2)}}{\partial y^2} \right)_{y=y_I}. \quad (8.2.24)$$

Finite-difference implementation

We begin developing the finite-difference method by dividing the lower layer into N_1 evenly spaced intervals defined by the $N_1 + 1$ grid points $y_i^{(1)}$, $i = 1, 2, \dots, N_1 + 1$, and the upper layer into N_2 evenly spaced intervals defined by the $N_2 + 1$ grid points $y_i^{(2)}$, $i = 1, 2, \dots, N_2 + 1$, as shown in figure 8.2.2. Moreover, for reasons that will soon become apparent, we extend the domain of definition of each layer into the adjacent layer by one artificial grid point labelled $N_1 + 2$ for the lower layer or 0 for the upper layer.

Approximating now the derivatives in (8.2.23) and (8.2.24) with centered finite differences, we derive two equations relating the values of the velocity at the extended nodes, $u_{N_1+2}^{(1)}$ and $u_0^{(2)}$,

$$\mu_1 \frac{u_{N_1+2}^{(1)} - u_{N_1}^{(1)}}{2 \Delta y_1} = \mu_2 \frac{u_2^{(2)} - u_0^{(2)}}{2 \Delta y_2}, \quad (8.2.25)$$

and

$$-\frac{1}{\rho_1} \frac{\partial p}{\partial x} + \nu_1 \frac{u_{N_1+2}^{(1)} - 2u_{N_1+1}^{(1)} + u_{N_1}^{(1)}}{\Delta y_1^2} = -\frac{1}{\rho_2} \frac{\partial p}{\partial x} + \nu_2 \frac{u_2^{(2)} - 2u_1^{(2)} + u_0^{(2)}}{\Delta y_2^2}, \quad (8.2.26)$$

where we have denoted

$$u_i^{(1)} \equiv u_x^{(1)}(y_i^{(1)}), \quad u_i^{(2)} \equiv u_x^{(2)}(y_i^{(2)}), \quad (8.2.27)$$

and we have defined $\Delta y_1 \equiv h_1/N_1$ and $\Delta y_2 \equiv h_2/N_2$. Setting $u_{N_1+1}^{(1)} = u_1^{(2)}$, and introducing the ratios

$$\lambda \equiv \frac{\mu_2}{\mu_1}, \quad \gamma \equiv \frac{\nu_2}{\nu_1}, \quad \delta \equiv \frac{\rho_2}{\rho_1}, \quad \beta \equiv \frac{\Delta y_2}{\Delta y_1}, \quad (8.2.28)$$

we recast equations (8.2.25) and (8.2.26) into the form of a system of two linear equations for the velocity at the extended nodes,

$$\beta u_{N_1+2}^{(1)} + \lambda u_0^{(2)} = \beta u_{N_1}^{(1)} + \lambda u_2^{(2)}, \quad (8.2.29)$$

and

$$\beta^2 u_{N_1+2}^{(1)} - \gamma u_0^{(2)} = 2(\beta^2 - \gamma) u_{N_1+1}^{(1)} - \beta^2 u_{N_1}^{(1)} + \gamma u_2^{(2)} + \frac{\Delta y_2^2}{\mu_1} \left(1 - \frac{1}{\delta}\right) \frac{\partial p}{\partial x}. \quad (8.2.30)$$

Solving for the velocity at the lower extended node, we find

$$u_{N_1+2}^{(1)} = a_1 u_{N_1}^{(1)} + a_2 u_{N_1+1}^{(1)} + a_3 u_2^{(2)} + a_4 \frac{\partial p}{\partial x}, \quad (8.2.31)$$

where

$$a_1 = \frac{\gamma - \beta\lambda}{\gamma + \beta\lambda}, \quad a_2 = 2\lambda \frac{\beta^2 - \gamma}{\beta(\gamma + \beta\lambda)}, \quad a_3 = \frac{2\gamma\lambda}{\beta(\gamma + \beta\lambda)},$$

$$a_4 = \frac{\lambda}{\beta(\gamma + \beta\lambda)} \frac{\Delta y_2^2}{\mu_1} \left(1 - \frac{1}{\delta}\right). \quad (8.2.32)$$

When the physical properties of the layers are matched, $\lambda = \gamma = \delta = 1$, and the lower and upper grid sizes are equal, $\beta = 1$, then $u_{N_1+2}^{(1)} = u_2^{(2)}$ by equation (8.2.31), and $u_0^{(2)} = u_{N_1}^{(1)}$ by equation (8.2.29), as required.

Explicit method

Working as in the case of single-fluid flow discussed earlier, we derive the explicit finite-difference equation

$$u_i^{(1)}(t + \Delta t) = \alpha_1 u_{i+1}^{(1)}(t) + (1 - 2\alpha_1) u_i^{(1)}(t) + \alpha_1 u_{i-1}^{(1)}(t) - \frac{\Delta t}{\rho_1} \frac{\partial p}{\partial x}(t) + \Delta t g_x \quad (8.2.33)$$

for the lower layer, and the corresponding equation

$$u_i^{(2)}(t + \Delta t) = \alpha_2 u_{i+1}^{(2)}(t) + (1 - 2\alpha_2) u_i^{(2)}(t) + \alpha_2 u_{i-1}^{(2)}(t) - \frac{\Delta t}{\rho_2} \frac{\partial p}{\partial x}(t) + \Delta t g_x \quad (8.2.34)$$

for the upper layer, where

$$\alpha_1 \equiv \frac{\Delta t \nu_1}{\Delta y_1^2}, \quad \alpha_2 \equiv \frac{\Delta t \nu_2}{\Delta y_2^2} \quad (8.2.35)$$

are the numerical diffusivities for the lower and upper layer. The numerical procedure involves the following steps:

1. Compute the velocity at the extended node $u_{N_1+2}^{(1)}$ from equation (8.2.31).
2. Use equation (8.2.33) to update the velocity at the grid points of the lower layer, $i = 2, \dots, N_1 + 1$.
3. Set $u_1^{(2)} = u_{N_1+1}^{(1)}$.
4. Use equation (8.2.34) to update the velocity at the internal grid points of the upper layer, for $i = 2, \dots, N_2$.
5. Use the boundary conditions to update the velocity at the lower and upper wall.
6. Return to step 1 and repeat the computation for another step.

Problems

Problem 8.2.1 *Steady state.*

Derive the system (8.2.12) departing from the explicit finite-difference formula (8.2.3).

Problem 8.2.2 *Two-layer channel flow.*

(a) Derive a system of finite-difference equations governing the velocity profile of the two-layer channel flow at steady state.

(b) Develop an implicit finite-difference method for computing the evolution of the two-layer flow discussed in the text.

Problem 8.2.3 *Flow in a circular tube.*

Develop an explicit finite-difference method based on the velocity / pressure formulation for computing the velocity profile developing in a circular tube due to a suddenly imposed constant pressure gradient.

Computer problems

Problem c.8.2.1 *Thomas's algorithm*

Subdirectory *01_num_meth/03_lin_eq* of *FDLIB* includes the program *thomas* that solves a tridiagonal system of linear equations using the Thomas algorithm discussed in the text. Use the program to solve a system of equations of your choice, and verify the accuracy of the solution by confirming that it satisfies the chosen system of equations.

Problem c.8.2.2 *Single-fluid channel flow.*

(a) Write a program that computes the evolution of the velocity profile in a channel with stationary walls due to the sudden application of a constant pressure gradient, based on the explicit finite-difference method discussed in the text. Run the program for fluid properties and flow conditions of your choice, and for several sizes of the time step corresponding to numerical diffusivity α larger and lower than 0.5, and discuss the performance of the numerical method.

(b) Repeat (a) for the implicit finite-difference method discussed in the text.

Problem c.8.2.3 *Two-layer channel flow.*

Write a program that computes the evolution of the velocity profile of two-layer flow in a channel with stationary walls due to the sudden application of a constant pressure gradient, based on the explicit finite-difference method discussed in the text. Run the program for fluid properties and flow conditions of your choice and for several sizes of the time step, and discuss the performance of the numerical method.

8.3 Unidirectional flow; velocity/vorticity formulation

In the case of unsteady unidirectional flow, the vorticity transport equation reduces to the unsteady diffusion equation for the strength of

the vorticity ω_z ,

$$\frac{\partial \omega_z}{\partial t} = \nu \frac{\partial^2 \omega_z}{\partial y^2}, \quad (8.3.1)$$

where ν is the kinematic viscosity. Using the definition of the vorticity shown in equation (8.1.1), we find that the strength of the vorticity is related to the x component of the velocity u_x by the differential relation

$$\omega_z = -\frac{\partial u_x}{\partial y}. \quad (8.3.2)$$

Integrating (8.3.2) with respect to y from the lower wall up to an arbitrary point, we obtain an integral representation for the velocity in terms of the vorticity,

$$u_x(y) = U_1 - \int_0^y \omega_z(y') dy'. \quad (8.3.3)$$

Without loss of generality, we have chosen to satisfy the boundary condition at the lower wall; it remains to ensure that the boundary condition at the upper wall will also be satisfied.

The numerical method involves computing the evolution of the vorticity from a specified initial state using (8.3.1), and simultaneously recovering the evolution of the velocity field based on equation (8.3.2) or its integrated version (8.3.3). Since the velocity does not appear in equation (8.3.1), the two steps are decoupled.

8.3.1 Boundary conditions for the vorticity

Now, because the unsteady diffusion equation (8.3.1) is a second-order differential equation with respect to y , two boundary conditions for the vorticity are required, one at each end of the solution domain located at $y = 0$ and h . These boundary conditions must be such that: (a) the integral condition

$$\int_0^h \omega_z(y') dy' = U_1 - U_2 \quad (8.3.4)$$

is observed so that the right-hand side of (8.3.3) satisfies the no-slip boundary condition $u_x(y = h) = U_2$, and (b) either the flow rate through the channel has a specified value $Q(t)$, or the streamwise pressure gradient has a specified value $\partial p(t)/\partial x$.

Considering flow subject to a specified pressure gradient, we recast the x component of the equation of motion for unidirectional flow into the form

$$\frac{\partial u_x}{\partial t} = -\frac{1}{\rho} \frac{\partial p}{\partial x} + \nu \frac{\partial^2 u_x}{\partial y^2} + g_x = -\frac{1}{\rho} \frac{\partial p}{\partial x} - \nu \frac{\partial \omega_z}{\partial y} + g_x. \quad (8.3.5)$$

Evaluating (8.3.5) at the lower and upper wall, and rearranging, we obtain boundary conditions for the slope of the vorticity,

$$\begin{aligned} \left(\frac{\partial \omega_z}{\partial y}\right)_{y=0} &= -\frac{1}{\nu} \frac{dU_1}{dt} - \frac{1}{\mu} \frac{\partial p}{\partial x} + \frac{1}{\nu} g_x, \\ \left(\frac{\partial \omega_z}{\partial y}\right)_{y=h} &= -\frac{1}{\nu} \frac{dU_2}{dt} - \frac{1}{\mu} \frac{\partial p}{\partial x} + \frac{1}{\nu} g_x. \end{aligned} \quad (8.3.6)$$

Special attention must be paid to the case of impulsive motion. If a wall moves suddenly in an impulsive fashion, with the velocity changing from one value to another over an infinitesimal period of time, the corresponding time derivative on the right-hand side of one or both of (8.3.6) will develop an infinite spike described by the Dirac delta function, to be discussed in Chapter 11. This singular behavior is too demanding to be handled by the numerical method.

To this end, we must investigate whether the vorticity boundary conditions (8.3.6) ensure the satisfaction of the integral constraint (8.3.4) which is necessary for the satisfaction of the no-slip boundary condition at the upper wall. For this purpose, we integrate both sides of (8.3.1) with respect to y from 0 to h , interchange the order of the integration and time differentiation on the left-hand side, and use (8.3.6) to simplify the right-hand side finding

$$\frac{d}{dt} \int_0^h \omega_z(y') dy' = \frac{d}{dt} (U_1 - U_2). \quad (8.3.7)$$

Time-integration of (8.3.7) reproduces (8.3.4) up to a time-independent constant that is determined by the initial state. Thus, if (8.3.4) is satisfied at the initial instant, it will also be satisfied at all subsequent times.

8.3.2 Alternative set of equations

In a simpler approach, we take the derivative of (8.3.2) with respect to y , and derive the second-order equation

$$\frac{\partial^2 u_x}{\partial y^2} = -\frac{\partial \omega_z}{\partial y} \equiv -q, \quad (8.3.8)$$

where $q \equiv \partial \omega_z / \partial y$ is the slope of the vorticity. To compute the velocity, we integrate the second-order equation (8.3.8) with respect to y using the velocity boundary conditions $u_x(y=0) = U_1$ and $u_x(y=h) = U_2$. The important benefit stemming from the use of (8.3.8) instead of (8.3.2), is that, to compute the velocity, the slope of the vorticity q instead of the vorticity itself is required.

An evolution equation for q arises by differentiating both sides of (8.3.1) with respect to y , finding

$$\frac{\partial q}{\partial t} = \nu \frac{\partial^2 q}{\partial y^2}. \quad (8.3.9)$$

Boundary conditions are provided by equations (8.3.6).

In summary, the numerical procedure involves integrating in time equation (8.3.9) from an initial state subject to the derived boundary conditions (8.3.6), while simultaneously computing the velocity by solving the second-order equation (8.3.8) subject to the velocity boundary conditions $u_x(y=0) = U_1$ and $u_x(y=h) = U_2$.

Explicit finite-difference method

To implement a finite-difference method, we divide the flow domain $0 \leq y \leq h$ into N intervals separated by $N + 1$ grid points, as shown in figure 8.2.1, and evaluate both sides of (8.3.9) at time t at the interior nodes corresponding to $i = 2, 3, \dots, N$. Approximating the time derivative on the left-hand side with a first-order finite difference, and the y derivative on the left-hand side with a second-order finite difference, we obtain

$$\frac{q_i(t + \Delta t) - q_i(t)}{\Delta t} = \nu \frac{q_{i+1}(t) - 2q_i(t) + q_{i-1}(t)}{\Delta y^2}, \quad (8.3.10)$$

where we have defined $q_i \equiv q(y_i)$. Solving for $q_i(t + \Delta t)$ on the left-hand side, we find

$$q_i(t + \Delta t) = \alpha q_{i-1}(t) + (1 - 2\alpha) q_i(t) + \alpha q_{i+1}(t), \quad (8.3.11)$$

where $\alpha \equiv \nu \Delta t / \Delta y^2$ is the numerical diffusivity. Equation (8.3.11) allows us to explicitly update the values of q at the grid points, subject to boundary conditions for q_1 and q_{N+1} given by the right-hand sides of equations (8.3.6).

The centered-difference discretization of equation (8.3.8) leads to the linear system (8.2.13), where the coefficient matrix \mathbf{C} is given in (8.2.14), and the constant vector on the right-hand side is given by

$$\mathbf{d} = \begin{bmatrix} \Delta y^2 q_2 + U_1 \\ \Delta y^2 q_3 \\ \vdots \\ \Delta y^2 q_{N-1} \\ \Delta y^2 q_N + U_2 \end{bmatrix}. \quad (8.3.12)$$

The linear system may be solved efficiently using Thomas's algorithm (8.2.21).

8.3.3 Comparison with the velocity-pressure formulation

Comparing the vorticity-velocity formulation discussed in this section with the velocity-pressure formulation discussed in Section 8.2, we find that the latter is significantly simpler in development and implementation. While this is undoubtedly true in the case of unidirectional flow, we shall see later in this chapter that the vorticity-velocity is more competitive in the more general case of two- and three-dimensional flow.

Problems

Problem 8.3.1 *Steady flow.*

Discuss the implementation of the velocity-vorticity formulation for steady channel flow subject to a specified pressure gradient.

Problem 8.3.2 *Two-layer flow.*

Develop the velocity-vorticity formulation for two-layer channel flow discussed in Section 8.2.

Problem 8.3.3 *Flow in a circular tube.*

Develop an explicit method based on the velocity-vorticity formulation for computing the velocity profile developing in a circular tube due to a suddenly imposed constant pressure gradient.

Computer problem

Problem c.8.3.1 *Explicit finite-difference method.*

Write a program that computes the evolution of the velocity profile in a channel with stationary walls due to the sudden application of a constant pressure gradient, based on the explicit finite-difference method discussed in the text. Run the program for fluid properties and flow conditions of your choice and for several sizes of the time step corresponding to numerical diffusivity α larger and lower than 0.5, and discuss the performance of the numerical method.

8.4 Unidirectional flow stream function/vorticity formulation

In Sections 8.2 and 8.3, we discussed methods for computing the evolution of the velocity profile in channel flow subject to a specified pressure gradient. In this section, we consider the complementary case of flow subject to a specified flow rate, and develop a numerical method descending from the vorticity-velocity formulation.

For reasons that will soon become apparent, we introduce the stream function ψ satisfying $u_x = \partial\psi/\partial y$. In the case of unidirectional flow, u_x and thus ψ is a function of y and t . The flow rate across a line beginning and ending at two planes located at $y = y_1$ and y_2 is equal to the difference in the corresponding values of the stream function, $Q_{12} = \psi(y_2) - \psi(y_1)$; the flow rate through the channel is equal to $Q = \psi(y = h) - \psi(y = 0)$. Using equation (8.3.2), we find that the strength of the vorticity is related to the stream function by the equation

$$\omega_z = -\frac{\partial^2\psi}{\partial y^2}. \quad (8.4.1)$$

The numerical method involves computing the evolution of the vorticity from a specified initial state using (8.3.1), and simultaneously recovering the evolution of the stream function using (8.4.1). Since equations (8.3.1) and (8.4.1) are both of second order with respect to y , two boundary conditions for the vorticity and two boundary conditions for the stream function are required, one at each end of the solution domain located at $y = 0$ and h .

To this end, we note that adding to the stream function an arbitrary constant does not affect the velocity, which means that the base level of the stream function may be arbitrary; accordingly, we stipulate $\psi(y = 0) = 0$, in which case $\psi(y = h) = Q(t)$. It is evident now that, by introducing the stream function, we have considerably facilitated the implementation of the condition on the flow rate.

8.4.1 Boundary conditions for the vorticity

The boundary conditions for the vorticity must involve the specified wall velocities U_1 and U_2 by means of the no-slip boundary condition. To illustrate the implementation of this condition, we divide the flow domain $0 \leq y \leq h$ into N intervals defined by $N + 1$ grid points, as shown in figure 8.2.1, and evaluate both sides of (8.4.1) at time t at the boundary nodes corresponding to $i = 1$ and $N + 1$. Approximating the y derivative on the left-hand side with a combination of finite differences, we obtain

$$\begin{aligned}\omega_1 &= -\frac{(\frac{\partial\psi}{\partial y})_{\frac{1}{2}(y_1+y_2)} - (\frac{\partial\psi}{\partial y})_{y_1}}{\frac{1}{2}\Delta y} = -2\frac{\psi_2 - \psi_1 - U_1}{\Delta y} \\ &= 2\frac{\psi_1 - \psi_2}{\Delta y^2} + 2\frac{U_1}{\Delta y},\end{aligned}\tag{8.4.2}$$

and

$$\begin{aligned}\omega_{N+1} &= -\frac{(\frac{\partial\psi}{\partial y})_{y_{N+1}} - (\frac{\partial\psi}{\partial y})_{\frac{1}{2}(y_N+y_{N+1})}}{\frac{1}{2}\Delta y} = -2\frac{U_2 - \frac{\psi_{N+1} - \psi_N}{\Delta y}}{\Delta y} \\ &= 2\frac{\psi_{N+1} - \psi_N}{\Delta y^2} - 2\frac{U_2}{\Delta y},\end{aligned}\tag{8.4.3}$$

where we have denoted $\omega_i \equiv \omega_z(y_i)$ and $\psi_i \equiv \psi(y_i)$.

It is somewhat alarming to realize that the no-slip condition has been implemented in an indirect fashion in terms of the vorticity. Specifically, it is not clear that solving (8.4.1) for the stream function and subsequently differentiating it to compute the velocity will generate a velocity field that is consistent with the prescribed velocity boundary conditions. Fortunately, a thorough analysis of the numerical method reveals that this will be the case except under unusual circumstances associated with singular boundary conditions involving discontinuous behavior.

8.4.2 A semi-implicit method

Proceeding with the finite-difference method, we evaluate both sides of (8.3.1) at the interior nodes corresponding to $i = 2, 3, \dots, N$ at time t , and approximate the time derivative on the left-hand side with a first-order finite difference, and the y derivative on the left-hand side with a second-order second finite difference, obtaining

$$\frac{\omega_i(t + \Delta t) - \omega_i(t)}{\Delta t} = \nu \frac{\omega_{i+1}(t) - 2\omega_i(t) + \omega_{i-1}(t)}{\Delta y^2}. \quad (8.4.4)$$

Solving for $\omega_i(t + \Delta t)$, we find

$$\omega_i(t + \Delta t) = \alpha \omega_{i+1}(t) + (1 - 2\alpha) \omega_i(t) + \alpha \omega_{i-1}(t), \quad (8.4.5)$$

where $\alpha \equiv \Delta t \nu / \Delta y^2$ is the numerical diffusivity. Equation (8.4.5) allows us to explicitly update the values of ω at the interior grid points, subject to boundary conditions for ω_1 and ω_{N+1} given by the right-hand sides of (8.4.2) and (8.4.3); the stream function at time t is assumed to be known.

Now, the implicit discretization of equation (8.4.1) leads to the linear system

$$\mathbf{C} \cdot \psi(t + \Delta t) = \mathbf{d}, \quad (8.4.6)$$

where the coefficient matrix \mathbf{C} is given in (8.2.14), the vector ψ is defined as

$$\psi = \begin{bmatrix} \psi_2 \\ \psi_3 \\ \vdots \\ \psi_{N-1} \\ \psi_N \end{bmatrix}, \quad (8.4.7)$$

and the vector on the right-hand side of (8.4.6) is given by

$$\mathbf{d} = \begin{bmatrix} \Delta y^2 \omega_2 \\ \Delta y^2 \omega_3 \\ \vdots \\ \Delta y^2 \omega_{N-1} \\ \Delta y^2 \omega_N + Q(t + \Delta t) \end{bmatrix}. \quad (8.4.8)$$

The system (8.4.6) may be solved efficiently using Thomas's algorithm (8.2.21).

The numerical method involves the following steps:

1. Assign initial values to the stream function and vorticity at all nodes.
2. Compute the vorticity at the boundary nodes using (8.4.2) and (8.4.3).
3. Update the vorticity at the internal nodes using (8.4.5).
4. Update the stream function at the internal nodes by solving the linear system (8.4.6).
5. Return to step 2 and repeat.

The velocity profile arises by numerically differentiating the stream function with respect to y .

Problems

Problem 8.4.1 *Steady flow.*

Develop a finite-difference method based on the stream function / vorticity formulation for computing the velocity profile of steady channel flow subject to a specified flow rate.

Problem 8.4.2 *Two-layer flow.*

Develop a finite-difference method based on the stream function / vorticity formulation for unsteady two-layer channel flow discussed in Section 8.2.

Problem 8.4.3 *Flow in a circular tube.*

Develop a finite-difference method based on the stream function/vorticity formulation for computing the developing velocity profile in a circular tube, subject to a specified flow rate.

Computer problem

Problem c.8.4.1 *Explicit finite-difference method.*

Write a program that computes the evolution of the velocity profile in a channel with stationary walls using the explicit finite-difference

method, subject to a flow rate that increases gradually toward a steady value according to the equation

$$Q(t) = Q_0 \left[1 - \exp\left(-\frac{\beta \nu t}{h^2}\right) \right], \quad (8.4.9)$$

where Q_0 is the constant flow rate prevailing of long times, and β is a dimensionless constant. Run the program for fluid properties and flow conditions of your choice, and for several sizes of the time step corresponding to α larger and lower than 0.5, and discuss the performance of the numerical method.

8.5 Two-dimensional flow; stream function/vorticity formulation

Having discussed finite-difference methods for unidirectional flow, we proceed to address the more general case of two-dimensional flow where further considerations concerning the satisfaction of the continuity equation and choice of boundary conditions arise. We begin in this section by considering the vorticity / stream function formulation, to be developed as an extension of the corresponding formulation for unidirectional flow discussed in Section 8.4.

Texts on computer language programming introduce elementary programming procedures by explaining the structure of a program entitled “world” which prints out the important message “Hello World”. Correspondingly, texts on computational fluid dynamics explain elementary numerical methods by discussing the prototypical example of flow in a two-dimensional cavity driven by a moving lid, known as the “driven-cavity flow”. We shall follow this time-honored tradition.

8.5.1 Flow in a cavity

Consider flow in a cavity driven by the motion of a lid translating parallel to itself with a generally time-dependent velocity $U(t)$, as illustrated in figure 8.5.1, and introduce the stream function defined by the relations $u_x = \partial\psi/\partial y$ and $u_y = -\partial\psi/\partial x$. The no-penetration condition requires that the component of the velocity normal to each one of the four walls vanish. In terms of the stream function,

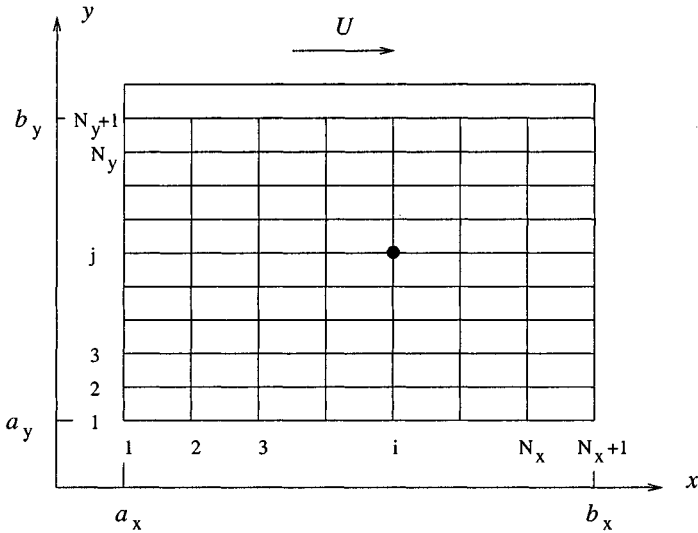


Figure 8.5.1 A finite-difference grid used to compute flow in a cavity driven by a moving lid.

$$\psi = 0 \quad \text{over all walls,} \quad (8.5.1)$$

so that the tangential derivative of the stream function, being proportional the normal component of the velocity, vanishes. The zero on the right-hand side of (8.5.1) may be replaced by an arbitrary constant with no consequence on the structure of the flow.

The no-slip boundary condition requires that the tangential component of the velocity vanish over the bottom, left, and right walls, and be equal to $U(t)$ on the upper wall. In terms of the stream function,

$$\begin{aligned} \frac{\partial \psi}{\partial y} = 0 \quad \text{at the bottom,} \quad \frac{\partial \psi}{\partial x} = 0 \quad \text{at the sides,} \\ \frac{\partial \psi}{\partial y} = U(t) \quad \text{at the top.} \end{aligned} \quad (8.5.2)$$

Based on the boundary conditions for the velocity, we may derive simplified expressions for the boundary values of the strength of the vorticity, $\omega_z \equiv -\partial u_x / \partial y + \partial u_y / \partial x$, in terms of the stream function. For example, taking into account that $u_y = 0$ and thus $\partial u_y / \partial x = 0$ over

the bottom wall, we find $\omega_z = -\partial u_x / \partial y = -\partial^2 \psi / \partial y^2$. Working in this fashion, we find

$$\begin{aligned}\omega_z &= -\frac{\partial^2 \psi}{\partial y^2} && \text{at the top and bottom,} \\ \omega_z &= -\frac{\partial^2 \psi}{\partial x^2} && \text{at the sides,}\end{aligned}\tag{8.5.3}$$

which are simplified versions of the more general expression for the vorticity in terms of the stream function, $\omega_z = -(\partial^2 \psi / \partial x^2 + \partial^2 \psi / \partial y^2)$.

8.5.2 Finite-difference grid

To prepare the ground for the implementation of the finite-difference method, we discretize the rectangular solution domain into a uniform two-dimensional Cartesian grid consisting of N_x intervals in the x direction and N_y intervals in the y direction, as shown in figure 8.5.1. The grid lines are separated by the uniform intervals Δx and Δy , called the grid sizes. The intersections of the grid lines define grid points labelled by the integer pair (i, j) , where $i = 1, 2, \dots, N_x + 1$ and $j = 1, 2, \dots, N_y + 1$. The side walls correspond to $i = 1$ and $N_x + 1$, and the bottom and top walls correspond to $j = 1$ and $N_y + 1$.

The goal of the finite-difference method is to produce the values of the flow variables at the grid points. For simplicity, we denote

$$\omega_{i,j} \equiv \omega_z(x_i, y_j), \quad \psi_{i,j} \equiv \psi(x_i, y_j),\tag{8.5.4}$$

and similarly for others variables.

8.5.3 Unsteady flow

Following the general procedure of methods based on the vorticity transport equation, we compute the evolution of the flow by advancing the vorticity field using the vorticity transport equation for two-dimensional flow written in the form of an evolution equation for the vorticity,

$$\frac{\partial \omega_z}{\partial t} = -u_x \frac{\partial \omega_z}{\partial x} - u_y \frac{\partial \omega_z}{\partial y} + \nu \left(\frac{\partial^2 \omega_z}{\partial x^2} + \frac{\partial^2 \omega_z}{\partial y^2} \right),\tag{8.5.5}$$

subject to appropriate *derived* boundary conditions for the vorticity, while obtaining the simultaneous evolution of the stream function by solving the Poisson equation

$$\nabla^2 \psi \equiv \frac{\partial^2 \psi}{\partial x^2} + \frac{\partial^2 \psi}{\partial y^2} = -\omega_z, \quad (8.5.6)$$

subject to *specified* boundary conditions for the stream function.

A simple method of computing the evolution of the flow when the lid starts translating suddenly from rest involves the following steps:

1. At the initial instant, set the stream function and velocity at all interior and boundary grid points equal to zero. Then set the x component of the velocity at the grid points over the lid equal to $U(t = 0)$.
2. Differentiate the velocity to produce the vorticity using the definition $\omega_z \equiv -\partial u_x / \partial y + \partial u_y / \partial x$. For the interior grid points, use centered differences, as shown in equation (2.5.18), to obtain

$$\omega_{i,j} = -\frac{(u_x)_{i,j+1} - (u_x)_{i,j-1}}{2\Delta y} + \frac{(u_y)_{i+1,j} - (u_y)_{i-1,j}}{2\Delta x}. \quad (8.5.7)$$

For the top wall, use backward differences to obtain

$$\omega_{i,N_y+1} \simeq -\left(\frac{\partial u_x}{\partial y}\right)_{i,N_y+1} \simeq \frac{-3U + 4(u_x)_{i,N_y} - (u_x)_{i,N_y-1}}{2\Delta y}. \quad (8.5.8)$$

involving values at interior grid points. Over the bottom and side walls, use forward or backward differences to obtain

$$\omega_{i,1} \simeq -\left(\frac{\partial u_x}{\partial y}\right)_{i,1} \simeq \frac{-4(u_x)_{i,2} + (u_x)_{i,3}}{2\Delta y}, \quad (8.5.9)$$

and

$$\begin{aligned} \omega_{1,j} &\simeq \left(\frac{\partial u_y}{\partial x}\right)_{1,j} \simeq \frac{4(u_y)_{2,j} - (u_y)_{3,j}}{2\Delta x}, \\ \omega_{N_x+1,j} &\simeq \left(\frac{\partial u_y}{\partial x}\right)_{N_x+1,j} \simeq \frac{-4(u_y)_{N_x,j} + (u_y)_{N_x-1,j}}{2\Delta x}, \end{aligned} \quad (8.5.10)$$

3. Integrate in time equation (8.5.5) to compute the vorticity at the interior grid points at time $t + \Delta t$. Choosing a fully explicit method, we set

$$\omega_{i,j}(t + \Delta t) = \omega_{i,j}(t) + G_{(i,j)}(t), \quad (8.5.11)$$

where $G_{(i,j)}(t)$ is the right-hand side of (8.5.5) evaluated at the (i, j) grid point, at time t . To evaluate $G_{(i,j)}(t)$, we approximate the first spatial derivatives and the Laplacian of the vorticity using centered differences. For example, the Laplacian of the vorticity may be approximated with the finite-difference formula shown in equation (3.3.13), written for ω_z .

4. Solve the Poisson equation (8.5.6) for the stream function subject to the boundary condition (8.5.1) using a slightly generalized version of the finite-difference method for Laplace's equation discussed in Section 3.3. Approximating the second derivatives with centered differences, we obtain the counterpart of equation (3.3.14)

$$\psi_{i+1,j} - 2(1 + \beta)\psi_{i,j} + \psi_{i-1,j} + \beta\psi_{i,j+1} + \beta\psi_{i,j-1} = -\Delta x^2 \omega_{i,j}, \quad (8.5.12)$$

where

$$\beta \equiv \left(\frac{\Delta x}{\Delta y}\right)^2. \quad (8.5.13)$$

5. Differentiate the stream function to compute the components of the velocity at time $t + \Delta t$ at the interior grid points.
6. Return to step 2 and repeat the computation for another time step.

8.5.4 Steady flow

To compute the structure of a steady flow, we follow a modified approach. In this case, the left-hand side of (8.5.5) vanishes, yielding a differential relation between the velocity and the vorticity. Solving for the Laplacian of the vorticity, we find

$$\frac{\partial^2 \omega_z}{\partial x^2} + \frac{\partial^2 \omega_z}{\partial y^2} = \frac{1}{\nu} \left(u_x \frac{\partial \omega_z}{\partial x} + u_y \frac{\partial \omega_z}{\partial y} \right), \quad (8.5.14)$$

which may be regarded as a Poisson equation for the vorticity, forced by the *a priori* unknown source function on the right-hand side. Computing the flow in terms of the stream function and vorticity involves simultaneously solving equations (8.5.6) and (8.5.14) according to the following steps:

1. Guess the distribution of the stream function and associated distribution of the vorticity.
2. Solve the Poisson equation (8.5.6) for the stream function subject to boundary condition (8.5.1).
3. Compute the right-hand side of (8.5.14).
4. Derive boundary conditions for the vorticity using the stream function obtained at step 2.
5. Solve the Poisson equation (8.5.14) for the vorticity.
6. Check to see whether the vorticity computed at step 5 agrees with that assigned in step 1 within a specified tolerance. If it does not, replace the latter with the former and return to step 2, otherwise stop.

The method is implemented according to the following steps:

1. Assign values to the stream function at all $(N_x + 1) \times (N_y + 1)$ interior and boundary grid points, and to the vorticity at all $N_x \times N_y$ interior grid points. A simple choice is to set them all equal to zero.
2. Solve the Poisson equation (8.5.6) subject to the boundary condition (8.5.1) using an iterative method. To perform the iterations, we approximate the second derivatives with centered differences and obtain equation (8.5.12), which we then express in the form

$$R_{i,j} \equiv \psi_{i+1,j} - 2(1+\beta)\psi_{i,j} + \psi_{i-1,j} + \beta\psi_{i,j+1} + \beta\psi_{i,j-1} + \Delta x^2 \omega_{i,j} = 0, \quad (8.5.15)$$

where $R_{i,j}$ is defined as the *residual*. The iterative method involves computing a time-like sequence of grid values parametrized by the index l , computed using the formula

$$\psi_{i,j}^{(l+1)} = \psi_{i,j}^{(l)} + \rho_1 R_{i,j}^{(l)}, \quad (8.5.16)$$

for $l = 1, 2, \dots$, where ρ_1 is a specified *relaxation factor* used to control the iterations.

3. Compute the vorticity at the boundary grid points taking into consideration the velocity boundary conditions. Considering the grid points on the lid, we expand the stream function in a Taylor series with respect to y about a top grid point, and evaluate the expansion at the grid point immediately below, to obtain

$$\psi_{i,N_y} \simeq \psi_{i,N_y+1} - \Delta y \left(\frac{\partial \psi}{\partial y} \right)_{i,N_y+1} + \frac{\Delta y^2}{2} \left(\frac{\partial^2 \psi}{\partial y^2} \right)_{i,N_y+1}. \quad (8.5.17)$$

Setting $(\partial \psi / \partial y)_{i,N_y+1} = U$, and $\omega_{i,N_y+1} = -(\partial^2 \psi / \partial y^2)_{i,N_y+1}$, as discussed in the paragraph following equation (8.5.2), and solving for ω_{i,N_y+1} , we find

$$\omega_{i,N_y+1} = 2 \frac{\psi_{i,N_y+1} - \psi_{i,N_y}}{\Delta y^2} - 2 \frac{U}{\Delta y}. \quad (8.5.18)$$

Working in a similar fashion, we derive analogous expressions for the bottom, left, and right walls,

$$\begin{aligned} \omega_{i,1} &= 2 \frac{\psi_{i,1} - \psi_{i,2}}{\Delta y^2}, & \omega_{1,j} &= 2 \frac{\psi_{1,j} - \psi_{2,j}}{\Delta y^2}, \\ \omega_{N_x+1,j} &= 2 \frac{\psi_{N_x+1,j} - \psi_{N_x,j}}{\Delta y^2}. \end{aligned} \quad (8.5.19)$$

4. Differentiate the stream function to produce the velocity at the interior grid points subject to the no-penetration condition expressed by (8.5.1).
5. Differentiate the vorticity to produce its x and y derivatives at the interior grid points subject to the boundary values computed at step 3.
6. Compute the right-hand side of (8.5.14) at the interior grid points.

7. Solve equation (8.5.14) by iteration, as discussed in step 2. The counterparts of equations (8.5.15) and (8.5.16) are:

$$R'_{i,j} \equiv \omega_{i+1,j} - 2(1+\beta)\omega_{i,j} + \omega_{i-1,j} + \beta\omega_{i,j+1} + \beta\omega_{i,j-1} - \Delta x^2 N_{i,j} = 0, \quad (8.5.20)$$

and

$$\omega_{i,j}^{(l+1)} = \omega_{i,j}^{(l)} + \rho_2 R'_{i,j}^{(l)}, \quad (8.5.21)$$

where $N_{i,j}$ is the right-hand side of (8.5.14) evaluated at the (i, j) grid point, and ρ_2 is a new relaxation factor.

Velocity vector fields computed using this method for Reynolds number $Re = 1$ and 100 are shown in figure 8.5.2. As the Reynolds number is raised, the center of the eddy developing inside the cavity is shifted toward the right wall due to the effects of fluid inertia.

8.5.5 Features of the stream function/vorticity formulation

The vorticity/stream function formulation is distinguished by the following characteristics:

1. Since expressing the velocity in terms of the stream function ensures the satisfaction of the continuity equation, the latter does not need to be considered.
2. The pressure does not appear during the solution, which is highly desirable: if we had to solve for the pressure, we would have to derive appropriate boundary conditions, as will be discussed in later sections.
3. Enforcing the no-penetration and no-slip boundary conditions is done in a sequential instead of a simultaneous fashion; the no-penetration condition is enforced in the process of solving for the stream function, and the no-slip condition is enforced in the process of deriving boundary conditions for the vorticity. In spite of this dichotomy, the overall method is consistent.

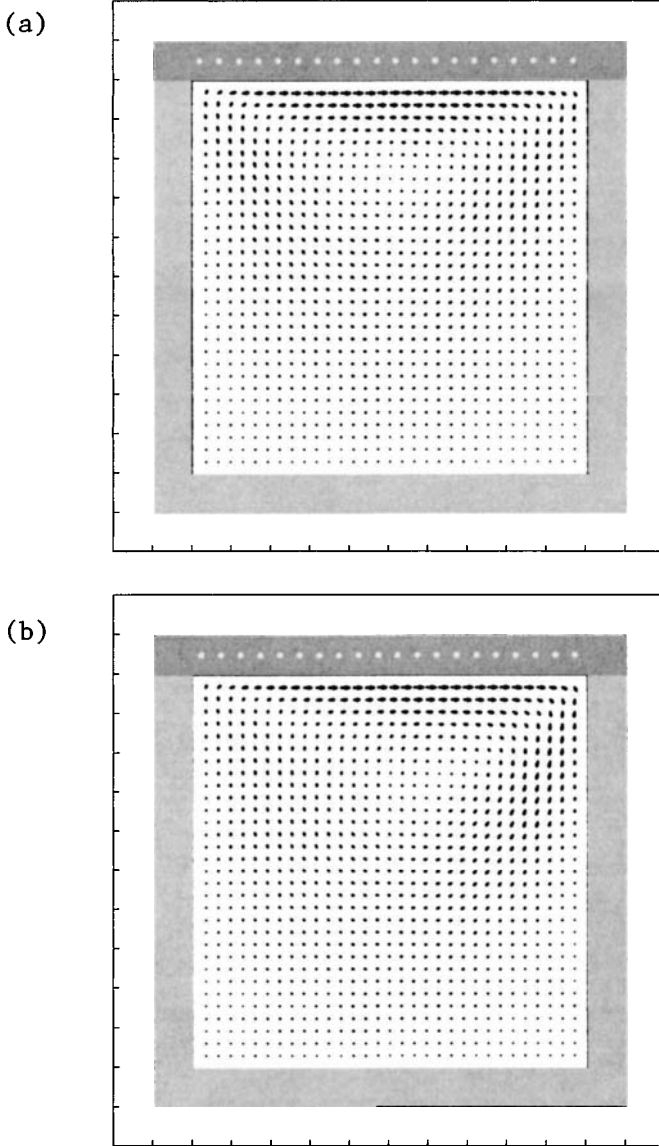


Figure 8.5.2 Velocity vector field of steady flow in a square cavity driven by a moving lid at Reynolds number (a) $Re \equiv UL/\nu = 1$, and (b) $Re = 100$, where U is the lid velocity and L is the cavity side-length. The flow was computed using program *11-fdm/cvt_sv* of *FDLIB*.

Problems

Problem 8.5.1 *Computation of the pressure.*

Show that the pressure distribution in an incompressible fluid satisfies Poisson's equation

$$\nabla^2 p = 2\rho \left[\frac{\partial^2 \psi}{\partial x^2} \frac{\partial^2 \psi}{\partial y^2} - \left(\frac{\partial^2 \psi}{\partial x \partial y} \right)^2 \right]. \quad (8.5.22)$$

Hint: Take the divergence of the Navier-Stokes equation and use the continuity equation.

Problem 8.5.2 *Axisymmetric flow.*

Develop a finite-difference method based on the stream function / vorticity formulation for flow in an axisymmetric cavity depressed on a circular cylinder, where the flow is driven by a sleeve sliding along the cylinder.

Computer problem

Problem c.8.5.1 *Steady flow in a cavity.*

Subdirectory `11_fdm/cvt_sv` of *FDLIB* contains a program that computes steady flow in a rectangular cavity using the stream function / vorticity formulation discussed in the text. Run the program for two flow conditions of your choice, prepare velocity vector fields, and discuss the performance of the numerical method and the changes in the structure of the flow with increasing Reynolds number $Re = UL/\nu$, where U is the lid velocity, L is the length of the top or bottom wall, and ν is the kinematic viscosity.

8.6 Velocity/pressure formulation

The stream function/vorticity formulation discussed in Section 8.5 is simple and efficient, but its extension to three-dimensions and its generalization to flows in the presence of interfaces are cumbersome. To be able to handle more general flow configurations, we develop a direct formulation in primary variables including the velocity and the pressure.

To compute the evolution of an unsteady flow, we require an evolution equation for the velocity and another evolution equation for the pressure. The former is provided by the Navier-Stokes equation written in the form

$$\frac{\partial \mathbf{u}}{\partial t} = \mathbf{N}(\mathbf{u}) - \frac{1}{\rho} \nabla p + \nu \mathbf{L}(\mathbf{u}), \quad (8.6.1)$$

where we have introduced the nonlinear convective operator \mathbf{N} and the linear diffusive operator \mathbf{L} , defined as

$$\mathbf{N}(\mathbf{u}) \equiv -\mathbf{u} \cdot \nabla \mathbf{u}, \quad \mathbf{L}(\mathbf{u}) \equiv \nabla^2 \mathbf{u}. \quad (8.6.2)$$

If the fluid were compressible, the continuity equation would provide us with an evolution equation for the density, as shown in equations (2.7.10) and (2.7.11). An evolution equation for the pressure could then be obtained by introducing an equation of state relating the density to the local pressure and temperature.

In the case of incompressible flow, an explicit evolution equation for the pressure is not available. Instead, the continuity equation requires the kinematic constraint

$$\nabla \cdot \mathbf{u} = 0, \quad (8.6.3)$$

which demands that the pressure field evolve so that the rate of expansion $\nabla \cdot \mathbf{u}$ vanishes throughout the domain of flow at all times. To translate this requirement into a mathematical restriction, we take the divergence of the Navier-Stokes equation (8.6.1), interchange the divergence with the time derivative on the left-hand side, and thereby derive an evolution equation for the rate of expansion,

$$\frac{\partial \nabla \cdot \mathbf{u}}{\partial t} = \nabla \cdot \mathbf{N}(\mathbf{u}) - \frac{1}{\rho} \nabla^2 p + \nu \nabla \cdot \mathbf{L}(\mathbf{u}). \quad (8.6.4)$$

Note that the divergence operator and the nonlinear operator \mathbf{N} do not commute on the right-hand side, $\nabla \cdot \mathbf{N}(\mathbf{u}) \neq \mathbf{N}(\nabla \cdot \mathbf{u})$. For simplicity, we have assumed that the density and the viscosity are uniform throughout the domain of flow.

Equation (8.6.3) requires that the left-hand side of (8.6.4) should vanish at all times, and this will be true if the pressure satisfies the pressure Poisson equation, PPE,

$$\nabla^2 p = \rho \nabla \cdot \mathbf{N}(\mathbf{u}) + \mu \nabla \cdot \mathbf{L}(\mathbf{u}). \quad (8.6.5)$$

It can be argued that, since the divergence and the linear operator \mathbf{L} commute, $\nabla \cdot \mathbf{L}(\mathbf{u}) = \mathbf{L}(\nabla \cdot \mathbf{u})$, the last term on the right-hand side of (8.6.5) should be set equal to zero yielding the simplified pressure Poisson equation, SPPE,

$$\nabla^2 p = \rho \nabla \cdot \mathbf{N}(\mathbf{u}). \quad (8.6.6)$$

In practice, however, the magnitude of the last term on the right-hand side of (8.6.5) is non-zero due to numerical error associated with the approximation of the partial derivatives with finite differences. It turns out that the complete absence of this term, however small, may be detrimental to the performance of the numerical method by fostering the growth of small oscillations. To avoid the onset of these oscillations, the PPE is preferred over its simplified counterpart.

8.6.1 Alternative system of governing equations

The preceding discussion suggests a numerical procedure for computing the evolution of an unsteady flow based on equations (8.6.1) and (8.6.5) or (8.6.6): compute the evolution of the velocity using (8.6.1), while obtaining the simultaneous evolution of the pressure by solving the Poisson equation (8.6.5) or (8.6.6). The process is analogous to that employed in the stream function / vorticity formulation discussed in Section 8.5. One important difference is that, by employing the stream function, the satisfaction of the continuity equation (8.6.3) is guaranteed, independent of the magnitude of the numerical error.

To examine whether the velocity-pressure formulation ensures the satisfaction of (8.6.3), we substitute (8.6.5) into the right-hand side of the PPE (8.6.4) and obtain the expected result

$$\frac{\partial \nabla \cdot \mathbf{u}}{\partial t} = 0, \quad (8.6.7)$$

which ensures that, if the rate of expansion vanishes at the initial instant by a sensible choice of the initial condition, it will also vanish at all times.

Substituting (8.6.6) into the right-hand side of the SPPE (8.6.4), we obtain an unsteady diffusion equation for the rate of expansion,

$$\frac{\partial \nabla \cdot \mathbf{u}}{\partial t} = \nu \nabla \cdot \mathbf{L}(\mathbf{u}), \quad (8.6.8)$$

which ensures that, if the rate of expansion vanishes at the initial instant by an appropriate choice of an initial condition, it will vanish at all times provided that the boundary values of the rate of expansion also vanish at all times. The additional condition underlines the importance of accurately satisfying mass conservation at the boundaries, and provides additional justification as to why (8.6.5) is preferred over its simplified counterpart (8.6.6).

8.6.2 Pressure boundary conditions

To solve the pressure Poisson equation, we require a boundary condition to be derived from specified boundary conditions for the velocity. The pressure boundary condition emerges by evaluating the Navier-Stokes equation (8.6.1) at the boundaries, and then taking the inner product of both sides with the unit vector normal to the boundaries pointing outward, \mathbf{n} . The result is the *Neumann boundary condition*

$$\mathbf{n} \cdot \nabla p = \rho \mathbf{n} \cdot \left[-\frac{\partial \mathbf{u}}{\partial t} + \mathbf{N}(\mathbf{u}) + \nu \mathbf{L}(\mathbf{u}) \right], \quad (8.6.9)$$

where the left-hand side expresses the derivative of the pressure normal to the boundaries, that is, the rate of change of the pressure with respect to distance normal to the boundaries. The right-hand side is then simplified by use of the no-slip and no-penetration boundary conditions.

For example, in the case of flow over a horizontal stationary wall located at $y = 0$, we require $u_x = 0$ and $u_y = 0$ at $y = 0$, and obtain

$$\mathbf{n} \cdot \nabla p = \frac{\partial p}{\partial y} = \mu \frac{\partial^2 u_y}{\partial y^2}. \quad (8.6.10)$$

The left-hand side is the normal derivative of the pressure, and the right-hand side is the negative of the normal derivative of the vorticity multiplied by the fluid viscosity.

8.6.3 Compatibility condition

The Poisson equation governing the pressure distribution in an incompressible fluid is analogous to the Poisson equation governing the steady-state distribution of temperature in a conductive medium identified with the domain of flow, subject to a homogeneous heat production term expressed by the right-hand side. The boundary condition (8.6.9)

specifies the boundary distribution of heat flux in terms of the instantaneous velocity. Now, physical reasoning suggests that a steady distribution of temperature will exist only if the total rate of heat production is balanced by the total rate of heat removal across the boundaries, so that heat does not accumulate to elevate the temperature.

In the case of two-dimensional flow, the mathematical expression of this requirement is the following compatibility condition: the areal integral of the right-hand side of (8.6.5) or (8.6.6) over the domain of flow must be equal to the line integral of the right-hand side of (8.6.9) or (8.6.10) over the boundaries, otherwise a solution for the pressure cannot be found. In the case of three-dimensional flow, the compatibility condition requires that the volume integral of the right-hand side of (8.6.5) or (8.6.6) over the domain of flow be equal to the surface integral of the right-hand side of (8.6.9) or (8.6.10) over the boundaries, otherwise a solution for the pressure cannot be found. In numerical practice, this compatibility condition is enforced either implicitly or explicitly depending on the particular implementation of the numerical method.

Problem

Problem 8.6.1 *Pressure boundary condition.*

Derive the pressure boundary condition (8.6.10).

8.7 Operator splitting and solenoidal projection

In practice, the velocity/pressure formulation is implemented in a manner that simplifies and, more important, expedites the numerical solution. For illustration, we discuss the computation of an evolving two-dimensional flow; extensions to three dimensions are straightforward in principle and implementation.

In the most popular implementation of the velocity/pressure formulation, the Navier-Stokes equation (8.6.1) is decomposed into the two constituent equations

$$\frac{\partial \mathbf{u}}{\partial t} = \mathbf{N}(\mathbf{u}) + \nu \mathbf{L}(\mathbf{u}), \quad (8.7.1)$$

and

$$\frac{\partial \mathbf{u}}{\partial t} = -\frac{1}{\rho} \nabla p, \quad (8.7.2)$$

where the operators \mathbf{N} and \mathbf{L} are defined in equations (8.6.2). The right-hand sides of (8.7.1) and (8.7.2) arise by splitting the full Navier-Stokes operator on the right-hand side of (8.6.1) into two parts, subject to the following interpretation.

Consider the change in the velocity field over a small time interval Δt following the current time t . The decomposition (8.7.1) and (8.7.2) is inspired by the idea of updating the velocity in two sequential steps, where the first update is due to inertia and viscosity, and the second update is due to the pressure gradient; the time is reset to $t + \Delta t$ upon completion of the second step. We shall see that this decomposition significantly simplifies the implementation of the numerical method by allowing the convection-diffusion and pressure-gradient steps to be handled independently using appropriate numerical methods.

Certain ambiguities, however, arise. First, the boundary conditions for the velocity to be used for integrating (8.7.1) cannot be the same as the specified boundary conditions, otherwise the second step mediated by (8.7.2) will cause a departure. Second, the boundary conditions for the pressure may no longer be computed from (8.6.9), and should be derived instead on the basis of equation (8.7.2).

The second observation suggests that p in equation (8.7.2) may no longer be considered to be the hydrodynamic pressure, and should be regarded as a modified pressure whose role is to ensure that the velocity field becomes solenoidal at the end of the second step. To make this distinction clear, we replace (8.7.2) with the equation

$$\frac{\partial \mathbf{u}}{\partial t} = -\frac{1}{\rho} \nabla \chi, \quad (8.7.3)$$

where χ is a *projection function*. Equation (8.7.3) receives the velocity field delivered by the convection-diffusion equation (8.7.1), which is not necessarily solenoidal, and removes the non-solenoidal component by a process that is described as *projection into the space of solenoidal functions*.

The choice of boundary conditions for the projection function χ has been the subject of extensive discussion. It can be shown that the *homogeneous Neumann boundary condition*, requiring that the derivative of the projection function χ with respect to distance normal to a boundary vanishes, is appropriate. The associated boundary conditions for the velocity will be discussed later in this section.

Next, we discuss the implementation of numerical methods for carrying out the convection-diffusion and projection steps expressed by equations (8.7.1) and (8.7.3).

8.7.1 Convection-diffusion step

To prevent numerical instabilities, we perform the convection-diffusion step expressed by (8.7.1) using an implicit finite difference method, updating the velocity by solving linear systems of algebraic equations.

Evaluating the x and y components of equation (8.7.1) at the (i, j) grid point at time $t + \Delta t$, and approximating the time derivatives with backward differences and the spatial derivatives with differences of our choice, we derive a system of equations for the unknown velocity vector containing the x and y velocity components at the grid points at time $t + \Delta t$. The size of the velocity vector is equal to twice the number of grid points. For a 32×32 grid, we obtain a velocity vector with nearly 2000 unknowns and an equal number of equations whose solution requires a prohibitive amount of computational effort.

As an alternative, we split the operator on the right-hand side of (8.7.1) into its two spatial components expressing convection-diffusion in the x or y direction, given by

$$\frac{\partial \mathbf{u}}{\partial t} = -u_x \frac{\partial \mathbf{u}}{\partial x} + \nu \frac{\partial^2 \mathbf{u}}{\partial x^2}, \quad (8.7.4)$$

and

$$\frac{\partial \mathbf{u}}{\partial t} = -u_y \frac{\partial \mathbf{u}}{\partial y} + \nu \frac{\partial^2 \mathbf{u}}{\partial y^2}, \quad (8.7.5)$$

and advance the velocity over the time interval Δt in a sequential fashion.

To achieve second-order accuracy, we discretize equation (8.7.4) using the Crank-Nicolson method by (a) evaluating (8.7.4) at the (i, j) grid point at time $t + \frac{1}{2}\Delta t$, (b) approximating the time and space derivatives with central differences, and (c) averaging the space derivatives over the time levels t and $t + \Delta t$, to find

$$\begin{aligned} \frac{\mathbf{u}_{i,j}^* - \mathbf{u}_{i,j}(t)}{\Delta t} &= \frac{1}{2}(u_x)_{i,j}(t) \left[\left(\frac{\mathbf{u}_{i+1,j} - \mathbf{u}_{i-1,j}}{2\Delta x} \right)(t) + \frac{\mathbf{u}_{i+1,j}^* - \mathbf{u}_{i-1,j}^*}{2\Delta x} \right] \\ &+ \frac{1}{2} \nu \left[\left(\frac{\mathbf{u}_{i+1,j} - 2\mathbf{u}_{i,j} + \mathbf{u}_{i-1,j}}{\Delta x^2} \right)(t) + \frac{\mathbf{u}_{i+1,j}^* - 2\mathbf{u}_{i,j}^* + \mathbf{u}_{i-1,j}^*}{\Delta x^2} \right]. \end{aligned} \quad (8.7.6)$$

The asterisk designates the first intermediate velocity field. To simplify the notation, we define

$$\mathbf{u}_{i,j}^n \equiv \mathbf{u}_{i,j}(t), \quad (8.7.7)$$

where the superscript n denotes the time level corresponding to time t . Rearranging equation (8.7.6), we derive the finite-difference equation

$$\begin{aligned} & -(c_x + 2\alpha_x) \mathbf{u}_{i-1,j}^* + 4(1 + \alpha_x) \mathbf{u}_{i,j}^* + (c_x - 2\alpha_x) \mathbf{u}_{i+1,j}^* \\ & = (c_x + 2\alpha_x) \mathbf{u}_{i-1,j}^n + 4(1 - \alpha_x) \mathbf{u}_{i,j}^n - (c_x - 2\alpha_x) \mathbf{u}_{i+1,j}^n, \end{aligned} \quad (8.7.8)$$

involving the local x convection number

$$c_x \equiv \frac{(u_x)_{i,j}^n \Delta t}{\Delta x}, \quad (8.7.9)$$

and the x diffusion number

$$\alpha_x \equiv \frac{\nu \Delta t}{\Delta x^2}. \quad (8.7.10)$$

The right-hand side of (8.7.8) may be computed from knowledge of the velocity at the grid points at the n th time level, which is assumed to be available.

Evaluating (8.7.8) at grid points that lie along y grid lines corresponding to fixed values of j , we obtain tridiagonal systems of equations for the x and y components of the first intermediate velocity. The paramount advantage of the method of directional splitting is that these tridiagonal systems may be solved efficiently using the Thomas algorithm discussed in Section 8.2.5, subject to boundary conditions to be discussed shortly.

An analogous discretization of equation (8.7.5) yields

$$\begin{aligned} & -(c_y + 2\alpha_y) \mathbf{u}_{i,j-1}^{**} + 4(1 + \alpha_y) \mathbf{u}_{i,j}^{**} + (c_y - 2\alpha_y) \mathbf{u}_{i,j+1}^{**} \\ & = (c_y + 2\alpha_y) \mathbf{u}_{i,j-1}^* + 4(1 - \alpha_y) \mathbf{u}_{i,j}^* - (c_y - 2\alpha_y) \mathbf{u}_{i,j+1}^*, \end{aligned} \quad (8.7.11)$$

where

$$c_y \equiv \frac{(u_y)_{i,j}^n \Delta t}{\Delta y} \quad (8.7.12)$$

is the local y convection number, and

$$\alpha_y \equiv \frac{\nu \Delta t}{\Delta y^2} \quad (8.7.13)$$

is the y diffusion number.

The double asterisk in (8.7.11) designates the second intermediate velocity field.

The right-hand side of (8.7.11) may be computed from knowledge of the first intermediate velocity delivered by equation (8.7.8). Evaluating (8.7.11) at grid points that lie along x grid lines corresponding to fixed values of i , we obtain tridiagonal systems of equations for the x and y components of the second intermediate velocity, which may be solved using the Thomas algorithm subject to boundary conditions to be discussed shortly.

8.7.2 Projection step

Next, we advance the velocity field using the projection step (8.7.3), where the projection function is computed so as to satisfy the continuity equation at the end of this step. Evaluating (8.7.4) at the (i, j) grid point, and approximating the time derivative with a finite difference, we find

$$\frac{\mathbf{u}_{i,j}(t + \Delta t) - \mathbf{u}_{i,j}^{**}}{\Delta t} = -\frac{1}{\rho} (\nabla \chi)_{i,j}^n, \quad (8.7.14)$$

which may be rearranged to give

$$\mathbf{u}_{i,j}(t + \Delta t) = \mathbf{u}_{i,j}^{**} - \frac{\Delta t}{\rho} (\nabla \chi)_{i,j}^n. \quad (8.7.15)$$

The gradient on the right-hand side of (8.7.15) may be approximated using centered, forward, or backward differences.

To this end, we consider the continuity equation $\nabla \cdot \mathbf{u} = 0$, and use centered differences to approximate the rate of expansion at the (i, j) grid point with the discrete form

$$D_{i,j} \equiv (\nabla \cdot \mathbf{u})_{i,j} \simeq \frac{(u_x)_{i+1,j} - (u_x)_{i-1,j}}{2\Delta x} + \frac{(u_y)_{i,j+1} - (u_y)_{i,j-1}}{2\Delta y}. \quad (8.7.16)$$

Evaluating (8.7.16) at the $n + 1$ time level corresponding to time $t + \Delta t$, requiring that the left-hand side vanishes, and using (8.7.15) to express $\mathbf{u}(t + \Delta t)$ on the right-hand side in terms of (a) the second intermediate velocity denoted by the double asterisk, and (b) the projection function, we find

$$\frac{\rho}{\Delta t} D_{i,j}^{**} = \frac{(\frac{\partial \chi}{\partial x})_{i+1,j} - (\frac{\partial \chi}{\partial x})_{i-1,j}}{2\Delta x} + \frac{(\frac{\partial \chi}{\partial y})_{i,j+1} - (\frac{\partial \chi}{\partial y})_{i,j-1}}{2\Delta y}. \quad (8.7.17)$$

The right-hand side of (8.7.17) is recognized as the discrete divergence of the gradient of the projection function χ .

Next, we consider grid points that are not adjacent to a wall, approximate the partial derivatives of the right-hand side of (8.7.17) with centered differences, and simplify to obtain

$$\frac{\rho}{\Delta t} D_{i,j}^{**} = \frac{\chi_{i+2,j} - 2\chi_{i,j} + \chi_{i-2,j}}{4\Delta x^2} + \frac{\chi_{i,j+2} - 2\chi_{i,j} + \chi_{i,j-2}}{4\Delta y^2}. \quad (8.7.18)$$

The right-hand side of (8.7.18) is recognized as the finite-difference approximation of the Laplacian of χ , computed with spatial intervals equal to $2\Delta x$ and $2\Delta y$.

For points that are adjacent to a wall, we derive corresponding formulas incorporating the homogeneous Neumann boundary condition. For example, applying (8.7.17) for $i = 2$ and $j = 2$, and setting $(\partial\chi/\partial y)_{2,1} = 0$ and $(\partial\chi/\partial x)_{1,2} = 0$, we obtain

$$\frac{\rho}{\Delta t} D_{2,2}^{**} = \frac{\chi_{4,2} - \chi_{2,2}}{4\Delta x^2} + \frac{\chi_{2,4} - \chi_{2,2}}{4\Delta y^2}. \quad (8.7.19)$$

Returning to (8.7.17), we reduce the intervals of the centered spatial differences to Δx and Δy , and derive the alternative expression

$$\frac{\rho}{\Delta t} D_{i,j}^{**} = \frac{\chi_{i+1,j} - 2\chi_{i,j} + \chi_{i-1,j}}{\Delta x^2} + \frac{\chi_{i,j+1} - 2\chi_{i,j} + \chi_{i,j-1}}{\Delta y^2}, \quad (8.7.20)$$

which may be applied at all interior grid points. This finite-difference equation could have been derived directly from (8.7.14) by taking the divergence of both sides, and then approximating the emerging Laplacian of χ on the right-hand side with the five-point formula, as shown in (8.7.20).

Evaluating (8.7.18) or (8.7.20) at the interior grid points, and the counterparts of the former for the wall-adjacent points, and introducing boundary conditions for χ , we obtain a system of linear equations for the grid values of χ , which is the counterpart of the linear system descending from the pressure Poisson equation discussed in Section 8.6. Having computed the grid values of the projection function, we return

to equation (8.7.15) and perform the final step, advancing the velocity to the $n + 1$ time level corresponding to time $t + \Delta t$.

It is important to note that the coefficient matrix of the linear system associated with (8.7.18) or (8.7.20) is independent of time, and this allows us to either compute its inverse at the outset and then solve the system at each step by simple matrix-vector multiplication, or else design and use efficient custom-made iterative solution algorithms.

8.7.3 Boundary conditions for the intermediate velocity

To this end, we address the issue of boundary conditions for the intermediate velocities denoted by a single or double asterisk. The choice of these conditions stems from a key observation: because of the homogeneous Neumann condition chosen for the projection function, the projection step introduces a tangential but not a normal component of boundary velocity. Accordingly, the boundary conditions for the intermediate velocity should be designed such that the tangential velocity introduced by the projection step brings the total velocity to the specified value. In practice, this can be done by estimating the magnitude of the intermediate slip velocity and then improving the guess by iteration, as will be explained later in this section.

8.7.4 Flow in a cavity

The implementation of the numerical method involves further considerations that are best illustrated with reference to the familiar problem of flow in a cavity driven by a translating lid.

Implementation of the homogeneous Neumann boundary condition for the projection function

Consider the implementation of the condition of zero normal derivative of the projection function along the boundaries of the cavity illustrated in figure 8.5.1. Requiring $\partial\chi/\partial y = 0$ at the bottom and top walls, and approximating the first derivative with a second-order forward or backward finite differences, we find

$$\left(\frac{\partial\chi}{\partial y}\right)_{i,1} \simeq \frac{-3\chi_{i,1} + 4\chi_{i,2} - \chi_{i,3}}{2\Delta y} = 0, \quad (8.7.21)$$

and

$$\left(\frac{\partial \chi}{\partial y}\right)_{i, N_y+1} \simeq \frac{\chi_{i, N_y-1} - 4\chi_{i, N_y} + 3\chi_{i, N_y+1}}{2\Delta y} = 0. \quad (8.7.22)$$

Requiring $\partial\chi/\partial x = 0$ at the left and right walls, and approximating the first derivative with a second-order forward or backward finite-difference formula, we find

$$\left(\frac{\partial \chi}{\partial y}\right)_{1, j} \simeq \frac{-3\chi_{1, j} + 4\chi_{2, j} - \chi_{3, j}}{2\Delta x} = 0, \quad (8.7.23)$$

and

$$\left(\frac{\partial \chi}{\partial y}\right)_{N_x+1, j} \simeq \frac{-\chi_{N_x-1, j} + 4\chi_{N_y, j} - 3\chi_{N_y+1, j}}{2\Delta x} = 0. \quad (8.7.24)$$

Compatibility condition for system (8.7.18)

The linear system descending from (8.7.18) accompanied by the homogeneous Neumann boundary conditions is singular, which means that it has either no solution or an infinite number of solutions depending on the right-hand side. If a multiplicity of solutions exists, then any particular solution may be altered by adding to it an arbitrary constant vector with equal elements, which means that the value of the projection function at the grid points may be shifted by a physically irrelevant constant. Reference to (8.7.15) ensures that this constant has no effect on the structure of the flow.

It can be shown that, when the discrete divergence of the second intermediate velocity is computed using (8.7.16), the linear system has a multiplicity of solutions; that is, the discrete form of the compatibility condition discussed at the end of Section 8.6 is fulfilled. A solution may then be found by assigning an arbitrary value to one of the unknowns, discarding one equation, and solving the rest of the equations for the remaining unknowns. Unfortunately, the numerical solution computed in this manner is contaminated by artificial oscillations described as *odd-even coupling*.

Compatibility condition for system (8.7.20)

The linear system descending from (8.7.20) accompanied by the homogeneous Neumann boundary conditions is also singular, reflecting the arbitrary level of the projection function. Unfortunately, when the discrete divergence of the second intermediate velocity is computed using

(8.7.16), the discrete form of the compatibility condition is not satisfied, which means that one of the equations of the linear system may not be fulfilled. Resisting the temptation to discard one equation, we implement a more elegant approach which involves adding a small term to the right-hand side of (8.7.20), and then adjusting its magnitude to satisfy the compatibility condition of the modified system of equations obtained in this fashion. If $\mathbf{A} \cdot \mathbf{x} = \mathbf{b}$ is the linear system corresponding to (8.7.20), then the modified system is

$$\mathbf{A} \cdot \mathbf{x} = \mathbf{b} + \epsilon \mathbf{c}, \quad (8.7.25)$$

where ϵ is an *a priori* unknown constant, and \mathbf{c} is a constant vector that emerges by replacing the left-hand side of (8.7.17) with an arbitrary value, while retaining the linear equations implementing the homogeneous Neumann boundary conditions. Our objective is to adjust the value of the constant ϵ so that the system (8.7.25) has an infinite number of solutions, and this can be done working as follows:

1. Set the value of the last component of \mathbf{x} equal to zero, discard the last equation of $\mathbf{A} \cdot \mathbf{x} = \mathbf{b}$, solve the remaining equations, and call the solution $\mathbf{x}^{(1)}$. Then evaluate the difference $r^{(1)}$ between the left-hand side and the right-hand of the last equation.
2. Set the value of the last component of \mathbf{x} equal to zero, discard the last equation of $\mathbf{A} \cdot \mathbf{x} = \mathbf{c}$, solve the remaining equations, and call the solution \mathbf{x}^{Ref} . Then evaluate the difference r^{Ref} between the left-hand side and the right-hand of the last equation.
3. The desired solution is

$$\mathbf{x} = \mathbf{x}^{(1)} + \epsilon \mathbf{x}^{Ref}, \quad (8.7.26)$$

where $\epsilon = -r^{(1)}/r^{Ref}$.

Boundary conditions for the intermediate velocity

The boundary conditions for the intermediate velocity must be such that the right-hand side of (8.7.15) is consistent with the specified boundary conditions at time $t + \Delta t$. Requiring that the left-hand side of (8.7.15) vanishes over a stationary boundary, we obtain the boundary condition

$$\mathbf{u}_{i,j}^{**} = \frac{\Delta t}{\rho} (\nabla \chi)_{i,j}^n. \quad (8.7.27)$$

Now, because the projection function was required to satisfy the homogeneous Neumann boundary condition, the right-hand side of (8.7.27) has only a tangential component expressing a numerical wall slip. An apparent difficulty in computing the tangential component of the boundary condition for the intermediate velocity is that the right-hand side of (8.7.27) is not available during the convection-diffusion step. One way to circumvent this difficulty is to approximate the projection function with that at the previous step, proceed to the projection step, and then improve the approximation by repeating the convection-diffusion step until the slip velocity has become sufficiently small.

Velocity vector fields of the developing flow at Reynolds number $Re = 1$ computed by the numerical discussed in this section are shown in figure 8.7.1. During the early stages of the motion, the flow is similar to that generated by the impulsive translation of a plate. At later times, a fully developed recirculating flow is established.

8.7.5 Computation of the pressure

Two methods are available for recovering the pressure field, if desired. The first method involves combining, for example, equations (8.7.8), (8.7.11), and (8.7.15) to produce a relationship between \mathbf{u}^n and $\mathbf{u}^{(n+1)}$. Requiring that, in the limit as Δt tends to zero, this relationship reduces to a spatially discretized version of the Navier-Stokes equation, we derive an expression for an effective pressure. If the boundary conditions satisfied by the effective pressure are consistent with the Neumann boundary condition satisfied by the actual pressure, then the former can be accepted as an approximation of the latter. The second method involves substituting the velocity into the Navier-Stokes equation, and solving the resulting equation for the pressure subject to the Neumann boundary condition, as discussed in Section 8.6.2.

Problems

Problem 8.7.1 *Singular system for the projection function.*

Show that equation (8.7.26) provides us with the solution of (8.7.25) subject to the homogeneous Neumann boundary condition.

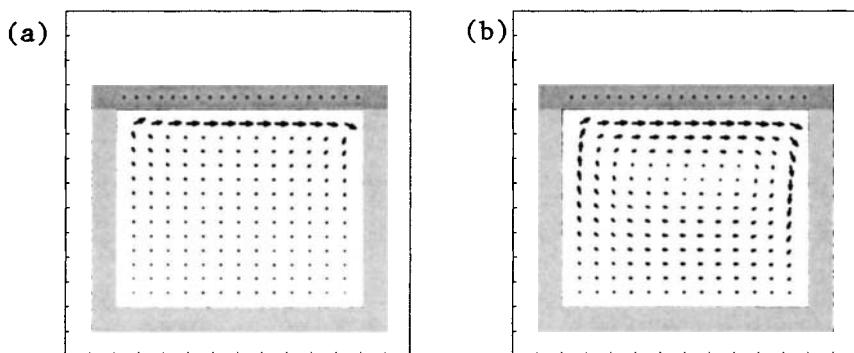


Figure 8.7.1 Velocity vector fields of the flow developing in a rectangular cavity due to the translation of the lid at Reynolds number $Re \equiv UL/\nu = 1$, where U is the lid velocity, and L is the cavity side length, computed using program *11_fdm/cvt_pm* of *FDLIB*. (a) Early, and (b) well-developed stages of the flow.

Computer problem

Problem c.8.7.1 *Developing flow in a cavity.*

Subdirectory *11_fdm/cvt_pm* of *FDLIB* contains a program that computes the flow developing in a rectangular cavity using the projection method discussed in the text. Run the program for two sets of conditions of your choice, prepare velocity vector fields, and discuss the structure of the flow and the performance of the numerical method.

Chapter 9

Flow at Low Reynolds Numbers

- 9.1 Flow in narrow channels**
- 9.2 Film flow on a horizontal or down a plane wall**
- 9.3 Two-layer channel flow**
- 9.4 Flow due to the motion of a sphere**
- 9.5 Point forces and point sources in Stokes flow**
- 9.6 Two-dimensional flow**
- 9.7 Flow near corners**

Newton's second law of motion requires that the rate of change of momentum of a fluid parcel be balanced by the body force exerted on its volume and the surface force exerted on its boundary. Under certain conditions, the rate of change of momentum is small compared to the body and surface force, and may be neglected without introducing serious error. This occurs, in particular, when the viscosity of the fluid is high, when the density is small, when the velocity changes rapidly over a small distance yielding a sharp spatial gradient, or when the velocity by which a fluid parcel is convected by the flow is sufficiently small. The formal requirement for fluid inertia to be negligible is that a properly defined Reynolds number be sufficiently small. How small it should be, depends on the particular problem under consideration. In this chapter, we consider a family of flows occurring at small Reynolds numbers, and discuss the solution of the simplified system of governing equations that arises by dropping the inertial terms from the equation of motion. This simplification will allow us to address a multitude of physical problems and obtain solutions by a host of analytical and numerical methods.

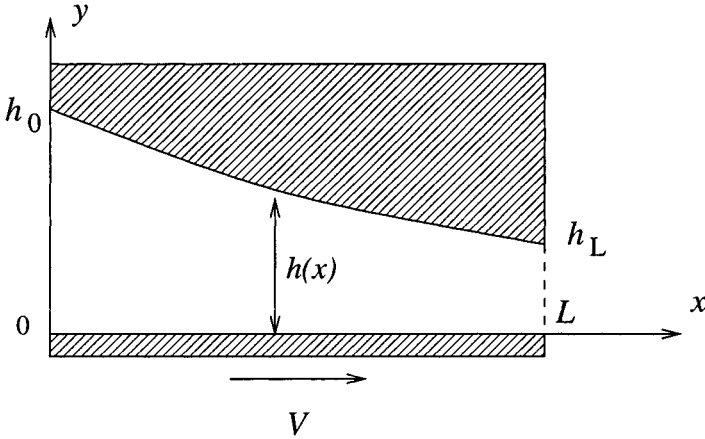


Figure 9.1.1 Schematic illustration of flow in a narrow channel: lubrication flow in a slider bearing with a curved upper surface.

9.1 Flow in narrow channels

We begin by considering steady, nearly unidirectional flow in a two-dimensional channel confined between a gently sloped upper surface and a perfectly flat lower surface, as illustrated in Figure 9.1.1. The flow is driven by the translation of the upper wall parallel to itself with velocity V , and possibly by a pressure drop imposed across the length of the channel subtended between $x = 0$ and L .

In the Cartesian system of coordinates depicted in figure 9.1.1, the lower wall is located at $y = 0$, and the upper wall is located at $y = h(x)$; if the channel width is constant, we obtain steady unidirectional flow in a channel with parallel-sided walls considered earlier in Section 7.1. Our present objective is to compute the velocity and pressure field, and also evaluate the force exerted on the walls, for more general flow configurations.

9.1.1 Governing equations

The motion of the fluid is governed by (a) the steady version of the Navier-Stokes equation for an incompressible fluid whose x and y scalar components read

$$\rho \left(u_x \frac{\partial u_x}{\partial x} + u_y \frac{\partial u_x}{\partial y} \right) = -\frac{\partial p}{\partial x} + \mu \left(\frac{\partial^2 u_x}{\partial x^2} + \frac{\partial^2 u_x}{\partial y^2} \right) + \rho g_x, \quad (9.1.1)$$

and

$$\rho \left(u_x \frac{\partial u_y}{\partial x} + u_y \frac{\partial u_y}{\partial y} \right) = -\frac{\partial p}{\partial y} + \mu \left(\frac{\partial^2 u_y}{\partial x^2} + \frac{\partial^2 u_y}{\partial y^2} \right) + \rho g_y, \quad (9.1.2)$$

and (b) by the continuity equation

$$\frac{\partial u_x}{\partial x} + \frac{\partial u_y}{\partial y} = 0. \quad (9.1.3)$$

Our first task is to show that, under certain conditions, a number of terms in equations (9.1.1) and (9.1.2) are negligible compared to others, and may thus be discarded yielding a simplified system of governing equations known as the equations of *lubrication flow*.

9.1.2 Scaling arguments

Consider the term $\partial u_x / \partial x$ on the left-hand side of equation (9.1.1). If the upper wall were perfectly flat and parallel to the lower wall, the flow would be unidirectional and this term would be identically equal to zero. More generally, suppose that $U_x(x_1)$ is the maximum of the magnitude of the x component of the velocity at a particular location $x = x_1$, and $U_x(x_2)$ is the corresponding maximum at the location $x = x_2$, where the maximum is defined with respect to y . Scaling arguments suggest that the magnitude of the term $\partial u_x / \partial x$ is comparable to the magnitude of the ratio $[U_x(x_2) - U_x(x_1)] / (x_2 - x_1)$.

To this end, we identify the distance $x_2 - x_1$ with the length necessary for the difference $U_x(x_2) - U_x(x_1)$ to become comparable to $U_x(x_1)$, and scale the partial derivative $\partial u_x / \partial x$ with the ratio $U_x(x_1) / (x_2 - x_1)$. If the upper wall were perfectly flat and parallel to the lower wall, then the distance $x_2 - x_1$ would be infinite, and this ratio would vanish.

Similar arguments can be made to show that the term $\partial u_x / \partial y$ evaluated at $x = x_1$, scales with $U_x(x_1) / h(x_1)$, the term $\partial^2 u_x / \partial x^2$ evaluated at $x = x_1$ scales with $U_x(x_1) / (x_2 - x_1)^2$, and the term $\partial^2 u_x / \partial y^2$ evaluated at $x = x_1$, scales with $U_x(x_1) / h^2(x_1)$.

Next, we consider the continuity equation (9.1.3), and scale the partial derivative $\partial u_y / \partial y$ evaluated at $x = x_1$ with $U_y(x_1) / h(x_1)$, where

$U_y(x_1)$ is the maximum of the magnitude of the y component of the velocity at $x = x_1$. The continuity equation requires that the magnitude of $\partial u_y / \partial y$ be comparable to the magnitude of $\partial u_x / \partial x$, which was found to be of order $U_x(x_1)/(x_2 - x_1)$. This will be true only if $U_y(x_1)$ scales with $U_x(x_1) h(x_1)/(x_2 - x_1)$.

9.1.3 Relative magnitudes

Using the preceding scalings, we find that the ratio of the magnitude of the first term on the left-hand side of (9.1.1) to the magnitude of the penultimate term on the right-hand side is

$$\frac{\rho U_x(x_1) \frac{U_x(x_1)}{x_2 - x_1}}{\mu \frac{U_x(x_1)}{h^2(x_1)}} = \frac{\rho h(x_1) U_x(x_1)}{\mu} \frac{h(x_1)}{x_2 - x_1}. \quad (9.1.4)$$

The ratio of the magnitude of the second term on the left-hand side of (9.1.1) to the magnitude of the penultimate term on the right-hand side is

$$\frac{\rho h(x_1) \frac{U_x(x_1)}{x_2 - x_1} \frac{U_x(x_1)}{h(x_1)}}{\mu \frac{U_x(x_1)}{h^2(x_1)}} = \frac{\rho h(x_1) U_x(x_1)}{\mu} \frac{h(x_1)}{x_2 - x_1}. \quad (9.1.5)$$

And the ratio of the magnitude of the second term on the right-hand side of (9.1.1) to the magnitude of the penultimate term on the right-hand side is

$$\frac{\mu \frac{U_x(x_1)}{(x_2 - x_1)^2}}{\mu \frac{U_x(x_1)}{h^2(x_1)}} = \left(\frac{h(x_1)}{x_2 - x_1} \right)^2. \quad (9.1.6)$$

9.1.4 Equations of lubrication flow

The first fraction on the right-hand sides of (9.1.4) and (9.1.5) is the local Reynolds number of the flow defined with respect to the local channel width. If the magnitude of the local Reynolds number and the magnitude of the ratio $h(x_1)/(x_2 - x_1)$ are such that the right-hand sides of equations (9.1.4)-(9.1.6) are much smaller than unity, then the first and penultimate terms on the right-hand side of (9.1.1) will dominate the x component of the equation of motion, leading to the simplified form

$$0 = -\frac{\partial p}{\partial x} + \mu \frac{\partial^2 u_x}{\partial y^2} + \rho g_x, \quad (9.1.7)$$

which describes locally unidirectional flow.

Consider next the distribution of the pressure. Equation (9.1.7) requires that the magnitude of the term $-\partial p/\partial x + \rho g_x$ be comparable to the magnitude of $\mu \partial^2 u_x/\partial y^2$, which scales with $\mu U_x(x_1)/h^2(x_1)$. Consideration of the individual terms on both sides of the y component of the equation of motion (9.1.2) shows that the term $-\partial p/\partial y + \rho g_y$ scales with $\mu U_x(x_1)/[(x_2 - x_1)h(x_1)]$. It is evident then that, when the ratio $h(x_1)/(x_2 - x_1)$ is small, non-hydrostatic pressure variations in the y direction may be neglected. Accordingly, the y component of the equation of motion (9.1.2) reduces to

$$0 = -\frac{\partial p}{\partial y} + \rho g_y. \quad (9.1.8)$$

Differentiating (9.1.8) once with respect to x , we find that the axial pressure gradient $\partial p/\partial x$ is independent of the lateral position y , and is only a function of the axial position x .

Physically, the flow may be assumed to be locally unidirectional and parallel to the x axis. At every station x , the upper and lower walls appear to be parallel, separated by a distance that is equal to the local channel width, $h(x)$.

9.1.5 Lubrication in a slider bearing

As an application, we consider flow in the lubrication zone of a slider bearing illustrated in figure 9.1.2. The lower wall is horizontal and the upper wall is gently sloped by the angle α . The pressure is held constant at either end of the lubrication zone extending from $x = 0$ to L . For example, if the fluid at one end of the lubrication zone is exposed to the atmosphere, then the pressure at that end is equal to the pressure of the atmosphere. Hydrostatic pressure variations in the y direction are assumed to be negligibly small.

Reviewing the scaling arguments discussed in Sections 9.1.2 and 9.1.3, we identify the distance $x_2 - x_1$ with the length of the lubrication zone L . A special case arises when the two walls are parallel: the distance $x_2 - x_1$ becomes infinite, and no error is introduced by dropping the inertial terms in the equation of motion.

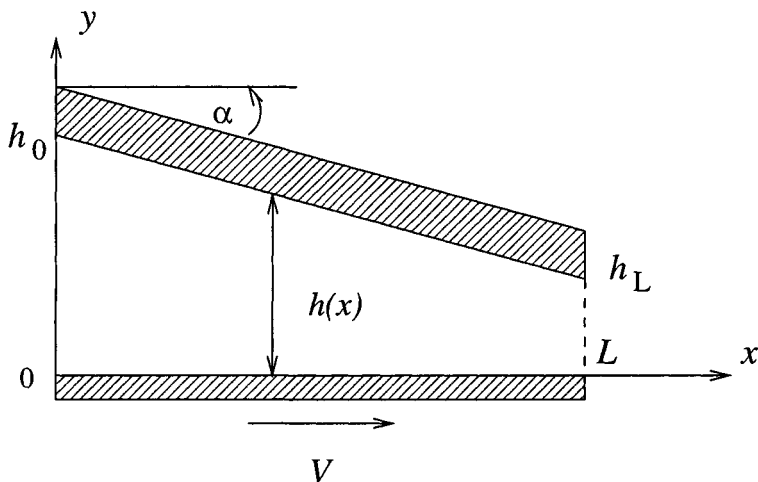


Figure 9.1.2 Lubrication flow in a slider bearing with a planar upper surface.

Velocity and flow rate

Proceeding with the solution, we approximate $\tan \alpha \simeq \alpha$, and express the local channel width in the simplified form $h(x) = h_0 - \alpha x$, where $h_0 \equiv h(x = 0)$ is the channel width at the beginning of the lubrication zone. Next, we use the velocity profile derived in Section 7.1 for flow in a two-dimensional channel with parallel-sided walls, and find that the solution of (9.1.7) is given by

$$u_x(x, y) = V \left(1 - \frac{y}{h(x)}\right) - \frac{1}{2\mu} y [h(x) - y] \frac{dp}{dx}(x). \quad (9.1.9)$$

The local axial pressure gradient $(dp/dx)(x)$ is an unknown that must be computed as part of the solution. The local flow rate along the channel corresponding to (9.1.9) is given by

$$Q(x) \equiv \int_0^{h(x)} u_x(x, y) dy = \frac{1}{2} V h(x) - \frac{h^3(x)}{12 \mu} \frac{dp}{dx}(x). \quad (9.1.10)$$

A key observation is that, because in a stationary frame of reference the flow is steady, the flow rate $Q(x)$ is not only constant in time, but also independent of the streamwise position x . To verify this statement, we

perform a mass balance over a control area confined between two cross-sections of the channel that are separated by an infinitesimal distance, and note that fluid neither enters nor escapes from the control volume through the bottom or top.

Computation of the pressure

Solving equation (9.1.10) for the axial pressure gradient, and substituting $h(x) = h_0 - \alpha x$ for the channel width, we find

$$\frac{dp}{dx} = \frac{6\mu V}{(h_0 - \alpha x)^2} - \frac{12\mu Q}{(h_0 - \alpha x)^3}. \quad (9.1.11)$$

To compute the flow rate Q , we exercise our knowledge of the pressure at the two ends of the lubrication zone: equation (9.1.11) provides us with the local pressure gradient whose integral with respect to x across the lubrication zone must produce a specified pressure drop. This mathematical condition is a reflection of the physical environment in which the lubrication flow takes place. Performing the integration, we find

$$\begin{aligned} -\Delta p \equiv p(x=L) - p(x=0) &= \int_0^L \frac{dp}{dx} dx \\ &= \int_0^L \left(\frac{6\mu V}{(h_0 - \alpha x)^2} - \frac{12\mu Q}{(h_0 - \alpha x)^3} \right) dx, \end{aligned} \quad (9.1.12)$$

where Δp is the pressure drop.

For simplicity, we assume that the end-pressures are equal, so that $\Delta p = 0$. Carrying out the integration on the right-hand side of (9.1.12), solving for Q , and then simplifying, we derive the expression

$$Q = V \frac{h_0 h_L}{h_0 + h_L}, \quad (9.1.13)$$

where $h_L = h_0 - \alpha L$ is the channel width at the end of the lubrication zone. Note that, if either h_0 or h_L vanishes, in which case the channel is closed at one end, the flow rate is equal to zero, as expected.

Substituting the right-hand side of (9.1.13) for the flow rate into the right-hand side of (9.1.12), and carrying out the integration, we find the pressure distribution

$$\begin{aligned}
 p(x) &= p(x=0) + \int_0^x \frac{dp}{dx} dx \\
 &= p(x=0) + \frac{6\mu V}{h_0 + h_L} \frac{\alpha x(L-x)}{(h_0 - \alpha x)^2}.
 \end{aligned}
 \tag{9.1.14}$$

It is reassuring to confirm that the second term on the right-hand side of (9.1.14) vanishes when $x = L$, yielding the specified zero pressure drop.

Lift force

The y component of the hydrodynamic force exerted on the upper sloped surface may be approximated with the integral

$$F_y = \int_0^L p(x) dx. \tag{9.1.15}$$

Substituting the pressure distribution (9.1.14) into the integrand, and carrying out the integration, we find

$$F_y = p(x=0) L + \frac{6\mu VL^2}{h_0^2} \kappa^2 \left(\ln \frac{h_0}{h_L} - 2 \frac{h_0 - h_L}{h_0 + h_L} \right). \tag{9.1.16}$$

We have introduced the geometrical factor

$$\kappa \equiv \frac{h_0}{\alpha L}, \tag{9.1.17}$$

taking values in the range $(-\infty, 0)$ or $(1, \infty)$; a negative value corresponds to an upper wall sloping upward, and a positive value corresponds to an upper wall sloping downward. Values of κ in the range $[0, 1]$ are prohibited by the requirement that the upper wall does not slope downward so much as to touch the lower wall before the end of the lubrication zone. When, in particular, $\kappa = 1$, the two walls meet at $x = L$, and the channel is closed at the right end.

In summary, we have derived expressions for the flow rate, pressure distribution, and normal force given, respectively, by equations (9.1.13), (9.1.14), and (9.1.16), and this concludes the goal of our analysis. To interpret the results in physical terms, we restate expression (9.1.16) in the form

$$F_y = p(x=0) L + \frac{6\mu VL^2}{h_0^2} G(\kappa), \tag{9.1.18}$$

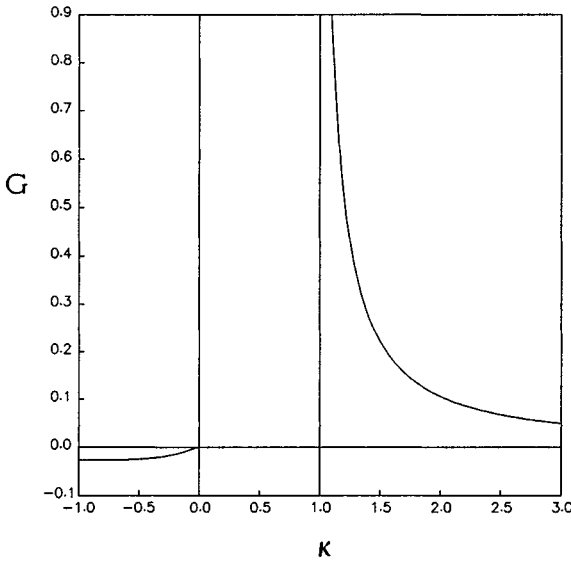


Figure 9.1.3 Graph of the function $G(\kappa)$ expressing the hydrodynamic lift force exerted on the inclined plane shown in figure 9.1.1.

where the function $G(\kappa)$, expressing the hydrodynamic lift or load force, is given by

$$G(\kappa) \equiv \kappa^2 \left(\ln \frac{\kappa}{\kappa - 1} - \frac{2}{2\kappa - 1} \right). \quad (9.1.19)$$

Figure 9.1.3 displays the graph of $G(\kappa)$ in its domain of definition. The results show that the lubrication force is positive when the plane wall moves towards the minimum gap, and negative when the plane wall moves towards the maximum gap. In the former case, the lift force is able to balance the weight of an overlying object whose lower surface is represented by the inclined plane, provided that κ is sufficiently close to unity. In the latter case, the lubrication force pulls the object toward the plane wall closing the gap and choking the flow.

9.1.6 Flow in a wavy channel

The preceding analysis may be extended in a straightforward fashion to arbitrary channel geometries. A fundamental assumption is that the

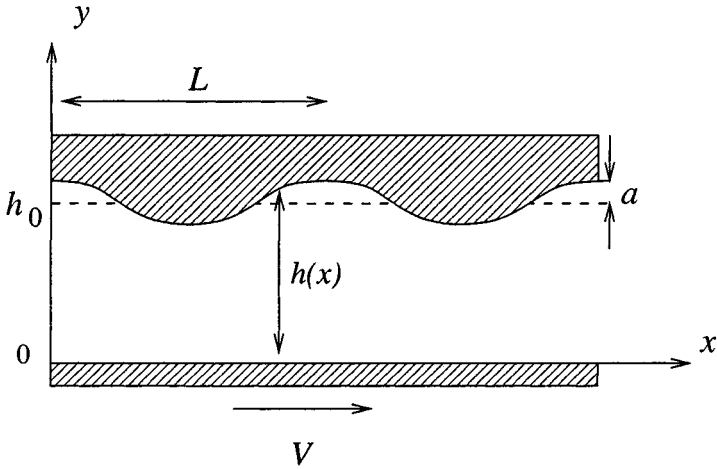


Figure 9.1.4 Lubrication flow in a furrowed channel confined between a plane and a wavy wall.

conditions for the right-hand sides of (9.1.4)-(9.1.6) to be small must be satisfied; that is, the local Reynolds number and the ratio $h(x_1)/(x_2 - x_1)$ must both be small.

Consider, for example, flow in a periodic channel confined between a plane and a wavy wall, as illustrated in figure 9.1.4. The local channel width is given by

$$h(x) = h_0 + a \cos \frac{2\pi x}{L}, \tag{9.1.20}$$

where h_0 is the average channel width, L is the period, and a is the amplitude of the corrugations. The streamwise velocity and flow rate are given by equations (9.1.9) and (9.1.10), with $h(x)$ given in (9.1.20). The counterpart of equation (9.1.11) is

$$\frac{dp}{dx} = \frac{6\mu V}{(h_0 + a \cos \frac{2\pi x}{L})^2} - \frac{12\mu Q}{(h_0 + a \cos \frac{2\pi x}{L})^3}, \tag{9.1.21}$$

and the negative of the pressure drop over one period is given by

$$\begin{aligned} -\Delta p \equiv p(x=L) - p(x=0) &= \int_0^L \frac{dp}{dx} dx \\ &= \int_0^L \left(\frac{6\mu V}{(h_0 + a \cos \frac{2\pi x}{L})^2} - \frac{12\mu Q}{(h_0 + a \cos \frac{2\pi x}{L})^3} \right) dx. \end{aligned} \tag{9.1.22}$$

Solving for Q , we find

$$Q = \frac{\frac{\Delta p}{6\mu} + V \int_0^L \frac{dx}{(h_0 + a \cos \frac{2\pi x}{L})^2}}{2 \int_0^L \frac{dx}{(h_0 + a \cos \frac{2\pi x}{L})^3}}, \quad (9.1.23)$$

which provides us with an expression for the flow rate in terms of the specified wall velocity and pressure drop.

The definite integrals on the right-hand side of (9.1.23) are best computed by numerical methods. Interestingly, because the integrands are periodic, best results are obtained by using the simplest algorithm of numerical integration expressed by the *trapezoidal rule*: divide the integration domain $(0, L)$ into N intervals of equal length $\Delta x = L/N$, and introduce the approximation

$$\int_0^L \frac{dx}{(h_0 + a \cos \frac{2\pi x}{L})^2} \simeq \Delta x \sum_{i=1}^N \frac{1}{(h_0 + a \cos \frac{2\pi x_i}{L})^2}, \quad (9.1.24)$$

where $x_i = (i - 1) \Delta x$ are the end-points of the intervals; similarly for the integral in the denominator of (9.1.23). It can be shown that, as the number of divisions N becomes larger, the difference between the left- and right-hand side of (9.1.24), defined as the numerical error, decreases faster than any power of $1/N$, allowing for rapid convergence.

Once the flow rate has been found, the result may be substituted into the right-hand side of (9.1.22), and the expression thus obtained may be integrated by analytical or numerical methods to yield the pressure distribution along the channel; the velocity follows from (9.1.9).

9.1.7 Dynamic lifting

An extension of the preceding analysis allows us to develop a method of simulating the motion of a two-dimensional body pressing against a horizontal wall that translates along the x axis with velocity V , as illustrated in figure 9.1.5. The clearance between the body and the translating wall is occupied by a lubricating fluid, with the lubrication zone extending from $x = -b$ and a . This configuration serves as a two-dimensional model of the flow between a piston ring pressing against the cylinder of a combustion chamber in an internal combustion engine.

The lubrication flow generates a pressure field, and the associated lifting force causes the body to move along the y axis with velocity $V_B = dc/dt$, where c is the minimum film thickness; that is, the minimum

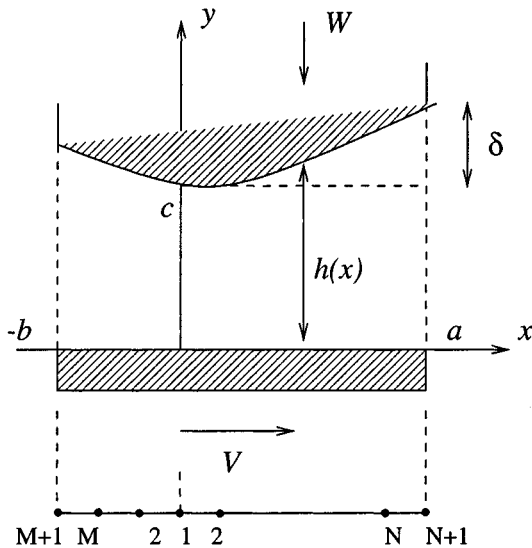


Figure 9.1.5 A two-dimensional body pressing against a sliding wall under the influence of its weight. The lubrication force developing between the body and the wall repels the body away from the wall.

clearance between the body and the translating wall. Our objective is to compute the evolution of the function $c(t)$ from a specified initial state. Hydrostatic pressure variations in the y direction are assumed to be negligibly small.

We begin by writing a mass balance for the lubricating fluid requiring,

$$\frac{dc}{dt} = -\frac{\partial Q}{\partial x}. \quad (9.1.25)$$

Evaluating the flow rate from the right-hand side of (9.1.10), we derive a partial-differential equation for the pressure,

$$\frac{\partial}{\partial x} \left(\frac{h^3}{\mu} \frac{\partial p}{\partial x} \right) = 6V \frac{\partial h}{\partial x} + 12 \frac{dc}{dt}, \quad (9.1.26)$$

which is to be solved subject to the specified, and possibly time-dependent, boundary conditions $p(x = -b) = P_1(t)$ and $p(x = a) = P_2(t)$. The vertical velocity of the body $V_B = dc/dt$ is determined by the balance between the weight of the body, denoted by W , and the lifting force due to the pressure, expressed by

$$W = \int_{-b}^a p(x, t) dx. \quad (9.1.27)$$

The solution may be computed using the following algorithm:

1. Solve the following simplified version of equation (9.1.26),

$$\frac{\partial}{\partial x} \left(\frac{h^3}{\mu} \frac{\partial p}{\partial x} \right) = 6V \frac{\partial h}{\partial x}, \quad (9.1.28)$$

subject to the required boundary conditions $p(x = -b) = P_1(t)$ and $p(x = a) = P_2(t)$, and call the solution $p_1(x)$.

2. Solve the following simplified version of equation (9.1.26),

$$\frac{\partial}{\partial x} \left(\frac{h^3}{\mu} \frac{\partial p}{\partial x} \right) = 12, \quad (9.1.29)$$

subject to the *homogeneous* boundary conditions $p(x = -b) = 0$ and $p(x = a) = 0$, and call the solution $p_2(x)$.

3. Set

$$p(x) = p_1(x) + \frac{dc}{dt} p_2(x). \quad (9.1.30)$$

4. Substitute the pressure distribution (9.1.30) into the force balance (9.1.27), and carry out the integration to compute dc/dt .
5. Having evaluated dc/dt , update the minimum clearance c .
6. Return to step 1 and repeat.

Straightforward substitution shows that the pressure distribution (9.1.30) satisfies the governing equation (9.1.26) and the pressure boundary conditions specified at either end.

Problems

Problem 9.1.1 *Lubrication in a slider bearing.*

Confirm that the function $G(\kappa)$ defined in equation (9.1.19) satisfies the symmetry property $H(\kappa-0.5) = -H(0.5-\kappa)$, and explain in physical terms why.

Problem 9.1.2 *Flow in a symmetric channel.*

Consider pressure-drive flow in a symmetric channel with stationary wavy walls located at $y = h(x) = \pm(h_0 + a \cos(2\pi x/L))$. Derive an expression for the flow rate in terms of the pressure drop over one period.

Computer problems

Problem c.9.1.1 *Flow in a wavy channel.*

(a) Consider flow in a channel confined between a plane and a wavy wall, as discussed in the text, driven by an imposed pressure drop; in this case, $V = 0$. Prepare a graph of the dimensionless flow rate $\hat{Q} \equiv 12\mu LQ/(h_0^3 \Delta P)$ against the reduced amplitude a/h_0 , and discuss its functional form. The integral on the right-hand side of (9.1.23) should be computed using the trapezoidal rule, as shown in equation (9.1.24).

(b) Repeat (a) for flow driven by boundary motion, corresponding to $\Delta p = 0$. Prepare a graph of the dimensionless flow rate $\hat{Q} \equiv 2Q/(V h_0)$ against the reduced amplitude a/h_0 , and discuss its functional form.

Problem c.9.1.2 *Dynamical simulation of the lifting of a body due to lubrication.*

Directory *05_lub/bear_2d* of *FDLIB* contains a program that simulates the lateral motion a body pressing against a translating wall, using the numerical method discussed in the text. The geometry of the body is specified by the lengths a , b , and δ defined in figure 9.1.5. In the finite-difference implementation, the left part of the lubrication zone, extending over $-b < x < 0$, is divided into M intervals, and the right part of the lubrication zone, extending over $0 < x < a$, is divided into N intervals, as depicted at the bottom of figure 9.1.5. The derivatives with respect to x in equations (9.1.28) and (9.1.29) are approximated with second-order finite differences, yielding a tridiagonal systems of algebraic equations for the pressure at the nodes.

Run the program for two sets of conditions of your choice, prepare a plot of the minimum film thickness as a function of time, and discuss the results of your simulations.

9.2 Film flow on a horizontal or down a plane wall

One distinguishing feature of the flow in narrow channels discussed in Section 9.1, is that the velocity profile may be approximated locally with the parabolic profile corresponding to unidirectional flow in a channel confined between two parallel plane walls. An analogous simplification is possible in the case of a liquid film bounded by a free surface over which the shear stress is required to vanish, discussed in this section, and in the case of a liquid layer bounded by a fluid interface, to be discussed in Section 9.3.

Consider the unsteady flow of a liquid film over a horizontal wall or down an inclined plane wall, as illustrated in figure 9.2.1. In the inclined system of coordinates depicted in this figure, the wall is located at $y = 0$, and the free surface is located at $y = h(x, t)$. The components of the gravity vector are given by

$$g_x = g \sin \theta_0, \quad g_y = -g \cos \theta_0, \quad (9.2.1)$$

where g is the acceleration of gravity, and θ_0 is the inclination angle of the wall; if the wall is horizontal, $\theta_0 = 0$, and if the wall is vertical, $\theta_0 = \pi/2$. The pressure above the film is assumed to be uniform and equal to the atmospheric pressure P_{Atm} . Our objective is to derive a differential equation governing the evolution of the film thickness $h(x, t)$ from a specified initial configuration.

9.2.1 Governing equations

Repeating the scaling arguments of Section 9.1, we find that, when the free surface is gently sloped, that is, the magnitude of $|\partial h/\partial x|$ is uniformly small, the x and y components of the equation of motion reduce to the lubrication equations (9.1.7) and (9.1.8). Integrating equation (9.1.8) with respect to y from an arbitrary location y up to the location of the free surface, we find

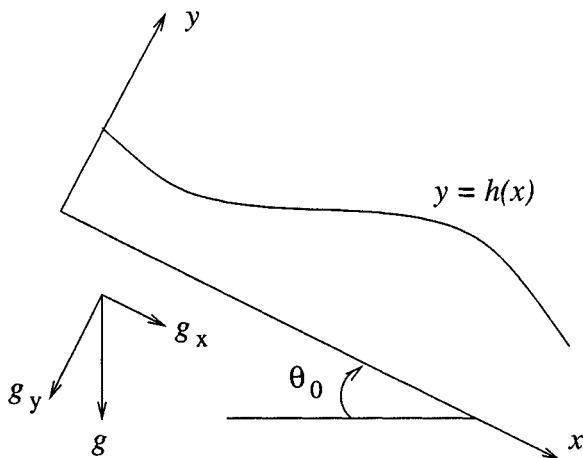


Figure 9.2.1 Illustration of a viscous film flowing down an inclined plane wall. The motion of the fluid is governed by the simplified equations of lubrication flow.

$$p(x, y, t) = p_{FS} - \rho g_y (h - y), \quad (9.2.2)$$

where $p_{FS} = p(x, y = h(t), t)$ is the pressure on the side of the liquid at the free surface.

The simple form of the lubrication equation (9.1.7) allows us to pretend that the flow is locally unidirectional and parallel to the x axis. Approximating the velocity profile across the uneven film with the Nusselt parabolic profile across a flat film with a planar free surface, given in equation (7.2.3), we find

$$u_x(x, y, t) = \left(-\frac{\partial p}{\partial x} + \rho g_x\right) \frac{1}{2\mu} y (2h - y), \quad (9.2.3)$$

Note that the x dependence enters in a parametric fashion through the pressure gradient. The term enclosed by the first set of parentheses on the right-hand side of (9.2.3) incorporates the effective body force due to gravity and the streamwise pressure gradient due to surface tension, as will be discussed shortly. The flow rate is given by

$$Q(x, t) \equiv \int_0^{h(x, t)} u_x(x, y, t) dy = \left(-\frac{\partial p}{\partial x} + \rho g_x\right) \frac{1}{3\mu} h^3(x, t). \quad (9.2.4)$$

Further analysis involves two key steps.

9.2.2 Evaluation of the pressure gradient

First, we observe that the normal stress undergoes a jump across the interface due to the surface tension γ , as required by the interfacial condition (4.2.22). In the context of locally unidirectional flow, the normal stress can be approximated with the negative of the pressure, yielding the pressure jump condition

$$p_{FS} = P_{Atm} + \gamma \kappa. \quad (9.2.5)$$

Moreover, the curvature of the mildly sloped free surface may be approximated with the simple form

$$\kappa(x) \simeq -\frac{\partial^2 h}{\partial x^2}. \quad (9.2.6)$$

Substituting (9.2.6) into (9.2.5), and the result into (9.2.2), we obtain the pressure distribution inside the film in terms of the film thickness,

$$p(x, y, t) \simeq P_{Atm} - \rho g_y (h - y) - \gamma \frac{\partial^2 h}{\partial x^2}. \quad (9.2.7)$$

Substituting further (9.2.7) into the right-hand side of (9.2.4), we derive an expression for the flow rate in terms of the film thickness,

$$Q(x, t) = \frac{\rho}{3\mu} h^3 \left(g_x + g_y \frac{\partial h}{\partial x} + \frac{\gamma}{\rho} \frac{\partial^3 h}{\partial x^3} \right). \quad (9.2.8)$$

9.2.3 Mass balance

Second, we perform a mass balance over a control area that is confined between (a) two parallel planes that are normal to the plane wall and are separated by an infinitesimal distance, (b) the corresponding section of the evolving free surface, and (c) the wall. The mass balance requires that the rate of accumulation of mass within the control volume be equal to the difference between the flow rates into and out from the control volume. In differential form,

$$\frac{\partial h}{\partial t} = -\frac{\partial Q}{\partial x}. \quad (9.2.9)$$

9.2.4 Evolution equation for the film thickness

To complete the mathematical formulation, we substitute the right-hand side of (9.2.8) into the right-hand side of (9.2.9), and thus obtain a partial differential equation governing the evolution of the film thickness,

$$\frac{\partial h}{\partial t} + \frac{\rho}{3\mu} \frac{\partial}{\partial x} [h^3 (g_x + g_y \frac{\partial h}{\partial x} + \frac{\gamma}{\rho} \frac{\partial^3 h}{\partial x^3})] = 0. \quad (9.2.10)$$

Several features of this equation are worth noting:

- Carrying out the differentiation with respect to x on the left-hand side, we find that the fourth derivative $\partial^4 h / \partial x^4$ springs off from the term involving the surface tension. Since (9.2.10) is a fourth-order equation, *two* boundary conditions at each end of the solution domain, involving h , $\partial h / \partial x$, or $\partial^2 h / \partial x^2$, are required. If the film is periodic, the boundary conditions are replaced by periodicity conditions for the film thickness and its spatial derivatives.

In the absence of surface tension, $\gamma = 0$, (9.2.10) becomes a second-order differential equation, in which case only *one* boundary condition at each end of the solution domain, involving h or $\partial h / \partial x$, is required. If the film is periodic, the boundary conditions are replaced by periodicity conditions.

- Equation (9.2.10) is a first-order differential equation in time t . To compute the solution, an initial condition for $h(x, t = 0)$ at the origin of computational time is required.
- Because of the presence of products of the film thickness h and its spatial derivatives, equation (9.2.10) is highly nonlinear.
- At steady state, $\partial h / \partial t = 0$, the shape of the free surface is described by the ordinary differential equation

$$\frac{d}{dx} [h^3 (g_x + g_y \frac{dh}{dx} + \frac{\gamma}{\rho} \frac{d^3 h}{dx^3})] = 0, \quad (9.2.11)$$

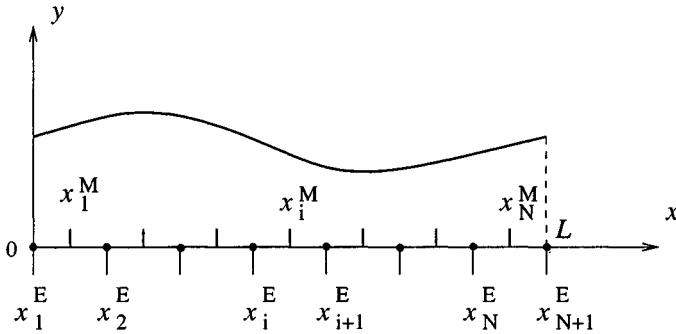


Figure 9.2.2 A finite-volume grid used to compute the evolution of a periodic film.

which admits the flat-film Nusselt solution derived in Section 7.2 for constant film thickness.

9.2.5 Solution by the finite-volume method

Several numerical methods are available for solving the differential equation (9.2.10), including finite-difference, finite-volume, finite-element, and spectral methods. Finite-difference methods have been discussed on several previous occasions. To illustrate an alternative, we discuss the implementation of an entry-level finite-volume method.

Consider the evolution of a film that is, and remains, spatially periodic with period L . To implement the finite-volume method, we divide the computational domain extending from $x = 0$ to L into N intervals of equal length $\Delta x = L/N$, also called finite volumes, as depicted in figure 9.2.2. The end-points of the i th interval are denoted by $x_i^E = (i - 1)\Delta x$, and the mid-point is denoted by $x_i^M = (i - 0.5)\Delta x$, where $i = 1, 2, \dots, N$. The values of the film-thickness corresponding to x_i^E and x_i^M are denoted, respectively, by h_i^E and h_i^M .

The distinguishing feature of the finite-volume method is that the governing equation (9.2.10) is integrated over the length of each element to eliminate the highest derivative. Considering the i th element, we write

$$\int_{x_i^E}^{x_{i+1}^E} \frac{\partial h}{\partial t} dx + \frac{\rho}{3\mu} \{ [h^3(g_x + g_y \frac{\partial h}{\partial x} + \frac{\gamma}{\rho} \frac{\partial^3 h}{\partial x^3})]_{x_{i+1}^E} - h^3(g_x + g_y \frac{\partial h}{\partial x} + \frac{\gamma}{\rho} \frac{\partial^3 h}{\partial x^3})_{x_i^E} \} = 0. \quad (9.2.12)$$

Using the mid-point rule to approximate the integral on the left-hand side of (9.2.12), we obtain

$$\int_{x_i^E}^{x_{i+1}^E} \frac{\partial h}{\partial t} dx \simeq \left(\frac{\partial h}{\partial t} \right)_{x_i^M} \Delta x. \quad (9.2.13)$$

Approximating further the time-derivative on the right-hand side of (9.2.13) with a first-order forward-difference, we obtain

$$\left(\frac{\partial h}{\partial t} \right)_{x_i^M} \simeq \left(\frac{h(t + \Delta t) - h(t)}{\Delta t} \right)_{x_i^M}. \quad (9.2.14)$$

Next, we substitute (9.2.14) into (9.2.13) and the result into (9.2.12), and solve the emerging expression for $h(x_i^M, t + \Delta t)$, to find

$$\begin{aligned} h(x_i^M, t + \Delta t) &= h(x_i^M, t) - \frac{\Delta t}{\Delta x} \frac{\rho}{3\mu} \{ [h^3(g_x + g_y \frac{\partial h}{\partial x} + \frac{\gamma}{\rho} \frac{\partial^3 h}{\partial x^3})]_{x_{i+1}^E} \\ &\quad - [h^3(g_x + g_y \frac{\partial h}{\partial x} + \frac{\gamma}{\rho} \frac{\partial^3 h}{\partial x^3})]_{x_i^E} \}, \end{aligned} \quad (9.2.15)$$

where the right-hand side is evaluated at t .

Finally, we express the values of the function h and its spatial derivatives at the element end-points in terms of values at the mid-points using a combination of averaging and finite-difference approximations, writing, for example,

$$\begin{aligned} h(x_{i+1}^E) &\simeq \frac{1}{2} [h(x_i^M) + h(x_{i+1}^M)], & \frac{\partial h}{\partial x}(x_{i+1}^E) &\simeq \frac{h(x_{i+1}^M) - h(x_i^M)}{\Delta x}, \\ \frac{\partial^3 h}{\partial x^3}(x_{i+1}^E) &\simeq \frac{h(x_{i+2}^M) - 3h(x_{i+1}^M) + 3h(x_i^M) - h(x_{i-1}^M)}{\Delta x^3}. \end{aligned} \quad (9.2.16)$$

The periodicity condition requires

$$\begin{aligned} h(x_{-1}^M) &= h(x_{N-1}^M), & h(x_0^M) &= h(x_N^M), \\ h(x_{N+1}^M) &= h(x_1^M), & h(x_{N+2}^M) &= h(x_2^M), \end{aligned} \quad (9.2.17)$$

which allow the evaluation of the right-hand sides of (9.2.16) at the ends of the computational domain extending over one period.

The numerical procedure involves the following steps:

1. Specify the values of h_i^M at the origin of computational time.
2. Choose a time step Δt .
3. Evaluate (9.2.16) and (9.2.17) at the element end-points.
4. Compute the right-hand side of (9.2.15), and thereby obtain the updated value of the film thickness at the mid-points.
5. Return to step 3 and repeat for another step.

9.2.6 Multi-film flow

Consider now the more general case of several superimposed layers flowing down an inclined plane, as illustrated in figure 9.2.3. For this flow configuration to be stable, the density of the layers must be constant or decrease with distance from the wall, otherwise a gravitational instability due to unstable density stratification, known as the Rayleigh-Taylor instability, will arise. Multi-layer flows occur in the manufacturing of photographic films during the process of *slide coating*, as discussed in Section 7.2.1.

For the sake of generality, we allow the inclined plane to exhibit periodic corrugations around a mean value. In the inclined system of coordinates defined in figure 9.2.3, the wall is described by the equation $y = y_0(x)$, and the interfaces are described by the equations $y = y_i(x, t)$, where $i = 1, 2, \dots, N$; the N th interface is the free surface. The i th film is confined between the interfaces labelled i and the $i - 1$, with the understanding that the zeroth interface represents the wall.

When the wall and the interfaces are nearly flat, $|\partial y_i / \partial x| < 1$, for $i = 0, 1, \dots, N$, the flow inside each layer may be assumed to be locally

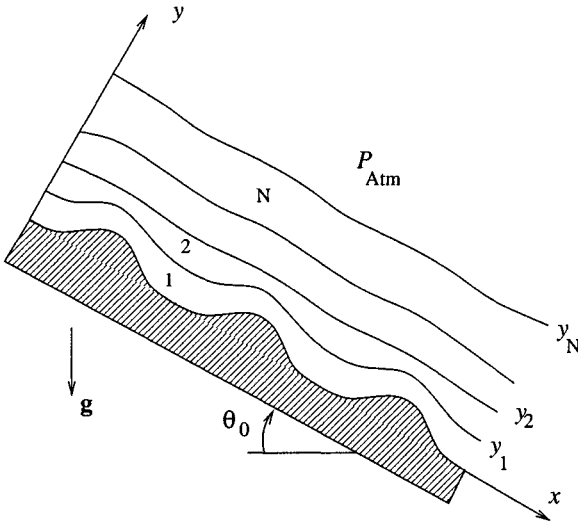


Figure 9.2.3 Multi-film flow down an inclined wall with periodic corrugations.

unidirectional along the x axis. The x and y components of the equation of motion then simplify to

$$\frac{\partial p^{(i)}}{\partial x} = \mu_i \frac{\partial^2 u_x^{(i)}}{\partial y^2} + \rho_i g_x, \quad \frac{\partial p^{(i)}}{\partial y} = \rho_i g_y, \quad (9.2.18)$$

where μ_i and ρ_i is the viscosity and density of the i th layer.

Continuity of velocity across the interfaces requires

$$u_x^{(i)}(y = y_i) = u_x^{(i+1)}(y = y_i), \quad (9.2.19)$$

for $i = 1, 2, \dots, N - 1$. The no-slip boundary condition at the wall requires

$$u_x^{(1)}(y = y_0) = 0. \quad (9.2.20)$$

Continuity of shear stress across the interfaces requires

$$\mu_i \left(\frac{\partial u_x^{(i)}}{\partial y} \right)_{y=y_i} = \mu_{i+1} \left(\frac{\partial u_x^{(i+1)}}{\partial y} \right)_{y=y_i}, \quad (9.2.21)$$

with the understanding that $\mu_{N+1} = 0$, which ensures that the shear stress vanishes at the free surface. Finally, a balance of the normal stresses on either side of the i th interface involving the interfacial tension γ_i , requires

$$(p^{(i)})_{y=y_i} = (p^{(i+1)})_{y=y_i} + \gamma_i \kappa_i, \quad (9.2.22)$$

where κ_i is the curvature of the i th interface or free surface, with the understanding that $p^{(N+1)} = P_{Atm}$. The statement of the problem is now complete, and we proceed to formulate the solution.

Pressure gradient

Our first task is to compute the pressure gradient on either side of each interface. We begin by integrating the second of equations (9.2.18) with respect to y from the i th interface up to an arbitrary point, and use the interfacial condition (9.2.22) to find

$$p^{(i)}(x, y) = p^{(i+1)}(x, y = y_i) + \gamma_i \kappa_i + \rho_i g_y [y - y_i(x)], \quad (9.2.23)$$

for $i = 1, 2, \dots, N$, with the understanding that $p^{(N+1)} = P_{Atm}$.

Next, we differentiate equation (9.2.23) with respect to x , and use the chain rule to write

$$\frac{\partial p^{(i)}}{\partial x} = \frac{\partial p^{(i+1)}}{\partial x} + \frac{\partial p^{(i+1)}}{\partial y} \frac{\partial y_i}{\partial x} + \gamma_i \frac{\partial \kappa_i}{\partial x} - \rho_i g_y \frac{\partial y_i}{\partial x}. \quad (9.2.24)$$

Evaluating $\partial p^{(i+1)}/\partial y$ from the second of equations (9.2.18), we obtain

$$\frac{\partial p^{(i)}}{\partial x} = \frac{\partial p^{(i+1)}}{\partial x} + \gamma_i \frac{\partial \kappa_i}{\partial x} + (\rho_{i+1} - \rho_i) g_y \frac{\partial y_i}{\partial x}. \quad (9.2.25)$$

Writing equation (9.2.25) for the interfaces numbered $i, i+1, \dots, N$, and adding corresponding sides, we obtain

$$\frac{\partial p^{(i)}}{\partial x} = \sum_{j=i}^N \gamma_j \frac{\partial \kappa_j}{\partial x} + \sum_{j=i}^N (\rho_{j+1} - \rho_j) g_y \frac{\partial y_j}{\partial x}. \quad (9.2.26)$$

Finally, we introduce the familiar approximation $\kappa_j \simeq -\partial^2 y_j / \partial x^2$, and obtain

$$\frac{\partial p^{(i)}}{\partial x} = - \sum_{j=i}^N \gamma_j \frac{\partial^3 y_j}{\partial x^3} + \sum_{j=i}^N (\rho_{j+1} - \rho_j) g_y \frac{\partial y_j}{\partial x}. \quad (9.2.27)$$

The right-hand side of (9.2.27) may be evaluated from knowledge of the instantaneous interfacial profiles.

Velocity profiles

The velocity profile inside the i th layer arises by integrating the first of equations (9.2.18) with respect to y , obtaining

$$u_x^{(i)} = A_i(x) + B_i(x) y - G_i(x) y^2, \quad (9.2.28)$$

where we have defined

$$G_i(x) \equiv \frac{1}{2\mu_i} \left[-\frac{\partial p^{(i)}}{\partial x} + \rho_i g_x \right]. \quad (9.2.29)$$

To compute the unknown functions $A_i(x)$ and $B_i(x)$, we use the interfacial and wall conditions expressed by (9.2.19) - (9.2.21), and find the following four relations:

$$A_i(x) + B_i(x) y_i - G_i(x) y_i^2 = A_{i+1}(x) + B_{i+1}(x) y_i - G_{i+1}(x) y_i^2, \quad (9.2.30)$$

for $i = 1, 2, \dots, N - 1$,

$$A_1(x) + B_1(x) y_0 - G_1(x) y_0^2 = 0, \quad (9.2.31)$$

$$\mu_i [B_i(x) - 2 G_i(x) y_i] = \mu_{i+1} [B_{i+1}(x) - 2 G_{i+1}(x) y_i], \quad (9.2.32)$$

and

$$B_N(x) = 2 G_N(x) y_N. \quad (9.2.33)$$

A straightforward substitution allows us to replace the recursion relation (9.2.33) with the explicit formula

$$B_i(x) = 2 G_i(x) y_i + 2 \sum_{k=i+1}^N \frac{\mu_k}{\mu_i} G_k(x) (y_k - y_{k-1}), \quad (9.2.34)$$

for $i = 1, 2, \dots, N - 1$. Equations (9.2.33) and (9.2.34) provide us with expressions for evaluating the coefficients $B_i(x)$. Once these are available, $A_1(x)$ follows from (9.2.31), and the rest of the coefficients $A_i(x)$ follow from (9.2.30).

Evolution equations

The counterpart of the mass balance equation (9.2.9) for the i th film is

$$\frac{\partial h_i}{\partial t} = \frac{\partial y_i}{\partial t} - \frac{\partial y_{i-1}}{\partial t} = -\frac{\partial Q_i}{\partial x}, \quad (9.2.35)$$

where h_i is the film thickness, and

$$\begin{aligned} Q_i(x, t) &\equiv \int_y^{y_{i-1}} u^{(i)} dy \\ &= A_i(x) (y_i - y_{i-1}) + \frac{1}{2} B_i(x) (y_i^2 - y_{i-1}^2) - \frac{1}{3} G_i(x) (y_i^3 - y_{i-1}^3) \end{aligned} \quad (9.2.36)$$

is the local flow rate. Writing equation (9.2.35) for $i = 1, 2, \dots, N$, and combining the expressions thus obtained, we derive the evolution equations

$$\frac{\partial y_i}{\partial t} = -\sum_{j=1}^i \frac{\partial Q_j}{\partial x}, \quad (9.2.37)$$

for $i = 1, 2, \dots, N$. Substituting equation (9.2.27) into (9.2.29), the result into (9.2.36), and the outcome into (9.2.37), we derive a system of fourth-order nonlinear partial differential equations governing the evolution of the interfaces and free surface.

One-layer flow on a plane

In the case of one film, $N = 1$, and a plane wall corresponding to $y_0 = 0$, equations (9.2.33) and (9.2.31) yield $B_1(x) = 2 G_1(x) y_1$ and $A_1(x) = 0$. The evolution equation (9.2.37) then reduces to (9.2.10) for single-film flow.

Two-layer flow on a plane

In the case of two films, $N = 2$, and a plane wall corresponding to $y_0 = 0$, we find

$$\begin{aligned} B_2(x) &= 2 G_2(x) y_2, & B_1(x) &= 2 G_1(x) y_1 + 2 \lambda_1 G_2(x) (y_2 - y_1), \\ A_1(x) &= 0, & A_2(x) &= G_1(x) y_1^2 + G_2(x) y_1 [2 \lambda_1 (y_2 - y_1) - 2 y_2 + y_1], \end{aligned} \quad (9.2.38)$$

where $\lambda_1 \equiv \mu_2/\mu_1$. Using (9.2.27) and (9.2.29), we obtain

$$G_2(x) = \frac{\rho_2}{2\mu_2} \left[g_x + g_y \frac{\partial y_2}{\partial x} + \frac{\gamma_2}{\rho_2} \frac{\partial^3 y_2}{\partial x^3} \right], \quad (9.2.39)$$

and

$$G_1(x) = \frac{\rho_2}{2\mu_2} \lambda_1 \left[\frac{1}{\beta_1} g_x + g_y \left(\frac{1}{\beta_1} - 1 \right) \frac{\partial y_1}{\partial x} + g_y \frac{\partial y_2}{\partial x} + \frac{\gamma_1}{\rho_2} \frac{\partial^3 y_1}{\partial x^3} + \frac{\gamma_2}{\rho_2} \frac{\partial^3 y_2}{\partial x^3} \right], \quad (9.2.40)$$

where $\beta_1 \equiv \rho_2/\rho_1$. The evolution of the interfaces is governed by the equations

$$\frac{\partial y_1}{\partial t} = -\frac{\partial Q_1}{\partial x}, \quad \frac{\partial y_2}{\partial t} = -\frac{\partial Q_1}{\partial x} - \frac{\partial Q_2}{\partial x}, \quad (9.2.41)$$

subject to a specified initial condition.

Numerical solution

The solution of equation (9.2.37) for $i = 1, 2, \dots, N$, may be found using a standard finite difference method. An explicit finite difference method involves introducing a one-dimensional grid along the x axis, applying equations (9.2.37) at a grid point, evaluating the right-hand sides by numerical differentiation, approximating the time derivatives on the left-hand side with forward differences using a sufficiently small time step Δt , and then advancing the position of the interfaces to a new position (problem c.9.2.2).

Problem

Problem 9.2.1 Two-layer flow.

Consider a two-layer flow with fluids of equal viscosity and density, $\lambda_1 = 1$ and $\beta_1 = 1$, in the absence of interfacial tension, $\gamma_1 = 0$. Show that the second of the evolution equations (9.2.41) reduces to (9.2.10) for single-film flow, and discuss the significance of the first of the evolution equations (9.2.41).

Computer problems

Problem c.9.2.1 *Finite-volume method for single-film flow.*

Write a computer code that uses the finite-volume method described in the text to simulate the evolution of a periodic film resting on a horizontal wall or flowing down an inclined wall. Compute the evolution of a film with an initially sinusoidal free surface resting on a horizontal wall, investigate and discuss the effect of surface tension by numerical experimentation.

Problem c.9.2.2 *Multi-film flow.*

Directory 05_lub/films of *FDLIB* contains a computer code that uses an explicit finite-difference method to simulate the evolution of a number of superimposed films resting on a horizontal periodic wall or flowing down an inclined periodic wall, as discussed in the text. Run the code for two multi-layer configuration of your choice involving a horizontal and an inclined wall. Investigate and discuss the significance of the interfacial tensions.

9.3 Two-layer channel flow

Multi-layer channel flows are encountered in the industrial processes of polymer co-extrusion and in the manufacturing of composites and laminated materials. Consider the unsteady flow of two superposed layers in a channel confined between two parallel plane walls that are separated by the distance $2h$, as illustrated in figure 9.3.1; the lower layer is labelled 1, and the upper layer is labelled 2. The flow is driven partly by the parallel translation of the lower and upper walls with respective velocities equal to U_1 and U_2 , partly by a pressure gradient imposed along the x axis, and partly by the gravitational body force. Our goal is to derive an evolution equation for the layer thicknesses, under the assumption that the interface is only gently sloped.

9.3.1 Equations of lubrication flow

We begin by describing the interface by the equation $y = y_I(x, t)$, and assume that the flow within each layer is governed by the following

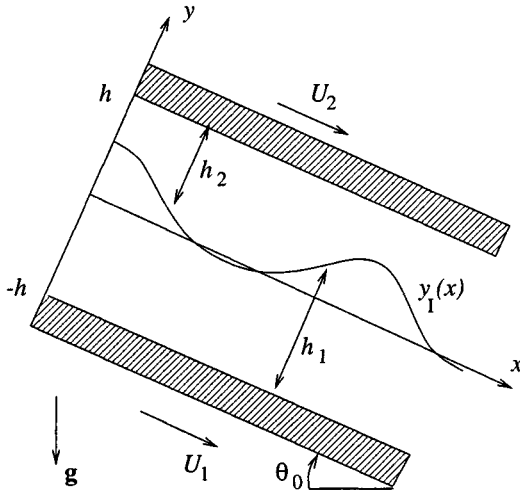


Figure 9.3.1 Flow of two layers in a channel confined between two parallel plane walls, driven by gravity, boundary motion, or an imposed pressure gradient.

simplified x and y components of the equation of motion,

$$\begin{aligned}
 0 &= -\frac{\partial p^{(1)}}{\partial x} + \mu_1 \frac{\partial^2 u_x^{(1)}}{\partial y^2} + \rho_1 g_x, \\
 0 &= -\frac{\partial p^{(1)}}{\partial y} + \rho_1 g_y,
 \end{aligned}
 \tag{9.3.1}$$

and

$$\begin{aligned}
 0 &= -\frac{\partial p^{(2)}}{\partial x} + \mu_2 \frac{\partial^2 u_x^{(2)}}{\partial y^2} + \rho_2 g_x, \\
 0 &= -\frac{\partial p^{(2)}}{\partial y} + \rho_2 g_y,
 \end{aligned}
 \tag{9.3.2}$$

where the components of the acceleration of gravity are given in (9.2.1). The y component of the equation of motion states that the pressure within each layer changes in the y direction only because of gravity.

9.3.2 Velocity profiles

Integrating the first of equations (9.3.1) and (9.3.2) twice with respect to y , while treating the streamwise pressure gradient as a constant, we obtain the parabolic profile

$$u_x^{(1)}(y, t) = -\frac{1}{2\mu_1} \left[-\frac{\partial p^{(1)}}{\partial x} + \rho_1 g_x \right] (y - y_I)^2 + \xi_1 (y - y_I) + u_I \quad (9.3.3)$$

for the lower fluid extending over $-h < y < y_I(x)$, and

$$u_x^{(2)}(y, t) = -\frac{1}{2\mu_2} \left[-\frac{\partial p^{(2)}}{\partial x} + \rho_2 g_x \right] (y - y_I)^2 + \xi_2 (y - y_I) + u_I \quad (9.3.4)$$

for the upper fluid extending over $y_I(x) < y < h$, where u_I is the *a priori* unknown streamwise velocity at the position of the interface, and $\xi_1 \equiv (\partial u_x^{(1)} / \partial y)_{y=y_I}$ and $\xi_2 \equiv (\partial u_x^{(2)} / \partial y)_{y=y_I}$ are the *a priori* unknown shear rates evaluated on either side of the interface. If the interface is flat, u_I , ξ_1 and ξ_2 are given by expressions (7.1.14) and (7.1.15).

9.3.3 Shear rate and interface velocity

To compute the interfacial shear rates, we use the no-slip boundary condition at the upper and lower wall, requiring $u_x^{(1)}(y = -h) = U_1$ and $u_x^{(2)}(y = h) = U_2$. Evaluating the velocity from (9.3.3) and (9.3.4), and solving for the shear rates, we find

$$\begin{aligned} \xi_1 &= -\frac{h_1}{2\mu_1} \left[-\frac{\partial p^{(1)}}{\partial x} + \rho_1 g_x \right] + \frac{u_I - U_1}{h_1}, \\ \xi_2 &= \frac{h_2}{2\mu_2} \left[-\frac{\partial p^{(2)}}{\partial x} + \rho_2 g_x \right] - \frac{u_I - U_2}{h_2}, \end{aligned} \quad (9.3.5)$$

where $h_1(x, t) = h + y_I(x, t)$ and $h_2(x, t) = h - y_I(x, t)$ are the local and instantaneous layer thicknesses. If the interface is flat, the streamwise pressure gradients are equal, and expressions (9.3.5) reduce to those given in (7.1.15) with $\partial p^{(1)} / \partial x = \partial p^{(2)} / \partial x = -\chi$.

Substituting the right-hand sides of equations (9.3.5) into the equation $\mu_1 \xi_1 = \mu_2 \xi_2$ expressing continuity of shear stress across the interface, we find

$$u_I = \frac{1}{2\mu_1} \frac{h_1 h_2}{\lambda + \delta} \left[-\frac{\partial p^{(1)}}{\partial x} - \delta \frac{\partial p^{(2)}}{\partial x} + \rho_1 g_x (1 + \beta \delta) \right] + \frac{\delta U_1 + \lambda U_2}{\delta + \lambda}, \tag{9.3.6}$$

where $\lambda \equiv \mu_2/\mu_1$, $\beta \equiv \rho_2/\rho_1$, and $\delta \equiv h_2/h_1$ is the ratio of the local layer thicknesses. If the interface is flat, the streamwise pressure gradients are equal, and expression (9.3.6) reduces to that given in (7.1.14) with $\partial p^{(1)}/\partial x = \partial p^{(2)}/\partial x = -\chi$.

9.3.4 Streamwise pressure field

Next, we note that the pressure undergoes a jump across the interface due to the surface tension γ , and write

$$p^{(1)}(x, y = y_I) = p^{(2)}(x, y = y_I) + \gamma \kappa, \tag{9.3.7}$$

where κ is the interfacial curvature. Adopting the familiar approximation $\kappa(x) \simeq -\partial^2 h/\partial x^2$, and differentiating both sides of (9.3.7) with respect to x using the chain rule, we find

$$\frac{\partial p^{(1)}}{\partial x} + \frac{\partial p^{(1)}}{\partial y} \frac{\partial y_I}{\partial x} = \frac{\partial p^{(2)}}{\partial x} + \frac{\partial p^{(2)}}{\partial y} \frac{\partial y_I}{\partial x} - \gamma \frac{\partial^3 h}{\partial x^3}, \tag{9.3.8}$$

where both sides are evaluated at the interface. Using the second of equations (9.3.1) and (9.3.2) to evaluate the derivatives of the pressure with respect to y , and rearranging, we obtain

$$\frac{\partial p^{(2)}}{\partial x} = \frac{\partial p^{(1)}}{\partial x} + (\rho_1 - \rho_2) g_y \frac{\partial y_I}{\partial x} + \gamma \frac{\partial^3 h}{\partial x^3}. \tag{9.3.9}$$

Substituting this expression into (9.3.6) to eliminate $p^{(2)}$, we derive an alternative expression for the interfacial velocity

$$u_I = \frac{1}{2\mu_1} \frac{h_1 h_2}{\lambda + \delta} \left[-(1 + \delta) \frac{\partial p^{(1)}}{\partial x} - \delta (\rho_1 - \rho_2) g_y \frac{\partial y_I}{\partial x} - \delta \gamma \frac{\partial^3 h}{\partial x^3} + \rho_1 g_x (1 + \beta \delta) \right] + \frac{\delta U_1 + \lambda U_2}{\delta + \lambda}, \tag{9.3.10}$$

involving the pressure gradient in the lower layer and the instantaneous shape of the interface.

9.3.5 Flow rates and mass conservation

We proceed by integrating the velocity profiles (9.3.3) and (9.3.4) with respect to y over their respective domain of definition to derive the following expressions for the streamwise flow rates

$$\begin{aligned}
 Q_1 &\equiv \int_{-h}^{y_I} u_x^{(1)} dy = -\frac{h_1^3}{6\mu_1} \left[-\frac{\partial p^{(1)}}{\partial x} + \rho_1 g_x \right] - \frac{1}{2} \xi_1 h_1^2 + u_I h_1, \\
 Q_2 &\equiv \int_{y_I}^h u_x^{(2)} dy = -\frac{h_2^3}{6\mu_2} \left[-\frac{\partial p^{(2)}}{\partial x} + \rho_2 g_x \right] + \frac{1}{2} \xi_2 h_2^2 + u_I h_2.
 \end{aligned}
 \tag{9.3.11}$$

Using expressions (9.3.5) to eliminate the shear rates ξ_1 and ξ_2 from the right-hand sides, we find

$$\begin{aligned}
 Q_1 &= \frac{h_1^3}{12\mu_1} \left[-\frac{\partial p^{(1)}}{\partial x} + \rho_1 g_x \right] + \frac{1}{2} (u_I + U_1) h_1, \\
 Q_2 &= \frac{h_2^3}{12\mu_2} \left[-\frac{\partial p^{(2)}}{\partial x} + \rho_2 g_x \right] + \frac{1}{2} (u_I + U_2) h_2.
 \end{aligned}
 \tag{9.3.12}$$

A mass balance over a control area that is confined between (a) two parallel planes that are normal to the channel walls and are separated by an infinitesimal distance, (b) the enclosed sections of the walls, and (c) the enclosed section of the evolving interface, requires that the rate of accumulation of mass of each layer within this control area should be equal to the difference between the mass flow rates into and out from the control volume. In differential form,

$$\frac{\partial h_1}{\partial t} = \frac{\partial y_I}{\partial t} = -\frac{\partial Q_1}{\partial x}, \quad \frac{\partial h_2}{\partial t} = -\frac{\partial y_I}{\partial t} = -\frac{\partial Q_2}{\partial x},
 \tag{9.3.13}$$

Since $h_1 + h_2 = 2h$ is constant, $\partial h_1/\partial t + \partial h_2/\partial t = 0$, and

$$\frac{\partial Q_1}{\partial x} + \frac{\partial Q_2}{\partial x} = 0 \quad \text{or} \quad Q_1 + Q_2 = f(t),
 \tag{9.3.14}$$

where $f(t)$ is an unspecified function of time. To compute this function, we use the expressions for the flow rates and interfacial velocity given in equations (9.3.12) and (9.3.10). Eliminating the pressure gradient in the second layer using expression (9.3.9), we find

$$\frac{\partial p^{(1)}}{\partial x} = \frac{N + \mu_1 f(t)}{D}, \quad (9.3.15)$$

where

$$\begin{aligned} N = & -(\rho_1 - \rho_2) g_y (h_2 + \frac{6 \lambda}{\lambda + \delta} h) h_2^2 \frac{\partial h_1}{\partial x} - \gamma (h_2 + \frac{6 \lambda}{\lambda + \delta} h) h_2^2 \frac{\partial^3 h_1}{\partial x^3} \\ & + \rho_1 g_x (\lambda h_1^3 + \beta h_2^3 + \frac{12 \lambda}{\lambda + \delta} h \frac{1 + \lambda \delta}{1 + \delta} h^2 h_2) \\ & + 12 \mu_2 h (\frac{U_1 + \delta U_2}{1 + \delta} + \frac{\delta U_1 + \lambda U_2}{\lambda + \delta}), \end{aligned} \quad (9.3.16)$$

and

$$D = \lambda h_1^3 + h_2^3 + \frac{12 \lambda}{\lambda + \delta} h^2 h_2. \quad (9.3.17)$$

Integrating both sides of (9.3.15) with respect to x over the length L , and solving for $f(t)$, we find

$$f(t) = \frac{\Delta p - \int_0^L \frac{N}{D} dx}{\mu_1 \int_0^L \frac{dx}{D}}, \quad (9.3.18)$$

where $\Delta p \equiv p(x = L) - p(x = 0)$ is the negative of the pressure drop over the length L . The integrals on the right-hand side of (9.3.18) may be computed from knowledge of the instantaneous shape of the interface using numerical methods.

9.3.6 Evolution equation

Having obtained the function $f(t)$, we evaluate the streamwise pressure gradient from (9.3.15), compute the interfacial velocity from (9.3.10), evaluate the flow rate Q_1 from the first of equations (9.3.12), and use the first of equations (9.3.13) to derive an expression for the rate of change of the lower film thickness or interface position. Symbolically, we write

$$\frac{\partial y_I}{\partial t} = F(y_I, \frac{\partial y_I}{\partial x}, \frac{\partial^2 y_I}{\partial x^2}, \frac{\partial^3 y_I}{\partial x^3}, \frac{\partial^4 y_I}{\partial x^4}), \quad (9.3.19)$$

where F is a nonlinear function of its arguments defined implicitly in terms of the aforementioned substitutions.

9.3.7 Numerical methods

Equation (9.3.19) may be solved using a standard finite difference method based on a one-dimensional grid with nodes deployed along the x axis. An explicit method involves applying (9.3.19) at a grid point at a certain time t , and approximating the time derivatives on the left-hand side with a *forward* finite difference using a small time step Δt , obtaining

$$\frac{y_I(x, t + \Delta t) - y_I(x, t)}{\Delta t} = F(t). \quad (9.3.20)$$

Evaluating the right-hand side by numerical differentiation, and solving for $y_I(x, t + \Delta t)$, we obtain the position of the interface at the new time $t + \Delta t$.

The explicit method requires a small time step to prevent the onset of numerical instabilities manifested by growing oscillations in the position of interfacial marker points. This restriction can be overcome by applying equations (9.3.19) at a grid point at a certain time $t + \Delta t$, and approximating the time derivatives on the left-hand side with a *backward* finite difference using a small time step Δt , to obtain

$$\frac{y_I(x, t + \Delta t) - y_I(x, t)}{\Delta t} = F(t + \Delta t). \quad (9.3.21)$$

Evaluating the right-hand side by numerical differentiation, and solving for $y_I(t + \Delta t)$, we obtain a nonlinear system of algebraic equations for the interface position at the nodes, at time $t + \Delta t$. A drawback of the implicit method is that computing the solution of the nonlinear algebraic system at each time step requires a substantial amount of computational effort.

Computer problem

Problem c.9.3.1 *Two-layer flow in a channel.*

Directory `05_lub/chan_2d_2l_exp` of *FDLIB* contains a program that simulates the evolution of a periodic interface between two layers in a channel using an explicit finite difference method.

- (a) Outline the numerical method implemented in the program.
 (b) Run the program for two sets of conditions of your choice, display sequences of evolving profiles, and discuss the nature of the motion.

9.4 Flow due to the motion of a sphere

A variety of natural and engineering applications involve particle motions in a viscous fluid. An elementary configuration involves a spherical particle settling with constant velocity under the influence of its weight in a virtually infinite quiescent ambient fluid, thereby generating an axisymmetric flow, as illustrated in figure 9.4.1.

When the radius of the particle a is small, or the fluid viscosity μ is large, or the fluid density ρ is low, or the particle velocity U is small, inertial forces near the particle are negligible, and the left-hand side of the Navier-Stokes equation may be set equal to zero without introducing serious error. The result is a simplified equation of motion which, together with the continuity equation, comprise the equations of *Stokes* or *creeping* flow, given by

$$\begin{aligned}\frac{\partial p}{\partial x} &= \mu \left(\frac{\partial^2 u_x}{\partial x^2} + \frac{\partial^2 u_x}{\partial y^2} + \frac{\partial^2 u_x}{\partial z^2} \right) + \rho g_x, \\ \frac{\partial p}{\partial y} &= \mu \left(\frac{\partial^2 u_y}{\partial x^2} + \frac{\partial^2 u_y}{\partial y^2} + \frac{\partial^2 u_y}{\partial z^2} \right) + \rho g_y, \\ \frac{\partial p}{\partial z} &= \mu \left(\frac{\partial^2 u_z}{\partial x^2} + \frac{\partial^2 u_z}{\partial y^2} + \frac{\partial^2 u_z}{\partial z^2} \right) + \rho g_z,\end{aligned}\tag{9.4.1}$$

and

$$\frac{\partial u_x}{\partial x} + \frac{\partial u_y}{\partial y} + \frac{\partial u_z}{\partial z} = 0.\tag{9.4.2}$$

The formal requirement for fluid inertia to be negligible is that the Reynolds number, defined with respect to the particle radius, $Re = a\rho U/\mu$, be small. We shall see, however, that this assumption does not guarantee that inertia will be *uniformly* negligible throughout the domain of the flow and, in particular, far from the sphere. Having noted this exception, we proceed to compute the solution on the assumption that inertia is negligible throughout the domain of flow, and then return to assess the validity of our conclusions.

- (a) Outline the numerical method implemented in the program.
- (b) Run the program for two sets of conditions of your choice, display sequences of evolving profiles, and discuss the nature of the motion.

9.4 Flow due to the motion of a sphere

A variety of natural and engineering applications involve particle motions in a viscous fluid. An elementary configuration involves a spherical particle settling with constant velocity under the influence of its weight in a virtually infinite quiescent ambient fluid, thereby generating an axisymmetric flow, as illustrated in figure 9.4.1.

When the radius of the particle a is small, or the fluid viscosity μ is large, or the fluid density ρ is low, or the particle velocity U is small, inertial forces near the particle are negligible, and the left-hand side of the Navier-Stokes equation may be set equal to zero without introducing serious error. The result is a simplified equation of motion which, together with the continuity equation, comprise the equations of *Stokes* or *creeping* flow, given by

$$\begin{aligned}\frac{\partial p}{\partial x} &= \mu \left(\frac{\partial^2 u_x}{\partial x^2} + \frac{\partial^2 u_x}{\partial y^2} + \frac{\partial^2 u_x}{\partial z^2} \right) + \rho g_x, \\ \frac{\partial p}{\partial y} &= \mu \left(\frac{\partial^2 u_y}{\partial x^2} + \frac{\partial^2 u_y}{\partial y^2} + \frac{\partial^2 u_y}{\partial z^2} \right) + \rho g_y, \\ \frac{\partial p}{\partial z} &= \mu \left(\frac{\partial^2 u_z}{\partial x^2} + \frac{\partial^2 u_z}{\partial y^2} + \frac{\partial^2 u_z}{\partial z^2} \right) + \rho g_z,\end{aligned}\tag{9.4.1}$$

and

$$\frac{\partial u_x}{\partial x} + \frac{\partial u_y}{\partial y} + \frac{\partial u_z}{\partial z} = 0.\tag{9.4.2}$$

The formal requirement for fluid inertia to be negligible is that the Reynolds number, defined with respect to the particle radius, $Re = a\rho U/\mu$, be small. We shall see, however, that this assumption does not guarantee that inertia will be *uniformly* negligible throughout the domain of the flow and, in particular, far from the sphere. Having noted this exception, we proceed to compute the solution on the assumption that inertia is negligible throughout the domain of flow, and then return to assess the validity of our conclusions.

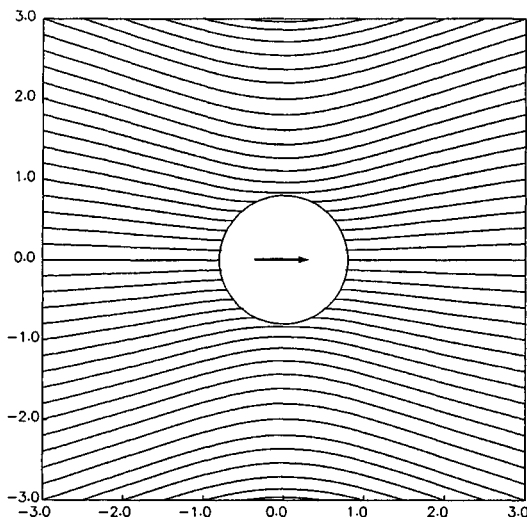


Figure 9.4.1 Streamline pattern in a meridional plane of the axisymmetric Stokes flow due to the translation of a sphere in an infinite fluid.

9.4.1 Formulation in terms of the stream function

To simplify the process, we take advantage of the assumed axial symmetry of the flow with respect to the direction of translation, and refer to spherical polar coordinates with the x axis pointing in the direction of translation. Moreover, to bypass the computation of the pressure, we work with the vorticity transport equation (6.6.7) for the non-vanishing component of the vorticity pointing in the azimuthal direction, ω_φ . In the absence of fluid inertia, we obtain the simplified form

$$E^2(\sigma \omega_\varphi) = 0, \quad (9.4.3)$$

where $\sigma = r \sin \varphi$ is the distance from the x axis; the second-order linear differential operator E^2 was defined in equation (2.9.12) and (2.9.15). Expressing the strength of the vorticity in terms of the stream function using equation (2.9.11), we find

$$E^4 \psi \equiv E^2 E^2 \psi = 0. \quad (9.4.4)$$

Our task is to solve the fourth-order differential equation (9.4.4) for the stream function in the flow regime confined between $r = a$ and infinity, subject to appropriate boundary and far-field conditions.

On the surface of the sphere, located at $r = a$, the no-slip and no-penetration boundary conditions require that the fluid velocity be equal to the velocity of the sphere,

$$\mathbf{u}(r = a) = U \mathbf{e}_x, \quad (9.4.5)$$

where \mathbf{e}_x is the unit vector along the x axis. The far-field condition must ensure that, as r tends to infinity, the velocity tends to vanish so that the fluid becomes quiescent.

Using the relations between the velocity and the stream function shown in equations (2.9.13), we find that, in terms of the stream function, the boundary and far-field conditions assume the forms

$$\psi(r = a) = \frac{1}{2} U a^2 \sin^2 \theta, \quad \left(\frac{\partial \psi}{\partial r}\right)_{r=a} = U a \sin^2 \theta, \quad (9.4.6)$$

and

$$\frac{\psi}{r^m} \rightarrow 0 \quad \text{as} \quad r \rightarrow \infty, \quad (9.4.7)$$

for $m \geq 2$. Condition (9.4.7) allows the stream function to diverge at infinity, but requires that the rate of divergence be less than quadratic, otherwise the velocity will not decay.

Motivated by the functional form of the boundary conditions (9.4.6), we search for a solution by separation of variables, writing

$$\psi = q(r) \sin^2 \theta, \quad (9.4.8)$$

The unknown function $q(r)$ is required to satisfy the boundary conditions

$$q(r = a) = \frac{1}{2} U a^2, \quad \left(\frac{\partial q}{\partial r}\right)_{r=a} = U a, \quad (9.4.9)$$

and the far-field condition

$$\frac{q(r)}{r^m} \rightarrow 0 \quad \text{as} \quad r \rightarrow \infty, \quad (9.4.10)$$

for $m \geq 2$. Substituting (9.4.8) into (9.4.4), and carrying out the differentiations, we derive the fourth-order linear ordinary differential equation

$$\left(\frac{d^2}{dr^2} - \frac{2}{r^2}\right)\left(\frac{d^2}{dr^2} - \frac{2}{r^2}\right)q = 0, \quad (9.4.11)$$

which may be decomposed into two second-order component equations,

$$\left(\frac{d^2}{dr^2} - \frac{2}{r^2}\right)w = 0, \quad \left(\frac{d^2}{dr^2} - \frac{2}{r^2}\right)q = w. \quad (9.4.12)$$

The second equation merely defines the intermediate function w . The general solution of the first of equations (9.4.12) is readily found to be $w = Ar^2 + B/r$, where A and B are two constants. Substituting this expression into the second of equations (9.4.12), we obtain

$$\left(\frac{d^2}{dr^2} - \frac{2}{r^2}\right)q = Ar^2 + \frac{B}{r}. \quad (9.4.13)$$

The solution of (9.4.13) is the sum of (a) the general solution of the homogeneous equation computed by setting the right-hand side equal to zero, given by $q = Cr^2 + D/r$, where C and D are two new constants, and (b) a particular solution found by inspection. The result is

$$q = \frac{A}{10}r^4 - \frac{B}{2}r + Cr^2 + \frac{D}{r}. \quad (9.4.14)$$

To ensure the satisfaction of condition (9.4.10), we set A and C equal to zero. Substituting the remaining expression into the boundary conditions (9.4.9), and solving for the coefficients B and D , we find

$$B = -\frac{3}{2}Ua, \quad D = -\frac{1}{4}Ua^3. \quad (9.4.15)$$

Substituting these values into (9.4.14) and the result into (9.4.8), we obtain the desired stream function

$$\psi = Ur^2 \frac{1}{4} \left[3 \frac{a}{r} - \left(\frac{a}{r}\right)^3 \right] \sin^2 \theta. \quad (9.4.16)$$

The radial and azimuthal components of the velocity arise by substituting (9.4.16) into equations (2.9.13), yielding

$$u_r = U \frac{1}{2} \left[3 \frac{a}{r} - \left(\frac{a}{r}\right)^3 \right] \cos \theta, \quad u_\theta = -U \frac{1}{4} \left[3 \frac{a}{r} + \left(\frac{a}{r}\right)^3 \right] \sin \theta. \quad (9.4.17)$$

Substituting these expressions into the r and θ spherical polar components of the Stokes equations, we derive expressions for the partial derivatives of the pressure $\partial p/\partial r$ and $\partial p/\partial \theta$. Integrating these expressions, we obtain the pressure distribution

$$p = \frac{3}{2} \frac{\mu U}{a} \left(\frac{a}{r}\right)^2 \cos \theta + \rho(g_x x + g_y y + g_z z) + c, \quad (9.4.18)$$

where $\mathbf{g} = (g_x, g_y, g_z)$ is the acceleration of gravity vector, and c is a constant determined by the level of the pressure far from the sphere (problem 9.4.1).

9.4.2 Validity of the equations of creeping flow

To this end, we return to evaluate the assumptions under which the preceding analysis is valid. Equations (9.4.17) reveal that, in the absence of fluid inertia, the velocity decays like Ua/r far from the sphere; the cubic term $U(a/r)^3$ decays much faster and may be neglected. Differentiating this asymptotic form with respect to r , we find that the derivative $\partial u_r/\partial r$ involved in the nonlinear convective term on the left-hand side of the Navier-Stokes equation decays like Ua/r^2 , and the derivative $\partial^2 u_r/\partial r^2$ involved in the viscous term on the right-hand side of the Navier-Stokes equation decays like Ua/r^3 .

Furthermore, we note that the time derivative $\partial u_r/\partial t$ scales with u_r/T , where T the characteristic time scale of the flow. In the absence of time-dependence due to external action, T is comparable to the ratio between the distance from the center of the sphere and the velocity of the sphere, $T = r/U$.

Using the preceding scaling, we find that the ratio of the magnitude of the nonlinear inertial term to the magnitude of the viscous term in the equation of motion is on the order of

$$\frac{\rho U \frac{a}{r} U \frac{a}{r^2}}{\mu U \frac{a}{r^3}} = \frac{\rho a U}{\mu} \equiv Re, \quad (9.4.19)$$

and the ratio of the magnitude of the time-dependent inertial term to the magnitude of the viscous term is on the order of

$$\frac{\rho(U \frac{a}{r})/(\frac{r}{U})}{\mu U \frac{a}{r^3}} = \frac{\rho r U}{\mu} \equiv Re_r = Re \frac{r}{a}. \quad (9.4.20)$$

We have introduced the global Reynolds number Re defined with respect to the radius of the sphere, and the local Reynolds number Re_r defined with respect to distance from the center of the sphere.

Equations (9.4.19) and (9.4.20) reveal that, for inertial forces to be negligible, both Re and Re_r must be far less than unity. The former can be made small by adjusting one of the flow constants involved in its definition, including ρ , a , U , and μ . There is no way, however, that the latter can be uniformly small throughout the domain of flow. Even if Re is exceedingly small, the ratio r/a will become arbitrary large far from the sphere, and the local Reynolds number Re_r will increase linearly with respect to distance rendering the effects of fluid inertia significant.

We conclude that the approximation of creeping flow ceases to be accurate far from the sphere, with a disturbing consequence. If the governing equations are not valid all the way up to infinity, requiring the far-field boundary condition expressed by (9.4.7) may not be valid. Fortunately, a more detailed analysis using the method of matched asymptotic expansions shows that retaining this far-field condition introduces an error that is comparable to that introduced by dropping the inertial terms in the equation of motion, which is of order Re .

9.4.3 Traction, force, and the Archimedes-Stokes law

Having derived expressions for the velocity and pressure fields, given, respectively, by equations (9.4.17) and (9.4.18), we proceed to evaluate the traction on the surface of the sphere and then integrate it to compute the force. For simplicity, we assume that gravity is directed along the x axis; that is, $g_x = g$, $g_y = 0$, and $g_z = 0$, where g is the acceleration of gravity.

Using the definition of the Newtonian stress tensor shown in equations (4.6.7), we derive an expression for the normal component of the traction

$$\sigma_{rr}(r = a) = (-p + 2\mu \frac{\partial u_r}{\partial r})_{r=a} = -\frac{3}{2} \frac{\mu U}{a} \cos \theta - \rho g x - c, \quad (9.4.21)$$

where the constant c is associated with the pressure, and an expression for the tangential component of the traction,

$$\sigma_{r\theta}(r = a) = \sigma_{\theta r}(r = a) = [r \frac{\partial}{\partial r} (\frac{u_\theta}{r}) + \frac{1}{r} \frac{\partial u_r}{\partial \theta}]_{r=a} = \frac{3}{2} \frac{\mu U}{a} \sin \theta. \quad (9.4.22)$$

Note that, because of the no-slip boundary condition, viscous stresses do not contribute to the normal component of the traction, in agreement with our discussion in Section 4.7.

Combining (9.4.21) and (9.4.22), we find that the traction exerted on the surface of the sphere is given by

$$\mathbf{f} = \sigma_{rr}(r = a) \mathbf{e}_r + \sigma_{r\theta}(r = a) \mathbf{e}_\theta, \quad (9.4.23)$$

where \mathbf{e}_r and \mathbf{e}_θ are the unit vectors in the radial and azimuthal directions. Expressing \mathbf{e}_r and \mathbf{e}_θ in terms of Cartesian unit vectors using relations (1.3.26), substituting the results along with expressions (9.4.21) and (9.4.22) into equation (9.4.23), and simplifying the resulting expression, we derive the remarkably simple result

$$\mathbf{f} = -\frac{3}{2} \frac{\mu U}{a} \mathbf{e}_x - (\rho g x + c) \mathbf{e}_r, \quad (9.4.24)$$

which shows that, hydrostatic contributions aside, the traction over the surface of the sphere points opposite to the direction of translation, and has a uniform magnitude.

To compute the force exerted on the sphere, \mathbf{F} , we integrate the traction over the surface of the sphere. Noting that $x = r \cos \theta$, we find

$$\begin{aligned} \mathbf{F} &= \iint_{\text{Sphere}} \mathbf{f} dS = \int_0^{2\pi} \int_0^\pi \mathbf{f} a^2 \sin \theta d\theta d\varphi \\ &= -6\pi\mu U a \mathbf{e}_x - \frac{4}{3} \pi a^3 \rho g \mathbf{e}_x. \end{aligned} \quad (9.4.25)$$

The first term on the right-hand side of (9.4.25) expresses *Stokes's law*. The second term is Archimedes's buoyancy force familiar from our discussion in Chapter 5 of hydrostatics: the force exerted on an immersed body is equal in magnitude and opposite in direction to the weight of the fluid displaced by the body.

9.4.4 Terminal velocity of a settling sphere

As an application of the Archimedes-Stokes law (9.4.25), we compute the terminal velocity of a sphere of density ρ_s settling in an infinite ambient fluid along the x axis. Balancing the weight of the sphere and the force given in (9.4.25), we find

$$\frac{4}{3} \pi a^3 \rho_s g \mathbf{e}_x - 6\pi\mu U a \mathbf{e}_x - \frac{4}{3} \pi a^3 \rho g \mathbf{e}_x = \mathbf{0}. \quad (9.4.26)$$

Solving for U , we find

$$U = \frac{2}{9} \frac{a^2(\rho_s - \rho)g}{\mu}. \quad (9.4.27)$$

In practice, this equation is used to estimate the viscosity of a fluid from observation of the terminal velocity of a sphere in a device called the falling-ball viscometer.

Problems

Problem 9.4.1 *Pressure distribution around a sphere.*

Derive the pressure distributon (9.4.18).

Problem 9.4.2 *Flow past a stationary sphere.*

Consider steady uniform flow with velocity V along the x axis past a stationary sphere, and derive expressions for the stream function, velocity components, pressure field, traction and force on the surface of the sphere. Show that, for the fluid inertia to be negligible, throughout the domain of flow, both Re and Re_r defined in equations (9.4.19) and (9.4.20) must both be considerably less than unity.

9.5 Point forces and point sources in Stokes flow

Consider the stream function of the flow due to a translating sphere, given in equation (9.4.16). The right-hand side involves two terms that decay like the inverse or inverse cubic power of r/a . To make this distinction clear, we recast equation (9.4.16) into the form

$$\psi = s_x \psi^{3D-ST-x} + d_x \psi^{3D-PSD-x}, \quad (9.5.1)$$

where

$$s_x = \frac{3}{4} Ua, \quad d_x = -\pi Ua^3, \quad (9.5.2)$$

are two constant coefficients,

$$\psi^{3D-ST-x} \equiv r \sin^2 \theta \quad (9.5.3)$$

is the stream function associated with a fundamental solution of the equations of Stokes flow called the three-dimensional *Stokeslet*, as will be discussed later in this section, and

$$\psi^{3D-PSD-x} \equiv \frac{1}{4\pi r} \sin^2 \theta \tag{9.5.4}$$

is the stream function of irrotational flow representing the flow due to a three-dimensional point-source dipole pointing in the direction of the x axis, as discussed in Section 3.6.

The expressions for the velocity, pressure, and stress, may be resolved into analogous component forms corresponding to the Stokeslet and potential dipole. For example, the Cartesian components of the velocity are given by

$$\begin{pmatrix} u_x \\ u_y \\ u_z \end{pmatrix} = s_x \begin{pmatrix} \frac{1}{r} + \frac{x^2}{r^3} \\ \frac{xy}{r^3} \\ \frac{xz}{r^3} \end{pmatrix} + \frac{dx}{4\pi} \begin{pmatrix} -\frac{1}{r^3} + \frac{3x^2}{r^5} \\ \frac{3xy}{r^5} \\ \frac{3xz}{r^5} \end{pmatrix}. \tag{9.5.5}$$

The first and second set of parentheses on the right-hand side of (9.5.5) represent, respectively, the velocity field due to a Stokeslet or a potential dipole parallel to the x axis, both situated at the origin.

9.5.1 The Oseen tensor and the point force

Generalizing the expressions enclosed by the first set of parentheses on the right-hand side of (9.5.5), we derive the velocity field at the point $\mathbf{x} = (x, y, z)$ due to a three-dimensional Stokeslet with vectorial strength $\mathbf{s} = (s_x, s_y, s_z)$ situated at the point $\mathbf{x}_0 = (x_0, y_0, z_0)$, given by

$$\begin{pmatrix} u_x \\ u_y \\ u_z \end{pmatrix}(\mathbf{x}, \mathbf{x}_0) = \mathbf{S}(\mathbf{x}, \mathbf{x}_0) \cdot \begin{pmatrix} s_x \\ s_y \\ s_z \end{pmatrix} \tag{9.5.6}$$

where \mathbf{S} is the 3×3 *Oseen tensor* for three-dimensional flow, defined as

$$\mathbf{S}(\mathbf{x}, \mathbf{x}_0) = \begin{pmatrix} \frac{1}{r} + \frac{(x-x_0)^2}{r^3} & \frac{(x-x_0)(y-y_0)}{r^3} & \frac{(x-x_0)(z-z_0)}{r^3} \\ \frac{(y-y_0)(x-x_0)}{r^3} & \frac{1}{r} + \frac{(y-y_0)^2}{r^3} & \frac{(y-y_0)(z-z_0)}{r^3} \\ \frac{(z-z_0)(x-x_0)}{r^3} & \frac{(z-z_0)(y-y_0)}{r^3} & \frac{1}{r} + \frac{(z-z_0)^2}{r^3} \end{pmatrix}, \quad (9.5.7)$$

and $r = \sqrt{(x-x_0)^2 + (y-y_0)^2 + (z-z_0)^2}$ is the distance of the field point \mathbf{x} from the location of the Stokeslet \mathbf{x}_0 . The three columns of the Oseen tensor represent, respectively, the x , y , and z components of the velocity associated with a Stokeslet of unit strength pointing in the direction of the x , y , or z axis. The corresponding pressure field is given by

$$p(\mathbf{x}, \mathbf{x}_0) = 2\mu \begin{pmatrix} \frac{x-x_0}{r^3} \\ \frac{y-y_0}{r^3} \\ \frac{z-z_0}{r^3} \end{pmatrix} \cdot \begin{pmatrix} s_x \\ s_y \\ s_z \end{pmatrix}, \quad (9.5.8)$$

where the dot denotes the inner vector product.

It can be shown by direct substitution that the velocity (9.5.6) and accompanying pressure field (9.5.8) satisfy the equations of Stokes flow (9.4.1) and (9.4.2) with the gravity term absent, for any Stokeslet strength represented by the vector \mathbf{s} , everywhere except at the point \mathbf{x}_0 where the velocity and pressure become infinite. The streamline pattern in the xy plane induced by a Stokeslet pointing in the x direction is shown in figure 9.5.1.

9.5.2 Force on a surface enclosing the Stokeslet

Consider a surface D enclosing the singular point \mathbf{x}_0 of a Stokeslet. It can be shown that the force exerted on this closed surface is given by

$$\mathbf{F} \equiv \int \int_D \boldsymbol{\sigma} \cdot \mathbf{n} \, dS = -8\pi\mu \mathbf{s}, \quad (9.5.9)$$

independent of the geometry of the surface; $\boldsymbol{\sigma}$ is the stress tensor, and \mathbf{n} is the unit vector normal to D pointing outward. The corresponding torque with respect to the point \mathbf{x}_0 is equal to zero,

$$\mathbf{T} \equiv \int \int_D (\mathbf{x} - \mathbf{x}_0) \times (\boldsymbol{\sigma} \cdot \mathbf{n}) \, dS = \mathbf{0}. \quad (9.5.10)$$

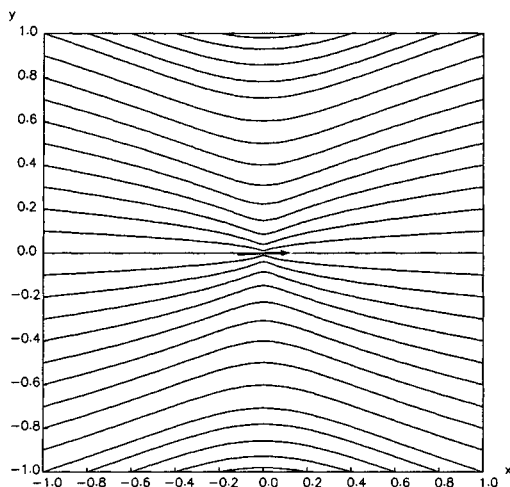


Figure 9.5.1 Streamline pattern in a meridional plane of the axisymmetric flow induced by a three-dimensional point force pointing along the x axis.

The force and torque exerted on a closed surface that *does not* enclose the singular point \mathbf{x}_0 , vanish.

Equation (9.5.9) illustrates that the Stokeslet expresses the flow due to a three-dimensional point force applied at the singular point \mathbf{x}_0 . In physical terms, this flow may be identified with the flow induced by the motion of a small particle located at the point \mathbf{x}_0 ; the strength of the point force counterbalances the force exerted on the particle due, for example, to gravity.

9.5.3 Point source and point-source dipoles

It can be shown by straightforward substitution that the irrotational velocity field due to a point source or point-source dipole discussed in Section 3.6 also satisfies the equations of Stokes flow (9.4.1) and (9.4.2) with the gravity term absent, with a corresponding constant pressure. Further analysis reveals that the induced force and torque on a closed surface vanish independent of whether the singular point \mathbf{x}_0 lies inside or outside the surface.

9.5.4 Flow representation in terms of singularities

We have discussed three singular fundamental solutions of the equations of Stokes flow, including the point force, and point source, and the point-source dipole. To this end, we employ these singularities to generate desired solutions by linear superposition. The key idea is to express a flow of interest in terms of a linear combination of singularities, and then compute the strengths in the singularities with the objective of satisfying the required boundary conditions. Linear superposition is permissible by the linearity of the equations of Stokes flow, resulting by dropping the nonlinear convective terms in the equation of motion.

For example, we have already seen that the flow due to the translation of a sphere may be represented *exactly* by a point force and a point-source dipole placed at the center of the sphere, where the coefficients of the singularities are given in equations (9.5.2). Using equation (9.5.9), we find that the hydrodynamic force exerted on the sphere is given by

$$\mathbf{F} = -8\pi\mu \mathbf{s} = -6\pi\mu U a \mathbf{e}_x, \quad (9.5.11)$$

which is in agreement with expression (9.4.25) derived by a more detailed computation.

Exact representations, however, are rare, and we confine ourselves to deriving approximate solutions. Illustrative examples are discussed in the remainder of this section.

9.5.5 Motion of a sphere along the axis of a tube in Poiseuille flow

Consider a spherical particle of radius a moving with velocity U along the axis of cylindrical tube of radius b under the action of pressure-driven flow, as illustrated in figure 9.5.2. In the absence of the sphere, the velocity profile is given by equation (7.3.4), repeated here for ready reference,

$$u_x^P = U_{Max}^P \left(1 - \frac{\sigma^2}{b^2}\right), \quad (9.5.12)$$

where the superscript “ P ” denotes the unperturbed parabolic flow, U_{Max}^P is the maximum velocity at the centerline, and $\sigma = \sqrt{y^2 + z^2} = r \sin \theta$ is the distance from the x axis. The corresponding stream function is defined by the equation

$$\frac{1}{\sigma} \frac{d\psi^P}{d\sigma} = u_x^P. \quad (9.5.13)$$

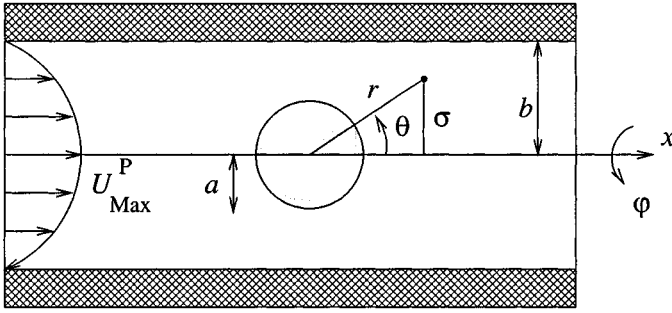


Figure 9.5.2 A sphere moving along the axis of a circular tube in Poiseuille flow.

Integrating with respect to σ , we find

$$\psi^P = U^P_{Max} \left(\frac{1}{2} \sigma^2 - \frac{1}{4} \frac{\sigma^4}{b^2} \right) + c, \tag{9.5.14}$$

where c is an unspecified constant.

An approximate representation of the flow in the presence of the sphere emerges by superposing the unperturbed parabolic flow, the flow due to a point force, and the flow due to a point-source dipole, where the two singularities are located at the center of the sphere and point along the x axis. The composite stream function is given by

$$\psi = \psi^P + s_x \psi^{3D-ST-x} + d_x \psi^{3D-PSD-x}, \tag{9.5.15}$$

where s_x and d_x are the unknown strengths of the singularities. Expressing (9.5.3) and (9.5.4) in cylindrical polar coordinates, we find

$$\psi^{3D-ST-x} \equiv r \sin^2 \theta = \frac{\sigma^2}{(x^2 + \sigma^2)^{1/2}}, \tag{9.5.16}$$

and

$$\psi^{3D-PSD-x} \equiv \frac{1}{4\pi r} \sin^2 \theta = \frac{1}{4\pi} \frac{\sigma^2}{(x^2 + \sigma^2)^{3/2}}, \tag{9.5.17}$$

where $r = \sqrt{x^2 + \sigma^2}$.

The boundary conditions require that the velocity at the surface of the sphere be equal to $\mathbf{u} = U \mathbf{e}_x$, where U is the velocity of the sphere, and \mathbf{e}_x is the unit vector along the x axis. In terms of the stream function,

$$u_x(r = a) = \frac{1}{\sigma} \left(\frac{\partial \psi}{\partial \sigma} \right)_{r=a} = U, \quad u_\sigma(r = a) = -\frac{1}{\sigma} \left(\frac{\partial \psi}{\partial x} \right)_{r=a} = 0, \quad (9.5.18)$$

where the derivative with respect to σ is taken holding x constant, and vice versa.

Substituting (9.5.14), (9.5.16), and (9.5.17) into the right-hand side of (9.5.15), and the resulting expression into the boundary conditions (9.5.18), and simplifying, we find

$$\left[U_{Max}^P \left(1 - \frac{\sigma^2}{b^2} \right) + \frac{s_x}{a} \left(2 - \frac{\sigma^2}{a^2} \right) + \frac{d_x}{4 \pi a^3} \left(2 - 3 \frac{\sigma^2}{a^2} \right) \right]_{r=a} = U, \quad (9.5.19)$$

and

$$s_x + \frac{3}{4 \pi a^2} d_x = 0. \quad (9.5.20)$$

Using (9.5.20) to eliminate d_x in favor of s_x from (9.5.19), we find

$$\left[U_{Max}^P \left(1 - \frac{\sigma^2}{b^2} \right) + \frac{4}{3} \frac{s_x}{a} \right]_{r=a} = U. \quad (9.5.21)$$

We note that, over the surface of the sphere, $\sigma = a \sin \theta$, and find that it is impossible to satisfy the boundary condition (9.5.21) all over the surface of the sphere, except in the absence of the parabolic flow. This difficulty underlines the limitations of the approximate representation (9.5.15). As a compromise, we require the satisfaction of (9.5.21) integrated over the surface of the sphere.

Substituting $\sigma = a \sin \theta$, and recalling that the integral of an axisymmetric function $f(\theta)$ over the surface of the sphere is given by $\iint f(\theta) dS = 2\pi a^2 \int_0^\pi f(\theta) \sin \theta d\theta$, and the surface area of the sphere is equal to $4\pi a^2$, we find

$$U_{Max}^P \left(4\pi a^2 - \frac{1}{b^2} 2\pi a^4 \int_0^\pi \sin^3 \theta d\theta \right) + \frac{4}{3} \frac{s_x}{a} 4\pi a^2 = U 4\pi a^2. \quad (9.5.22)$$

Computing $\int_0^\pi \sin^3 \theta d\theta = \frac{4}{3}$, and simplifying, we obtain

$$U_{Max}^P \left(1 - \frac{2}{3} \frac{a^2}{b^2} \right) + \frac{4}{3} \frac{s_x}{a} = U. \quad (9.5.23)$$

Now, according to (9.5.11), the x component of the hydrodynamic force exerted on the sphere is given by

$$F_x = -8\pi\mu s_x. \quad (9.5.24)$$

Using this expression to eliminate s_x in favor of F_x in (9.5.23), we obtain

$$U_{Max}^P \left(1 - \frac{2}{3} \frac{a^2}{b^2}\right) - \frac{F_x}{6\pi\mu a} = U, \quad (9.5.25)$$

which provides us with a relationship between the velocity profile of the Poiseuille flow determined by U_{Max}^P and b , the force exerted on the sphere F_x , and the velocity of the sphere U . If the tube is vertical with the x axis pointing downward, a force balance over the sphere requires that F_x be equal and opposite to the weight of the sphere minus the buoyancy force, $F_x = -\frac{4\pi}{3}a^3(\rho_s - \rho)g$, where ρ_s is the density of the sphere and g is the acceleration of gravity.

The second term on the left-hand side of (9.5.25) is a consequence of Stokes's law given in (9.4.25). The first term on the left-hand side expresses the velocity of the sphere in terms of the maximum velocity of the unperturbed parabolic flow and the tube radius. This expression shows that the velocity of a neutrally buoyant sphere lags behind the local fluid velocity U_{Max}^P by a factor that is determined by the ratio of the sphere to tube radius a/b .

An implicit approximation underlines the preceding derivations: the no-slip and no-penetration conditions on the surface of the tube were not required. As a consequence, expression (9.5.25) is strictly valid for a sphere that is immersed in infinite parabolic flow; the presence of the tube in the preceding discussion is relevant only insofar as to establish the curvature of the velocity profile.

Remarkably, in spite of the approximate satisfaction of the boundary condition on the surface of the sphere expressed by (9.5.22), expression (9.5.25) turns out to be exact for infinite parabolic flow, but not for wall-bounded parabolic flow.

9.5.6 Integral representations

Consider an incident flow with velocity \mathbf{u}^∞ past a stationary, translating, or rotating particle, and discretize the surface of the particle into a collection of N surface elements such as curved quadrilaterals or triangles, as illustrated in figure 9.5.3. An approximate representation of

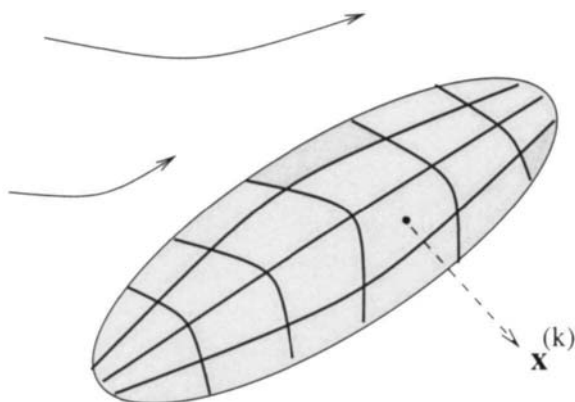


Figure 9.5.3 Stokes flow past a particle may be represented by a superposition of point forces located at designated centers of boundary elements.

the flow may be obtained by adding to the incident flow the flow due to a collection of point forces located at designated centers of the surface elements.

Expressing the Stokeslet in terms of the Oseen tensor, as shown in equation (9.5.6), we find that the velocity at a point \mathbf{x} that lies in the fluid is given by

$$\mathbf{u}(\mathbf{x}) = \mathbf{u}^\infty(\mathbf{x}) - \frac{1}{8\pi\mu} \sum_{k=1}^N \mathbf{S}(\mathbf{x}, \mathbf{x}^{(k)}) \cdot \mathbf{F}^{(k)}, \quad (9.5.26)$$

where $\mathbf{x}^{(k)}$ is the designated center of the k th element, and $\mathbf{F}^{(k)}$ is the corresponding vectorial strength of the point force.

Straightforward rearrangement of (9.5.26) yields

$$\mathbf{u}(\mathbf{x}) = \mathbf{u}^\infty(\mathbf{x}) - \frac{1}{8\pi\mu} \sum_{k=1}^N \mathbf{S}(\mathbf{x}, \mathbf{x}^{(k)}) \cdot \mathbf{f}^{(k)} \Delta S^{(k)}, \quad (9.5.27)$$

where $\Delta S^{(k)}$ is the surface area of the k th element, and we have defined the average traction $\mathbf{f}^{(k)} \equiv \frac{1}{\Delta S^{(k)}} \mathbf{F}^{(k)}$. In the limit as the number of elements N tends to infinity, and correspondingly the surface areas $\Delta S^{(k)}$ tend to zero, the sum on the right-hand side of (9.5.27) reduces to a surface integral yielding the integral representation

$$\mathbf{u}(\mathbf{x}) = \mathbf{u}^\infty(\mathbf{x}) - \frac{1}{8\pi\mu} \int \int_{\text{Particle}} \mathbf{S}(\mathbf{x}, \mathbf{x}') \cdot \mathbf{f}(\mathbf{x}') dS(\mathbf{x}'), \quad (9.5.28)$$

which expresses the flow in terms of a distribution of point forces over the particle surface. It can be shown that the density of the distribution \mathbf{f} is, in fact, the hydrodynamic traction exerted on the particle surface, $\mathbf{f} = \sigma \cdot \mathbf{n}$, where \mathbf{n} is the unit vector normal to the particle surface pointing into the fluid.

The integral representation (9.5.28) suggests a practical method of computing the flow: apply this equation at a point \mathbf{x} on the particle surface, use the required boundary conditions for the velocity to evaluate the left-hand side, and then solve the resulting integral equation for the traction \mathbf{f} . In practice, the solution is found numerically by approximating (9.5.28) with a discrete form in terms of boundary elements, as shown in equation (9.5.27). Identifying the point \mathbf{x} in (9.5.27) with the designated center of each element, we obtain a system of linear equations for the strengths of the point forces $\mathbf{F}^{(k)}$. The overall procedure is described as a boundary-element/collocation method.

Problems

Problem 9.5.1 *Force on a surface enclosing a Stokeslet.*

Verify relation (9.5.9) for a spherical surface centered at the singular point \mathbf{x}_0 .

Problem 9.5.2 *Point source.*

Verify that the force exerted on a spherical surface centered at a point source vanishes. Recall that the pressure field associated with a point is uniform throughout the domain of a Stokes flow.

9.6 Two-dimensional Stokes flow

It would appear that the discussion of three-dimensional flow in Sections 9.4 and 9.5 carries over to two-dimensional flow without any further difficulties or added considerations. While this is true, in general, there is one important exception: the flow due to the motion of a two-dimensional

body in an infinite and otherwise quiescent fluid is not defined, in the sense that a solution that satisfies the condition of vanishing velocity at infinity cannot be obtained. We shall consider this problematic case first, and then discuss flows that are well-defined.

9.6.1 Flow due to the motion of a cylinder

Consider the flow due to a circular cylinder of radius a translating along the x axis with velocity U . If the Reynolds number $Re = \rho a U / \mu$ is small, then sufficiently close to the cylinder inertial forces are negligible compared to pressure and viscous forces, and the motion of the fluid is governed by the linear equations of Stokes flow. In Section 9.4, we emphasized that the smallness of the Reynolds number does not guarantee that inertial forces will be insignificant far from the cylinder, and the consistency of a solution derived working exclusively on the equations of Stokes flow should be verified.

To bypass the computation of the pressure, we seek a solution based on the vorticity transport equation for the strength of the vorticity ω_z ,

$$\rho \left(\frac{\partial \omega_z}{\partial t} + u_x \frac{\partial \omega_z}{\partial x} + u_y \frac{\partial \omega_z}{\partial y} \right) = \mu \nabla^2 \omega_z, \quad (9.6.1)$$

where $\nabla^2 \equiv \partial^2 / \partial x^2 + \partial^2 / \partial y^2$ is the two-dimensional Laplacian operator. In terms of the stream function, the strength of the vorticity is given by equation (2.9.7). Setting the right-hand side of (9.6.1) equal to zero, and substituting (2.9.7) into the right-hand side, we derive a fourth-order linear differential equation for the stream function,

$$0 = -\nabla^2 \nabla^2 \psi \equiv -\nabla^4 \psi, \quad (9.6.2)$$

where

$$\nabla^4 \equiv \nabla^2 \nabla^2 = \left(\frac{\partial^2}{\partial x^2} + \frac{\partial^2}{\partial y^2} \right) \left(\frac{\partial^2}{\partial x^2} + \frac{\partial^2}{\partial y^2} \right) = \frac{\partial^4}{\partial x^4} + 2 \frac{\partial^4}{\partial x^2 \partial y^2} + \frac{\partial^4}{\partial y^4} \quad (9.6.3)$$

is the *biharmonic* operator in two dimensions. Our task is to solve the fourth-order differential equation (9.6.3) in the flow regime confined between $r = a$ and infinity, subject to appropriate boundary and far-field conditions.

Repeating the analysis of Section 9.4 for the analogous problem of flow due to a translating sphere, we find that, in terms of the stream

function, the boundary and far-field conditions in plane polar coordinates (r, θ) take the form

$$\psi(r = a) = Ua \sin \theta, \quad \left(\frac{\partial \psi}{\partial r}\right)_{r=a} = U \sin \theta, \quad (9.6.4)$$

and

$$\frac{\psi}{r^m} \rightarrow 0 \quad \text{as} \quad r \rightarrow \infty, \quad (9.6.5)$$

for $m \geq 1$. Condition (9.6.5) allows the stream function to diverge at infinity, but requires that the rate of growth be less than linear for the velocity to decay.

Motivated by the functional form of the boundary conditions (9.6.4), we seek a solution for the stream function by separation of variables in plane polar coordinates, writing

$$\psi = q(r) \sin \theta. \quad (9.6.6)$$

The unknown function $q(r)$ is required to satisfy the boundary conditions

$$q(r = a) = Ua, \quad \left(\frac{\partial q}{\partial r}\right)_{r=a} = U, \quad (9.6.7)$$

and the far-field condition

$$\frac{q(r)}{r^m} \rightarrow 0 \quad \text{as} \quad r \rightarrow \infty, \quad (9.6.8)$$

for $m \geq 1$.

Equation (3.2.25) provides us with the Laplacian operator in planar polar coordinates. The corresponding biharmonic operator is

$$\nabla^4 = \left[\frac{1}{r} \frac{\partial}{\partial r} \left(r \frac{\partial}{\partial r} \right) + \frac{1}{r^2} \frac{\partial^2}{\partial \theta^2} \right] \left[\frac{1}{r} \frac{\partial}{\partial r} \left(r \frac{\partial}{\partial r} \right) + \frac{1}{r^2} \frac{\partial^2}{\partial \theta^2} \right]. \quad (9.6.9)$$

Substituting (9.6.6) into (9.6.2), expressing the biharmonic operator in the form provided by (9.6.9), and carrying out the differentiations, we derive the fourth-order linear ordinary differential equation

$$\left(\frac{d^2}{dr^2} + \frac{1}{r} \frac{d}{dr} - \frac{1}{r^2} \right) \left(\frac{d^2}{dr^2} + \frac{1}{r} \frac{d}{dr} - \frac{1}{r^2} \right) q = 0. \quad (9.6.10)$$

Working as in Section 9.4 for flow due to the motion of a sphere, we derive the general solution

$$q(r) = A r^3 + B r \ln r + C r + \frac{D}{r}, \quad (9.6.11)$$

where A , B , C and D , are four constants. For the far-field condition (9.6.8) to be satisfied, A , B , and C must all be equal to zero, and this leaves us with only one coefficient to satisfy the two remaining boundary conditions (9.6.7), which is impossible. Thus, the problem of flow due to the motion of a cylinder in Stokes flow does not admit a solution.

To probe the origin of this catastrophe, we examine the magnitude of the inertial and viscous terms in the equation of motion, as discussed in Section 9.4, and find that the approximations underlying the notion of creeping flow cease to be accurate far from the cylinder. As a consequence, requiring the far field condition (9.6.8) leads to irreconcilable behavior. In the case of three-dimensional flow due to the motion of a sphere, this difficulty is shielded by the decay of the flow due to a three-dimensional Stokeslet expressing a point force. In contrast, in the case of two-dimensional flow, the velocity field due to a point force exhibits a logarithmic divergence contributed by the second term on the right-hand side of (9.6.11), and a decaying solution cannot be found.

To remedy the situation, we use the method of *matched asymptotic expansions*, dividing the flow into an inner regime where the motion of the fluid is governed by the equations of creeping flow with the boundary conditions on the surface of the cylinder required, and an outer regime where the motion of the fluid is governed by another simplified system of equations, called the equations of Oseen flow, with the far-field condition (9.6.8) required. Matching conditions arise by inspecting the functional forms of the two solutions. The analysis involves sophisticated arguments that are outside the scope of an introductory exposition.

9.6.2 Flow due to the rotation of a circular cylinder

Not all problems of two-dimensional infinite flow are ill-posed, in the sense that a solution that satisfies the boundary and far-field conditions cannot be found. If the force exerted on the internal boundaries vanishes, then a perfectly acceptable solution can be found.

Consider, for example, the flow generated by a circular cylinder of radius a rotating with angular velocity Ω about its center. The induced flow is identical to that due to a point vortex with strength $\kappa = 2\pi \Omega a^2$

placed at the center of cylinder, as discussed in Section 3.7. Using expressions (3.6.1), we find that the velocity field is given by

$$u_r = 0, \quad u_\theta = \frac{\Omega a^2}{r}. \quad (9.6.12)$$

The corresponding pressure field is uniform throughout the domain of flow.

To sustain the rotation of the cylinder, an external torque must be applied counterbalancing the hydrodynamic torque due to the fluid motion. The torque with respect to the center of the cylinder is given by

$$T_z = \oint_{Cylinder} \sigma_{r\theta} a \, dl. \quad (9.6.13)$$

Substituting (9.6.12) into (4.6.19), we find that the stress component $\sigma_{r\theta}$ is given by $-2\mu\Omega a^3/r^2$. Substituting this expression into (9.6.13), setting $dl = a \, d\theta$, and integrating with respect to θ from 0 to 2π , we find

$$T_z = -4\pi\mu \Omega a^2. \quad (9.6.14)$$

9.6.3 The Oseen tensor and the point force

The second term on the right-hand side of (9.6.11), involving the logarithm, represents the flow due to a two-dimensional point force oriented along the x axis. Differentiating with respect to x or y to obtain the corresponding velocity field, and repeating for the y direction, we obtain the velocity field at the point $\mathbf{x} = (x, y)$ due to a two-dimensional Stokeslet with vectorial strength $\mathbf{s} = (s_x, s_y)$ situated at the point $\mathbf{x}_0 = (x_0, y_0)$, expressed by

$$\begin{pmatrix} u_x \\ u_y \end{pmatrix}(\mathbf{x}, \mathbf{x}_0) = \mathbf{S}(\mathbf{x}, \mathbf{x}_0) \cdot \begin{pmatrix} s_x \\ s_y \end{pmatrix}, \quad (9.6.15)$$

where \mathbf{S} is the 2×2 Oseen tensor for two-dimensional flow defined as

$$\mathbf{S}(\mathbf{x}, \mathbf{x}_0) = \begin{pmatrix} -\ln r + \frac{(x-x_0)^2}{r^2} & \frac{(x-x_0)(y-y_0)}{r^2} \\ \frac{(y-y_0)(x-x_0)}{r^2} & -\ln r + \frac{(y-y_0)^2}{r^2} \end{pmatrix}, \quad (9.6.16)$$

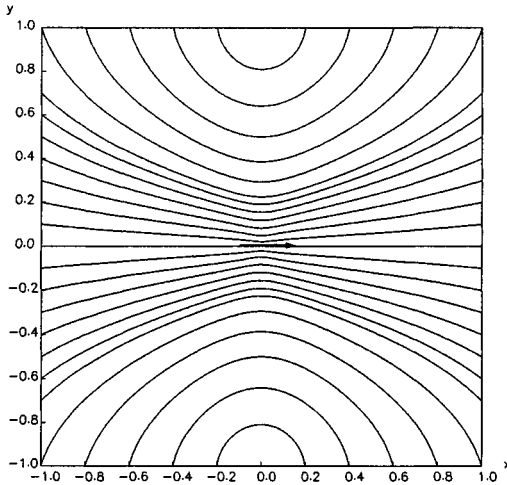


Figure 9.6.1 Streamline pattern of the flow induced by a two-dimensional point force pointing along the x axis.

and $r = \sqrt{(x - x_0)^2 + (y - y_0)^2}$ is the distance of the field point \mathbf{x} from the location of the Stokeslet, \mathbf{x}_0 .

The two columns of the Oseen tensor represent, respectively, the x and y velocity components associated with a Stokeslet of unit strength pointing in the direction of the x or y axis. The corresponding pressure field is given by

$$p(\mathbf{x}, \mathbf{x}_0) = 2\mu \begin{pmatrix} \frac{x-x_0}{r^2} \\ \frac{y-y_0}{r^2} \end{pmatrix} \cdot \begin{pmatrix} s_x \\ s_y \end{pmatrix}, \quad (9.6.17)$$

where a dot denotes the inner vector product. The streamline pattern of the flow induced by a two-dimensional Stokeslet oriented along the x axis is shown in figure 9.6.1.

Consider a closed contour C enclosing the singular point \mathbf{x}_0 . It can be shown that the force exerted on the contour is given by

$$\mathbf{F} = \int_C \boldsymbol{\sigma} \cdot \mathbf{n} \, dS = -4\pi\mu \mathbf{s}. \quad (9.6.18)$$

independent of the shape of the contour; $\boldsymbol{\sigma}$ is the stress tensor, and \mathbf{n} is the unit vector normal to C pointing outward. The torque with respect

to the point \mathbf{x}_0 is equal to zero. The force and torque exerted on a closed contour that *does not* enclose the singular point \mathbf{x}_0 , vanish. These results confirm our earlier assertion that the two-dimensional Stokeslet expresses the flow due to a two-dimensional point force.

Problem

Problem 9.6.1 *Simple shear flow past a freely-suspended cylinder.*

Consider simple shear flow along the x axis past a circular cylinder of radius a centered at the origin. The incident velocity field is given by $\mathbf{u}^\infty = (ky, 0)$, where k is the shear rate. The cylinder rotates about its center with angular velocity $\Omega = -\frac{1}{2}k$; if k is positive, the cylinder rotates in the clockwise direction. The components of the velocity field corresponding to this flow are known to be

$$u_r = \frac{k}{2} \left(r - \frac{2}{r} + \frac{1}{r^3} \right) \sin(2\theta), \quad u_\theta = \frac{k}{2} \left\{ r + \left[r - \frac{1}{r^3} \cos(2\theta) \right] \right\}. \quad (9.6.19)$$

(a) Compute the associated pressure field to satisfy the Stokes equations.

(b) Show that the torque exerted on the cylinder is equal to zero.

These results suggest that a freely-suspended cylinder rotates at an angular velocity that is equal to the negative of half the shear rate of the simple shear flow.

9.7 Flow near corners

The boundaries of a flow often involve walls, interfaces, and dividing streamlines that meet at sharp corners or cusps. Deep into the corners and cusps, the magnitude of the velocity diminishes rapidly, fluid inertia becomes negligible, and the Reynolds number of the local flow is small. The structure of the flow may then be studied in the context of Stokes flow, with the far flow playing the role of an external mechanism that determines the intensity and selects the geometrical mode of the local flow.

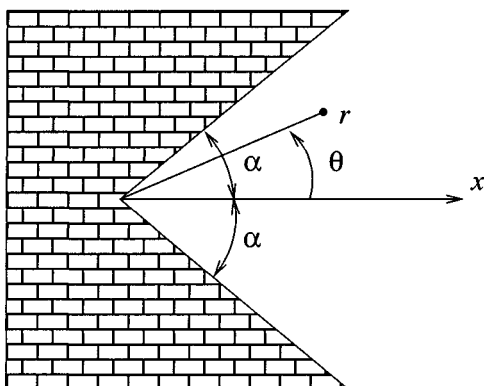


Figure 9.7.1 The local Reynolds number of the flow near a corner is small, and the motion of the fluid is governed by the equations of Stokes flow. Similarity solutions may be derived working in local plane polar coordinates.

9.7.1 Local solutions

Consider two-dimensional flow between two planes intersecting at an angle 2α , as illustrated in figure 9.7.1. To facilitate the impending implementation of the boundary conditions, we introduced plane polar coordinates (r, θ) with origin at the apex. Moreover, to bypass the computation of the pressure, we introduce the stream function ψ and express it in the separated form

$$\psi = q(r) f(\theta). \quad (9.7.1)$$

Note that (9.7.1) is a generalization of (9.6.6) describing flow due to the motion of a cylinder.

We begin by stipulating that the component functions $q(r)$ and $f(\theta)$ exhibit, respectively, a power-law and an exponential dependence on their respective arguments,

$$q(r) = r^\lambda, \quad f(\theta) = A \exp(\kappa\theta), \quad (9.7.2)$$

where λ and κ are two constants, and A is a constant coefficient.

The exponent κ is allowed to be complex, expressed in the form $\kappa = \kappa_r + i\kappa_i$, where i is the imaginary unit defined by the equation $i^2 = -1$, and κ_r and κ_i are two real constants. Using the Euler decomposition of the complex exponential, we write

$$f(\theta) = A \exp(\kappa_r \theta) [\cos(\kappa_i \theta) + i \sin(\kappa_i \theta)], \quad (9.7.3)$$

with the understanding that either the real or the imaginary part may be selected on the right-hand side of (9.7.1).

Substituting (9.7.2) into (9.7.1), and the result into the biharmonic equation $\nabla^4 \psi = 0$ expressed in plane polar coordinates, as shown in (9.6.9), we derive a bi-quadratic algebraic equation for κ parametrized by the exponent λ ,

$$\kappa^4 + 2(\lambda^2 - 2\lambda + 2)\kappa^2 + \lambda^2(\lambda - 2)^2 = 0, \quad (9.7.4)$$

whose roots are found readily by use of the quadratic formula. Solving for κ , substituting the result into (9.7.3), and rearranging the emerging expression, we obtain the general solution

$$f(\theta) = \begin{cases} B \sin(\lambda\theta - \beta) + C \sin[(\lambda - 2)\theta - \gamma] & \text{if } \lambda \neq 0, 1, 2 \\ B \sin(2\theta - \beta) + C\theta + D & \text{if } \lambda = 0, 2 \\ B \sin(\theta - \beta) + C\theta \sin(\theta - \gamma) & \text{if } \lambda = 1 \end{cases}, \quad (9.7.5)$$

where B, C are complex constants, and β, γ are real constants.

A variety of flows may be generated by selecting, or solving for, the exponent λ . Examples will be illustrated in the remainder of this section.

9.7.2 Stagnation-point flow on a plane wall

First, we consider flow near a stagnation point on a plane wall, illustrated in figure 9.7.2. The no-slip and no-penetration boundary conditions demand that $f = 0$ and $df/d\theta = 0$ at $\theta = 0$ and π . The structure of the flow is determined by requiring that $f = 0$ along the dividing streamline located at $\theta = \alpha$, where the angle α is a free parameter.

Making the judicious selection $\lambda = 3$, and using the general solution given by the first of equations (9.7.5), we find

$$f(\theta) = B \sin(3\theta - \beta) + C \sin(\theta - \gamma). \quad (9.7.6)$$

Requiring the no-slip and no-penetration boundary conditions, and specifying the orientation of the dividing streamline, we obtain a system of

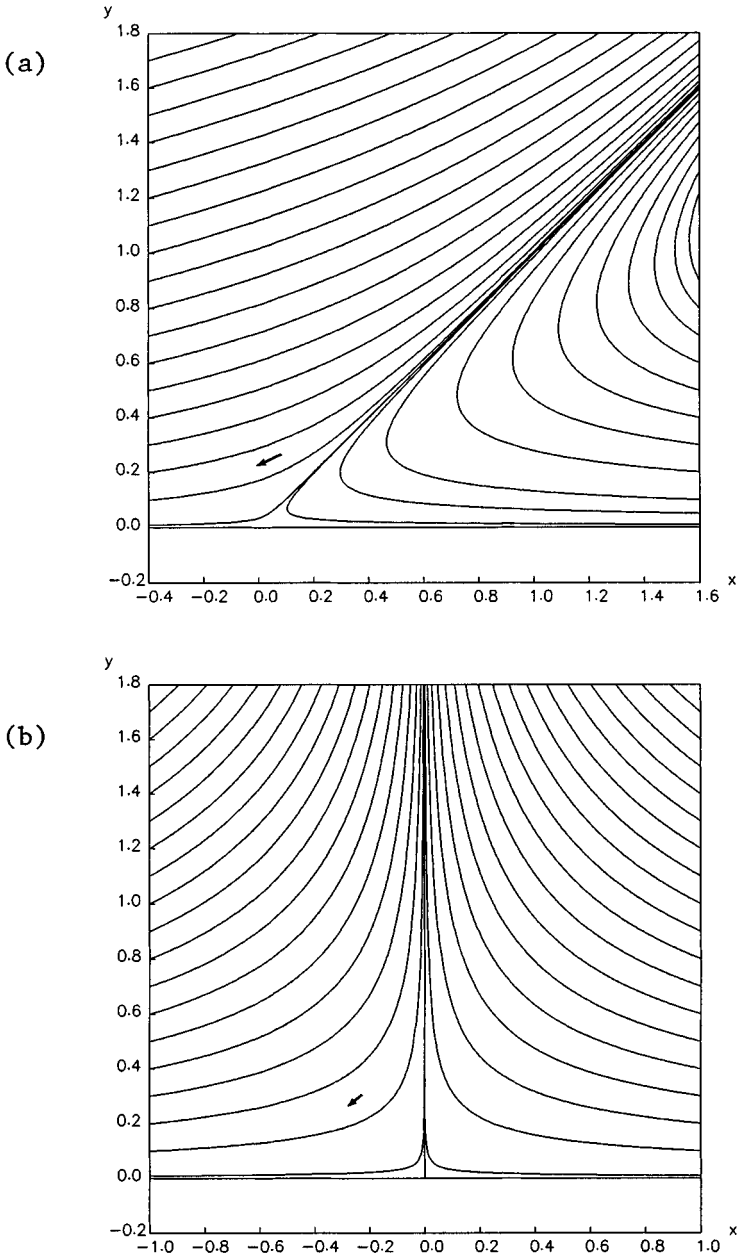


Figure 9.7.2 Streamline pattern of flow in the neighborhood of a stagnation point on a plane wall. The angle subtended between the dividing streamline and the wall is (a) $\alpha = \pi/4$, and (b) $\pi/2$.

three scalar homogenous equations for B and C involving the unknown parameters β and γ .

$$f(0) = f(\pi) = -B \sin \beta - C \sin \gamma = 0,$$

$$\left(\frac{df}{d\theta}\right)_{\theta=0} = -\left(\frac{df}{d\theta}\right)_{\theta=\pi} = 3B \cos \beta + C \cos \gamma = 0,$$

$$f(\alpha) = B \sin(3\alpha - \beta) + C \sin(\alpha - \gamma) = 0. \quad (9.7.7)$$

The first two equations in (9.7.7) require

$$\tan \beta = -3 \tan \gamma, \quad (9.7.8)$$

and the second and third equations require

$$3 \frac{\cos \beta}{\sin(3\alpha - \beta)} = -\frac{\cos \gamma}{\sin(\alpha - \gamma)}. \quad (9.7.9)$$

The system of equations (9.7.8) and (9.7.9) may be used to express β and γ in terms of α . Using any one of equations (9.7.7) to express B in terms of C , or vice versa, substituting the result into (9.7.6), and making use of the trigonometric identity $\sin 3a = 3 \sin a - 4 \sin^3 a$, where a is arbitrary, we derive the final form

$$f(\theta) = G \sin^2 \theta \sin(\theta - \alpha), \quad (9.7.10)$$

where G is an arbitrary constant. Substituting (9.7.10) into (9.7.1), we obtain the desired solution for the stream function,

$$\psi = G r^3 \sin^2 \theta \sin(\theta - \alpha). \quad (9.7.11)$$

The value of the constant G is determined by the strength of the flow far from the stagnation point. Streamline patterns for $\alpha = \pi/4$ and $\pi/2$ are depicted in figure 9.7.2. A distinguishing feature of Stokes flow is that the dividing streamlines are straight lines emanating from the stagnation point on the wall.

9.7.3 Flow near a corner

As a second application, we consider flow inside a corner that is confined between two intersecting stationary planes located at $\theta = \pm\alpha$,

as illustrated in figure 9.7.1. The no-slip and no-penetration boundary conditions require $f = 0$ and $df/d\theta = 0$ at $\theta = \pm\alpha$. We confine our attention to flow that is antisymmetric with respect to the mid-plane located at $\theta = 0$, and require the condition $df/d\theta = 0$ at $\theta = 0$, which states that the radial velocity vanishes at the mid-plane.

In this case, the value of the exponent λ cannot be specified *a priori*, as in the case of stagnation-point flow discussed earlier, but must be found as part of the solution. Assuming that $\lambda \neq 0, 1, 2$, we use the first of equations (9.7.5), set $\beta = \pi/2$ and $\gamma = \pi/2$ to satisfy the condition $df/d\theta = 0$ at $\theta = 0$, and find

$$f(\theta) = Q \cos(\lambda\theta) + G \cos[(\lambda - 2)\theta], \quad (9.7.12)$$

where Q and G are two constants. Requiring the boundary conditions $f = 0$ and $df/d\theta = 0$ at $\theta = \pm\alpha$, we obtain a homogeneous system of two equations for the constants Q and G ,

$$\begin{bmatrix} \cos(\lambda\alpha) & \cos[(\lambda - 2)\alpha] \\ \lambda \sin(\lambda\alpha) & (\lambda - 2) \sin[(\lambda - 2)\alpha] \end{bmatrix} \cdot \begin{bmatrix} Q \\ G \end{bmatrix} = \begin{bmatrix} 0 \\ 0 \end{bmatrix}. \quad (9.7.13)$$

For a nontrivial solution to exist, the determinant of the coefficient matrix on the left-hand side must be equal to zero, yielding

$$\cos(\lambda\alpha)(\lambda - 2) \sin[(\lambda - 2)\alpha] - \lambda \sin(\lambda\alpha) \cos[(\lambda - 2)\alpha] = 0, \quad (9.7.14)$$

which may be restated in the form of the nonlinear algebraic equation

$$\sin[2\alpha(\lambda - 1)] = (1 - \lambda) \sin(2\alpha). \quad (9.7.15)$$

An obvious solution is $\lambda = 1$. For this value, however, the third instead of the first of equations (9.7.5) should have been selected, and this disqualifies the obvious choice.

We anticipate that equation (9.7.15) will have a generally complex solution for λ , and write

$$\lambda = \lambda_r + i\lambda_i, \quad (9.7.16)$$

where i is the imaginary unit. Substituting (9.7.16) into (9.7.15), and using standard formulas of complex calculus, we derive a system of two real equations for the real components λ_r and λ_i ,

$$\begin{aligned} \sin[2\alpha(\lambda_r - 1)] \cosh(2\alpha\lambda_i) &= (1 - \lambda_r) \sin(2\alpha), \\ \sin[2\alpha(\lambda_r - 1)] \sinh(2\alpha\lambda_i) &= -\lambda_i \sin(2\alpha). \end{aligned} \quad (9.7.17)$$

To simplify the notation, we introduce the auxiliary variables

$$\xi = 2\alpha(\lambda_r - 1), \quad \eta = 2\alpha\lambda_i \quad \kappa = \frac{\sin(2\alpha)}{2\alpha}, \quad (9.7.18)$$

and express the system (9.7.17) in the more convenient form

$$\begin{aligned} f_1(\xi, \eta) &\equiv \sin \xi \cosh \eta + \kappa \xi = 0, \\ f_2(\xi, \eta) &\equiv \cos \xi \sinh \eta + \kappa \eta = 0. \end{aligned} \quad (9.7.19)$$

Using the first two equations of (9.7.18), we find

$$\lambda = \frac{1 + \xi}{2\alpha} + i \frac{\eta}{2\alpha}. \quad (9.7.20)$$

Our task is to solve the system of equations (9.7.19) for ξ and η , subject to a specified value for κ ; that is, subject to a specified angle α .

Newton's method

The solution of the nonlinear algebraic equations must be found by iteration: guess values for ξ and η that allegedly satisfy equations (9.7.19), and then improve the guess in a sensible fashion.

In Newton's method, the solution is found by guessing the values ξ^G and η^G , replacing the functions $f_1(\xi, \eta)$ and $f_2(\xi, \eta)$ with their linearized Taylor series expansion, and then solving a linear system for the unknowns using elementary analytical or numerical methods. The linearized Taylor series expansion provides us with the approximations

$$\begin{aligned} f_1(\xi, \eta) &\simeq f_1(\xi^G, \eta^G) + \left(\frac{\partial f_1}{\partial \xi}\right)_{\xi=\xi^G, \eta=\eta^G} (\xi - \xi^G) \\ &\quad + \left(\frac{\partial f_1}{\partial \eta}\right)_{\xi=\xi^G, \eta=\eta^G} (\eta - \eta^G), \\ f_2(\xi, \eta) &\simeq f_2(\xi^G, \eta^G) + \left(\frac{\partial f_2}{\partial \xi}\right)_{\xi=\xi^G, \eta=\eta^G} (\xi - \xi^G) \\ &\quad + \left(\frac{\partial f_2}{\partial \eta}\right)_{\xi=\xi^G, \eta=\eta^G} (\eta - \eta^G). \end{aligned} \quad (9.7.21)$$

Setting the right-hand sides equal to zero to satisfy (9.7.19), we find

$$\begin{pmatrix} \frac{\partial f_1}{\partial \xi} & \frac{\partial f_1}{\partial \eta} \\ \frac{\partial f_2}{\partial \xi} & \frac{\partial f_2}{\partial \eta} \end{pmatrix}_{\xi=\xi^G, \eta=\eta^G} \cdot \begin{pmatrix} \xi - \xi^G \\ \eta - \eta^G \end{pmatrix} = \begin{pmatrix} -f_1(\xi^G, \eta^G) \\ -f_2(\xi^G, \eta^G) \end{pmatrix}. \quad (9.7.22)$$

The matrix on the left-hand side of (9.7.22) is the *Jacobian* of the algebraic system (9.7.19). Newton's algorithm involves the following steps:

1. Guess the values ξ^G and η^G .
2. Evaluate the right-hand side of (9.7.22) and the coefficient matrix on the left-hand side.
3. Solve the system of two linear equations (9.7.22) for the differences $\Delta\xi \equiv \xi - \xi^G$ and $\Delta\eta \equiv \eta - \eta^G$. Remember that ξ and η are unknown.
4. Improve the guesses by replacing the guessed values with the new values

$$\xi^N = \xi^G + \Delta\xi, \quad \eta^N = \eta^G + \Delta\eta. \quad (9.7.23)$$

5. Return to step 2 and repeat the procedure with the new values of ξ and η .

It can be shown that the iterations converge as long as the initial guess is sufficiently close to the exact solution.

System (9.7.19) has a family of solution branches obtained by making different selections for the initial guess. The most physically relevant branch is the one associated with the smallest value of λ_r , corresponding to the flow that decays at the lowest possible rate in the limit as the distance from the apex r tends to zero.

Figure 9.7.3 shows graphs of the real and imaginary part of λ plotted against the semi-angle α , computed using Newton's method. When $0.41\pi < \alpha < \pi$, λ is real; the fluid moves uninterrupted along the walls, and regions of recirculating flow do not develop, as depicted in figure 9.7.4(a). When $0 < \alpha < 0.41\pi$, the exponent λ is complex; the flow develops an infinite sequence of regions of recirculating fluid, also called eddies, as shown in figure 9.7.4(b).

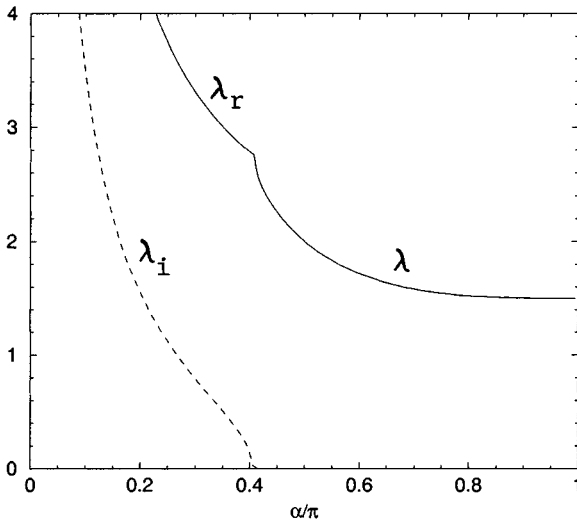


Figure 9.7.3 The exponent λ with the smallest real part for antisymmetric flow between two walls intersecting at the angle 2α . When $0.41\pi < \alpha < \pi$, λ is real; when $0 < \alpha < 0.41\pi$, λ is complex.

Problem

Problem 9.7.1 *Flow near a scraper.*

Derive a local solution for the flow near two intersecting plates, where one of the plates is held stationary and the second moves parallel to itself with constant velocity. This idealized configuration is a model of the flow due to a plate scrapping a fluid off a flat surface, viewed in a frame of reference moving with the scraper.

Computer problem

Problem c.9.7.1 *Computation of the exponent.*

Write a computer program that uses Newton's method to solve the nonlinear algebraic system (9.7.19), and reproduce the graph shown in figure 9.7.3.

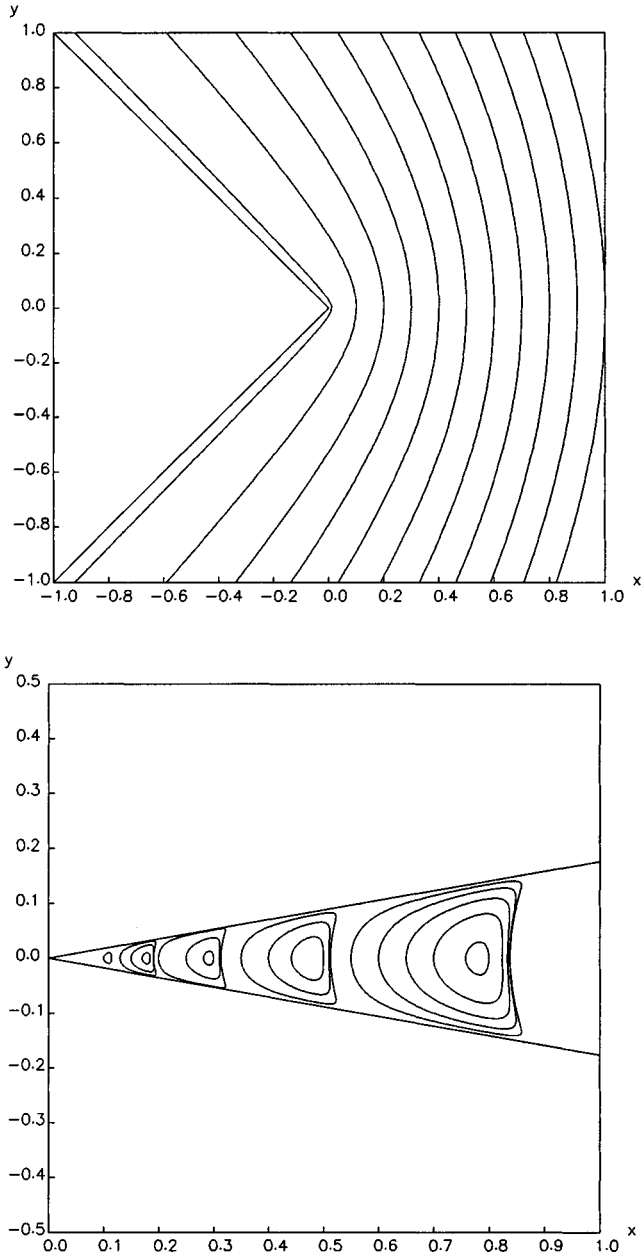


Figure 9.7.4 Streamline pattern of antisymmetric flow in a corner with half-angle (a) $\alpha = 135^\circ$, and (b) 10° .

Chapter 10

Flow at high Reynolds numbers

- 10.1 Changes in the structure of a flow with increasing Reynolds number
- 10.2 Prandtl boundary-layer analysis
- 10.3 Prandtl boundary layer on a flat surface
- 10.4 Von Kàrmàn's integral method
- 10.5 Instability of shear flows
- 10.6 Turbulent motion
- 10.7 Analysis of turbulent motion

Having discussed viscous flows at vanishing Reynolds numbers, we turn our attention to the diametrically opposite limit of inertia-dominated flows at high Reynolds numbers. Examining the changes in the structure of a flow with increasing Reynolds number, we encounter a broad variety of protocols accompanied by a rich phenomenology. In all cases, when the Reynolds number exceeds a critical threshold, flow instability arises and a small-scale turbulent motion is established. The theoretical study of the structure and dynamics of flows at high Reynolds numbers encompasses several complementary topics including potential-flow theory, boundary-layer theory, theory of hydrodynamic stability, theory of turbulent motion, and dynamics of vortex motion. Potential flow was considered in earlier sections; boundary-layer theory, hydrodynamic stability, and turbulent motion will be discussed in this chapter; and vortex motion will be the exclusive topic of Chapter 11.

10.1 Changes in the structure of a flow with increasing Reynolds number

As the Reynolds number of a flow is raised by increasing, for example, the magnitude of the velocity, the structure of the flow changes in a way that depends strongly on the particular flow configuration. Even though a general statement regarding the protocol of change cannot be made, several generic features may be identified:

- As the Reynolds number is raised, diffusion of vorticity from the boundaries into the bulk of the flow is hindered by strong convection along and toward the boundaries. As a result, the vorticity tends to be confined inside boundary layers and free shear layers developing along fluid interfaces and free surfaces. Viscous forces are significant inside the boundary and free shear layers, but may be neglected outside their edges.
- Vorticity that has entered the flow by diffusion across the boundaries may accumulate to form compact regions of rotational motion identified as vortices. Vortices are typically generated behind bluff bodies and at the trailing edges of streamlined objects.
- Vortex interaction causes the flow to become unsteady in a regular or chaotic fashion. Spatial, temporal, and spatio-temporal chaos, may be established even at moderate Reynolds numbers.
- When the Reynolds number exceeds a critical threshold, small disturbances amplify, altering the local or even the global structure of the base flow.
- Instability is followed by transition leading to turbulent flow, whereupon a small-scale unsteady motion is superimposed on a large-scale steady or unsteady flow. The small-scale motion affects, and is affected significantly by the large-scale structure and global properties of the flow.

Figure 10.1.1 illustrates the changes in the structure of streaming flow past a circular cylinder with increasing Reynolds number $Re \equiv \rho D U / \mu$, where D is the cylinder diameter, and U is the velocity of the incoming stream far from the cylinder. When the Reynolds number is less than unity, inertial forces are negligible near the cylinder, the motion of the fluid is governed by the equations of Stokes flow, and the streamline

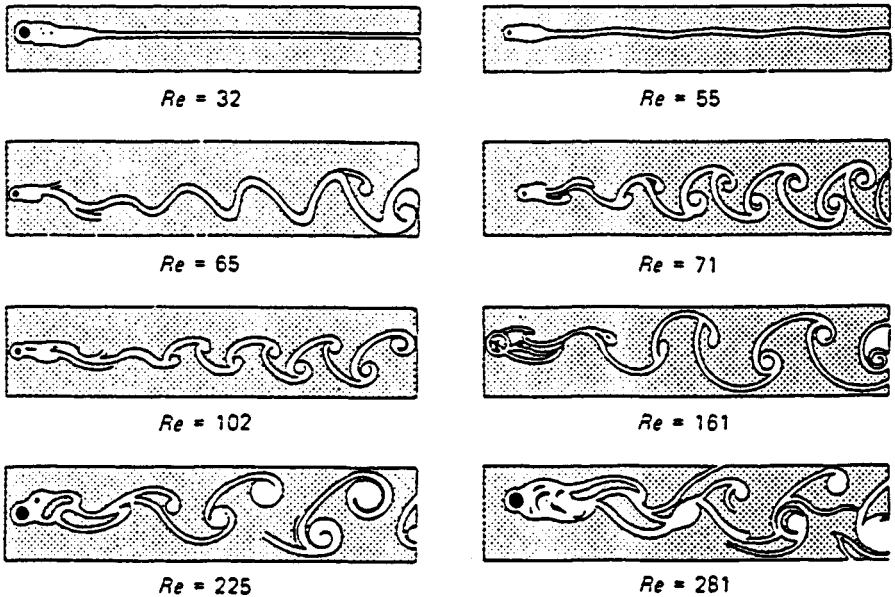


Figure 10.1.1 Illustration of the changes in the structure of streaming flow past a circular cylinder with increasing Reynolds numbers, showing boundary-layer separation and the development of a wake, after F. Homann (1936, Einfluss grosser Zähigkeit bei Strömung um Zylinder, *Forsch. Ing.-Wes.* 7, 1-10).

pattern is symmetric with respect to the vertical plane that is normal to the incident stream and passes through the center of the cylinder.

As the Reynolds number is raised, inertial forces become significant, and a boundary layer, identified as a region of increased vorticity, is established around the surface of the cylinder. The rotational fluid inside the boundary layer is convected along the cylinder and accumulates behind it to form two regions of recirculating flow followed by a slender wake.

Further increase in the Reynolds number causes the flow to become unstable. The pair of vortices developed behind the cylinder are shed downstream in an alternating fashion at a frequency that depends weakly on the Reynolds number, only to be replaced by newly formed vor-

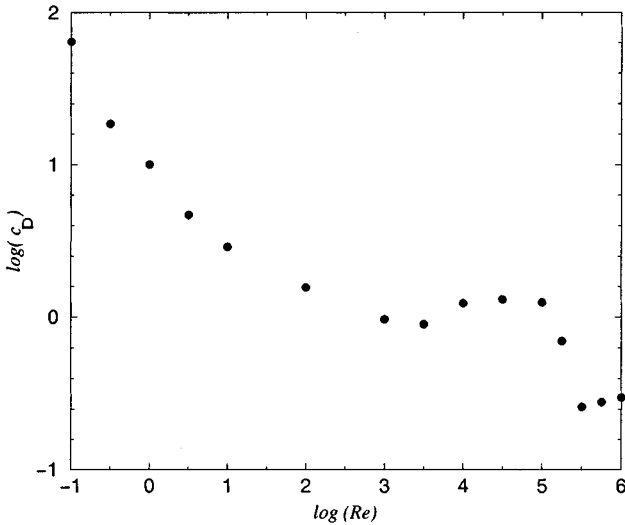


Figure 10.1.2 Drag coefficient of a circular cylinder held stationary in streaming flow, plotted against the Reynolds number defined with respect to the cylinder diameter.

tices. The frequency of shedding, denoted by f , is expressed by the dimensionless Strouhal number $St = fD/U$; in the case of a circular cylinder, $St \simeq 0.2$. Far from the cylinder, the wake consists of two rows of counter-rotating vortices arranged in a staggered formation known as the von Kàrmàn vortex street. At even higher Reynolds numbers, turbulent motion is established, and the edges of the wake becomes blurred and less well-defined.

The changes in the structure of the flow described in the preceding paragraphs have a strong influence on the drag force exerted on the cylinder. Figure 10.1.2 shows a graph of the drag coefficient

$$c_D \equiv \frac{2F}{\rho U^2 D}, \quad (10.1.1)$$

where F is the drag force per unit length exerted on the cylinder, plotted against the Reynolds number on a log-log scale. In the limit of vanishing Reynolds numbers, theoretical analysis shows that the drag force is given by the modified Stokes law

$$F \simeq \frac{4\pi\mu U}{\ln \frac{7.4}{Re}}. \quad (10.1.2)$$

Correspondingly, the drag coefficient is given by

$$c_D \simeq \frac{8\pi}{Re \log \frac{7.4}{Re}}. \quad (10.1.3)$$

The change in the functional form of the drag coefficient at a critical Reynolds number on the order of 10^3 , shown in figure 10.1.2, is due to the detachment of the boundary layer from the surface of the cylinder at a certain point on the rear surface of the cylinder, as will be discussed in Section 10.4, in a process that is described as flow separation. When the Reynolds number becomes on the order of 10^5 , the flow becomes turbulent and the boundary layer reattaches causing a sudden decline in the drag coefficient.

The non-monotonic dependence of the drag coefficient on the Reynolds number, illustrated in figure 10.1.2, is a manifestation of the complexity of fluid motion in the world of high-Reynolds-numbers flow.

Problem

Problem 10.1.1 *Flow in a channel through an expansion.*

Consider flow through a channel with a sudden expansion, as illustrated in figure 6.2.1. Discuss the expected changes in the structure of the flow with increasing a properly defined Reynolds number.

10.2 Prandtl boundary-layer analysis

In Section 10.1, we identified a boundary layer as a region of increased vorticity developing over a solid boundary in a high-Reynolds-number flow. To make the concept of a boundary layer more specific, we consider a model flow consisting of (a) an *outer* regime wherein the curl of the vorticity or the vorticity itself vanishes and the motion of the fluid is described by the equations of inviscid flow, including Euler's equation and the continuity equation, and (b) a boundary layer wherein the curl of the vorticity is substantial and viscous forces are significant, as illustrated

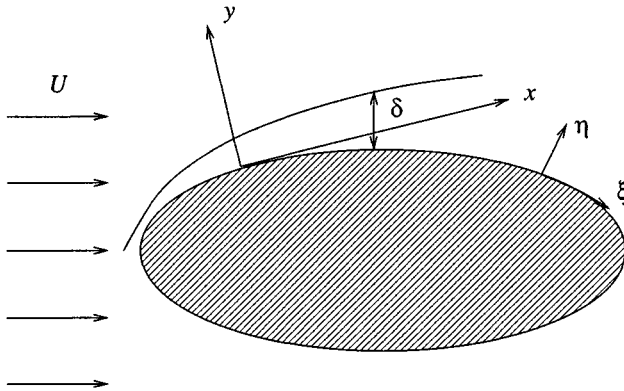


Figure 10.2.1 Schematic illustration of a Prandtl boundary layer developing around the surface of a two-dimensional curved body.

in figure 10.2.1. Wakes and regions of recirculating flow are allowed, but are significant only insofar as to determine the structure of the outer flow.

The slenderness of the boundary layer, compared to the typical size of the boundaries, allows us to simplify the equation of motion for the flow inside the boundary layer, and thereby derive approximate solutions valid in the asymptotic limit of high Reynolds numbers. To illustrate the physical arguments involved in the formulation of boundary-layer theory, and simultaneously demonstrate the important mathematical simplifications, we consider the boundary layer developing along a mildly-curved two-dimensional rigid body that is held stationary in an incident irrotational flow, as depicted in figure 10.2.1. Extensions to axisymmetric and three-dimensional configurations are straightforward.

10.2.1 Continuity equation

We begin the analysis by introducing Cartesian coordinates with the x axis tangential to the body at a point, and the y axis perpendicular to the body at that point, as shown in figure 10.2.1, and apply the continuity equation

$$\frac{\partial u_x}{\partial x} + \frac{\partial u_y}{\partial y} = 0 \quad (10.2.1)$$

at a point in the vicinity of the origin.

viscous term and may be neglected, yielding the boundary-layer equation

$$\frac{\partial u_x}{\partial t} + u_x \frac{\partial u_x}{\partial x} + u_y \frac{\partial u_x}{\partial y} = -\frac{\partial P}{\partial x} + \nu \frac{\partial^2 u_x}{\partial y^2}. \quad (10.2.4)$$

Second, the magnitude of the last viscous term must be comparable to the magnitude of the inertial terms on the left-hand side, requiring

$$\frac{U^2}{L} \sim \nu \frac{U}{\delta^2} \quad \text{or} \quad \delta \sim \sqrt{\frac{\nu L}{U}} = \frac{L}{Re^{1/2}}, \quad (10.2.5)$$

where $Re = UL/\nu$ is the Reynolds number defined with respect to the size of the boundaries.

10.2.3 y -component of the equation of motion

Next, we consider the individual terms in the y component of the equation of motion

$$\begin{aligned} \frac{\partial u_y}{\partial t} + u_x \frac{\partial u_y}{\partial x} + u_y \frac{\partial u_y}{\partial y} &= -\frac{1}{\rho} \frac{\partial P}{\partial y} + \nu \left(\frac{\partial^2 u_y}{\partial x^2} + \frac{\partial^2 u_y}{\partial y^2} \right), \\ \downarrow \quad \quad \downarrow \quad \quad \quad \quad \downarrow \quad \quad \downarrow & \\ \frac{U^2}{L^2} \delta \quad \quad \frac{U^2}{L^2} \delta \quad \quad \quad \frac{U^2}{L^2} \delta \quad \quad \frac{U^2}{L^2} \delta & \end{aligned} \quad (10.2.6)$$

and scale u_y with V , $\partial u_y/\partial x$ with V/L , u_x with U , $\partial u_y/\partial y$ with V/δ , the second derivative $\partial^2 u_y/\partial x^2$ with V/L^2 , and $\partial^2 u_y/\partial y^2$ with V/δ^2 . Moreover, we express the kinematic viscosity ν in terms of δ using the first of equations (10.2.5), replacing it with $U\delta^2/L$, and find that the magnitude of the various terms is as shown by the arrows underneath equation (10.2.6).

The magnitude of all nonlinear convective and viscous terms is of order δ . Unless the magnitude of the temporal derivative on the left-hand side is of order unity, the dynamic pressure gradient across the boundary layer must also be of order δ , $\partial P/\partial y \simeq \delta$, and this suggests the leading-order approximation

$$\frac{\partial P}{\partial y} \simeq 0. \quad (10.2.7)$$

Thus, non-hydrostatic pressure variations across the boundary layer are negligible, and the dynamic pressure inside the boundary layer is primarily a function of arc length along the boundary.

10.2.4 Boundary-layer equations

To compute the streamwise pressure gradient, we evaluate the x component of the Euler equation (6.4.2) at the edge of the boundary layer, obtaining

$$-\frac{1}{\rho} \frac{\partial P}{\partial x} = \frac{\partial U_x}{\partial t} + U_x \frac{\partial U_x}{\partial x}, \quad (10.2.8)$$

where U_x is the tangential component of the velocity of the outer flow. The boundary-layer equation (10.2.4) then becomes

$$\frac{\partial u_x}{\partial t} + u_x \frac{\partial u_x}{\partial x} + u_y \frac{\partial u_x}{\partial y} = \frac{\partial U_x}{\partial t} + U_x \frac{dU_x}{dx} + \nu \frac{\partial^2 u_x}{\partial y^2}. \quad (10.2.9)$$

Equations (10.2.1) and (10.2.9) provide us with a system of two second-order, nonlinear partial-differential equations for u_x and u_y , to be solved subject to: (a) the no-slip and no-penetration boundary conditions requiring that u_x and u_y vanish along the body, and (b) the far-field condition requiring that, as y/δ tends to infinity, u_x tends to the tangential component of the outer velocity U_x . Because the boundary-layer equations do not involve the second partial derivative of u_y with respect to y , a far-field condition for u_y is not required. The pressure follows from knowledge of the structure of the outer flow and plays the role of a forcing function, computed by solving the equations governing the structure of the outer irrotational flow.

10.2.5 Favorable and adverse pressure gradient

Considering a steady flow, we evaluate (10.2.9) at the origin, and enforce the no-slip and no-penetration conditions to obtain

$$\left(\frac{\partial^2 u_x}{\partial y^2}\right)_{y=0} = -\frac{1}{\nu} U_x \frac{dU_x}{dx}, \quad (10.2.10)$$

which shows that the sign of the curvature of the velocity profile at the boundary is opposite to the sign of the streamwise acceleration of the outer flow, dU_x/dx . Thus, the flow inside the boundary layer in a decelerating outer flow, corresponding to $dU/dx < 0$, reverses direction

causing convection of vorticity away from the boundary and consequent formation of vortices within the bulk of the fluid.

When $dU_x/dx > 0$, the pressure gradient is negative, $dP/dx < 0$, and the boundary layer is subjected to a *favorable* pressure gradient. In the opposite case $dU_x/dx < 0$, the pressure gradient is positive, $dP/dx > 0$, and the boundary layer is subjected to an *adverse* pressure gradient. Equation (10.2.10) shows that an adverse pressure gradient promotes flow separation.

10.2.6 Boundary-layer equations in curvilinear coordinates

The Prandtl boundary-layer equation (10.2.9) was developed with reference to the local Cartesian system of axes shown in figure 10.2.1, and is valid at a point in the vicinity of the origin. To avoid redefining the Cartesian axes at every point along the boundary, we introduce a curvilinear coordinate system with the ξ axis tangential to the boundary and the η axis perpendicular to the boundary, as shown in figure 10.2.1, and denote the corresponding velocity components by u_ξ and u_η .

Repeating the preceding arguments, we find that the boundary layer equations (10.2.1), (10.2.7), and (10.2.9) remain valid to leading-order approximation, provided that the Cartesian x and y coordinates are replaced by corresponding arc lengths in the ξ and η direction denoted, respectively, by l_ξ and l_η . Equation (10.2.7), in particular, becomes

$$\frac{\partial P}{\partial l_\eta} = \frac{\rho U_\xi^2}{R}, \quad (10.2.11)$$

where R is the radius of curvature of the boundary. Thus, the dynamic pressure drop across the boundary layer is of order δ , provided that R is not too small; that is, provided that the boundary is not too sharply curved. For simplicity, in the remainder of this chapter we shall denote l_ξ and l_η , respectively, by x and y .

10.2.7 Parabolization

The absence of a second partial derivative with respect to x renders the boundary-layer equation (10.2.9) a *parabolic* partial differential equation with respect to x . This classification has important consequences on the nature and method of computing the solution. Most important, the system of equations (10.2.1) and (10.2.9) may be solved using a marching

method with respect to x , beginning from a particular x station where the structure of the boundary layer is somehow known; examples will be discussed in subsequent sections. In contrast, the Navier-Stokes equation is an *elliptic* partial differential equation with respect to x and y , and the solution must be found simultaneously and at once at every point in the flow, even when the velocity and pressure at the points of entrance are specified.

The parabolic nature of (10.2.9) with respect to x implies that, if a perturbation is introduced at some point along the boundary layer, it will modify the structure of the flow downstream, but will leave the upstream flow unaffected. The absence of the second partial derivative with respect to x due to the boundary-layer approximation precludes a mechanism for upstream propagation.

10.2.8 Flow separation

Boundary-layer analysis for laminar flow is based on two key assumptions: the Reynolds number is sufficiently large, but not so large that the flow becomes turbulent; and the vorticity remains confined inside boundary layers that wrap around the boundaries.

The physical relevance of the second assumption depends on the structure of the incident flow and the geometry of the boundaries. Streamlined bodies allow laminar boundary layers to develop over a large portion, or even the whole, of their surface area, whereas bluff bodies cause the vorticity to concentrate within compact regions forming steady or unsteady wakes. For example, the alternating ejection of vortices of opposite sign into the wake is responsible for the von Kàrmàn vortex street illustrated in figure 10.1.1. These limitations should be born in mind when carrying out a boundary layer analysis.

10.3 Prandtl boundary layer on a flat surface

Having established simplified equations of motion for the flow inside a boundary layer over a solid surface, we proceed to derive solutions by analytical and numerical methods. First, we consider the simplest possible boundary layer developing on a flat surface in a constant, accelerating, or decelerating flow.

10.3.1 Boundary layer on a semi-infinite plate

Consider the boundary layer established over a semi-infinite flat plate that is held stationary and parallel to an incident streaming flow with velocity U , as illustrated in figure 10.3.1 (a). Since the tangential velocity of the outer flow is constant, $dU_x(x)/dx = 0$, the boundary layer equation (10.2.9) for steady flow simplifies to the convection-diffusion equation

$$u_x \frac{\partial u_x}{\partial x} + u_y \frac{\partial u_x}{\partial y} = \nu \frac{\partial^2 u_x}{\partial y^2} \quad (10.3.1)$$

The problem has been reduced to solving the simplified equation of motion (10.3.1) along with the continuity equation (10.2.1) for the velocity components u_x and u_y , subject to the no-slip, no-penetration, and far-field conditions.

Because the length of the plate is infinite, our only choice for the length L introduced in Section 10.2 is the streamwise distance x . The second of relations (10.2.5) then provides us with an expression for the boundary layer thickness in terms of the local Reynolds number $Re_x \equiv Ux/\nu$,

$$\delta(x) \sim \sqrt{\frac{\nu x}{U}} = \frac{x}{Re_x^{1/2}}. \quad (10.3.2)$$

Recall that this scaling arose by balancing the magnitudes of the inertial and viscous forces inside the boundary layer.

Self-similarity

Blasius noted that computing the solution of the system of partial differential equations (10.2.1) and (10.3.1) may be reduced to solving a single ordinary differential equation. To carry out this reduction, we assume that the flow develops in a self-similar manner, such that the streamwise velocity profile across the boundary layer is a function of the scaled transverse position expressed by the *similarity variable*

$$\eta \equiv \frac{y}{\delta(x)} = y \sqrt{\frac{U}{\nu x}}, \quad (10.3.3)$$

according to the functional form

$$u_x(x, y) = U F(\eta), \quad (10.3.4)$$

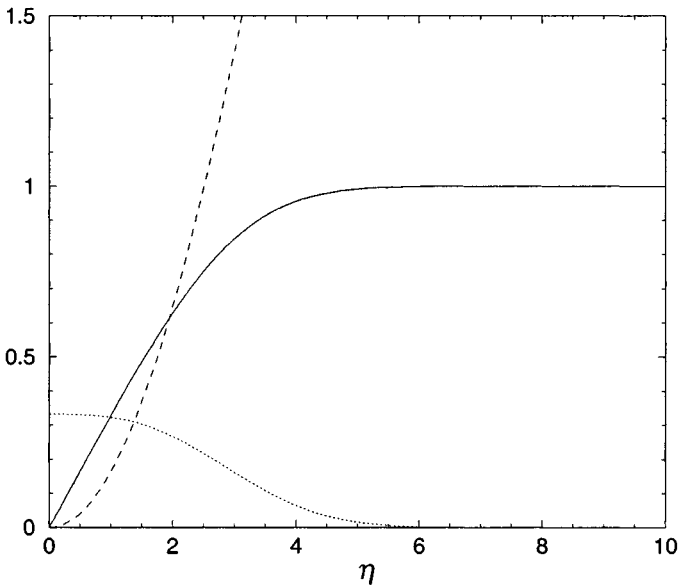
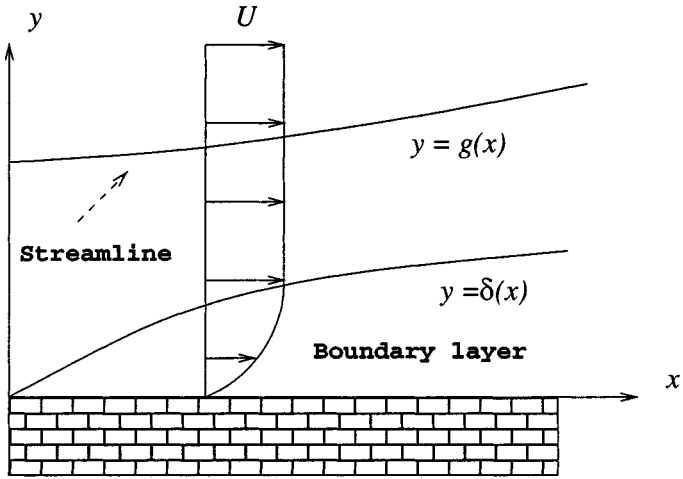


Figure 10.3.1 (a) Schematic illustration of a boundary layer developing along a semi-infinite flat plate placed parallel to a uniform incident stream. (b) Graphs of the self-similar streamwise velocity profile $u/U = f'$ (solid line), and of its integral and derivative functions f and f'' (dashed and dotted line).

where $F(\eta)$ is an unknown function. A key observation is that this self-similar streamwise profile derives from the stream function

$$\psi(x, y) = \sqrt{\nu U x} f(\eta), \quad (10.3.5)$$

where f is the indefinite integral or antiderivative of F , satisfying $df/d\eta = F$. The principal advantage of using the stream function is that the continuity equation is satisfied automatically and does not need to be further considered.

Differentiating (10.3.5) with respect to y or x , we find

$$\begin{aligned} u_x(x, y) &= \frac{\partial \psi}{\partial y} = U \frac{df}{d\eta}, \\ u_y(x, y) &= -\frac{\partial \psi}{\partial x} = \frac{1}{2} \sqrt{\frac{\nu U}{x}} \left(\eta \frac{df}{d\eta} - f \right). \end{aligned} \quad (10.3.6)$$

Substituting these expressions into the boundary layer equation (10.3.1), we obtain a third-order, nonlinear ordinary differential equation for the function $f(\eta)$,

$$\frac{d^3 f}{d\eta^3} + \frac{1}{2} f \frac{d^2 f}{d\eta^2} = 0, \quad (10.3.7)$$

first derived by Blasius in 1908. Using the no-slip and no-penetration conditions, and requiring that, far from the plate, the flow in the boundary layer reduces to the outer uniform flow, we obtain

$$f = 0 \quad \text{and} \quad \frac{df}{d\eta} = 0 \quad \text{at} \quad \eta = 0, \quad (10.3.8)$$

and

$$\frac{df}{d\eta} \rightarrow 1 \quad \text{as} \quad \eta \rightarrow \infty. \quad (10.3.9)$$

These equations provide us with boundary and far-field conditions to be used in solving the Blasius equation (10.3.7).

Before proceeding to compute the solution, it is instructive to apply the Blasius equation (10.3.7) at the plate, and use the first of the boundary conditions (10.3.8) to find $d^3 f/d\eta^3(\eta = 0) = 0$, which shows that the curvature of the streamwise velocity profile vanishes at the wall, in agreement with equation (10.2.10).

Solution of the Blasius equation

To solve the Blasius equation (10.3.6), we denote the first and second derivative of the function f by $g \equiv df/d\eta$ and $q \equiv dg/d\eta = d^2f/d\eta^2$, and decompose the third-order equation into a system of three first-order nonlinear equations,

$$\frac{df}{d\eta} = g, \quad \frac{dg}{d\eta} = q, \quad \frac{dq}{d\eta} = -\frac{1}{2} f g. \quad (10.3.10)$$

This system is accompanied by the boundary conditions $f(\eta = 0) = 0$, $g(\eta = 0) = 0$, and $g(\eta = \infty) = 1$, stemming from (10.3.8) and (10.3.9).

Since boundary conditions are provided at both ends of the solution domain with respect to η , extending from 0 to ∞ , we are faced with a two-point boundary value problem involving a third-order differential equation. The solution may be computed using a shooting method according to the following steps:

1. Guess the value of $q(\eta = 0) \equiv \frac{d^2f}{d\eta^2}(\eta = 0)$.
2. Integrate the Blasius equation (10.3.7) from $\eta = 0$ to $\eta = \infty$ subject to the initial conditions (10.3.8) using the guessed value of $q(\eta = 0)$. In practice, integrating up to $\eta = 10$ yields satisfactory accuracy.
3. Check whether the far-field condition $g(\eta = \infty) = 1$ is fulfilled; if not, improve the guess for $q(\eta = 0)$, and return to step 2.

The profile of the streamwise velocity $u/U = f' \equiv df/d\eta$ computed in this manner is shown with the solid line in figure 10.3.1(b), along with the profiles of f and $f'' \equiv d^2f/d\eta^2$ drawn with the dashed and dotted lines. The numerical solution reveals that $f'''(0) = 0.332$ and $u/U = 0.99$ when $\eta = 4.9$. Based on this result, we may define the 99% boundary-layer thickness

$$\delta_{99} = 4.9 \sqrt{\frac{\nu x}{U}} \quad \text{or} \quad \frac{\delta_{99}}{x} = \frac{4.9}{Re_x}, \quad (10.3.11)$$

where $Re_x \equiv Ux/\nu$. The 99.5% boundary-layer thickness is defined in a similar fashion; the numerical solution shows that the corresponding coefficient on the right-hand side of equations (10.3.11) is equal to 5.3.

Wall shear stress and drag force on the plate

The wall shear stress and drag force exerted on the wall are of particular interest in the engineering design of equipment handling high-speed flows. According to the similarity solution, the wall shear stress is given by

$$\begin{aligned}\sigma_{xy}(x, y = 0) &= \mu \left(\frac{\partial u_x}{\partial y} \right)_{y=0} = \frac{f''(0)}{\sqrt{Re_x}} \rho U^2 \\ &= \frac{0.332}{\sqrt{Re_x}} \rho U^2.\end{aligned}\tag{10.3.12}$$

Thus, the wall shear stress takes an infinite value at the leading edge, and decreases like the inverse square root of streamwise distance or local Reynolds number Re_x along the plate. The physical significance of the singular behavior at the origin, however, is diminished by the observation that the assumptions that led us to the boundary-layer equations cease to be valid at the leading edge.

Even though the shear stress is infinite at the leading edge, the inverse-square-root singularity is integrable, and the drag force exerted on any finite section of the plate extending from the leading edge up to an arbitrary point is finite. Using the similarity solution, we find that the drag force exerted on *both* sides of the plate over a length extending from the leading edge up to a certain distance x , is given by

$$\begin{aligned}D(x) &\equiv 2 \int_0^x \sigma_{xy}(x', y' = 0) dx' = 0.664 \frac{\rho U^{3/2}}{\nu^{1/2}} \int_0^x \frac{1}{\sqrt{x}} dx' \\ &= \frac{1.328}{\sqrt{Re_x}} \rho U^2 x.\end{aligned}\tag{10.3.13}$$

Based on this expression, we define the dimensionless drag coefficient

$$c_D \equiv \frac{D}{\frac{1}{2} \rho U^2 x} = \frac{2.656}{\sqrt{Re_x}}.\tag{10.3.14}$$

The predictions provided by (10.3.13) and (10.3.14) agree well with laboratory measurements up to about $Re_x = 1.2 \times 10^5$, whereupon the flow in the boundary layer develops a wavy pattern and ultimately becomes turbulent. Above the critical value of Re_x , the function $c_D(Re_x)$ jumps to a different branch with a significantly higher value of c_D .

Vorticity transport

Neglecting the velocity component along the y axis, we find that the strength of the vorticity inside the boundary layer is given by

$$\omega_z(x, y) \simeq -\frac{\partial u_x}{\partial y} = -\frac{f''(\eta)}{\sqrt{Re_x}} \frac{U^2}{\nu} = -f''(\eta) \frac{U}{\delta(x)}, \quad (10.3.15)$$

which shows that, at a particular location η , the strength of the vorticity decreases like the inverse of the local boundary-layer thickness due to the broadening of the velocity profile. The streamwise rate of convection of vorticity across a plane that is perpendicular to the plate is given by

$$\int_0^\infty u_x(x, y) \omega_z(x, y) dy \simeq -\int_0^\infty u_x(x, y) \frac{\partial u_x}{\partial y} dy = -\frac{1}{2} U^2, \quad (10.3.16)$$

which is independent of the downstream position x .

One consequence of this result is that the flux of vorticity across the plate is equal to zero, which is consistent with our earlier observation that the gradient of the vorticity vanishes, and viscous diffusion of vorticity does not occur at the wall, $U \partial f''' / \partial y = \partial^2 u_x / \partial y^2 = -\partial \omega / \partial y = 0$. Another consequence is that all convected vorticity is generated at the leading edge where the boundary-layer approximation ceases to be valid. Viscous stresses at the leading edge somehow generate the proper amount of vorticity needed for the self-similar flow to be established.

Displacement thickness

Because of the widening of the streamwise velocity profile in the streamwise direction, the streamlines are deflected upward, away from the plate, as shown in figure 10.3.1(a). Let us consider a streamline outside the boundary layer, described it by the equation $y = g(x)$, and write a mass balance over a control area that is enclosed by (a) the streamline, (b) a vertical plane at $x = 0$, (c) a vertical plane located at a certain distance x , and (d) the plate. Taking into consideration that the streamwise velocity profile at the leading edge located at $x = 0$ is flat, we obtain

$$\int_0^{g(0)} U dy = \int_0^{g(x)} u_x(x, y) dy. \quad (10.3.17)$$

Straightforward rearrangement yields

$$U [g(x) - g(0)] = \int_0^{g(x)} [U - u_x(x, y)] dy. \quad (10.3.18)$$

Taking the limit as the streamline under consideration moves far from the plate, we find

$$\lim[g(x) - g(0)] = \delta^*(x), \quad (10.3.19)$$

where we have introduced the displacement thickness

$$\delta^*(x) \equiv \int_0^\infty \left(1 - \frac{u_x}{U}\right) dy. \quad (10.3.20)$$

Using the numerical solution of the Blasius equation to evaluate the integral on the right-hand side of (10.3.20), we derive the precise relation

$$\delta^*(x) = \sqrt{\frac{\nu x}{U}} \int_0^\infty \left[1 - \frac{df}{d\eta}\right] d\eta = 1.721 \sqrt{\frac{\nu x}{U}}, \quad (10.3.21)$$

which shows that the displacement thickness, like the 99% boundary-layer thickness, increases like the square root of the streamwise position.

Physically, the displacement thickness represents the vertical displacement of the streamlines far from the plate with respect to their elevation at the leading edge. Laboratory observation has shown that the laminar boundary layer undergoes a transition to the turbulent state when the displacement thickness reaches the value $\delta^* \sim 600\nu/U$, at which point turbulent shear stresses become significant and the present analysis based on the assumption of laminar flow ceases to be accurate.

The displacement thickness describes the surface of a fictitious impenetrable body held stationary in the incident irrotational flow. An improved boundary-layer theory may be developed by replacing the tangential velocity of the outer flow along the plate, U , with the corresponding tangential component of the velocity of the irrotational flow past this fictitious body. The irrotational flow past the fictitious body must be computed after the displacement thickness has been established, as discussed in this section. This iterative improvement provides us with a basis for describing the flow in the context of asymptotic expansions.

Momentum thickness

It is both illuminating and useful to perform a momentum integral balance over the control area used previously to define the displacement thickness. Since the upper boundary of the control volume is a streamline, it does not contribute to the rate of momentum input. Assuming that the normal stresses on the vertical sides are equal in magnitude and opposite in sign, which is justified by the assumption that the pressure drop across the boundary layer is negligibly small, and neglecting the traction along the top streamline, we obtain

$$\int_0^{g(0)} U (\rho U) dy - \int_0^{g(x)} u_x (\rho u_x) dy - \frac{1}{2} D(x) = 0, \quad (10.3.22)$$

where $D(x)$ is the drag force exerted on *both* sides of the plate, defined in equation (10.3.13). Making the upper limits of integration equal, we recast (10.3.22) into the form

$$-\rho U^2 [g(x) - g(0)] - \rho \int_0^{g(x)} (U^2 - u_x^2) dy - \frac{1}{2} D(x) = 0. \quad (10.3.23)$$

Taking now the limit as the streamline defining the top of the control area moves far from the plate, and using the definitions (10.3.19) and (10.3.20), we obtain the relation

$$D(x) = 2 \rho U^2 \Theta(x), \quad (10.3.24)$$

where Θ is the momentum thickness defined as

$$\Theta(x) \equiv \int_0^\infty \frac{u_x}{U} \left(1 - \frac{u_x}{U}\right) dy. \quad (10.3.25)$$

Using the numerical solution of the Blasius equation, we find

$$\Theta(x) = \sqrt{\frac{\nu x}{U}} \int_0^\infty f'(\eta) [1 - f'(\eta)] d\eta = 0.664 \sqrt{\frac{\nu x}{U}}. \quad (10.3.26)$$

where $f'(\eta) = df/d\eta$.

Shape factor

The ratio between the displacement and the momentum thickness,

$$H \equiv \frac{\delta^*}{\Theta}, \quad (10.3.27)$$

is called the shape factor. Inspecting the definitions of δ^* and Θ shown in equations (10.3.20) and (10.3.24), we find that the shape factor is greater than unity, as long as the u is less than U over a substantial portion of the boundary layer; the satisfaction of this restriction is expected by physical intuition. The smaller the value of H , the more blunt the velocity profile across the boundary layer. Substituting the right-hand sides of expressions (10.3.21) and (10.3.25) into (10.3.27), we find that, for the boundary layer over a flat plate, $H = 2.591$.

Relation between the wall shear stress and momentum thickness

The momentum thickness is related to the wall shear stress, and vice versa, by the momentum integral balance expressed by (10.3.24): differentiating (10.3.13) with respect to x , we find $dD(x)/dx = 2\sigma_{xy}(x, y = 0)$; expressing the drag force in terms of the momentum thickness using (10.3.24), we obtain

$$\sigma_{xy}(x, y = 0) = \rho U^2 \frac{d\Theta(x)}{dx}. \quad (10.3.28)$$

Thus, if the shear stress is known, the momentum thickness may be computed by integration; and if the momentum thickness is known, the shear stress may be computed by differentiation.

10.3.2 Von Kàrmàn's approximate method

Given the velocity profile across the boundary layer, we have two ways of computing the wall shear stress: directly by differentiation, or indirectly by evaluating the momentum thickness and then differentiating it with respect to streamwise position x to obtain the shear stress according to equation (10.3.28). The indirect method is more forgiving, in the sense that it is less sensitive to the structure of the velocity profile near the wall. For the velocity profile that arises by solving the Blasius equation, the two methods are equivalent (problem 10.3.1).

Consider now a self-similar velocity profile with some reasonable form involving an unspecified function which is either obtained by exercising physical intuition or suggested by laboratory observation. Is it possible to adjust the unspecified function so that the two methods of computing the wall shear stress discussed in the preceding paragraph are equivalent? and, if the answer is affirmative, will the velocity profile obtained in this manner be a good approximation to the exact solution?

To answer these questions, we consider the velocity profile

$$\frac{u_x}{U} = \frac{df(\eta)}{d\eta} = \begin{cases} \sin \frac{\pi y}{2\Delta(x)} & \text{for } 0 < y < \Delta(x) \\ 1 & \text{for } y > \Delta(x) \end{cases}, \quad (10.3.29)$$

where

$$\eta \equiv \frac{y}{\Delta(x)}, \quad (10.3.30)$$

and $\Delta(x)$ is an unspecified function playing the role of a boundary-layer thickness, similar to the δ_{99} thickness introduced in equation (10.3.11). Note that the velocity distribution (10.3.29) conforms with the required boundary conditions $f'(0) = 0$, $f'''(0) = 0$, and $f'(\infty) = 1$, where a prime denotes a derivative with respect to η , but does *not* satisfy the Blasius equation.

Differentiating the profile (10.3.29) with respect to y , we obtain the wall shear stress

$$\sigma_{xy}(x, y = 0) = \frac{\pi \mu U}{2 \Delta(x)}. \quad (10.3.31)$$

The displacement thickness, momentum thicknesses, and shape factor defined in (10.3.20), (10.3.24), and (10.3.27), are found to be

$$\delta^*(x) = \left(1 - \frac{2}{\pi}\right) \Delta(x) = 0.363 \Delta(x),$$

$$\Theta(x) = \left(\frac{2}{\pi} - \frac{1}{2}\right) \Delta(x) = 0.137 \Delta(x),$$

$$H = 2.660. \quad (10.3.32)$$

It is reassuring to observe that the shape factor is remarkably close to that arising by solving the Blasius equation, $H = 2.591$.

Substituting the expressions for the momentum thickness and wall shear stress into the integral momentum balance (10.3.28), we obtain an ordinary differential equation for $\Delta(x)$,

$$\frac{\pi \mu U}{2 \Delta(x)} = 0.137 \rho U^2 \frac{d\Delta(x)}{dx}. \quad (10.3.33)$$

Rearranging, and integrating with respect to x subject to the initial condition $\Delta = 0$ at $x = 0$, we find

$$\Delta(x) = 4.80 \sqrt{\frac{\nu x}{U}}. \quad (10.3.34)$$

Substituting now this expression back into (10.3.31) and into the first and second of relations (10.3.32), we find

$$\begin{aligned}\sigma_{xy}(x, y = 0) &= \frac{0.327}{\sqrt{Re_x}} \rho U^2, \\ \delta^*(x) &= 1.743 \sqrt{\frac{\nu x}{U}}, \\ \Theta(x) &= 0.665 \sqrt{\frac{\nu x}{U}}.\end{aligned}\tag{10.3.35}$$

These expressions are in excellent agreement with their exact counterparts shown in equations (10.3.12), (10.3.21), and (10.3.25). This kind of agreement, however, is fortuitous and atypical of the accuracy of the approximate method (problem 8.2.2).

10.3.3 Boundary layers in accelerating or decelerating flow

Having examined the Blasius boundary layer developing along a flat plate that is aligned with a uniform incident flow, distinguished by the uniformity of the tangential velocity of the outer flow along the plate, we proceed to consider the more general case of Falkner-Skan boundary layers developing in an accelerating or decelerating incident flow. Examples of physical situations where these boundary layers occur are illustrated in figure 10.3.2.

We consider, in particular, an outer flow whose tangential velocity $U_x(x)$ exhibits a power-law dependence on streamwise distance x along a flat plate,

$$U_x(x) = c x^m,\tag{10.3.36}$$

where c is a positive coefficient and m is a positive or negative exponent. When $m = 0$, we recover the Blasius boundary layer over a flat plate at zero angle of attack; when $m = 1$, we obtain the boundary layer in orthogonal stagnation-point flow; intermediate values of m correspond to symmetric flow past a wedge of semi-angle $\alpha = \pi m/(m+1)$, as illustrated in figure 10.3.2(a).

Differentiating (10.3.36) with respect to x , we obtain the streamwise acceleration or deceleration of the outer flow,

$$\frac{dU_x}{dx}(x) = c m x^{m-1}.\tag{10.3.37}$$

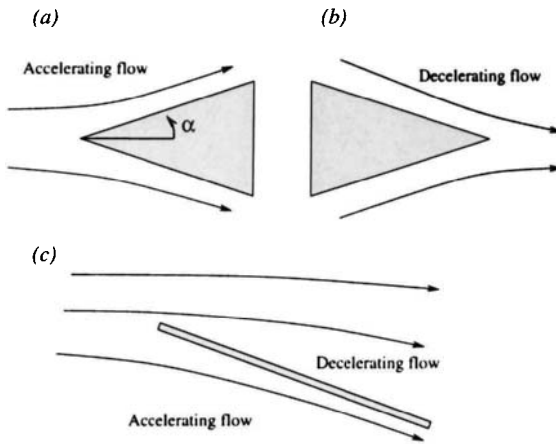


Figure 10.3.2 Boundary layers developing in accelerating or decelerating flow: (a, b) flow past a wedge, and (c) uniform flow past a flat plate at non-zero angle of attack.

Thus, the outer flow accelerates when $m > 0$, and decelerates when $m < 0$. In the first case, conservation of mass expressed by the continuity equation requires that the y derivative of the velocity component normal to the wall, denoted by U_y , be negative, $\partial U_y / \partial y < 0$. Since U_y vanishes on the wall, it must be negative at the edge of the boundary layer; the associated motion of the outer fluid toward the wall confines the vorticity and reduces the thickness of the boundary layer with respect to that in a non-accelerating flow.

Substituting (10.3.37) into the boundary-layer equation (10.2.9) at steady state, we obtain the specific form

$$u_x \frac{\partial u_x}{\partial x} + u_y \frac{\partial u_x}{\partial y} = c^2 m x^{2m-1} + \nu \frac{\partial^2 u_x}{\partial y^2}. \quad (10.3.38)$$

Working as in the case of the Blasius boundary layer, we identify the characteristic length L with the current streamwise position x , and use (10.3.2) to define the boundary layer thickness

$$\delta(x) \sim \sqrt{\frac{\nu x}{U_x(x)}} = \sqrt{\frac{\nu}{c x^{m-1}}}. \quad (10.3.39)$$

Self-similarity

To this end, we assume that the velocity profile across the boundary is self-similar, that is, u_x is a function of the similarity variable

$$\eta \equiv \frac{y}{\delta(x)} = \sqrt{\frac{c}{\nu}} \frac{y}{x^{(1-m)/2}}, \quad (10.3.40)$$

and write $u_x(x, y) = U_x(x) F(\eta)$. This self-similar velocity profile can be derived from the stream function shown in (10.3.5), where $F = df/d\eta$ and $U = U_x(x)$ is given in (10.3.36). Differentiating (10.3.39) with respect to x , and using the relation

$$\frac{\partial \eta}{\partial x} = \frac{m-1}{2} \frac{y}{x} \sqrt{\frac{U_x(x)}{\nu x}}, \quad (10.3.41)$$

we obtain expressions for the two components of the velocity

$$u_x(x, y) = \frac{\partial \psi}{\partial y} = U_x(x) \frac{df}{d\eta},$$

$$u_y(x, y) = -\frac{\partial \psi}{\partial x} = \frac{1}{2} \sqrt{\frac{\nu U_x(x)}{x}} [(1-m)\eta \frac{df}{d\eta} - (1+m)f]. \quad (10.3.42)$$

Substituting these expressions into (10.3.38), we derive the Falkner-Skan ordinary differential equation for the function f ,

$$\frac{d^3 f}{d\eta^3} + \frac{1}{2} (m+1) f \frac{d^2 f}{d\eta^2} - m \left(\frac{df}{d\eta} \right)^2 + m = 0, \quad (10.3.43)$$

which is to be solved subject to the boundary conditions expressed by (10.3.8) and (10.3.9). When $m = 0$, we obtain the Blasius equation (10.3.7). Since boundary conditions are specified at both ends of the solution domain $(0, \infty)$, we are faced with a two-point boundary-value problem involving a third-order differential equation.

The solution of the boundary-value problem may be found using the shooting method described earlier in this section for the Blasius equation. Convergence is achieved when $f''(0) = 1.493$ for $m = 1.5$, $f''(0) = 1.232$ for $m = 1$, $f''(0) = 0.675$ for $m = 0.25$, $f''(0) = 0.332$ for $m = 0.25$, and $f''(0) = 0$ for $m = -0.0904$. Figure 10.3.3 illustrates streamwise velocity profiles expressed by the derivative $f'(\eta)$ for several values of m . Note that the profiles for $m < 0$, corresponding to decelerating flow, exhibit an inflection point near the wall.

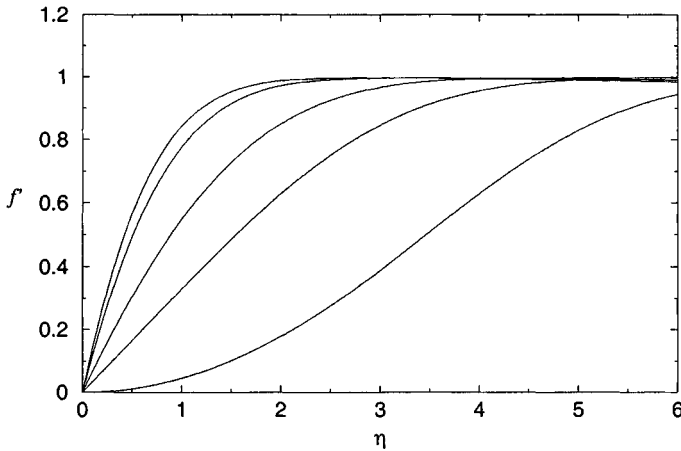


Figure 10.3.3 Velocity profiles across Falkner-Skan boundary layers for several values of the acceleration parameter; from top to bottom, $m = 1.5, 1.0, 0.25, 0.0,$ and -0.0904 .

Problems

Problem 10.3.1 *Computation of the wall shear stress.*

Show that the wall shear stress computed directly by differentiating the velocity profile across the Blasius boundary layer is the same as that arising by evaluating the momentum thickness and then differentiating it with respect to streamwise position x according to equation (10.3.28).

Problem 10.3.2 *Von Kármán's method.*

Assume that the velocity profile across the Blasius boundary layer is described by a hyperbolic tangent function $u_x = U \tanh[y/\Delta(x)]$. Show that the effective boundary-layer thickness, wall shear stress, displacement thickness, and momentum thicknesses are given by the right-hand sides of equations (10.3.34) and (10.3.35), except that the numerical coefficients are equal, respectively, to 2.553, 0.392, 1.770, and 0.783. Discuss the accuracy of these results with reference to the exact solution.

Problem 10.3.3 *Orthogonal stagnation-point flow.*

The Falkner-Skan profile with $m = 1$ corresponds to irrotational orthogonal stagnation point flow against a flat plate.

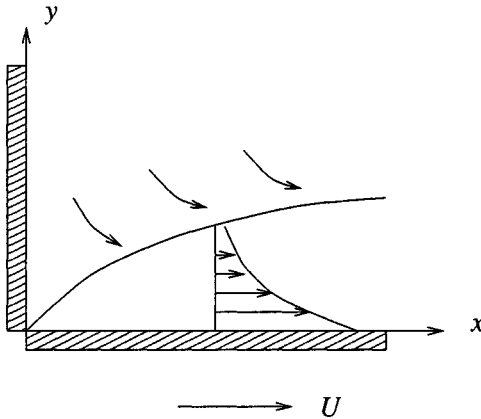


Figure 10.3.4 The Sakiadis boundary layer developing on a semi-infinite translating belt.

- (a) Derive the complete velocity field of the outer irrotational flow.
 (b) Show that the Falkner-Skan boundary-layer solution satisfies the unsimplified Navier-Stokes equation, and it thus provides us with an exact solution.

Computer problems

Problem c.10.3.1 Blasius boundary layer.

Directory `10-bl/fal_scan` of `FDLIB` contains a program that solves the Blasius and Falkner-Skan differential equations using the shooting method described in the text. Run the program to compute, and then plot the velocity profiles shown in figure 10.3.1(b) and 10.3.3.

Problem c.10.3.2 Sakiadis's boundary layer.

Consider flow due to the motion of a semi-infinite belt translating along the x axis with velocity U normal to a vertical stationary wall, as illustrated in figure 10.3.4. A boundary layer identified by Sakiadis is established along the belt ¹.

¹Sakiadis, B. C. 1961, Boundary-layer behavior on continuous solid surfaces: I. Boundary-layer equations for two-dimensional and axisymmetric flow, *A.I.Ch.E. J.* **7**, 26-28; II. The boundary layer on a continuous flat surface, *A.I.Ch.E. J.* **7**, 221-225

(a) Show that the flow in the boundary layer is governed by the Blasius equation (10.3.7) subject to the modified boundary conditions $f = 0$ and $f' = 0$ at $\eta = 0$, and $f' \rightarrow 0$ as η tends to infinity.

(b) Obtain the solution using a numerical method of your choice. Plot and discuss the streamwise velocity profile, the displacement thickness, the momentum thickness, and the shape factor. *Hint:* the shooting method converges when $f''(0) = 0.44375$.

(c) Deduce the nature of the flow field far from the moving belt.

10.4 Von Kàrmàn's integral method

In Section 10.3, we discussed methods for solving the boundary layer equations over a flat surface subject to a constant, accelerating, or decelerating outer flow with a power-law dependence on streamwise position. To compute boundary layers developing over a curved surface and for more general types of outer flow, we resort to numerical methods.

Von Kàrmàn developed an elegant method of computing the flow inside a two-dimensional boundary layer developing over a surface with arbitrary shape, based on an integral momentum balance. The formulation culminates in an ordinary differential equation for a properly defined boundary-layer thickness with respect to arc length along the surface.

To illustrate the method, we consider the boundary layer developing over a flat surface located at $y = 0$, and introduce a control area that is confined by (a) two vertical planes located at x_1 and x_2 , (b) the planar surface, and (c) a horizontal plane located at the elevation $y = h$. Consistent with our previous notation, we denote the tangential component of the outer flow along the surface by $U_x(x)$. For simplicity, we shall assume that the physical properties of the fluid are uniform throughout the domain of flow.

We begin by applying the x component of the integral momentum balance (6.2.14) combined with the Newtonian constitutive equation for the stress tensor. Neglecting the normal viscous stresses over the vertical and top planes, and considering the effects of gravity secondary, we find

$$\begin{aligned}
& \int_{x_1}^{x_2} \int_0^h \rho \frac{\partial u_x}{\partial t}(x, y) dy dx - \int_0^h [u_x (\rho u_x)](x = x_1, y) dy \\
& + \int_0^h [u_x (\rho u_x)](x = x_2, y) dy + \int_{x_1}^{x_2} [u_y (\rho u_x)](x, y = h) dx \\
& = \int_0^h (-p)(x = x_1, y) dy - \int_0^h (-p)(x = x_2, y) dy \\
& - \int_{x_1}^{x_2} \sigma_{xy}(x, y = 0) dx.
\end{aligned} \tag{10.4.1}$$

Next, we take the limit as x_1 tends to x_2 , recall that the pressure remains constant across the boundary layer, set $u_x(x, y = h) = U_x(x)$, and rearrange to obtain the integro-differential relation

$$\begin{aligned}
\rho \int_0^h \frac{\partial u_x}{\partial t} dy &= h \left(\frac{\partial p}{\partial x} \right)_{y=h} \\
-\rho \frac{\partial}{\partial x} \int_0^h u_x^2(x, y) dy &- \rho U_x(x) u_y(x, y = h) - \sigma_{xy}(x, y = 0).
\end{aligned} \tag{10.4.2}$$

To reduce the number of unknowns, we eliminate $u_y(x, y = h)$ in favor of u_x using the continuity equation, setting

$$u_y(x, y = h) = - \int_0^h \frac{\partial u_x}{\partial x}(x, y') dy'. \tag{10.4.3}$$

Moreover, we use the x component of Euler's equation (6.4.3) to evaluate the streamwise pressure gradient, finding

$$\frac{\partial p}{\partial x} = -\rho \left(\frac{\partial U_x}{\partial t} + U_x \frac{\partial U_x}{\partial x} \right). \tag{10.4.4}$$

Substituting expressions (10.4.3) and (10.4.4) into (10.4.2), and rearranging, we find

$$\begin{aligned}
\rho \int_0^h \frac{\partial(U_x - u_x)}{\partial t} dy &= -\rho \frac{\partial}{\partial x} \int_0^h u_x (U_x - u_x) dy \\
&- \rho \frac{\partial}{\partial x} \int_0^h U - x (U_x - u_x) dy + \rho U_x \frac{\partial}{\partial x} \int_0^h (U_x - u_x) dy \\
&+ \sigma_{xy}(x, y = 0),
\end{aligned} \tag{10.4.5}$$

which may be interpreted as an evolution law for the momentum deficit $\rho(U_x - u_x)$.

To this end, we let the reduced height h/δ tend to infinity, and use the definitions of the displacement and momentum thickness stated in equations (10.3.20) and (10.3.25) to derive the von Kàrmàn integral momentum balance

$$\begin{aligned}
\rho \frac{\partial(U_x \delta^*)}{\partial t} + \rho \frac{\partial(U_x^2 \Theta)}{\partial x} \\
+ \rho \frac{\partial(U_x^2 \delta^*)}{\partial x} - \rho U_x \frac{\partial(U_x \delta^*)}{\partial x} - \sigma_{xy}(x, y = 0) = 0.
\end{aligned} \tag{10.4.6}$$

Rearranging, we obtain an expression for the wall shear stress in terms of the displacement and momentum thickness,

$$\frac{\sigma_{xy}(x, y = 0)}{\rho U_x^2} = \frac{\partial(U_x \delta^*)}{\partial t} + \frac{\partial \Theta}{\partial x} + (2\Theta + \delta^*) \frac{1}{U_x} \frac{\partial U_x}{\partial x}. \tag{10.4.7}$$

If the flow is steady, the first term on the right-hand side does not appear. It is reassuring to confirm that, when U_x is constant and independent of x , equation (10.4.7) reduces to (10.3.28) describing the boundary layer developing over a flat plate that is held stationary in an incident stream at zero angle of attack.

If fluid is injected into, or withdrawn from the flow through a porous wall with normal velocity V , the right-hand side of (10.4.7) contains the additional term $-V/U_x$, where V is positive in the case of injection and negative in the case of suction.

10.4.1 The von Kàrmàn - Pohlhausen method

Von Kàrmàn and Pohlhausen developed an approximate method for computing the boundary layer thickness and associated structure of the

flow on the basis of the momentum integral balance (10.4.7). The main idea was discussed in Section 10.3.2: assume a sensible velocity profile across the boundary layer in the form $u_x = F(\eta)$, where $\eta \equiv y/\Delta(x)$ and $\Delta(x)$ is a boundary-layer thickness similar to the δ_{99} boundary-layer thickness; then compute $\Delta(x)$ to satisfy the integral momentum balance (10.4.7).

The implementation of the method for flow over a flat plate at zero angle of attack, where $F(\eta)$ is a quarter of a period of a sinusoidal function, as shown in (10.3.30), was discussed in Section 10.3.2. In the remainder of this section, we illustrate the implementation of the method for more general types of steady flow.

10.4.2 Pohlhausen polynomials

Pohlhausen identified the velocity profile $F(\eta)$ across the boundary layer with a fourth-order polynomial, setting

$$\frac{u}{U_x} = F(\eta) = \begin{cases} \eta [a(x) + b(x)\eta + c(x)\eta^2 + d(x)\eta^3] & \text{for } 0 < \eta < 1 \\ 1 & \text{for } \eta > 1 \end{cases}, \quad (10.4.8)$$

where $a(x)$, $b(x)$, $c(x)$, and $d(x)$ are four position-dependent coefficients to be computed as part of the solution. Note that the functional form (10.4.8) satisfies the no-slip boundary condition at the wall, corresponding to $\eta = 0$. To compute the four coefficients a , b , c and d , we require four equations.

First, we demand that the overall velocity profile is continuous and has smooth first and second derivatives at the edge of the boundary layer, corresponding to $\eta = 1$, and thus obtain the three conditions

$$F(\eta = 1) = 1, \quad \frac{dF}{d\eta}(\eta = 1) = 0, \quad \frac{d^2F}{d\eta^2}(\eta = 1) = 0. \quad (10.4.9)$$

A fourth condition arises by applying the boundary-layer equation (10.2.4) at the wall located at $y = 0$, and then using the no-slip and no-penetration boundary conditions to set the left-hand side equal to zero. Evaluating the streamwise pressure gradient from (10.4.4) with the time derivative on the right-hand side set equal to zero, we find

$$\left(\frac{\partial u_x^2}{\partial y^2}\right)_{y=0} = -\frac{1}{\nu} U_x \frac{dU_x}{dx}. \quad (10.4.10)$$

Expressing now the velocity in terms of the function $F(\eta)$ introduced in (10.4.8), we obtain

$$\frac{d^2 F}{d\eta^2}(\eta = 0) = -\Lambda, \quad (10.4.11)$$

where

$$\Lambda(x) \equiv \frac{\Delta^2(x)}{\nu} \frac{dU_x}{dx}, \quad (10.4.12)$$

is a dimensionless function expressing the ratio of the magnitude of the inertial acceleration forces of the outer irrotational flow, to the magnitude of the viscous forces developing inside the boundary layer; if $dU_x/dx = 0$, then $\Lambda = 0$.

By definition, the effective boundary layer thicknesses $\Delta(x)$ is related to $\Lambda(x)$ by

$$\Delta(x) \equiv \sqrt{\frac{\nu \Lambda}{U'_x}}, \quad (10.4.13)$$

where $U'_x \equiv dU_x/dx$.

Requiring now that the Pohlhausen profile (10.4.8) satisfies equations (10.4.9) and (10.4.11), we obtain

$$a = 2 + \frac{\Lambda}{6}, \quad b = -\frac{\Lambda}{2}, \quad c = -2 + \frac{\Lambda}{2}, \quad d = 1 - \frac{\Lambda}{6}. \quad (10.4.14)$$

Substituting these expressions into (10.4.8), and rearranging, we obtain the velocity profile in terms of the parameter Λ ,

$$\frac{u}{U_x} = F(\eta) = \begin{cases} \eta(2 - 2\eta^2 + \eta^3) + \frac{\Lambda}{6}\eta(1 - \eta)^3 & \text{for } 0 < \eta < 1 \\ 1 & \text{for } \eta > 1 \end{cases}. \quad (10.4.15)$$

Program *pohl_pol* in directory *10.bl/pohl_pol* of *FDLIB* computes polynomial profiles by evaluating the right-hand side of (10.4.15). A family of profiles corresponding to $\Lambda = 20, 12$ (heavy line), 6, 0, -6, -12, and -15, is shown in figure 10.4.1. When $\Lambda > 12$, corresponding to a strongly accelerating external flow according to (10.4.12), the profile overshoots, placing a limit on the physical relevance of the fourth-order polynomial expansion. When $\Lambda = -12$, the slope of the velocity profile at the wall is equal to zero, suggesting that the flow is on the verge of reversal. At that point, the approximations that led us to the boundary-layer equations cease to be valid, and the boundary layer is expected to separate from the wall developing regions of recirculating flow.

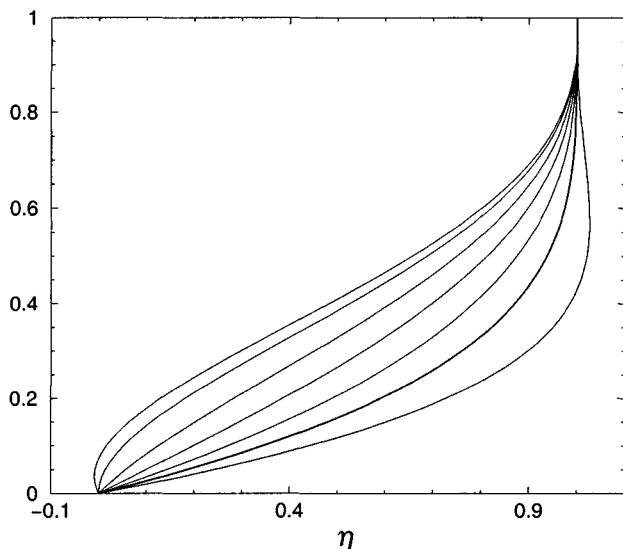


Figure 10.4.1 Profiles of the Pohlhausen polynomials for $\Lambda = 20, 12$ (heavy line), 6, 0, -6, -12, -15.

The displacement thickness, momentum thickness, and wall shear stress may be computed in terms of $\Delta(x)$ and $\Lambda(x)$ using the profiles (10.4.15), and are found to be

$$\begin{aligned}\delta^* &= \frac{\Delta}{10} \left(3 - \frac{\Lambda}{12} \right), \\ \Theta &= \frac{\Delta}{315} \left(37 - \frac{\Lambda}{3} - \frac{5}{144} \Lambda^2 \right), \\ \sigma_{xy}(x, y = 0) &= \frac{\mu U_x}{\Delta} \left(2 + \frac{\Lambda}{6} \right).\end{aligned}\tag{10.4.16}$$

Expressing $\Delta(x)$ in terms of $\Lambda(x)$ using the definition (10.4.13), we obtain corresponding expressions in terms of Λ alone.

The key idea is to substitute expressions (10.4.16) into the momentum integral balance (10.4.7), and thus derive a first-order nonlinear ordinary differential equation for $\Lambda(x)$ with respect to x . Having solved this equation, we recover the boundary-layer thickness $\Delta(x)$ from the definition (10.4.13).

10.4.3 Numerical solution

To solve the von Kàrmàn boundary-layer equation, it is convenient to introduce the Holstein-Bohlen parameter defined as

$$\lambda(x) \equiv \frac{\Theta^2(x)}{\Delta^2(x)} \Lambda(x) = \frac{\Theta^2(x)}{\nu} \frac{dU_x}{dx}, \quad (10.4.17)$$

whose physical interpretation is similar to that of Λ discussed after the definition (10.4.12). Using the expression for the momentum thickness given in the second of equations (10.4.16), we obtain a relationship between λ and Λ ,

$$\sqrt{\frac{\lambda}{\Lambda}} = \frac{1}{315} \left(37 - \frac{\Lambda}{3} - \frac{5}{144} \Lambda^2 \right). \quad (10.4.18)$$

The value $\Lambda = -12$ corresponds to $\lambda = -0.15673$, whereupon the boundary layer is expected to separate according to figure 10.4.1.

To expedite the solution, we multiply both sides of the momentum integral balance (10.4.7) at steady state with Θ , and rearrange to obtain

$$\frac{d}{dx} \left(\frac{\lambda}{dU_x/dx} \right) \equiv \frac{1}{\nu} \frac{d^2\Theta}{dx^2} = \frac{2}{U_x} \{ S(\lambda) - [2 + H(\lambda)] \lambda \}, \quad (10.4.19)$$

where H is the shape factor defined in (10.3.27), and S is the *shear function* defined as

$$S(\lambda) \equiv \frac{\Theta \sigma_{xy}(x, y = 0)}{\mu U_x}. \quad (10.4.20)$$

Physically, the shear function expresses the ratio between the wall shear stress and the average value of the shear stress across the boundary layer; thus, it is another measure of the sharpness of the velocity profile across the boundary layer. Using expressions (10.4.16), we find

$$H = \frac{315}{10} \frac{3 - \frac{\Lambda}{12}}{37 - \frac{\Lambda}{3} - \frac{5}{144} \Lambda^2},$$

$$S = \frac{1}{315} \left(2 + \frac{\Lambda}{6} \right) \left(37 - \frac{\Lambda}{3} - \frac{5}{144} \Lambda^2 \right), \quad (10.4.21)$$

where Λ can be expressed in terms of λ using equation (10.4.18).

The numerical procedure involves the following steps:

1. Given the value of λ at a particular position x , compute the corresponding value of Λ by solving the nonlinear algebraic equation (10.4.18).
2. Evaluate the functions S and H using expressions (10.4.21).
3. Compute the right-hand side of (10.4.19), and thus obtain the rate of change of the ratio on the left-hand side with respect to x .
4. Advance the value of λ over a small increment Δx .
5. Return to step 1 and repeat.

Evaluation at a stagnation point

The numerical integration typically begins at a stagnation point where the tangential velocity U_x vanishes and the right-hand side of (10.4.19) is undefined. To avoid the occurrence of a singularity, we require that the numerator be equal to zero at that point, and thus obtain a nonlinear algebraic equation for Λ . A physically acceptable solution is $\Lambda = 7.052$ corresponding to $\lambda = 0.0770$. This value is used to initialize the computation.

To evaluate the right-hand side of (10.4.19) at a stagnation point located at $x = 0$, we denote the expression enclosed by the angular brackets on the right-hand side by $Q(\lambda)$. Applying the l'Hôpital rule to evaluate the fraction, we find

$$\begin{aligned} \frac{d}{dx} \left(\frac{\lambda}{dU_x/dx} \right)_{x=0} &= \left(\frac{dQ/dx}{dU_x/dx} \right)_{x=0} = \left(\frac{dQ/d\lambda}{dU_x/dx} \frac{d\lambda}{dx} \right)_{x=0} \\ &= \left(\frac{dQ}{d\lambda} \right)_{x=0} \left[\frac{d}{dx} \left(\frac{\lambda}{dU_x/dx} \right) + \lambda \frac{d^2 U_x/dx^2}{(dU_x/dx)^2} \right]_{x=0}. \end{aligned} \quad (10.4.22)$$

Combining the left-hand side with the first term within the square brackets on the right-hand side, we find

$$\frac{d}{dx} \left(\frac{\lambda}{dU_x/dx} \right)_{x=0} = \left[\frac{\lambda}{1 - dQ/d\lambda} \frac{dQ}{d\lambda} \frac{d^2 U_x/dx^2}{(dU_x/dx)^2} \right]_{x=0}. \quad (10.4.23)$$

Evaluating the expression on the right-hand side using the definition of $Q(\lambda)$, we obtain the required initial value

$$\frac{d}{dx} \left(\frac{\lambda}{dU_x/dx} \right)_{x=0} = -0.0652 \left[\frac{d^2 U_x/dx^2}{(dU_x/dx)^2} \right]_{x=0}. \quad (10.4.24)$$

10.4.4 Boundary layer around a curved body

The Kàrmàn-Pohlhausen method was developed with reference to a planar boundary where the x coordinate increases along the boundary in the direction of the velocity of the outer flow. To tackle the more general case of a curved boundary, we simply replace x with the arc length l measured along the boundary in the direction of the tangential velocity of the incident flow, and begin the integration from a stagnation point. A difficulty arises at the critical point where the acceleration dU_l/dl vanishes or assumes an infinite value, but the ambiguity may be removed by carrying out the integration at that point using the Falkner-Skan similarity solution with a proper value for the exponent m .

10.4.5 Boundary layer around a circular cylinder

As an application, we consider uniform flow past a stationary circular cylinder of radius a , with vanishing circulation around the cylinder, as shown at the top of figure 10.4.2. Far from the cylinder, the flow occurs toward the negative direction of the x axis, and the velocity tends to the uniform value $-U\mathbf{e}_x$, where $U > 0$ is the magnitude of the streaming flow and \mathbf{e}_x is the unit vector along the x axis. Using the velocity potential for irrotational flow past a circular cylinder given by equation (3.5.28) with $V_x = -U$, we find that the tangential component of velocity of the outer flow is given by

$$U_\theta(\theta) = \left(\frac{\partial \phi}{\partial \theta} \right)_{r=a} = 2U \sin \theta, \quad (10.4.25)$$

where θ is the polar angle measured around the cylinder in the counter-clockwise direction, as shown in figure 10.4.2. The arc length around the cylinder, measured from the front stagnation point, is given by $l = a\theta$. The required derivatives of the velocity with respect to arc length are then

$$\begin{aligned}\frac{dU_\theta}{dl} &= \frac{1}{a} \frac{dU_\theta}{d\theta} = 2 \frac{U}{a} \cos \theta, \\ \frac{d^2U_\theta}{dl^2} &= \frac{1}{a^2} \frac{d^2U_\theta}{d\theta^2} = -2 \frac{U}{a^2} \sin \theta.\end{aligned}\tag{10.4.26}$$

Equation (10.4.24) yields

$$\frac{d}{dl} \left(\frac{\lambda}{dU_\theta/dl} \right)_{l=0} = 0,\tag{10.4.27}$$

which is used to start up the computation.

Graphs of the solution computed using program *10.bl/kp.cc* of *FDLIB* are shown in figure 10.4.2. The velocity profiles across the boundary layer at different stations around the cylinder may be inferred from the scaled profiles shown in figure 10.4.1, using the local value of Λ . The numerical solution reveals that $\Lambda = -12$ when $\theta = 109.5^\circ$, at which point the shear stress vanishes and the boundary layer is expected to separate. Comparing this result with the experimentally observed value $\theta = 80.5^\circ$, we find a serious disagreement attributed to the fact that, in practice, the outer flow deviates substantially from the potential flow distribution described by (10.4.25) due to the presence of a wake. To improve the solution, we may describe the tangential velocity U_θ by interpolation based on data gathered in the laboratory; when this is done, the results of the boundary-layer analysis are found to be in excellent agreement with observation.

Problem

Problem 10.4.1 *Von Kàrmàn's method for the Blasius boundary layer.*

Assume that the velocity profile across the Blasius boundary layer is given by the Pohlhausen polynomial (10.4.15). Show that the effective boundary-layer thickness, wall shear stress, displacement thickness, and momentum thicknesses are given by the right-hand sides of equations (10.3.34) and (10.3.35), except that the numerical coefficients are equal, respectively, to 5.863, 0.343, 1.751, and 0.685. Discuss the accuracy of these results with reference to the exact solution obtained by numerical methods.

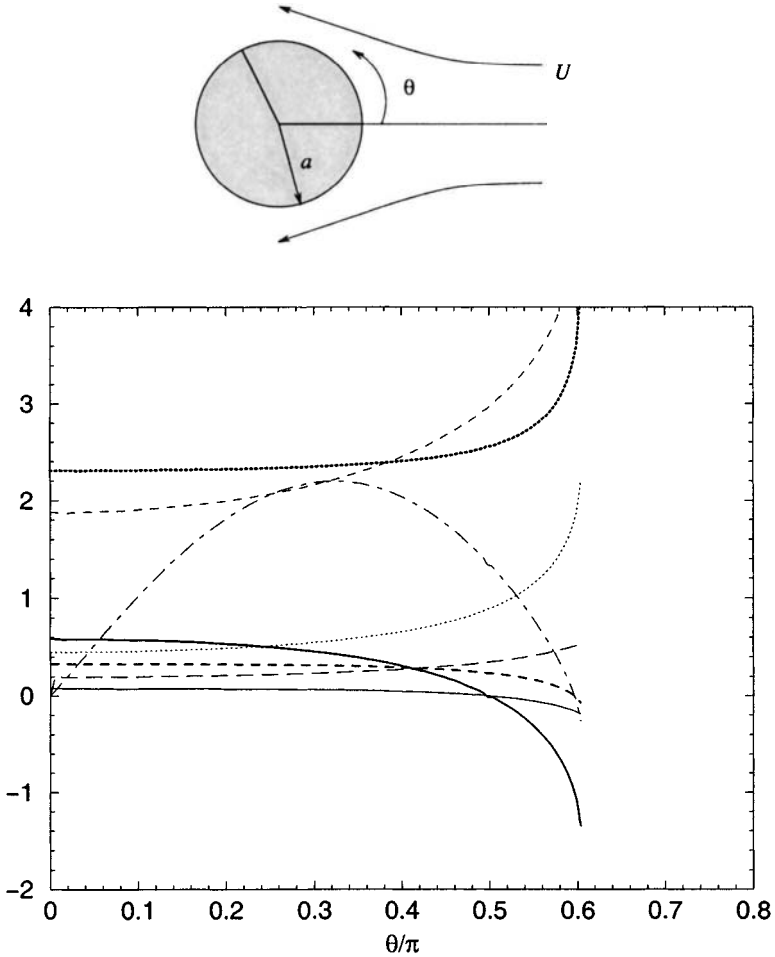


Figure 10.4.2 Features of the Prandtl boundary layer around a circular cylinder of radius a held stationary in an incident streaming flow with velocity U , computed using the von Kàrmàn - Pohlhausen method. Distributions of the dimensionless parameters $\frac{1}{12}\Lambda$ (heavy solid line) and λ (solid line); reduced boundary-layer thickness $\hat{\Delta} \equiv \Delta^* \sqrt{U/\nu a}$ (dashed line); reduced displacement thickness $\hat{\delta}^* \equiv \delta^* \sqrt{U/\nu a}$ (dotted line); reduced momentum thickness $\hat{\Theta} \equiv \Theta \sqrt{U/\nu a}$ (long dashed line); reduced shear stress $\hat{\sigma}_S \equiv \sigma_S \sqrt{a/\mu U}$ (dot-dashed line); shape factor S (heavy dashed line); and shear function H (heavy dotted line).

Computer problem

Problem c.10.4.1 *Boundary layer around a circular cylinder.*

Directory `10-bl/kp-cc` of *FDLIB* contains a program that computes the boundary layer around a circular cylinder using the numerical method discussed in the text. Run the program and reproduce the graphs shown in figure 10.4.2.

10.5 Instability of shear flows

In Chapter 7, we derived exact solutions of problems involving various kinds of steady channel and tube flow, under one important assumption: the flow is steady and unidirectional with rectilinear or circular streamlines. The physical relevance of this assumption is corroborated by laboratory observation at small and moderate Reynolds numbers. At high Reynolds numbers, however, small perturbations inherent in any real flow amplify, initiating unsteady motion and possibly leading to a new steady state that is different than that computed under the assumption of unidirectional flow.

The following questions then arise: what is the threshold value of the Reynolds number above which a flow becomes unstable, and what are the salient modes of amplification? One way to answer these questions is by carrying out a linear stability analysis.

10.5.1 Linear stability analysis

The main idea is to consider a certain flow of interest at steady state, introduce small perturbations, and describe the time evolution of the perturbations by solving simplified versions of the governing equations that arise by linearization.

To illustrate the procedure, we consider a steady unidirectional flow along the x axis whose velocity, pressure, and vorticity are given by

$$\begin{aligned} u_x^B &= U(y), & u_y^B &= 0, & p^B &= -G x, \\ \omega_z^B &= -\frac{dU(y)}{dy}. \end{aligned} \tag{10.5.1}$$

Computer problem

Problem c.10.4.1 *Boundary layer around a circular cylinder.*

Directory `10-bl/kp_cc` of *FDLIB* contains a program that computes the boundary layer around a circular cylinder using the numerical method discussed in the text. Run the program and reproduce the graphs shown in figure 10.4.2.

10.5 Instability of shear flows

In Chapter 7, we derived exact solutions of problems involving various kinds of steady channel and tube flow, under one important assumption: the flow is steady and unidirectional with rectilinear or circular streamlines. The physical relevance of this assumption is corroborated by laboratory observation at small and moderate Reynolds numbers. At high Reynolds numbers, however, small perturbations inherent in any real flow amplify, initiating unsteady motion and possibly leading to a new steady state that is different than that computed under the assumption of unidirectional flow.

The following questions then arise: what is the threshold value of the Reynolds number above which a flow becomes unstable, and what are the salient modes of amplification? One way to answer these questions is by carrying out a linear stability analysis.

10.5.1 Linear stability analysis

The main idea is to consider a certain flow of interest at steady state, introduce small perturbations, and describe the time evolution of the perturbations by solving simplified versions of the governing equations that arise by linearization.

To illustrate the procedure, we consider a steady unidirectional flow along the x axis whose velocity, pressure, and vorticity are given by

$$\begin{aligned} u_x^B &= U(y), & u_y^B &= 0, & p^B &= -G x, \\ \omega_z^B &= -\frac{dU(y)}{dy}. \end{aligned} \tag{10.5.1}$$

The superscript B designates the base flow whose stability is to be examined, $U(y)$ is the unperturbed velocity profile, and G is the negative of the streamwise pressure gradient. Now, unless the velocity profile is parabolic, the base flow will not satisfy the *steady* version of the equation of motion. We will assume, however, that in such cases the base flow evolves at a rate that is much slower than that of the perturbations, and may thus be considered to be in a quasi-steady state.

Next, we introduce a two-dimensional perturbation whose velocity, pressure, and vorticity are described by

$$u_x^P(x, y, t) = \epsilon u_x^D(x, y, t),$$

$$u_y^P(x, y, t) = \epsilon u_y^D(x, y, t),$$

$$p^P(x, y, t) = \epsilon p^D(x, y, t),$$

$$\omega_z^P(x, y, t) = \epsilon \omega^D(x, y, t) = \epsilon \left(\frac{\partial u_y^D}{\partial x} - \frac{\partial u_x^D}{\partial y} \right)(x, y, t), \quad (10.5.2)$$

where the superscript P designates the perturbation, the superscript D designates the disturbance, and ϵ is a dimensionless coefficient whose magnitude is small compared to unity.

The complete flow arises by adding corresponding variables of the base and perturbation flow shown in (10.5.1) and (10.5.2). For example, the x velocity component of the perturbed flow is

$$u_x(x, y, t) = u_x^B(y) + \epsilon u_x^D(x, y, t). \quad (10.5.3)$$

Substituting this sum and its counterparts into the vorticity transport equation for two-dimensional flow, equation (6.6.6), we obtain

$$\begin{aligned} & \epsilon \frac{\partial \omega_z^D}{\partial t} + \epsilon u_x^B \frac{\partial \omega_z^D}{\partial x} + \epsilon^2 u_x^D \frac{\partial \omega_z^D}{\partial x} + \epsilon u_y^D \frac{\partial \omega_z^B}{\partial y} + \epsilon^2 u_y^D \frac{\partial \omega_z^D}{\partial y} \\ & = \nu \left[\frac{\partial^2 \omega^B}{\partial x^2} + \frac{\partial^2 \omega^B}{\partial y^2} + \epsilon \left(\frac{\partial^2 \omega^D}{\partial x^2} + \frac{\partial^2 \omega^D}{\partial y^2} \right) \right], \end{aligned} \quad (10.5.4)$$

where ν is the kinematic viscosity. Since, at quasi-steady state, the vorticity of the base flow satisfies the steady version of the vorticity

transport equation for unidirectional flow, the sum of the first two terms on the right-hand side of (10.5.4) is equal to zero.

Because ϵ has been assumed small, quadratic terms that are proportional to ϵ^2 are small compared to linear terms that are proportional to ϵ , and may be discarded from both sides of (10.5.4). Collecting the linear terms, and setting their sum equal to zero, we obtain the linearized vorticity transport equation

$$\frac{\partial \omega_z^D}{\partial t} + u_x^B \frac{\partial \omega_z^D}{\partial x} + u_y^D \frac{\partial \omega_z^B}{\partial y} = \nu \left(\frac{\partial^2 \omega_z^D}{\partial x^2} + \frac{\partial^2 \omega_z^D}{\partial y^2} \right). \quad (10.5.5)$$

Substituting into (10.5.5) the expressions for the base flow given in (10.5.1), we derive the more specific form

$$\frac{\partial \omega_z^D}{\partial t} + U(y) \frac{\partial \omega_z^D}{\partial x} - u_y^D \frac{d^2 U}{dy^2} = \nu \left(\frac{\partial^2 \omega_z^D}{\partial x^2} + \frac{\partial^2 \omega_z^D}{\partial y^2} \right). \quad (10.5.6)$$

The problem has been reduced to solving the *linear* equation (10.5.6) for the disturbance flow, subject to a specified initial condition and appropriate boundary conditions.

10.5.2 Disturbance stream function

It is convenient to express the disturbance flow in terms of the disturbance stream function $\psi^D(x, y, t)$ defined by the equations

$$\begin{aligned} u_x^D &= \frac{\partial \psi^D}{\partial y}, & u_y^D &= -\frac{\partial \psi^D}{\partial x}, \\ \omega_z^D &= -\left(\frac{\partial^2 \psi^D}{\partial x^2} + \frac{\partial^2 \psi^D}{\partial y^2} \right) = -\nabla^2 \psi^D, \end{aligned} \quad (10.5.7)$$

where $\nabla^2 \equiv \partial^2/\partial x^2 + \partial^2/\partial y^2$ is the Laplacian operator in two dimensions. Substituting these expressions into (10.5.6), and rearranging, we find

$$\frac{\partial \nabla^2 \psi^D}{\partial t} + U(y) \frac{\partial \nabla^2 \psi^D}{\partial x} - \nu \nabla^4 \psi^D = \frac{\partial \psi^D}{\partial x} \frac{d^2 U}{dy^2}, \quad (10.5.8)$$

where $\nabla^4 = \nabla^2 \nabla^2$ is the biharmonic operator in two dimensions.

10.5.3 Normal-mode analysis

To study the evolution of each and every possible disturbance is practically impossible. As an alternative, we exploit the linearity of equation (10.5.8) and deduce the nature of the general solution corresponding to an arbitrary initial condition from the behavior of an infinite family of solutions corresponding to disturbances that are sinusoidal functions of the streamwise position x , called *normal modes*. The general solution may be constructed by linear superposition.

Consider a normal mode with wave length L and corresponding wave number $k = 2\pi/L$. The disturbance stream function may be expressed in the form

$$\psi^D(x, y, t) = \chi_r(y, t) \cos(kx) + \chi_i(y, t) \sin(kx), \quad (10.5.9)$$

where $\chi_r(y, t)$ and $\chi_i(y, t)$ are two real functions. To simplify the notation, we introduce the complex function

$$\chi(y, t) \equiv \chi_r(y, t) - i \chi_i(y, t), \quad (10.5.10)$$

where i is the imaginary unit defined by the equation $i^2 = -1$, and use the Euler decomposition of the imaginary exponential, $\exp(ikx) = \cos(kx) + i \sin(kx)$ to recast (10.5.9) into the form

$$\psi^D(x, y, t) = \text{Real}\{\Psi^D(x, y, t)\}, \quad (10.5.11)$$

where Real designates the real part of the complex quantity enclosed by the angular brackets, and

$$\Psi^D(x, y, t) \equiv \chi(y, t) \exp(ikx) \quad (10.5.12)$$

is a complex stream function.

To simplify the analysis, we require that the imaginary part of Ψ^D also satisfies equation (10.5.8). Substituting (10.5.12) into (10.5.8), carrying out the differentiation with respect to x , and noting that

$$\nabla^2 \Psi^D = (-k^2 \chi + \frac{\partial^2 \chi}{\partial y^2}) \exp(ikx), \quad (10.5.13)$$

we find

$$\begin{aligned} -k^2 \frac{\partial \chi}{\partial t} + \frac{\partial^3 \chi}{\partial y^2 \partial t} + i k U(y) (-k^2 \chi + \frac{\partial^2 \chi}{\partial y^2}) \\ -\nu (k^4 \chi - 2k^2 \frac{\partial^2 \chi}{\partial y^2} + \frac{\partial^4 \chi}{\partial y^4}) = i k \chi \frac{d^2 U}{dy^2}. \end{aligned} \quad (10.5.14)$$

A solution of (10.5.14) may be found by expressing $\chi(x, t)$ in the separated form

$$\chi(y, t) = f(y) \exp(-i \sigma t) = f(y) \exp(-i k c t), \quad (10.5.15)$$

where $f(y)$ is a complex function, σ is a complex constant called the *complex growth rate*, and $c \equiv \sigma/k$ is another complex constant called the *complex phase velocity*. Substituting (10.5.15) into (10.5.12), we derive the corresponding complex disturbance stream function

$$\Psi(x, y, t) = f(y) \exp[i(kx - \sigma t)] = f(y) \exp[ik(x - ct)]. \quad (10.5.16)$$

Next, we decompose σ and c into their real and imaginary parts, writing $\sigma = \sigma_R + i \sigma_I$ and $c = c_R + i c_I$, where the subscripts R and I stand for Real and Imaginary, and obtain

$$\Psi(x, y, t) = f(y) \exp[i k (x - c_r t)] \exp(\sigma_I t). \quad (10.5.17)$$

Expression (10.5.17) illustrates two important features:

- c_r is the real phase velocity of the disturbance. The crest or trough of the sinusoidal perturbation, but not the fluid itself, travels along the x axis with velocity c_r .
- σ_I is the growth rate of the disturbance; if σ_I is positive, the disturbance grows at an exponential rate in time; if σ_I is negative, the disturbance decays at an exponential rate in time; if $\sigma_I = 0$, the amplitude of the disturbance remains constant in time. In the first case, the flow is unstable; in the second case, the flow is stable; and in the third case, the flow is neutrally stable.

10.5.4 Orr-Sommerfeld equation

To compute the function $f(y)$, and simultaneously obtain the complex phase velocity c , we substitute (10.5.15) into (10.5.14), and rearrange the resulting expression to derive the Orr-Sommerfeld equation

$$k^4 f - 2k^2 \frac{d^2 f}{dy^2} + \frac{d^4 f}{dy^4} = \frac{ik}{\nu} \{ [U(y) - c] \left(\frac{d^2 f}{dy^2} - k^2 f \right) - \frac{d^2 U}{dy^2} f \}, \quad (10.5.18)$$

A trivial solution is $f = 0$. Nontrivial solutions expressing normal modes exist for certain values of c that are the eigenvalues of the Orr-Sommerfeld equation. The main objective of linear stability analysis is to compute these eigenvalues, and thereby assess whether a normal mode will grow, decay, or remain constant in time.

10.5.5 Rayleigh's equation

When viscous forces are negligible, the left-hand side of the Orr-Sommerfeld equation (10.5.18) may be set equal to zero, yielding Rayleigh's equation

$$[U(y) - c] \left(\frac{d^2 f}{dy^2} - k^2 f \right) - \frac{d^2 U}{dy^2} f = 0, \quad (10.5.19)$$

also available in the alternative form

$$\frac{d^2 f}{dy^2} - \left(k^2 + \frac{1}{U(y) - c} \frac{d^2 U}{dy^2} \right) f = 0. \quad (10.5.20)$$

Because of the absence of viscous forces, the Rayleigh equation is a second-order differential equation, whereas the inclusive Orr-Sommerfeld equation is a fourth-order differential equation. Both equations are linear, but the coefficients multiplying the derivatives of the complex function f are not necessarily constant.

10.5.6 Numerical solution of the Orr-Sommerfeld and Rayleigh equation

Analytical solutions to the Orr-Sommerfeld and Rayleigh equation are possible only for a limited class of purely viscous or inviscid flows. To study the stability of more general flows, we resort to numerical methods.

To illustrate the implementation of finite-difference methods, we consider the stability of a shear flow in a channel confined between two parallel walls located at $y = -A$ and B , as illustrated in figure 10.5.1. Assuming that the effects of viscosity are negligible, we consider Rayleigh's equation (10.5.19) and express it in the form

$$U(y) \frac{d^2 f}{dy^2} - [U(y) k^2 + \frac{d^2 U}{dy^2}] f = c \left(\frac{d^2 f}{dy^2} - k^2 f \right). \quad (10.5.21)$$

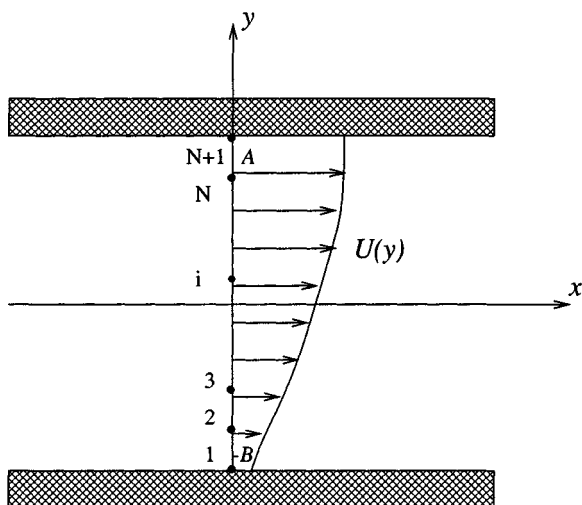


Figure 10.5.1 A finite-difference grid used to solve the Rayleigh equation determining the growth rate of two-dimensional perturbation in unidirectional shear flow.

Note that the unknown eigenvalue c has been moved to the right-hand side.

Next, we introduce a one-dimensional uniform grid of nodes separated by the grid spacing Δy , located at y_i , $i = 0, 1, \dots, N + 1$, where $y_0 = -A$ and $y_{N+1} = B$, as illustrated in figure 10.5.1. For simplicity, we denote the value of f at the i th node by f_i . To satisfy the no-penetration condition, we require that the stream function is constant over the lower and upper walls, setting

$$f_0 = 0 \quad \text{and} \quad f_{N+1} = 0. \quad (10.5.22)$$

Because the values of the stream function over the two walls are equal, the disturbance flow will not generate a net flow rate in the stream-wise direction. Applying equation (10.5.21) at the i th node, where $i = 1, 2, \dots, N$, and approximating the second derivative $d^2 f / dy^2$ with centered differences, we obtain the difference equation

$$\begin{aligned}
 & U(y_i) \frac{f_{i+1} - 2 f_i + f_{i-1}}{\Delta y^2} - [U(y_i) k^2 + \frac{d^2 U}{dy^2}(y_i)] f_i \\
 &= c \left(\frac{f_{i+1} - 2 f_i + f_{i-1}}{\Delta y^2} - k^2 f_i \right).
 \end{aligned}
 \tag{10.5.23}$$

Denoting $U_i \equiv U(y_i)$ and $U_i'' \equiv (d^2 U/dy^2)(y_i)$, and rearranging, we obtain

$$\begin{aligned}
 & U_i f_{i-1} - [2 U_i + \Delta y^2 (U_i k^2 + U_i'')] f_i + U_i f_{i+1} \\
 &= c [f_{i-1} - (2 + k^2 \Delta y^2) f_i + f_{i+1}].
 \end{aligned}
 \tag{10.5.24}$$

Applying equation (10.5.24) for $i = 1, 2, \dots, N$, we obtain a system of linear equations, which we then compile into the matrix form

$$\mathbf{A} \cdot \mathbf{f} = c \mathbf{B} \cdot \mathbf{f},
 \tag{10.5.25}$$

where

$$\mathbf{f} \equiv \begin{bmatrix} f_1 \\ f_2 \\ \dots \\ f_{N-1} \\ f_N \end{bmatrix}
 \tag{10.5.26}$$

is the N -dimensional solution vector, \mathbf{A} is an $N \times N$ tridiagonal matrix defined as

$$\mathbf{A} \equiv \begin{bmatrix} -2 U_1 & U_1 & 0 & 0 & \dots & 0 \\ -\Delta y^2 (U_1 k^2 + U_1'') & & & & & \\ U_2 & -2 U_2 & U_2 & 0 & \dots & 0 \\ -\Delta y^2 (U_2 k^2 + U_2'') & & & & & \\ \dots & \dots & \dots & \dots & \dots & \dots \\ 0 & 0 & 0 & \dots & U_N & -2 U_N \\ & & & & & -\Delta y^2 (U_N k^2 + U_N'') \end{bmatrix},
 \tag{10.5.27}$$

and \mathbf{B} is another $N \times N$ tridiagonal matrix defined as

$$\mathbf{B} \equiv \begin{bmatrix} -2 - k^2 \Delta y^2 & 1 & 0 & 0 & \dots & 0 \\ 1 & -2 - k^2 \Delta y^2 & 1 & 0 & \dots & 0 \\ \dots & \dots & \dots & \dots & \dots & \dots \\ 0 & 0 & 0 & \dots & 1 & -2 - k^2 \Delta y^2 \end{bmatrix}. \quad (10.5.28)$$

Note that the elements of the matrix \mathbf{B} are independent of the velocity profile $U(y)$.

Equation (10.5.25) presents us with a *generalized algebraic eigenvalue problem* that can be stated as follows: compute the value of c so that (10.5.25) has a nontrivial solution for the vector \mathbf{f} ; that is, a solution other than the null vector.

One way to compute the eigenvalue c is to recast equation (10.5.25) into the homogeneous equation

$$\mathbf{E} \cdot \mathbf{f} = 0, \quad (10.5.29)$$

where \mathbf{E} is a tridiagonal matrix given by

$$\mathbf{E} \equiv \begin{bmatrix} -2 - \Delta y^2(k^2 + \frac{U_1''}{U_1 - c}) & 1 & 0 & 0 & \dots & 0 \\ 1 & -2 - \Delta y^2(k^2 + \frac{U_2''}{U_2 - c}) & 1 & 0 & \dots & 0 \\ \dots & \dots & \dots & \dots & \dots & \dots \\ 0 & 0 & 0 & \dots & 1 & -2 - \Delta y^2(k^2 + \frac{U_N''}{U_N - c}) \end{bmatrix}. \quad (10.5.30)$$

For system (10.5.29) to have a nontrivial solution, the coefficient matrix \mathbf{E} must be singular: the eigenvalue c must be such that the determinant of the complex matrix \mathbf{E} is equal to zero. This observation provides us with a basis for a numerical method involving the following steps:

1. Guess a complex value for c .
2. Compute the determinant of \mathbf{E} using the algorithm discussed in the following subsection.
3. Improve c to reduce the magnitude of the determinant.

The improvement in step 3 can be made using Newton's method, setting

$$c^{New} = c^{Old} - \frac{\text{Det}[\mathbf{E}(c^{Old})]}{(\frac{d \text{Det}[\mathbf{E}(c^{Old})]}{dc})_{c=c^{Old}}}. \quad (10.5.31)$$

The derivative in the denominator on the right-hand side of (10.5.31) may be approximated with a finite difference, setting

$$\frac{d \text{Det}[\mathbf{E}(c^{Old})]}{dc} \Big|_{c=c^{old}} \simeq \frac{\text{Det}[\mathbf{E}(c^{Old} + \epsilon)] - \text{Det}[\mathbf{E}(c^{Old})]}{\epsilon}, \quad (10.5.32)$$

where ϵ is a real or complex increment with small magnitude.

Determinant of a tridiagonal matrix

To compute the determinant of the tridiagonal matrix \mathbf{E} , we use an efficient algorithm applicable to general tridiagonal matrices of the form

$$\mathbf{T} \equiv \begin{bmatrix} a_1 & b_1 & 0 & 0 & \dots & 0 & 0 \\ c_2 & a_2 & b_2 & 0 & \dots & 0 & 0 \\ \dots & \dots & \dots & \dots & \dots & \dots & \dots \\ 0 & 0 & 0 & 0 & \dots & c_{N-1} & a_{N-1} & b_{N-1} \\ 0 & 0 & 0 & 0 & \dots & 0 & c_N & a_N \end{bmatrix}, \quad (10.5.33)$$

where $a_i, b_i,$ and c_i are real or complex constants.

The algorithm involves computing the sequence of numbers P_i based on the recursion relation

$$\begin{aligned} P_0 &= 0, \\ P_1 &= a_1, \\ &\dots \\ P_i &= a_i P_{i-1} - b_{i-1} c_i P_{i-2}, \end{aligned} \quad (10.5.34)$$

for $i = 2, 3, \dots, N$; then $\text{Det}(\mathbf{T}) = P_N$.

Instability of a shear flow with hyperbolic tangent profile

As an example, we consider an inviscid shear flow with velocity profile

$$U(y) = U_0 \tanh \frac{y}{b}, \quad (10.5.35)$$

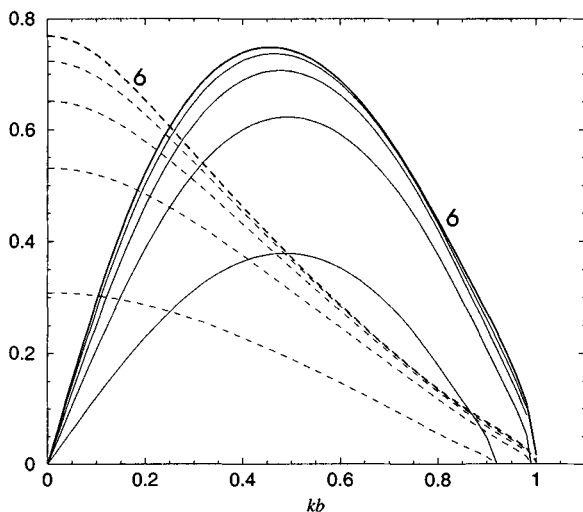


Figure 10.5.2 Instability of an inviscid shear flow whose velocity profile is described by equation (10.5.35). Graphs of the reduced imaginary part of the phase velocity $\hat{c}_I \equiv c_I/U_0$ (dashed lines) and reduced growth rate $\hat{\sigma}_I \equiv 4b\sigma_I/U_0$ (solid lines) for $A/b = B/b = 2.0, 2.5, 3.0, 4.0,$ and 6.0 (heavy lines), in the regime of unstable wave numbers.

where U_0 is the uniform velocity of the flow far above and below the shear layer, and b is the shear layer half-thickness.

The dashed lines in figure 10.5.2 represent the dimensionless imaginary part of the phase velocity of unstable perturbations, $\hat{c}_I \equiv c_I/U_0$, for a sequence of channel widths with $A = B$, computed using the numerical method discussed in this section, implemented in program *08.stab/sf.inv* of *FDLIB*; the heavy line corresponds to $A/b = B/b = 6.0$. The solid lines represent the corresponding reduced growth rate $\hat{\sigma}_I \equiv 4b\sigma_I/U_0$. When the reduced wave number kb is larger than a critical value kb_{cr} that depends on A/b , the growth rate vanishes and the perturbations are neutrally stable. As A/b tends to infinity, we obtain infinite shear flow in the absence of side walls; in this limit the critical wave number for neutral stability is known to be $kb_{cr} = 1.0$.

The results in figure 10.5.2 suggest that the walls reduce the growth rate of the perturbations by restricting the lateral extent over which normal motions are allowed to develop. Maximum growth rate occurs at a certain wave number $kb_{max} \simeq 0.50$; the corresponding perturbation is

expected to dominate the instability, and therefore spontaneously arise in a randomly perturbed flow.

Finite difference methods for the Orr-Sommerfeld equation

Finite-difference methods for the Orr-Sommerfeld equation may be developed working along similar lines. The no-penetration and no-slip boundary conditions over a stationary solid surface require that the boundary values of f and its first derivative with respect to transverse distance y vanish. The discretization of the Orr-Sommerfeld equation yields a system of linear equations similar to that shown in (10.5.25). In the case of viscous flow, however, because of the presence of the fourth derivative $f^{(iv)}$, the matrix \mathbf{A} is complex pentadiagonal; *penta* derives from the Greek word $\pi\epsilon\nu\tau\epsilon$ which means five. The algebraic system descending from the finite-difference discretization may be placed in a form that is analogous to that shown in (10.5.29), where the matrix \mathbf{E} is now pentadiagonal. Unfortunately, the determinant of this matrix may no longer be computed using an efficient numerical method.

To illustrate the effect of viscosity, we consider an infinite shear flow whose velocity profile is described by equation (10.5.35). Figure 10.5.3 shows a contour plot of the reduced growth rate $\hat{\sigma}_I \equiv b\sigma_I/U_0$ in the $kb - Re$ (wave number - Reynolds number) plane, where $Re \equiv U_0 b/\nu$. The contour $\hat{\sigma}_I = 0$ corresponds to neutrally stable perturbations; a perturbation whose wave number lies in the shaded area below this contour is unstable, and a perturbation whose wave number lies in the unshaded area above this contour are stable. As the Reynolds number tends to infinity, we recover the results presented in figure 10.5.2 for inviscid flow. Figure 10.5.3 reveals that the flow is unstable, no matter how small the Reynolds number. The stabilizing effect of viscosity becomes evident by observing that, as the Reynolds number is raised, the range of unstable wave numbers $(0, kb_{cr})$ expands, thereby allowing a wider range of perturbations to grow at higher growth rates.

Problem

Problem 10.5.1 *Instability of an inviscid shear flow.*

Consider an infinite shear flow whose velocity profile is described by (10.5.35). Show that an eigenvalue and the corresponding eigenfunction of Rayleigh's equation describing a neutrally stable perturbation is given by $c = 0$ and $f(y) = d \operatorname{sech}(y/b)$, where d is an arbitrary constant.

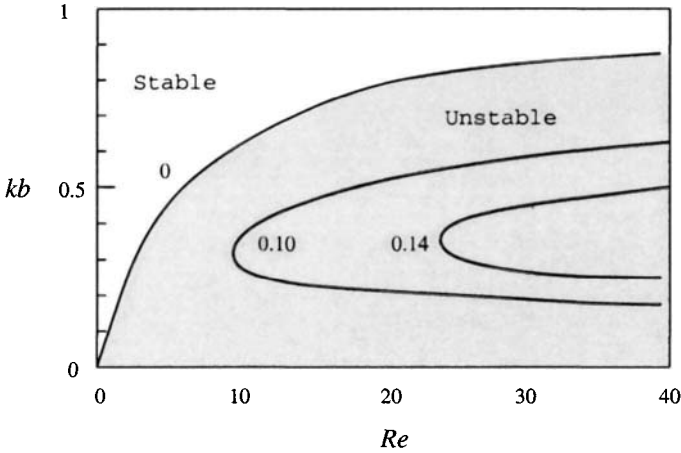


Figure 10.5.3 Contour plot of the reduced growth rate $\hat{\sigma}_I \equiv b\sigma_I/U_0$ for viscous shear flow whose velocity profile is described by equation (10.5.35); the Reynolds number is defined as $Re \equiv U_0 b/\nu$.

Computer problem

Problem c.10.5.1 *Instability of inviscid shear flows.*

Directory *08_stab/sf_inv* of *FDLIB* includes the program *sf_inv* that computes the complex phase velocity of perturbations using the finite-difference method discussed in the text.

(a) Consider a family of inviscid shear flows with velocity profile

$$U(y) = U_0 \left\{ \delta \tanh \frac{y}{b} + (\delta - 1) \exp\left[-\left(\frac{y}{b}\right)^2\right] \right\}, \quad (10.5.36)$$

where the parameter δ takes values in the range $[0, 1]$. The limiting values $\delta = 1$ and 0 correspond, respectively, to a shear layer with a hyperbolic tangent velocity profile, and a symmetric wake with a Gaussian velocity profile.

Assuming that the flow is confined between two parallel walls located at $y = \pm A$ where the no-penetration condition is required, use the program to generate a graph of a properly defined dimensionless growth rate versus the reduced wave number kb , for $\delta = 0, 0.50,$ and 1.0 , in each case for $A/b = 2.0, 3.0,$ and 4.0 , and discuss the results of your computations.

(b) Repeat (a) for a shear flow with velocity profile

$$U(y) = U_0 \left[\delta \tanh \frac{y}{b} + (1 - \delta) \operatorname{sech}^2 \frac{y}{b} \right], \quad (10.5.37)$$

where the parameter δ takes values in the range $[0, 1]$. The limiting values $\delta = 1$ and 0 correspond, respectively, to a shear layer with a hyperbolic tangent velocity profile and to the Bickley jet.

10.6 Turbulent motion

Turbulent flow is established when the Reynolds number $Re = \rho V L / \mu$, defined in an appropriate fashion for the particular flow under consideration, exceeds a certain threshold, usually on the order of 10^3 ; V is a characteristic macroscopic velocity, and L is a characteristic macroscopic length scale typically associated with the size of the boundaries. Both V and L are classified as *external scales*. For example, in the case of tube flow, V can be identified with the mean velocity or with the maximum velocity occurring at the centerline, and L can be identified with the tube radius or diameter.

Turbulence is characterized by random motion in *both* time and space. Thus, a graph of a velocity component, denoted by v , plotted against time at a particular location in a turbulent flow reveals random fluctuations, as illustrated in figure 10.6.1(a). An analogous graph of v against the spatial coordinate x at a particular instant in time reveals similar random fluctuations, as illustrated in figure 10.6.1(b).

10.6.1 Transition

The transition from the laminar to the turbulent state with increasing Reynolds number is not sudden, but occurs through a sequence of events eventually leading to randomly fluctuating motion. For example, pressure-driven flow in a circular tube is laminar when the Reynolds number, defined with respect to the tube radius and the maximum velocity at the centerline, is less than 1,100; transition occurs when the Reynolds number lies in the range between 1,100 and 1,500; and fully developed turbulent motion is established at higher Reynolds numbers. Wall roughness and entrance conditions affect the precise thresholds for transition.

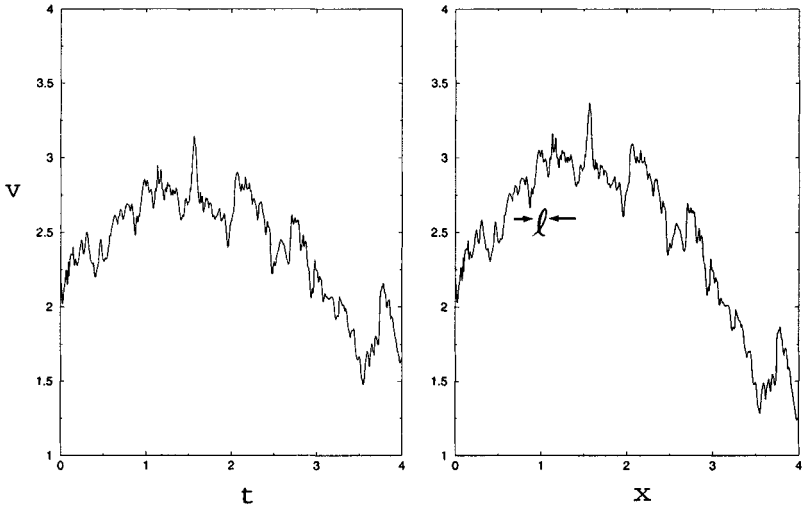


Figure 10.6.1 (a) Temporal, and (b) spatial variation of a velocity component in a turbulent flow; l is the scale of the energy-containing turbulent motion.

Figure 10.6.2 shows a recording of the streamwise component of the velocity in streaming flow past a flat plate of length L , at a sequence of increasing Reynolds numbers defined with respect to the length of the plate². The velocity probe was placed 0.02 in above the plate and 56 in behind the leading edge. The graphs illustrate the onset of oscillations, the development of turbulent spots, and the ultimate establishment of turbulent motion.

Logistic mapping

A simple model illustrating the process of transition from simple to complex behavior is provided by the logistic mapping. Given a number $x^{(0)}$, the logistic mapping generates a sequence of numbers $x^{(1)}, x^{(2)}, \dots$ computed by the recursion formula

$$x^{(k+1)} = \lambda x^{(k)} (1 - x^{(k)}), \quad (10.6.1)$$

²Cebeci T., & Smith, A. M. O. 1974, *Analysis of Turbulent Boundary Layers*, Academic Press.

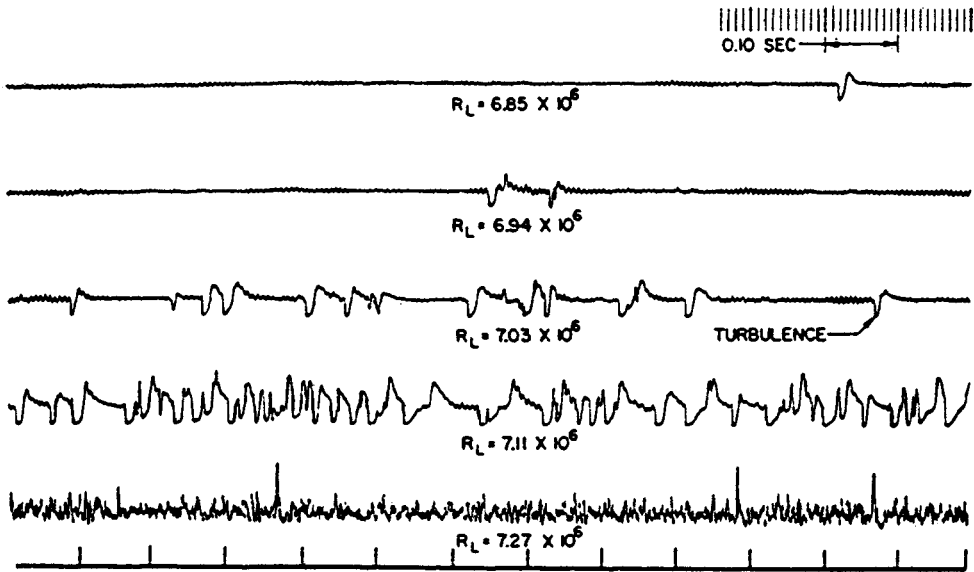


Figure 10.6.2 Recording of the streamwise component of the velocity in flow past a flat plate at a sequence of increasing Reynolds numbers R_L defined with respect to the length of the plate, L . The signal shows the onset of oscillations, the development of turbulent spots, and the ultimate establishment of turbulent motion.

for $k = 0, 1, \dots$, where λ is a specified positive constant. The special choices $x^{(0)} = 0$ and $(\lambda - 1)/\lambda$ are the fixed points of the mapping; for these choices, $x^{(k)} = x^{(0)}$ for all k , and the logistic sequence is stationary.

To illustrate the transition, we introduce the λx plane, and perform a series of computations according to the following steps:

1. Choose a value for λ .
2. Select a value for $x^{(0)}$ that lies between 0 and 1, but is not exactly equal to 0 or 1.

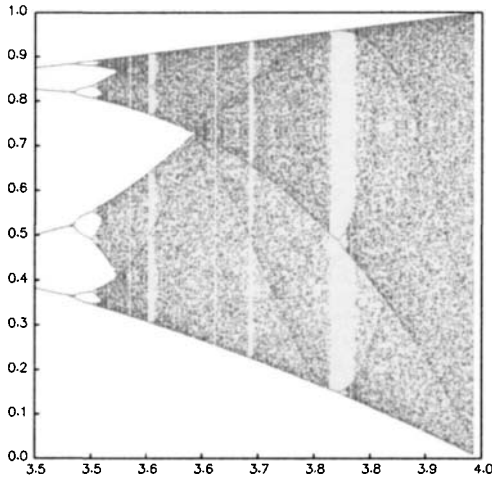


Figure 10.6.3 Behavior of sequences generated by the logistic mapping (10.6.1), illustrating the process of transition: cascade of bifurcations in the λx plane.

3. Compute a few hundred terms based on the logistic mapping (10.6.1).
4. Skip the first one hundred terms, and graph the rest of them in the λx plane with dots.
5. Return to step 1 and repeat.

The result of this computation is shown in figure 10.6.3. As λ is raised, a cascade of bifurcations and a random behavior reminiscent of turbulent motion is established.

10.6.2 Eulerian and Lagrangian turbulence

Point particles in a certain class of unsteady two-dimensional *laminar* flows, and steady or unsteady three-dimensional *laminar* flows, have been observed to move in a random fashion described as *Lagrangian turbulent motion*. Fluid motion in a turbulent flow should be distinguished from the seemingly random motion of point particles in these laminar chaotic flows: a distinguishing feature of a turbulent flow is significant kinematic and molecular diffusion accompanied by high levels of viscous dissipation.

10.6.3 Nature of turbulent motion

Turbulence has defied a simple physical interpretation in terms of elementary fluid motions. In the traditional approach, a turbulent flow is regarded as a random or stochastic process amenable to statistical analysis. Certain important features, however, distinguish the turbulent motion from a generic random process, including the following:

- Turbulence is *intermittent*. A recording of the velocity at a certain point in a turbulent flow may appear regular for a period of time, only to be interrupted by periods of violent turbulent motion in an intermittent fashion.
- A turbulent flow contains small-scale short-lived, and large-scale long-lived *coherent motions* associated with eddies and vortices with a well-defined structure. Examples include horse-shoe vortices developing near boundary layers and in regions of high shear rates.
- An intimate connection exists between *vortex dynamics*, to be discussed in Chapter 11, and the dynamics of turbulent flow, but the precise relationship remains unclear.
- Eddy motions in a turbulent flow carry turbulent kinetic energy that is distributed over a broad range of scales; from the external scale L , to the energy dissipating Kolmogorov scale η to be defined later in this section. Energy is transferred across the scales in the forward or backward direction, and a balance is achieved at dynamic equilibrium. The dynamics of, and distribution of energy among the length scales is not universal, but depends on the particular flow under consideration. Thus, the properties of wall-bounded turbulent shear flow are different than those of unbounded shear flow, and different than those of grid-turbulent flow generated behind a grid intercepting a high-speed flow. The diverse behavior reflects differences in the physical mechanisms by which energy is supplied into a turbulent flow, only to be dissipated by the small-scale motion.
- The non-slip boundary condition sedates the turbulent motion near a wall where a viscous sublayer of unsteady laminar flow is established. A buffer zone separates the viscous sublayer from the regime of fully-developed turbulent flow. Figure 10.6.4 shows the temporal velocity signal of a turbulent flow at different radial positions

in a circular pipe of radius 15 cm, illustrating the cessation of the turbulent motion near the wall³.

Figure 10.6.4 Temporal velocity fluctuations in turbulent pipe flow at different distances from the wall, showing the presence of the laminar sublayer and buffer zone near the wall.



(a) $r = 0$ (on axis)



(b) $r = 4.5$ cm



(c) $r = 7.5$ cm



(d) $r = 9.5$ cm



(e) $r = 14.5$ cm

³Corrsin, S. 1943, Investigation of flow in an axially asymmetric heated jet-air, *NACA Rep. 3L23*

10.6.4 Decomposition into mean and fluctuating components

One way to describe a turbulent flow is to decompose it into a smoothly varying or mean component, and a rapidly fluctuating component. The smoothly varying component may be identified with the time average over a period of time t_0 that is large compared to the time scale of the fluctuations, but small compared to the external time scale L/V . Thus, the mean velocity at the position \mathbf{x} , designated by an overbar, is defined as

$$\bar{\mathbf{u}}(\mathbf{x}, t) \equiv \frac{1}{t_0} \int_{t-t_0/2}^{t+t_0/2} \mathbf{u}(\mathbf{x}, t + t') dt'. \quad (10.6.2)$$

The fluctuating velocity, designated by a prime, is defined by the decomposition

$$\mathbf{u}(\mathbf{x}, t) = \bar{\mathbf{u}}(\mathbf{x}, t) + \mathbf{u}'(\mathbf{x}, t). \quad (10.6.3)$$

The definition (10.6.2) implies that the time-average value of the fluctuating velocity vanishes by construction,

$$\overline{\mathbf{u}'}(\mathbf{x}, t) \equiv \frac{1}{t_0} \int_{t-t_0/2}^{t+t_0/2} \mathbf{u}'(\mathbf{x}, t + t') dt' = \mathbf{0}. \quad (10.6.4)$$

In contrast, the time average of the square of the x component of the fluctuating velocity,

$$\overline{u_x'^2}(\mathbf{x}, t) \equiv \frac{1}{t_0} \int_{t-t_0/2}^{t+t_0/2} u_x'^2(\mathbf{x}, t + t') dt', \quad (10.6.5)$$

is not equal to zero; similarly for the y and z components of the fluctuating velocity. In fact, the square root of these time averages, called the root-mean-square values, RMS, normalized by an external velocity scale V , expressed by the ratios

$$i_x \equiv \frac{\sqrt{\overline{u_x'^2}}}{V}, \quad i_y \equiv \frac{\sqrt{\overline{u_y'^2}}}{V}, \quad i_z \equiv \frac{\sqrt{\overline{u_z'^2}}}{V}, \quad (10.6.6)$$

are measures of the intensity of the turbulent motion in the three spatial directions.

Laboratory measurements have shown that the three intensities defined in (10.6.6) have different magnitudes, except in the idealized case of isotropic turbulence occurring in the absence of boundaries. Nearly

isotropic turbulence may be realized in the laboratory by placing eight fans at the vertices of a cube, and turning them toward the cube center. In the case of channel or tube flow, the turbulence intensity in the direction of the flow is significantly greater than that in directions perpendicular to the flow, especially near the walls.

A single measure of the magnitude of the turbulent velocity fluctuations is provided by the velocity scale

$$u \equiv \sqrt{\frac{u'^2_x + u'^2_y + u'^2_z}{3}}. \quad (10.6.7)$$

In the case of isotropic turbulence, the three terms in the numerator on the right-hand side are equal.

As an example, consider pressure-driven turbulent flow through a circular tube of radius a . Figure 10.6.5 shows a schematic illustration of the mean velocity profile (solid line), distribution of the streamwise turbulence intensity (dashed line), and distribution of the lateral turbulence intensity (dotted line); the intensities have been normalized by the maximum velocity at the centerline. The mean velocity profile may be approximated with the algebraic form

$$\bar{u}_x(\sigma) = V \left(1 - \frac{\sigma}{a}\right)^{1/7}, \quad (10.6.8)$$

where $V \equiv (\bar{u}_x)_{Max}$ is the maximum mean velocity occurring at the centerline, which may be contrasted with its parabolic counterpart shown in equation (7.3.4) for laminar flow.

10.6.5 Inviscid scales

A turbulent flow contains an infinite collection of interacting eddies, defined and regarded as elementary fluid motions. Inspecting the turbulence signal shown in figure 10.6.1(b), we identify spatial scales with a broad range of magnitudes. One important scale, classified as inviscid, is the scale of the *energy containing turbulent motion*, denoted by l . Using l and the magnitude of the velocity fluctuations u defined in (10.6.7), we deduce that the time scale of the energy containing eddies is comparable to l/u .

The actual size of l varies according to the particular flow under consideration, as follows:

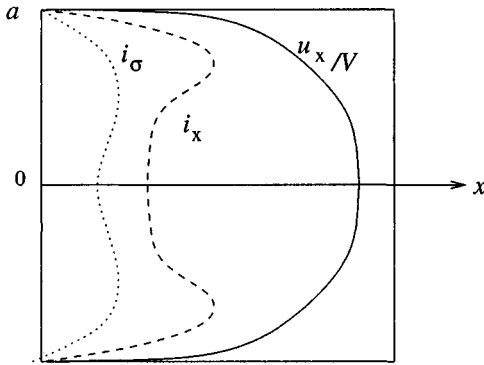


Figure 10.6.5 Turbulent flow in a circular tube: schematic illustration of the mean velocity profile (solid line), and distributions of the streamwise (dashed line) and lateral (dotted line) turbulence intensities, reduced by the maximum mean velocity at the centerline.

- In the case of boundary-layer flow, l is comparable to the local boundary-layer thickness.
- In the case of turbulent jet flow, l is comparable to the local jet diameter.
- In the case of a wake, l is comparable to the local width of the wake.
- In the case of tube flow, l is comparable to the tube diameter.
- In the case of infinite shear flow over a wall, l in the buffer zone is proportional to the distance from the wall.
- In the case of free turbulence generated by placing a grid in a uniform stream, l is comparable to the grid size behind the grid, and then it increases with downstream position.

10.6.6 Viscous scales

Energy is dissipated in a turbulent flow even if the mean flow has a uniform velocity profile, and this requires external action to sustain the

motion. The rate of viscous dissipation, with units of kinetic energy per mass per time, is denoted by ϵ . One distinguishing property of turbulent flow is that dissipation occurs primarily due to the small-scale motion.

Kolmogorov argued that the rate of dissipation is determined by the fluid properties alone, and combined ϵ with the kinematic viscosity ν to form the Kolmogorov length scale

$$\eta \equiv \left(\frac{\nu^3}{\epsilon}\right)^{1/4}, \quad (10.6.9)$$

and accompanying Kolmogorov velocity scale

$$u_K \equiv (\nu \epsilon)^{1/4}. \quad (10.6.10)$$

The two scales are related by

$$\frac{u_K \eta}{\nu} = 1. \quad (10.6.11)$$

The left-hand side of (10.6.11) defines the Reynolds number of the energy dissipating motion; by design, this is equal to unity underlying the dominance of viscous forces responsible for converting kinetic to thermal energy in a viscous flow.

10.6.7 Relation of inviscid and viscous scales

Conservation of energy requires that the rate of viscous dissipation ϵ scales as

$$\epsilon \simeq \frac{u^3}{l}. \quad (10.6.12)$$

Substituting this estimate into (10.6.9) and rearranging, we find

$$\frac{\eta}{l} \simeq \left(\frac{\nu}{u l}\right)^{4/3}. \quad (10.6.13)$$

Now, the magnitude of the velocity fluctuations, u , is typically comparable to the external velocity scale V , and the inviscid length scale l is comparable to the external length scale L . As a result, the inverse of the ratio on the right-hand side of (10.6.13) is comparable to the Reynolds number $Re = V L/\nu$, yielding the scaling

$$\frac{\eta}{l} \simeq Re^{-3/4}. \quad (10.6.14)$$

Working in a similar fashion with (10.6.10), we find the scaling law

$$\frac{u_K}{u} \simeq Re^{-1/4}. \quad (10.6.15)$$

These equations allow us to estimate the scales of the energy-dissipating motion from measurable inviscid scales and the Reynolds number of the flow.

10.6.8 Fourier analysis

To analyze the distribution of energy across the scales of a turbulent flow, we decompose a recording of the velocity at a particular location into a Fourier series with respect to time, and then examine the magnitude of the Fourier coefficients. In the laboratory, the velocity is typically measured by two methods: hot-wire anemometry based on a calibration that associates velocity to heat loss from a small wire probe placed in a flow; and laser-doppler velocimetry based on the scattering of a laser beam caused by small particles that have been seeded into the flow.

To develop the Fourier decomposition, we consider a *times series* of a function $f(x)$, which is a sequence of values of the function recorded at evenly-spaced time intervals separated by the sampling time Δt . Suppose that the time series contains N recordings corresponding to times $0, \Delta t, 2\Delta t, \dots, (N-1)\Delta t$. Using the Fourier representation theory, we assume that $f(N\Delta t) = f(0)$, and express the function $f(t)$ over the time interval $(0, T)$, where $T = N \Delta t$, in the form of a complete Fourier series

$$f(t) \simeq \frac{1}{2} a_0 + \sum_{p=1}^M a_p \cos\left(\frac{2\pi p}{N} \frac{t}{\Delta t}\right) + \sum_{p=1}^M b_p \sin\left(\frac{2\pi p}{N} \frac{t}{\Delta t}\right), \quad (10.6.16)$$

where M is a specified truncation level, p is an integer, and a_p, b_p are the cosine and sine Fourier coefficients. The complex Fourier coefficients are defined by

$$c_p \equiv \frac{1}{2} (a_p + i b_p), \quad (10.6.17)$$

where i is the imaginary unit. In terms of the complex Fourier coefficients, the Fourier series (10.6.16) can be recast into the more compact form

$$f(t) \simeq \sum_{p=-M}^M c_p \exp\left(-i \frac{2\pi p}{N} \frac{t}{\Delta t}\right), \quad (10.6.18)$$

where the negative-indexed complex Fourier coefficients are given by

$$c_{-p} = c_p^* = \frac{1}{2} (a_p - i b_p), \quad (10.6.19)$$

and an asterisk denotes the complex conjugate.

Fourier theory provides us with a remarkably simple method for evaluating the Fourier coefficients. Denoting the data by $f_l \equiv f(t_l)$, where $t_1 = 0, t_2 = \Delta t, \dots, t_N = (N - 1) \Delta t$, we obtain ⁴

$$a_p = \frac{2}{N} [f_1 + \cos(2\pi \frac{p}{N}) f_2 + \cos(2\pi \frac{2p}{N}) f_3 + \dots + \cos(2\pi \frac{(N-1)p}{N}) f_N],$$

$$b_p = \frac{2}{N} [f_1 + \sin(2\pi \frac{p}{N}) f_2 + \sin(2\pi \frac{2p}{N}) f_3 + \dots + \sin(2\pi \frac{(N-1)p}{N}) f_N]. \quad (10.6.20)$$

In practice, the number of data points N can be on the order of several thousand or even higher, and the direct evaluation of the sums on the right-hand sides of expressions (10.6.20) and (10.6.21) requires a prohibitive amount of computational time. Fortunately, the computations can be expedited considerably by use of an ingenious algorithm for computing the Fourier coefficients, known as the Fast Fourier Transform, FFT. Subroutine *fft* in directory *13.turbo/stats* of *FDLIB* performs the FFT of a time series whose size is a power of 2, that is $N = 2^q$ where q is an integer.

10.6.9 Power spectrum

Taking the square of both sides of (10.6.18), expanding out the square of the product on the right-hand side, integrating the resulting expression with respect to time from $t = 0$ to $T \equiv N \Delta t$, and using trigonometric identities to set the integral of a large number of terms equal to zero, we find

$$\int_0^T f^2(t) dt \simeq T \sum_{p=-M}^M c_p c_p^*, \quad (10.6.21)$$

which may be rearranged to give

⁴See, for example, C. Pozrikidis 1998, *Numerical Computation in Science and Engineering*, Oxford University Press.

$$\overline{f^2} \equiv \frac{1}{T} \int_0^T f^2(t) dt \simeq \sum_{p=-M}^M |c_p|^2 = c_0^2 + \sum_{p=1}^M 2 |c_p|^2, \quad (10.6.22)$$

where $|c_p|^2 = c_p c_p^* = \frac{1}{2} (a_p^2 + b_p^2)$ is the square of the magnitude of the p th complex Fourier coefficient.

- A graph of the coefficients $2 |c_p|^2$ against the *angular frequency* $\omega_p \equiv 2 \pi p / \Delta t$ for $p = 1, 2, \dots$, is the *discrete temporal power spectrum* of the function $f(t)$. Of particular interest is the behavior at high values of p corresponding to high angular frequencies.
- A graph of the coefficients $2 |c_p|^2$ against the *spatial wave number* $k_p \equiv \omega_p V = 2 \pi p V / \Delta t$, where V is a specified velocity, is the *discrete power spectrum* of the function $f(t)$. Of particular interest is the behavior at high values of p corresponding to high wave numbers.

Identifying now the generic function $f(t)$ with the x , y , or z component of the velocity, we obtain the discrete energy spectrum of a turbulent flow, which provides us with information on how kinetic energy is distributed among the different scales. In practice, the discrete power spectrum is computed by taking the Fourier transform of a time series comprised of sets of data points on the order of $2^{12} = 4096$. The power spectrum computed using one data set shows large fluctuations. To obtain a smooth spectrum, we average the Fourier coefficients over sets corresponding to different realizations or different time periods for the same flow conditions.

As the sample size N and total sampling time $T = N \Delta t$ tend to infinity, the sum on the right-hand side of (10.6.18) reduces to an infinite Fourier integral. Correspondingly, the right-hand side of (10.6.22) takes the form

$$\overline{f^2} = \int_0^\infty E_t(\omega) d\omega = \int_0^\infty E(k) dk, \quad (10.6.23)$$

where $E_t(\omega)$ and $E(k)$ are the temporal and spatial energy density functions. Making a correspondence between (10.6.23) and (10.6.22), we obtain the relations

$$E_t(\omega_p) = \frac{\Delta t}{2\pi} 2 |c_p|^2, \quad E(k_p) = \frac{V \Delta t}{2\pi} 2 |c_p|^2, \quad (10.6.24)$$

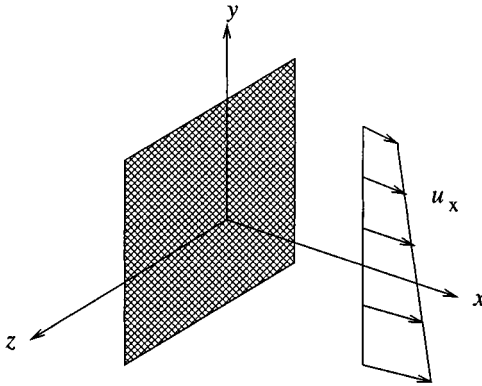


Figure 10.6.6 Stratified turbulent shear flow behind a vertical grid. A time series of the velocity and temperature recorded by Kurt Keller is placed in file *keller.dat* of directory *13_turbo/stats* of *FDLIB*.

which allow us to prepare graphs and study the shape of the energy density function. Taylor's hypothesis prescribes setting V equal to the local mean value of the streamwise velocity.

Problems

Problem 10.6.1 *Turbulent mean velocity profile in tube flow.*

Consider turbulent flow in a tube whose mean velocity profile is given by (10.6.8). Derive a relationship between the mean flow rate and the mean velocity at the centerline, and compare it with its counterpart for laminar flow.

Problem 10.6.2 *Kolmogorov length scale for pipe flow.*

Laboratory data for turbulent flow in a circular tube with diameter D has shown that (a) the length scale of the energy containing turbulent motion l is comparable to D , and (b) the magnitude of the turbulent velocity fluctuations is comparable to V , where V is the maximum mean velocity occurring at the centerline. Based on this information, compute the Kolmogorov length and velocity scale for a tube with diameter $D=10$ cm, at Reynolds number $Re \equiv U D/\nu = 10^6$.

Computer problem

Problem c.10.6.1 Stratified shear flow.

Consider stratified turbulent shear flow behind a vertical grid, as illustrated in figure 10.6.6, with mean velocity profile $\bar{u}_x(y)$ and mean temperature field $\bar{T}(y)$. Kurt Keller recorded a time series of the x and y velocity components and temperature at a point located 457.2 cm behind the grid, at the sampling frequency 5 KHz corresponding to sampling time 0.0002 s^{-1} , for the following conditions: grid spacing 2.54 cm; mean shear rate $d\bar{u}_x/dy = -7.63 \text{ s}^{-1}$; mean temperature gradient $d\bar{T}/dy = 35.8 \text{ K m}^{-1}$; local microscale Reynolds number $Re \equiv \lambda u/\nu = 91.2$, where $u \equiv \sqrt{u_x'^2}$ is the RMS value of the fluctuations of the streamwise component of the velocity, and λ is the *Taylor microscale* defined by the relation

$$\frac{u^2}{\lambda^2} = \overline{\left(\frac{du'}{dy}\right)^2}. \quad (10.6.25)$$

The data are placed in the three columns of file *keller.dat* in directory *13_turbo/stats* of *FDLIB*. Use program *stats* in this directory to compute and plot (a) the mean and RMS values, and (b) the discrete power spectrum of the x and y components of the velocity and temperature, and discuss the results of your computation.

10.7 Analysis of turbulent motion

Deriving exact solutions of the Navier-Stokes equation for turbulent flow is out of the question. Direct numerical simulation, DNS, on the other hand, is prohibited by pragmatic constraints associated with finite grid-size: to capture the dynamics of a turbulent flow, we must resolve a prohibitively broad range of length scales. Progress can be made by developing approximate models and phenomenological theories based on empirical correlations inspired by laboratory observation.

10.7.1 Reynolds stresses

A point of departure for developing phenomenological theories is the decomposition of the velocity into a mean and a fluctuating component, as shown in equation (10.6.3). A similar decomposition of the pressure yields

$$p(\mathbf{x}, t) = \bar{p}(\mathbf{x}, t) + p'(\mathbf{x}, t), \quad (10.7.1)$$

where

$$\bar{p}(\mathbf{x}, t) \equiv \frac{1}{t_0} \int_{t-t_0/2}^{t+t_0/2} p(\mathbf{x}, t+t') dt' \quad (10.7.2)$$

is the mean pressure. Substituting the decompositions (10.6.3) and (10.7.2) into Cauchy's equation of motion (6.3.13), expanding out the derivatives of the products, taking the time average of both sides, and simplifying, we derive a modified equation of motion for the mean component. The fluctuating component appears as an effective inertial hydrodynamic volume force.

Considering, for example, the term $\partial(\rho u_x u_y)/\partial y$ on the left-hand side of the x component of the equation of motion (6.3.13), we write

$$\begin{aligned} \frac{\partial}{\partial y}(\rho u_x u_y) &= \frac{\partial}{\partial y}[\rho(\bar{u}_x + u'_x)(\bar{u}_y + u'_y)] \\ &= \frac{\partial}{\partial y}(\rho \bar{u}_x \bar{u}_y) + \frac{\partial}{\partial y}(\rho \bar{u}_x u'_y) + \frac{\partial}{\partial y}(\rho u'_x \bar{u}_y) + \frac{\partial}{\partial y}(\rho u'_x u'_y). \end{aligned} \quad (10.7.3)$$

Taking the time average of both sides, defined in equations (10.6.2) and (10.7.2), and interchanging the order of time-averaging and space differentiation, we find

$$\begin{aligned} \frac{\partial}{\partial y}(\overline{\rho u_x u_y}) &= \frac{\partial}{\partial y}(\overline{\rho \bar{u}_x \bar{u}_y}) + \frac{\partial}{\partial y}(\overline{\rho \bar{u}_x u'_y}) + \frac{\partial}{\partial y}(\overline{\rho u'_x \bar{u}_y}) + \frac{\partial}{\partial y}(\overline{\rho u'_x u'_y}) \\ &= \frac{\partial}{\partial y}(\rho \bar{u}_x \bar{u}_y) + \frac{\partial}{\partial y}(\rho \bar{u}_x \bar{u}'_y) + \frac{\partial}{\partial y}(\rho \bar{u}'_x \bar{u}_y) + \frac{\partial}{\partial y}(\overline{\rho u'_x u'_y}). \end{aligned} \quad (10.7.4)$$

Because of (10.6.4), the second and third terms in the second line of (10.7.4) are equal to zero, leaving the simplified expression

$$\frac{\partial}{\partial y}(\overline{\rho u_x u_y}) = \frac{\partial}{\partial y}(\rho \bar{u}_x \bar{u}_y) + \frac{\partial}{\partial y}(\overline{\rho u'_x u'_y}). \quad (10.7.5)$$

Working in a similar fashion with the other terms on the left-hand side of Cauchy's equation of motion, we derive an equation of motion for the time-average variables

$$\rho \left(\frac{\partial \bar{\mathbf{u}}}{\partial t} + \bar{\mathbf{u}} \cdot \nabla \bar{\mathbf{u}} \right) = \nabla \cdot \bar{\boldsymbol{\sigma}} - \nabla \cdot \boldsymbol{\sigma}^R + \rho \mathbf{g}, \quad (10.7.6)$$

or

$$\frac{\partial (\rho \bar{\mathbf{u}})}{\partial t} + \nabla \cdot (\rho \bar{\mathbf{u}} \bar{\mathbf{u}}) = \nabla \cdot \bar{\boldsymbol{\sigma}} - \nabla \cdot \boldsymbol{\sigma}^R + \rho \mathbf{g}. \quad (10.7.7)$$

where $\boldsymbol{\sigma}^R$ is the Reynolds stress tensor with components

$$\sigma_{ij}^R = \overline{\rho u'_i u'_j}, \quad (10.7.8)$$

expressing the transfer of momentum from the i to the j direction, and vice versa, by turbulence fluctuations.

Phenomenological theories seek to establish a relationship between the Reynolds stresses and the structure of the time-averaged flow. Once this is done, the averaged equation of motion (10.7.6) or (10.7.7) can be solved subject to the continuity equation

$$\nabla \cdot \bar{\mathbf{u}} = 0, \quad (10.7.9)$$

to produce the velocity distribution in a turbulent flow.

10.7.2 Prandtl's mixing length model

Prandtl developed a theoretical model that relates the Reynolds stresses to the velocity profile of the mean flow. Motivation for this model is provided by a tentative analogy between eddy motion in a turbulent flow and molecular motion in a gas. The derivation is analogous to that discussed in Section 4.4.5 concerning the fluid viscosity.

Consider unidirectional turbulent shear flow along the x axis with mean velocity profile $\bar{u}_x = U(y)$, as illustrated in figure 10.7.1. Suppose now that, because of the turbulent motion, a small fluid parcel with volume δV_p initially located at $y = y_1$ is displaced to the position $y = y_2$, where it travels in the streamwise direction with the new local velocity. The accompanying change in the x component of the momentum is

$$\begin{aligned} \delta M_x &= \rho \delta V_p [u_x(y = y_2, t) - u_x(y = y_1, t)] \\ &\simeq \rho \delta V_p [U(y = y_2) - U(y = y_1)]. \end{aligned} \quad (10.7.10)$$

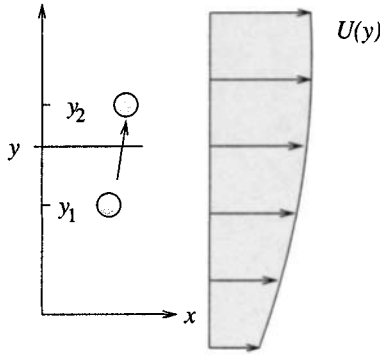


Figure 10.7.1 Profile of turbulent shear flow along the x axis, illustrating the random displacement of a fluid parcel by a distance that is comparable to Prandtl's mixing length.

Because the turbulent fluctuations have been assumed small, the total velocity has been approximated with the mean velocity to yield the expression shown in the second line of (10.7.10).

Consider next the transport of momentum across a horizontal line at the y elevation shown in figure 10.7.1. During a small period of time Δt , all parcels residing within a layer of thickness $u_y(y, t) \Delta t$ adjacent to this line will cross the line to find themselves on the other side. The transport of x momentum over a horizontal length Δx due to this motion is

$$\begin{aligned} \sum \delta M_x &\simeq \rho [U(y = y_2) - U(y = y_1)] \sum \delta V_p \\ &\simeq \rho (y_2 - y_1) \left(\frac{\partial U}{\partial y}\right)_y \sum \delta V_p. \end{aligned} \quad (10.7.11)$$

Setting $\sum \delta V_p = u_y(y, t) \Delta t \Delta x$, we obtain

$$\sum \delta M_x \simeq \rho u_y(y, t) (y_2 - y_1) \left(\frac{\partial U}{\partial y}\right)_y \Delta t \Delta x. \quad (10.7.12)$$

Averaging now this expression over all time intervals Δt , we find

$$\overline{\sum \delta M_x} \simeq \overline{\rho u_y(y, t) (y_2 - y_1) \left(\frac{\partial U}{\partial y}\right)_y \Delta t \Delta x}. \quad (10.7.13)$$

According to Newton's second law of motion, this averaged transfer of momentum is tantamount to a force pointing in the x direction, expressed by the Reynolds shear stress σ_{xy}^R . Setting

$$\frac{\overline{\sum \delta M_x}}{\Delta t} = \sigma_{xy}^R \Delta x, \quad (10.7.14)$$

we obtain

$$\sigma_{xy}^R = \rho \overline{u_y(y, t) \Delta y} \left(\frac{\partial U}{\partial y} \right)_y, \quad (10.7.15)$$

where we have defined $\Delta y \equiv y_2 - y_1$.

The next key step is the scaling

$$\overline{u_y(y, t) \Delta y} \simeq \sqrt{\overline{u_y^2}} l_P \simeq \left| \frac{\partial U}{\partial y} \right| l_P^2, \quad (10.7.16)$$

where l_P is Prandtl's mixing length. Substituting (10.7.16) into (10.7.15), we obtain the constitutive equation

$$\sigma_{xy}^R(y) = \rho l_P^2 \left| \frac{\partial U}{\partial y} \right| \left(\frac{\partial U}{\partial y} \right). \quad (10.7.17)$$

The product of the first three terms on the right-hand side of (10.7.17) plays the role of an eddy viscosity first introduced by Boussinesq.

If the reader is overwhelmed by uneasiness regarding the physical relevance of the various steps involved in the preceding derivation, she is not alone. Constitutive relations similar to that shown in (10.7.17) have been proposed by several authors on the basis of tentative analogies and laboratory observation.

Logarithmic law in the outer layer of wall-bounded shear flow

As an application, we use Prandtl's mixing length model expressed by equation (10.7.17) to deduce the functional form of the velocity profile in a wall-bounded shear flow, away from the viscous sublayer and the buffer zone. Assuming that the sign of $\partial U / \partial y$ is positive, neglecting the viscous shear stress $\mu \partial U / \partial y$ in comparison to the Reynolds shear stress, and ignoring the variation of the shear stress in the y direction due to a streamwise pressure drop, we find

$$\sigma_{xy}^R(y) = \rho l_P^2 \left(\frac{\partial U}{\partial y} \right)^2 = \tau_W, \quad (10.7.18)$$

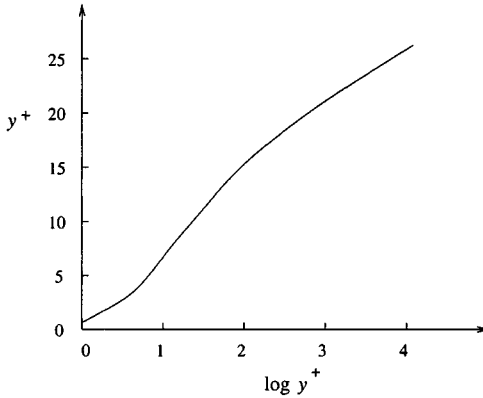


Figure 10.7.2 Wall-bounded turbulent shear flow: schematic illustration of the distribution of the mean velocity in the dimensionless variables defined in equations (10.7.23).

where τ_W is the wall shear stress. Rearranging (10.7.18), we obtain

$$l_P^2 \left(\frac{\partial U}{\partial y} \right)^2 = \frac{\tau_W}{\rho} \equiv u_*^2, \quad (10.7.19)$$

where u_* is the *friction velocity*.

Next, we set the Prandtl mixing length l_P proportional to the distance from the wall, setting $l_P = \kappa y$, where κ is von Kármán's dimensionless constant. For flow in a circular tube, measurements suggest that $\kappa \simeq 0.36$. Substituting the relation $l_P = \kappa y$ into (10.7.19), taking the square root of the emerging equation, and rearranging, we find

$$\frac{\partial U}{\partial y} = \frac{u_*}{\kappa y}. \quad (10.7.20)$$

Integrating both sides of (10.7.20) with respect to y , we find the logarithmic relationship

$$\frac{U(y)}{u_*} = \frac{1}{\kappa} \log y + A, \quad (10.7.21)$$

where A is a dimensionless constant.

In dimensionless variables, expression (10.7.21) takes the form

$$u^+ = \frac{1}{\kappa} \log y^+ + B, \quad (10.7.22)$$

where B is a dimensionless constant, and we have defined

$$u^+ \equiv \frac{\bar{u}_x(y)}{u_*} = \frac{U(y)}{u_*}, \quad y^+ \equiv \frac{y u_*}{\nu}, \quad (10.7.23)$$

Laboratory measurements have shown that equation (10.7.22) with $B=3.6$ describes well the velocity profile for $y^+ > 26$, as illustrated in figure 10.7.2. In the viscous sublayer attached to the wall, laboratory data suggest the linear relation $u^+ = y^+$, for $0 < y^+ < 5$. In the buffer zone, extending over $5 < y^+ < 26$, a more involved relation is required.

10.7.3 Correlations

One way of extracting information on the small-scale structure of a turbulent flow is by means of space-time correlations. Consider the i th component of the fluctuating velocity at the point \mathbf{x}_1 at time t , and the j th component of the fluctuating velocity at the point \mathbf{x}_2 at time $t + \tau$, where τ is the time delay. The corresponding second-order space-time correlation is defined as

$$\begin{aligned} R_{ij}(\mathbf{x}_1, \mathbf{x}_2, t, \tau) &\equiv \overline{u'_i(\mathbf{x}_1, t) u'_j(\mathbf{x}_2, t + \tau)} \\ &= \frac{1}{t_0} \int_{t-t_0/2}^{t+t_0/2} u'_i(\mathbf{x}_1, t + t') u'_j(\mathbf{x}_2, t + \tau + t') dt'. \end{aligned} \quad (10.7.24)$$

Two special correlations are of particular interest: the spatial correlation corresponding to $\tau = 0$, and the time-delayed correlation arising when the points \mathbf{x}_1 and \mathbf{x}_2 coincide.

Taylor's frozen-field hypothesis provides us with a relationship between the time-delayed and the spatial correlation: in a low-intensity turbulent flow, the mean velocity sweeps the turbulence so fast that the eddies do not evolve significantly during the time it takes them to cross a fixed point in space; that is, the velocity vector field appears to be frozen in time. If the mean velocity is in the direction of the x axis, we may write

$$\begin{aligned} R_{ij}(\mathbf{x}_1, \mathbf{x}_2, t, \tau) &\simeq R_{ij}(\mathbf{x}_1, \mathbf{x}_1 + \Delta x \mathbf{e}_x, t, \tau) \\ &= R_{ij}(\mathbf{x}_1, \mathbf{x}_1, t, \tau = -\frac{\Delta x}{\bar{u}_x}), \end{aligned} \quad (10.7.25)$$

where \mathbf{e}_x is the unit vector along the x axis. This expression provides us with a convenient method of obtaining the spatial correlation in terms of the more easily measured time-delayed counterparts.

The usefulness of the second-order correlations lie in their ability to produce information on the geometrical structure and dynamics of eddy motion in a turbulent flow. As the point \mathbf{x}_2 tends to the point \mathbf{x}_1 , the local fluid motions are coordinated and the correlations are significant. As the points \mathbf{x}_1 and \mathbf{x}_2 are moved far apart, the fluid motions become independent or decorrelated, and the correlations decay to zero.

In the case of homogeneous turbulent flow, the correlations depend on the vectorial distance between the points \mathbf{x}_1 and \mathbf{x}_2 , but not on the actual location of the two points; to signify this, we write $R_{ij}(\mathbf{x}_2 - \mathbf{x}_1, t, \tau)$. In the case of isotropic turbulent flow, the correlations depend on the scalar distance between the two points \mathbf{x}_1 and \mathbf{x}_2 ; to signify this, we write $R_{ij}(|\mathbf{x}_2 - \mathbf{x}_1|, t, \tau)$.

Evolution equations for the second-order correlations may be derived departing from the Navier-Stokes equation. Just as the averaged Navier-Stokes equation (10.7.6) involves the Reynolds stresses, the evolution equations for the second-order correlations involve third-order correlations defined as the time averages of products of three scalar fluctuating variables. An important field of study of turbulent flow seeks to relate high-order correlations to the structure of the mean flow, thereby achieving closure.

Problem

Problem 10.7.1 Deissler correlation.

Deissler replaced Prandtl's constitutive equation (10.7.17) with the following more involved equation suggested by laboratory measurements,

$$\sigma_{xy}^R(y) = n^2 \rho y U(y) \left(\frac{\partial U}{\partial y} \right) \left[1 - \exp\left(-\frac{n^2 U y}{\nu}\right) \right], \quad (10.7.26)$$

where $n = 0.124$ is an experimentally determined dimensionless constant. Substitute this relation into (10.7.18), integrate to compute the velocity profile, and then compare the oprofile with that shown in (10.7.22).

Computer problem

Problem c.10.7.1 *Stratified shear flow.*

Compute, plot, and discuss the form of the time-delayed correlation of the velocity components and temperature recorded in file *keller.dat* in directory *13_turbo/stats* of *FDLIB*.

Chapter 11

Vortex Motion

- 11.1 Vorticity and circulation in two-dimensional flow
- 11.2 Motion of point vortices
- 11.3 Two-dimensional flow with distributed vorticity
- 11.4 Vorticity, circulation,
and three-dimensional flow induced by vorticity
- 11.5 Axisymmetric flow induced by vorticity
- 11.6 Three-dimensional vortex motion

Flows at high Reynolds numbers tend to develop islands of concentrated vorticity, concisely called vortices, embedded in a low-vorticity or virtually irrotational ambient fluid. The velocity field may be decomposed into two constituents: an irrotational component prevailing in the absence of the vortices, and a rotational component associated with the localized vorticity distribution. The latter may be expressed in the convenient form of an integral over the volume occupied by the vortices, involving the vorticity distribution. At high Reynolds numbers, viscous forces are insignificant away from flow boundaries, and the vortices evolve according to simplified rules dictated by the vorticity transport equation for inviscid fluids. In this chapter, we derive the integral representation of the velocity in terms of the vorticity, discuss the simplified laws governing vortex motion in a flow with negligible viscous forces, and develop numerical methods for describing the dynamics of a prototypical class of vortex flows with specifically chosen vorticity distributions. The study of these flows will allow us to develop insights into the dynamics of more high-Reynolds-number flows characterized by vortex interactions.

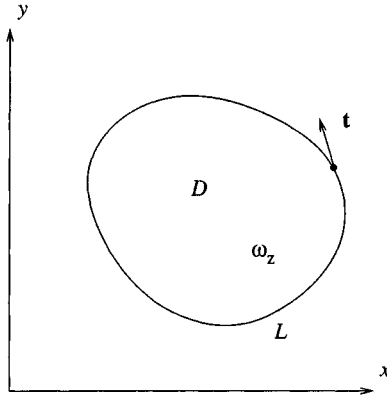


Figure 11.1.1 A closed loop in the xy plane, denoted by L , enclosing the area D . The circulation around the loop is equal to the areal integral of the strength of the vorticity, ω_z , over D .

11.1 Vorticity and circulation in two-dimensional flow

In Section 3.7, we defined the circulation around a closed loop in a two-dimensional flow as the line integral of the tangential component of the velocity with respect to arc length around the loop, as shown in equation (3.7.9), repeated here for ready reference,

$$C \equiv \oint_L u_t \, dl = \oint_L \mathbf{u} \cdot \mathbf{t} \, dl, \quad (11.1.1)$$

where L denotes the loop, $dl = \sqrt{dx^2 + dy^2}$ is the differential of the arc length around the loop, and the unit tangent vector \mathbf{t} points in the counterclockwise direction along L , as illustrated in figure 11.1.1.

If the loop is *reducible*, that is, if it can be shrunk to a point without crossing flow boundaries or singular points, we may use Stokes's circulation theorem to express the circulation around the loop as the areal integral of the strength of the vorticity over the area D enclosed by the loop, as shown in equation (3.7.10), repeated here for ready reference,

$$C = \int_D \omega_z \, dx \, dy, \quad (11.1.2)$$

(problem 11.1.1). With this expression as a point of departure, and using the vorticity transport equation discussed in Section 6.6, we shall now derive an important theorem that considerably facilitates the study of two-dimensional vortex flow.

Consider a reducible *material* loop consisting of a fixed collection of point particles with a permanent identity, as illustrated in figure 11.1.1. The fluid enclosed by the loop also has a permanent identity; that is, it is composed of the same collection of point particles at all times. The vorticity transport equation for a flow with uniform density and negligible viscous forces requires that the point particles maintain their vorticity as they move about the domain of flow, $D\omega_z/Dt = 0$, as shown in equation (6.6.5), where D/Dt is the material derivative. Moreover, because the fluid has been assumed incompressible, the area $dx dy$ occupied by an infinitesimal patch of fluid located inside the loop remains constant in time, $D(dx dy)/Dt = 0$.

Combining these arguments, we find that the integral on the right-hand side of (11.1.2) remains constant in time. Formally, we write

$$\begin{aligned} \frac{dC}{dt} &= \frac{d}{dt} \int_D \omega_z dx dy = \int_D \frac{D(\omega_z dx dy)}{Dt} \\ &= \int_D \frac{D\omega_z}{Dt} dx dy + \int_D \omega_z \frac{D(dx dy)}{Dt} = 0. \end{aligned} \quad (11.1.3)$$

We have found that, when viscous forces are negligible, the circulation around a reducible material loop remains constant in time. In Section 11.4, we shall see that the circulation around an irreducible loop also remains constant in time, and thus the vorticity of point particles residing inside any loop is preserved during the motion.

Problem

Problem 11.1.1 *Stokes's circulation theorem.*

Prove that the circulation around a reducible loop can be expressed in terms of the vorticity, as shown in equation (11.1.2). *Hint:* Apply Gauss's divergence theorem stated in equation (2.6.20) for the vector functions $\mathbf{h} = (u_y, 0)$ and $\mathbf{h} = (0, u_x)$.

11.2 Motion of point vortices

We begin the study of vortex dynamics by considering the motion of point vortices in a flow with negligible viscous forces. Expressions (3.7.1) provide us with the plane polar component of the velocity induced at the point $\mathbf{x} = (x, y)$ by a point vortex with strength κ located at the point $\mathbf{x}_0 = (x_0, y_0)$. The corresponding Cartesian components of the velocity are given by

$$\begin{aligned} u_x(x, y) &= -\frac{\kappa}{2\pi} \frac{y - y_0}{(x - x_0)^2 + (y - y_0)^2}, \\ u_y(x, y) &= \frac{\kappa}{2\pi} \frac{x - x_0}{(x - x_0)^2 + (y - y_0)^2}. \end{aligned} \quad (11.2.1)$$

The denominator on the right-hand sides of equations (11.2.1) is the square of the distance of the field point \mathbf{x} from the location of the point vortex \mathbf{x}_0 . Since the numerator is a linear function of the difference in the x or y coordinates, the velocity due to a point vortex decays like the inverse of the distance from the point vortex, in agreement with (3.7.1).

One may readily verify by straightforward differentiation that the strength of the vorticity $\omega_z \equiv \partial u_y / \partial x - \partial u_x / \partial y$ vanishes everywhere in the flow except at the location of the point vortex where the right-hand sides of equations (11.2.1) and their derivatives are not defined. Dirac's delta function in two dimensions provides us with a convenient means of expressing this singular vorticity distribution in compact form using the concept of generalized functions.

11.2.1 Dirac's delta function in a plane

To construct the Dirac delta function in two dimensions, we introduce a family of test functions $g_\lambda(x, y)$ parametrized by the variable λ . The test functions are radially symmetric with respect to a specified point (x_0, y_0) , that is, they depend only on the distance between the field point \mathbf{x} and the chosen point \mathbf{x}_0 ; they peak at the point (x_0, y_0) ; they rapidly decay to zero with distance from this point; and their areal integral over the entire xy plane is equal to unity.

One such family of test functions is given by

$$g_\lambda(r) = \frac{\lambda}{\pi} \exp(-\lambda r^2), \quad (11.2.2)$$

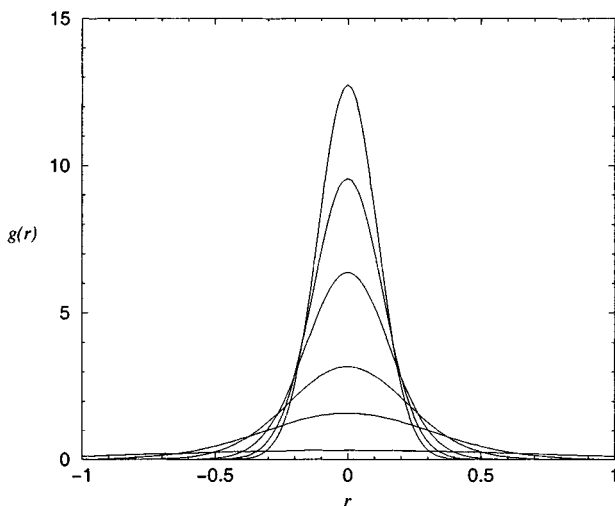


Figure 11.2.1 A family of test functions described by equation (11.2.2), for $\lambda = 1, 5, 10, 20, 30,$ and 40 . In the limit as λ tends to infinity, we obtain Dirac's delta function in two dimensions.

where $r = \sqrt{(x - x_0)^2 + (y - y_0)^2}$; the graphs of these functions are displayed in figure 11.2.1. Taking the limit as λ tends to infinity, whereupon the support of these functions shrinks down to zero, we obtain Dirac's delta function in the xy plane, denoted by $\delta_2(x - x_0, y - y_0)$. By construction then, $\delta_2(x - x_0, y - y_0)$ is endowed with the following properties:

1. $\delta_2(x - x_0, y - y_0)$ vanishes everywhere except at the point $x = x_0$ and $y = y_0$, where it takes an infinite value.
2. The integral of the delta function over an area D that contains the point (x_0, y_0) is equal to unity

$$\int_D \delta_2(x - x_0, y - y_0) dx dy = 1. \quad (11.2.3)$$

This property requires that the delta function in two dimensions has units of inverse squared length.

3. The integral of the product of an arbitrary function $f(x, y)$ and the delta function over an area D that contains the point (x_0, y_0)

is equal to value of the function at the singular point,

$$\int_D \delta_2(x - x_0, y - y_0) f(x, y) dx dy = f(x_0, y_0). \quad (11.2.4)$$

Note that identity (11.2.3) arises from (11.2.4) by setting $f(x, y)$ equal to unity. The integral of the product of an arbitrary function $f(x, y)$ and the delta function over an area D that does *not* contain the point (x_0, y_0) is equal to zero.

11.2.2 Vorticity associated with a point vortex

The vorticity distribution associated with the velocity field (11.2.1) may now be expressed in terms of the delta function in the compact form

$$\omega_z(x, y) = \kappa \delta_2(x - x_0, y - y_0) = \kappa \delta_2(\mathbf{x} - \mathbf{x}_0). \quad (11.2.5)$$

The strength of the point vortex, κ , has units of circulation, velocity multiplied by length, and the delta function has units of inverse length squared; their product has units of velocity over length, which is consistent with the definition of the vorticity in terms of spatial derivatives of the velocity.

Reviewing the process by which the delta function arose from a family of smooth functions with increasingly narrow supports and high peaks, we interpret a point vortex as an idealized vortex structure arising in the limit as the size of a compact vortex region in the xy plane tends to zero, while the circulation around the vortex is held constant.

It is instructive to confirm equation (3.7.11), stating that the circulation around a closed loop that encloses a point vortex is equal to the strength of the point vortex. Substituting (11.2.5) into the integrand on the right-hand side of (11.1.2), and using property (11.2.3), we find $C = \kappa$.

11.2.3 Evolution of the point vortex strength

When viscous forces are negligible, the circulation around any material loop that encloses a point vortex, and therefore the strength of the point vortex, must remain constant in time,

$$\frac{d\kappa}{dt} = 0. \quad (11.2.6)$$

Thus, the point vortex maintains its strength as it moves with the fluid velocity in the domain of flow.

11.2.4 Velocity of a point vortex

The computation of the fluid velocity at the position of a point vortex is prohibited by the singular nature of the right-hand side of (11.2.1). To circumvent this difficulty, we observe that, although the fluid in the vicinity of a point vortex spins about the point vortex with a velocity that increases like the inverse of the distance from the point vortex, radial symmetry prevents it from exhibiting a net translational motion. This observation suggests that the *self-induced* velocity of a point vortex vanishes; that is, a point vortex is convected with a velocity other than that associated with its own vorticity distribution. For example, a point vortex embedded in uniform flow simply translates with the velocity of the uniform flow.

11.2.5 Motion of a collection of point vortices

A collection of N point vortices move under the influence of their mutually-induced velocity. The rate of change of position of the i th point vortex, (X_i, Y_i) , is governed by the differential equations

$$\begin{aligned} \frac{dX_i}{dt} &= - \sum_{j=1, \dots, i-1, i+1, \dots, N} \frac{\kappa_j}{2\pi} \frac{Y_i - Y_j}{(X_i - X_j)^2 + (Y_i - Y_j)^2}, \\ \frac{dY_i}{dt} &= \sum_{j=1, \dots, i-1, i+1, \dots, N} \frac{\kappa_j}{2\pi} \frac{X_i - X_j}{(X_i - X_j)^2 + (Y_i - Y_j)^2}, \end{aligned} \quad (11.2.7)$$

for $i = 1, 2, \dots, N$. Note that the sum over j excludes the term $j = i$ to bypass the vanishing self-induced contribution. Equation (11.2.6) requires that the strength of each point vortex remain constant during the motion.

Equations (11.2.7) comprise a system of $2N$ first-order differential equations for the point vortex coordinates, (X_i, Y_i) . Having specified

the initial position, we may compute the subsequent motion using a standard method for solving ordinary equations, such as the explicit modified Euler method discussed in earlier sections.

11.2.6 Presence of boundaries

When the domain of flow is bounded by impermeable surfaces, the right-hand sides of equations (11.2.1) and (11.2.6) must be modified with the addition of a complementary flow whose purpose is to ensure the satisfaction of the no-penetration boundary condition. For simple boundary geometries, the complementary flow may be identified with the flow induced by point vortices located at image positions.

Point vortex above a plane wall

The complementary flow of a point vortex above a plane wall placed at $y = w$ is generated by reflecting the point vortex with respect to the wall. If a primary point vortex with strength κ is located at the point (x_0, y_0) , then an image point vortex with strength $-\kappa$ is located at $(x_0, 2w - y_0)$. The velocity field induced by the primary point vortex and its image is given by

$$\begin{aligned} u_x(x, y) &= -\frac{\kappa}{2\pi} \left[\frac{y - y_0}{(x - x_0)^2 + (y - y_0)^2} - \frac{y - 2w + y_0}{(x - x_0)^2 + (y - 2w + y_0)^2} \right], \\ u_y(x, y) &= \frac{\kappa}{2\pi} \left[\frac{x - x_0}{(x - x_0)^2 + (y - y_0)^2} - \frac{x - x_0}{(x - x_0)^2 + (y - 2w + y_0)^2} \right]. \end{aligned} \quad (11.2.8)$$

The streamline pattern induced by the vortex pair is illustrated in figure 11.2.2(a), and a subroutine that evaluates the velocity field is included in subdirectory *09_vortex/pv* of *FDLIB*.

The x component of the velocity induced by the image vortex at the location of the primary vortex is $v_x \equiv u(x_0, y_0) = \kappa/[4\pi(y_0 - w)]$, and the y component vanishes, $v_y \equiv u_y(x_0, y_0) = 0$. Thus, the primary point vortex translates parallel to the wall with constant velocity.

Point vortex inside or outside a circular cylinder

The complementary flow of a point vortex located inside or outside a circular cylinder of radius a centered at the point (x_c, y_c) is generated

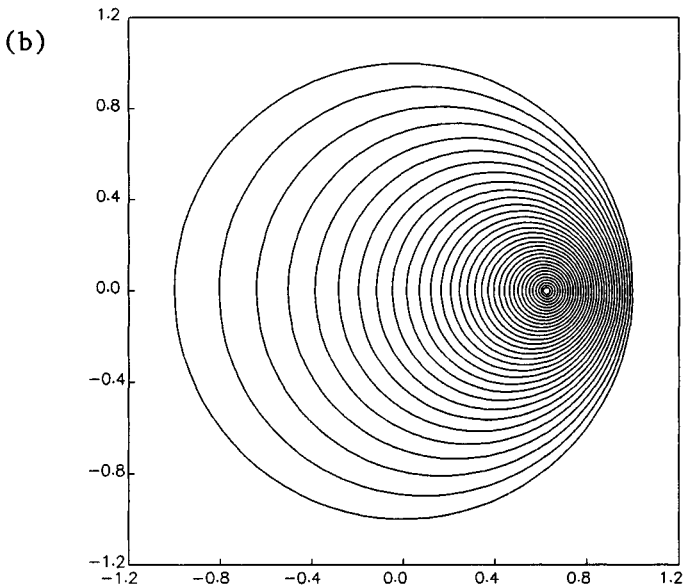
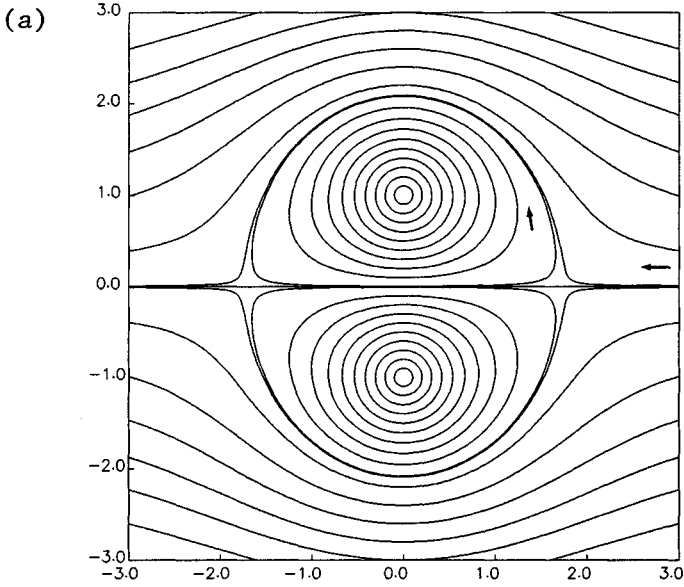


Figure 11.2.2 Streamline pattern of the flow due to (a) a pair of point vortices with opposite strength, (b) a point vortex inside a circular cylinder; (c) a point vortex outside a circular cylinder.

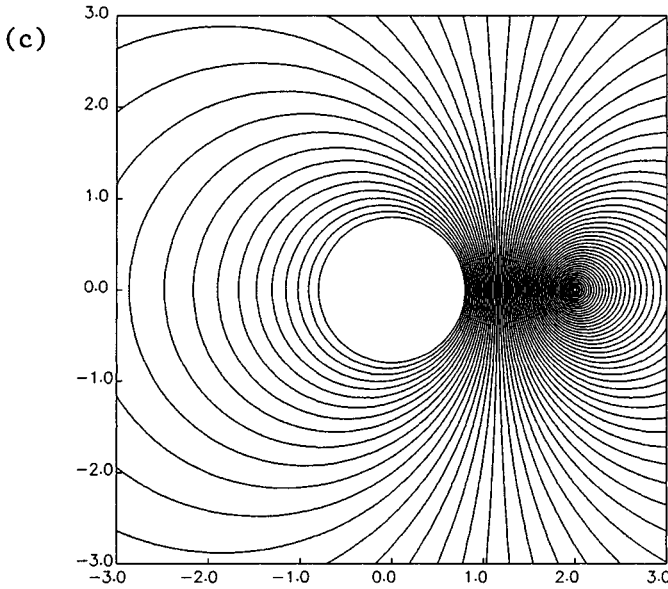


Figure 11.2.2 Continued.

by an image point vortex located at the inverse point of the primary point vortex with respect to the cylinder. If a primary point vortex with strength κ is located at (x_0, y_0) , then an image point vortex with strength $-\kappa$ is located at

$$x_0^I = x_c + (x_0 - x_c) \frac{a^2}{d^2}, \quad y_0^I = y_c + (y_0 - y_c) \frac{a^2}{d^2}, \quad (11.2.9)$$

where $d = \sqrt{(x_0 - x_c)^2 + (y_0 - y_c)^2}$ is the distance of the primary point vortex from the center of the cylinder. The velocity field induced by the primary point vortex and its image is given by

$$u_x(x, y) = -\frac{\kappa}{2\pi} \left[\frac{y - y_0}{(x - x_0)^2 + (y - y_0)^2} - \frac{y - y_0^I}{(x - x_0^I)^2 + (y - y_0^I)^2} \right],$$

$$u_y(x, y) = \frac{\kappa}{2\pi} \left[\frac{x - x_0}{(x - x_0)^2 + (y - y_0)^2} - \frac{x - x_0^I}{(x - x_0^I)^2 + (y - y_0^I)^2} \right]. \quad (11.2.10)$$

The streamline pattern induced by the vortex pair is illustrated in figure 11.2.2 (b, c), and a subroutine that evaluates the velocity field is included in subdirectory *09_vortex/pv* of *FDLIB*.

Examining the velocity induced by the image point vortex at the location of the primary vortex, we find that the latter rotates around the center of the cylinder in the direction of the polar angle θ measured around the center of the cylinder in the counterclockwise direction, with velocity

$$v_\theta = \frac{\kappa}{2\pi} \frac{d}{a^2 - d^2}. \quad (11.2.11)$$

11.2.7 A periodic array of point vortices

Consider a periodic array of a point vortices with identical strengths deployed along the x axis and separated by the distance a , as illustrated in figure 11.2.3. The m th point vortex is located at the position $x_m = x_0 + ma$, $y_m = y_0$, where (x_0, y_0) is the position of a randomly chosen point vortex labelled 0, and m is an integer. If we attempt to compute the velocity induced by the array simply by summing the individual contributions, we will encounter divergent infinite sums.

To overcome this difficulty, we consider the stream function corresponding to the velocity field induced by the individual point vortices, defined by the equations $u_x = \partial\psi/\partial y$ and $u_y = -\partial\psi/\partial x$, and express it in the form

$$\psi_0(x, y) = -\frac{\kappa}{2\pi} \ln \frac{r_0}{a}, \quad \psi_m(x, y) = -\frac{\kappa}{2\pi} \ln \frac{r_m}{|m|a}, \quad (11.2.12)$$

for $m = \pm 1, \pm 2, \dots$, where $r_m^2 \equiv (x - x_m)^2 + (y - y_m)^2$ is the square of the distance of the field point (x, y) from the location of the m th point vortex. The denominators of the fractions in the arguments of the logarithms on the right-hand sides of (11.2.12) have been chosen judiciously to facilitate the forthcoming algebraic manipulations.

It is important to observe that, as m tends to $\pm\infty$, the fraction on the right-hand side of the second of equations (11.2.12) tends to unity and its logarithm tends to vanish, thereby ensuring that remote point vortices make small contributions. In contrast, if the denominators had not been included, remote point vortices would make contributions that are proportional to the logarithm of the distance between a point vortex and the point (x, y) where the stream function is evaluated.

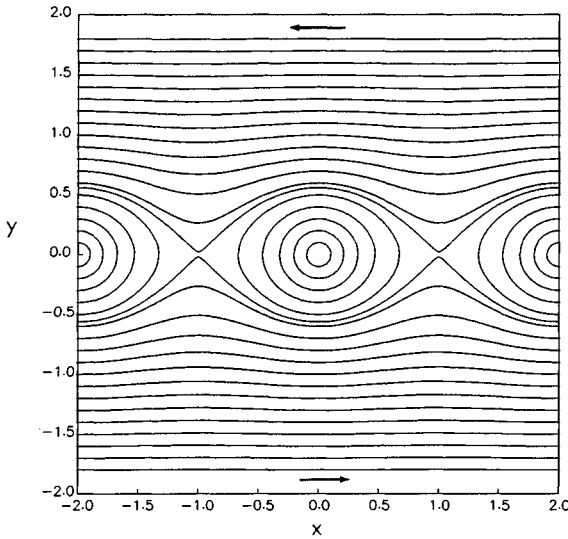


Figure 11.2.3 Streamline pattern of the flow due to an infinite array of point vortices evenly-spaced along the x axis.

Next, we express the stream function due to the infinite array as the sum of (a) a constant expressed by the term after the first equal sign in equation (11.2.13), and (b) the individual stream functions stated in expressions (11.2.12), obtaining

$$\begin{aligned}
 \psi(x, y) &= -\frac{\kappa}{2\pi} \ln(\sqrt{2}\pi) + \sum_{m=-\infty}^{\infty} \psi_m(x, y) \\
 &= -\frac{\kappa}{2\pi} \ln \frac{\sqrt{2} \pi r_0}{a} - \frac{\kappa}{2\pi} \sum_{m=\pm 1, \pm 2, \dots} \ln \frac{r_m}{|m| a} \\
 &= -\frac{\kappa}{2\pi} \ln \left[\frac{\sqrt{2} \pi r_0}{a} \prod_{m=\pm 1, \pm 2, \dots} \frac{r_m}{|m| a} \right], \tag{11.2.13}
 \end{aligned}$$

where Π denotes the product. An identity allows us to compute the infinite product on the right-hand side of (11.2.13) in closed form, obtaining

$$\frac{\sqrt{2} \pi r_0}{a} \prod_{m=\pm 1, \pm 2, \dots} \frac{r_m}{|m| a} = \{ \cosh[k(y - y_0)] - \cos[k(x - x_0)] \}^{1/2}. \tag{11.2.14}$$

Substituting the right-hand side of (11.2.14) into (11.2.13), we derive the desired stream function

$$\psi(x, y) = -\frac{\kappa}{4\pi} \ln\{\cosh[k(y - y_0)] - \cos[k(x - x_0)]\}, \quad (11.2.15)$$

where $k = 2\pi/a$ is the wave number. Differentiating the right-hand side of (11.2.15) with respect to x or y , we obtain the corresponding velocity components

$$\begin{aligned} u_x(x, y) &= -\frac{\kappa}{2a} \frac{\sinh[k(y - y_0)]}{\cosh[k(y - y_0)] - \cos[k(x - x_0)]}, \\ u_y(x, y) &= \frac{\kappa}{2a} \frac{\sin[k(x - x_0)]}{\cosh[k(y - y_0)] - \cos[k(x - x_0)]}. \end{aligned} \quad (11.2.16)$$

The streamline pattern due to the periodic array illustrated in figure 11.2.3, and a subroutine that evaluates the velocity field is included in subdirectory *09.vortex/pv* of *FDLIB*.

Because of symmetry, the velocity at the location of one point vortex induced by all other point vortices vanishes, and the array is stationary. Far above or below the array, the x component of the velocity tends to the value $-\kappa/a$ or κ/a , while the y component vanishes at an exponential rate. This behavior renders the infinite array a reasonable model of the flow generated by the instability of a shear layer separating two streams that merge at different velocities. The Kelvin-Helmholtz instability causes the shear layer to roll up into compact vortices represented by the point vortices of the periodic array.

Motion of a collection of point vortices in periodic arrangement

The motion of a periodic collection of N point vortices, each repeated in the x direction with period a , is governed by the counterpart of equations (11.2.7) for periodic flow. Using the velocity field (11.2.16), we find

$$\begin{aligned} \frac{dX_i}{dt} &= - \sum_{j=1, \dots, i-1, i+1, \dots, N} \frac{\kappa_j}{2a} \frac{\sinh[k(Y_i - Y_j)]}{\cosh[k(Y_i - Y_j)] - \cos[k(X_i - X_j)]}, \\ \frac{dY_i}{dt} &= \sum_{j=1, \dots, i-1, i+1, \dots, N} \frac{\kappa_j}{2a} \frac{\sin[k(X_i - X_j)]}{\cosh[k(Y_i - Y_j)] - \cos[k(X_i - X_j)]}, \end{aligned} \quad (11.2.17)$$

for $i = 1, 2, \dots, N$. The sum over j excludes the term $j = i$ corresponding to the vanishing velocity induced by the host array. The strength of each point vortex remains constant during the motion.

11.2.8 A point vortex between two parallel walls

The image system for a point vortex placed between two parallel walls that are separated by the distance h , as illustrated in figure 11.2.4(a), consists of the reflections of the point vortex, and the reflections of the reflections of the point vortex with respect to both walls. The result is an image system consisting of two infinite periodic arrays of point vortices separated by the distance $2h$. One array contains the primary point vortex, and the second array contains the reflection of the primary array with respect to one of the walls. The strength of the point vortices in the second array is equal in magnitude and opposite in sign to that of the point vortices in the first array.

The stream function and velocity field may be deduced from expressions (11.2.15) and (11.2.16). A subroutine that evaluates the velocity is included in subdirectory *09_vortex/pv* of *FDLIB*.

11.2.9 A point vortex in a semi-infinite strip

The image system of a point vortex placed between two parallel walls that are separated by the distance h and intersect at a right angle a third plane wall, thereby forming a semi-infinite rectangular strip, as illustrated in figure 11.2.4(b), consists of the image system associated with the two parallel walls discussed in Section 11.2.8, and the reflection of the image system with respect to the intersecting wall. The strength of the reflected point vortices is the negative of that of their images. A subroutine that evaluates the velocity field is provided in subdirectory *09_vortex/pv* of *FDLIB*.

Problems

Problem 11.2.1 Dirac delta function in one dimension.

The Dirac delta function in one dimension, denoted by $\delta_1(x - x_0)$, is distinguished by the following properties:

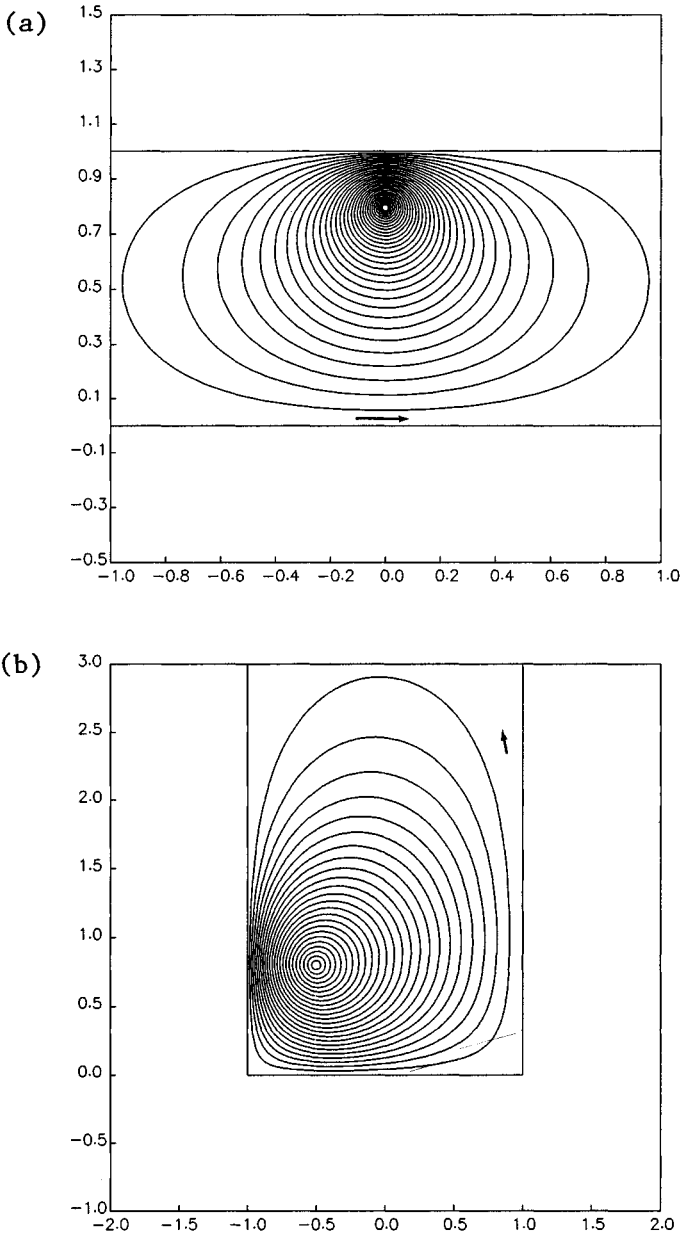


Figure 11.2.4 Streamline pattern of the flow due to (a) a point vortex placed between two parallel plane walls, and (b) a point vortex in a semi-infinite rectangular strip.

1. $\delta_1(x - x_0)$ vanishes everywhere except at the point $x = x_0$ where it becomes infinite.
2. The integral of the delta function over an interval I that contains the point x_0 is equal to unity,

$$\int_I \delta_1(x - x_0) dx = 1. \quad (11.2.18)$$

This property reveals that the delta function in one dimension has units of inverse length.

3. The integral of the product of an arbitrary function $f(x)$ and the delta function over an interval I that contains the point x_0 is equal to value of the function at the singular point,

$$\int_D \delta_1(x - x_0) f(x) dx = f(x_0). \quad (11.2.19)$$

The integral of the product of an arbitrary function $f(x)$ and the delta function over an interval I that does *not* contain the point x_0 vanishes. Note that identity (11.2.18) arises from (11.2.19) by setting $f(x)$ equal to unity.

(a) Show that δ_1 arises from the family of test functions

$$q_\lambda(|x - x_0|) = \left(\frac{\lambda}{\pi}\right)^{1/2} \exp[-\lambda(x - x_0)^2], \quad (11.2.20)$$

in the limit as the parameter λ tends to infinity.

(b) Show that the test functions $g_\lambda(r)$ defined in (11.2.2) derive from the test functions q_λ defined in (11.2.20) as

$$g_\lambda(r) = q_\lambda(|x - x_0|) q_\lambda(|y - y_0|), \quad (11.2.21)$$

and explain why we may write

$$\delta_2(x - x_0, y - y_0) = \delta_1(x - x_0) \delta_1(y - y_0). \quad (11.2.22)$$

(c) Show that the integral of $\delta_1(x - x_0)$ is the *Heaviside* function that is equal to zero when $x < x_0$ or unity when $x > x_0$. Is there a corresponding Heaviside function in two dimensions?

Problem 11.2.2 *Dirac delta function in three dimensions.*

State the distinguishing properties of the Dirac delta function in three dimensions, and devise an appropriate family of test functions corresponding to those discussed in the text for the delta function in two dimensions.

Problem 11.2.3 *A point vortex near a corner.*

Show that the image flow associated with a point vortex located between two semi-infinite walls intersecting at right-angle is represented by three point vortices located at the reflections, and the reflection of the reflections of the primary vortex with respect to the two walls. Then introduce plane polar coordinates (r, θ) with origin at the apex and the walls located at $\theta = 0$ and $\pi/2$, and show that the primary point vortex moves along a path described by $r = c/\sin(2\theta)$, where the constant c is determined by the initial position.

Problem 11.2.4 *Point vortex between two parallel walls.*

Consider a point vortex between two parallel walls separated by the distance h . Show that the point vortex travels parallel to the walls with velocity

$$v = \frac{\kappa}{4h} \frac{\sinh(2kb)}{1 - \cos(2kb)}, \quad (11.2.23)$$

where $k = \pi/h$, and b is the distance of the point vortex from the upper or lower wall. Confirm that, in the limit as b tends to zero, v tends to the value $\kappa/(4\pi b)$ corresponding to a point vortex above a plane wall.

Problem 11.2.5 *Point vortex in a rectangular box.*

Discuss how the image system for a point vortex located in a semi-infinite rectangular strip discussed in Section 11.2.9 can be extended to describe flow in a rectangular box.

Computer problems

Problem c.11.2.1 *Motion of a polygonal collection of point vortices.*

Subdirectory `09_vortex/pvm` of *FDLIB* contains a program that simulates the motion of a collection of point vortices in an unbounded domain of flow.

Run the program to simulate the motion of a collection of N point vortices with identical strengths placed at the vertices of an N -sided

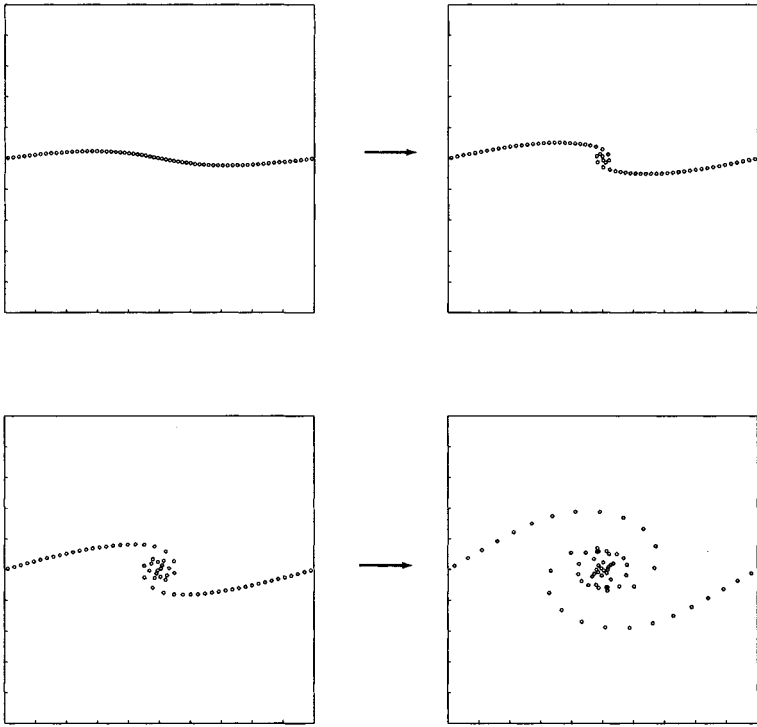


Figure 11.2.5 Stages in the evolution of a perturbed periodic array of point vortices, showing periodic roll up and eventual disorganized motion; one period is shown.

regular polygon of radius a . Carry out simulations for $N = 2, 4, 8,$ and 16 , and discuss the nature of the motion at long times.

Problem c.11.2.2 *Motion of a solitary collection of point vortices in a bounded domain.*

Subdirectory *09_vortex/pv* of *FDLIB* contains a collection of subroutines that generate the velocity field due to a point vortex in the presence of boundaries with various geometries. With these subroutines as a foundation class, modify the main program *09_vortex/pvm* discussed in problem c.11.2.1 to include the presence of a boundary of your choice. Compute the motion of a collection of point vortices of your choice, and discuss the nature of the motion.

Problem c.11.2.3 *Motion of a periodic collection of point vortices.*

Subdirectory *09_vortex/pvm.pr* of *FDLIB* contains a program that simulates the motion of a periodic row of point vortices perturbed from the planar configuration. The motion is known to suffer from severe numerical instabilities that cause the appearance of small-scale irregularities at an early stage of the motion. One way to suppress these instabilities, is to smooth out the coordinates of the point vortices by replacing them with weighted averages involving the neighbors. The five-point formula of Longuet-Higgins and Coker replaces the old positions with the new positions, as

$$f_i^{new} = \frac{1}{16} (-f_{i-2} + 4f_{i-1} + 10f_i + 4f_{i+1} - f_{i+2}), \quad (11.2.24)$$

where f stands for x or y . Results of a simulation with smoothing applied after each time step are shown in figure 11.2.5.

Run the program to compute the motion subject to an initial condition of your choice with and without smoothing, and discuss the nature of the motion in each case.

11.3 Two-dimensional flow with distributed vorticity

Broadening the scope of our discussion, we consider two-dimensional flow in the xy plane containing a non-infinitesimal region of concentrated vorticity embedded in a perfectly or nearly irrotational fluid, and subdivide the vortex region into a collection of N parcels with small areas δA_i , where $i = 1, 2, \dots, N$, as illustrated in figure 11.3.1. If $\omega_i \equiv \omega_z(\mathbf{x}_i)$ is the strength of the vorticity at the designated center of the i th parcel denoted by \mathbf{x}_i , then the strength of the parcel, defined as the integral of the vorticity over the area of the parcel, is approximately equal to $\kappa_i \equiv \omega_i \delta A_i$.

For the purpose of evaluating the velocity at a point in the flow, we now replace the parcels with point vortices located at the designated parcel centers. Using equations (11.2.1), we find that the velocity induced by the collection of the point vortices is given by

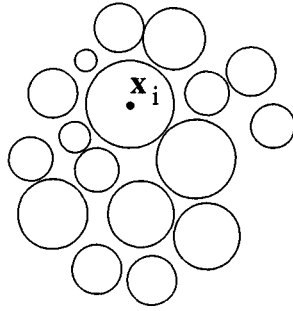


Figure 11.3.1 A vortex in a two-dimensional flow is discretized into small parcels, and each parcel is replaced by a point vortex located at the designated parcel center. As the number of parcels tends to infinity, the velocity induced by the point vortices is expressed by the integral representation (11.3.2).

$$\begin{aligned}
 u_x(x, y) &= -\frac{1}{2\pi} \sum_{i=1}^N \frac{y - y_i}{(x - x_i)^2 + (y - y_i)^2} \omega_i \delta A_i, \\
 u_y(x, y) &= \frac{1}{2\pi} \sum_{i=1}^N \frac{x - x_i}{(x - x_i)^2 + (y - y_i)^2} \omega_i \delta A_i.
 \end{aligned}
 \tag{11.3.1}$$

In the limit as the number of parcels N tends to infinity, the sums reduce to areal integrals, yielding an integral representation for the velocity in terms of the vorticity,

$$\begin{aligned}
 u_x(x, y) &= -\frac{1}{2\pi} \iint_{Vortex} \frac{y - y'}{(x - x')^2 + (y - y')^2} \omega_z(x', y') dx' dy', \\
 u_y(x, y) &= \frac{1}{2\pi} \iint_{Vortex} \frac{x - x'}{(x - x')^2 + (y - y')^2} \omega_z(x', y') dx' dy'.
 \end{aligned}
 \tag{11.3.2}$$

Equations (11.3.2) allow us to compute the velocity field associated with a specified distribution of vorticity in the xy plane. The stream function is given by the corresponding representation

$$\psi(x, y) = -\frac{1}{4\pi} \int \int_{V_{\text{ortex}}} \ln[(x - x')^2 + (y - y')^2] \omega_z(x', y') dx' dy'. \quad (11.3.3)$$

It is instructive to observe that the velocity field due to a point vortex arises by substituting the singular vorticity distribution (11.2.5) into expressions (11.3.2), and then using property (11.2.4) to evaluate the integrals. The delta function simply switches x' to x_0 and y' to y_0 , and thereby produces the flow due to a point vortex expressed by (11.2.1).

11.3.1 Vortex patches with uniform vorticity

Consider now a compact vortex with uniform vorticity Ω enclosed by the contour C , as illustrated in figure 11.3.2(a). Extracting the vorticity from the integral on the right-hand side of (11.3.3), we obtain the stream function

$$\psi(x, y) = -\frac{\Omega}{4\pi} \int \int_{V_{\text{ortex}}} \ln[(x - x')^2 + (y - y')^2] dx' dy'. \quad (11.3.4)$$

By definition, the x and y components of the velocity derive from the stream function as $u_x = \partial\psi/\partial y$ and $u_y = -\partial\psi/\partial x$. Differentiating both sides of (11.3.4) with respect to x or y , transferring the derivatives on the right-hand sides into the integrals, and then writing

$$\begin{aligned} \frac{\partial}{\partial x} \ln[(x - x')^2 + (y - y')^2] &= -\frac{\partial}{\partial x'} \ln[(x - x')^2 + (y - y')^2], \\ \frac{\partial}{\partial y} \ln[(x - x')^2 + (y - y')^2] &= -\frac{\partial}{\partial y'} \ln[(x - x')^2 + (y - y')^2], \end{aligned} \quad (11.3.5)$$

we obtain

$$\begin{aligned} u_x(x, y) &= \frac{\Omega}{4\pi} \int \int_{V_{\text{ortex}}} \frac{\partial}{\partial y'} \ln[(x - x')^2 + (y - y')^2] dx' dy', \\ u_y(x, y) &= -\frac{\Omega}{4\pi} \int \int_{V_{\text{ortex}}} \frac{\partial}{\partial x'} \ln[(x - x')^2 + (y - y')^2] dx' dy'. \end{aligned} \quad (11.3.6)$$

These manipulations have been motivated by our ability to convert the areal integral of the x or y derivative of a function over a region identified with the vortex, to a line integral along the boundary of the vortex. The conversion is done using the Gauss divergence theorem stated in equation (2.6.20) for an arbitrary vector function $\mathbf{h} = (h_x, h_y)$. Setting $h_x = 0$ and $h_y = \ln[(x - x')^2 + (y - y')^2]$, we find

$$u_x(x, y) = \frac{\Omega}{4\pi} \int_C \ln[(x - x')^2 + (y - y')^2] n_y(x', y') dl(x', y'), \quad (11.3.7)$$

where n_y is the y component of the unit vector normal to the vortex contour C pointing outward from the vortex, and dl is the differential arc length along C .

Working in a similar fashion for the y component of the velocity, we find

$$u_y(x, y) = -\frac{\Omega}{4\pi} \int_C \ln[(x - x')^2 + (y - y')^2] n_x(x', y') dl(x', y'). \quad (11.3.8)$$

To recast the component equations (11.3.7) and (11.3.8) into a unified vector form, we note that $n_x = t_y$ and $n_y = -t_x$, where $\mathbf{t} = (t_x, t_y)$ is the unit vector tangent to the vortex contour oriented in the counter-clockwise direction, as shown in figure 11.3.2(a). The velocity induced by the patch may now be expressed in the vector form

$$\mathbf{u}(x, y) = -\frac{\Omega}{4\pi} \int_C \ln[(x - x')^2 + (y - y')^2] \mathbf{t}(x', y') dl(x', y'). \quad (11.3.9)$$

A collection of patches

If the flow contains a collection of M vortex patches with uniform vorticity Ω_l , where $l = 1, 2, \dots, M$, then the velocity field arises by integrating around the contour of each individual patch, and then summing the contributions according to the generalized version of (11.3.9)

$$\mathbf{u}(x, y) = -\frac{1}{4\pi} \sum_{l=1}^M \Omega_l \int_{C_l} \ln[(x - x')^2 + (y - y')^2] \mathbf{t}(x', y') dl(x', y'), \quad (11.3.10)$$

where C_l is the contour of the l th patch.

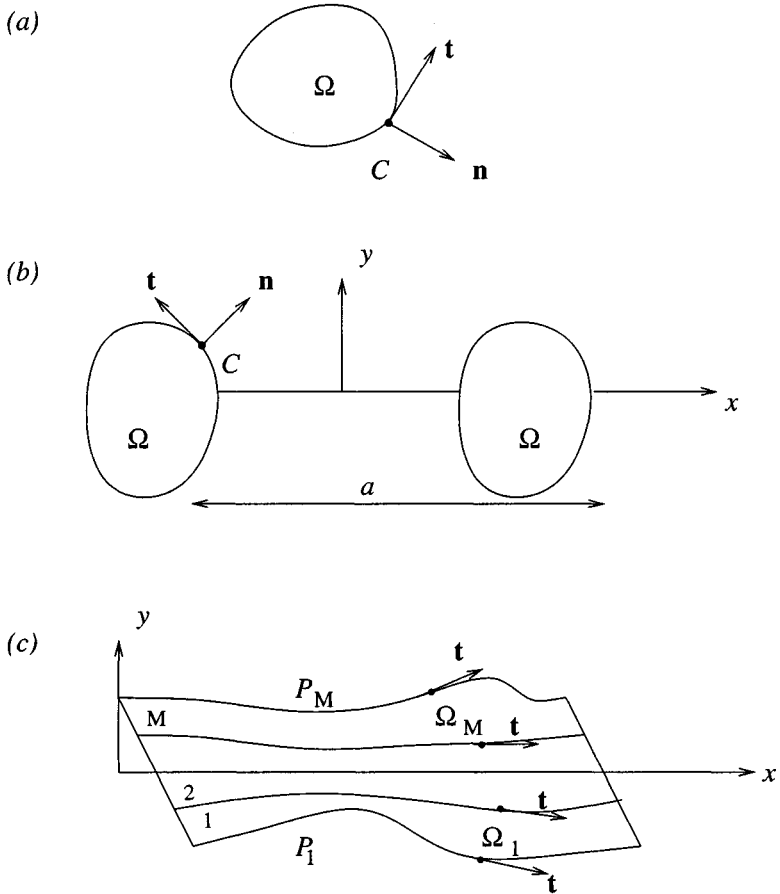


Figure 11.3.2 Patches of constant vorticity in the xy plane of a two-dimensional flow: (a) solitary, (b) periodic, and (c) in the form of periodic vortex layers.

Periodic patches

To develop a contour integral representation of the flow induced by a vortex patch that is repeated periodically in the x direction with period a , as illustrated in figure 11.3.2(b), we repeat the preceding analysis using the stream function of the flow induced by a periodic array of point vortices given in (11.2.15). Straightforward generalization provides us with the counterpart of (11.3.10) for a flow containing a collection of M periodic vortex patches,

$$\mathbf{u}(x, y) = -\frac{1}{4\pi} \sum_{l=1}^M \Omega_l \int_{C_l} \ln\{\cosh[k(y - y')] - \cos[k(x - x')]\} \\ \times \mathbf{t}(x', y') dl(x', y'), \quad (11.3.11)$$

where $k = 2\pi/a$ is the common wave number of the patches. For the configuration depicted in figure 11.3.2(b), $M = 1$.

Periodic layers

A judicious rearrangement of (11.3.11) allows us to obtain a contour integral representation of the flow induced by a number of adjacent periodic vortex layers with constant vorticity, as illustrated in figure 11.3.2(c). To develop this representation, we identify one period of a vortex layer with a periodic patch, and note that the contour integrals over periodic segments cancel. The result is the integral representation

$$\mathbf{u}(x, y) = -\frac{1}{4\pi} \sum_{l=1}^M (\Omega_l - \Omega_{l+1}) \\ \times \int_{P_l} \ln\{\cosh[k(y - y')] - \cos[k(x - x')]\} \mathbf{t}(x', y') dl(x', y'), \quad (11.3.12)$$

with the understanding that $\Omega_{M+1} = 0$, where P_l is one period of the l th contour, as illustrated in figure 11.3.2(c). A group of adjacent layers with gradually varying uniform vorticity is a model of a shear layer with smoothly varying vorticity separating two streams.

11.3.2 Contour dynamics

The vorticity transport equation (6.6.5) requires that, when viscous forces are insignificant, the vorticity inside a patch with uniform vorticity remain constant in time. To compute the evolution of the flow, it suffices then to pursue the motion of the vortex contour. This can be done by (a) tracing the contour with a collection of point particles, (b) evaluating the velocity at the position of the point particles using the contour integral representation, and (c) advancing the position of the point particles using a numerical method for integrating ordinary differential equations.

Consider a solitary vortex patch immersed in an infinite fluid, as depicted in figure 11.3.2(a). The numerical method involves the following steps:

1. Trace the vortex contour with $N + 1$ marker points located at $\mathbf{X}_i = (X_i, Y_i)$, where $i = 1, 2, \dots, N + 1$; points numbered 1 and $N + 1$ coincide.
2. Describe the shape of the contour by interpolation. In the simplest approach, the contour is approximated with the polygonal line connecting successive marker points, consisely called a *polyline*.
3. Compute the velocity of each marker point by evaluating the integral on the right-hand side of (11.3.9) for $x = X_i$ and $y = Y_i$, where $i = 1, 2, \dots, N$.

In the numerical method, the contour integral is replaced with the sum of integrals over the individual straight elements. Observing that the unit tangent vector over the j th element is constant and equal to $\mathbf{t}^{(j)} = \frac{1}{\Delta l_j}(\mathbf{X}_{j+1} - \mathbf{X}_j)$, where Δl_j is the element length, we write

$$\mathbf{u}(X_i, Y_i) \simeq -\frac{\Omega}{4\pi} \sum_{j=1}^N \mathbf{t}^{(j)} \int_{E_j} \ln[(X_i - x')^2 + (Y_i - y')^2] dl(x', y'). \quad (11.3.13)$$

where E_j denotes the j th element.

To facilitate the logistics, we introduce the dimensionless influence coefficients A_j and recast equation (11.3.13) into the compact form

$$\mathbf{u}(X_i, Y_i) = -\frac{\Omega}{2\pi} \sum_{j=1}^N A_j(X_i, Y_i) (\mathbf{X}_{j+1} - \mathbf{X}_j), \quad (11.3.14)$$

where we have defined

$$A_j(X_i, Y_i) \equiv \frac{1}{\Delta l_j} \int_{E_j} \ln[(X_i - x')^2 + (Y_i - y')^2]^{1/2} dl(x', y'). \quad (11.3.15)$$

Because, as the integration point (x', y') approaches the evaluation point (X_i, Y_i) the integrand diverges at a logarithmic rate, the integrals over the elements numbered $i - 1$ and i are singular. Fortunately, these integrals may be computed analytically, and the influence coefficients are found to be

$$A_j(X_i, Y_i) = \ln r_{i,j} - 1, \quad (11.3.16)$$

for $j = i - 1$ or i , where

$$r_{i,j} \equiv \sqrt{(X_i - X_j)^2 + (Y_i - Y_j)^2} \quad (11.3.17)$$

is the distance between the marker points (problem 11.3.1).

The rest of the integrals defining the influence coefficients are non-singular and may be computed using standard numerical methods. Choosing, for example, the trapezoidal rule, we replace the integrand in (11.3.15) with the average of the values corresponding to the ends of the integration domain, finding

$$A_j(X_i, Y_i) = \frac{1}{2} (\ln r_{i,j} + \ln r_{i,j+1}), \quad (11.3.18)$$

for $j = 1, \dots, i - 2, i + 1, \dots, N$.

4. Compute the motion of the marker points by integrating in time the ordinary differential equations

$$\frac{dX_i}{dt} = u_x(X_i, Y_i), \quad \frac{dY_i}{dt} = u_y(X_i, Y_i). \quad (11.3.19)$$

If the flow contains a collection of vortex patches, the right-hand side of (11.3.14) is summed over all contours to account for all induced contributions. Figure 11.3.3 illustrates stages in the evolution of three vortex patches computed using program *09_vortex/vp_2d* of *FDLIB*.

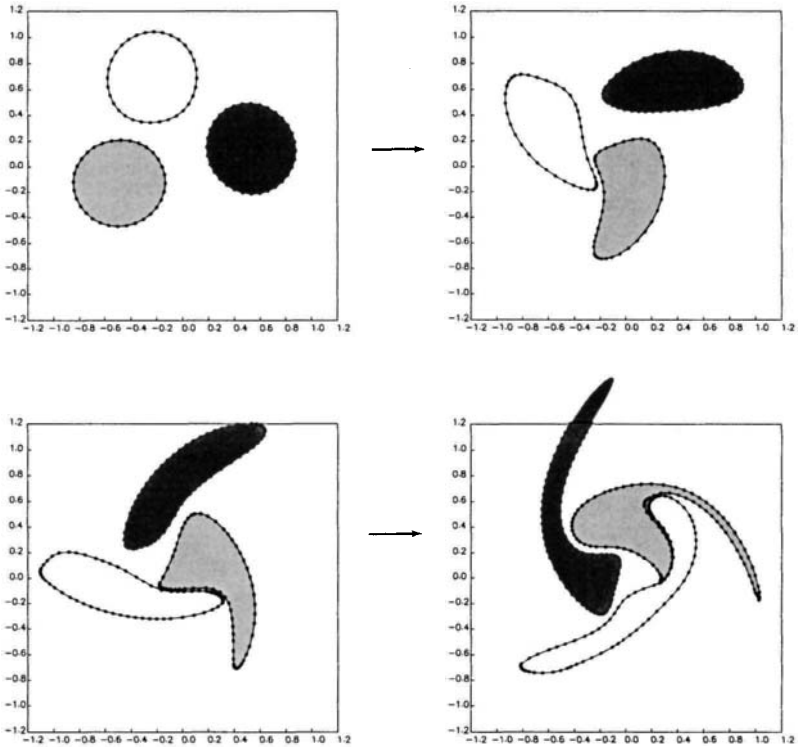


Figure 11.3.3 Evolution of three vortex patches computed using the method of contour dynamics for two-dimensional flow, implemented in program *09_vortex/vp_2d* of *FDLIB*. The dots around the contours mark the adaptively redistributed marker points. The three vortices merge into a larger vortex with spiral filaments.

Periodic flow

To compute the evolution of a periodic flow, we replace equation (11.3.9) with its counterpart originating from equation (11.3.11). In the case of one vortex patch repeated in the x direction with period a , corresponding to $M = 1$, we find

$$\begin{aligned} \mathbf{u}(X_i, Y_i) = & -\frac{\Omega}{4\pi} \sum_{j=1}^N \mathbf{t}^{(j)} \\ & \times \int_{E_j} \ln\{\cosh[k(Y_i - y')] - \cos[k(X_i - x')]\} \mathbf{t}(x', y') dl(x', y'), \end{aligned} \quad (11.3.20)$$

where $k = 2\pi/a$ is the wave number.

The periodic integrand in (11.3.20) exhibits a logarithmic singularity over the two elements hosting a marker point. To remove this singularity, we add and subtract the non-periodic kernel corresponding to a solitary point vortex, writing

$$\begin{aligned} & \ln\{\cosh[k(Y_i - y')] - \cos[k(X_i - x')]\} \\ & = \ln \frac{\cosh[k(Y_i - y')] - \cos[k(X_i - x')]}{(X_i - x')^2 + (Y_i - y')^2} + \ln[(X_i - x')^2 + (Y_i - y')^2]. \end{aligned} \quad (11.3.21)$$

As x' tends to X_i and y' tends to Y_i , the fraction on the right-hand side of (11.3.21) tends to a finite value, and the integral of the corresponding logarithmic term may be computed using a standard numerical method. The improper integral of the last term on the right-hand side of (11.3.21) may be computed analytically, as discussed previously in this section for non-periodic flow.

Figure 11.3.4 illustrates stages in the Kelvin-Helmholtz instability of a periodic vortex layer, computed using program *09_vortex/vp_2d_pr* of *FDLIB*. The initially sinusoidal vortex contours roll up into a periodic sequence of compact vortices connected by thinning braids.

11.3.3 Gaussian integration quadrature

Various modifications of the basic procedure described in Section 11.3.2 can be made to improve the accuracy of the numerical method.

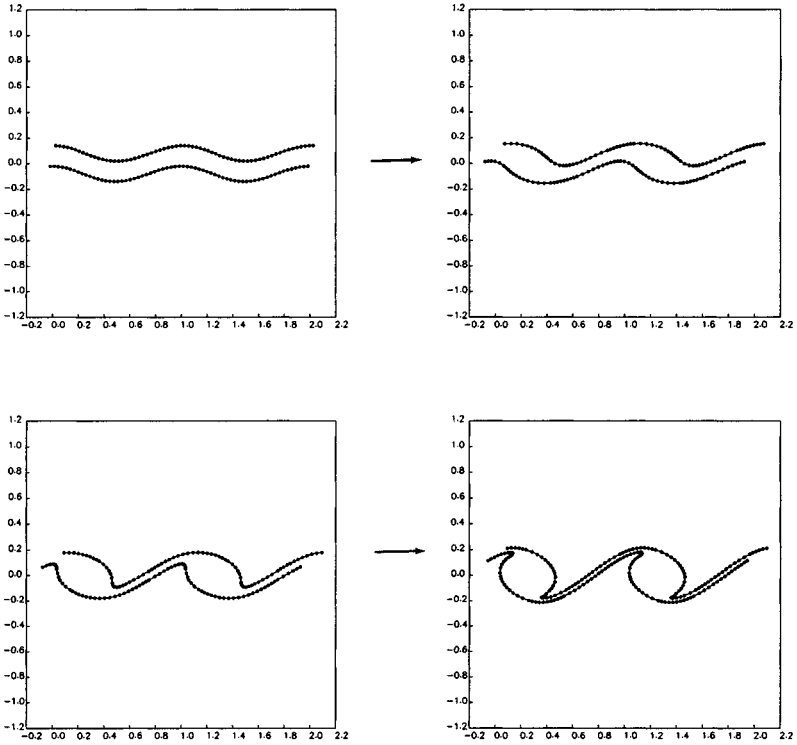


Figure 11.3.4 The Kelvin-Helmholtz instability of an infinite vortex layer with uniform vorticity computed by the method of contour dynamics, implemented in program *09_vortex/vl_2d* of *FDLIB*.

Consider, for example, the evaluation of the influence coefficients A_j defined in equation (11.3.14) over non-singular elements. The trapezoidal rule expressed by (11.3.18) replaces the integral with a weighted average of the values of integrand at the two end-points, where both weights are equal to 1/2. Generalizing this approximation, we evaluate the integral by a quadrature, which is weighted average of the integrand at craftily selected quadrature points,

$$\int_{E_j} \ln[(X_i - x')^2 + (Y_i - y')^2]^{1/2} dl(x', y') \\ \simeq \frac{\Delta l_j}{2} \sum_{k=1}^{N_Q} w_k \ln[(X_i - x_k)^2 + (Y_i - y_k)^2]^{1/2}, \quad (11.3.22)$$

where N_Q is a chosen number of quadrature points, and w_k are integration weights. The base points (x_k, y_k) lie on element E_j , and their position is given by

$$x_k = \frac{1}{2} (X_{j+1} + X_j) + \frac{1}{2} (X_{j+1} - X_j) t_k, \\ y_k = \frac{1}{2} (Y_{j+1} + Y_j) + \frac{1}{2} (Y_{j+1} - Y_j) t_k, \quad (11.3.23)$$

where the scaled base-point positions t_k take values in the range [-1, 1]. The left extreme value $t_k = -1$ corresponds to $x_k = X_j$, $y_k = Y_j$, and the right extreme value $t_k = 1$ corresponds to $x_k = X_{j+1}$, $y_k = Y_{j+1}$. The trapezoidal rule expressed by (11.3.18) corresponds to $N_Q = 2$ with $t_1 = -1$ and $t_2 = 1$, and equal weights $w_1 = w_2 = 1.0$.

Handbooks of mathematical functions provide us with tables of the optimal positioning of the base points, t_k , and corresponding weights, w_k , for a specified number of quadrature points N_Q , where $k = 1, 2, \dots, N_Q$. The base points are the zeros of selected classes of orthogonal polynomials, and the weights arise by integrating interpolating polynomials defined in terms of the base points. For smooth integrands that do not exhibit singularities, the tables come under the header of the Gauss-Legendre quadrature. For integrands with integrable singularities, or integrals over infinite domains, the tables come under different headers.

Directory 01_num_meth/07_integration of *FDLIB* includes subroutines that tabulate base points and weights, and programs that perform numerical integration.

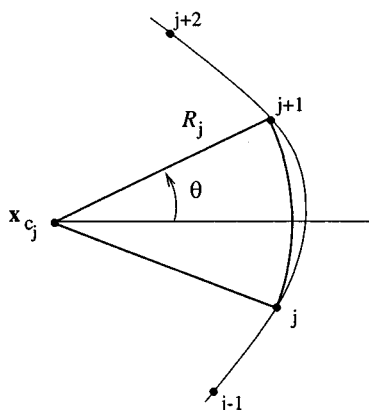


Figure 11.3.5 A vortex contour may be approximated locally with a circular arc passing through three marker points.

11.3.4 Representation with circular arcs

To account for the curvature of a vortex contour, we replace the straight segment connecting two adjacent marker points with a circular arc, as illustrated in figure 11.3.5. The backward arc passes through the trio of points numbered $j - 1, j$, and $j + 1$, and the forward arc passes through the trio of points numbered $j, j + 1$, and $j + 2$. Each arc is specified by its center and radius, computed by solving a system of linear equations using interpolation constraints. The blended arc arises by averaging the geometrical properties of the forward and backward arc.

The position of a point on the j th arc may be expressed in the parametric form

$$x = x_{c_j} + R_j \cos \theta, \quad y = y_{c_j} + R_j \sin \theta, \quad (11.3.24)$$

where (x_{c_j}, y_{c_j}) are the coordinates of the arc center, R_j is the arc radius, and the polar angle θ varies between two limits corresponding to the arc end-points. The components of the unit tangent vector are given by

$$t_x(\theta) = -\pm \sin \theta, \quad t_y(\theta) = \pm \cos \theta, \quad (11.3.25)$$

and the differential arc length is given by $dl = \pm R_j d\theta$, where the plus sign is chosen when the arc is traced in the counterclockwise direction from point j to point $j + 1$, and the minus sign otherwise.

The x and y components of the integral on the right-hand side of (11.3.9) over the j arc, evaluated at the point (X_i, Y_i) , are given by

$$\begin{aligned}
 & -R_j \int_{\theta_j}^{\theta_{j+1}} \ln[(X_i - x_{c_j} - R_j \cos \theta)^2 + (Y_i - y_{c_j} - R_j \sin \theta)^2] \sin \theta \, d\theta, \\
 & R_j \int_{\theta_j}^{\theta_{j+1}} \ln[(X_i - x_{c_j} - R_j \cos \theta)^2 + (Y_i - y_{c_j} - R_j \sin \theta)^2] \cos \theta \, d\theta.
 \end{aligned} \tag{11.3.26}$$

The integrals with respect to θ on the right-hand sides may be computed using, for example, the Gauss-Legendre quadrature.

When the evaluation point (X_i, Y_i) lies on the j th arc, the integrands in (11.3.26) are singular. To handle this special case, we express the coordinates (X_i, Y_i) in local plane polar coordinates, writing

$$X_i = x_{c_j} + R_j \cos \theta_i, \quad Y_i = y_{c_j} + R_j \sin \theta_i, \tag{11.3.27}$$

and then substitute these expressions into (11.3.26), simplify, and rearrange to find

$$\begin{aligned}
 & -R_j \int_{\theta_j}^{\theta_{j+1}} \ln\{2 R_j^2 [1 - \cos(\theta - \theta_i)]\} \sin \theta \, d\theta, \\
 & R_j \int_{\theta_j}^{\theta_{j+1}} \ln\{2 R_j^2 [1 - \cos(\theta - \theta_i)]\} \cos \theta \, d\theta.
 \end{aligned} \tag{11.3.28}$$

As the integration angle θ tends to the evaluation angle θ_i , the integrands in (11.3.28) exhibit a logarithmic singularity. To remove this singularity, we manipulate the x component as follows,

$$\begin{aligned}
 & \int_{\theta_j}^{\theta_{j+1}} \ln\{2 R_j^2 [1 - \cos(\theta - \theta_i)]\} \sin \theta \, d\theta \\
 & = \ln(2R_j^2) \int_{\theta_j}^{\theta_{j+1}} \sin \theta \, d\theta + \int_{\theta_j}^{\theta_{j+1}} \ln[1 - \cos(\theta - \theta_i)] \sin \theta \, d\theta \\
 & = -\ln(2R_j^2) (\cos \theta_j - \cos \theta_{j+1}) + \int_{\theta_j}^{\theta_{j+1}} \ln \frac{1 - \cos(\theta - \theta_i)}{(\theta - \theta_i)^2} \sin \theta \, d\theta \\
 & + \int_{\theta_j}^{\theta_{j+1}} \ln(\theta - \theta_i)^2 (\sin \theta - \sin \theta_i) \, d\theta + \sin \theta_i \int_{\theta_j}^{\theta_{j+1}} \ln(\theta - \theta_i)^2 \, d\theta.
 \end{aligned} \tag{11.3.29}$$

Using the Taylor series expansion of the cosine with respect to θ about the point θ_i , we find that, as θ tends to θ_i , the fraction in the first integral on the right-hand side of (11.3.29) tends to the finite value of 0.5. Thus, this integral is non-singular and may be computed using a standard method. The second integral on the right-hand side is also non-singular. The singularity has been shifted to the third integral which, however, may be evaluated by analytical methods. The y component expressed by the second of equations (11.3.28) may be treated in a similar fashion.

An alternative method of computing the singular integrals (11.3.28) involves using a quadrature that is specifically designed for integrals with a logarithmic singularity, as discussed in texts on numerical methods cited in the bibliography.

Problems

Problem 11.3.1 *Influence coefficient over a singular element.*

(a) Derive the influence coefficients shown in (11.3.16). *Hint:* Work in local Cartesian coordinates with the x axis tangential to the singular element.

(b) Derive the analytical form of the last integral on the right-hand side of (11.3.29).

(c) Derive the counterpart of (11.3.29) for the y component of the induced velocity.

Problem 11.3.2 *Periodic kernel.*

Evaluate the limit of the fraction after the logarithm on the right-hand side of (11.3.21) as the integration point tends to the evaluation point.

Computer problems

Problem c.11.3.1 *Motion of vortex patches.*

Subdirectory *09_vortex/vp_2d* of *FDLIB* contains a program that simulates the motion of vortex patches with uniform vorticity using the method of contour dynamics discussed in the text. In the numerical implementation, the contour of each patch is approximated with a collection of blended circular arcs. The marker points are redistributed

adaptively during the motion to capture the development of regions of large curvature and prevent point clustering and dilution.

Run the program to simulate the motion of an arrangement of your choice, and discuss the nature of the motion.

Problem c.11.3.2 *Motion of vortex layers.*

Subdirectory *09_vortex/vl.2d* of *FDLIB* contains a program that simulates the motion of adjacent vortex layers with uniform vorticity using the method of contour dynamics discussed in the text. The numerical method is similar to that described in problem c.11.3.2 for vortex patches.

Run the program to simulate the motion of an arrangement of your choice, and discuss the nature of the motion.

11.4 Vorticity, circulation, and three-dimensional flow induced by vorticity

The circulation around a loop L in three-dimensional flow is defined as the line integral of the tangential component of the velocity around the loop,

$$C \equiv \oint_L u_t dl = \oint_L (u_x t_x + u_y t_y + u_z t_z) dl = \oint_L \mathbf{u} \cdot \mathbf{t} dl, \quad (11.4.1)$$

where $\mathbf{t} = (t_x, t_y, t_z)$ is the unit vector tangent to L , and $dl = (dx^2 + dy^2 + dz^2)^{1/2}$ is the differential arc length around the loop measured from an arbitrary point, as depicted in figure 11.4.1. The definition (11.4.1) is a generalization of that stated in equation (11.1.1) for two-dimensional flow.

If the loop is *reducible*, that is, if it can be shrunk to a point without crossing flow boundaries or singular lines, we may use Stokes's circulation theorem to express the circulation around the loop as an integral of the component of the vorticity vector normal to *any* three-dimensional surface D bounded by the loop,

$$C = \int_D \omega \cdot \mathbf{n} dS, \quad (11.4.2)$$

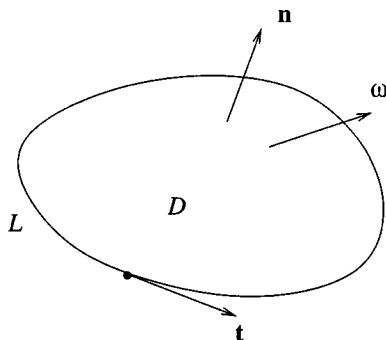


Figure 11.4.1 A closed loop in three-dimensional flow, L , enclosing an open area, D . The circulation around the loop is equal to the surface integral of the normal component of the vorticity, $\omega \cdot \mathbf{n}$, over D .

where dS is the differential surface area of D . The orientation of the unit normal vector \mathbf{n} is such that, as we look down from the positive direction of the normal vector, the unit tangent vector \mathbf{t} points in a direction corresponding to counterclockwise rotation.

In the case of two-dimensional flow in the xy plane, the loop L and surface D enclosed by L may be chosen to lie in the xy plane. The unit normal vector \mathbf{n} is then parallel to the z axis, and expression (11.4.2) reduces to (11.1.2) where the vorticity vector is given by $\omega = \omega_z \mathbf{n}$.

11.4.1 Preservation of circulation in a flow with negligible viscous forces

To compute the rate of change of circulation around a material loop consisting of a fixed collection of point particles with a permanent identity, we take the time derivative of both sides of the definition (11.4.1), and find

$$\frac{dC}{dt} = \frac{d}{dt} \oint_L \mathbf{u} \cdot \mathbf{t} \, dl = \oint_L \frac{D\mathbf{u}}{Dt} \cdot \mathbf{t} \, dl + \oint_L \mathbf{u} \cdot \frac{D(\mathbf{t} \, dl)}{Dt}, \quad (11.4.3)$$

where D/Dt is the material derivative.

If viscous forces are negligible, we may use Euler's equation (6.4.2) to express the first integral on the right-hand side of (11.4.3) in the form

$$\oint_L \frac{D\mathbf{u}}{Dt} \cdot \mathbf{t} \, dl = \oint_L \left(-\frac{1}{\rho} \nabla p + \mathbf{g}\right) \cdot \mathbf{t} \, dl. \quad (11.4.4)$$

Now, if \mathbf{X} is the position of a point particle around the loop, then $\mathbf{t} = \frac{1}{dl} d\mathbf{X}$. Using this expression, and assuming that the fluid density is uniform throughout the domain of flow, we find

$$\begin{aligned} \oint_L \frac{D\mathbf{u}}{Dt} \cdot \mathbf{t} \, dl &= -\frac{1}{\rho} \oint_L d\mathbf{X} \cdot \nabla p + \mathbf{g} \cdot \oint_L d\mathbf{X} \\ &= -\frac{1}{\rho} \oint_L dp + \mathbf{g} \cdot \oint_L d\mathbf{X}. \end{aligned} \quad (11.4.5)$$

Because the loop is closed, the domain of integration may be regarded as periodic. Since the two integrands on the right-hand side of (11.4.5) are exact differentials, their integrals vanish.

Considering the second integral on the right-hand side of (11.4.3), we express it in the form

$$\oint_L \mathbf{u} \cdot \frac{D(\mathbf{t} \, dl)}{Dt} = \oint_L \mathbf{u} \cdot \frac{Dd\mathbf{X}}{Dt}. \quad (11.4.6)$$

The material derivative $D(d\mathbf{X})/Dt$ expresses the rate of change of the components of an infinitesimal material vector beginning at a certain point particle and ending at another point particle. If the two point particles move with the same velocity, the material vector will simply translate, and $D(d\mathbf{X})/Dt = \mathbf{0}$. This observation suggests that $D(d\mathbf{X})/Dt$ is proportional to the local rate of change of the velocity with respect to arc length along the material vector. Using Taylor series expansions, we find

$$\begin{aligned} \frac{DdX}{Dt} &= dX \frac{\partial u_x}{\partial x} + dY \frac{\partial u_x}{\partial y} + dZ \frac{\partial u_x}{\partial z}, \\ \frac{DdY}{Dt} &= dX \frac{\partial u_y}{\partial x} + dY \frac{\partial u_y}{\partial y} + dZ \frac{\partial u_y}{\partial z}, \\ \frac{DdZ}{Dt} &= dX \frac{\partial u_z}{\partial x} + dY \frac{\partial u_z}{\partial y} + dZ \frac{\partial u_z}{\partial z}. \end{aligned} \quad (11.4.7)$$

Considering now the inner product on the right-hand side of (11.4.6), we write

$$\begin{aligned} u_x \frac{DdX}{Dt} &= dX u_x \frac{\partial u_x}{\partial x} + dY u_x \frac{\partial u_x}{\partial y} + dZ u_x \frac{\partial u_x}{\partial z} \\ &= dX \frac{1}{2} \frac{\partial u_x^2}{\partial x} + dY \frac{1}{2} \frac{\partial u_x^2}{\partial y} + dZ \frac{1}{2} \frac{\partial u_x^2}{\partial z} = \frac{1}{2} \frac{du_x^2}{dl}. \end{aligned} \quad (11.4.8)$$

Because the right-hand side of (11.4.8) is an exact differential, its line integral over the closed loop vanishes. Working in a similar manner with the projections of the y and z components, we find that the second integral on the right-hand side of (11.4.3) also vanishes, yielding the conservation law

$$\frac{dC}{dt} = 0, \quad (11.4.9)$$

which expresses Kelvin's circulation theorem: when viscous forces are negligible, the circulation around a closed material loop in a three-dimensional flow remains constant in time.

11.4.2 Flow induced by vorticity

Given the velocity field, we may compute the associated vorticity field using the definition of the vorticity

$$\boldsymbol{\omega} \equiv \nabla \times \mathbf{u}, \quad (11.4.10)$$

by analytical or numerical differentiation. Is there a way of doing the inverse, that is, expressing the velocity in terms of the vorticity?

In the case of two-dimensional flow, the velocity field associated with a specified vorticity distribution in the xy plane arises from the integral representation (11.3.2). The corresponding formula for three-dimensional flow is

$$\begin{aligned} \mathbf{u}(x, y, z) &= -\frac{1}{4\pi} \int \int \int_{Flow} \\ &\quad \frac{(\mathbf{x} - \mathbf{x}') \times \boldsymbol{\omega}(x', y', z')}{[(x - x')^2 + (y - y')^2 + (z - z')^2]^{3/2}} dx' dy' dz', \end{aligned} \quad (11.4.11)$$

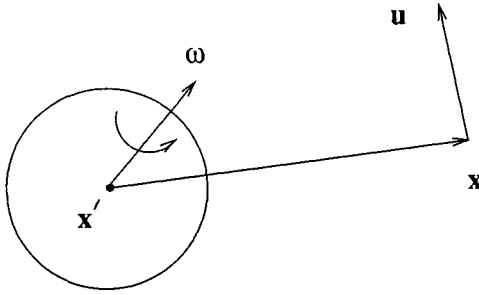


Figure 11.4.2 The flow induced by the rotation of a small fluid parcel is expressed by the Biot-Savart integral shown in (11.4.12).

In index notation,

$$u_i(x, y, z) = -\frac{1}{4\pi} \iiint_{Flow} \frac{\epsilon_{ijk} (x_j - x'_j) \omega_k(x', y', z')}{[(x - x')^2 + (y - y')^2 + (z - z')^2]^{3/2}} dx' dy' dz'. \tag{11.4.12}$$

The second set of parentheses in the numerators on the right-hand sides of (11.4.11) and (11.4.12) enclose the arguments of the vorticity.

The numerator of the integrand in (11.4.11) consists of the cross product of (a) the vectorial distance between the evaluation point $\mathbf{x} = (x, y, z)$ and the integration point $\mathbf{x}' = (x', y', z')$, and (b) the vorticity. The denominator is the cubic power of the scalar distance between the evaluation point and the integration point, $|\mathbf{x} - \mathbf{x}'|^3$. Thus, far from the integration point \mathbf{x}' , the integrand decays like $1/r^2$, where $r = [(x - x')^2 + (y - y')^2 + (z - z')^2]^{1/2}$.

The physical interpretation of (11.4.11) becomes evident by replacing the integral with a sum of integrals over the volumes of elementary fluid parcels. The velocity induced by each individual parcel due to its rotation is illustrated in figure 11.4.2. The analogy with the magnetic field induced by an electrical current explains why the integral on the right-hand side of (11.4.11) is known as the *Biot-Savart integral* of vortex dynamics.

The integral representation (11.4.11) is applicable only for unbounded flow extending to infinity in all directions. In the presence of boundaries, an additional complementary flow must be included to ensure

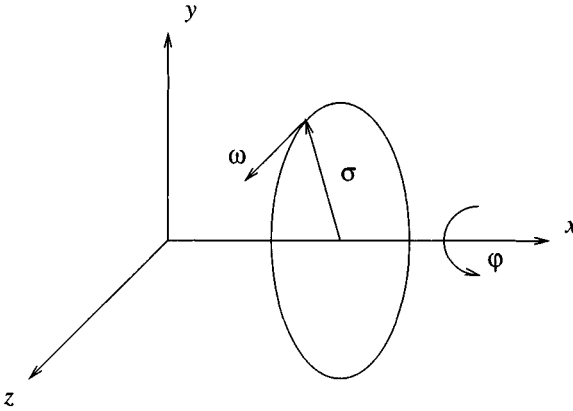


Figure 11.5.1 Illustration of an axisymmetric flow without swirling motion. The vorticity vector points in the meridional direction.

the solenoidality of the velocity field and the satisfaction of the no-penetration and no-slip boundary conditions.

11.5 Axisymmetric flow induced by vorticity

The vorticity of an axisymmetric vortex flow without swirling motion points in the direction of the meridional angle φ , as illustrated in figure 11.5.1. The known orientation of the vorticity field and accompanying axial symmetry of the velocity allow us to simplify the volume integral on the right-hand side of (11.4.11), thereby deriving representations that are more amenable to analytical and numerical methods.

In the cylindrical polar coordinates depicted in figure 11.5.1, the vorticity vector takes the form $\boldsymbol{\omega} = \omega_\varphi(x, \sigma) \mathbf{e}_\varphi$, where ω_φ is the scalar strength of the vorticity, and \mathbf{e}_φ is the unit vector pointing in the direction of the meridional angle φ . The Cartesian components of the vorticity are given by

$$\omega_x = 0, \quad \omega_y = -\omega_\varphi \sin \varphi, \quad \omega_z = \omega_\varphi \cos \varphi. \quad (11.5.1)$$

Considering the integral representation (11.4.11), we express the y and z coordinates of the evaluation point \mathbf{x} and integration point \mathbf{x}' in

terms of their cylindrical polar coordinates, writing

$$y = \sigma \cos \varphi, \quad z = \sigma \sin \varphi, \quad y' = \sigma' \cos \varphi', \quad z' = \sigma' \sin \varphi'. \quad (11.5.2)$$

The square of the distance between these two points is given by

$$\begin{aligned} r^2 &\equiv (x - x')^2 + (y - y')^2 + (z - z')^2 \\ &= (x - x')^2 + (\sigma \cos \varphi - \sigma' \cos \varphi')^2 + (\sigma \sin \varphi - \sigma' \sin \varphi')^2, \end{aligned} \quad (11.5.3)$$

Expanding out the squares, and using elementary trigonometric identities, we find

$$\begin{aligned} r^2 &= (x - x')^2 + (\sigma + \sigma')^2 - 2\sigma\sigma' \cos(\varphi - \varphi') \\ &= (x - x')^2 + (\sigma + \sigma')^2 - 4\sigma\sigma' \cos^2 \frac{\hat{\varphi}}{2}, \end{aligned} \quad (11.5.4)$$

where $\hat{\varphi} \equiv \varphi - \varphi'$.

Next, we consider the x component of (11.4.12), and express the differential volume $dx' dy' dz'$ in the alternative form $dx' d\sigma' \sigma' d\varphi'$ to obtain

$$\begin{aligned} u_x(x, \sigma) &= -\frac{1}{4\pi} \int_0^{2\pi} \int_{Flow} \int_{Flow} \\ &\quad \frac{(y - y') \omega_z(x', y', z') - (z - z') \omega_y(x', y', z')}{r^3} \sigma' dx' d\sigma' d\varphi'. \end{aligned} \quad (11.5.5)$$

Substituting relations (11.5.1) and (11.5.2) into the numerator of the integrand, simplifying by use of trigonometric identities, and rearranging, we find

$$u_x(x, \sigma) = \frac{1}{4\pi} \int \int_{Flow} \left[\int_0^{2\pi} \frac{-\sigma \cos \hat{\varphi} + \sigma'}{r^3} d\hat{\varphi} \right] \omega_\varphi(x', \sigma') \sigma' dx' d\sigma', \quad (11.5.6)$$

where r is equal to the square root of the right-hand side of (11.5.4).

To compute the σ component of the velocity, we work in a similar fashion departing from the equation $u_\sigma = u_y \cos \varphi + u_z \sin \varphi$. The result is

$$u_\sigma(x, \sigma) = \frac{1}{4\pi} \int \int_{Flow} \left[\int_0^{2\pi} \frac{(x - x') \cos \hat{\varphi}}{r^3} d\hat{\varphi} \right] \omega_\varphi(x', \sigma') \sigma' dx' d\sigma'. \quad (11.5.7)$$

To simplify the notation, we recast equations (11.5.6) and (11.5.7) into the forms

$$u_x(x, \sigma) = \frac{1}{4\pi} \int \int_{Flow} [-\sigma I_{31}(x - x', \sigma, \sigma') + \sigma' I_{30}(x - x', \sigma, \sigma')] \omega_\varphi(x', \sigma') \sigma' dx' d\sigma',$$

$$u_\sigma(x, \sigma) = \frac{1}{4\pi} \int \int_{Flow} (x - x') I_{31}(x - x', \sigma, \sigma') \omega_\varphi(x', \sigma') \sigma' dx' d\sigma'. \quad (11.5.8)$$

We have introduced the integrals

$$\begin{aligned} I_{30}(x - x', \sigma, \sigma') &\equiv \int_0^{2\pi} \frac{d\hat{\varphi}}{r^3} \\ &= \int_0^{2\pi} \frac{d\hat{\varphi}}{[(x - x')^2 + (\sigma + \sigma')^2 - 4\sigma\sigma' \cos^2 \frac{\hat{\varphi}}{2}]^{3/2}} \\ &= \frac{4}{[(x - x')^2 + (\sigma + \sigma')^2]^{3/2}} \int_0^{\pi/2} \frac{d\eta}{(1 - k^2 \cos^2 \eta)^{3/2}}, \end{aligned} \quad (11.5.9)$$

and

$$\begin{aligned} I_{31}(x - x', \sigma, \sigma') &\equiv \int_0^{2\pi} \frac{\cos \hat{\varphi}}{r^3} d\hat{\varphi} \\ &= \int_0^{2\pi} \frac{\cos \hat{\varphi}}{[(x - x')^2 + (\sigma + \sigma')^2 - 4\sigma\sigma' \cos^2 \frac{\hat{\varphi}}{2}]^{3/2}} d\hat{\varphi} \\ &= \frac{4}{[(x - x')^2 + (\sigma + \sigma')^2]^{3/2}} \int_0^{\pi/2} \frac{\cos(2\eta)}{(1 - k^2 \cos^2 \eta)^{3/2}} d\eta, \end{aligned} \quad (11.5.10)$$

where $\eta \equiv \hat{\varphi}/2$, and

$$k^2 \equiv \frac{4\sigma\sigma'}{(x - x')^2 + (\sigma + \sigma')^2}. \quad (11.5.11)$$

The integrals on the right-hand side of (11.5.9) and (11.5.10) are not known in analytical form. To evaluate them, we express them in terms of *complete elliptic integrals* of the first and second kind denoted, respectively, by F and E , defined as

$$F(k) = \int_0^{\pi/2} \frac{d\eta}{(1 - k^2 \sin^2 \eta)^{1/2}}, \quad E(k) = \int_0^{\pi/2} (1 - k^2 \sin^2 \eta)^{1/2} d\eta. \quad (11.5.12)$$

The complete elliptic integrals may be evaluated efficiently by iteration or approximation, as will be discussed later in this section.

Referring to standard integration tables, we find that the integrals on the right-hand side of (11.5.9) and (11.5.10) are given by

$$\int_0^{\pi/2} \frac{d\eta}{(1 - k^2 \cos^2 \eta)^{3/2}} = \frac{E(k)}{1 - k^2}, \quad (11.5.13)$$

and

$$\int_0^{\pi/2} \frac{\cos(2\eta)}{(1 - k^2 \cos^2 \eta)^{3/2}} d\eta = -\frac{2}{k^2} F(k) + \frac{2 - k^2}{k^2 (1 - k^2)} E(k). \quad (11.5.14)$$

The derivation of these expressions concludes the analytical part of our work.

*Evaluation of the complete elliptic integrals
of the first and second kind*

An efficient method of evaluating the complete integrals is based on the following expressions involving rapidly converging infinite products,

$$\begin{aligned} F(k) &= \frac{\pi}{2} (1 + K_1)(1 + K_2) \dots, \\ E(k) &= F(k) \left(1 - \frac{k^2}{2} P\right), \end{aligned} \quad (11.5.15)$$

where

$$P = 1 + \frac{K_1}{2} \left[1 + \frac{K_2}{2} \left(1 + \frac{K_3}{3} \dots\right)\right]. \quad (11.5.16)$$

The sequence K_p is computed using the recursive formula

$$K_p = \frac{1 - (1 - K_{p-1}^2)^{1/2}}{1 + (1 - K_{p-1}^2)^{1/2}}. \quad (11.5.17)$$

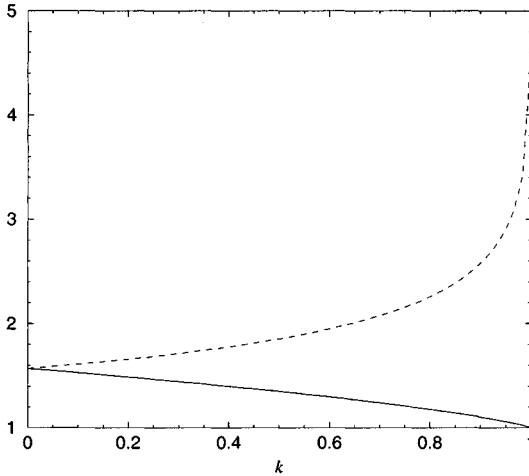


Figure 11.5.2 Graphs of the complete elliptic integral of the first kind, $E(k)$, drawn with the dashed line, and complete elliptic integral of the second kind, $F(k)$, drawn with the solid line, defined in equations (11.5.12).

beginning with $K_0 = k$. Graphs of the complete elliptic integrals computed using this method, implemented in subroutine *ell_int* located in directory *01_num_meth/12_spec_fnc* of *FDLIB*, are shown in figure 11.5.2.

11.5.1 Line vortex ring

We are in a position now to evaluate the velocity field associated with a specified axisymmetric vorticity distribution on the basis of the integral representations (11.5.8).

The simplest of vorticity distribution is associated with a line vortex ring, which is the axisymmetric counterpart of the point vortex in two-dimensional flow. The strength of the vorticity in a meridional plane is expressed by the generalized distribution

$$\omega_\varphi(x, \sigma) = \kappa \delta_2(x - x_r, \sigma - \sigma_r), \quad (11.5.18)$$

where δ_2 is the two-dimensional delta function in the $x\sigma$ plane; κ is the strength of the vortex ring, equal to the circulation around the ring; σ_r is the radius of the ring; and x_r is the axial position of the ring. Substituting (11.5.18) into expressions (11.5.8), and using the distinctive

properties of the delta function discussed in Section 11.2 to evaluate the integrals, we find

$$\begin{aligned} u_x(x, \sigma) &= \frac{\kappa \sigma_r}{4\pi} [-\sigma I_{31}(x - x_r, \sigma, \sigma_r) + \sigma' I_{30}(x - x_r, \sigma, \sigma_r)], \\ u_\sigma(x, \sigma) &= \frac{\kappa \sigma_r}{4\pi} (x - x_r) I_{31}(x - x_r, \sigma, \sigma_r). \end{aligned} \quad (11.5.19)$$

The streamline pattern of the flow induced by the ring is shown in figure 11.5.3(a).

Motion in the presence of boundaries

In the presence of boundaries, the velocity field expressed by (11.5.19) must be enhanced with a complementary velocity that ensures the satisfaction of the no-penetration boundary condition at impermeable walls. For simple boundary geometries involving one or two parallel walls, the complementary flow may be expressed in terms of image vortex rings.

Figure 11.5.3(b-c) illustrates the streamline pattern of the axisymmetric flow induced by a vortex ring in front of a plane wall and in the exterior of a sphere. Programs that evaluate the velocity field are provided in directory *09_vortex/lvr* of *FDLIB*. The streamline patterns shown in figure 11.5.3 were generated using program *04_various/strmll* of *FDLIB*.

11.5.2 Vortex rings with finite core

Consider now the flow induced by a slender vortex ring of radius σ_r located at the axial position x_r . We will assume that the ring has a circular core of radius a , as illustrated in figure 11.5.4. It will be convenient to introduce plane polar coordinates in a meridional plane with origin at the center of the core, denoted by (q, χ) , as depicted in figure 11.5.4. The vorticity is assumed to vanish outside the core; that is, $\omega_\varphi = 0$ when $q > a$.

Using expression (11.4.2), we find that the circulation around the core is given by

$$C = \int_{core} \omega_\varphi(x', \sigma') dx' d\sigma' = \int_0^{2\pi} \int_0^a \omega_\varphi(x', \sigma') q dq d\chi, \quad (11.5.20)$$

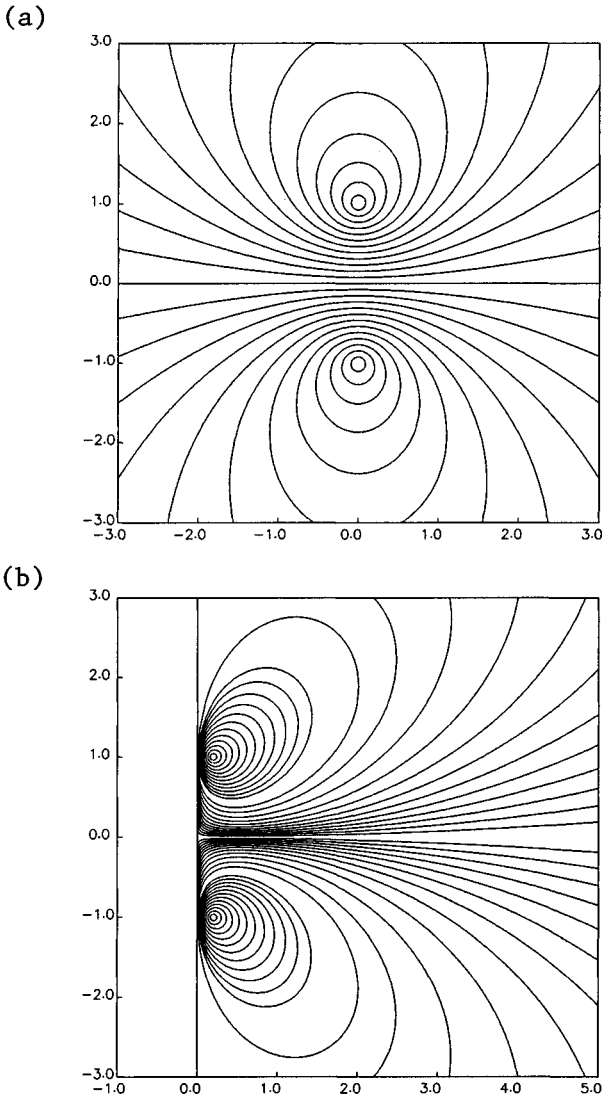


Figure 11.5.3 Streamline pattern of the flow induced by a line vortex ring (a) in an unbounded domain of flow, (b) in a semi-infinite domain bounded by a plane wall, and (c) in the exterior of a sphere.

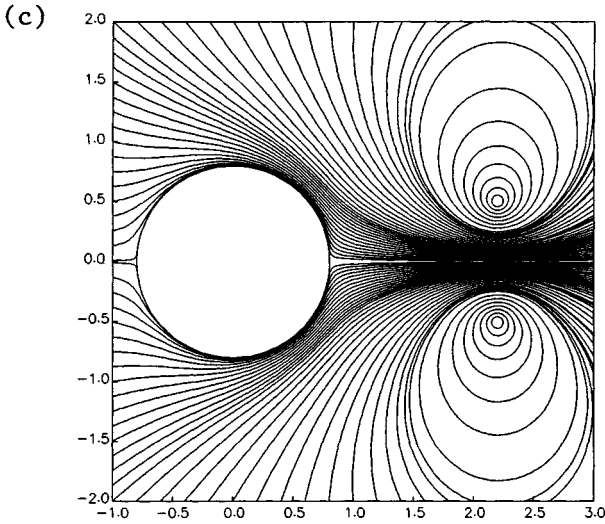


Figure 11.5.3 Continued.

According to our earlier discussion, the circulation may be identified with the conserved strength of the vortex ring, denoted by κ .

Considering the integral representation for the velocity given in (11.5.8) we perform the integration in the plane polar coordinates (q, χ) defined in figure 11.5.4, and find

$$u_x(x, \sigma) = \frac{1}{4\pi} \int_0^{2\pi} \int_0^a (-\sigma I_{31} + \sigma' I_{30}) \omega_\varphi(x', \sigma') \sigma' q dq d\chi,$$

$$u_\sigma(x, \sigma) = \frac{1}{4\pi} \int_0^{2\pi} \int_0^a (x - x') I_{31} \omega_\varphi(x', \sigma') \sigma' q dq d\chi. \quad (11.5.21)$$

Note that, because of the singular behavior of the complete elliptic integral $F(k)$, the integrands in (11.5.21) exhibit a logarithmic singularity when the evaluation point (x, σ) lies inside the core.

The simplest way of evaluating the double integrals on the right-hand sides of (11.5.21) is by the double-trapezoidal rule: divide the domain of integration with respect to q and χ into evenly spaced intervals defining circular sectors, approximate the integrand over each sector with the value at the center, and add all contributions.

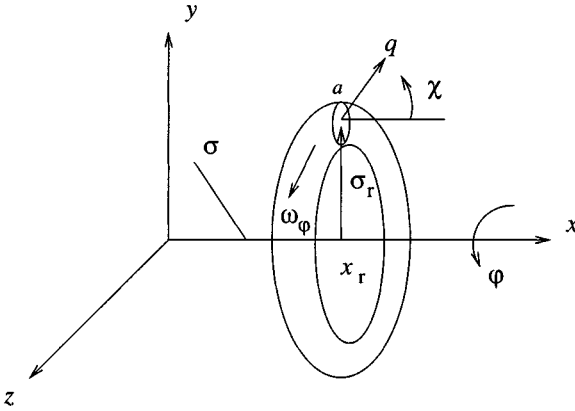


Figure 11.5.4 Illustration of a vortex ring of radius σ_r with a circular core of radius a .

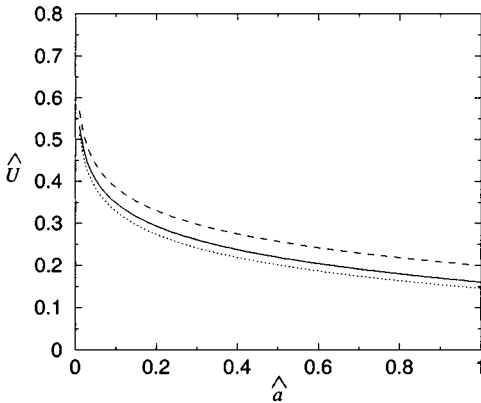


Figure 11.5.5 The reduced self-induced velocity of a vortex ring with radius σ_r and circulation κ , plotted against the reduced core radius $\hat{a} \equiv a/\sigma_r$. The solid and dashed line correspond, respectively, to a ring with uniform or gradual vorticity distribution described by equation (11.5.22) or (11.5.23). The dotted line represents Helmholtz's asymptotic prediction for small core radius, expressed by equation (11.5.24).

Self-induced velocity

The self-induced velocity of a vortex ring propagating along the x axis with velocity U_x , may be identified with the x component of the fluid velocity evaluated at the center of the vortex core, which may be computed using the first of expressions (11.5.21) for $x = x_r$ and $\sigma = \sigma_r$.

Figure 11.5.5 shows a graph of the dimensionless self-induced velocity $\hat{U} \equiv U_x \sigma_r / \kappa$, plotted against the reduced core radius $\hat{a} \equiv a / \sigma_r$, evaluated using the double-trapezoidal approximation described in the last paragraph, neglecting the weak logarithmic singularity of the integrand. The numerical method is implemented in program *09_vortex/ring* of *FDLIB*. The solid line corresponds to a core with uniform vorticity

$$\omega_\varphi = \frac{\kappa}{\pi a^2}, \quad (11.5.22)$$

and the dashed line corresponds to a core with distributed vorticity described by

$$\omega_\varphi = \frac{2\pi\kappa}{(\pi^2 - 4)a^2} \left(1 + \cos \frac{\pi q}{a}\right), \quad (11.5.23)$$

for $0 < q < a$, and $\omega_\varphi = 0$ for $q > a$.

The results show that, as the size of the core tends to zero while the strength of the ring is held constant, the self-induced velocity obtains increasingly larger values irrespective of the form of the vorticity distribution over the core. Thus, the self-induced velocity of a line vortex ring with infinitesimal core, which is the axisymmetric counterpart of a point vortex, is not defined. We shall see later in this chapter that this is a more general result applicable to vortex filaments with non-rectilinear shapes.

An asymptotic analysis of the self-induced velocity in the limit of small core size shows that, to leading order, the self-induced velocity of a slender vortex ring is given by Helmholtz's formula

$$U_x = \frac{C}{4\pi\sigma_r} \left(-\ln \frac{8a}{\sigma_r} - \frac{1}{4}\right). \quad (11.5.24)$$

This formula explicitly illustrates that the self-induced velocity diverges at a logarithmic rate with respect to the reduced core radius a/σ_r . The predictions of (11.5.24), represented by the dotted line in figure 11.5.5, are in fair agreement with the exact values represented by the solid and dashed lines, even when the size of the core is not small compared to the ring radius.

11.5.3 Motion of a collection of vortex rings

A vortex ring belonging to a collection of coaxial vortex rings translates under the influence of its self-induced velocity as well as of the velocity induced by its peers. When the ring core size is small, the self-induced velocity is given by Helmholtz's formula (11.5.24).

Now, the vorticity transport equation (6.6.7) requires that, as the radius of a ring, σ_r changes during the motion, the strength of the vorticity, ω_φ , should increase or decrease by the same proportion. In response to this change, the radius of the core, a , is adjusted to preserve the ring strength and core volume,

$$\frac{d}{dt}[(2\pi\sigma_r)\pi a^2] = 0. \quad (11.5.25)$$

Expanding out the derivative on the left-hand side, and rearranging, we obtain an evolution equation for the core radius

$$\frac{da}{dt} = -\frac{1}{2} \frac{a}{\sigma_r} \frac{d\sigma_r}{dt} = -\frac{1}{2} \frac{a}{\sigma_r} U_\sigma, \quad (11.5.26)$$

where $U_\sigma \equiv d\sigma_r/dt$ is the rate of expansion of the ring centerline.

Appending equation (11.5.26) to the equation of motion for the ring centerline, we obtain a system of differential equations governing the ring axial position, centerline, and core radius. A numerical method for integrating this system in time is implemented in program *09_vortex/lvrm* of *FDLIB*. Figure 11.5.6 shows stages in the motion of four vortex rings computed using this program. The simulation reveals that two neighboring vortex rings pass through one another in an alternating fashion, exhibiting a type of motion that can be described as leap-frogging.

11.5.4 Vortex patches in axisymmetric flow

Consider an axisymmetric flow containing an annular vortex whose vorticity is proportional to the distance from the x axis,

$$\omega_\varphi = \Omega \sigma, \quad (11.5.27)$$

where Ω is a constant. The flow outside the vortex is assumed to be irrotational. Substituting the vorticity distribution (11.5.27) into the integral representation (11.5.8), and using the Gauss divergence theorem, we derive a contour integral representation that is analogous to that for a two-dimensional vortex patch with uniform vorticity discussed in Section 11.2,

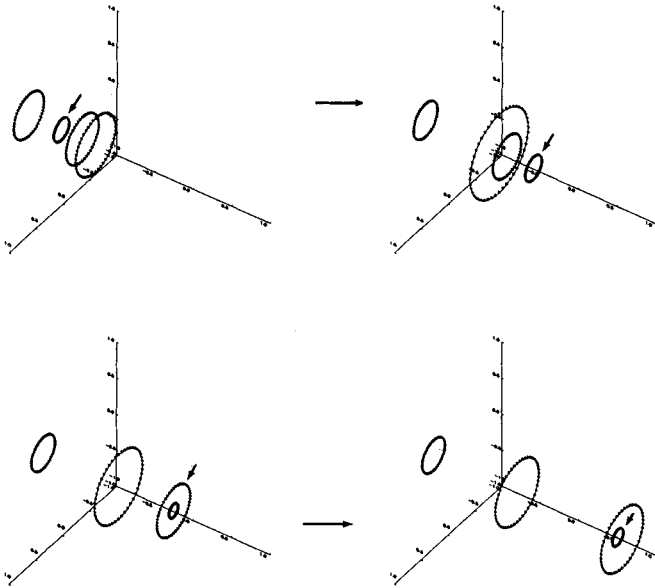


Figure 11.5.6 Motion of a collection of coaxial vortex rings computed using program *09_vortex/lvrm* of *FDLIB*, showing leap-frogging.

$$u_x(x, \sigma) = -\frac{\Omega}{4\pi} \int_C [(x - x') I_{10}(x - x', \sigma, \sigma') n_x(x', \sigma') + \sigma I_{11}(x - x', \sigma, \sigma') n_\sigma(x', \sigma')] \sigma' dl(x', \sigma'),$$

$$u_\sigma(x, \sigma) = \frac{\Omega}{4\pi} \int_C I_{11}(x - x', \sigma, \sigma') n_x(x', \sigma') \sigma'^2 dl(x', \sigma'),$$

(11.5.28)

where C is the trace of the vortex contour in a meridional plane. We have introduced the integrals

$$\begin{aligned}
I_{10}(x-x', \sigma, \sigma') &\equiv \int_0^{2\pi} \frac{d\hat{\varphi}}{r} \\
&= \int_0^{2\pi} \frac{d\hat{\varphi}}{[(x-x')^2 + (\sigma + \sigma')^2 - 4\sigma\sigma' \cos^2 \frac{\hat{\varphi}}{2}]^{1/2}} \\
&= \frac{4}{[(x-x')^2 + (\sigma + \sigma')^2]^{1/2}} \int_0^{\pi/2} \frac{d\eta}{(1-k^2 \cos^2 \eta)^{1/2}} \\
&= \frac{4 F(k)}{[(x-x')^2 + (\sigma + \sigma')^2]^{1/2}}, \tag{11.5.29}
\end{aligned}$$

and

$$\begin{aligned}
I_{11}(x-x', \sigma, \sigma') &\equiv \int_0^{2\pi} \frac{\cos \hat{\varphi}}{r} d\hat{\varphi} \\
&= \int_0^{2\pi} \frac{\cos \hat{\varphi}}{[(x-x')^2 + (\sigma + \sigma')^2 - 4\sigma\sigma' \cos^2 \frac{\hat{\varphi}}{2}]^{1/2}} d\hat{\varphi} \\
&= \frac{4}{[(x-x')^2 + (\sigma + \sigma')^2]^{1/2}} \int_0^{\pi/2} \frac{\cos(2\eta)}{(1-k^2 \cos^2 \eta)^{1/2}} d\eta, \tag{11.5.30}
\end{aligned}$$

where $\eta \equiv \hat{\varphi}/2$, k^2 is defined in (11.5.11), and $F(k)$ is the complete elliptic integral of the first kind defined in the first of equations (11.5.12). The integral on the right-hand side of (11.5.30) may be expressed in terms of complete elliptic integral of the first and second kind, as

$$\int_0^{\pi/2} \frac{\cos(2\eta)}{(1-k^2 \cos^2 \eta)^{1/2}} d\eta = \frac{2-k^2}{k^2} F(k) - \frac{2}{k^2} E(k). \tag{11.5.31}$$

11.5.5 Contour dynamics

The vorticity transport equation for axisymmetric flow with negligible viscous forces, equation (6.6.8), requires that the vorticity inside an axisymmetric patch whose vorticity distribution is linear with respect to distance from the x axis, σ , remain linear at all times. To compute the evolution of the flow, it suffices then to simulate the motion of the vortex contour using the counterpart of the contour dynamics formulation for two-dimensional flow discussed in Section 11.3.

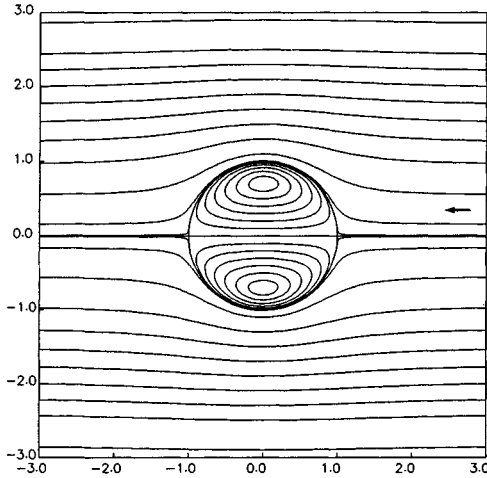


Figure 11.5.7 Streamline pattern associated with Hill's spherical vortex, in a frame of reference translating with the vortex.

Problems

Problem 11.5.1 *Velocity induced by vorticity.*

Derive the representation (11.5.7).

Problem 11.5.2 *Hill's spherical vortex.*

Hill's spherical vortex is a paradigm of an axisymmetric vortex patch with distributed vorticity. Inside the vortex, the strength of the vorticity is proportional to the distance from the x axis, σ , as shown in equation (11.5.27); outside the vortex, the flow is irrotational. The streamline pattern in a frame of reference translating with the vortex is shown in figure 11.5.7. Hill's vortex is the extreme member of a family of vortex rings, arising in the limit as the core spreads out and the ring contour touches and then extends over the x axis. The opposite extreme member of this family is a line vortex ring with a core of infinitesimal radius discussed in Section 11.5.1.

(a) Verify that, in a stationary frame of reference, the axisymmetric stream function of the flow inside and outside Hill's vortex is given, respectively, by

$$\psi^{in} = \frac{\Omega}{10} (a^2 - x^2 - \sigma^2),$$

$$\psi^{out} = -\frac{\Omega}{15} a^2 \sigma^2 \left(1 - \frac{a^3}{(x^2 + \sigma^2)^{3/2}}\right). \quad (11.5.32)$$

(b) Show that the velocity is continuous across the spherical interface.

(c) Explain why the unperturbed vortex translates along the x axis with velocity $U = \frac{2}{15} \Omega a^2$.

Problem 11.5.3 *Contour dynamics for three-dimensional flow.*

Is it possible to derive a contour dynamics method for a three-dimensional (non-axisymmetric) vortex flow?

Computer problems

Problem c.11.5.1 *Motion of line vortex rings.*

Subdirectory *09_vortex/lvrm* of *FDLIB* contains a program that simulates the motion of a collection of line vortex rings in an unbounded domain of flow. Run the program to simulate the motion of a collection of rings of your choice, and discuss the nature of the motion.

Problem c.11.5.2 *Motion of vortex patches.*

Subdirectory *09_vortex/vp_ax* of *FDLIB* contains a program that simulates the motion of a specified number of axisymmetric vortex patches using the method of contour dynamics. In the numerical method, the contour of each patch is approximated with blended circular arcs, as discussed in Section 11.3. The marker points are redistributed adaptively during the motion to capture the development of regions of high curvature and prevent point clustering and dilution.

Run the program to simulate the motion of a patch of your choice, and discuss the nature of the motion.

11.6 Three-dimensional vortex motion

In previous sections, we have studied the dynamics of two-dimensional and axisymmetric vortex flows using (a) the integral representation of

the velocity in terms of the vorticity expressed by the Biot-Savart integral, and (b) simplified versions of the vorticity transport equation for inviscid flow. Extensions to three dimensions are straightforward in principle, but subtle in numerical implementation.

11.6.1 Vortex particles

The vortex-particle method arises by replacing the Biot-Savart integral shown in (11.4.11) with a sum of integrals over parcels of rotational fluid, and then condensing the vorticity of each parcel into a designated center. This approximation replaces the rotational fluid with a collection of three-dimensional singularities called *rotlets* or *vortons*. The strength of the vortons evolves according to rules stemming from the vorticity transport equation for three-dimensional flow, expressing stretching and reorientation.

The vorton discretization is analogous to the point-vortex or circular-line-vortex discretization of two-dimensional or axisymmetric flow. Because, however, the three-dimensional discretization breaks the continuity of the vortex lines, some fundamental difficulties arise in three dimensions. These difficulties, combined with high computational cost, explain why the vorton method is less attractive compared to its counterparts for two-dimensional and axisymmetric flow.

11.6.2 Line vortices and the local induction approximation

A simplified model of the self-induced motion of a three-dimensional vortex filament with small core size, as illustrated in figure 11.6.1, can be devised using our earlier results for vortex rings with small but non-infinitesimal core radius.

To compute the motion of the filament centerline, we evaluate the velocity at the position of point particles distributed over the centerline using the Biot-Savart integral (11.4.11), and then advance the position of the point particles using a standard numerical method. Our earlier discussion for vortex rings suggests that the self-induced velocity of the filament is determined, primarily, by the ratio between the local filament core radius and the local radius of curvature of the centerline, as shown in equation (11.5.24). This observation provides us with a basis for computing the motion of the centerline according to the *local induction approximation*.

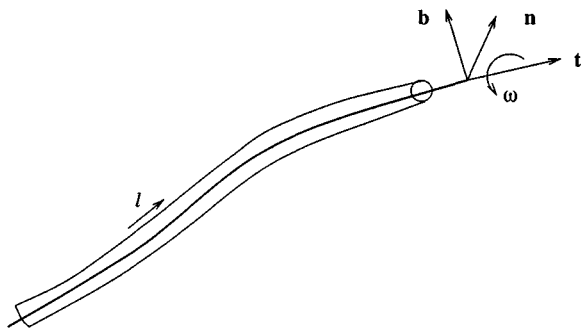


Figure 11.6.1 The motion of a thin vortex filament may be computed using the local induction approximation expressed by equations (11.6.1) and (11.6.2).

In this approximation, the velocity at a point along the centerline is assumed to be parallel to the local unit binormal vector \mathbf{b} , defined as the cross product of the unit tangent vector \mathbf{t} and the unit normal vector \mathbf{n} ,

$$\mathbf{b} = \mathbf{t} \times \mathbf{n}. \quad (11.6.1)$$

The unit tangent vector arises by differentiating the position vector \mathbf{x} with respect to arc length l along the centerline,

$$\mathbf{t} = \frac{d\mathbf{x}}{dl}, \quad (11.6.2)$$

and the unit normal vector arises by further differentiating the unit tangent vector with respect to arc length, obtaining

$$\mathbf{n} = -\frac{1}{R} \frac{d\mathbf{t}}{dl}. \quad (11.6.3)$$

The scalar coefficient R is the radius of curvature of the filament centerline. The self-induced velocity of the filament is given by

$$\mathbf{u} = u_b \mathbf{b}, \quad (11.6.4)$$

where κ is the strength of the filament. The magnitude of the velocity u_b derives from Helmholtz's formula (11.5.24) as

$$u_b = \frac{\kappa}{4\pi R} \left(-\ln \frac{8a}{R} - \frac{1}{4} \right), \quad (11.6.5)$$

where a is the local filament core radius, allowed to vary with position along the centerline.

The vorticity transport equation requires that the vorticity inside the filament core increase or decrease depending on whether the filament centerline undergoes stretching or compression. This constraint allows us to derive an evolution equation for the filament core radius, by requiring conservation of volume of rotational fluid composing the core. If δl is an infinitesimal arc length along the centerline corresponding to a material segment that begins and ends at two point particles, then conservation of volume requires

$$\frac{d}{dt}(\delta l \pi a^2) = 0, \quad (11.6.6)$$

which is the counterpart of equation (11.5.25) for axisymmetric flow. Expanding out the derivative of the product on the right-hand side of (11.6.6), and rearranging, we obtain the evolution equation

$$\frac{da}{dt} = -\frac{1}{2} \frac{a}{\delta l} \frac{d\delta l}{dt}, \quad (11.6.7)$$

which is the counterpart of equation (11.5.26) for axisymmetric flow.

A numerical method for computing the evolution of the centerline of a closed filament involves the following steps:

1. Trace the centerline with $N + 1$ marker points, and assign initial values to the core radius. Point 1 coincides with point $N + 1$.
2. Approximate the centerline over the interval subtended between points numbered $i - 1$ and $i + 1$ with a circular arc passing through the three points labelled $i - 1$, i , and $i + 1$, and compute the arc center and radius for $i = 1, 2, \dots, N$.
3. Compute the unit tangent, normal, and binormal vector at the i th marker point using equations (11.6.1) - (11.6.3), for $i = 1, 2, \dots, N$.
4. Set the radius of curvature of the line vortex at each point equal to the radius of the arc, R .
5. Advance the position of the marker points with the velocity computed from (11.6.4).
6. Update the core radius by requiring conservation of volume expressed by (11.6.6).

The motion of marker points computed using this method suffers from numerical instabilities that cause the onset of strong oscillations due to the violent amplification of numerical or round-off error. Smoothing the position of the marker points by the five-point formula (11.2.24) applied for the Cartesian coordinates of the marker points filters out the oscillations and allows the motion to be pursued for an extended period of time.

Stages in the evolution of a closed line vortex computed using program *09_vortex/lv_lia* of *FDLIB* are shown in figure 11.6.2. The numerical method incorporates adaptive point redistribution to capture the development of regions of high curvature. The simulation shows that the ring travels while exhibiting wobbly oscillations familiar to the cigar smoker.

Problem

Problem 11.6.1 *LIA for a circular line vortex ring.*

Confirm that the local induction approximation consistently describes the motion of a circular line vortex ring discussed in Section 11.5.

Computer problem

Problem c.11.6.1 *Motion of line vortex.*

Subdirectory *09_vortex/lv_lia* of *FDLIB* contains a program that simulates the motion of a closed line vortex using the local induction approximation. Run the program to simulate the evolution of a line vortex with initial shape and core radius of your choice, and discuss the nature of the motion.

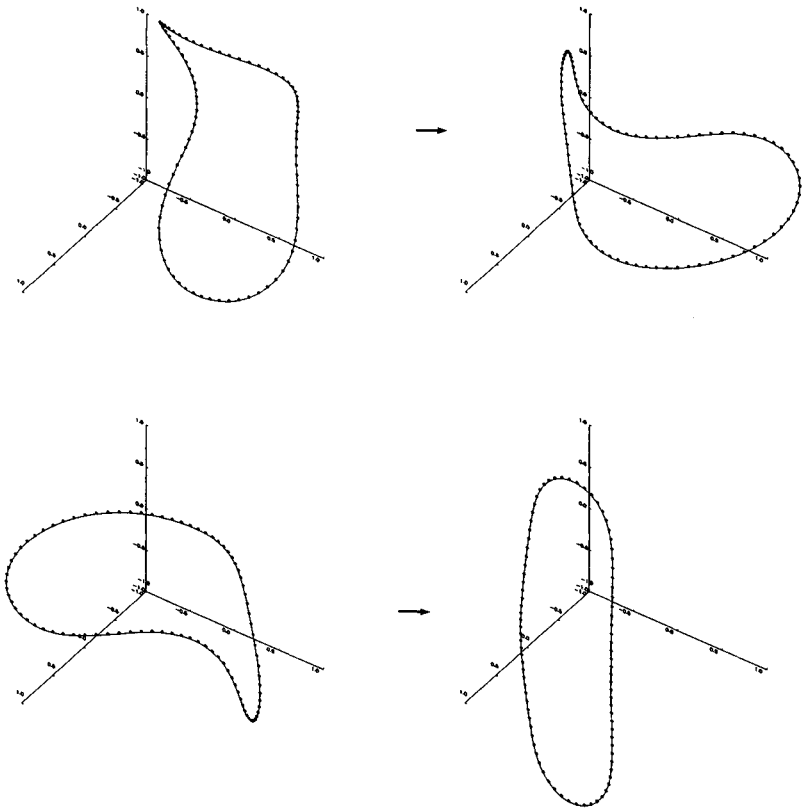


Figure 11.6.2 Stages in the evolution of a closed line vortex resembling a smoke ring, computed by program *09_vortex/lv_lia* of *FDLIB*.

Chapter 12

Aerodynamics

- 12.1 General features of flow past an aircraft**
- 12.2 Airfoils and the Kutta-Joukowski condition**
- 12.3 Vortex panels**
- 12.4 Vortex panel method**
- 12.5 Vortex sheet representation**
- 12.6 Point-source-dipole panels**
- 12.7 Point-source panels and Green's third identity**

Flows past airplane wings and high-speed ground vehicles have captured the attention of fluid dynamicists, applied mathematicians, and computational scientists and engineers, not only because of their obvious technological significance, but also because of the opportunity they present to perform elegant mathematical analyses and develop realistic and efficient numerical models. Although these flows occur at high Reynolds numbers, and often at transonic or supersonic speeds that are comparable to or even exceed the speed of sound, the effects of viscosity are important in two ways. First, viscous stresses determine the drag force exerted on the moving surfaces, and thus the energy required to sustain the motion; second, viscous stresses are responsible for the production of vorticity which generates circulation and thereby induces lift. A comprehensive analysis of a high-speed flow in aerodynamics incorporates the effects of fluid compressibility and turbulent motion, and accounts for the presence of boundary layers and regions of recirculating flow. In this chapter, we discuss the most basic configuration by neglecting the presence of boundary layers and wakes, and by assuming that the fluid is inviscid and incompressible. The simplified model, involving irrotational flow in the presence of global circulatory motion, is amenable to efficient numerical methods that illustrate the importance of computational fluid dynamics in the practical field of aerodynamics.

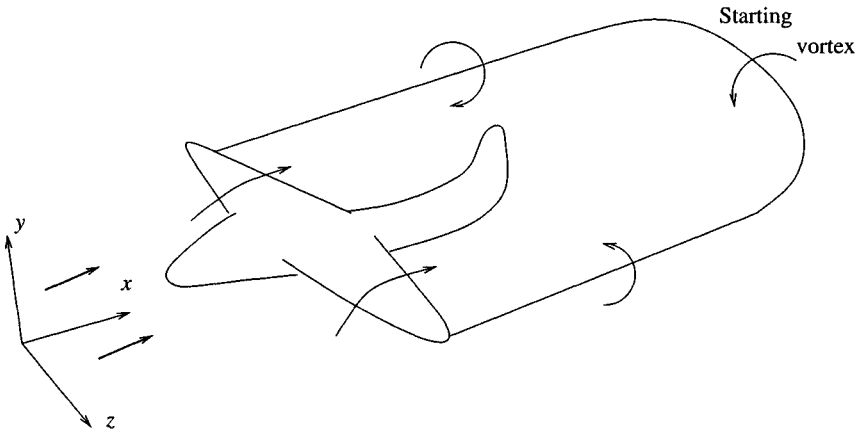


Figure 12.1.1 Schematic illustration of flow past an aircraft in a frame of reference moving with the aircraft.

12.1 General features of flow past an aircraft

Figure 12.1.1 shows a schematic illustration of flow past an aircraft after it has taken off and travelled by a certain distance, in a frame of reference moving with the aircraft. If the flow is subsonic, the following features are most significance:

- A thin vortex loop resembling a line vortex is established behind the aircraft. The loop extends from the left wing tip, back at a length comparable to the distance that the aircraft has travelled, and then forward up to the right wing tip. The trailing vortex at the back of the loop was generated when the airplane started moving, and is accordingly called the *starting vortex*. The vortex loop may be extended artificially into the wings to form a closed line vortex.

The circulation around any closed loop that encloses the line vortex is constant, independent of the shape and location of the loop. Thus, the circulation around a simple loop that encloses a wing is equal to the circulation around a simple loop that encloses the trailing vortex.

- Viscous stresses cause the vortex loop to diffuse and its vortex core to be smeared out. The circulation around any loop that encloses

the smeared vortex loop, however, is equal to the circulation around a loop that encloses a wing, no matter how far the vorticity has spread out.

- The circulation around a loop that encloses a wing is determined by the speed of the aircraft and the geometry and orientation of the wings with respect to the incoming wind, as will be discussed in Section 12.2.
- If the aircraft suddenly changes its speed or direction of flight, a new vortex loop will be ejected, contributing an additional amount of circulation around the wings.
- Each wing experiences a lift force normal to the direction of flight, and a drag force parallel to the direction of flight. The latter must be compensated by the thrust produced by the engines.

The lift force may be computed with surprisingly good accuracy by neglecting the effects of viscosity, and by assuming that the flow around the airfoil is irrotational. To compute the drag force, we may carry out a boundary-layer analysis of the basic irrotational flow, as discussed in Chapter 10.

It is important to bear in mind that the main features of the flow past an aircraft discussed in this section assume that the wings are only slightly tilted with respect to the direction of the incoming wind. When this condition is not met, regions of recirculating flow develop over the upper surface of the airfoil, seriously affecting the structure of the flow and the performance of the aircraft.

To study the flow past the wings and compute the lift force per unit span exerted on them, we may assume that the flow is locally two-dimensional occurring in the xy plane that is normal to the line connecting the wing tips. It turns out that neglecting the third dimension provides us with a theoretical model whose predictions are in good or even excellent agreement with laboratory measurements conducted in wind tunnels. Accordingly, in the remainder of this chapter, we concentrate on the two-dimensional flow, regarding the three-dimensional flow as an advanced topic suitable for a second course in aerodynamics.

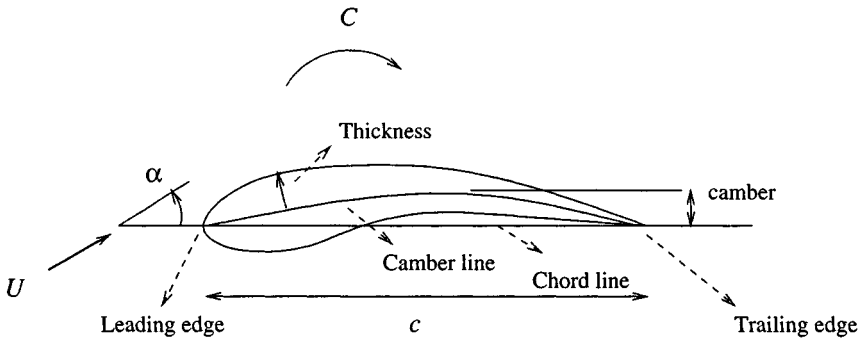


Figure 12.2.1 An airfoil and its standard geometrical properties.

12.2 Airfoils and the Kutta-Joukowski condition

An airfoil is a section of a wing, as depicted in figure 12.2.1. The shape of an airfoil is described by the following geometrical properties:

- The *chord line*, defined as the straight line connecting the leading to the trailing edge.
- The *chord*, denoted by c , defined as the distance between the leading and the trailing edge.
- The *camber line*, defined as the locus of points located halfway between the upper and lower surface of the airfoil.
- The *camber*, defined as the maximum distance between the camber line and the chord line. When the camber vanishes, the airfoil is symmetric.
- The airfoil *thickness* distribution along the camber line.

The angle α subtended between the incoming wind and the chord line is called the *angle of attack*.

12.2.1 NACA airfoils

The National Advisory Committee for Aeronautics of the United States, NACA, the ancestor of today's NASA, has standardized airfoil

shapes to facilitate engineering design. NACA airfoils are produced by specifying the geometry of the camber line, and then wrapping around the camber line the airfoil contour to obtain a desired distribution of half-thickness. The dated four-digit NACA $efgh$ airfoils, where e, f, g, h are four integers, has a camber of $0.0f \times c$ occurring at a distance $0.0f \times c$ from the leading edge, where c is the chord; the maximum airfoil thickness is $0.gh \times c$. Modern five- and six-digit airfoils are coded with additional geometrical and flow properties.

12.2.2 The Kutta-Joukowski theorem

It can be shown that the lift force per unit span exerted on an airfoil, L , is determined by the incoming wind speed, U , and the circulation around the airfoil, C , by means of the Kutta-Joukowski theorem expressed by

$$L = -\rho U C, \quad (12.2.1)$$

where ρ is the density of the fluid. Note that positive lift requires negative circulation associated with clockwise rotation around the airfoil, as illustrated in figure 12.2.1. If the circulation vanishes, the lift force is equal to zero.

The Kutta-Joukowski can be proved most readily making use of the theory of analytical functions of a complex variable, as discussed in the texts cited in the bibliography.

Flow past a cylinder

To confirm the validity of the Kutta-Joukowski theorem, we consider uniform flow past a circular cylinder with radius a , as discussed in Section 3.7. Applying Bernoulli's equation (6.4.14) at infinity and at a point on the surface of the cylinder, and evaluating the tangential velocity on the surface of the cylinder using formula (3.7.8), we derive an expression for the surface pressure,

$$p(r = a) = p_\infty - 2\rho V_\infty^2 (\sin \theta + \beta)^2, \quad (12.2.2)$$

where p_∞ is the pressure at infinity, and β is the dimensionless circulation parameter defined in equation (3.7.7). In the absence of viscous stresses, the force per unit span exerted on the cylinder is given by

$$\mathbf{F} = \oint [-p(r = a)] \mathbf{n} dl = - \int_0^{2\pi} p(r = a) \mathbf{n} a d\theta, \quad (12.2.3)$$

where $dl = a d\theta$ is the differential arc length around the cylinder, and $\mathbf{n} = (\cos \theta, \sin \theta)$ is the unit vector normal to the cylinder pointing into the fluid. Substituting (12.2.2) into (12.2.3), and carrying out the integration with respect to θ , we find that the x component of the force vanishes, and the y component is given by $L = 4\pi a \rho V_x^2 \beta$. Recalling the definition of β given in (3.7.7), we derive

$$L = -\rho V_x \kappa, \quad (12.2.4)$$

which is in agreement with the Kutta-Joukowski theorem expressed by (12.2.1).

12.2.3 The Kutta-Joukowski condition

In the context of irrotational flow theory, the circulation around an airfoil, or any two-dimensional body, may be arbitrary. Kutta and Joukowski observed independently that, in practice, when the angle of attack α is small, the flow on the upper side of an airfoil joins smoothly with the flow on the lower side of the airfoil at the trailing edge. This observation provides us with a physical basis for the Kutta-Joukowski condition stipulating that the amount of circulation established around an airfoil is such that a singular flow is not established at the trailing edge. In the context of irrotational flow theory, the Kutta-Joukowski condition requires that the fluid does not turn around a cornered or cusped trailing edge.

Considering the Kutta-Joukowski theorem expressed by (12.2.1), we see that a well-designed airfoil should be able to produce a high degree of circulation while minimizing the drag force exerted on the airfoil.

Problem

Problem 12.2.1 *Flow past a cylinder.*

Carry out the integration in (12.2.3) with the pressure given in (12.2.2) to derive expression (12.2.4).

Computer problem

Problem c.12.2.1 *Airfoil shapes by mapping.*

Airfoil shapes may be produced by mapping a closed contour in the (ξ, η) plane to the airfoil contour in the xy plane, using an appropriate mapping function. In theoretical aerodynamics, the mapping function arises from a function of a complex variable f , by setting $z = f(\zeta)$, where $z \equiv x + iy$, $\zeta \equiv \xi + i\eta$ are two complex variables, and i is the imaginary unit. Joukowski's transformation employs the mapping function

$$f(\zeta) = \zeta + \frac{\lambda^2}{\zeta}, \quad (12.2.5)$$

where λ is a real constant. A circle in the ζ plane passing through the point $(-\lambda, 0)$ and enclosing the reflected point $(\lambda, 0)$ is mapped to a cusped airfoil whose camberline and camber are determined by the location of the center of the circle in the ζ plane.

Program `07_ptf/airf_2d/joukowski` of *FDLIB* produces airfoil shapes using the Joukowski mapping function (12.2.5). Run the program to generate and graph several airfoil shapes of your choice.

12.3 Vortex panels

We begin the study of two-dimensional flow past an airfoil by introducing a class of elementary flows associated with vortex panels. Our ultimate objective is to use these elementary flows as fundamental building blocks for describing the flow past an airfoil with arbitrary shape, where the circulation around the airfoil is determined by the Kutta-Joukowski condition.

In Section 3.7, we introduced the two-dimensional irrotational flow with circulatory motion induced by a point vortex. The x and y components of the velocity at the point (x, y) due to a point vortex with strength κ located at the point (x_0, y_0) were given in equations (11.2.1), repeated here for ready reference,

$$\begin{aligned} u_x(x, y) &= -\frac{\kappa}{2\pi} \frac{y - y_0}{(x - x_0)^2 + (x - y_0)^2}, \\ u_y(x, y) &= \frac{\kappa}{2\pi} \frac{x - x_0}{(x - x_0)^2 + (x - y_0)^2}. \end{aligned} \quad (12.3.1)$$

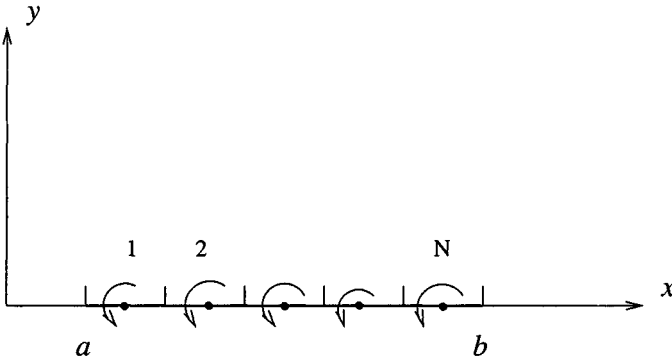


Figure 12.3.1 A collection of N point vortices deployed along the x axis over the interval (a, b) . As N tends to infinity, we obtain a vortex panel.

The corresponding stream function and velocity potential are given, respectively, by

$$\psi(x, y) = -\frac{\kappa}{4\pi} \log[(x - x_0)^2 + (y - y_0)^2], \quad (12.3.2)$$

and

$$\phi(x, y) = \frac{\kappa}{2\pi} \arctan \frac{y - y_0}{x - x_0}. \quad (12.3.3)$$

12.3.1 From point vortices to vortex panels

Consider a collection of N point vortices distributed evenly along the x axis over the interval (a, b) , separated by the distance $\Delta x = (b - a)/N$, as illustrated in figure 12.3.1. The i th point vortex is situated at the position $x_i = a + \frac{i}{2} \Delta x$, $y_i = 0$, where $i = 1, 2, \dots, N$, and its strength is equal to κ_i ; the first point vortex is located at $x_1 = a + \frac{1}{2} \Delta x$, and the last point vortex is located at $x_N = b - \frac{1}{2} \Delta x$.

Superposing the stream functions associated with the individual point vortices, we find that the stream function of the flow induced by the point vortex collection is given by

$$\psi(x, y) = -\sum_{i=1}^N \frac{\kappa_i}{4\pi} \log[(x - x_i)^2 + (y - y_i)^2], \quad (12.3.4)$$

which can be recast into the form

$$\psi(x, y) = - \sum_{i=1}^N \frac{1}{4\pi} \log[(x - x_i)^2 + (y - y_i)^2] \frac{\kappa_i}{\Delta x} \Delta x, \quad (12.3.5)$$

with the understanding that $y_i = 0$.

In the limit as N tends to infinity, and correspondingly Δx tends to zero, while the strength of the point vortices is reduced so that the ratio $\gamma_i \equiv \kappa_i/\Delta x$ remains constant, the sum on the right-hand side of (12.3.5) reduces to a line integral over the domain of distribution of the point vortices, yielding the integral representation

$$\psi^{VP}(x, y) = - \frac{1}{4\pi} \int_a^b \log[(x - x')^2 + (y - y')^2] \gamma(x') dx', \quad (12.3.6)$$

with the understanding that $y' = 0$. The right-hand side of (12.3.6) expresses the flow due to a two-dimensional *finite vortex sheet* or *vortex panel* with strength density $\gamma(x)$, subtended between the points $x = a$ and b , as indicated by the superscript VP. The circulation around the panel, defined as the strength of the panel, is equal to the line integral of the strength density,

$$\Gamma_p \equiv \int_a^b \gamma(x) dx. \quad (12.3.7)$$

Following the discussion in Section 3.7, we find that the circulation around a closed loop that does not enclose the panel vanishes, whereas the circulation around a simple closed loop that wraps around the panel once is equal to the strength of the panel, Γ_p . If the strength of the panel is equal to zero, the circulation vanishes.

12.3.2 Vortex panels with constant strength density

Consider a vortex panel with constant strength density equal to $\gamma^{(0)}$; according to (13.3.7), the circulation around the panel is equal to $\Gamma_p = (b - a) \gamma^{(0)}$. Using (12.3.6) with $y' = 0$, we find that the stream function of the induced flow is given by

$$\psi^{(0)}(x, y) = - \frac{\gamma^{(0)}}{4\pi} \int_a^b \log[(x - x')^2 + y^2] dx'. \quad (12.3.8)$$

The integral on the right-hand side of (12.3.8) may be computed in closed form with the aid of standard mathematical tables, and the result is

$$\begin{aligned} \psi^{(0)}(x, y) = & -\frac{\gamma^{(0)}}{4\pi} [-(x-b) \log[(x-b)^2 + y^2] \\ & + (x-a) \log[(x-a)^2 + y^2] \\ & + 2y (\arctan \frac{y}{x-b} - \arctan \frac{y}{x-a}) - 2(b-a)]. \end{aligned} \quad (12.3.9)$$

The velocity components are found by straightforward differentiation, and are given by

$$u_x^{(0)}(x, y) = \frac{\partial \psi^{(0)}}{\partial y} = -\frac{\gamma^{(0)}}{2\pi} [\arctan \frac{y}{x-b} - \arctan \frac{y}{x-a}], \quad (12.3.10)$$

and

$$u_y^{(0)}(x, y) = -\frac{\partial \psi^{(0)}}{\partial x} = -\frac{\gamma^{(0)}}{4\pi} \ln \frac{(x-b)^2 + y^2}{(x-a)^2 + y^2}. \quad (12.3.11)$$

The streamline pattern induced by a vortex panel subtended between the points $x = -b$ and b is shown in figure 12.3.2. Far from the panel, the flow reduces to that due to a point vortex with strength $\kappa = \Gamma_p = \gamma^{(0)}(b-a) = 2b\gamma^{(0)}$ situated at the origin.

Jump in velocity across the panel

Expression (12.3.11) shows that the y component of the velocity is continuous throughout the domain of flow as well as across the vortex panel. In contrast, because of the presence of the inverse tangent function on the right-hand side of (12.3.10), the x component of the velocity undergoes a discontinuity across the vortex panel. To demonstrate this jump, we evaluate the velocity at a point on the upper surface of the panel, for $a < x < b$ and $y = +\epsilon$, where ϵ is a small positive number, and find

$$\begin{aligned} u_x^{(0)}(x, y \rightarrow 0+) = & -\frac{\gamma^{(0)}}{2\pi} [-\arctan(-\infty) + \arctan(+\infty)] \\ = & -\frac{\gamma^{(0)}}{2\pi} \left[\frac{\pi}{2} + \frac{\pi}{2} \right] = -\frac{\gamma^{(0)}}{2}, \end{aligned} \quad (12.3.12)$$

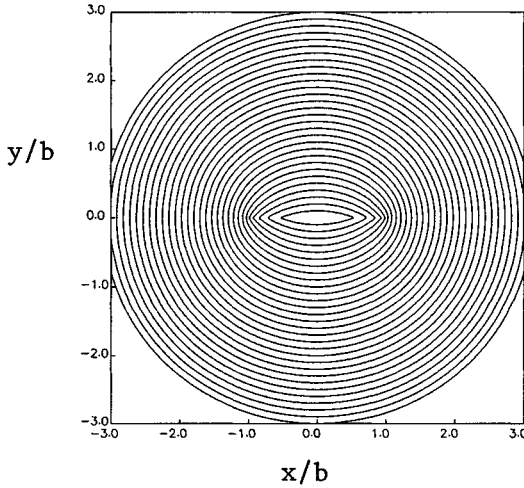


Figure 12.3.2 Streamline pattern of the flow induced by a vortex panel with constant strength situated on the x axis over the interval $-b < x < b$.

independent of x , as long as $a < x < b$. The corresponding velocity at a point on the lower surface of the panel, located at $x < b$ and $x > a$, is given by

$$\begin{aligned} u_x^{(0)}(x, \rightarrow 0-) &= -\frac{\gamma^{(0)}}{2\pi} [-\arctan(+\infty) + \arctan(-\infty)] \\ &= -\frac{\gamma^{(0)}}{2\pi} \left[-\frac{\pi}{2} - \frac{\pi}{2}\right] = \frac{\gamma^{(0)}}{2}, \end{aligned} \quad (12.3.13)$$

independent of x , as long as $a < x < b$. Thus, as the vortex panel is crossed from the upper to the lower side, the velocity undergoes a discontinuity whose magnitude is equal to the strength of the vortex sheet,

$$u_x(x, -\epsilon) - u_x(x, +\epsilon) = \gamma^{(0)}. \quad (12.3.14)$$

In contrast, no discontinuity occurs when the x axis is crossed beyond the edges of the vortex panel.

These observations identify a vortex sheet with a surface across which the tangential component of the velocity undergoes a discontinuity; the magnitude of the discontinuity is the strength of the vortex sheet.

13.3.3 Vortex panel with linear strength density

Next, we consider a vortex panel with linear strength density distribution given by

$$\gamma(x) = \gamma^{(0)} + \gamma^{(1)}(x - a). \quad (12.3.15)$$

Using (13.2.7), we find that the circulation around the panel is given

$$\begin{aligned} \Gamma_p &= \int_a^b \gamma \, dx = (b - a) \left[\gamma^{(0)} + \frac{1}{2} \gamma^{(1)}(b - a) \right] \\ &= (b - a) \gamma \left(\frac{a + b}{2} \right). \end{aligned} \quad (12.3.16)$$

Applying (12.3.6) with $y' = 0$, and rearranging, we find that the stream function of the flow induced by the panel is given by

$$\begin{aligned} \psi^{(01)}(x, y) &= -\frac{\gamma^{(0)} + \gamma^{(1)}(x - a)}{4\pi} \int_a^b \ln[(x - x')^2 + y^2] \, dx' \\ &\quad - \frac{\gamma^{(1)}}{4\pi} \int_a^b (x' - x) \ln[(x - x')^2 + y^2] \, dx'. \end{aligned} \quad (12.3.17)$$

The first integral on the right-hand side of (12.3.17) is equal to the expression enclosed by the square brackets following the fraction on the right-hand side of (12.3.9). The second integral is found with the help of standard tables of integrals to be

$$\begin{aligned} \int_a^b (x' - x) \ln[(x - x')^2 + y^2] \, dx' &= \frac{1}{2} [(x - b)^2 + y^2] \ln[(x - b)^2 + y^2] \\ &\quad - \frac{1}{2} [(x - a)^2 + y^2] \ln[(x - a)^2 + y^2] - \frac{1}{2} (x - b)^2 + \frac{1}{2} (x - a)^2. \end{aligned} \quad (12.3.18)$$

Combining (12.3.8), (12.3.18), and (12.3.6), and consolidating various terms, we find

$$\psi^{(01)}(x, y) = \psi^{(0)}(x, y) + \psi^{(1)}(x, y), \quad (12.3.19)$$

where $\psi^{(0)}$ is given by (12.3.9), and

$$\begin{aligned} \psi^{(1)}(x, y) = & -\frac{\gamma^{(1)}}{4\pi} \left[\frac{1}{2} [y^2 - (x-b)(x+b-2a)] \ln[(x-b)^2 + y^2] \right. \\ & - \frac{1}{2} [y^2 - (x-a)^2] \ln[(x-a)^2 + y^2] \\ & + 2y(x-a) \left(\arctan \frac{y}{x-b} - \arctan \frac{y}{x-a} \right) \\ & \left. - \frac{1}{2}(x-b)^2 + \frac{1}{2}(x-a)^2 - 2(x-a)(b-a) \right]. \end{aligned} \quad (12.3.20)$$

The velocity components may be resolved into the corresponding forms

$$u_x^{(01)}(x, y) = u_x^{(0)}(x, y) + u_x^{(1)}(x, y), \quad (12.3.21)$$

and

$$u_y^{(01)}(x, y) = u_y^{(0)}(x, y) + u_y^{(1)}(x, y), \quad (12.3.22)$$

where $u_x^{(0)}$ and $u_y^{(0)}$ are given in (12.3.10) and (12.3.11). Tedious differentiation yields

$$\begin{aligned} u_x^{(1)}(x, y) = & \frac{\partial \psi^{(1)}}{\partial y} = -\frac{\gamma^{(1)}}{4\pi} \left[y \ln \frac{(x-b)^2 + y^2}{(x-a)^2 + y^2} \right. \\ & \left. + 2(x-a) \left(\arctan \frac{y}{x-b} - \arctan \frac{y}{x-a} \right) \right], \end{aligned} \quad (12.3.23)$$

and

$$\begin{aligned} u_y^{(1)}(x, y) = & -\frac{\partial \psi^{(1)}}{\partial x} = -\frac{\gamma^{(1)}}{4\pi} \left[(x-a) \ln \frac{(x-b)^2 + y^2}{(x-a)^2 + y^2} \right. \\ & \left. - 2y \left(\arctan \frac{y}{x-b} - \arctan \frac{y}{x-a} \right) + 2(b-a) \right]. \end{aligned} \quad (12.3.24)$$

Using these expressions, we find that, as the vortex panel is crossed normal to the x axis, the x component of the velocity undergoes a discontinuity whose magnitude is equal to the local strength of the vortex sheet.

The streamline pattern of the flow induced by a vortex panel subtended between the points $x = -b$ and b , with linear strength density

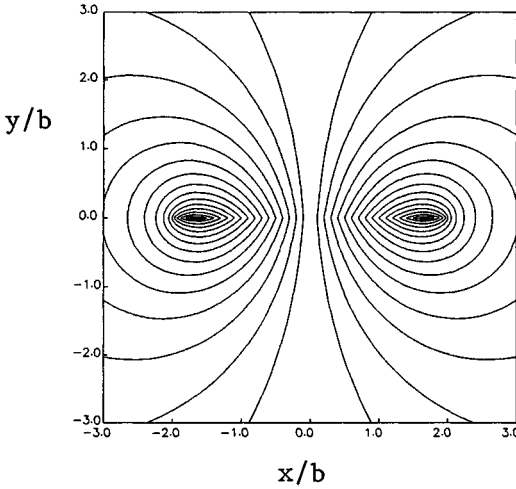


Figure 12.3.3 Streamline pattern of flow due to a vortex panel with linear strength distribution extending between $x = -b$ and b , for vanishing circulation around the panel.

distribution given by $\gamma^{(1)} = -2\gamma^{(0)}/(b - a) = -\gamma^{(0)}/b$, is shown in figure 12.3.3. Because the circulation around the panel vanishes, as required by equation (12.3.16), far from the panel the flow reduces to that due to a point-vortex dipole situated at the center of the panel and pointing along the x axis, which is identical to the flow due to a point-source dipole placed at the same location and pointing along the y axis.

Problem

Problem 12.3.1 *Velocity potential due to vortex panels.*

Show that the velocity potentials corresponding to the stream functions (12.3.9) and (12.3.20) are given, respectively, by

$$\begin{aligned} \phi^{(0)}(x, y) = & -\frac{\gamma^{(0)}}{2\pi} \left[(x - b) \arctan \frac{y}{x - b} - (x - a) \arctan \frac{y}{x - a} \right. \\ & \left. + \frac{1}{2} y \ln \frac{(x - b)^2 + y^2}{(x - a)^2 + y^2} \right], \end{aligned} \tag{12.3.25}$$

and

$$\begin{aligned}
 \phi^{(1)}(x, y) = & -\frac{\gamma^{(1)}}{4\pi} \left\{ (x-a)y \ln \frac{(x-b)^2 + y^2}{(x-a)^2 + y^2} \right. \\
 & + [(x-a)^2 - (b-a)^2 - y^2] \arctan \frac{y}{x-b} \\
 & \left. - [(x-a)^2 - y^2] \arctan \frac{y}{x-a} + y(b-a) \right\}.
 \end{aligned}
 \tag{12.3.26}$$

12.4 Vortex panel method

In Section 12.3, we considered the flow induced by vortex panels with constant or linear density distributions. Having available these elementary panel flows, we proceed to develop the vortex-panel method that allows us to compute irrotational flow past a two-dimensional airfoil with the Kutta-Joukowski condition satisfied at the trailing edge.

The key idea is to represent the flow in terms of a superposition of (a) the incident streaming flow, and (b) a collection of flows induced by vortex panels with *a priori* unknown strength densities deployed around the contour of an airfoil, and then compute the panel strength densities to satisfy the no-penetration boundary condition around the airfoil.

12.4.1 Contour discretization

Consider uniform flow with velocity $\mathbf{U} = (U_x, U_y)$, past an airfoil at angle of attack α , as illustrated in figure 12.4.1. As a preliminary, we trace the contour of the airfoil with $N + 1$ marker points distributed around the airfoil in the clockwise sense, where points numbered 1 and $N + 1$ coincide with the trailing edge. A pair of successive points $\mathbf{x}^{(i)}$ and $\mathbf{x}^{(i+1)}$ define a flat vortex panel labelled i . The collection of the N vortex panels defines a polygonal contour which is an approximation to the generally curved contour of the airfoil.

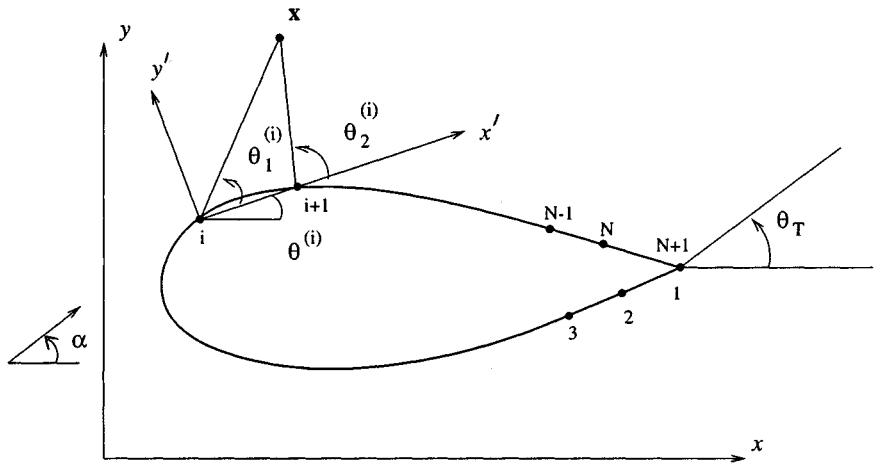


Figure 12.4.1 Discretization of the contour of an airfoil into flat panels defined by a sequence of marker points.

12.4.2 Flow representation

In the vortex-panel method, the velocity at the point (x, y) is expressed by the superposition

$$\mathbf{u}(x, y) = \mathbf{U} + \sum_{i=1}^N \mathbf{u}^{(i)}(x, y), \tag{12.4.1}$$

where $\mathbf{u}^{(i)}(x, y)$ is the velocity induced by the i th vortex panel.

In the implementation discussed in this section, we use panels with linear strength density. The strength density of the i th panel varies in a linear fashion from the value γ_i assigned to the i th marker point, which is the first point of the i th panel, to the value γ_{i+1} assigned to the $i + 1$ marker point, which is the last point of the i th panel. The $N + 1$ *a priori* unknown values $\gamma_i, i = 1, 2, \dots, N + 1$ must be computed to satisfy the no-penetration condition around the airfoil in some approximate fashion.

We proceed by observing that the velocity induced by the i th panel, denoted by $\mathbf{u}^{(i)}(x, y)$, is determined by the position and strength density of the panel at the two end-points. To signify this dependence, we write

$$\mathbf{u}^{(i)}(x, y) = \mathbf{u}^{LVP}(x, y; \mathbf{x}^{(i)}, \mathbf{x}^{(i+1)}, \gamma^{(i)}, \gamma^{(i+1)}), \tag{12.4.2}$$

where the superscript *LVP* stands for “linear vortex panel”.

12.4.3 Panel-induced velocity in global coordinates

Our first task is to develop a numerical method for computing \mathbf{u}^{LVP} as a function of its arguments listed in (12.4.2), using the formulas developed in Section 12.3. For this purpose, we introduce a local coordinate system (x', y') with the x' axis passing through the two end points of the i th panel, $\mathbf{x}^{(i)}$ and $\mathbf{x}^{(i+1)}$, and set the origin at the first end-point $\mathbf{x}^{(i)}$, as depicted in figure 12.4.1. The coordinates of a point in the local system (x', y') are related to those in the global system (x, y) by the equations

$$\begin{aligned}x' &= (x - x^{(i)}) \cos \theta^{(i)} + (y - y^{(i)}) \sin \theta^{(i)}, \\y' &= -(x - x^{(i)}) \sin \theta^{(i)} + (y - y^{(i)}) \cos \theta^{(i)},\end{aligned}\tag{12.4.3}$$

where $\theta^{(i)}$ is the inclination of the i th panel defined in figure 12.4.1.

Next, we express the strength density of the i th panel in the linear form

$$\gamma(x') = \gamma^{(0)} + \gamma^{(1)}(x' - x'^{(i)}),\tag{12.4.4}$$

with the understanding that $x'^{(i)} = 0$, and require

$$\begin{aligned}\gamma(x' = x'^{(i)}) &= \gamma^{(0)} = \gamma^{(i)}, \\ \gamma(x' = x'^{(i+1)}) &= \gamma^{(0)} + \gamma^{(1)}(x'^{(i+1)} - x'^{(i)}) = \gamma^{(i+1)},\end{aligned}\tag{12.4.5}$$

to find

$$\gamma^{(0)} = \gamma^{(i)}, \quad \gamma^{(1)} = \frac{\gamma^{(i+1)} - \gamma^{(i)}}{x'^{(i+1)} - x'^{(i)}}.\tag{12.4.6}$$

The length of the panel is given by $x'^{(i+1)} = \sqrt{(x_{i+1} - x_i)^2 + (y_{i+1} - y_i)^2}$.

Reviewing the results of Section 12.3, we find that the x' and y' components of the velocity induced by the i th panel are given by equations (12.3.21) and (12.3.22), subject to the following substitutions:

$$\begin{aligned}
a &\rightarrow 0 \\
b &\rightarrow x'^{(i+1)} \\
\gamma^{(0)} &\rightarrow \gamma^{(i)} \\
\gamma^{(1)} &\rightarrow \frac{\gamma^{(i+1)} - \gamma^{(i)}}{x'^{(i+1)} - x'^{(i)}} \\
x &\rightarrow x' \\
y &\rightarrow y'
\end{aligned} \tag{12.4.7}$$

Carrying out some algebra, we find that the velocity components of the flow induced by the i th panel in the local frame are given by

$$\begin{aligned}
u_{x'}^{(i)}(x', y') &= a_{x'}^{(i,1)} \gamma^{(i)} + a_{x'}^{(i,2)} \gamma^{(i+1)}, \\
u_{y'}^{(i)}(x', y') &= a_{y'}^{(i,1)} \gamma^{(i)} + a_{y'}^{(i,2)} \gamma^{(i+1)},
\end{aligned} \tag{12.4.8}$$

where $a_{x'}^{(i,1)}$, $a_{x'}^{(i,2)}$, $a_{y'}^{(i,1)}$, and $a_{y'}^{(i,2)}$ are *local* influence coefficients given by

$$\begin{aligned}
a_{x'}^{(i,1)} &= \frac{1}{2\pi x'_2} [y' c + (x' - x'_2) \Delta\theta'], \\
a_{y'}^{(i,1)} &= \frac{1}{2\pi x'_2} [(x' - x'_2) c - y' \Delta\theta' + x'_2], \\
a_{x'}^{(i,2)} &= -\frac{1}{2\pi x'_2} [y' c + x' \Delta\theta'], \\
a_{y'}^{(i,2)} &= -\frac{1}{2\pi x'_2} [x' c - y' \Delta\theta' + x'_2],
\end{aligned} \tag{12.4.9}$$

and we have defined

$$\begin{aligned}
x'_2 &\equiv x'^{(i+1)}, \quad \Delta\theta' \equiv \theta'_2 - \theta'_1, \quad \theta'_2 \equiv \arctan \frac{y'}{x' - x'_2}, \\
\theta'_1 &\equiv \arctan \frac{y'}{x'}, \quad c \equiv \ln\left(\frac{(x' - x'_2)^2 + y'^2}{x'^2 + y'^2}\right)^{1/2}.
\end{aligned} \tag{12.4.10}$$

To obtain the velocity components in the global frame, we use the inverse of the coordinate transformation shown in (12.4.3), finding

$$\begin{aligned}
 u_x^{(i)}(x, y) &= u_{x'}^{(i)}(x', y') \cos \theta^{(i)} - u_{y'}^{(i)}(x', y') \sin \theta^{(i)}, \\
 u_y^{(i)}(x, y) &= u_{x'}^{(i)}(x', y') \sin \theta^{(i)} + u_{y'}^{(i)}(x', y') \cos \theta^{(i)}.
 \end{aligned}
 \tag{12.4.11}$$

Substituting expressions (12.4.8) into the right-hand sides of equations (12.4.11), and rearranging, we obtain explicit relations in terms of the strength of the vortex sheet at the end points,

$$\begin{aligned}
 u_x^{(i)}(x, y) &= a_x^{(i,1)} \gamma^{(i)} + a_x^{(i,2)} \gamma^{(i+1)}, \\
 u_y^{(i)}(x, y) &= a_y^{(i,1)} \gamma^{(i)} + a_y^{(i,2)} \gamma^{(i+1)},
 \end{aligned}
 \tag{12.4.12}$$

where $a_x^{(i,1)}$, $a_x^{(i,2)}$, $a_y^{(i,1)}$, and $a_y^{(i,2)}$ are *global* influence coefficients given by

$$\begin{aligned}
 a_x^{(i,1)}(x, y) &= a_{x'}^{(i,1)}(x', y') \cos \theta^{(i)} - a_{y'}^{(i,1)}(x', y') \sin \theta^{(i)}, \\
 a_x^{(i,2)}(x, y) &= a_{x'}^{(i,2)}(x', y') \cos \theta^{(i)} - a_{y'}^{(i,2)}(x', y') \sin \theta^{(i)}, \\
 a_y^{(i,1)}(x, y) &= a_{x'}^{(i,1)}(x', y') \sin \theta^{(i)} + a_{y'}^{(i,1)}(x', y') \cos \theta^{(i)}, \\
 a_y^{(i,2)}(x, y) &= a_{x'}^{(i,2)}(x', y') \sin \theta^{(i)} + a_{y'}^{(i,2)}(x', y') \cos \theta^{(i)}.
 \end{aligned}
 \tag{12.4.13}$$

Given the coordinates of the evaluation point (x, y) , we evaluate these coefficients by carrying out the following steps:

1. Compute the panel inclination angle $\theta^{(i)}$ and the panel length $x'_2 \equiv x'^{(i+1)} = \sqrt{(x_{i+1} - x_i)^2 + (y_{i+1} - y_i)^2}$.
2. Compute the local coordinates (x', y') using (12.4.3).
3. Compute the local influence coefficients using (12.4.9).
4. Compute the global influence coefficients using (12.4.13).

12.4.4 Velocity in terms of the strength of the vortex panels at the nodes

Substituting expressions (12.4.12) into the right-hand side of (12.4.1), we obtain explicit expressions for the global components of the velocity in terms of the strength of the vortex panels at the nodes,

$$\begin{aligned}
 u_x(x, y) &= U_x + \sum_{i=1}^N [a_x^{(i,1)}(x, y) \gamma^{(i)} + a_x^{(i,2)}(x, y) \gamma^{(i+1)}] \\
 &= \sum_{i=1}^{N+1} b_x^{(i)}(x, y) \gamma^{(i)}, \\
 u_y(x, y) &= U_y + \sum_{i=1}^N [a_y^{(i,1)}(x, y) \gamma^{(i)} + a_y^{(i,2)}(x, y) \gamma^{(i+1)}] \\
 &= \sum_{i=1}^{N+1} b_y^{(i)}(x, y) \gamma^{(i)},
 \end{aligned} \tag{12.4.14}$$

where we have introduced the new influence coefficients

$$\begin{aligned}
 b_x^{(1)}(x, y) &= b_x^{(1,1)}(x, y), \\
 b_x^{(2)}(x, y) &= b_x^{(1,2)}(x, y) + b_x^{(2,1)}(x, y), \\
 b_x^{(3)}(x, y) &= b_x^{(2,2)}(x, y) + b_x^{(3,1)}(x, y), \\
 &\dots \\
 b_x^{(N)}(x, y) &= b_x^{(N-1,2)}(x, y) + b_x^{(N,1)}(x, y), \\
 b_x^{(N+1)}(x, y) &= b_x^{(N,2)}(x, y).
 \end{aligned} \tag{12.4.15}$$

The coefficients $b_y^{(i)}$ are defined by corresponding expressions.

12.4.5 Point collocation

If we knew the strength of the vortex panels at the nodes, we could use equations (12.4.14) to evaluate the velocity at any point in the flow. The main idea underlying the vortex-panel method is that the $N + 1$

a priori unknown values $\gamma^{(i)}$, $i = 1, 2, \dots, N$, should be computed to satisfy the no-penetration condition

$$\mathbf{u}(\mathbf{x}) \cdot \mathbf{n}(\mathbf{x}) = 0, \quad (12.4.16)$$

where the point \mathbf{x} is located at the contour of the airfoil, and \mathbf{n} is the unit vector normal to the contour of the airfoil.

In the panel-collocation method, N equations emerge by requiring the satisfaction of (12.4.16) at the mid-point of each panel, located at

$$\mathbf{x}_M^{(j)} = \frac{1}{2} (\mathbf{x}^{(j)} + \mathbf{x}^{(j+1)}), \quad (12.4.17)$$

where $j = 1, 2, \dots, N$. Using (12.4.14) to express the velocity in terms of the strength of the vortex sheet, and rearranging, we find

$$\sum_{i=1}^{N+1} A_{i,j} \gamma^{(i)} = -U_x n_x(x_M^{(j)}, y_M^{(j)}) - U_y n_y(x_M^{(j)}, y_M^{(j)}), \quad (12.4.18)$$

where we have defined

$$A_{i,j} \equiv b_x^{(i)}(x_M^{(j)}, y_M^{(j)}) n_x(x_M^{(j)}, y_M^{(j)}) + b_y^{(i)}(x_M^{(j)}, y_M^{(j)}) n_y(x_M^{(j)}, y_M^{(j)}). \quad (12.4.19)$$

It is important to bear in mind that, when $i = j$, the self-induced velocity is evaluated at the mid-point of the panel *on the side of the flow*. With reference to equations (12.4.9), this means that $y' = 0$, $c = 0$, and $\Delta\theta' = \pi$.

Applying equation (12.4.18) for $j = 1, 2, \dots, N$, we obtain a system of N linear algebraic equations for the $N + 1$ unknowns $\gamma^{(i)}$. One degree of freedom is available and can be used to arbitrarily specify the amount of circulation around the airfoil. In Section 12.2, we saw that, in practice, the circulation established around the airfoil is such that the Kutta-Joukowski condition is fulfilled at the trailing edge. In the present formulation, this condition is implemented by requiring that the strength of the vortex sheet on the upper side of the airfoil at the trailing edge is equal in magnitude and opposite in sign to the strength of the vortex sheet on the lower side of the airfoil at the trailing edge. The mathematical statement of the Kutta-Joukowski condition is then

$$\gamma^{(1)} = -\gamma^{(N+1)}. \quad (12.4.20)$$

Appending this equation to equation (12.4.18) written for $j = 1, 2, \dots, N$, we obtain the desired system of $N + 1$ equations for the $N + 1$ unknowns $\gamma^{(i)}$. The solution may be computed using, for example, the method of Gauss elimination discussed in Section 3.4.

12.4.6 Pressure coefficient and lift force

Once the strength of the vortex sheet has been computed, the tangential velocity, $u_t = \mathbf{u} \cdot \mathbf{t}$, may be evaluated from the discrete representation (12.4.14), where \mathbf{t} is the unit vector tangent to the airfoil pointing along the local x' axis. The circulation around the airfoil may be approximated with either one of the expressions

$$C = - \sum_{i=1}^N u_t(\mathbf{x}_M^{(i)}) = \frac{1}{2} \sum_{i=1}^N (\gamma^{(i)} + \gamma^{(i+1)}) \Delta l^{(i)}, \quad (12.4.21)$$

where $\Delta l^{(i)}$ is the length of the i th panel. The second expression implements the trapezoidal rule for integrating the strength of the vortex sheet with respect to arc length around the airfoil.

The dimensionless pressure coefficient at the panel mid-points is defined by the expression

$$c_p^{(i)}(\mathbf{x}_M^{(i)}) \equiv \frac{p(\mathbf{x}_M^{(i)}) - p_\infty}{\frac{1}{2} \rho U^2} = 1 - \frac{u_t^2(\mathbf{x}_M^{(i)})}{U^2}, \quad (12.4.22)$$

where p_∞ is the pressure at infinity, and $U^2 \equiv U_x^2 + U_y^2$.

The distribution of the pressure coefficient and the streamline pattern around a NACA airfoil computed by the linear vortex panel method described in this section, implemented in program *07_ptf/airf_2d.lvp* of *FDLIB*, are illustrated in figure 12.4.2. High pressure coefficient corresponds to the lower surface of the airfoil, and low pressure coefficient corresponds to the upper surface of the airfoil; the difference produces a lift force.

In the absence of viscous stresses, the force exerted on the airfoil is given by the pressure integral

$$\mathbf{F} = \oint (-p) \mathbf{n} dl = \frac{1}{2} \rho U^2 \oint (-c_p + p^\infty) \mathbf{n} dl = -\frac{1}{2} \rho U^2 \oint c_p \mathbf{n} dl, \quad (12.4.23)$$

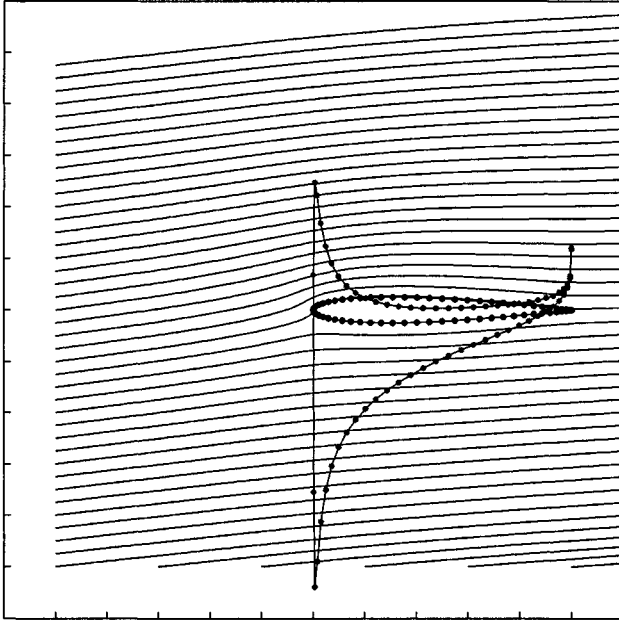


Figure 12.4.2 Distribution of the pressure coefficient around the upper and lower surface of a NACA airfoil for angle of attack 5° , computed using the linear vortex panel method implemented in program *07_ptf/airf_2d_lvp* of *FDLIB*.

where \mathbf{n} is the unit vector normal to the airfoil pointing into the fluid. The last expression arises by noting that the integral of the unit normal vector over a closed contour vanishes. Using the trapezoidal rule to approximate the two scalar components of the last integral, we find the following expressions for the reduced x and y components of the force,

$$\begin{aligned}\hat{F}_x &\equiv \frac{F_x}{\frac{1}{2}\rho U^2} = - \sum_{i=1}^N c_p^{(i)} \Delta l^{(i)} n_x^{(i)}, \\ \hat{F}_y &\equiv \frac{F_y}{\frac{1}{2}\rho U^2} = - \sum_{i=1}^N c_p^{(i)} \Delta l^{(i)} n_y^{(i)}.\end{aligned}\quad (12.4.24)$$

The reduced lift force with respect to the wind axis, defined as the component of the force that is normal to the direction of the incident flow,

is given by

$$\hat{L}_w = \hat{F}_y \cos \alpha - \hat{F}_x \sin \alpha, \quad (12.4.25)$$

where α is the angle of attack, as depicted in figure 12.4.1. According to the Kutta-Joukowski theorem expressed by equation (12.2.1),

$$\hat{L}_w = -2 \frac{C}{U}. \quad (12.4.26)$$

The difference in the values of the lift computed from (12.4.25) or (12.4.26) serves as an index of the accuracy of the numerical method.

Computer problem

Problem c.12.4.1 *Linear vortex panel method.*

Program *07_ptf/airf_2d.lvp* of *FDLIB* computes the flow past an airfoil using the linear vortex panel method discussed in the text.

(a) Run the code for an airfoil of your choice offered in the menu, prepare graphs and discuss the distribution of the pressure coefficient and the streamline pattern.

(b) Evaluate the velocity at points *inside*, the airfoil and discuss your results.

12.5 Vortex sheet representation

Consider the vortex panel method for flow past a two-dimensional airfoil discussed in Section 12.4. In the limit as the number of panels N tends to infinity, the piecewise linear strength distributions over the individual panels join to yield a smooth distribution defined over the airfoil contour. Correspondingly, the sum on the right-hand side of equation (12.4.1) reduces to an integral with respect to arc length around the airfoil contour, representing the velocity induced by a vortex sheet with a generally curved shape.

Generalizing expression (12.3.6), we find that the stream function associated with this vortex sheet is given by

$$\psi^{VS}(x, y) = -\frac{1}{4\pi} \oint \ln[(x - x')^2 + (y - y')^2] \gamma(x') dl', \quad (12.5.1)$$

where the integration is performed over the airfoil contour, and $dl' = \sqrt{dx'^2 + dy'^2}$ is the differential arc length around the airfoil measured in the clockwise direction starting at the trailing edge.

Conversely, the vortex panel representation may be viewed as the result of the discretization of the integral on the right-hand side of (12.5.1) into geometrical elements represented by the vortex panels. In Section 12.4, we discussed straight elements with linear strength distribution. In more advanced implementations, curved elements - such as sections of a parabola and circular arcs - and quadratic or higher-order strength density distributions are employed.

12.5.1 Internal flow

Although the vortex sheet representation is physically meaningful only when it is used to evaluate the stream function or the velocity at a point in the flow, nothing prevents us from using it to perform corresponding evaluations at a point inside the airfoil. When this is done, we find that the stream function is constant, and the velocity vanishes inside the airfoil (problem c.12.4.1).

To explain this result, we observe that the strength of the vortex sheet is computed to satisfy the no-penetration boundary condition. Because the normal component of the velocity is continuous across the vortex sheet, the interior flow occurs under vanishing normal boundary velocity. Since tangential velocity on the interior side of the airfoil is prohibited by the condition of irrotational motion, the internal flow must vanish.

12.5.2 Thin airfoil theory

Consider flow past a thin cambered airfoil, as illustrated in figure 12.5.1, and introduce a system of coordinates such that the leading edge lies at the origin of the x axis, and the trailing edge lies on the x at the point $x = c$. The camberline of the airfoil is described by the equation

$$y = \epsilon \eta_c(x), \quad (12.5.2)$$

where ϵ is a small dimensionless number, and $\eta_c(x)$ is the camberline shape function required to satisfy $\eta_c(0) = 0$ and $\eta_c(c) = 0$. If $\eta_c = 0$ for all x , then the camberline is flat.

Now, because both sides of the airfoil are close to the x axis, the corresponding line integrals in (12.5.1) may be approximated with integrals

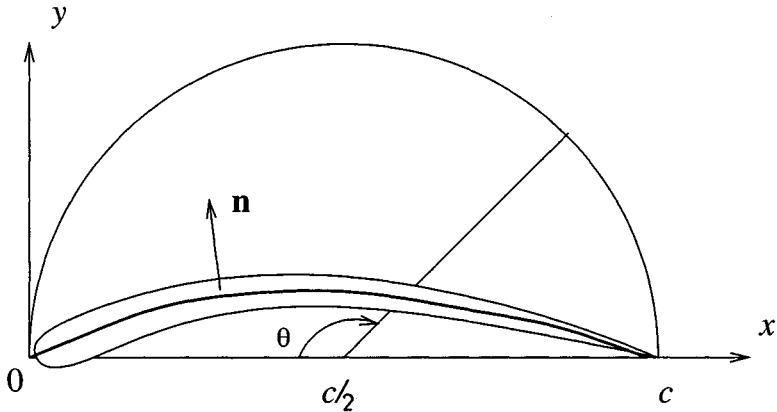


Figure 12.5.1 Illustration of the camberline of a thin airfoil, and definition of variables used to develop the slender-airfoil theory.

with respect to x from $x = 0$ to c . Setting $y' = 0$, tracing the airfoil in the clockwise direction beginning at the trailing edge, and noting that on the upper side $dl' = dx'$ while on the lower side $dl' = -dx'$, we find

$$\psi^{VS}(x, y) \simeq -\frac{1}{4\pi} \int_0^c \ln[(x - x')^2 + y^2] (\gamma^+ - \gamma^-)(x') dx', \quad (12.5.3)$$

where the superscripts $+$ and $-$ denote, respectively, the upper and lower side of the airfoil. Defining $\chi \equiv \gamma^+ - \gamma^-$, we obtain a representation in terms of an effective flat vortex sheet subtended between the leading and trailing edge,

$$\psi^{VS}(x, y) \simeq -\frac{1}{4\pi} \int_0^c \ln[(x - x')^2 + y^2] \chi(x') dx'. \quad (12.5.4)$$

The corresponding velocity potential is given by

$$\phi^{VS}(x, y) \simeq \frac{1}{2\pi} \int_0^c \arctan\left(\frac{y}{x - x'}\right) \chi(x') dx'. \quad (12.5.5)$$

Our goal is to compute the strength of the effective vortex sheet, χ , to satisfy the no-penetration condition over the airfoil.

Velocity on either side of the vortex sheet

As a preliminary, we consider the velocity induced by the effective vortex sheet on the upper and lower side of the airfoil. Consider first the limit of the velocity potential as the point (x, y) approaches the vortex sheet from the upper side, that is, as $y \rightarrow 0+$ with $0 < x < c$. In this limit, the inverse tangent function on the right-hand side of (12.5.5) is equal to zero when $x' < x$, or π when $x' > x$. Consequently, the potential takes the value

$$\phi^{VS}(x, y \rightarrow 0+) = \frac{1}{2} \int_x^c \chi(x') dx'. \quad (12.5.6)$$

Differentiating both sides of (12.5.6) with respect to x , we find that the x component of the velocity is given by

$$u_x^{VS}(x, y \rightarrow 0+) = -\frac{1}{2}\chi(x). \quad (12.5.7)$$

Working in a similar fashion for the lower side, we find

$$u_x^{VS}(x, y \rightarrow 0-) = \frac{1}{2}\chi(x). \quad (12.5.8)$$

The last two equations illustrate, once again, that the velocity undergoes a discontinuity whose magnitude is equal to the strength of the vortex sheet.

The y component of the velocity over the airfoil may be found by differentiating either (12.5.4) with respect to x , or (12.5.5) with respect to y . The result is

$$u_y(x, y = 0) = \frac{1}{2\pi} \int_0^c \frac{\chi(x')}{x - x'} dx'. \quad (12.5.9)$$

Unlike the x component of the velocity, the y component remains continuous across the vortex sheet.

Asymptotics

To compute the strength of the effective vortex sheet, χ , we require the no-penetration condition implemented through a series of approximations that may appear drastic but have a solid theoretical foundation.

First, we replace the disturbance flow due to the airfoil with the flow due to the effective vortex sheet expressed by (12.5.4) or (12.5.5). Applying the no-penetration boundary condition at the camberline, we obtain

$$\mathbf{n} \cdot [\mathbf{U} + \mathbf{u}^{VS}(x = \epsilon \eta_c)] = 0, \quad (12.5.10)$$

where \mathbf{n} is the unit vector normal to the camberline on the upper side pointing into the fluid. Using (12.5.2), we find

$$n_x = -\frac{\epsilon \frac{d\eta_c}{dx}}{\sqrt{1 + \epsilon^2 \left(\frac{d\eta_c}{dx}\right)^2}}, \quad n_y = \frac{1}{\sqrt{1 + \epsilon^2 \left(\frac{d\eta_c}{dx}\right)^2}}. \quad (12.5.11)$$

Because ϵ has been assumed small, the denominators can be replaced by unity, yielding the simplified expressions

$$n_x \simeq -\epsilon \frac{d\eta_c}{dx}, \quad n_y \simeq 1. \quad (12.5.12)$$

A second approximation arises by replacing the velocity on the upper side of the camberline with the velocity on the upper side of the effective vortex sheet, given by (12.5.7) and (12.5.9). Substituting (12.5.12), (12.5.7), and (12.5.9) into (12.5.10), we find

$$-\epsilon \frac{d\eta_c}{dx}(x) \left[U_x - \frac{1}{2} \chi(x) \right] + U_y + \frac{1}{2\pi} \int_0^c \frac{\chi(x')}{x - x'} dx' = 0. \quad (12.5.13)$$

Next, we confine our attention to flow that is nearly parallel to the x axis, meaning that U_y is small compared to U_x . Writing $U_y = \tan \alpha U_x \simeq \alpha U_x$, where α is the angle of attack, we obtain

$$-\epsilon \frac{d\eta_c}{dx}(x) \left[U_x - \frac{1}{2} \chi(x) \right] + \alpha U_x + \frac{1}{2\pi} \int_0^c \frac{\chi(x')}{x - x'} dx' = 0. \quad (12.5.14)$$

Inspecting the various terms on the left-hand side of (12.5.14), we find that the magnitude of χ is of order ϵ or α , both of which have been assumed small. Since χ is negligible compared to U_x , it may be discarded from the expression enclosed by the square brackets, leaving the equation

$$\frac{1}{2\pi U_x} \int_0^c \frac{\chi(x')}{x - x'} dx' = \epsilon \frac{d\eta_c}{dx}(x) - \alpha, \quad (12.5.15)$$

where $0 < x < c$. The problem has been reduced to computing the function $\chi(x)$ that satisfies the integral equation of the first kind (12.5.15).

Solution by Fourier expansion

One way to solve equation (12.5.15) is by expanding the unknown function χ in a Fourier series with respect to the angle θ defined such that

$$x = \frac{c}{2} (1 - \cos \theta), \quad (12.5.16)$$

and varying between 0 and π , as illustrated in figure 12.5.1. The Kutta-Joukowski condition requires that the strength of the vortex sheet vanish at the trailing edge, and wind tunnel evidence reveals a large peak at the leading edge. Accordingly, we express χ as the sum of the singular function $\cot \frac{\theta}{2}$ and a sine fourier series, in the form

$$\chi = 2 U_x \left[a_0 \cot \frac{\theta}{2} + \sum_{i=1}^{\infty} a_i \sin(i\theta) \right], \quad (12.5.17)$$

where a_i are constant coefficients. Substituting (12.5.16) and (12.5.17) into (12.5.15), we find

$$\frac{1}{\pi} \int_0^{\pi} \frac{\sin \theta'}{\cos \theta' - \cos \theta} \left[a_0 \cot \frac{\theta'}{2} + \sum_{i=1}^{\infty} a_i \sin(i\theta') \right] d\theta' = \epsilon \frac{d\eta_c}{dx}(x) - \alpha. \quad (12.5.18)$$

The integrals on the left-hand side of (12.5.18) may be evaluated with the aid of standard tables. First, we write $\cot(\theta'/2) = (1 + \cos \theta')/\sin \theta'$, and find

$$\int_0^{\pi} \frac{\sin \theta'}{\cos \theta' - \cos \theta} \cot \frac{\theta'}{2} d\theta' = \int_0^{\pi} \frac{1 + \cos \theta'}{\cos \theta' - \cos \theta} d\theta' = \pi. \quad (12.5.19)$$

Second, we find

$$\int_0^{\pi} \frac{\sin \theta'}{\cos \theta' - \cos \theta} \sin(i\theta') d\theta' = -\pi \cos(i\theta). \quad (12.5.20)$$

Substituting these results into (12.5.18), we derive the remarkably simple expression

$$a_0 - \sum_{i=1}^{\infty} a_i \cos(i\theta) = \epsilon \frac{d\eta_c}{dx}(x) - \alpha. \quad (12.5.21)$$

The left-hand side of (12.5.21) is the cosine Fourier expansion of the right-hand side with respect to θ . Multiplying both sides by $\cos(j\theta)$, where j is an integer, integrating with respect to θ from 0 to π , and using the identity

$$\int_0^\pi \cos(i\theta) \cos(j\theta) d\theta = \begin{cases} 0 & \text{if } i \neq j \\ \pi & \text{if } i = j = 0 \\ \pi/2 & \text{if } i = j \neq 0 \end{cases}, \quad (12.5.22)$$

we obtain the desired results

$$a_0 = -\alpha + \frac{\epsilon}{\pi} \int_0^\pi \frac{d\eta_c}{dx} d\theta, \quad a_i = -\frac{2\epsilon}{\pi} \int_0^\pi \frac{d\eta_c}{dx} \cos(i\theta) d\theta, \quad (12.5.23)$$

for $i = 1, 2, \dots$

Alternatively, we expand the camberline slope $d\eta_c/dx$ in a cosine Fourier series with respect to θ ,

$$\frac{d\eta_c}{dx}(x) = \frac{b_0}{2} + \sum_{i=1}^\infty b_i \cos(i\theta), \quad (12.5.24)$$

substitute the right-hand side of (12.5.24) into (12.5.21), and set the sum of like Fourier coefficients equal to zero to obtain

$$a_0 = -\alpha + \epsilon \frac{b_0}{2}, \quad a_i = -\epsilon b_i, \quad (12.5.25)$$

for $i = 1, 2, \dots$. These relations illustrate that only the leading coefficient a_0 is a function of the angle of attack, and the rest of the coefficients are determined by the geometry of the camberline.

Lift, lift coefficient, and lift slope

To compute the lift force per unit span exerted on the airfoil, we use the Kutta-Joukowski theorem expressed by equation (12.2.1), obtaining

$$L = -\rho U_x \int_0^c \chi(x) dx. \quad (12.5.26)$$

Substituting expansion (12.5.17) into the right-hand side, and evaluating the integrals, we find that only two terms make a non-zero contribution, yielding

$$L = -\rho U_x^2 c \pi \left(a_0 + \frac{1}{2} a_1 \right). \quad (12.5.27)$$

The lift coefficient is given by

$$c_L \equiv \frac{L}{\frac{1}{2} \rho U_x^2 c} = -2\pi \left(a_0 + \frac{1}{2} a_1 \right). \quad (12.5.28)$$

In practical aerodynamics, the performance of an airfoil is characterized by the *lift slope* defined as the slope $dc_L/d\alpha$; the preceding results show that the lift slope of a thin airfoil is constant and equal to 2π , independent of the camber.

Pressure difference and moment

The difference in pressure on either side of the vortex sheet representing the airfoil may be computed using Bernoulli's equation (6.4.14). Expressions (12.5.7) and (12.5.8) show that the velocity on the upper or lower side of the vortex sheet is, respectively, equal to $U_x - \frac{1}{2}\chi$ or $U_x + \frac{1}{2}\chi$. Using Bernoulli's equation, we evaluate the pressure difference

$$\begin{aligned} \Delta p &\equiv p(x, y \rightarrow 0-) - p(x, y \rightarrow 0+) \\ &= [p_\infty - \frac{1}{2}\rho (U_x + \frac{1}{2}\chi)^2] - [p_\infty + \frac{1}{2}\rho (U_x + \frac{1}{2}\chi)^2] = -\rho U_x \chi. \end{aligned} \quad (12.5.29)$$

The moment of the pressure forces with respect to the leading edge is expressed by the integral

$$M = - \int_0^c x \Delta p dx. \quad (12.5.30)$$

Substituting (12.5.29) and the expansion (12.5.17) into the right-hand side, and evaluating the emerging definite integrals with the aid of standard mathematical tables, we find

$$M = \frac{1}{4} \rho U_x^2 c^2 \pi \left(a_0 + a_1 - \frac{1}{2} a_2 \right), \quad (12.5.31)$$

which shows that only three coefficients make a contribution to the moment. The moment coefficient is defined by

$$c_M \equiv \frac{M}{\frac{1}{2} \rho U_x^2 c^2} = \frac{\pi}{2} \left(a_0 + a_1 - \frac{1}{2} a_2 \right). \quad (12.5.32)$$

The moment of the pressure forces with respect to an arbitrary point located at $x = d$ is given by

$$M_d = - \int_0^c (x - d) \Delta p dx = M + d L. \quad (12.5.33)$$

Substituting (12.5.27) and (12.5.31) into the right-hand side of (12.5.33), we find that, when $d = c/4$, the coefficient a_0 disappears, and M_d becomes independent of the angle of attack α . Accordingly, the quarter chord moment, $M_{c/4}$, and associated moment coefficient

$$c_{M_{c/4}} \equiv \frac{M_{c/4}}{\frac{1}{2} \rho U_x^2 c^2} \quad (12.5.34)$$

are used to characterize the performance of the airfoil.

Symmetric airfoils

Since the camber of a symmetric airfoil vanishes, we may set either $\epsilon = 0$ or $\eta_c(x) = 0$ in the preceding equations. Either way, equations (12.5.25) yield $a_0 = -\alpha$ and $a_i = 0$ for $i = 1, 2, \dots$, and expansion (12.5.17) reduces to

$$\chi = -2 \alpha U_x \cot \frac{\theta}{2}. \quad (12.5.35)$$

The lift force and lift coefficient computed from equations (12.5.27) and (12.5.28) are given by

$$L = \pi \alpha c \rho U_x^2, \quad c_L = 2 \pi \alpha. \quad (12.5.36)$$

and the moment and moment coefficient computed from equations (12.5.31) and (12.5.32) are given by

$$M = -\pi \alpha c^2 \rho U_x^2, \quad c_M = -\frac{\pi}{2} \alpha. \quad (12.5.37)$$

Problems

Problem 12.5.1 *Thin airfoil with parabolic camber.*

Consider a thin airfoil with parabolic camberline described by the shape function $\eta_c(x) = 4x(1 - \frac{x}{c})$. Note that the camber is equal to ϵc . Show that the lift and moment coefficients are given by

$$c_L = 2\pi(\alpha + 2\epsilon), \quad c_M = -\frac{\pi}{2}(\alpha + 4\epsilon). \quad (12.5.38)$$

Note that the lift vanishes when $\alpha = -2\epsilon$.

Problem 12.5.2 *NACA 23012 airfoil.*

The camberline of the NACA 23012 airfoil is described by

$$\hat{y} = \begin{cases} 2.6595(\hat{x}^3 - 0.6075\hat{x}^2 + 0.1147\hat{x}) & \text{for } 0 \leq \hat{x} \leq 0.2025 \\ 0.02208(1 - \hat{x}) & \text{for } 0.2025 \leq \hat{x} \leq 1 \end{cases}, \quad (12.5.39)$$

where $\hat{x} \equiv x/c$ and $\hat{y} \equiv y/c$. Derive expressions for the lift and moment coefficients in terms of the angle of attack, and compare your results with experimental measurements for $\alpha = 4^\circ$, showing that $c_L = 0.55$ and $c_{M_{c/4}} = -0.01$.

Computer problem

Problem c.12.5.1 *Comparison with the vortex panel method.*

Consider the NACA 23012 discussed in problem 12.5.2. Run the code `airf_2d.lvp` in directory `07_ptf` of `FDLIB` to compute the lift coefficient in wind axes, and compare the numerical results with the asymptotic predictions for small airfoil thickness.

12.6 Point-source-dipole panels

Consider the stream function of the flow induced by a vortex panel situated on the x axis and subtended between the point $x = a$ and b , as shown in equation (12.3.6). The distribution of circulation along the panel, denoted by $\mu(x)$, is defined as the integral of the strength density of the vortex sheet with respect to x from an arbitrary point $x = d$ up to the point x , where $x > a$ and $x < b$,

$$\mu(x) \equiv \int_d^x \gamma(x') dx'. \quad (12.6.1)$$

Using the rules of integral differentiation, we find

$$\frac{d\mu}{dx} = \gamma. \quad (12.6.2)$$

Substituting the left-hand side of (12.6.2) into the integral in (12.3.6), and integrating by parts, we find

$$\begin{aligned} \psi^{VP}(x, y) &= \frac{\mu(x=a)}{2\pi} \ln[(x-a)^2 + (y-y')^2] \\ &\quad - \frac{\mu(x=b)}{2\pi} \ln[(x-b)^2 + (y-y')^2] \\ &\quad + \frac{1}{4\pi} \int_a^b \frac{d \ln[(x-x')^2 + (y-y')^2]}{dx'} \mu(x') dx', \end{aligned} \quad (12.6.3)$$

with the understanding that $y' = 0$. Carrying out the differentiation under the integral sign, we derive the final form

$$\begin{aligned} \psi^{VP}(x, y) &= \frac{\mu(x=a)}{2\pi} \ln[(x-a)^2 + (y-y')^2] \\ &\quad - \frac{\mu(x=b)}{2\pi} \ln[(x-b)^2 + (y-y')^2] \\ &\quad - \frac{1}{2\pi} \int_a^b \frac{x-x'}{(x-x')^2 + (y-y')^2} \mu(x') dx'. \end{aligned} \quad (12.6.4)$$

The three terms on the right-hand side of (12.6.4) have the following physical interpretation:

- The first term represents the flow due to a point vortex with strength $-\mu(x=a)$ placed at the first panel end-point, and the second term represents the flow due to a point vortex with strength $\mu(x=b)$ placed at the second panel end-point.
- Recalling that, by definition, $u_x = \partial\psi/\partial y$ and $u_y = -\partial\psi/\partial x$, and comparing the third term on the right-hand side of (12.6.4) with expressions (3.5.23) and (3.5.24), we find that this term represents the flow due to a distribution of point-source dipoles with strength density $\mu(x)$ oriented normal to the panel.

If $\mu(x')$ is positive, the dipole at x' points toward the positive direction of the y axis; if $\mu(x')$ is negative, the dipole at x' points toward the negative direction of the y axis.

Denoting the stream function due to the point-source dipole distribution by ψ^{SDP} , where SDP stands for source-dipole panel, and rearranging equation (12.6.4), we obtain

$$\begin{aligned}\psi^{SDP}(x, y) &\equiv -\frac{1}{2\pi} \int_a^b \frac{x - x'}{(x - x')^2 + (y - y')^2} \mu(x') dx' \\ &= -\frac{\mu(x = a)}{2\pi} \ln[(x - a)^2 + (y - y')^2] \\ &\quad + \frac{\mu(x = b)}{2\pi} \ln[(x - b)^2 + (y - y')^2] + \psi^{VP}(x, y),\end{aligned}\tag{12.6.5}$$

which establishes a correspondence between the flow due to a source-dipole panel and the flow due to a vortex panel, subject to relation (12.6.2).

We note, in particular, that the first term on the right-hand side of (12.6.5) represents the flow due to a point vortex with strength $\mu(x = a)$ placed at the first panel end-point, and the second term represents the flow due to a point vortex with strength $-\mu(x = b)$ placed at the second panel end-point.

12.6.1 Panels with constant source-dipole strength density

When the strength density of the source-dipole distribution over a panel is constant, the strength of the vortex sheet vanishes, and the last term on the right-hand side of (12.6.5) disappears. In this case, the flow due to the panel is identical to the flow induced by two point vortices with strengths $\mu(0)$ and $-\mu(0)$ situated, respectively, at the first and second panel end-point.

Source-dipole panel method

The flow due to a point-source dipole panel may be used as a fundamental building block for representing, and subsequently computing, the flow past an airfoil. To develop the source-dipole panel method, we work

by analogy with the vortex panel method discussed in Section 12.4, with some variations. First, we trace the contour of the airfoil with $N + 1$ marker points distributed in the clockwise sense, as illustrated in figure 12.4.1. A pair of successive marker points $\mathbf{x}^{(i)}$ and $\mathbf{x}^{(i+1)}$ define a flat source-dipole panel labelled i .

In the source-dipole panel method, the velocity at the point (x, y) located in the flow is described by the superposition of the incident flow and the flows induced by the N source-dipole panels. An additional degree of freedom is required to be able to arbitrarily specify the circulation around the airfoil, and is provided by enhancing the source-dipole representation with an additional contribution associated with a point vortex of strength κ located at the trailing edge. The composite representation is

$$\mathbf{u}(x, y) = \mathbf{U} + \sum_{i=1}^N \mathbf{u}^{(i)}(x, y) + \mathbf{u}^{PV}(x, y), \quad (12.6.6)$$

where $\mathbf{u}^{(i)}(x, y)$ is the velocity induced by the i th panel, and $\mathbf{u}^{PV}(x, y)$ is the velocity induced by the point vortex.

According to our earlier discussion, if the source-dipole strength is constant over each panel, then the flow induced by the i th panel is identical to the flow induced by two point vortices with strengths $\mu^{(i)}$ and $-\mu^{(i)}$ located at the first and second panel end-points; $\mu^{(i)}$ is the constant value of the source dipole strength density over the i th panel. Consequently, the i th marker point, $i = 2, 3, \dots, N$, hosts two point-vortices: one with strength $-\mu^{(i-1)}$ contributed by the $i - 1$ panel, and the second with strength $\mu^{(i)}$ contributed by the i panel, for a combined strength of $\mu^{(i)} - \mu^{(i-1)}$. The first marker point hosts three point vortices: one due to the first panel, a second due to the last panel, and the circulation-producing point vortex at the trailing edge. The Kutta-Joukowski condition requires that the net strength of the trailing edge point vortex vanish,

$$\mu^{(1)} - \mu^{(N)} + \kappa = 0. \quad (12.6.7)$$

The $N + 1$ unknowns, including $\mu^{(i)}$, $i = 1, 2, \dots, N$, and κ , may be computed using the collocation method discussed in Section 12.3, incorporating the Kutta-Joukowski condition (12.6.7).

12.6.2 Source-dipole panel with linear strength density

When the strength density of a source dipole panel varies in a linear fashion with respect to arc length, all three terms on the right-hand side

of (12.6.5) make a non-zero contribution. Expression (12.6.2) shows that the strength density of the equivalent vortex sheet is constant and equal to the slope of the dipole density over the panel.

In the linear source-dipole panel method, the flow is represented by a superposition of the three components shown in equation (12.6.6), where the dipole density over the i th panel varies in a linear manner with respect to arc length from the initial value $\mu^{(i)}$ to the final value $\mu^{(i+1)}$. Summing up the flows due to the individual panels expressed by the right-hand side of (12.6.5), and consolidating the left- and right-panel point vortices at the panel end-points, we derive an equivalent representation in terms of point vortices and vortex panels with constant strength. The uniform strength density of the i th vortex panel is equal to

$$\gamma^{(i)} \equiv \frac{\mu^{(i+1)} - \mu^{(i)}}{\Delta l^{(i)}}, \quad (12.6.8)$$

where $\Delta l^{(i)}$ is the panel length.

Next, we observe that, because the dipole strength is continuous around the approximate polygonal contour of the airfoil, as described by the panels, the strength of the point vortices vanishes at all but the first point where it takes the value $\mu^{(1)} - \mu^{(N+1)} + \kappa$. Thus, the linear source-dipole panel representation is equivalent to the constant vortex panel representation supplemented by a point vortex at the trailing edge. The strength of the point vortex must vanish to satisfy the Kutta-Joukowski condition at the trailing edge, as required by equation (12.6.7).

12.6.3 Source-dipole representation

As the number of panels N tends to infinity, the individual panel strength density distributions join to yield a smooth distribution defined around the airfoil. Correspondingly, the sum on the right-hand side of (12.6.6) reduces to an integral with respect to arc length around the airfoil, yielding an integral representation in terms of a source-dipole sheet.

Equation (12.6.5) provides us with an expression for the stream function associated with a source-dipole panel situated over the x axis, where the source-dipoles pointing along the y axis. Generalizing this expression, we find that the stream function associated with source-dipole distribution around the airfoil is given by

$$\psi^{SD}(x, y) = -\frac{1}{2\pi} \oint \frac{(x - x') n_y - (y - y') n_x}{(x - x')^2 + (y - y')^2} \mu(x') dl', \quad (12.6.9)$$

where $dl' = \sqrt{dx'^2 + dy'^2}$ is the differential arc length around the airfoil measured in the clockwise direction from a designated origin. The associated velocity potential is given by

$$\phi^{SD}(x, y) = -\frac{1}{2\pi} \oint \frac{(x - x') n_x(\mathbf{x}') + (y - y') n_y(\mathbf{x}')}{(x - x')^2 + (y - y')^2} \mu(x') dl'. \quad (12.6.10)$$

The counterpart of the panel representation (12.6.6) is

$$\mathbf{u}(x, y) = \mathbf{U} + \mathbf{u}^{SD}(x, y) + \mathbf{u}^{PV}(x, y), \quad (12.6.11)$$

where $\mathbf{u}^{SD}(x, y)$ is the velocity corresponding to (12.6.9) and (12.6.10). The stream function and velocity potential are given by the corresponding expressions

$$\psi(x, y) = U_x y - U_y x + \psi^{SD}(x, y) + \psi^{PV}(x, y), \quad (12.6.12)$$

and

$$\phi(x, y) = U_x x + U_y y + \phi^{SD}(x, y) + \phi^{PV}(x, y). \quad (12.6.13)$$

Conversely, the source-dipole panel representation may be regarded as the result of the discretization of the integral on the right-hand side of (12.6.9) or (12.6.10) into geometrical elements representing the source-dipole panels. In this section, we have discussed straight elements with constant and linear strength density distributions. In more advanced implementations, curved elements such as sections of a parabola and circular arcs, and quadratic or higher-order strength density distributions are employed.

12.6.4 Solution of the interior problem

Assume that the strength of the source-dipole sheet satisfying the no-penetration condition around the airfoil is available. For reasons discussed in Section 12.3, if we evaluate the right-hand sides of (12.6.9)-(12.6.11) at a point located inside the airfoil, we will find that the velocity vanishes, and the stream function and potential take constant values.

This observation suggests an alternative method of computing the strength density of the source dipoles: instead of using the Neumann non-penetration boundary condition, use the Dirichlet condition requiring that the potential and stream function are constant along the *interior* side of the airfoil.

Panels with constant strength density

To illustrate the implementation of the method, we discretize the airfoil contour into N flat panels with constant strength density, as illustrated in figure 12.4.1. Identifying the flow induced by each panel with the flow induced by two point vortices located at the end-points, as discussed earlier in this section, we obtain the discrete representation

$$\phi(x, y) = U_x x + U_y y + \frac{1}{2\pi} \sum_{i=1}^N [\mu^{(i)} (\theta_1^{(i)} - \theta_2^{(i)})] + \frac{\kappa}{2\pi} \theta_T, \quad (12.6.14)$$

where the angles $\theta_1^{(i)}$, $\theta_2^{(i)}$, and θ_T are defined in figure 12.4.1.

To implement the collocation method, we evaluate (12.6.14) at the mid-point of the j panel $(x_M^{(j)}, y_M^{(j)})$, on the interior side of the airfoil. Noting that $\theta_1^{(j)} = 0$ and $\theta_2^{(j)} = -\pi$, and assigning to the potential the reference value of zero, we derive the algebraic equation

$$0 = U_x x_M^{(j)} + U_y y_M^{(j)} + \frac{1}{2\pi} \sum'_{i=1}^N [\mu^{(i)} (\theta_1^{(i)} - \theta_2^{(i)})] + \frac{1}{2} \mu^{(j+1)} + \frac{\kappa}{2\pi} \theta_T, \quad (12.6.15)$$

where the primed sum signifies that the term $i = j$ is excluded from the summation. Rearranging (12.6.15), we derive a linear equation relating the panel source-dipole densities to the strength of the trailing-edge point vortex,

$$\frac{1}{2} \mu^{(j+1)} + \frac{1}{2\pi} \sum'_{i=1}^N [\mu^{(i)} (\theta_1^{(i)} - \theta_2^{(i)})] + \frac{\kappa}{2\pi} \theta_T = -U_x x_M^{(j)} - U_y y_M^{(j)}. \quad (12.6.16)$$

Applying equation (12.6.16) for $j = 1, 2, \dots, N$, and appending to the resulting system of equations the Kutta-Joukowski condition expressed by (12.6.7), we obtain a linear system for the $N + 1$ unknowns $\mu^{(i)}$, $i = 1, 2, \dots, N$, and κ .

Distribution of the potential over the airfoil

Inspecting the third term on the right-hand side of (12.6.14), we find that the potential undergoes a discontinuity of magnitude $-\mu^{(i)}$ across the i th panel. Since the potential inside the airfoil is constant and equal to zero, the potential on the exterior side of the panel must be equal to $-\mu^{(i)}$.

This result is valid in a more general context: the potential on the outer side of the airfoil is equal to the negative of the strength density of the source dipoles. The tangential velocity may then be computed by numerically differentiating μ with respect to arc length along the airfoil.

Computer problem**Problem c.12.6.1** *Constant strength dipole panels.*

Program *07_ptf/airf_2d.cdp* of *FDLIB* computes flow past an airfoil using the constant-strength source-dipole-panel method.

(a) Run the code for an airfoil of your choice, prepare graphs, and discuss the distribution of the pressure coefficient.

(b) Evaluate the velocity at points *inside* the airfoil, and discuss your findings.

12.7 Point-source panels and Green's third identity

In previous sections, we have discussed flow representations in terms of vortex panels and point-source dipole panels expressed, respectively, by equations (12.5.1) and (12.6.10) or (12.6.11). In this section, we introduce a new representation in terms of a point source distribution. Working by analogy with (12.6.11), we find that the harmonic potential of the induced flow is given by

$$\phi^S(x, y) = \frac{1}{4\pi} \oint \ln[(x - x')^2 + (y - y')^2] \sigma(x') dl', \quad (12.7.1)$$

where σ is the strength density of the distribution.

The point-source representation carries an important restriction: conservation of mass requires that the total strength of the point sources,

defined as the integral of the strength density σ with respect to arc length around the airfoil, vanishes, otherwise a net radial flow due to an effective point source will arise. This restriction is satisfied automatically only in the case of symmetric flow past a symmetric non-lifting airfoil at zero angle of attack, and in the absence of circulatory motion.

In spite of this limitation, the point-source representation is not without merits. Its usefulness stems predominantly from Green's third identity, to be discussed in Section 12.7.2, stating that a judicious combination of the point source and source-dipole representation ensures the satisfaction of the condition of zero radial flow, and also allows the strength densities of the distributions to obtain simple physical interpretations.

12.7.1 Source panels with constant density

Consider a flat source panel with uniform strength density equal to $\sigma^{(0)}$ situated on the x axis, and subtended between $x = a$ and b . Using (12.7.1) with $y' = 0$, we find that the corresponding potential is given by

$$\phi^{(0)}(x, y) = \frac{\sigma^{(0)}}{4\pi} \int_a^b \ln[(x - x')^2 + y^2] dx'. \quad (12.7.2)$$

Note that this expression is identical to that for the stream function due to a vortex panel with constant strength density given in equation (12.3.8), subject to the substitution $\gamma^{(0)} = -\sigma^{(0)}$. Modifying (12.3.9) correspondingly, we find

$$\begin{aligned} \phi^{(0)}(x, y) &= \frac{\sigma^{(0)}}{4\pi} [-(x - b) \ln[(x - b)^2 + y^2] \\ &\quad + (x - a) \ln[(x - a)^2 + y^2] \\ &\quad + 2y (\arctan \frac{y}{x - b} - \arctan \frac{y}{x - a}) - 2(b - a)]. \end{aligned} \quad (12.7.3)$$

The components of the velocity are found by straightforward differentiation, and are given by

$$u_x^{(0)}(x, y) = \frac{\partial \phi^{(0)}}{\partial x} = -\frac{\sigma^{(0)}}{4\pi} \ln \frac{(x - b)^2 + y^2}{(x - a)^2 + y^2}, \quad (12.7.4)$$

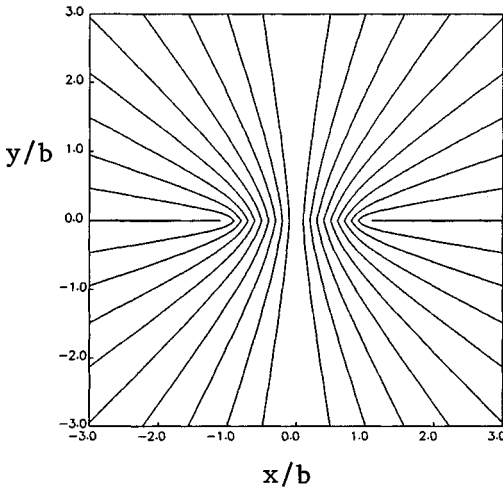


Figure 12.7.1 Streamline pattern of the flow due to a point-source panel with constant strength density subtended between the points $x = -b$ and b .

and

$$u_y^{(0)}(x, y) = \frac{\partial \phi^{(0)}}{\partial y} = \frac{\sigma^{(0)}}{2\pi} \left[\arctan \frac{y}{x-b} - \arctan \frac{y}{x-a} \right]. \quad (12.7.5)$$

The streamline pattern of the flow induced by a panel is shown in figure 12.7.1. Far from the panel, the flow reduces to that due to a point source with strength $\sigma^{(0)}(b-a)$ situated at the origin.

Jump in velocity across the panel

Expression (12.7.4) shows that the y component of the velocity is continuous throughout the domain of flow and across the source panel. In contrast, because of the presence of the inverse tangent functions on the right-hand side of (12.7.5), the y component of the velocity undergoes a discontinuity of magnitude $\sigma^{(0)}$ across the panel. Specifically, the y component of the velocity on the upper or lower side of the panel, for $a < x < b$, is given by

$$u_y^{(0)}(x, y \rightarrow \pm 0) = \pm \frac{\sigma^{(0)}}{2}. \quad (12.7.6)$$

Inverse tangent functions also appear on the right-hand side of (12.7.3). Because, however, these functions are multiplied by y which is equal to zero over the panel, a discontinuity in the potential does not arise.

12.7.2 Green's third identity

The source panels may be used in the familiar way to develop a representation of the flow past a symmetric airfoil at zero angle of attack. The numerical implementation is analogous to that of the vortex panel method discussed in Section 12.3. A more interesting and more general representation stems from Green's third identity discussed in the remainder of this section.

Consider a control area in the xy plane bounded by a collection of boundaries C , as illustrated in figure 12.7.2. Green's third identity states that the harmonic potential at a point \mathbf{x} that lies inside the control area may be represented in terms of a combined point-source / dipole-source distribution, in the form

$$\begin{aligned} \phi(x, y) = & \frac{1}{4\pi} \oint \log[(x - x')^2 + (y - y')^2] \mathbf{N}(\mathbf{x}') \cdot \nabla \phi(\mathbf{x}') dl' \\ & + \frac{1}{2\pi} \oint \frac{(x - x') N_x(\mathbf{x}') + (y - y') N_y(\mathbf{x}')}{(x - x')^2 + (y - y')^2} \phi(\mathbf{x}') dl', \end{aligned} \quad (12.7.7)$$

where \mathbf{N} is the unit vector normal to the boundaries C pointing into the control area, as shown in figure 12.7.2.

Comparing the two terms on the right-hand side of (12.7.7) with (12.7.1) and (12.6.11), we identify the strength density of the point-source distribution with the boundary values of the potential, and the strength density of the source-dipole distribution with the boundary values of the normal derivative of the potential.

Let us identify the control area with the area occupied by an airfoil, and apply Green's identity for the potential of the incident uniform flow. Writing $\mathbf{N} = -\mathbf{n}$, where \mathbf{n} is the unit vector normal to the airfoil pointing into the exterior, we obtain

$$\begin{aligned} \phi_\infty(x, y) = & -\frac{1}{4\pi} \oint \ln[(x - x')^2 + (y - y')^2] \mathbf{n}(\mathbf{x}') \cdot \nabla \phi_\infty(\mathbf{x}') dl' \\ & - \frac{1}{2\pi} \oint \frac{(x - x') n_x(\mathbf{x}') + (y - y') n_y(\mathbf{x}')}{(x - x')^2 + (y - y')^2} \phi_\infty(\mathbf{x}') dl', \end{aligned} \quad (12.7.8)$$

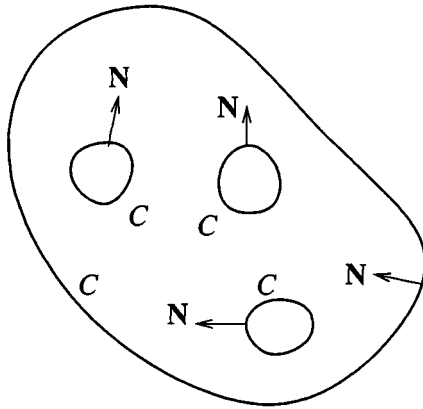


Figure 12.7.2 A control area in the xy plane confined by a collection of curves denoted by C , used to establish Green's third identity; \mathbf{N} is the unit vector normal to the boundaries pointing into the fluid.

where the point (x, y) is located in the *interior* of the airfoil.

Now, equation (12.6.14) expresses a double-layer representation in the form

$$\begin{aligned} \phi(x, y) &= \phi_\infty(x, y) + \frac{1}{2\pi} \oint \frac{(x - x') n_x(\mathbf{x}') + (y - y') n_y(\mathbf{x}')}{(x - x')^2 + (y - y')^2} \phi^{(+)}(\mathbf{x}') dl' \\ &+ \phi^{PV}(x, y), \end{aligned} \tag{12.7.9}$$

where $\phi^{(+)}$ is the potential on the exterior side of the airfoil. Since the point (x, y) is located in the interior of the airfoil, the left-hand side is a constant that may be set equal to zero.

Combining equations (12.7.8) and (12.7.9), we obtain

$$\begin{aligned} &\frac{1}{4\pi} \oint \ln[(x - x')^2 + (y - y')^2] \mathbf{n}(\mathbf{x}') \cdot \nabla \phi_\infty(\mathbf{x}') dl' \\ &= -\frac{1}{2\pi} \oint \frac{(x - x') n_x(\mathbf{x}') + (y - y') n_y(\mathbf{x}')}{(x - x')^2 + (y - y')^2} \mu(\mathbf{x}') dl' + \phi^{PV}(x, y), \end{aligned} \tag{12.7.10}$$

where we have defined

$$\mu \equiv -\phi^{(+)} + \phi_\infty. \tag{12.7.11}$$

Equation (12.7.10) is an integral equation for the dipole density μ . Once this equation has been solved using, for example, a panel method, the potential on the exterior side of the airfoil may be computed from equation (12.7.11) as

$$\phi^{(+)} = \phi_{\infty} - \mu. \quad (12.7.12)$$

Computer problems

Problem c.12.7.1 *Source-dipole panel method.*

Program `07_ptf/airf_2d_csdp` of *FDLIB* contains a code that computes flow past an airfoil using a panel method based on equation (12.7.10). Run the code for an airfoil of your choice, prepare graphs, and discuss the distribution of the pressure coefficient around the airfoil.

Problem c.12.7.2 *Constant source panel method.*

Write a code that computes flow past a symmetric airfoil at zero angle of attack using the point-source panel method. Run the code for an airfoil of your choice, prepare graphs, and discuss the distribution of the pressure coefficient around the airfoil.

Subject Index

<u>Index terms</u>	<u>Links</u>
A	
acceleration	14
of a point particle	95
aerodynamics	606
airfoil	609
thin-airfoil theory	630
alternating tensor	65
Archimedis principle	224 451
atmospheric pressure	
distribution	214
Avogadro number	184
axisymmetric	
flow	17
extensional	193
flow rate in	86
stream function	104
vorticity of	67 292
interfaces	246
B	
baroclinic production of vorticity	289
bearing	414
Beltrami flow	270
Bernoulli's equations	272

Links**Index terms**

Bessel functions	356	358	361
Bickley jet	525		
biharmonic operator	460		
Bingham plastic	195		
Biot-Savart integral	585		
Blasius equation	486		
body,			
force	165		
neutrally-buoyant	226		
rigid	3		
Bond number	305		
Boundary			
conditions,			
Dirichlet	119		
for Euler's equation	271		
for the Navier-Stokes equation	285		
Neumann	118		
no-penetration	107		
for the pressure	398		
no-slip	204		
slip	204		
elements	458		
layer,			
Falkner-Skan	496		
Prandtl	480	485	
Sakiadis	500		
Stokes	351		
traction	172		
Bubble, expanding	283		
Buoyancy force	219		
Burgers equation	100		
Boussinèsq eddy viscosity	543		

Index terms**Links****C**

capillary	
length	230
rise	233
Cauchy equation of motion	266
cavity flow	386 405
centrifugal force	268
CFDLAB	652
channel flow,	
finite-difference methods for	367 377 382
two-layer flow	373 436
steady	306 411
multi-layer	311
semi-infinite	333
two-layer	309
wavy	418
unsteady	339 346
circulation	159 549 581
circulatory flow	155
conjugate gradients	134
contact	
angle	228
line	228
continuum mechanics	20
contour dynamics,	
for axisymmetric flow	598
for two-dimensional flow	572
coordinates,	
Cartesian	4
cylindrical polar	6
plane polar	12
spherical polar	9

Links**Index terms**

Coriolis force	269		
corners, flow inside	465		
correlations	545		
Couette flow,			
circular	336		
plane or rectilinear	310	339	
Crank-Nicolson method	401		
creeping flow	443		
curl of a vector field	65		
curvature			
of an ellipse	179		
of an interface	232	247	
of a line	176		
of a surface	177		
cylinder, circular,			
boundary layer around	509		
flow past	476		
potential flow past	143	156	
Stokes flow due to the motion of	460		
D			
deformation	3		
of a fluid parcel	29	57	68
Deissler correlation	546		
delta function	551	561	
density	93		
difference,			
backward	72		
centered	73		
forward	72		
differentiation, numerical	72		
of a function of two variables	74	125	

<u>Index terms</u>	<u>Links</u>
dilatant fluid	194
dipole	
of a point source	139
of a point vortex	163
Dirac delta function	551 561
displacement thickness	491
divergence	
theorem	83 84 225
of a vector field	62
drop, resting on a plane	241 250
 E	
eigenvalues and eigenvectors	35 69
Einstein summation convention	52
ellipse, curvature of	179
elliptic integrals	335 589
error function	344
Euler	
equation	270
method	21
modified	24
for a system of equations	238
equation of motion	
for a parcel	254
for a point particle	266
evolution equation,	
for the density	90
for the velocity	267
for the velocity potential	273
for the vorticity	288
expansion of a parcel	29 56 61

Index terms

extensional flow	193
extensive property	93
F	
Falkner-Skan boundary layers	498
Fast Fourier transform	536
FDLIB	651 653
FFT	536
film flow,	
down an inclined plane	315 424
multi-layered	316 430
finite differences, <i>see</i> differences	
finite difference methods,	
for the continuity equation	91
for Laplace's equation	122
for the Navier-Stokes equation	364
finite-volume method	428
flow rate,	
areal and volumetric	77
mass	87
flux,	
areal and volumetric	77
mass	87
force,	
body force	165
hydrodynamic volume force	264
in polar coordinates	267
surface force	165
on an immersed surface	217
Fourier decomposition	535
frequency parameter of a flow	304
friction velocity	544

Index terms**Links**

Froude number	278	304	
fundamental			
modes of parcel motion	49		
solutions of Laplace's equation	135		
G			
Gauss			
divergence theorem	83	84	225
elimination	132		
quadrature	575		
-Siedel method	134		
gradient of a function	52	59	60
Green's third identity	648		
growth rate of a perturbation	516		
H			
Hagen flow,			
steady	308		
transient	346		
oscillatory	352		
harmonic functions	116	117	
Helmholtz			
velocity of a vortex ring	596		
high-Reynolds-number flow	303	475	
Hill's vortex	599		
Holstein-Bohlen parameter	507		
homogeneous boundary conditions	118		
hump, flow over	277	281	
hydrostatics	208		
stress tensor in	182		

Index terms**I**

ideal			
fluid			192
gas law			184
incompressible fluid			101
inner vector product			52
instability of shear flows			512
integration, numerical			81
intensive property			93
interface,			
shape in hydrostatics			227
traction exerted on			171
traction jump across			173
interpolation			
of a function			
of one variable			38
of two variables			43
of three variables			47
of the velocity			46
irreducible loop			159
irrotational flow			65
		99	112
			295

J

Jacobi method			134
Joukowski transformation			611

K

Kàrmàn, von			
constant			544
integral method			494
-Pohlhausen solution			503

Index terms**Links**

Kàrmàn, von (<i>Continued</i>)			
vortex street		478	
Kelvin			
circulation theorem		584	
functions		360	
-Helmholtz instability		560	575
kinematics		1	49 111
Kronecker delta		66	
Kutta-Joukowski			
condition		611	
theorem		610	
L			
laminar flow		303	
Laplace			
equation and operator		116	117
in polar coordinates		119	324
-Young equation		229	
LIA		464	
line vortex		161	601
linear			
equations		132	
momentum		100	
stability analysis		512	
linearization of a function		50	
local induction approximation		601	
logarithmic law of the wall in turbulent flow		543	
logistic mapping		526	
lubrication flow		303	

Index terms

M	
manometer	215
Marangoni traction	175
mass	
conservation of	88
flow rate and flux	87
material	
derivative	88
parcel	27
surface	27
mean free path	3 190
meniscus	235 246
mid-point rule	325 335
momentum	
integral balance	258
of a parcel	100
rate of change of	253
tensor	259
thickness	493
N	
Navier-Stokes equation	281
neutrally-buoyant body	226
Newton's	
method	
for a nonlinear equation	220
for two nonlinear equations	471
for eigenvalues	520
second law of motion for a parcel	252
Newtonian fluid	188
non-Newtonian fluid	194
Nusslet film	316 425

Index terms**Links****O**

operator splitting	399		
Orr-Sommerfeld equation	516		
oscillatory flow			
in a channel	347		
in a tube	354	360	
Oseen			
Flow	462		
tensor	451	463	
Ostwald - de Waele model	194		
outer vector product	63		

P

panel method	620		
parcel			
of a fluid	2	28	
deformation	29	68	
expansion	29	61	
Newton's law for the motion of	252		
rotation	28	55	62
phase velocity	516		
pipe flow,			
<i>see</i> tube and channel flow			
through an enlargement	261		
pivoting of a linear system	133		
plane polar coordinates	12		
path line	20		
plastic fluid	194		
flow due to the motion of	343		
point			
force	450	463	
particle	18		

Index terms

point (<i>Continued</i>)	
properties of	93
source	136 149
in bounded flow	144 152
panel	639
in Stokes flow	450
in uniform flow	138
source dipole	139
panel	640
vortex	154 551
dipole	163
periodic array of	558
Pohlhausen polynomials	504
Poiseuille	
flow	321
transient	354
oscillatory	360
law	321
potential of the velocity	114
power	
-law fluid	194 314 318
spectrum	536
Prandtl	
boundary layers	480
mixing length	541
pressure	
boundary conditions	398
in hydrostatics	183
force due to	283
Poisson equation	327
for the pressure	395
integral formula	324

Index terms**Links**

pump, ejector	263
pycnometer	223
R	
Rayleigh	
equation of hydrodynamic stability	517
equation for an expanding bubble	285
-Taylor instability	430
reducible loop	160
rescaling	298
Reynolds	
decomposition	531
number	297 301
stresses	539
rigid body	
motion	3 108
rotation	2 108
translation	2 108
rotation	
matrix	33
of a parcel	28 62
rotational flow	113
rotlet	601
S	
Sakiadis boundary layer	500
scraper, flow due to the motion of	473
secant method	240
separation of a flow	478 485
simple	
fluid	187
shear flow	121 188 256

Links**Index terms**

shape factor	493		
shear			
function	507		
-thinning and -thickening	194		
shooting method	239	244	249
	489		
similitude	296		
sloshing of a fluid	273		
smoothing, numerical	566		
solenoidal			
vector field	101		
projection	399		
solid	1		
source, <i>see</i> point source			
sparse matrix	130	134	
sphere			
floating	218		
potential flow past	151	281	
Stokes flow due to the motion of	443		
spherical polar coordinates	9		
stability, hydrodynamic	512		
stagnation point	18		
Stokes flow	467		
Stokes			
circulation theorem	549		
boundary layer	351		
flow	302	410	443
law	449		
streaklines	25		
stream function,			
for axisymmetric flow	104		
no-penetration condition	109		

Index terms**Links**

stream function (<i>Continued</i>)			
for two-dimensional flow		102	
-vorticity formulation		382	386
streamlines		18	25
stress		166	
in polar coordinates		197	
symmetry of		172	
tensor		168	
Strouhal number		478	
surface			
force		165	
material		27	
tension		174	
suspension		2	
swirling flow		17	336 362
T			
tangent vector		77	
Taylor			
hypothesis		538	545
microscale		539	
tensor		54	
thin-airfoil theory		632	
Thomas algorithm		371	377
thread of a fluid, extending		186	
Toricelli's law		275	
traction		166	
on a boundary		172	
jump across an interface		173	
on an interface		171	
trapezoidal rule		420	593

Links**Index terms**

tridiagonal matrix	371
determinant of	521
troposphere	216
tube flow,	
steady,	
annular	321 339
circular	319 525 532
elliptical	328
rectangular	330
triangular	334
transient and oscillatory in a tube	354
turbulent flow	303 476 525
two-dimensional flow	17
vorticity of	67

U

unidirectional flow,	
<i>see</i> channel and tube flow	
unit vectors	4

V

vector	
inner product	52
outer product	63
velocity	
fluid	16
gradient tensor	53
of a molecule	5
potential	114
-pressure formulation	395
Venturi flume	277

<u>Index terms</u>	<u>Links</u>
viscosity	188
extensional	186
of a gas	190
shear	187
viscous force	283
vortex	
flow	112
force	270
layer	571
line	601
motion	548
panel	612
patch,	
axisymmetric	596
two-dimensional	567
point-	154 551
ring,	
with finite-size core	591
line	590
sheet	614 629
stretching	292
vorticity	62
flow induced by	584 586
in terms of the stream function	103
transport equation	288
vorton	601
Y	
yield stress	196

Index terms**Links**

W	
wall stress	205
Weber number	305
wind tunnel	276
Womersley number	350 360